

Texas Tech University

Multidisciplinary Research in Transportation

Develop Guidelines for Evaluation of Embankment Conditions in Bridge Approach Slabs and Pavement Structures

Bishal Shakya, Pawan Bhandari, Byeonguk Ryu, Garima Thapa, and Hoyoung Seo

Performed in cooperation with the Texas Department of Transportation and the Federal Highway Administration

Research Project 0-7173

Research Report 0-7173-R1B

Technical Documentation Page

1. Report No. FHWA/TX-27/0-7173-R1B	2. Government Accession No.:	3. Recipient's Catalog No.:	
4. Title and Subtitle: Develop Guidelines for Evaluation of Embankment Conditions in Bridge Approach Slabs and Pavement Structures		5. Report Date: October 2026	
		6. Performing Organization Code	
7. Author(s): Bishal Shakya, Pawan Bhandari, Byeonguk Ryu, Garima Thapa, and Hoyoung Seo		8. Performing Organization Report No. 0-7173-R1B	
9. Performing Organization Name and Address: Texas Tech Center for Multidisciplinary Research in Transportation Texas Tech University Lubbock, Texas 79409-1023		10. Work Unit No.(TRAIS):	
		11. Contract or Grant No.: Project 0-7173	
12. Sponsoring Agency Name and Address: Texas Department of Transportation Research and Technology Implementation Office P.O. Box 5080 Austin, TX 78763-5080		13. Type of Report and Period Covered Technical Report: September 2023 – August 2026	
		14. Sponsoring Agency Code:	
15. Supplementary Notes: Project performed in cooperation with Texas Department of Transportation and the Federal Highway Administration			

16. Abstract:

Distress at bridge approach slabs (BAS), adjacent pavement, and roadway embankments remains a recurring maintenance concern, commonly appearing as settlement, bumps, faulting, lane separation, cracking, and voids beneath slabs. The performance of these systems is often related to the condition of the underlying embankment and support materials. However, current TxDOT documentation does not provide a unified guideline for evaluating in-service embankment conditions or selecting repairs based on the underlying distress mechanism. Project 0-7173 was conducted to develop guidance for characterizing BAS and adjacent pavement conditions in roadway embankment areas and for selecting maintenance and repair strategies that address both visible distress and probable root causes. The research included a literature review of current evaluation and post-construction repair practices, a statewide survey of TxDOT districts, selection of representative field sections, field and laboratory evaluations using falling weight deflectometer (FWD), ground-penetrating radar (GPR), coring, dynamic cone penetrometer (DCP), cone penetration test (CPT), and soil sampling, and classification of observed distress mechanisms. The field and analytical findings were used to classify four primary distress mechanisms: compression of materials, loss of materials or washout, lateral stress buildup behind retaining walls, and non-uniform slab support. Based on these mechanisms, a three-level repair-selection framework was developed to identify the active distress mechanism, address the root cause, and then apply corrective repair measures for remaining surface distress. The outcomes of this project provide TxDOT engineers with a consistent, mechanism-based approach for evaluating embankment-related BAS and pavement distress and selecting repair strategies that are better aligned with the cause of poor performance.

17. Key Words: Bridge Approach Slabs (BAS), Roadway Embankments, Distress Mechanisms, Embankment Evaluation, Forensic Investigation, Maintenance and Repair Strategies		18. Distribution Statement No Restrictions. This document is available to the public through the National Technical Information Service, Springfield, VA 22161, www.ntis.gov	
19. Security Classification (of this report) Unclassified	20. Security Classification (of this page) Unclassified	21. No. Of Pages 532	22. Price

Develop Guidelines for Evaluation of Embankment Conditions in Bridge Approach Slabs and Pavement Structures

by

Bishal Shakya
Graduate Research Assistant
Civil, Environmental and Construction Engineering
Texas Tech University

Pawan Bhandari
Former Graduate Research Assistant
Civil, Environmental and Construction Engineering
Texas Tech University

Byeonguk Ryu
Graduate Research Assistant
Civil, Environmental and Construction Engineering
Texas Tech University

Garima Thapa
Graduate Research Assistant
Civil, Environmental and Construction Engineering
Texas Tech University

Hoyoung Seo
Associate Professor, Ph.D., P.E.
Civil, Environmental and Construction Engineering
Texas Tech University

Project Report 0-7173-R1B
Project Number 0-7173

Performed in Cooperation with the
Texas Department of Transportation
and the
Federal Highway Administration

Center for Multidisciplinary Research in Transportation
Department of Civil, Environmental and Construction Engineering
Texas Tech University
Box 41023
Lubbock, TX 79409-1023

AUTHOR'S DISCLAIMER

The contents of this report reflect the views of the authors who are responsible for the facts and the accuracy of the data presented herein. The contents do not necessarily reflect the official view of policies of the Texas Department of Transportation or the Federal Highway Administration. This report does not constitute a standard, specification, or regulation.

PATENT DISCLAIMER

There was no invention or discovery conceived or first actually reduced to practice in the course of or under this contract, including any art, method, process, machine, manufacture, design or composition of matter, or any new useful improvement thereof, or any variety of plant which is or may be patentable under the patent laws of the United States of America or any foreign country.

ENGINEERING DISCLAIMER

Not intended for construction, bidding, or permit purposes.

TRADE NAMES AND MANUFACTURERS' NAMES

The United States Government and the State of Texas do not endorse products or manufacturers. Trade or manufacturers' names appear herein solely because they are considered essential to the object of this report.

ACKNOWLEDGMENTS

This research study was sponsored by the Texas Department of Transportation (TxDOT) in cooperation with the Federal Highway Administration (FHWA). The Research Team greatly appreciates the support and assistance provided by the TxDOT Project Manager Anne Smith, and members of the Project Monitoring Committee (PMC): Ruben Carrasco, Pan Gil Choi, Ryan Eaves, Mark Davis, SangIck Lee, Gyaneswor Pokharel, and Karen Voelkel. Their guidance, insightful feedback, and continuous support throughout the duration of this project were essential in bringing the research to its final outcome.

TABLE OF CONTENTS

LIST OF FIGURES xv
LIST OF TABLES xxix
Chapter 1 Introduction 1
1.1 Background 1
1.2 Report Organization 2
Chapter 2 Literature Review and Current Practice 4
2.1 Overview of Roadway Embankments 4
2.1.1 Components 4
2.1.2 Typical cross-sections of roadway embankments and specifications for backfills 5
2.2 Distresses of Roadway Embankments and Their Causes 10
2.2.1 Common distresses on roadway embankments 10
2.2.2 Possible causes of distresses 13
2.2.3 Criteria for quantification of performance of bridge approach system 17
2.3 State-of-the-practice for evaluation of in-service roadway embankments 22
2.3.1 Specifications on evaluation of in-service roadway embankments 22
2.3.2 Specifications related to backfill materials for embankments and MSE walls 25
2.3.3 Design standards of bridge approach slabs 30
2.3.4 Project-specific case studies 38
2.3.5 Synthesis and Summary 64
2.4 Review of repair and soil improvement methods 78
2.4.1 Classification of soil improvement methods 78
2.4.2 Common methods used to repair roadway embankment/BAS 79
Chapter 3 Survey of Current TxDOT District Practice 113
3.1 Survey Questionnaire 113
3.2 Survey Responses 114
3.2.1 Question 1: Common distress types 115
3.2.2 Question 2: Timing of distress appearance 116
3.2.3 Question 3: Methods to identify sections that need repairs 117
3.2.4 Question 4: Specific criterion used for making decisions for repairs 118
3.2.5 Question 5: Typical activities conducted to evaluate the condition of BAS and nearby pavement structures 119

3.2.6 Question 6: Typical activities conducted for condition evaluation of in-service embankment fills 120
3.2.7 Question 7: Properties of embankment fills that need to be determined to assess their conditions 121
3.2.8 Question 8: Major contributing factors to the distresses 123
3.2.9 Question 9: Common maintenance measures taken 124
3.2.10 Question 10: Typical frequency of performing repairs 125
3.2.11 Question 11: Potential sections for new investigation 126
3.2.12 Question 12: Sections that have been performing well after repair 128
3.2.13 Question 13: Recommendations for fill materials for embankments/retaining walls or for construction practices 129
3.2.14 Question 14: Recommendations for repair practices 130
3.3 Synthesis of Survey Responses 131
3.3.1 Current practice for evaluation of bridge approach slabs and nearby pavement section in roadway embankments/retaining walls 131
3.3.2 Current practice for repair of bridge approach slabs and nearby pavement section in roadway embankments/retaining walls 132
3.3.3 Recommendations to improve performance of bridge approach slabs and nearby pavement section in embankments/retaining walls 132
Chapter 4 Selection of Test Sections 134
4.1 Potential field test sections 134
4.1.1 Section ID: P-A-1 143
4.1.2 Section ID: P-A-2 146
4.1.3 Section ID: P-A-3 148
4.1.4 Section ID: P-A-4 151
4.1.5 Section ID: P-A-5 154
4.1.6 Section ID: P-B-1 157
4.1.7 Section ID: P-B-2 160
4.1.8 Section ID: P-B-4 163
4.1.9 Section ID: P-C-1 166
4.1.10 Section ID: P-C-2 168
4.1.11 Section ID: S-11-1 171
4.1.12 Section ID: S-11-2 173
4.1.13 Section ID: S-11-3 175

4.1.14 Section ID: S-11-4 178
4.1.15 Section ID: S-11-5 180
4.1.16 Section ID: S-11-6 182
4.1.17 Section ID: S-11-7 185
4.1.18 Section ID: S-11-8 187
4.1.19 Section ID: S-11-9 190
4.1.20 Section ID: S-11-10 193
4.1.21 Section ID: S-12-1 195
4.1.22 Section ID: S-12-2 198
4.1.23 Section ID: S-12-3 200
4.1.24 Section ID: S-12-4 (P-B-3) 201
4.1.25 Section ID: S-12-5 204
4.1.26 Section ID: S-12-6 204
4.1.27 Section ID: E-1 206
4.1.28 Section ID: E-2 208
4.1.29 Section ID: E-3 211
4.1.30 Section ID: E-4 213
4.2 Final field test sections 215
Chapter 5 Field Investigations 219
5.1 Section E-2: IH-10 in San Antonio 219
5.1.1 Overview 219
5.1.2 Falling Weight Deflectometer (FWD) tests 220
5.1.3 Coring 223
5.1.4 Dynamic Cone Penetrometer (DCP) tests and Cone Penetration Tests (CPT) 226
5.1.5 Soil sampling 232
5.1.6 Potential Distress Mechanisms 235
5.1.7 Repair Recommendation 237
5.2 Section E-3: SH-47 in College Station 240
5.2.1 Overview 240
5.2.2 Falling Weight Deflectometer (FWD) tests 241
5.2.3 Coring 243
5.2.4 Dynamic Cone Penetrometer (DCP) tests 247

5.2.5 Potential Distress Mechanism 250
5.2.6 Repair Recommendations: 253
5.3 Section P-B-2: US 290 in Brenham 256
5.3.1 Overview 256
5.3.2 Dynamic Cone Penetrometer (DCP) tests 257
5.3.3 Injection of polyurethane foam 263
5.3.4 Comparison of Dynamic Cone Penetrometer (DCP) test results before and after injection of polyurethane foam 267
5.3.5 Potential Distress Mechanism 269
5.3.6 Repair Recommendations 271
5.4 Section S-11-8: US-290 Frontage Road in Austin 274
5.4.1 Overview 274
5.4.2 Falling Weight Deflectometer (FWD) tests 278
5.4.3 Ground Penetration Radar (GPR) Utility Scan 280
5.4.4 Coring 282
5.4.5 Dynamic Cone Penetrometer (DCP) tests 283
5.4.6 Soil Sampling 284
5.4.7 Potential Distress Mechanisms 287
5.4.8 Repair Recommendation 292
5.5 Section P-A-3: IH 20 on-ramp in Fort Worth 294
5.5.1 Overview 294
5.5.2 Falling Weight Deflectometer 296
5.5.3 Ground Penetrating Radar (GPR) Utility Scan 298
5.5.4 Coring 299
5.5.5 Dynamic Cone Penetration (DCP) tests and CPT Tests 301
5.5.6 Soil sampling 304
5.5.7 Potential Distress Mechanism 305
5.5.8 Repair Recommendation 308
5.6 P-A-4: IH 820 on-ramp in Fort Worth 310
5.6.1 Overview 310
5.6.2 Falling Weight Deflectometer Test 313
5.6.3 Ground Penetrating Radar (GPR) Utility Scan 314
5.6.4 Coring 316

5.6.5 Dynamic Cone Penetration (DCP) tests and CPT Tests 317
5.6.6 Soil sampling 319
5.6.7 Potential Distress Mechanism 321
5.6.8 Repair Recommendation 325
5.7 Section E-5: Beltway-8 at IH-45 in Houston, Houston 326
5.7.1 Overview 326
5.7.2 Falling Weight Deflectometer (FWD) Tests 330
5.7.3 Coring 330
5.7.4 Dynamic Cone Penetrometer (DCP) tests and Cone Penetration Test (CPT) 332
5.7.5 Soil Sampling 335
5.7.6 Potential Distress Mechanism 337
5.7.7 Repair Recommendation 339
5.8 Section E-4: IH 35 Exit 368A in Hillsboro, Waco 342
5.8.1 Overview 342
5.8.2 Falling Weight Deflectometer (FWD) tests 346
5.8.3 Ground Penetration Radar (GPR) Utility Scan 348
5.8.4 Coring 350
5.8.5 Dynamic Cone Penetrometer (DCP) Test 352
5.8.6 Soil Sampling 353
5.8.7 Inclinometer Monitoring 355
5.8.8 Potential Distress Mechanism 358
5.8.9 Repair Recommendation 363
5.9 Section E-1: IH 27 in Keuka Street, Lubbock 364
5.9.1 Overview 364
5.9.2 Falling Weight Deflectometer (FWD) tests 366
5.9.3 Coring 370
5.9.4 Dynamic Cone Penetration (DCP) tests 375
5.9.5 Soil Sampling 377
5.9.6 Potential Distress Mechanism 382
5.9.7 Repair Recommendations 383
5.10 Section P-A-5: IH 27 Tulia, Lubbock 385
5.10.1 Overview 385

5.10.2 Falling Weight Deflectometer (FWD) tests 387
5.10.3 Coring 389
5.10.4 Dynamic Cone Penetration (DCP) tests 391
5.10.5 Potential Distress Mechanism 394
5.10.6 Repair Recommendations 397
5.11 Section P-B-1: IH 35 Northbound Frontage Road in Waco 398
5.11.1 Overview 398
5.11.2 Google Earth Satellite Image Investigation 400
5.11.3 Falling Weight Deflectometer (FWD) Tests 403
5.11.4 Coring 404
5.11.5 Dynamic Cone Penetration (DCP) tests and CPT tests 405
5.11.6 Potential Distress Mechanism 409
5.11.7 Repair Recommendation 411
Chapter 6 Evaluation Guidelines 412
6.1 Observations from Field Investigation Program 412
6.1.1 Falling Weight Deflectometer (FWD) Testing 412
6.1.2 Ground Penetrating Radar (GPR) Scanning 413
6.1.3 Coring 414
6.1.4 Dynamic Cone Penetrometer (DCP) and Cone Penetration Testing (CPT) 415
6.1.5 Soil Sampling and Laboratory Testing 416
6.2 Guideline for Interpreting FWD Data 417
6.2.1 Overall Deflection Distributions 417
6.2.2 Effect of Slab Thickness on Deflection 425
6.2.3 Segmentation of FWD Deflection 428
6.3 Guideline for Interpreting Dynamic Cone Penetrometer (DCP) Test Data for Evaluation of Embankment Fill Conditions 433
6.3.1 Overview 433
6.3.2 Minimum $\boldsymbol{Mr}$ value at different DCP locations. 433
6.3.3 Spatial context and thickness of layer corresponding to minimum M_r 435
6.3.4 Performance-based classification of embankment materials 437
6.4 Guideline for Interpreting Cone Penetration Test (CPT) Data for Evaluation of Embankment Fill Conditions 438
6.4.1 Overview 438

6.4.2 Point-wise interpolation 439
6.4.3 Layer-wise method 442
6.4.4 Depth-binned analysis 444
6.4.5 Summary and recommendations 449
Chapter 7 Distress Mechanisms and Classification 451
7.1 Classification of distress mechanisms 451
7.1.1 Compression of materials 451
7.1.2 Loss of materials (Washout) 453
7.1.3 Lateral stress buildup behind the retaining wall 454
7.1.4 Non-uniform slab support 456
7.1.5 Frequency of distress mechanisms observed from test sites 457
7.1.6 Interaction of Root Causes, Mechanisms, and Embankment Distresses 458
Chapter 8 Maintenance and Repair Strategies 461
8.1 Principles for selecting a repair strategy 461
8.2 Mechanism-Based Decision Flowchart for BAS and Embankment Repair Selection 462
8.2.1 Level 0: Identification of distress mechanism 462
8.2.2 Level 1: Repair for root cause and mechanism 463
8.2.3 Level 2: Corrective repair measures 467
8.3 Commonly Used Repair Methods 471
8.3.1 HMA Level-up and Overlay 471
8.3.2 Flowable Fill 472
8.3.3 Polyurethane Foam Injection 473
8.3.4 Full and Partial-Depth Repair 475
8.3.5 Dowel-bar Retrofit, Slot Stitching, and Cross Stitching 476
Chapter 9 Conclusions and Recommendations 478
9.1 Summary of the Research 478
9.2 Summary of Findings 478
9.2.1 Current Practice and the Need for Evaluation Guidance 478
9.2.2 Field Evaluation Methods and Interpretation Guidelines 479
9.2.3 Distress Mechanisms 480
9.2.4 Maintenance and Repair Strategy 481
9.3 Recommendations for Implementation 481

9.4 Limitations and Recommendations for Future Research 482
REFERENCES 484
APPENDIX A: Survey Questionnaire 492
APPENDIX B: Value of Research (VoR) 499

LIST OF FIGURES

Figure 2-1. Schematic illustrations of typical components of a roadway embankment and a bridge approach system (modified after Briaud et al. 1997) 5
Figure 2-2. Typical cross sections of roadway embankments: (a) slope-slope section, (b) retaining wall-slope section, and (c) retaining wall- retaining wall section 6
Figure 2-3. Graphical representations of density control requirements of compacted embankment fill per TxDOT Item 132 8
Figure 2-4. Graphical representations of gradation requirements for select backfills for retaining walls per TxDOT Item 423 9
Figure 2-5. Photos showing (a) a bump between bituminous approach roadway and a concrete bridge deck in Minnesota (ElBatanouny et al. 2021) and (b) a differential settlement between the bridge deck and the approach slab in Iowa (White et al. 2005) 10
Figure 2-6. Photos showing cracks in roadway embankments: (a) a longitudinal crack on continuously reinforced concrete pavement (CRCP) in Texas and (b) a transverse crack on asphalt overlay in Iowa (White et al. 2005) 11
Figure 2-7. Photos showing faulting in roadway embankments: (a) faulting of bridge approach concrete panels in Iowa (White et al. 2005) and (b) faulting between outside main lane and outside shoulder in Texas 12
Figure 2-8. Photos showing lane separations in roadway embankments in Texas: (a) lane separation between inner lane and middle lane and (b) lateral movement of MSE wall 13
Figure 2-9. Photos showing settlement of foundation soils in Texas (from Galvan 2007 and Galvan 2011) 14
Figure 2-10. Photos showing (a) fill materials washed out from the retaining wall and (b) soil-reinforcing mats exposed behind retaining walls due to soil erosion in Texas (from Galvan 2007 and Galvan 2011) 15
Figure 2-11. Range of most erodible soils (modified from Briaud et al. 1997) and select backfill materials for MSE walls per TxDOT Item 423 16
Figure 2-12. Illustration of definition of Bridge Approach Performance Index (BI): BI = deviation area/length (modified from White et al. 2005) 19
Figure 2-13. Bridge Approach Index for rating bridge approach performance (Source: White et al. 2005) 20
Figure 2-14. Comparison of gradation limits of select fill for MSE walls from US DOTs: (a) maximum percent passing and (b) minimum percent passing (from Marr and Stulgis 2013) 26
Figure 2-15. US DOTs specified placement moisture content for MSE wall select fill (Marr and Stulgis 2013) 27
Figure 2-16. TxDOT's bridge approach slab standard: (a) plan view and (b) section view at the interface between the bridge approach slab and concrete pavement 32
Figure 2-17. Illinois Tollway's bridge approach slab standard 33
Figure 2-18. Iowa DOT's bridge approach slab standard 34
Figure 2-19. Inverted T-shaped slab in Colorado DOT standard 35
Figure 2-20. Sleeper slab underlain by bedding material in Louisiana DOTD standard 36

Figure 2-21. Details of a sleeper slab used in Oklahoma: (a) plan view and (b) section view 37
Figure 2-22. Demonstration of use of stringline for settlement measurement (Chen and Yi 2015) 39
Figure 2-23. Deviation curve (Chen and Yi 2015) 39
Figure 2-24. Comparison of the FWD deflections before and after the polyurethane-foam injection (IH 35) (Chen and Yi 2015) 40
Figure 2-25. Reduction of roughness (shaded area) in deviation plot before and after polyurethane-foam injection (Chen and Yi 2015) 41
Figure 2-26. Test section along SH 6 (Puppala et al. 2011) 42
Figure 2-27. Sectional views of the west and east approach slabs of IH 410 in San Antonio (Puppala et al. 2011) 44
Figure 2-28. Testing layout of IH 410 in San Antonio (Puppala et al. 2011) 45
Figure 2-29. GPR scanning in progress on an approach slab (ElBatanouny et al. 2018) 48
Figure 2-30. Photos showing the presence of voids beneath the bridge approach slab: (a) view of core drop (1/4 in) indicating presence of minor void under the slab and (b) view of void from borescope (ElBatanouny et al. 2018) 48
Figure 2-31. (a) Installation plan of horizontal inclinometers and (b) installation of horizontal inclinometer casing and return pipe (Abu-Farsakh and Chen 2014) 51
Figure 2-32. Comparison of settlement prediction (Abu-Farsakh and Chen 2014) 52
Figure 2-33. Borehole locations for US-177 over Salt Fork in Oklahoma (Miller et al. 2013) ... 54
Figure 2-34. (a) CPT and borehole locations for SH-1 over SH-99 in Oklahoma and (b) CPT results for East Embankment for SH-1 over SH-99 (Miller et al. 2013) 56
Figure 2-35. Typical wheel path designation in a lane (Lu et al., 2018) 58
Figure 2-36. Proposed rating system for bridge approach/departure asphalt pavement (Lu et al. 2018) 60
Figure 2-37. Rehabilitation strategy selection procedure for bridge approach/departure asphalt pavements (Lu et al., 2018) 61
Figure 2-38. An example of Bridge Approach Slab Condition Sheet (MoDOT, 2004) 63
Figure 2-39. Projected x-intercept average deflection (mils) before and after undersealing (MoDOT, 2004) 64
Figure 2-40. Techniques used for concrete slab leveling (Onyango et al. 2018) 79
Figure 2-41. Grouting applications (Szynakiewicz, 2016) 86
Figure 2-42. Grouting types (Nicholson, 2014) 87
Figure 2-43. Grouting methods and gradation relationship (Nicholson, 2014) 87
Figure 2-44. Compaction grouting process (Szynakiewicz, 2016) 88
Figure 2-45. Common grouting pattern layout for bridge embankment (Szynakiewicz, 2016) .. 89
Figure 2-46. Compaction Grouting SPT Results (Scherer & Gay, 2000) 95
Figure 2-47. Illustrations of polyurethane injection (Ellis, 2015) 97
Figure 2-48. An example of layout for injecting polyurethane (Ellis, 2015) 98
Figure 2-49. Slab joint before and after polyurethane slab jacking (Soltesz, 2002) 103
Figure 2-50. Dowel bar retrofit in progress (Stevenson, 2021b) 106
Figure 2-51. Washington state example of dowel bar retrofit (Darter, 2017) 106
Figure 2-52. An example of cross stitching: section view (Darter, 2017) 107

Figure 3-1. Summary of survey responses: (a) districts responded (the number in the parentheses indicate that two responses were provided from these districts) and (b) survey participants by position. 115
Figure 3-2. Summary of survey responses to common distress types (Question 1). 115
Figure 3-3. Summary of survey responses to timing of distress appearance (Question 2). 116
Figure 3-4. Summary of survey responses to methods to identify sections that need repairs (Question 3). 117
Figure 3-5. Summary of survey responses to specific criterion used for making decisions for repairs (Question 4) 118
Figure 3-6. Summary of survey responses to typical activities conducted for condition evaluation of BAS and nearby pavement structures (Question 5). 119
Figure 3-7. Summary of survey responses to specific criterion used for conducted for condition evaluation of in-service embankment fills (Question 6). 120
Figure 3-8. Summary of survey responses to properties of embankment fills that need to be determined to assess their conditions (Question 7). 122
Figure 3-9. Summary of survey responses to major contributing factors to the distresses (Question 8). 123
Figure 3-10. Summary of survey responses to common maintenance measures taken (Question 9). 124
Figure 3-11. Summary of survey responses to typical frequency of performing repairs (Question 10). 125
Figure 3-12. Locations of potential sections for new investigation, collected from survey Question 11 127
Figure 3-13. Locations of sections that have been performing well after repair, collected from survey Question 12. 128
Figure 4-1. Location of potential test sections identified at the time of proposal writing 134
Figure 4-2. Locations of potential test sections identified from survey in response to (1) Question 11 (new section) and (b) Question 12 (sections that have been performing well after repair). 135
Figure 4-3. Location of Section P-A-1 144
Figure 4-4. Observed distresses at Section P-A-1: (a) a longitudinal crack on the leave side of the subject section, (b) a longitudinal crack on the approach side of the subject section, and (c) misalignment of the traffic rail in approach side BAS. 145
Figure 4-5. (a) Site location and (b) location of Section P-A-2 147
Figure 4-6. Observed distresses at section P-A-2: (a) rutting of ACP on EBML approach side, (b) rutting of ACP on EBML leave side, (c) Google historical image that suggests poor performance of MSE wall and (d) repair in progress. 148
Figure 4-7. (a) Site location and (b) location of Section P-A-3 149
Figure 4-8. Observed distresses at Section P-A-3: (a) initiation of longitudinal crack on the leave side of the subject section with signs of spalling, (b) propagation of longitudinal crack on the subject section, (c) initiation of another longitudinal crack on the leave side of the subject section with signs of spalling, (d) propagation of longitudinal crack, and (e) settlement of pavement and separation from railing. 151
Figure 4-9. (a) Site location of P-A-4 and (b) location of Section P-A-4 152

Figure 4-10. Observed distresses at section P-A-4 (Google Street view image, March 2022): (a) settlement and longitudinal crack in BAS, (b) overlay in the BAS and approaching road, and (c) spalling in the BAS joint. 154
Figure 4-11. (a) Site location and (b) location of Section P-A-5. 155
Figure 4-12. Observed distresses at Section P-A-5 (Google street view image, May 2023): (a) longitudinal crack on the approach side of SBML, (b) propagation of longitudinal crack with signs of spalling/punchout, (c) longitudinal crack with spalling and patchwork, and (d) repair-joint deterioration and longitudinal crack on the leave side of SBML. 156
Figure 4-13. Location of Section P-B-1 158
Figure 4-14. Observed distresses at Section P-B-1: (a) a longitudinal crack on the southside of the subject section, (b) faulting between inside lane and edge (c), voids under the approach side of BAS and signs of HDPF applications in the past, and (d) a severe longitudinal crack in CRCP nearby the leave side of BAS 160
Figure 4-15. (a) Site location and (b) location of Section P-B-2 161
Figure 4-16. Observed distresses at section P-B-2 (Google street view image, May 2023): (a) settlement in BAS on Westbound main lane leave side, (b) pavement condition near drainage inlet, (c) longitudinal crack with punchout on the westbound main lane leave side, and (d) longitudinal crack and spalling in the BAS overlay. 163
Figure 4-17. (a) Site location and (b) location of Section P-B-4 164
Figure 4-18. Observed distresses at Section P-B-4 (Google street view image, Feb 2022): (a) Settlement in BAS and separation of shoulder and pavement and (b) separation of shoulder and pavement with loss of material from the joint. 165
Figure 4-19. New BAS and CRCP of Section P-B-4 after repair (June 2024). 166
Figure 4-20. (a) Site location and (b) location of Section P-C-1 167
Figure 4-21. Settlement of P-C-1 northbound approach BAS 167
Figure 4-22. (a) Site location and (b) location of Section P-C-2 169
Figure 4-23. Observed distresses at Section P-C-2 (Google Street View images): (a) minor bumps and spalling in the BAS, (b) patch work and spalling in the BAS, (c) longitudinal crack in the pavement, and (d) spalling and minor longitudinal crack in the BAS and asphalt overlay in the pavement 171
Figure 4-24. (a) Site location and (b) location of Section S-11-1 172
Figure 4-25. Observed distresses at Section S-11-1: (a) severe settlement in bridge approach slab and (b) longitudinal cracks in the adjacent pavement (Google Street View images of March 2023). 172
Figure 4-26. (a) Site location and (b) location of Section S-11-2 174
Figure 4-27. Observed distresses at Section S-11-2: (a) settlement (bump) at the northbound approach bridge approach slab (BAS), (b) settlement (bump) at the southbound leave BAS, and (c) minor longitudinal crack in the nearby pavement of the northbound leave in Section 1 (Google Street View images of March 2023). 175
Figure 4-28. (a) Site location and (b) location of Section S-11-3 176
Figure 4-29. Observed distresses in WB approach side at Section S-11-3: minor bumps based on Google Street View images of (a) Sep 2019 and (b) July 2022 177

Figure 4-30. Observed distresses in EB leave side at Section S-11-3: (a) longitudinal cracks on EB Approach Side, May 2024, (b) longitudinal cracks on WB Approach Side shoulder, and (c) bump and longitudinal crack (Google Street View images of Sep 2019)..... 178
Figure 4-31. (a) Site location and (b) location of Section S-11-4..... 179
Figure 4-32. Observed distresses at Section S-11-4: (a) longitudinal crack in BAS, (b) longitudinal cracks in pavement with crack sealing, and (c) longitudinal cracks in pavement and BAS with crack sealing..... 180
Figure 4-33. (a) Site location and (b) location of Section S-11-5..... 181
Figure 4-34. Observed distresses at Section S-11-5: longitudinal cracks in BAS (a) on SB leave side and (b) SB approach Side..... 182
Figure 4-35. (a) Site location and (b) location of Section S-11-6..... 184
Figure 4-36. Observed distresses at Section S-11-6: (a) settlement (bump) in BAS in SB approach side, (b) longitudinal crack in BAS in SB approach side, (c) longitudinal crack and patchwork in SB approach side, (d) longitudinal crack in BAS in SB leave side, and (e) lateral movement of MSE wall in SB leave side..... 185
Figure 4-37. (a) Site location and (b) location of Section S-11-7..... 186
Figure 4-38. Observed distresses at Section S-11-7: (a) spalling and longitudinal crack in the pavement and (b) longitudinal crack in the pavement. 187
Figure 4-39. (a) Site location and (b) location of Section S-11-8..... 188
Figure 4-40. (a) EB Frontage Road Approach Side (May 2024), (b) EB Frontage Road Approach Side (May 2024), and (c) EB Frontage Road Leave Side (May 2024)..... 189
Figure 4-41. Google Street View images of (a) EB Leave side pavement before asphalt overlay in Feb 2020, (b) EB Leave side pavement after asphalt overlay in May 2024. 190
Figure 4-42. (a) Site location and (b) location of Section S-11-9..... 191
Figure 4-43. Observed distresses at Section S-11-9: (a) longitudinal crack in BAS on WBML approach side, (b) longitudinal crack in BAS on WBML leave side, (c) diagonal crack on WBML leave side, and (d) longitudinal crack on EBML approach side, and (e) settlement (bump) in westbound BAS 192
Figure 4-44. (a) Site location and (b) location of Section S-11-10..... 194
Figure 4-45. Observed distresses at Section S-11-10: (a) longitudinal crack in BAS on EBML leave side, (b) diagonal crack in BAS on WBML leave side, (c) longitudinal crack and settlement in BAS on WBML approach side, and (d) longitudinal crack and settlement in BAS on EBML approach side. 195
Figure 4-46. (a) Site location and (b) location of Section S-12-1..... 196
Figure 4-47. Distress observed at Section S-12-1: longitudinal cracks in (a) northbound approach, (b) southbound leave, (c) northbound leave, and (d) southbound approach..... 197
Figure 4-48. Google satellite images showing construction history and condition of Section S-12-1..... 197
Figure 4-49. (a) Site location and (b) location of Section S-12-2..... 199
Figure 4-50. Void discovered beneath the bridge approach slab on October 4, 2021, as identified by TxDOT (Source: Email communication with TxDOT)..... 199

Figure 4-51. Google Street View images of (a) NB Approach side pavement (May 2022), (b) NB leave side pavement (May 2022), (c) longitudinal crack observed in NB Leave side pavement (May 2022), and (d) SB approach side pavement (May 2024)..... 200
Figure 4-52. Longitudinal crack in approach pavement (March 2023). 201
Figure 4-53. Location of Section S-12-4 202
Figure 4-54. Distress observed at Section S-12-4 (P-B-3): (a) lane Separation between main lanes, (b) lane Separation ranges between main lane and shoulder as well as lane settlement, (c) tie-bar failure, and (d) MSE wall movement..... 203
Figure 4-55. (a) Site location and (b) location of Section S-12-6. 205
Figure 4-56. Distress observed at Section S-12-6: (a) settlement at approach pavement and (b) diagonal crack and PCC patch. 205
Figure 4-57. (a) Site location and (b) location of Section E-1 207
Figure 4-58. Lane separation observed in the approach pavement pre-repair, 2003 (Photo courtesy of Dr. Moon Won) 207
Figure 4-59. Distress observed at Section E-1 (a) longitudinal crack, (b) PCC Patches, (c) spalling in NB approach pavement and (d) settlement in BAS. 208
Figure 4-60. Location of Section E-2 (IH 10 main lanes in San Antonio, TX)..... 209
Figure 4-61. Observed distresses at Section E-2: (a) 7-inch-thick void beneath the bridge approach slab (BAS) and (b) severe joint opening between the outside two lanes of westbound (Image source: TxDOT)..... 211
Figure 4-62. Location of Section E-3 (SH-47 main lanes College station, TX)..... 212
Figure 4-63. Observed distresses at Section E-3: (a)Settlement at SB approach and (b) Settlement at NB leave (c) Misaligned railing at SB approach. 213
Figure 4-64. (a) Site location and (b) location of Section E-4 214
Figure 4-65. Distress observed at Section E-4 (a) settlement of departure BAS (b) lateral separation and faulting between gore area and ramp (c) MSE wall panel bulge (d) diagonal/halfmoon crack..... 215
Figure 4-66. Locations of final sections selected for this project 216
Figure 5-1. Location of Section E-2 on IH-10 in San Antonio, Texas 219
Figure 5-2. Typical section of Section E-2 on IH-10 in San Antonio, Texas..... 220
Figure 5-3. FWD drop location of Section E-2 on IH 10 in San Antonio, Texas..... 221
Figure 5-4. FWD testing location and deflections measured in the middle (R3) and inside (R4) lanes of eastbound main lanes..... 222
Figure 5-5. FWD testing location and deflections measured at inside lane (L4), middle lane (L3), and inside shoulder (IS) of westbound..... 223
Figure 5-6. Coring locations and images of core samples 224
Figure 5-7. Void thickness measured from coring operations in relation to FWD deflection: (a) eastbound and (b) westbound main lanes 225
Figure 5-8. Results from DCP tests: Cumulative blow counts vs. Penetration depth below the pavement surface 227
Figure 5-9. Resilient modulus determined from DCP tests (Notes: DCP4 and DCP5 are controls; the color scheme for M_r value is for illustrative purposes only.)..... 228
Figure 5-10. Cone tip resistance measured from CPTs 229

Figure 5-11. Soil behavior types estimated from CPT results 230
Figure 5-12. Correlation between resilient moduli from DCP tests and average cone resistances from CPTs for the corresponding layers (Note: For information purpose only) 231
Figure 5-13. Resilient moduli of embankment backfill soils estimated from CPT results: (a) whole data and (b) zoomed-in view (Note: For information purpose only) 232
Figure 5-14. Photos of soil sample taken from the locations of (a) C1 and (b) C4 232
Figure 5-15. Particle size distribution curves: (a) soil samples taken from C1 at various depths and (b) comparison between C1 and C4 at similar depth 234
Figure 5-16. Conceptual illustration of washout of fines due to water infiltration and ensuing volume decrease: (a) initial soil composition, (b) washout of fines due to water infiltration, and (c) decrease in volume after washout 235
Figure 5-17. Distress mechanism of void formation and BAS settlement in Section E-2 (Note: the color scheme for M_r value is for illustrative purposes only.) 236
Figure 5-18. Potential distress mechanism of material washout in Section E-2 237
Figure 5-19. Existing investigation (a) core hole temporarily patched with (b) HMA cold mix. 238
Figure 5-20. Recommended flowable fill injection locations 238
Figure 5-21. Location of Section E-3 on SH-47 in College Station, Texas 240
Figure 5-22. Typical section of Section E-3 on SH-47 in College Station, Texas 241
Figure 5-23. FWD testing location and deflections measured at inside and outside lanes of southbound 242
Figure 5-24. FWD testing location and deflections measured at inside lane, outside lane, and outside shoulder of northbound. 243
Figure 5-25. Coring locations and images of core samples: (a) southbound and (b) northbound 245
Figure 5-26. Void thickness measured from coring operations in relation to FWD deflection: (a) southbound and (b) northbound 246
Figure 5-27. Cumulative DCP blow counts vs. penetration depth below the pavement surface: (a) southbound and (b) northbound 248
Figure 5-28. Resilient modulus determined from DCP tests: (a) southbound and (b) northbound lanes (Note: the color scheme for M_r value is for illustrative purposes only.) 249
Figure 5-29. Illustration showing void development under BAS and settlement/bump on BAS and nearby pavement due to the settlement of embankment soil and water infiltration (Note: the color scheme for M_r value is for illustrative purposes only) 251
Figure 5-30. (a) Illustration showing the probable distresses mechanism in the embankment in SH 47, College Station and (b) fill materials washed out of MSE wall (Google Street View from April 2021) 253
Figure 5-31. Repair recommendations for SH 47 SB approach and NB departure areas 254
Figure 5-32. Repair recommendation for SH 47 SB departure. 255
Figure 5-33. Location of Section P-B-2 of US 290 in Brenham, Texas 256
Figure 5-34. Location of DCP tests 258
Figure 5-35. Results from DCP tests: (a) DCP1 through DCP5 in the excavated area (BAS area), (b) DCP6 through DCP14 (pavement area), and (c) DCP15 through DCP21 (pavement area). 260

Figure 5-36. Resilient modulus determined from DCP tests: (a) DCP1 through DCP5 in the excavated area (BAS area), (b) DCP6 through DCP14 (pavement area), and (c) DCP15 through DCP21 (pavement area) (Note: the color scheme for M_r value is for illustrative purposes only.) 261
Figure 5-37. Photos showing (a) water flowing out of the MSE wall, (b) backfill materials washed out of the MSE wall on the side of frontage road, and (c) backfill materials washed out of the MSE wall on the side of abutment wall 263
Figure 5-38. Photos showing the injection process of high-density polyurethane foam (HDPF): (a) installation of 0.5-in. diameter injection tubes on a 5-ft by 5-ft grid, (b) connection of an injection gun with the tube to supply HDPF from a truck where the chemical tanks and pumps are stored, (c) monitoring the ground movement throughout the injection process using a rotating laser level and a receiver, and (d) removal of excessive polyurethane material after the injection is completed. 266
Figure 5-39. Comparison of DCP test results before and after high-density polyurethane foam (HDPF) injection: (a) DCP1, (b) DCP2, (c) DCP3, and (d) DCP5 268
Figure 5-40. Illustration showing settlement of BAS and nearby pavement due to the compression of embankment soil and washout (Note: the color scheme for M_r value is for illustrative purposes only.) 270
Figure 5-41. Illustration showing the distress mechanism in the embankment in US-290, Brenham. 271
Figure 5-42. Extent of full depth repair (FDR) for US-290, Brenham (provided by TxDOT).. 273
Figure 5-43. Location of Section S-11-8 of US-290 in Austin, Texas 274
Figure 5-44. Observed distresses at bridge approach side in section S-11-8: (a) lateral movement of railing and sidewalk, (b) railing settlement, and (c) longitudinal cracks on pavement surface 276
Figure 5-45. Observed distress (a) on MSE wall panels and (b) on coping and riprap 277
Figure 5-46. FWD testing locations at the approach and departure side 278
Figure 5-47. FWD deflections measured at the approach outside (a) and inside (b) lanes 279
Figure 5-48. FWD deflections measured at the outside lane of departure side 280
Figure 5-49. GPR scanned locations and data of approach side for (a) outside lane and (b) inside lane 281
Figure 5-50. Coring Locations and images of core samples 282
Figure 5-51. Locations of DCP testing 283
Figure 5-52. (a) Cumulative DCP blow counts vs. penetration depth below the pavement surface. (b) Resilient modulus (M_r) determined from DCP tests (Note: the color scheme for M_r value is for illustrative purposes only.) 284
Figure 5-53. Sampling locations and moisture contents with various depths 286
Figure 5-54. Particle size distribution curves: (a) soil samples taken from C7B and (b) soil sample from C8A at various depths 287
Figure 5-55. Potential distress mechanism (Note: the color scheme for M_r value is for illustrative purposes only.) 290
Figure 5-56. Potential distress mechanism for MSE wall 292
Figure 5-57. Recommended repair area for short-term and long-term plans 293

Figure 5-58. Location of Section P-A-3 of IH20 on-ramp in Fort Worth, Texas 294
Figure 5-59. Distress observed at IH-20 on-ramp: (a) Half-moon shaped cracking (b) Settlement between pavement and base of railing at different DMI. 296
Figure 5-60. (a) FWD testing locations with coring location marked. (b) Deflections measured at the inside shoulder and on middle of lane on the Ramp and middle lane and inside lane of adjacent frontage road at different DMI along with coring location marked. 297
Figure 5-61. (a) GPR pass location. (b) Visualization of void and HDPF and GPR scan result at 2ft from the railing. 299
Figure 5-62. Coring location and images of cored samples. 300
Figure 5-63. Void thickness measured at cored location. 301
Figure 5-64. Detail DCP locations 301
Figure 5-65. Cumulative blow counts vs. penetration depth below the pavement surface and the resilient modulus determined from DCP tests (Note: the color scheme for M_r value is for illustrative purposes only.) 302
Figure 5-66. Locations of CPTs 303
Figure 5-67. CPT cone tip resistance vs. penetration depth below the pavement surface. 303
Figure 5-68. Soil sampling location and results from particle size distribution analysis. 305
Figure 5-69. Illustration showing formation of gap between base of railing and the pavement due to settlement of embankment soil and foundation soil. 306
Figure 5-70. Illustration showing Void development under BAS due to the settlement of embankment soil and foundation soil and water infiltration (Note: the color scheme for M_r value is for illustrative purposes only.) 307
Figure 5-71. Illustration showing void development under CRCP. 308
Figure 5-72. Short term repair recommendation for IH 20, Fort Worth using HDPF. 308
Figure 5-73. Long term repair recommendation for IH 20, Fort Worth Section 309
Figure 5-74. Location of Section P-A-4 of IH820 On-ramp in Fort Worth, Texas 310
Figure 5-75. Typical section view and pavement structure of IH820 Ramp. 311
Figure 5-76. (a) HMA overlay and (b) lateral movement of BAS railing. 312
Figure 5-77. Settlement between base of railing and the pavement with photos taken (a) at DMI 30 and 410 ft and (b) at DMI 160 ft 313
Figure 5-78. FWD testing locations and deflections measured at the outside shoulder (Ramp Shoulder) and middle of the lane (Ramp). 314
Figure 5-79. (a) GPR paths and (b) GPR results at 2ft, 10ft and 16ft from the railing 315
Figure 5-80. Coring location and images of cored samples. 317
Figure 5-81. Locations of DCP tests. 317
Figure 5-82. DCP Cumulative blow counts vs. penetration depth below the pavement surface and resilient modulus determined from DCP tests 318
Figure 5-83. Locations of CPTs 319
Figure 5-84. Results from CPT: (a) cone tip resistance and (b) sleeve friction vs. penetration depth below the pavement surface. 319
Figure 5-85. Soil sampling location and particle size distribution. 321

Figure 5-86. Illustration showing void development under BAS, settlement/bump on BAS and nearby pavement, and riprap settlement due to the settlement of embankment soil and water infiltration (Note: the color scheme for M_r value is for illustrative purposes only.) 322
Figure 5-87. (a) Illustration showing formation of gap between base of railing and the pavement due to settlement of embankment soil and foundation soil and (b) birds-eye-view illustration of the distresses in the embankment in IH-820, Fort Worth. 324
Figure 5-88. Repair recommendation for IH 820, Fort Worth, using HDPF and HMA overlay. 325
Figure 5-89. Location of the Beltway-8 test section at IH-45 in Houston. 326
Figure 5-90. Observed Distress (a) wide lane separation, (b) tie-bar failure, (c) faulting, (d) abutment Separation, and (e) MSE wall lateral movement. 329
Figure 5-91. Longitudinal FWD deflection profiles (d1) across BW-8 test site at Houston 330
Figure 5-92. Location of cores and drills at BW8 test section in Houston 331
Figure 5-93. Presence of HDPF and void under the slab at location (a) C2 and (b) C5 at BW-8 test site in Houston 331
Figure 5-94. Locations of DCP and CPT testing across the pavement width. 332
Figure 5-95. Cumulative blow counts and layer M_r vs. penetration depth for select locations, highlighting the contrast between control and distressed sections (Note: the color scheme for M_r value is for illustrative purposes only.) 333
Figure 5-96. Correlation between subgrade moduli from DCP and average cone resistance from CPT (Note: For information purpose only). 334
Figure 5-97. Moduli of backfill materials and founding soils determined from CPT data using the site-specific correlation at (a) CPT8, (b) CPT7, and (c) CPT6 (Note: For information purpose only) 335
Figure 5-98. Particle size distribution curves determined from wet sieve and hydrometer analysis 336
Figure 5-99. Illustration of (a) original embankment configuration and (b) vertical displacement due to weak founding soil 338
Figure 5-100. Illustration of lane separation triggered by rotation of wall 338
Figure 5-101. Illustration of subsequent void formation and faulting. 339
Figure 5-102. Proposed temporary repair plan (TxDOT item 721 & 401) to prevent rainwater infiltration 340
Figure 5-103. Illustration of proposed layout for Repair Option 1 with longitudinal FWD deflection profiles. 340
Figure 5-104. Illustration presenting proposed layout for Repair Option 2 with longitudinal FWD deflection profiles. 341
Figure 5-105. Location of the IH 35 Exit 368A test section in Hillsboro, Texas. 342
Figure 5-106. Wall configuration of IH 35 Exit 368A test section in Hillsboro, Texas 344
Figure 5-107. Comparison of test section after expansion 344
Figure 5-108. Observed distresses including (a) settlement of departure slab (b) lateral separation between gore area and ramp (c) faulting between gore area and ramp (d) MSE wall panel bulge (e) diagonal/halfmoon crack. 346

Figure 5-109. Longitudinal FWD deflection profiles (D1) for shoulder and wheel paths across IH35 SB (Exit 368A) test section 347
Figure 5-110. Spatial comparison of FWD surface deflections (D0), GPR-derived CRCP thickness with core locations (C1–C8), and potential HDPF injection areas. 348
Figure 5-111. GPR scan 4 showing the extent of void and HDPF under pavement..... 349
Figure 5-112. Potential HDPF extent determined using GPR and verified using field observation. 350
Figure 5-113. Coring locations and images of core samples 351
Figure 5-114. Cumulative DCP blow counts and layer M_r values..... 353
Figure 5-115 Inclinometer displacement profiles with depth by reading date: (a) lateral displacement, positive toward the MSE wall; (b) longitudinal displacement, positive toward the abutment..... 356
Figure 5-116. Inclinometer displacement time-history at selected depths..... 357
Figure 5-117. Rate of lateral movement between successive inclinometer readings at depths of 2 ft and 26 ft, showing the reduction in rate following the June 2020 buttress placement..... 358
Figure 5-118. Initial phase: Water infiltration leading to elevated lateral pressure and reduced reinforcement friction. 359
Figure 5-119. Progress of distress: (a) Lateral subgrade movement creates a void, (b) transferring immense load to the tie bars causing them to yield and fracture, and (c) lane separation and further MSE wall bulging 361
Figure 5-120. Proposed cracking sequence: Initial faulting causes halfmoon cracks, followed by shear movement causing parallel diagonal cracks. 362
Figure 5-121. Illustration of proposed layout for Repair Option 1 (cut-and-fill/overlay) 363
Figure 5-122. Location of Section E-1 on IH-27 in Lubbock, Texas 364
Figure 5-123. Typical section of Section E-1 on IH-27 in Lubbock, Texas..... 365
Figure 5-124. Current condition of patch to address lane separation observed in SB departure366
Figure 5-125. FWD testing locations and deflections measured at the outside lanes and shoulders of northbound and southbound main lanes 367
Figure 5-126. FWD testing locations and deflections measured at the outside lanes and shoulders of northbound main lanes..... 368
Figure 5-127. FWD testing locations and deflections measured at the outside lanes and shoulders of southbound main lanes 369
Figure 5-128. FWD deflection box plot summarizing data from all tested locations..... 370
Figure 5-129 Coring locations and images of core samples: (a) Northbound and (b) Southbound 372
Figure 5-130. Photo of inside of C4 cored hole (0.5-in-thick void is observed between CRCP bottom and top of sleeper slab)..... 373
Figure 5-131. Separation between pavement and sleeper slab measured from coring in relation to FWD deflection at (a) southbound and (b) northbound roads 374
Figure 5-132. Corrosion observed in (a) Pavement surface near longitudinal joint, (b) SB departure side Abutment (outside lane) 375
Figure 5-133. DCP test results for Southbound main lanes (a) Cumulative N plot (b) Resilient modulus determined from DCP test..... 376

Figure 5-134. DCP test results for Northbound main lanes (a) Cumulative N plot (b) Resilient modulus determined from DCP test..... 377
Figure 5-135. Location of collected soil sample and moisture content at (a) Northbound and (b) Southbound Road..... 378
Figure 5-136. Particle Size Distribution for Southbound Soils 380
Figure 5-137. Particle Size Distribution for Northbound Soils 382
Figure 5-138. Observed separation at the BAS-sleeper slab interface. 383
Figure 5-139. Location of Section P-A-5 on IH-27 in Tulia, Lubbock, Texas..... 385
Figure 5-140. Typical section of Section P-A-5 on IH-27 in Tulia, Lubbock, Texas 386
Figure 5-141. Observed white residue on the pavement surface. 387
Figure 5-142. FWD deflections along outside lane and outside shoulder on NB approach and SB departure 388
Figure 5-143. FWD deflections along outside lane and outside shoulder on NB departure and SB approach..... 389
Figure 5-144. Coring locations and pavement structure for Southbound Approach 390
Figure 5-145. Coring locations and pavement structure for Southbound Departure..... 390
Figure 5-146. DCP Results – Southbound (a) Cumulative DCP blow counts vs. penetration depth below the pavement surface. (b) Resilient modulus determined from DCP tests 392
Figure 5-147. DCP results – Northbound (a) Cumulative DCP blow counts vs. penetration depth below the pavement surface. (b) Resilient modulus determined from DCP tests 393
Figure 5-148. Illustration of IH27 Tulia site longitudinal cross section showing CRCP terminal anchor lug system 394
Figure 5-149. Longitudinal expansion and contraction of CRCP and anchorage system due to temperature variation 395
Figure 5-150. Illustration of formation of voids around anchor lugs due to cyclic thermal expansion and contraction of the CRCP. 396
Figure 5-151. Addition of Bridge Approach Slab (BAS) and expansion joint to accommodate thermal expansion. 396
Figure 5-152. Location of the IH 35 Northbound Frontage Road in Waco, Texas. 398
Figure 5-153. Typical section of Section P-B-1 on IH 35 in Waco. Texas 399
Figure 5-154. Observed distress on approach and departure side..... 400
Figure 5-155. Reconstruction of main lanes and ramp on IH35 Waco site 401
Figure 5-156. Google historical street view images on approach and departure side where longitudinal cracks were observed. 402
Figure 5-157. Pavement width of outside lane in approach and departure side. 403
Figure 5-158. FWD drop locations (a) and deflections (b) on bridge approach and departure side. 404
Figure 5-159. Coring locations and images of cored samples 405
Figure 5-160. DCP and CPT testing locations. Testing layout for field investigation in I35 Waco site. 406
Figure 5-161. Resilient modulus of embankment fills from initial five DCP tests conducted by TxDOT (Note: the color scheme for M_r value is for illustrative purposes only.)..... 407

Figure 5-162. Resilient modulus of embankment fills from additional five DCP tests conducted by TTU research team (Note: the color scheme for M_r value is for illustrative purposes only.) 408
Figure 5-163. Cone resistance versus depth each CPT test location 409
Figure 5-164. Distress mechanism for the observed longitudinal cracks: (a) initiation of early-age longitudinal crack due to warping/curling and (b) reduction of the lateral confinement due to excavation, causing lateral movement and settlement leading to widening of the longitudinal crack 411
Figure 6-1. Overall FWD deflection distribution by site 417
Figure 6-2. Comparison of deflection data obtained from Bridge Approach Slab (BAS) and pavement on embankment 418
Figure 6-3. Average and standard deviation of normalized D_0 deflection by site 419
Figure 6-4. Longitudinal D_0 deflection profile: IH10WB SAT DEP L4 422
Figure 6-5. Longitudinal D_0 deflection profile: IH820RMP FTW APP OL..... 423
Figure 6-6. Longitudinal D_0 deflection profile: SH47NB COL Dep IL 423
Figure 6-7. Longitudinal D_0 deflection: SH47NB COL APP OL..... 424
Figure 6-8. Longitudinal D0 Deflection: IH27SB TUL APP OSH 424
Figure 6-9. Slab thickness of well-performing CRCP vs normalized central deflection from FWD (modified after TxDOT Project 0-5445)..... 426
Figure 6-10. Observed FWD central deflection (D_0) vs CRCP thickness 427
Figure 6-11. Cumulative distribution of deflection ratios by condition type..... 428
Figure 6-12. Typical example of "elbow method" for determining the optimal number of segments 430
Figure 6-13. Iterative segmentation examples showing progression toward optimal segmentation (IH-20 Fort Worth Ramp)..... 431
Figure 6-14. Field-validated segmentation isolating thinner slab, HDPF, normal support, and voided bridge-approach regions (IH-20 Ramp)..... 432
Figure 6-15. Minimum Mr value at each test location associated with distress types 434
Figure 6-16. Minimum $\boldsymbol{Mr}$ value at each test location associated with distress types; Minimum $\boldsymbol{Mr}$ value was assigned to zero for locations with voids. 435
Figure 6-17. Minimum M_r value at each test location vs. mid depth of the layer corresponding to the M_r. 436
Figure 6-18. Minimum M_r value at each test location vs. thickness of the layer corresponding to the M_r. 437
Figure 6-19. Regression analysis between Mr from DCP and qc from CPT at the same depth using a pointwise data: (a) IH-20, Fort Worth (b) IH-820, Fort Worth (c) IH-45, Navarro (d) BW-8, Houston (e) IH-10, San Antonio, and (f) IH-35, Waco. 441
Figure 6-20. Regression analysis between M_r from DCP and q_c from CPT at the same depth using layer-wise data: (a) IH-20, Fort Worth, (b) IH-820, Fort Worth, (c) IH-45, Navarro, (d) BW-8, Houston, (e) IH-10, San Antonio, and (f) IH-35, Waco. 443
Figure 6-21. Regression analysis between M_r from DCP and q_c from CPT averaged for 6-in layer interval: (a) IH-20, Fort Worth, (b) IH-820, Fort Worth, (c) IH-45, Navarro, (d) BW-8, Houston, (e) IH-10, San Antonio, and (f) IH-35, Waco. 446

Figure 6-22. Regression analysis between M_r from DCP and q_c from CPT averaged for 12-in layer interval: (a) IH-20, Fort Worth, (b) IH-820, Fort Worth, (c) IH-45, Navarro, (d) BW-8, Houston, (e) IH-10, San Antonio, and (f) IH-35, Waco. 448
Figure 6-23. Combined regression analysis between M_r from DCP and q_c from CPT averaged for 12-in layer interval from four predominant clay sites (IH 20, Fort Worth; IH 820, Fort Worth; BW-8, Houston; and IH 35 Navarro) 449
Figure 7-1. Illustration of distress mechanism for compression of fill materials: (a) embankment condition right after construction; (b) resulting embankment condition 452
Figure 7-2. Illustration of distress mechanism for embankment condition resulted from compression of founding soil over time 453
Figure 7-3. Illustration of distress mechanism for loss of materials (washout) 454
Figure 7-4. Illustration of distress mechanism for lateral stress buildup: (a) weakening of fill materials due to water infiltration, (b) compression of fill materials (or void formation), development of pavement cracks, and lateral movement of wall due to increase of lateral pressure, (c) faulting due to weakened slab support and repeated traffic loading, and (d) lane separation and further lateral movement of the wall due to increased lateral pressure. 456
Figure 7-5. Illustration of distress mechanism for non-uniform slab support: (a) typical section of MSE-wall-type roadway embankment and (b) development of pavement cracks due to non-uniform slab support 457
Figure 7-6. Distress mechanisms identified at each site 458
Figure 7-7. Three-layer interaction diagram showing how root causes (Layer 1) can trigger embankment response mechanisms (Layer 2) that manifest as visible distresses (Layer 3) at bridge approach transitions. 460
Figure 7-8. Interaction of Root Causes, Mechanisms, and Visible Distresses with Highlighted Deterioration Loop for the IH-35 Hillsboro Site. 460
Figure 8-1. Three-level procedural framework for evaluating and repairing distress in BAS and embankment-pavement structures. 462
Figure 8-2. Flowchart to address compression of material for embankment-pavement system repair (this flowchart is for illustrative purposes only). 464
Figure 8-3. Flowchart to address loss of materials for embankment-pavement system repair (this flowchart is for illustrative purposes only). 465
Figure 8-4. Flowchart to address lateral stress buildup behind the retaining wall for embankment-pavement system repair (this flowchart is for illustrative purposes only). 466
Figure 8-5. Flowchart to address non-uniform slab support for embankment-pavement system repair (this flowchart is for illustrative purposes only). 467
Figure 8-6. Repair flowchart for void (this flowchart is for illustrative purposes only). 468
Figure 8-7. Repair flowchart for settlement and bump (this flowchart is for illustrative purposes only). 469
Figure 8-8. Repair flowchart for faulting and lane separation (this flowchart is for illustrative purposes only). 470
Figure 8-9. Leakage of flowable fill from riprap. (Image source: TxDOT Maintenance Division) 473
Figure 8-10. HDPF injection process (Image source: https://www.uretekusa.com/blogs/) 474

LIST OF TABLES

Table 2-1. Field density control requirements for embankment fills per TxDOT Item 132 7
Table 2-2. Gradation requirements for select backfills for retaining walls per TxDOT Item 423. 9
Table 2-3. Micro method in determining differential settlement scale (Zhang 2016) 17
Table 2-4. Macro method in determining differential settlement scale (Zhang 2016) 18
Table 2-5. Summary of IRI interval and threshold for determining poor bumps (Wang et al. 2023) 18
Table 2-6. Criteria based on differential settlement of bridge approach areas 21
Table 2-7. Condition rating for approach roadway from Washington State DOT 23
Table 2-8. Reinforced concrete approach slab condition states from Montana DOT 24
Table 2-9. Condition rating for Approach Embankment from Ohio DOT 25
Table 2-10. Comparison of electrochemical properties of MSE wall select fill 28
Table 2-11. Embankment fill specifications for bridge approach (from Hoppe 1999) 29
Table 2-12. Summary of design standards for bridge approach slabs from selected states 31
Table 2-13. Example of documentation from visual inspection (ElBatanouny et al. 2018) 46
Table 2-14. Crack characterization based on surface condition (Lu et al., 2018) 58
Table 2-15. Pavement condition evaluation based on condition rating (Lu et al., 2018) 59
Table 2-16. Criteria for maintenance (MoDOT 2004) 64
Table 2-17. Studies that have utilized FWD to assess the conditions of the BAS and nearby pavement in roadway embankments 66
Table 2-18. A summary of GPR testing procedure from various studies conducted for evaluations of bridge approach and nearby pavement 69
Table 2-19. A summary of surface profile measurements 72
Table 2-20. A summary of CPTs conducted to evaluate the conditions of roadway embankments 75
Table 2-21. A summary of DCP tests conducted to evaluate the conditions of roadway embankments 76
Table 2-22. Automatic FDR criteria (Krauss et al., 2009) 81
Table 2-23. State DOTs' specifications about FDR (Darter, 2017) 82
Table 2-24. PDR State DOTs' specifications on PDR (Darter, 2017) 82
Table 2-25. Treatment types and applicability (Fortunatus, 2018) 85
Table 2-26. State DOTs' specifications on cementitious grout (Vennapusa et al., 2016) 90
Table 2-27. State DOTs' specifications on high density polyurethane (HDP) (Vennapusa et al., 2016) 99
Table 2-28. Applicability of dowel bar retrofits, cross stitching, and slot stitching (Fortunatus, 2018) 108
Table 2-29. State DOTs' specifications for dowel bar retrofit (Darter, 2017) 108
Table 2-30. State DOT's specifications for cross-stitching (Darter, 2017) 109
Table 2-31. TxDOT District-wide survey on mitigation techniques for bridge approach settlement (Puppala et al., 2011) 111
Table 2-32. Cost comparison of slab faulting repair methods (Al-Eis & LaBarca, 2007) 112
Table 3-1. Survey response to Question 1 by districts 116

Table 3-2. Survey response to Question 2 by districts 117
Table 3-3. Survey response to Question 3 by districts 118
Table 3-4. Survey response to Question 5 by districts 120
Table 3-5. Survey response to Question 6 by districts 121
Table 3-6. Survey response to Question 7 by districts 122
Table 3-7. Survey response to Question 8 by districts 124
Table 3-8. Survey response to Question 9 by districts 125
Table 3-9. Survey response to Question 10 by districts 126
Table 3-10. Potential sections for new investigation from survey Question 11 127
Table 3-11. Sections that have been performing well after repair from survey Question 12 128
Table 4-1. A summary of potential field test sections 137
Table 4-2. Detailed descriptions of Section P-A-1 143
Table 4-3. Detailed descriptions of Section P-A-2 146
Table 4-4. Detailed descriptions of Section P-A-3 149
Table 4-5. Detailed descriptions of Section P-A-4 152
Table 4-6. Detailed descriptions of Section P-A-5 155
Table 4-7. Detailed descriptions of Section P-B-1 157
Table 4-8. Detailed descriptions of Section P-B-2 161
Table 4-9. Detailed descriptions of Section P-B-4 164
Table 4-10. Detailed Description of P-C-1 166
Table 4-11. Detailed descriptions of Section P-C-2 168
Table 4-12. Detailed description of Section S-11-1 171
Table 4-13. Detailed description of site S-11-2 173
Table 4-14. Detailed description of Section S-11-3 176
Table 4-15. Detailed descriptions of Section S-11-4 179
Table 4-16. Detailed descriptions of Section S-11-5 181
Table 4-17. Detailed descriptions of Section S-11-6 183
Table 4-18. Detailed descriptions of Section S-11-7 186
Table 4-19. Detailed description of site S-11-8 188
Table 4-20. Detailed descriptions of Section S-11-9 191
Table 4-21. Detailed descriptions of Section S-11-10 193
Table 4-22. Detailed Description of S-12-1 195
Table 4-23. Detailed description of Section S-12-2 198
Table 4-24. Detailed description of Section S-12-4 202
Table 4-25. Detailed description of Section E-1 206
Table 4-26. Detailed descriptions of Section E-2 209
Table 4-27. Detailed descriptions of Section E-3 212
Table 4-28. Detailed description of Section E-4 214
Table 4-29. Summary of final test sections selected 217
Table 5-1. Detailed descriptions of Section E-2 on IH-10 in San Antonio, Texas 220
Table 5-2. Summary of void thickness measured at core holes 226
Table 5-3. Summary of laboratory test results. 233
Table 5-4. Detailed descriptions of Section E-3 on SH-47 in College Station, Texas 241

Table 5-5. Detailed descriptions of Section P-B-2 of US 290 in Brenham, Texas 257
Table 5-6. Resilient moduli of backfill soils before and after HDPF injection 269
Table 5-7. Detailed descriptions of Section S-11-8 of US 290 in Austin, Texas..... 275
Table 5-8. Summary of laboratory test results 285
Table 5-9. Detailed descriptions of Section P-A-3 295
Table 5-10. Summary of measurement at cored locations 300
Table 5-11. Summary of lab test results..... 304
Table 5-12. Detailed descriptions of Section P-A-4 IH 820, Fort Worth, Texas..... 311
Table 5-13. Summary of measurement at cored locations. 316
Table 5-14. Summary of lab test results..... 320
Table 5-15. Detailed descriptions of the Beltway 8 test section at IH 45 in Houston. 327
Table 5-16. Summary of laboratory test results for backfill and subgrade soil samples. 336
Table 5-17. Detailed descriptions of IH-35 Exit 368A in Hillsboro, Texas. 343
Table 5-18. Summary of measurement at cored locations 350
Table 5-19. Summary of laboratory test results 354
Table 5-20. Summary of lab test results (Southbound)..... 379
Table 5-21. Summary of Laboratory Test Results for Northbound Soils 381
Table 5-22. Detailed descriptions of Section P-A-5 on IH-27 in Tulia, Lubbock, Texas..... 386
Table 5-23. Detailed descriptions of Section P-B-1 on IH 35 in Waco, Texas 399
Table 6-1. Average and standard deviation of normalized D_0 from FWD by site 420
Table 6-2. Recommended classification for evaluation of in-service roadway embankments using DCP data (draft). 438
Table 6-3. Summary of regression analysis using pointwise data for all sites..... 441
Table 6-4. Summary of correlation for DCP layer-wise averaging. 444
Table 6-5. Summary of correlation for 6” and 12” averaged data. 448
Table 6-6. Recommended classification for evaluation of in-service roadway embankments using CPT data (draft). 450

Chapter 1 Introduction

1.1 Background

Bridge approach slabs (BAS), adjacent pavement, and embankments form the transition between bridge structures and roadway pavement. In this report, the term "***bridge approach system***" or ***"bridge approach"*** is used to refer collectively to the BAS, adjacent pavement, embankment, backfill, retaining wall elements where present, and supporting foundation soils that influence the performance of this transition zone. When a specific component is discussed, such as the BAS, adjacent pavement, embankment fill, retaining wall, or foundation soil, that component is identified separately.

The bridge approach system is often difficult to maintain because the bridge is typically supported on stiffer deep foundations, while the approach pavement is supported by embankment fill and foundation soil that may continue to deform during the service. As a result, bridge approach systems are commonly affected by settlement, bumps, faulting, lateral movement, lane separation, void development, and loss of material. These distresses can reduce ride quality, increase maintenance needs, and shorten the service life of the bridge approach system.

The "bump at the end of the bridge" is one of the most recognized symptoms of poor bridge approach performance, but it is only one expression of a broader support-condition problem. Roadway embankments and bridge approach systems may experience compression of fill or foundation soil, water infiltration, material washout, erosion, and weakening of support under repeated traffic loading. The BAS is intended to provide a smoother transition across these changing support conditions; however, voids beneath the slab, differential movement at the sleeper slab and abutment end, and distress in the adjacent pavement can still develop when the underlying embankment or support condition deteriorates.

A central challenge is that similar surface distresses can be caused by different underlying mechanisms. For example, a bump, faulted joint, longitudinal crack, lane separation, or void beneath a slab may be associated with compression of materials, loss of material through washout, lateral stress buildup behind a retaining wall, non-uniform slab support, or a combination of these mechanisms. Therefore, the visible distress alone is not sufficient for selecting a repair strategy. A repair that restores the surface condition may improve ride quality in the short term, but the same distress may recur if the active mechanism remains untreated.

Current TxDOT practice includes several tools and repair methods for evaluating and maintaining bridge approach systems. However, available guidance does not provide a unified procedure for characterizing in-service embankment conditions and selecting repair strategies based on the underlying distress mechanism. TxDOT Project 0-7173: *Develop Guidelines for Evaluation of Embankment Conditions in Bridge Approach Slabs and Pavement Structures* was undertaken to address this need by developing guidelines for evaluating embankment conditions affecting BAS and adjacent pavement structures and for selecting maintenance and repair strategies that address both visible distress and probable root causes.

The Research Team (a) reviewed literature and current practice, (b) surveyed TxDOT districts, (c) selected field test sections representing different pavement structures, embankment configurations, distress conditions, and repair histories, (d) conducted field and laboratory evaluations, (e) classified observed distress mechanisms, and (f) developed a mechanism-based repair framework. The resulting guidance is intended to provide TxDOT engineers with a more consistent basis for evaluating in-service bridge approach systems and selecting repair strategies that are aligned with the causes of unsatisfactory performance.

1.2 Report Organization

This report documents the research conducted under TxDOT Project 0-7173, performed by Texas Tech University, and is organized into eight chapters:

a) Chapter 1 introduces the research problem, the need for improved evaluation guidance, and the overall scope of Project 0-7173.
b) Chapter 2 presents the literature review and current state of practice related to roadway embankments, BAS, pavement distress, field evaluation methods, post-construction soil improvement, and repair methods.
c) Chapter 3 presents the TxDOT district survey conducted to document current Texas practice. The survey results summarize commonly observed distress types, timing of distress development, methods used to identify repair needs, evaluation activities, repair practices, and recommendations from TxDOT districts.
d) Chapter 4 documents the field test section selection process. Potential sections were identified from proposal-stage locations, TxDOT district survey responses, and additional sections identified by the Research Team. The chapter explains how final sections were selected to represent different distress types, pavement structures, embankment configurations, repair histories, and suspected mechanisms of poor performance.
e) Chapter 5 documents the field and laboratory investigations conducted at the 11 evaluated test sections. The chapter presents the site conditions, observed distresses, testing layouts, and results from falling weight deflectometer (FWD), ground-penetrating radar (GPR), coring, dynamic cone penetrometer (DCP), cone penetration test (CPT), soil sampling, and laboratory testing used to characterize the condition of the BAS adjacent pavement, embankment fill, and founding soils.
f) Chapter 6 synthesizes the observations from the field investigation program and presents guidelines for interpreting evaluation data for BAS, adjacent pavement, and roadway embankments. The resulting thresholds and correlations are presented as screening guidance based on the sections evaluated and should be applied with consideration of the limitations identified in the chapter.
g) Chapter 7 uses the field and laboratory findings to classify the distress mechanisms observed in the evaluated sections. The discussion focuses on four primary mechanisms: compression of materials, loss of materials or washout, lateral stress buildup behind retaining walls, and non-uniform slab support.
h) Chapter 8 develops the maintenance and repair strategy based on the evaluation results and mechanism classification. The repair-selection framework separates the diagnosis of the

active mechanism, repair of the root cause, and corrective treatment of remaining surface distress.

i) Chapter 9 summarizes the major findings of the research and provides recommendations for implementing a mechanism-based approach to evaluating and repairing bridge approach systems in roadway embankment areas.

Chapter 2 Literature Review and Current Practice

This chapter reviews the literature and current practice related to the evaluation and repair of bridge approach systems in roadway embankment areas. The review first summarizes the major components of roadway embankments and bridge approach slabs (BAS), along with TxDOT specifications for embankment fill and backfill materials. It then discusses common distress types and contributing factors reported in the literature, including differential settlement, poor compaction, water infiltration, erosion or washout, void development, and loss of support. The chapter also reviews evaluation methods used by state DOTs and previous research studies, with emphasis on how visual inspection, ride-quality measurements, ground-penetrating radar (GPR), falling weight deflectometer (FWD), coring, dynamic cone penetrometer (DCP), cone penetration test (CPT), and laboratory testing have been used to assess in-service embankment and BAS conditions. Finally, the chapter summarizes post-construction soil improvement and repair methods for distressed BAS and adjacent pavement, and synthesizes the literature findings to identify the need for a combined evaluation approach and mechanism-based repair selection.

2.1 Overview of Roadway Embankments

Bridge approach system performance depends on the interaction among the bridge approach slab, adjacent pavement, embankment fill, backfill, drainage condition, retaining wall elements where present, and supporting foundation soils. Because distress at the surface may reflect different subsurface or support conditions, the literature review was organized to connect three related topics: the components and material requirements of roadway embankments, the causes and indicators of common bridge approach distresses, and the evaluation and repair methods used in current practice. This chapter first reviews roadway embankment and bridge approach system components and relevant TxDOT specifications, then summarizes commonly reported distress types and contributing factors, followed by evaluation methods and post-construction repair or soil improvement practices for in-service embankment areas.

2.1.1 Components

Roadway embankments and bridge approach systems provide a smooth transition from roadways to bridges by gradually increasing height of embankment. Typical components of roadway embankments and bridge approach systems are shown in **Figure 2-1**.

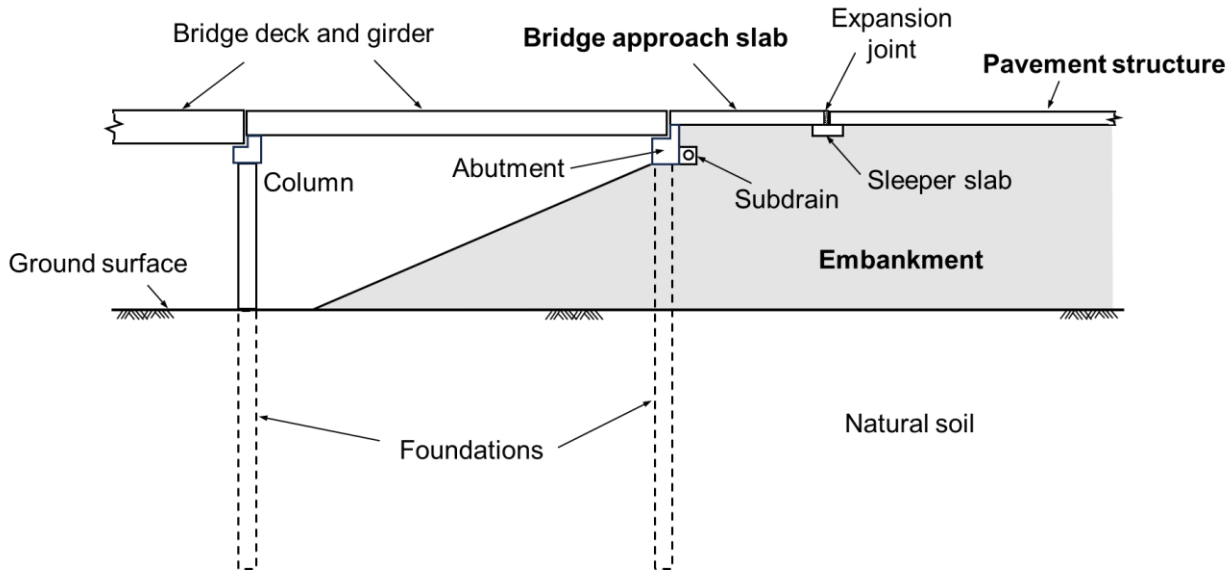
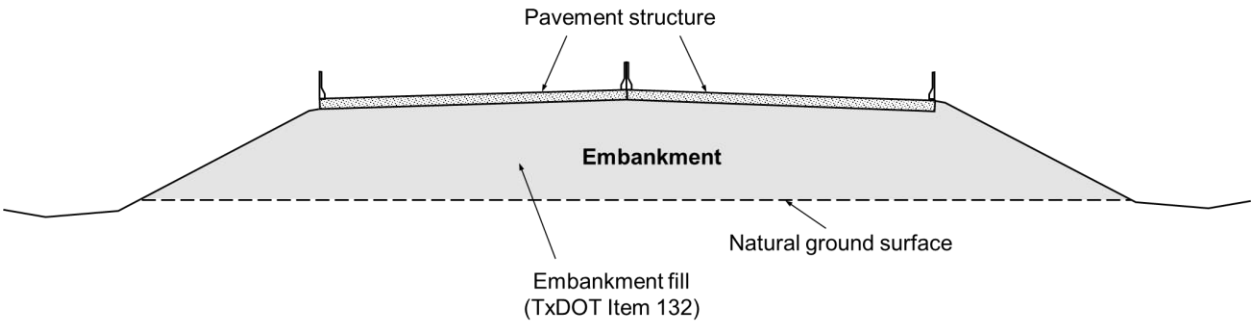


Figure 2-1. Schematic illustrations of typical components of a roadway embankment and a bridge approach system (modified after Briaud et al. 1997)

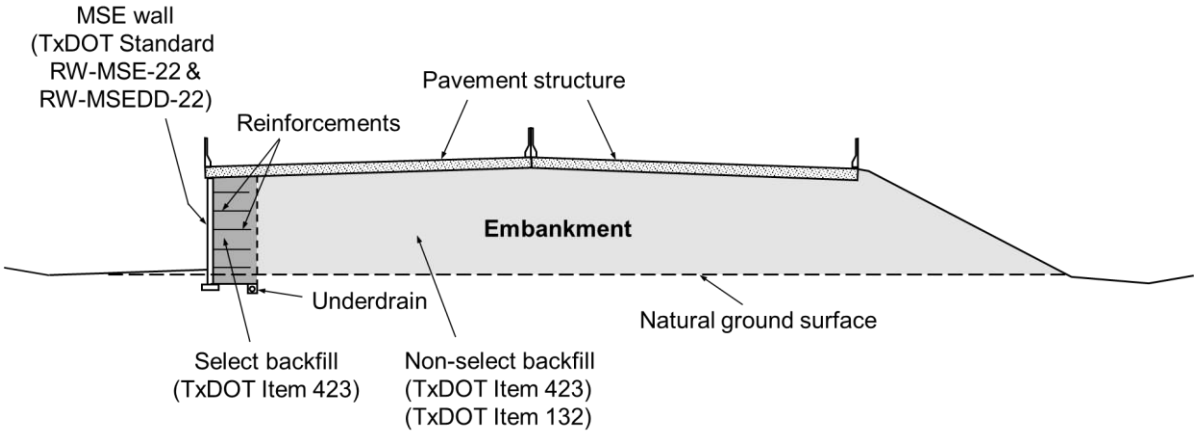
As shown in **Figure 2-1**, a bridge approach slab (BAS) acts as an intermediate bridge to span the end portion of the pavement on the roadway embankment directly behind the bridge abutment. In Texas, the bridge abutment is typically supported by drilled shafts whereas the BAS on the pavement side is supported by a sleeper slab. Such a difference in support system between one end of the bridge approach slab and the other end may be one of the factors that induce the differential settlement. Differential settlements (or bumps) are also commonly observed at the interface between the bridge deck and BAS due to a void development beneath the BAS. The development of void can be caused by the loss of fill materials due to water intrusions (Jayawickrama et al. 2005) and, therefore, drainage systems should be provided to remove water from critical areas around the abutments (surface drain) and, preferably, under the approach pavements (subsurface drain). However, according to Jayawickrama et al. (2005), subsurface drain system is rarely used in Texas.

2.1.2 Typical cross-sections of roadway embankments and specifications for backfills

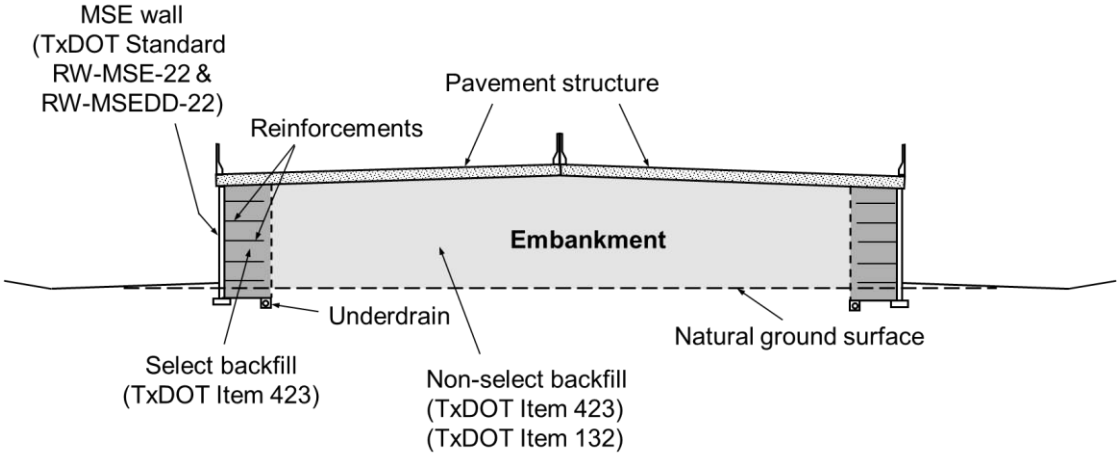
Cross-section profiles of typical roadway embankments are presented in **Figure 2-2**. Both sides of the roadway embankment can be sloping grounds (**Figure 2-2(a)**), one-side with a retaining wall and the other side with a sloping ground (**Figure 2-2(b)**), or both sides with retaining walls (**Figure 2-2(c)**).



(a)



(b)



(c)

Figure 2-2. Typical cross sections of roadway embankments: (a) slope-slope section, (b) retaining wall-slope section, and (c) retaining wall- retaining wall section

2.1.2.1 TxDOT's specifications for embankment fills

Item 132 "Embankment" in TxDOT *Standard Specifications for Construction and Maintenance of Highways, Streets, and Bridges* (TxDOT 2014) specifies requirements for embankment fills. Key requirements for embankment fills are summarized below:

- **Materials**
  - **Type A**: Granular material that is free from vegetation or other objectionable material and meets the following requirement:
    - Liquid Limit (LL) ≤ 45
    - Plasticity Index (PI) ≤ 15
    - Bar linear shrinkage ≥ 2
  - **Type B**: Materials such as rock, loam, clay, or other approved materials.
  - **Type C**: Material meeting the specification requirements shown on the plans.
  - **Type D**: Material from required excavation areas shown on the plans.

- **Density Control**: TEX-114-E (*Test Procedure for Laboratory Compaction Characteristics and Moisture-Density Relationship of Subgrade, Embankment Soils, and Backfill Material*) is used to determine the maximum dry density ($\gamma_{d,max}$) and optimum moisture content (w_{opt}) of the fill materials. Requirements for field density and moisture content are given in **Table 2-1**. TxDOT Item 132 further requires that the fill materials for embankments should be compacted in lifts and thickness of each layer should not exceed 16 in when loose or 12 in when compacted.

Table 2-1. Field density control requirements for embankment fills per TxDOT Item 132

Description	Density	Moisture Content
	TEX-115-E (Field Method for Determining In-Place Density of Soils and Base Materials)	
PI ≤ 15	≥ 98% $\gamma_{d,max}$	
15 < PI ≤ 35	≥ 98% $\gamma_{d,max}$ and ≤ 102%	≥ w_{opt}
PI > 35	≥ 95% $\gamma_{d,max}$ and ≤ 100%	≥ w_{opt}

The requirements shown in **Table 2-1** are graphically represented in **Figure 2-3**. Note that TxDOT requires that the moisture content of the compacted embankment fill to be on the wet-side of the optimum moisture content for fill materials that have PI greater than 15.

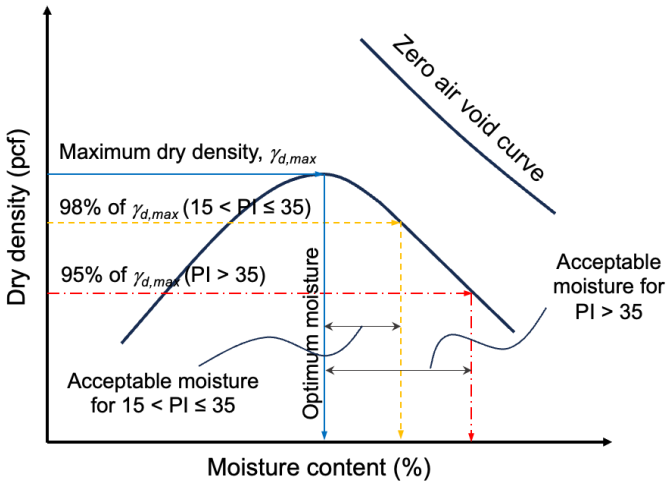


Figure 2-3. Graphical representations of density control requirements of compacted embankment fill per TxDOT Item 132

2.1.2.2 TxDOT's specifications for backfill materials behind the retaining walls

For roadway embankments that have a retaining wall on one or more side, two types of backfill materials are used: (i) select fill and (ii) non-select fill. Requirements for backfill materials behind retaining walls are specified in TxDOT Item 423, "Retaining Walls." Key requirements are summarized below:

- **Materials**
  - **Non-select backfill**: Non-select backfills are used for embankment areas other than temporary and permanent mechanically stabilized earth (MSE) and concrete block walls (refer to **Figure 2-2(b)** and **Figure 2-2(c)**). Non-select fill should meet TxDOT Item 132, "Embankment," of the type specified on the plans. If no type is specified, a fill material that has PI ≤ 30 should be provided.

  - **Select backfill**: Select backfill is required in specific areas of permanent and temporary MSE and concrete block-type retaining walls. TxDOT Item 423 lists four types of select backfill for retaining walls:
    - **Type BS:** Default backfill for permanent MSE walls.
    - **Type AS:** Coarser, higher quality backfill material.
    - **Type CS:** Used only on temporary MSE walls.
    - **Type DS:** Free-draining, rock backfill. Intended for use in MSE walls that are subjected to inundation.

    Select backfill should be free from organic or otherwise deleterious materials and should satisfy gradation limits shown in **Table 2-2**. Graphical representation of the gradation requirements is shown in **Figure 2-4**.

- **Cement-stabilized backfill**: Cement-stabilized backfill can be used when required or as approved. Type CS backfill is stabilized with 5% hydraulic cement by dry weight of the backfill material. TxDOT Item 423 further requires that special drainage provisions be provided when cement-stabilized backfill is used.

Table 2-2. Gradation requirements for select backfills for retaining walls per TxDOT Item 423

Type	Sieve Size	Percent Retained	Percent Passing
AS	3"	0	100
	1/2"	50-100	0-50
	#40	85-100	0-15
	#200	95-100	0-5
BS	3"	0	100
	#40	40-100	0-60
	#200	85-100	0-15
CS	3"	0	100
	#200	75-100	0-25
DS	3"	0	100
	3/8"	85-100	0-15
	#200	95-100	0-5

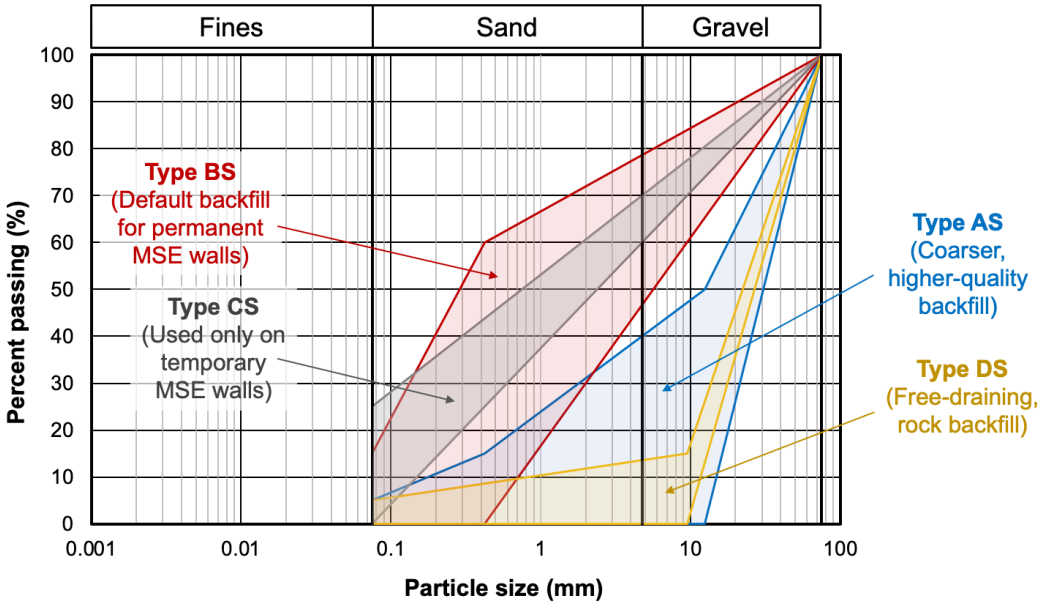


Figure 2-4. Graphical representations of gradation requirements for select backfills for retaining walls per TxDOT Item 423

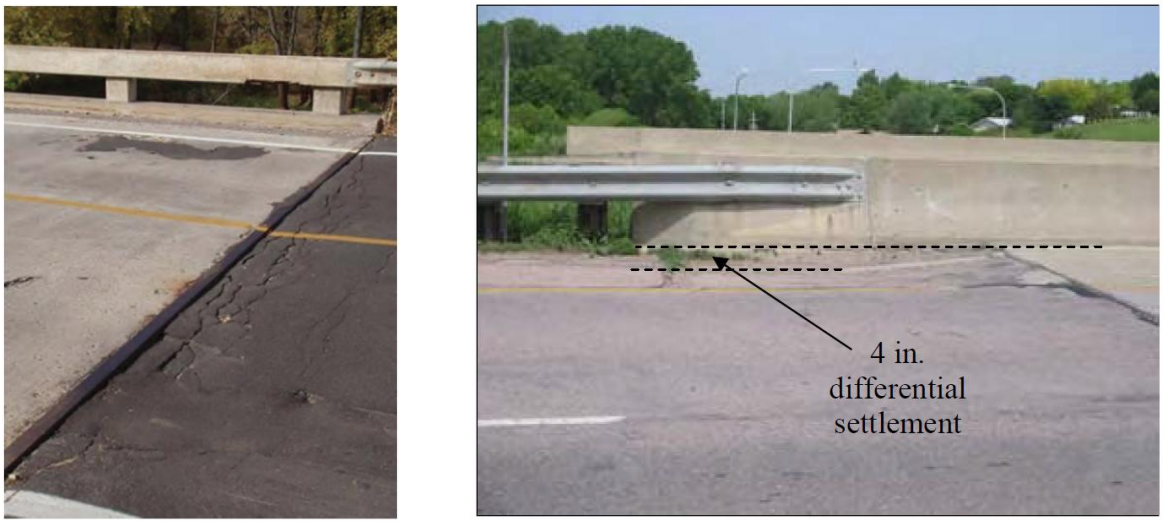
- **Density Control for Permanent MSE walls**: TxDOT Item 423 requires that select backfill should be placed in lifts of 8 in or less (loose measurement) and compacted to at least 95% of maximum dry density determined in accordance with TEX-114-E.

2.2 Distresses of Roadway Embankments and Their Causes

2.2.1 Common distresses on roadway embankments

2.2.1.1 Differential settlement (bump)

Roadway embankments are built on existing soil by adding fill materials and compacting them, and, therefore, undergo load-induced compression and settlements over time. In contrast, bridges are typically supported on deep foundations, and the total settlement of the bridge is usually much smaller than that of adjacent roadway embankment. As a result, a considerable differential settlement is often observed at the area between the bridge and roadway interface (Puppala et al. 2011). To minimize problems associated with the differential settlements, BASs are used to provide a smooth transition between the bridge and roadway. However, BASs also suffer from differential settlements either at the interface between the bridge and BAS or at the interface between the BAS and roadway, or at both interfaces. **Figure 2-5(a)** shows a bump between bituminous approach roadway and a concrete bridge deck in Minnesota, and **Figure 2-5(b)** shows a differential settlement between the bridge deck and the approach slab in Iowa.



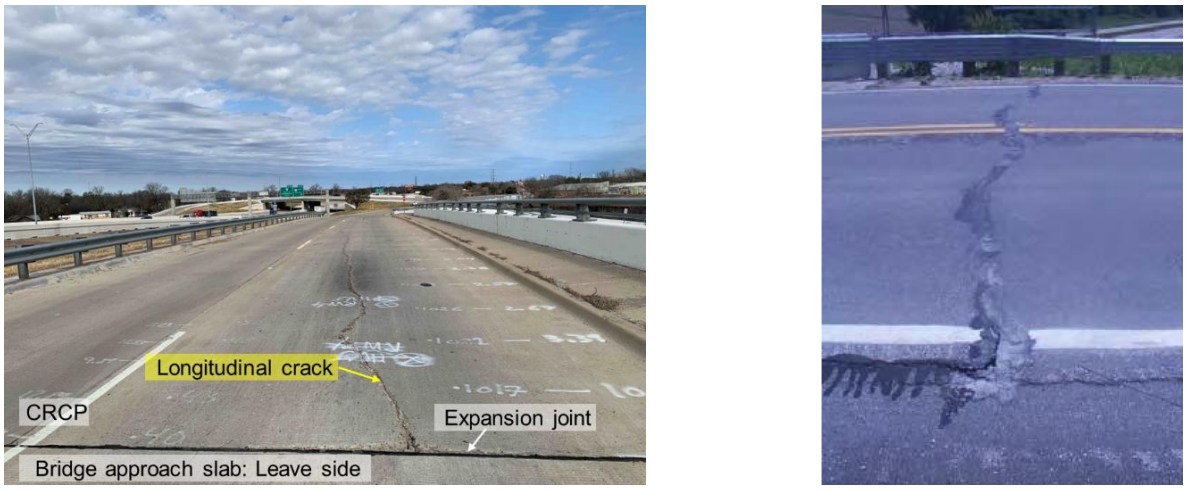
(a) (b)

Figure 2-5. Photos showing (a) a bump between bituminous approach roadway and a concrete bridge deck in Minnesota (ElBatanouny et al. 2021) and (b) a differential settlement between the bridge deck and the approach slab in Iowa (White et al. 2005)

2.2.1.2 Cracks on pavement

Another common type of distress in roadway embankments is the development of cracks in pavement structures. Cracking in pavement structures may indicate deterioration or movement

within the underlying roadway embankment; however, not all pavement cracks are associated with subgrade or slab-support problems. In CRCP, regularly spaced transverse cracks are an expected response to restrained temperature- and drying-shrinkage-induced strains and, by themselves, generally do not indicate loss of support. Nevertheless, intrusion of surface water into the embankment fill can not only weaken the subgrade but also cause internal soil erosion, often leading to void development near the bridge approach area. Under repeated traffic loading, weakened, lost, or nonuniform support may lead to additional cracking, including longitudinal cracks and, in some cases, atypical transverse cracking. Accordingly, the crack pattern, width, spacing, and associated signs of movement or settlement should be considered when evaluating whether the cracking is related to embankment/support conditions, or pavement surface layer. **Figure 2-6** shows such cracks developed in roadway embankments.



(a) (b)

Figure 2-6. Photos showing cracks in roadway embankments: (a) a longitudinal crack on continuously reinforced concrete pavement (CRCP) in Texas and (b) a transverse crack on asphalt overlay in Iowa (White et al. 2005)

2.2.1.3 Faulting

Water infiltrations into joints and cracks and ensuing weakening process of subgrade (or loss of backfill material) under the wheel load can also create faulting in the longitudinal direction (see **Figure 2-7(a)**). Furthermore, as described previously, roadway embankments undergo load-induced compression over time, leading to settlement of pavement surface. Uneven settlements between the two adjacent lanes (or between lanes and shoulder) can cause faulting in the transverse direction (See **Figure 2-7(b)**).



(a) (b)

Figure 2-7. Photos showing faulting in roadway embankments: (a) faulting of bridge approach concrete panels in Iowa (White et al. 2005) and (b) faulting between outside main lane and outside shoulder in Texas

2.2.1.4 Lane separation

Dupont and Allen (2002) argued that the most successful method to construct a roadway embankment is to select high-quality fill material with most of them being a coarse granular material with high internal frictional characteristics. However, roadway embankments are often constructed by using materials from nearby roadway excavation areas or convenient borrow pits close to the project site (Puppala et al. 2011). This implies that the slope stability of embankment, stability of retaining wall, or bearing capacity issues, depends on the geotechnical properties of the fill materials (Wahls 1990). The use of backfill materials that contain large amounts of materials passing No. 200 sieve, particularly highly plastic clays, and that can induce water pressure buildup due to low permeability can reduce the stability of roadway embankments. Considering that the sides of roadway embankments are sloping grounds or retaining walls as previously shown in **Figure 2-2**, lateral movements of slopes or retaining walls can cause displacements of pavement structures in the transverse direction, leading to lane separations. **Figure 2-8** shows lane separations between main lanes caused by lateral movement of MSE wall in Texas.



(a) (b)

Figure 2-8. Photos showing lane separations in roadway embankments in Texas: (a) lane separation between inner lane and middle lane and (b) lateral movement of MSE wall

Miller et al. (2013) also reported a significant lateral movement of wing walls near the bridge abutment due to downward movement of adjacent soil. Such lateral movements opened up joints between adjacent pavement structures causing lane separations and allowed water to enter the underlying soil and backfill contributing to the erosion problems (Miller et al. 2013).

2.2.2 Possible causes of distresses

Briaud et al. (1997) analyzed survey responses received from 48 states and listed factors contributing to poor performances in bridge approach area as follows:

- Compression of the fill material
- Settlement of natural soil under the embankment fill
- Poor construction practices/specifications
- Poor drainage
- Loos of fill by erosion
- Poor fill material
- Poor joints
- Temperature cycles
- Abutment type
- A too rigid bridge foundation relative to the approach
- Bridge type

Among these lists, several contributing factors are related to each other, and types of bridge and abutment were outside the scope of this study. Accordingly, we simplified the list into the following three factors: (i) consolidation settlement of foundation soil beneath the embankment

fill, (ii) poor compaction of backfill materials, and (iii) loss of fill by erosion and void formation due to water infiltration.

2.2.2.1 Consolidation settlement of foundation soil

Many researchers (Hopkins 1969; Tadros and Benak 1989; Wahls 1990; Dupont and Allen 2002) reported that consolidation of the foundation soil (*e.g.*, see **Figure 2-9**) is one of the most contributing factors to the settlement-related distresses of the roadway embankments. Soil consolidation is the process of the expulsion of water (*i.e.*, dissipation of excess pore pressure) under loads. This process, also known as primary consolidation, occurs rapidly for coarse-grained soils but may take up to 10 years for certain types of clays (Puppala et al. 2011). After the primary consolidation is completed, soils can further settle under a constant stress due to slow rearrangement of soil particles and this process is known as secondary consolidation or creep. Usually, secondary consolidation occurs over a much longer time period than the primary consolidation and can be as large as the primary consolidation for very soft, highly plastic or organic clays (Hopkins 1969). However, the settlement of the foundation soil is difficult to address for in-service roadway embankments because the foundation soil is buried deep below the pavement surface.



Figure 2-9. Photos showing settlement of foundation soils in Texas (from Galvan 2007 and Galvan 2011)

2.2.2.2 Poor compaction of backfill materials

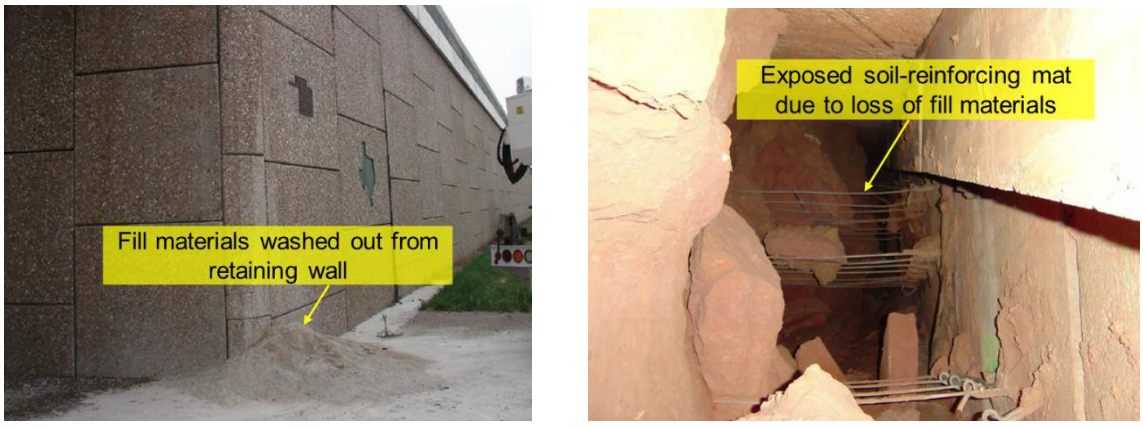
As discussed previously, TxDOT Item 132 and Item 423 requires that both non-select fill and select fill should satisfy the density control requirements after compaction. However, poor

compaction control of the embankment material has been reported to be another contributing factor to the distresses in roadway embankments (Wahls 1990; Briaud et al. 1997; Lenke 2006; White et al. 2007). It is a common practice to construct bridge abutments before placing and compacting embankment fill materials. This practice makes the compaction of the backfill materials near the bridge abutment very difficult because of limited accessibility of the compaction equipment. Survey responses from TxDOT district officials reported in the research report by Jayawickrama et al. (2005) also noted the difficulties in compacting fill materials near the abutment walls. The research report further stated that the Yoakum district initiated the use of hand compaction of material near abutment walls and they have observed less distresses at those bridge ends.

To address the difficulties in compacting the backfill materials near the abutment, TxDOT *Bridge Design Guide* (2023) states that "TxDOT supports the placement of a cement-stabilized abutment backfill (CSAB) wedge in the zone behind the abutment. CSAB solves the problem of difficult compaction behind the abutment, and it resists the moisture gain and loss of material common under approach slabs."

2.2.2.3 Loss of fill by erosion and void formation due to water infiltration

Soil erosion by poor drainage system of the bridge abutment and embankment area is considered as one of the most important factors that cause distresses in BAS and nearby pavement structure by many researchers (Wahls 1990; Jayawickrama et al. 2005; Mekkawy et al. 2005; White et al. 2005; Abu-Hejleh et al. 2006). The intrusion of surface water through faulty joints or cracked pavement sections can not only weaken the embankment fill but also cause internal erosion because the fines can be washed out from the fill material, often leading to developments of voids. **Figure 2-10** shows examples of loss of fill by erosion in roadway embankments.



(a) (b)

Figure 2-10. Photos showing (a) fill materials washed out from the retaining wall and (b) soil-reinforcing mats exposed behind retaining walls due to soil erosion in Texas (from Galvan 2007 and Galvan 2011)

The erodibility of soil is mainly influenced by the characteristics of particle size distributions, among others, and silts and fine sands are the most erodible types of soils (Briaud et al. 1997). TxDOT's experience also suggests that fine sands are prone to erosion, by stating that "incidence of backfill loss is most commonly associated with very fine, uniform 'sugar sands' that were allowed in past specifications, although some more recent cases have involved coarser backfills" in the document titled *Loss of Backfill in Mechanically Stabilized Earth Retaining Walls* (TxDOT 2019).

Figure 2-11 shows typical ranges of the most erodible soils. Select backfills Type AS and Type DS specified in TxDOT Item 423 generally do not fall in the range, but finer portions of Type BS and Type CS backfill materials do fall in the most erodible range. Furthermore, the current TxDOT requirements for embankment backfill materials specified in TxDOT Item 132 are based on liquid limit and plasticity index rather than particle gradations. Therefore, if the surface water intrudes into the embankment, the fines can be washed out from the fill material and create voids, which was reported as one of the major problems in roadway embankments in Texas (Jayawickrama et al. 2005).

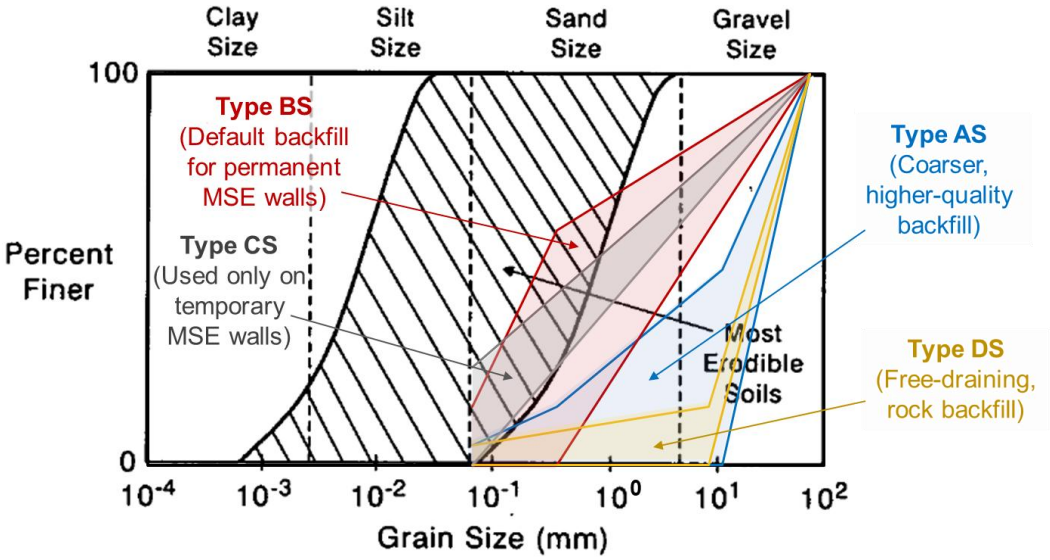


Figure 2-11. Range of most erodible soils (modified from Briaud et al. 1997) and select backfill materials for MSE walls per TxDOT Item 423

According to Jayawickrama et al. (2005), the dominant source for water intrusion at bridge ends is surface water inflow through cracks and poorly sealed joints. They emphasized that surface drainage system should be provided to move water from the bridge deck through adequate channels to prevent water from infiltrating into embankment fill material and stated that standard drainage provisions may not be adequate in some parts of the state that receive heavy rainfall. Jayawickrama et al. (2005) further reported that most TxDOT districts did not use a subsurface drainage system and recommended installing subsurface drainage system such as pipe underdrain to remove water that has entered the fill material and periodically inspect and maintain the subsurface drainage system.

Loss of backfill materials by erosion and continuous water infiltrations also reduce the stability of roadway embankments. Particularly, in areas that receive large amounts of rainfall, the continuous infiltration of water and poor drainage system can lead to a development of large water pressure behind the retaining wall and cause lateral movement of the wall, which in turn can induce lane separations.

2.2.3 Criteria for quantification of performance of bridge approach system

Currently, there are no well-accepted criteria that rate the performance of BASs and nearby pavements in roadway embankments to be used for consideration of when to initiate repair works. Nonetheless, many researchers have attempted to quantify the condition of bridge approach area, and a summary of our review is given below.

2.2.3.1 IRI (International Roughness Index)

The International Roughness Index (IRI) is an essential tool used globally for assessing road surface roughness and has been applied for bridge approach slabs as well. Using a quarter-car vehicle model, the IRI measures longitudinal road profiles to quantify roughness in units like m/km or in/mi. It has been widely used in determining maintenance needs for bridge approaches. Various instruments, such as rod and level, walking profilers, and inertial profilers, are used for these measurements, and inertial profilers are highly preferred by various DOTs for their non-destructive approach and minimal traffic disruption (Zang et al. 2018; Mishra et al. 2020; Henderson et al. 2016).

The Federal Highway Administration (FHWA) uses the IRI in its pavement rating system, where an IRI less than 60 in/mi (0.95 m/km) indicates excellent pavement conditions, while a value above 220 in/mi (3.47 m/km) suggests poor quality (Olmedo et al., 2015). However, there is no standard method for applying IRI to bridge approaches, especially for choosing a fixed IRI interval and defining the bump. Recent studies, including those by Wang et al. (2023), and Mishra et al. (2021), note the variation of IRI based on the interval adopted and indicate that smaller measurement intervals, such as 1 ft (0.3 m), might be more effective for this purpose. Zhang (2016) discusses two distinct approaches, micro and macro methods, for rating the differential settlement of bridge approaches (see **Table 2-3** and **Table 2-4**).

Table 2-3. Micro method in determining differential settlement scale (Zhang 2016)

Rating	**Description**	**Actual Settlement**	**IRI (mm/m)**
Very Good	No bump	0 inch	0 - 4
Good	Slight bump	0 ~1 inch	5 - 8
Fair	Moderate, easily recognizable bump	~2 inches	9 - 12
Poor	Significant bump requiring repair	~3 inches	13 - 16
Very Poor	Large bump, safety hazard	> 3 inches	> 17

Table 2-4. Macro method in determining differential settlement scale (Zhang 2016)

Rating	Description	Settlement Scale	Maintenance Requirement	Maintenance Action
Good	No bump or minimal/ slight bump	No or < 1.5 inch	No maintenance needed	No maintenance work on fixing differential settlement since opening
Fair	Moderate bump	1.5 to 3 inches	Repairs may be needed	1 to 3 times of maintenance work performed to fix differential settlement since opening
Poor	Severe bump	> 3 inches	Frequent maintenance	Maintenance work required every couple of years

Wang et al. (2023) conducted a review of criteria for characterizing the bridge approach slab condition based on IRI as summarized in **Table 2-5**.

Table 2-5. Summary of IRI interval and threshold for determining poor bumps (Wang et al. 2023)

Study	IRI Interval (ft)	Rating/Quality based on IRI (in/mi)				
		Very good	Good	Fair	Poor	Very Poor
Das et al. (1999)	-	0 - 253	253 - 506	506 - 633	633 - 760	> 760
McGhee (2002)	10				140	
Lenke (2006)	-				380	
Olmedo et al. (2015)	-	0 -60	60 - 95	95 - 170	170 - 220	> 220
Henderson et al. (2016)	-	0 -60	60 - 95	95 - 170	170 - 220	> 220
Lu et al. (2018)	-				95	
Mishra et al. (2021)	1, 10, 25				220	
Wang et al. (2023)	1		< 1200	1200 - 2400	2400	
Zhang (2016)		0 - 253	316 - 506	570 - 760	823 - 1013	> 1077

2.2.3.2 Bridge Approach Performance Index (BI)

White et al. (2005) expanded the definition of a "bridge approach" to include not just the approach slab but also the area extending from the bridge abutment to approximately 100 feet away from it. They created a rating method known as the Bridge Approach Performance Index (BI), which is

used in combination with the IRI to assess the condition of the bridge approach area. The BI is defined graphically as the area between the current bridge approach elevation profile and the original elevation profile normalized by the bridge approach length, as illustrated in **Figure 2-12**.

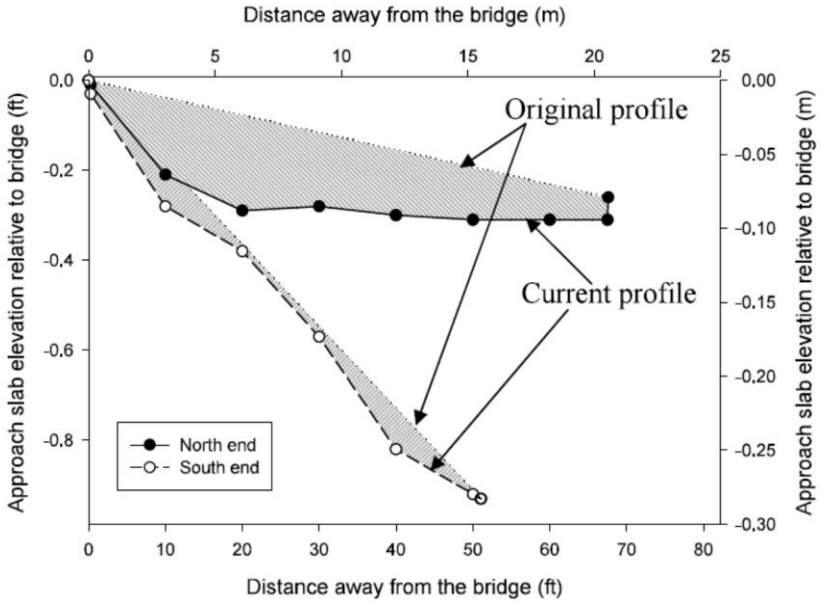


Figure 2-12. Illustration of definition of Bridge Approach Performance Index (BI): BI = deviation area/length (modified from White et al. 2005)

Based on the BI and the IRI, White et al. (2005) categorizes the condition of bridge approaches into different ratings from 'Good' to 'Very poor' as shown in **Figure 2-13.**

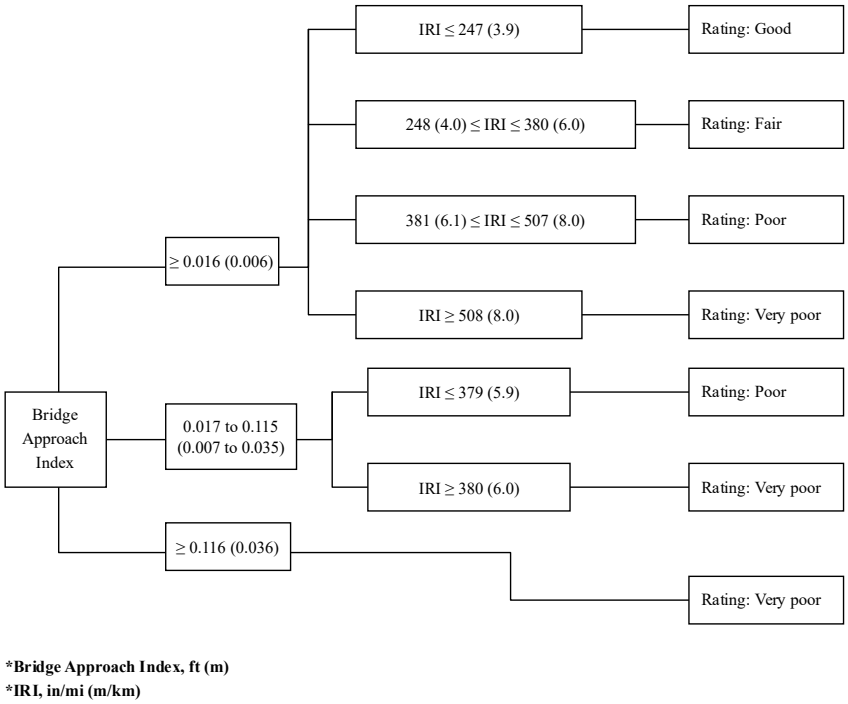


Figure 2-13. Bridge Approach Index for rating bridge approach performance (Source: White et al. 2005)

2.2.3.3 Settlement-based criteria

Another widely used criterion for defining the performance of bridge approach system is the magnitude of differential settlement or gradient of differential settlement. The gradient of differential settlement is defined as a difference in elevations at two measurement points (*i.e.*, often beginning and end of the BAS) divided by the distance between the two points.

Wahls (1990) suggested that a differential settlement of even 0.5 inches could lead to a noticeable bump and recommended a gradient of 1/100 (0.01) - 1/125 (0.008) as a criterion for repair, as settlements at this level could cause discomfort to riders. Similarly, Long et al. (1998) found that a settlement of 2 inches or greater usually leads to significant rider discomfort and established the approach-relative gradient with a threshold of 1/200 (0.005) as a measure for remedial action. A summary of our literature review on settlement-based criteria is presented in **Table 2-6**.

Table 2-6. Criteria based on differential settlement of bridge approach areas

Reference	**Criteria/Measure**	**Threshold**	**Characteristics/ Action**	**Remarks**
Bozozuk (1978)	Differential settlement	100 mm	Repair required	
Wahls (1990); Long et al. (1998)	Differential settlement gradient	1/100 - 1/125 (0.008 - 0.01)	Repair	Can cause discomfort to riders
Olmedo et al. (2015)	Differential settlement gradient	3.2 mm in 3.05 m (= 0.00105)	Bump	
Hsi (2007)	Differential settlement gradient	0.30% (0.003)	Repair required	On transition zones
	Residual settlement	100 mm		
Phares et al (2011)	Differential settlement gradient	1/200 (0.005)	Repair (levelling)	
Cai et al. (2005)	Approach Slab Settlement	152 mm	Loses support	

2.3 State-of-the-practice for evaluation of in-service roadway embankments

2.3.1 Specifications on evaluation of in-service roadway embankments

Based on the information available and the documents reviewed, it appears that specific guidelines or specifications for the evaluation or inspection of in-service roadway embankments are not explicitly detailed in the general construction specifications provided by various DOTs. Nonetheless, several DOTs have mentioned evaluation of embankment conditions in their *Bridge Inspection Manuals*, and the synthesized findings from our review are presented below:

- Connecticut DOT [10.14]: Their guidelines include rating the approaches on both sides of the channel based on sloughing and presence of vegetation in embankments. Areas with minimal vegetation or those in the path of roadway runoff are identified as particularly vulnerable to erosion.
- Washington State DOT (WsDOT) [4-4.6]: In their documentation, the roadway embankment is included in the evaluation of the *WsDOT Abutment Fill* section, which involves assessing the capacity of all abutments to transfer design loads to a foundation through structural elements. This includes evaluating embankments with non-monolithic concrete wingwalls, timber planking, and other abutment retaining systems. Additionally, the manual details the general condition rating of any retaining walls associated with the bridge, considering evidence of movement, cracking, or settling [p. 2-C-67].
- Ohio DOT: Their manual has provided condition ratings for MSE walls. This rating system provides a structured approach to evaluating the condition of in-service roadway embankments, considering factors like erosion, guardrail performance, and foundation settlement. In addition, this rating system provides condition rating to evaluate the condition of in-service roadway MSE walls, considering factors like erosion, cracking, spalling, and joint spacing.

Synthesized findings from our review of criteria for the condition assessment of bridge approach slabs are presented as follows:

- AASHTO Manual for Bridge Evaluation 2020 [4.3.5.11.1]: This manual specifies checking approach slabs for cracking, unevenness, settlement, or roughness. It notes that these defects may cause vehicles to induce undesirable impact stresses in the structure. The approach slabs are to be examined for their capacity, especially in cases of erosion of underlying fills, and the expansion joints between the slabs and the bridge's structural elements are to be inspected for deficiencies.
- Connecticut DOT (Revised 2019) [10.14; 10.10]: This document provides guidelines to assist in determining the condition rating of bridge approaches, including approach slabs, roadway embankment and relief joints. It includes criteria for evaluating their condition based on cracks, scaling, wear, and differential settlement.
- Montana DOT (2015): Montana DOT's Bridge Inspection Program describes bridge approach slabs as Bridge Management Elements (BMEs) constructed with concrete and mild or prestressed reinforcement. The document details the condition states of these slabs.

- New York State DOT (2017): This document outlines procedures for evaluating and documenting the condition of bridge approach elements, including approach slabs. It emphasizes inspecting approach slabs as part of a broader evaluation of bridge approach elements. This manual recommends that approach pavement should be checked for cracking, rutting, unevenness, settlement, and roughness [p. 292].
- North Dakota DOT (2023) [1.6.4]: North Dakota DOT provides maintenance recommendations for bridge approach slabs, including crack sealing, repair of spalled concrete, and leveling of approach slabs. The document specifies routine maintenance actions for these structures.
- Ohio DOT (2014) [Chapter 10]: The Ohio DOT has guidelines for the inspection of bridge approach slabs, which focus on ensuring a smooth transition onto and off the bridge and reducing impact forces on the structure. Inspectors should check the elevation, alignment, and safety features of bridge approach slabs, as well as for potential structural or hydraulic problems.
- Delaware DOT (2020): In Delaware DOT's bridge inspection manual [p. 3-15], it is advised to inspect the approach slab with a focus on delamination, spalls, exposed reinforcement or prestressing, cracking, wear, and settlement. This includes cleaning exposed reinforcement to assess section loss and remaining section. Inspectors are also instructed to observe live traffic or drive across the approach slab to evaluate any vertical offsets and the surface's rideability. Additionally, erosion below or adjacent to the slab should be noted, and its extent investigated.

Examples of condition rating for bridge approach slabs or roadway embankment from a few states are presented in **Table 2-7** through **Table 2-9**.

Table 2-7. Condition rating for approach roadway from Washington State DOT

WSBIS Code	Description
9	Not applicable.
8	Smooth approach onto the bridge structure.
6	Less than 1 inch of settlement of the approach roadway causing minor bouncing and load impact onto the bridge. Monitor the settlement.
3	More than 1 inch of settlement of the approach roadway causing bouncing and load impact onto the bridge. Needs to be ACP feather repaired to provide a smooth transition onto the bridge.

Note: *Code 6 is for well-maintained gravel roads. Code 3 is for gravel roads in rough condition.*
Source item: *WB76-81, Condition Rating for Approach Roadway.*

Table 2-8. Reinforced concrete approach slab condition states from Montana DOT

Defects	Condition States			
	1 - GOOD	**2 - FAIR**	**3 - POOR**	**4 - SEVERE**
Delamination/Spall/ Patched Area (1080)	None.	Delaminated. Spall 1 in. or less deep or 6 in. or less in diameter. Patched area that is sound.	Spall greater than 1 in. deep or greater than 6 in. diameter. Patched area that is unsound or showing distress. Does not warrant structural review.	The condition warrants a structural review to determine the effect on strength or serviceability of the element or bridge; OR a structural review has been completed and the defects impact strength or serviceability of the element or bridge.
Exposed Rebar (1090)	None.	Present without measurable section loss.	Present with measurable section loss but does not warrant structural review.	
Cracking (RC and Other) (1130)	Insignificant cracks or moderate-width cracks that have been sealed.	Unsealed moderate-width cracks or unsealed moderate pattern (map) cracking.	Wide cracks or heavy pattern (map) cracking.	
Abrasion/Wear (PSC/RC) (1190)	No abrasion or wearing.	Abrasion or wearing has exposed coarse aggregate but the aggregate remains secure in the concrete.	Coarse aggregate is loose or has popped out of the concrete matrix due to abrasion or wear.	
Settlement (4000)	None.	Exists within tolerable limits or arrested with no observed structural distress.	Exceeds tolerable limits but does not warrant structural review.	

Damage (7000)	Not applicable.	The element has impact damage. The specific damage caused by the impact has been captured in Condition State 2 under the appropriate material defect entry.	The element has impact damage. The specific damage caused by the impact has been captured in Condition State 3 under the appropriate material defect entry.	The element has impact damage. The specific damage caused by the impact has been captured in Condition State 4 under the appropriate material defect entry.

Table 2-9. Condition rating for Approach Embankment from Ohio DOT

Rating	Description
1-Good	Moderate rutting from drainage. Minor bare soil exposed.
2-Fair	Erosion caused by drainage or channel; Erosion to embankment impacting guardrail performance or encroaching on shoulder. Evidence of minor or stable foundation settlement.
3-Poor	Major erosion caused by drainage or channel; Erosion to embankment impacting guardrail performance or encroaching on shoulder. Evidence of foundation settlement.
4-Critical	Several guardrail posts are hanging due to major erosion. A lane of traffic is closed, tension cracks in asphalt due to embankment movement.

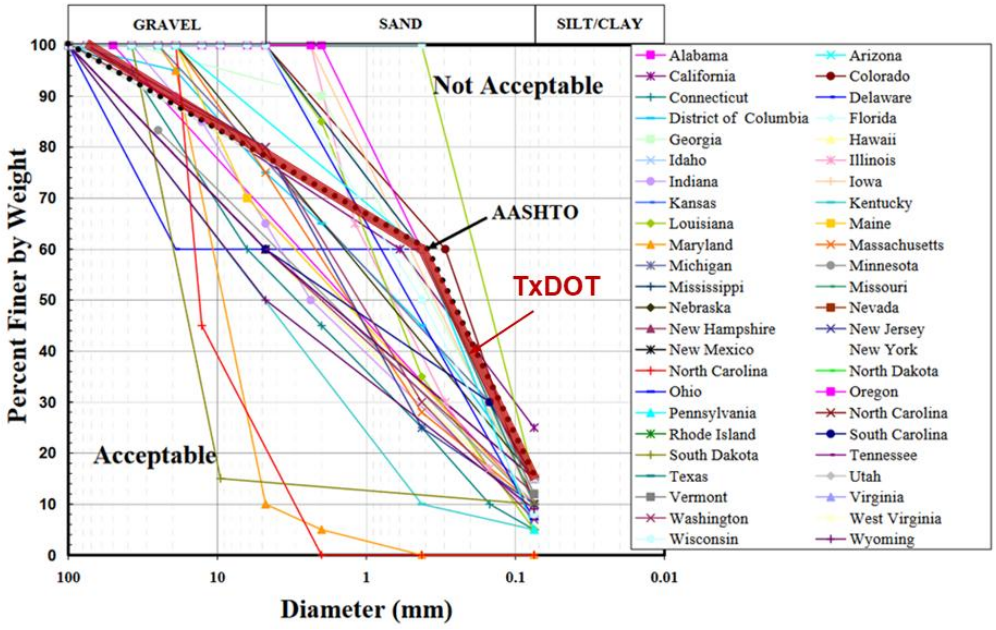
2.3.2 Specifications related to backfill materials for embankments and MSE walls

2.3.2.1 Select fill (or Reinforced fill)

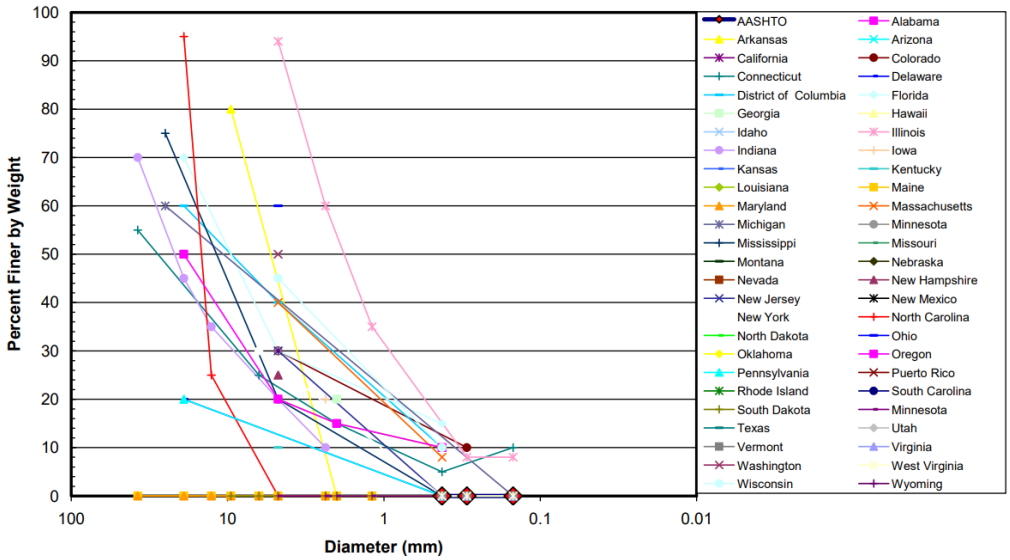
In 2013, a report on selecting backfill materials for MSE retaining walls was published by the NCHRP Transportation Research Board (Marr and Stulgis 2013). This report included a 2004 survey of all US states on their specifications for backfill materials. Out of the 52 state DOTs, 49 responded, giving a good representation of the specifications for MSE wall fills in the US. This survey reviewed the reinforced fill for MSE walls, also known as "select" fill. It was found that most state DOTs (48 participants) follow or modify the AASHTO guidelines for select fill in MSE walls, which includes AASHTO class A-1a soils, fines < 15%, and a PI < 6% (Marr and Stulgis 2013).

Based on the results of the survey, the "upper and lower limits" of gradations of the select fill for MSE wall for each US state was found and presented in **Figure 2-14**. As can be seen in the plot,

many states have a particle size distribution considered acceptable by AASHTO standard, but some states have modified their standard in a way that is not considered acceptable. To make TxDOT's percent passing easier to compare to the other state DOTs, TxDOT's upper limit in terms of gradation has been exaggerated with a thick red line in **Figure 2-14**. As can be seen in the graph, TxDOT's maximum percent passing is almost identical to that from AASHTO (black dashed line).



(a)



(b)

Figure 2-14. Comparison of gradation limits of select fill for MSE walls from US DOTs: (a) maximum percent passing and (b) minimum percent passing (from Marr and Stulgis 2013)

For other factors, such as compaction and moisture content, 37 of the participants reported that the fill is compacted to a minimum of 95% standard Proctor density, and 29 of the participants reported the specified placement moisture content being between ± 4% of the optimum moisture content (Marr and Stulgis 2013). TxDOT Item 423 requires that select backfill should be compacted to at least 95% of maximum dry density but does not specify the moisture content requirement. The figure below shows the ranges of acceptable moisture content for each state.

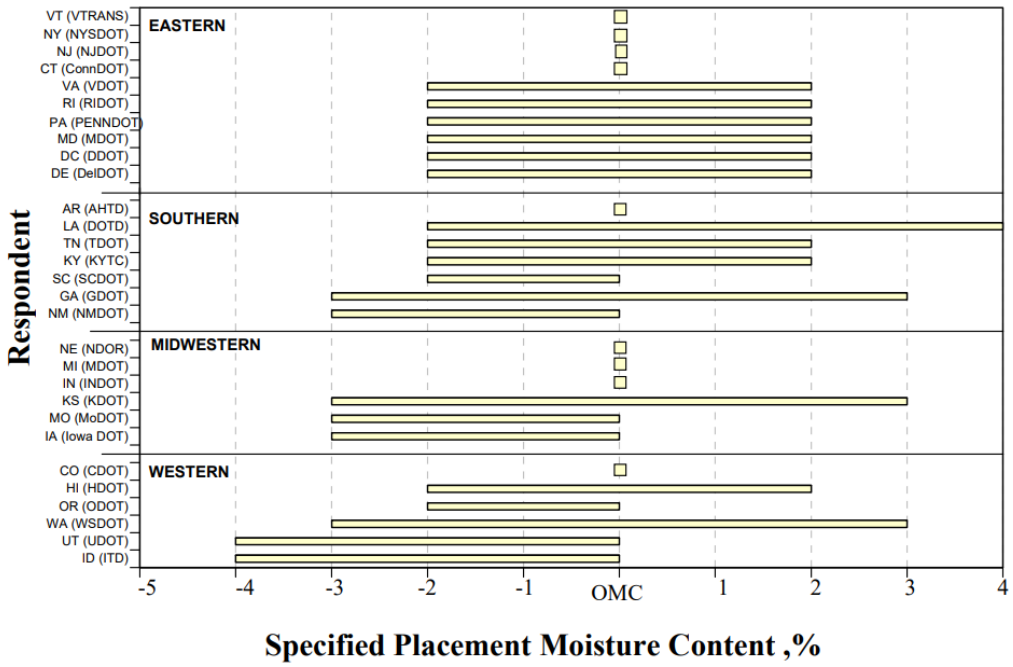


Figure 2-15. US DOTs specified placement moisture content for MSE wall select fill (Marr and Stulgis 2013)

Regarding electrochemical properties, including resistivity, *pH*, sulfate content, and chloride content, the majority of responses followed AASHTO guidelines as can be seen in **Table 2-10**. TxDOT's specification is in compliance with AASHTO guidelines.

Table 2-10. Comparison of electrochemical properties of MSE wall select fill

Property	AASHTO requirements	Number of states that follow AASHTO guidelines	TxDOT's requirements per Item 423
Resistivity	≥ 3000 Ω-cm	32 states	> 3000 Ω-cm
pH	5.0 to 10.0	29 states	5.5 to 10.0
Sulfate content	≤ 200 ppm	35 states	< 200 ppm
Chloride content	≤ 100 ppm	35 states	< 100 ppm

Regarding mechanical properties, including friction angle and cohesion, the majority of responses followed AASHTO guidelines for a friction angle of 34° and a cohesion of zero (Marr and Stulgis, 2013). TxDOT RW-MSE-22 (TxDOT 2022) also requires that the select backfill should have a friction angle of 34°, a cohesion of zero, unit weight of 105 pcf for stability analyses of pullout, sliding, overturning, and eccentricity, and 125 pcf for stability analyses of rupture and bearing.

2.3.2.2 Embankment fill or Non-select fill (or Retained fill)

As for embankment fill or non-select fill (also known as retained backfill) behind MSE walls, not many states provide specifications for this. Hoppe (1999) studied specifications for embankment fills from various DOTs. The results from his survey are presented in **Table 2-11** and show that about half of DOTs use more rigorous material specifications for bridge approach fill than for a regular roadway embankment fill. One common requirement is to limit the percentage of passing No. 200 sieve in the bridge-approach fill to reduce the plasticity of the material. **Table 2-11** shows the allowable percentage of passing No. 200 sieve for the bridge approach fill varies from less than 4% to less than 20%.

Puppala et al. (2011) conducted a literature review on limiting the percent fines used for the embankment fill in the bridge approach. They noted several research studies that recommended limiting the percentage of passing No. 200 sieve in bridge approach fill. For example, Wahls (1990) recommended that the bridge approach fill materials should have a PI less than 15 with percent fines not exceeding 5%. Similarly, the FHWA (2000) recommended that bridge approach backfill materials be less than 15% passing No. 200 sieve. Seo (2003) also recommended the use of a backfill material with a PI less than 15 with percent fines less than 20% and with a coefficient of uniformity greater than 3 within 100 ft (30.5 m) of the bridge abutment.

As previously presented in **Section 2.1.2.1**, TxDOT Item 132 lists various types of embankment fill materials and Type A should satisfy LL ≤ 45, PI ≤ 15, and bar linear shrinkage ≥ 2. For the other types of embankment fills (Types B, C, and D), TxDOT Item 132 states that the requirements are given on the plans, indicating that these are handled on a project-specific basis. According to Item 423 of TxDOT specifications, non-select backfills behind MSE walls should have a maximum plasticity index of 30 unless otherwise specified, as presented in **Section 2.1.2.2**. Both TxDOT Items 132 and 423 specify the PI requirements for embankment fills but do not limit the percentage passing No. 200 sieve.

Table 2-11. Embankment fill specifications for bridge approach (from Hoppe 1999)

State	Same/Different from Regular Embankment	% Passing 75 µm (No. 200) Sieve	Miscellaneous
AL	Same		A-1 to A-7
AZ	Different		
CA		<4	Compacted pervious material
CT	Different	<5	Pervious material
DE	Different		Borrow type C
FL	Same		A-1,A-2-4 through A-2-7,A-4,A-5,A-6,A-7 (LL<50)
GA	Same		GA Class I, II or III
ID			A yielding material
IL	Different		Porous, granular
IN	Different	<8	
IO	Different		Granular; can use Geogrid
KS			Can use granular, flowable or light weight
KY		<10	Granular
LA			Granular
ME	Different	<20	Granular borrow
MA	Different	<10	Gravel Borrow" type B, M1.03.0
MI	Different*	<7	*Only top 0.9 m (3 ft) are different (granular materials Class II)
MN		<10	Fairly clean granular
MS	Different		Sandy or loamy, non-plastic
MO			Approved material
MT	Different	<4	Pervious
NE			Granular
NV	Different		Granular
NH	Same	<12	
NJ	Different	<8	Porous fill (Soil Aggregate I-9)
NM	Same		
NY		<15	<30% Magnesium Sulfate loss
ND	Different		Graded mix of gravel and sand
OH	Same		Can use granular material
OK	Different*		*Granular just next to backwall
OR	Different		Better materials
SC	Same		
SD	Varies*		*Different for integral; same for conventional
TX	Same		
VT	Same		Granular
VA	Same		Porous backfill
WA			Gravel borrow
WI	Different	<15	Granular
WY	Different		Fabric reinforced

2.3.3 Design standards of bridge approach slabs

The design details of BASs vary nationwide. According to the study conducted by Hoppe (1999), the typical span length of BAS among 39 state DOTs who responded to the survey was 20 ft (6.1 m) with an average thickness of 12 in (0.3 m). Thiagarajan et al. (2010) collected design standards of BASs from 40 states and synthesized the data collected. According to the data collected by Thiagarajan et al. (2010), the span length of BAS varied from 10 ft to 33 ft and the thickness varied from 5 in to 17 in. After the study by Thiagarajan et al. (2010), there have been updates in the BAS standards by various DOTs and we have conducted a review of BAS standards of 10 selected states including states neighboring Texas such as Arkansas, Colorado, Louisiana, and Oklahoma. **Table 2-12** summarizes our review on BAS standards from the 10 states.

Among the 10 selected states, the span lengths of BASs varied from 16 to 100 ft with the shortest span length of 16 ft in Arkansas, the longest span length of 100 ft from Illinois Tollway, and the second longest span length of 70 ft from Iowa DOT. The thickness of BAS varied from 9 in (Arkansas) to 18 in (Louisiana). TxDOT uses 20-ft-long and 13-in-thick BAS as shown in **Figure 2-16(a)**. Most DOTs use a sleeper slab as a foundation at the interface between BAS and pavement, and the widths of the sleeper slabs vary from 3 ft (Arkansas) to 8 ft (Indiana). The thicknesses of the sleeper slabs vary from 9 in (Florida) to 21 in (Arkansas). TxDOT also uses a sleeper slab with a width of 5 ft and a thickness of 10 in, as shown in **Figure 2-16(b)**.

The 100-ft-long approach slab that the Illinois Tollway uses consists of a 30-ft-long slab that is directly connected to a bridge abutment and 70-ft-long transition slab that is connected to the pavement, as shown in **Figure 2-17**. The opposite side of the abutment of the 30-ft-long slab is supported on a pile bent and the 70-ft-long transition slab is supported on a subgrade aggregate.

Iowa DOT uses 70-ft-long approach slab with a thickness of 12 in. The 70-ft-long slab consists of 20-ft-long double-reinforced slab, 20-ft-long single reinforced slab, and 30-ft-long non-reinforced slab, as shown in **Figure 2-18**. The double-reinforced slab is supported on sleeper slab and other slabs are connected using dowel bars.

Although most DOTs use a rectangular sleeper slab, placed directly on fill materials, as a foundation at the interface between BAS and pavement, some DOTs use other configurations. For example, Colorado DOT uses an inverted T-shaped sleeper slab (see **Figure 2-19**), and Louisiana DOTD requires a 12-in-thick bedding material, underlain by geosynthetic-reinforced soil, to be placed beneath the sleeper slab (see **Figure 2-20**). Also, the configuration of the sleeper slab used by Louisiana DOTD is non-symmetric: 3.5-ft section into the BAS side and 1.5-ft section into the pavement side. Oklahoma DOT uses an H pile in conjunction with a sleeper slab (see **Figure 2-21**).

Table 2-12. Summary of design standards for bridge approach slabs from selected states

State	BAS length (ft)	BAS thickness (in)	Foundation at the interface between BAS and pavement	Foundation width (ft)	Foundation thickness (in)	Notes
Texas	20	13	Sleeper slab	5	10	
Arkansas	16 – 36.5	9 – 14.5	Sleeper slab	3	21	
Colorado	≥ 20	12	Inverted T-shaped sleeper slab	4	12	Height of T stem = 15 in and width = 12 in
Florida	≥ 30	12	Sleeper slab	5	9	
Illinois DOT	30	15	Sleeper slab	6	10	The sleeper slab is placed on 12-in-thick improved subgrade.
Illinois Tollway	100	15	Pile bent and Subgrade aggregate	-	-	30-ft BAS + 70-ft transition slab; 30-ft slab is supported on pile bent.
Indiana	20.5	12	Sleeper slab	8	10	
Iowa	70	12	Sleeper slab + modified subbase	6.25	≥ 12	20-ft double-reinforced slab + 20-ft single reinforced slab + 30-ft non-reinforced slab; The double-reinforced slab is supported on sleeper slab and other slabs are connected using dowel bars.
Louisiana	≥ 20	18	Sleeper slab + bedding material	5	12	Sleeper slab: 3.5 ft into BAS side and 1.5 ft into pavement side; 12-in bedding material beneath it
Minnesota	20	12	Sleeper slab	4	18	
Ohio	≥ 15	≥ 12	Sleeper slab + aggregate base	8	9	
Oklahoma	≥ 20	13	Sleeper slab + H pile	3	23	

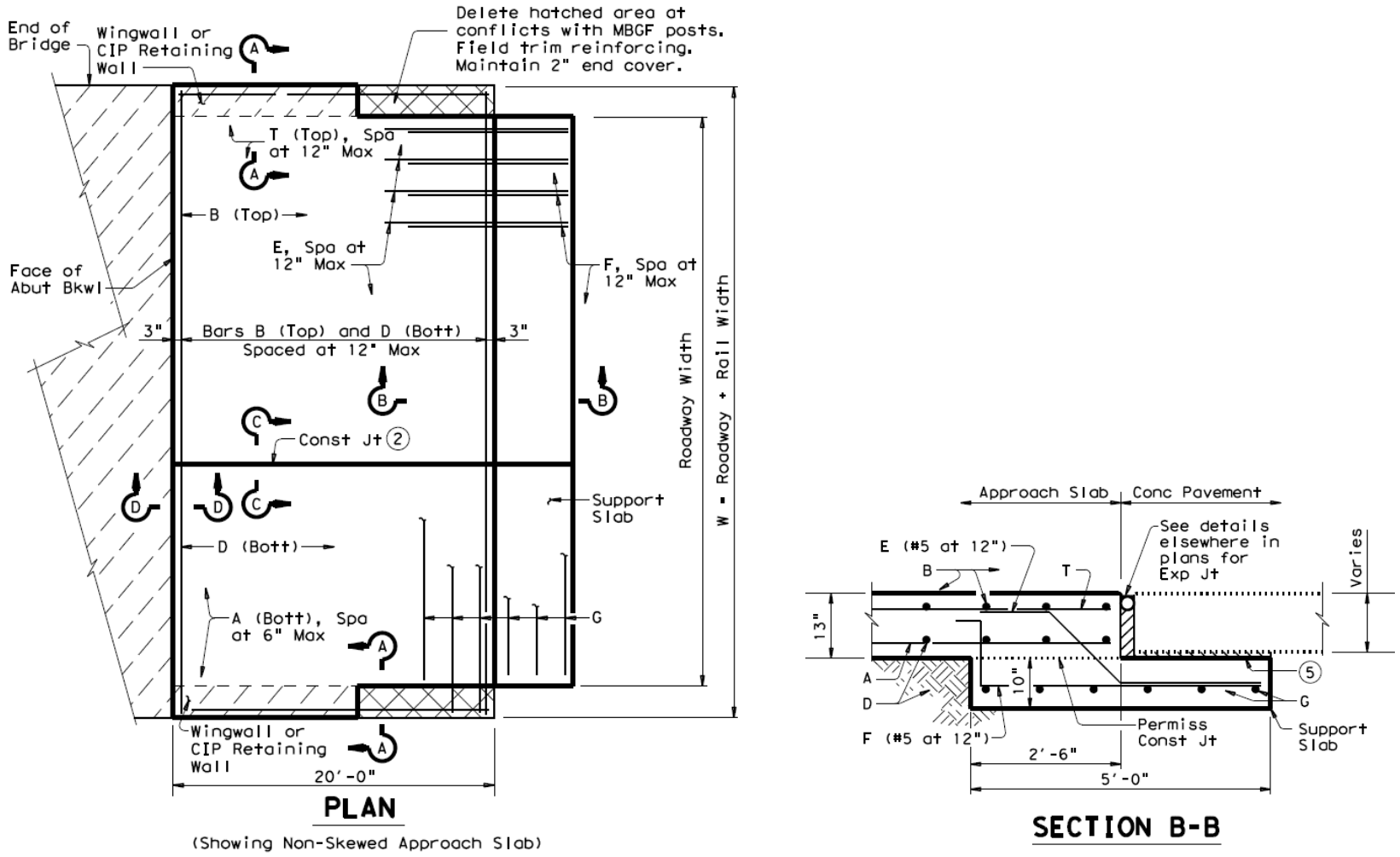


Figure 2-16. TxDOT's bridge approach slab standard: (a) plan view and (b) section view at the interface between the bridge approach slab and concrete pavement

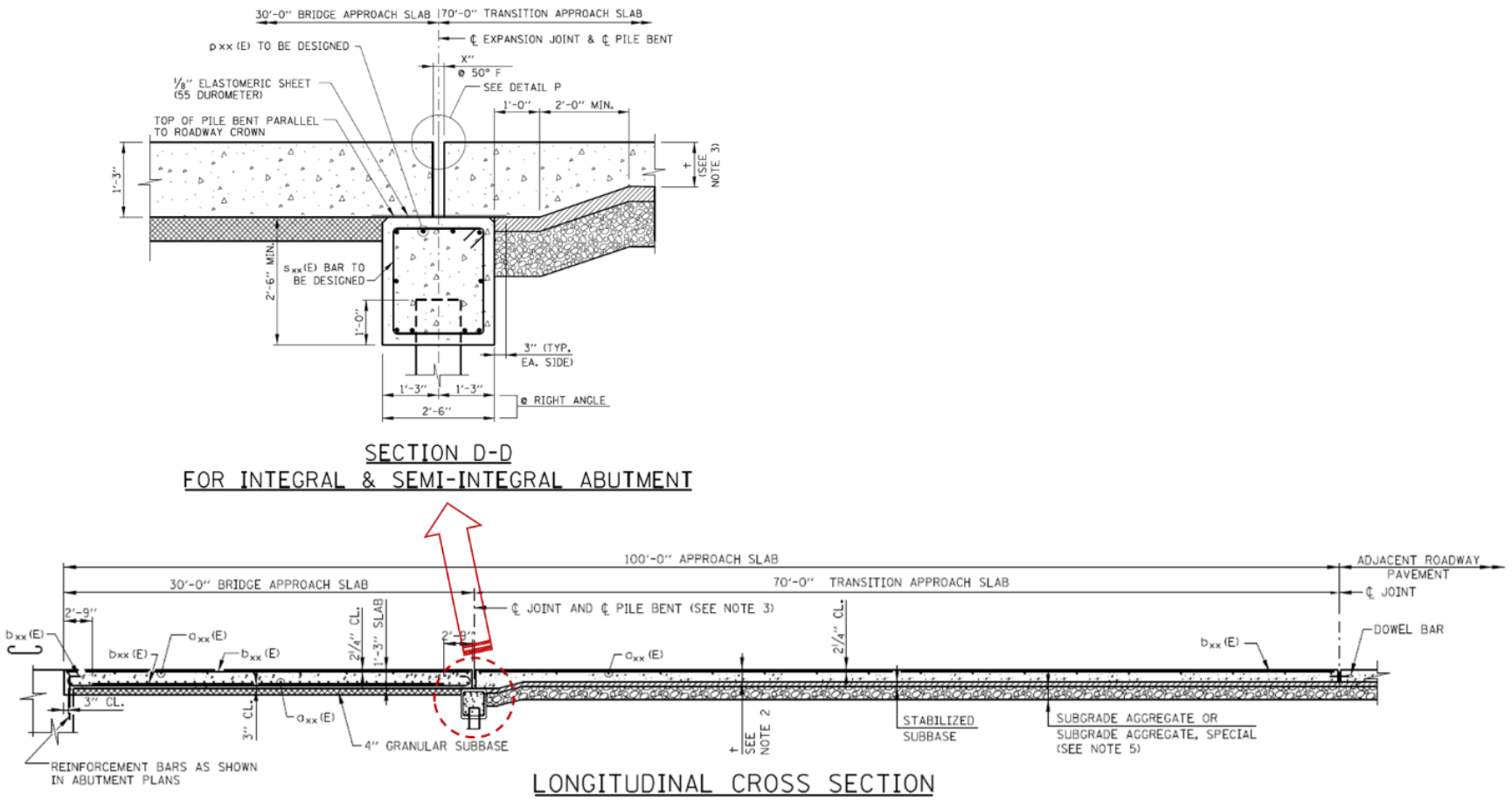


Figure 2-17. Illinois Tollway's bridge approach slab standard

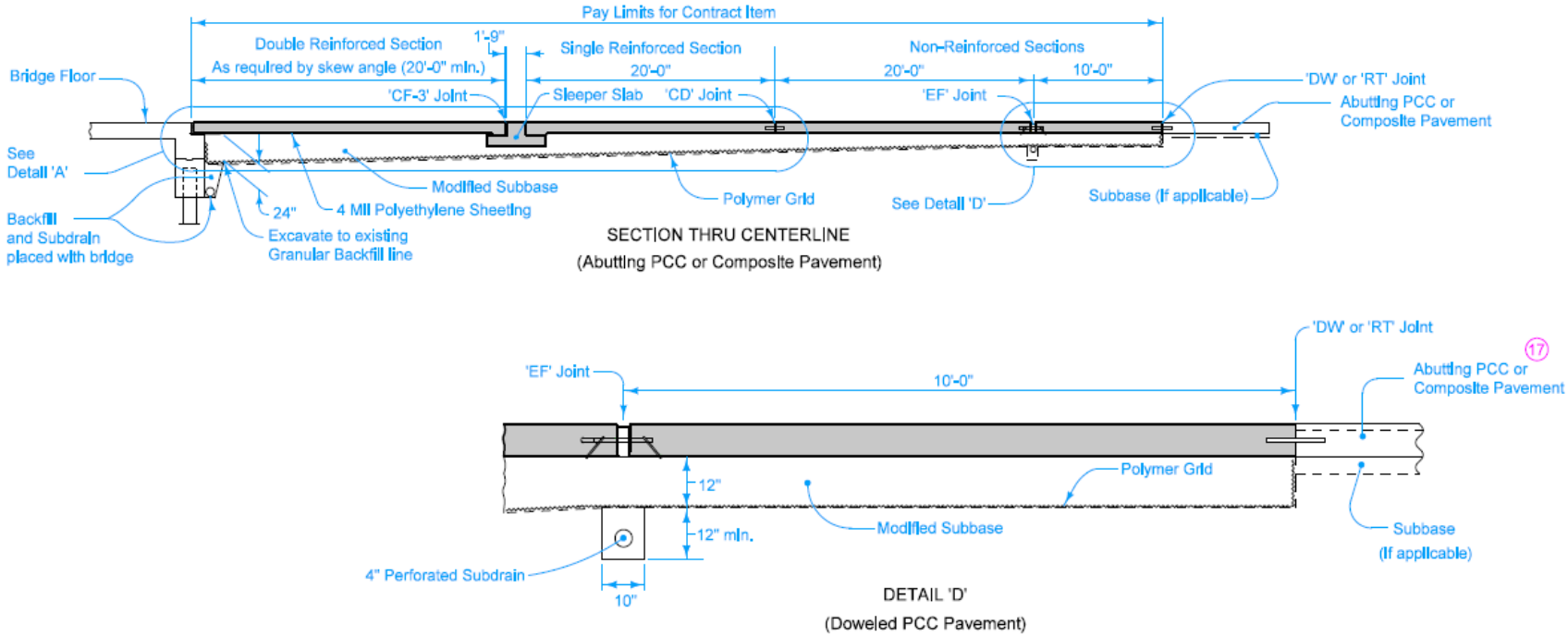


Figure 2-18. Iowa DOT's bridge approach slab standard

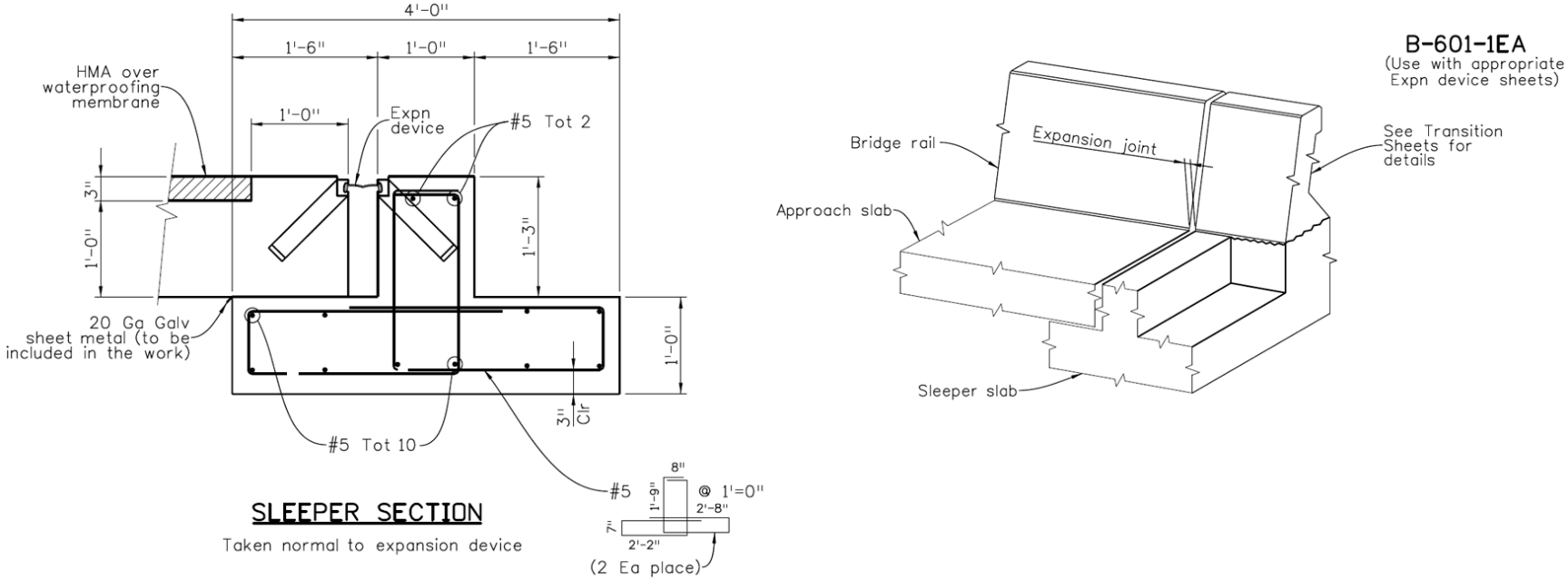
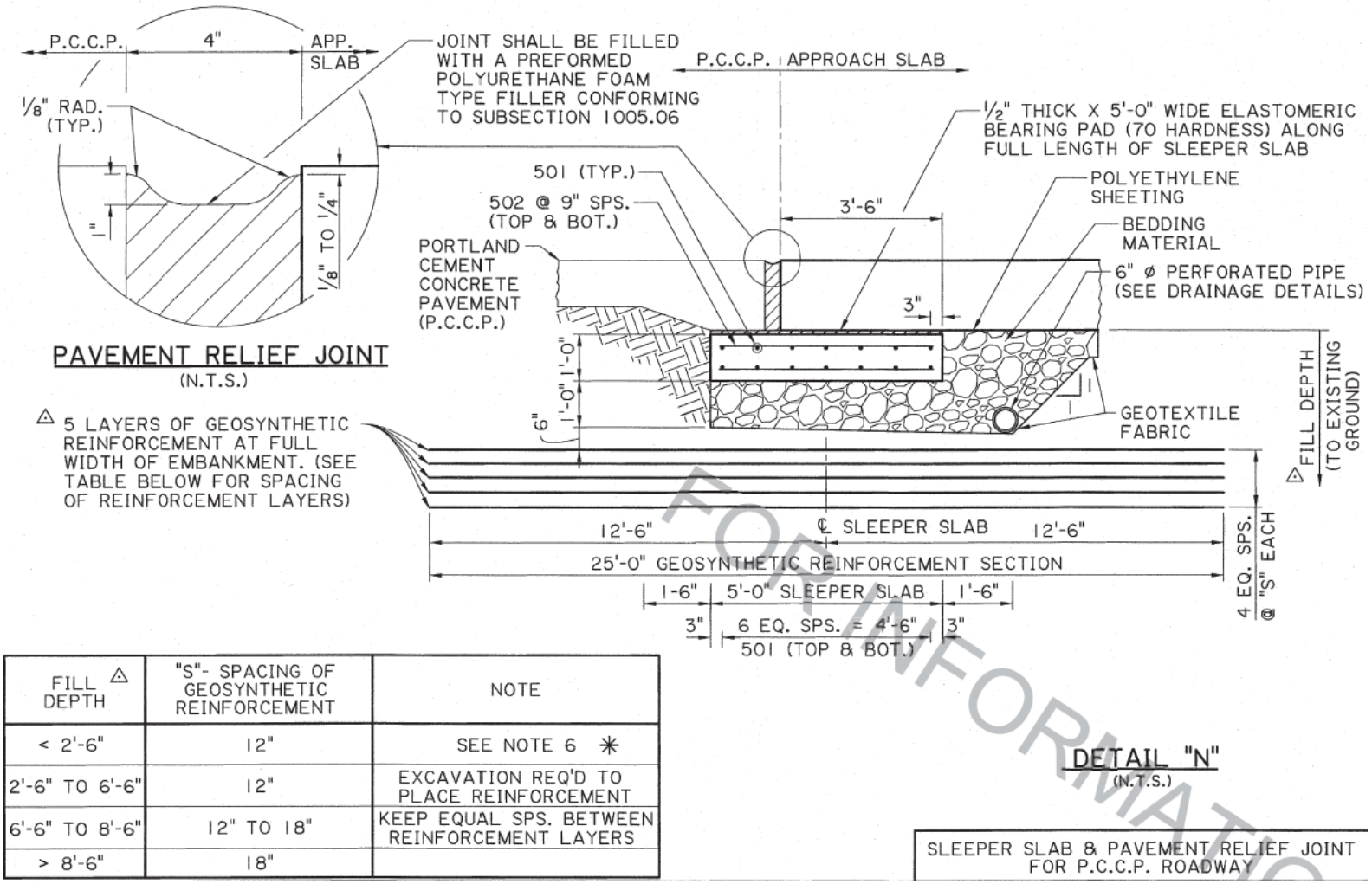
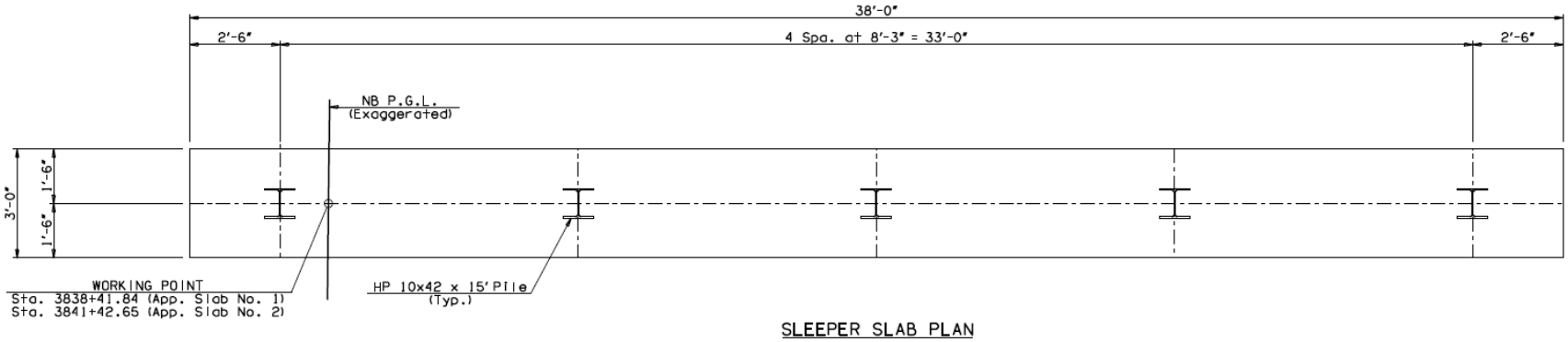


Figure 2-19. Inverted T-shaped slab in Colorado DOT standard

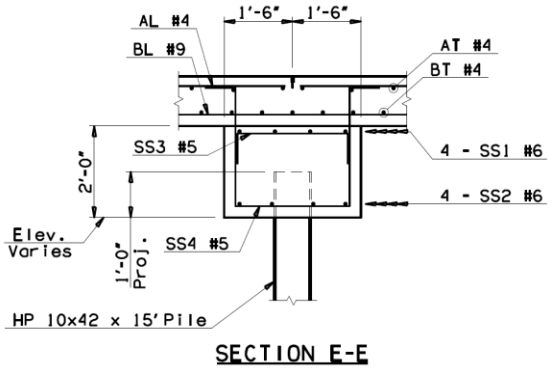


FILL DEPTH △	"S"- SPACING OF GEOSYNTHETIC REINFORCEMENT	NOTE
< 2'-6"	12"	SEE NOTE 6 ✳
2'-6" TO 6'-6"	12"	EXCAVATION REQ'D TO PLACE REINFORCEMENT
6'-6" TO 8'-6"	12" TO 18"	KEEP EQUAL SPS. BETWEEN REINFORCEMENT LAYERS
> 8'-6"	18"	

Figure 2-20. Sleeper slab underlain by bedding material in Louisiana DOTD standard



(a)



(b)

Figure 2-21. Details of a sleeper slab used in Oklahoma: (a) plan view and (b) section view

2.3.4 Project-specific case studies

2.3.4.1 Texas

2.3.4.1.1 Study by Chen and Yi (2015)

Chen and Yi (2015) evaluated the performance of BAS in Texas repaired by two distinct polyurethane-foam injection processes. This study provides detailed insights into the field investigation tools and procedures used for the condition assessment of bridge approaches using results from falling weight deflectometer (FWD) tests and elevation profile:

1) Localized Roughness Characterization: The study focuses on evaluating the localized roughness of bridge-approach settlements using deviation curves. Localized roughness of with a deviation over 0.15 in (3.8 mm) within a 25-ft (7.62-m) segment marking is considered to be significant (Olmedo et al. 2015).

2) Polyurethane-Foam Injection: Two processes of polyurethane-foam injection were investigated for slab lifting and leveling: a patented deep-injection process and a non-patented injection process.

3) Tools and Techniques:

    a. Elevation Surveys: These surveys are conducted using total station to measure and characterize the extent of settlement. The original profile is assumed to be linear between the bridge joint and the other end at 10 ft beyond the pavement-slab joint.

    b. Surface Profiles Using High-Speed Laser Profiler: This tool is used to gather the surface profile data of the approach slab for the calculation of IRI.

    c. Settlement Measurements with a String Line: The method involves stretching a string line in a straight line along the longitudinal direction of the bridge and pavement. One end of the string is anchored at the bridge joint, while the other end extends 10 feet beyond the joint where the pavement and the slab meet. Vertical measurements are taken at various points along this string line (see **Figure 2-22**). The largest measurement recorded is used to determine the severity of the slab settlement.



Figure 2-22. Demonstration of use of stringline for settlement measurement (Chen and Yi 2015)

d. FWD test: FWD tests were used to measure the deflection and to compare the condition of approach slab before and after treatment.

e. Performance Evaluation Based on Deviation Curves: The study presented a new method for measuring roughness by calculating the total area within deviation plots. This method utilized the TxDOT test procedure Tex-1001-S, which focuses on operating inertial profilers for pavement profile evaluations. To effectively measure profile deviations in these shorter spans, it is recommended using a 25-ft (7.62-m) moving baseline, ensuring more accurate deviation assessments for these shorter bridge approaches. The localized roughness is calculated for every 25 ft (7.62 m) by calculating the area of the deviation curve represented as shaded area in **Figure 2-23**.

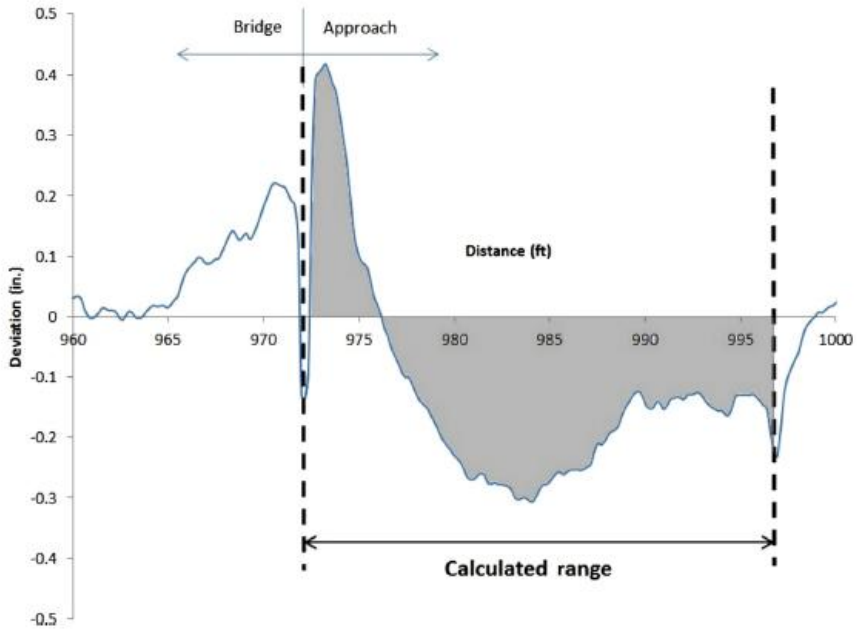


Figure 2-23. Deviation curve (Chen and Yi 2015)

The typical field-testing procedure for this study is outlined as follows:

1) Evaluation of Settlement:

   - The initial step involves evaluating the extent of the slab settlement. This includes measuring the deviation in the slab's elevation and assessing the roughness of the pavement surface using elevation surveys, surface profiles using a high-speed laser profiler, and settlement measurements with a string line. The string line measurements were much less time consuming than the elevation survey using total station.

2) FWD Tests:

   - FWD tests are conducted at 40 – 48 evenly distributed points throughout the approach/departure slabs both before and after the polyurethane-foam injection treatment (see **Figure 2-24**). The tests are normalized to 9000-lb (40-kN) load.

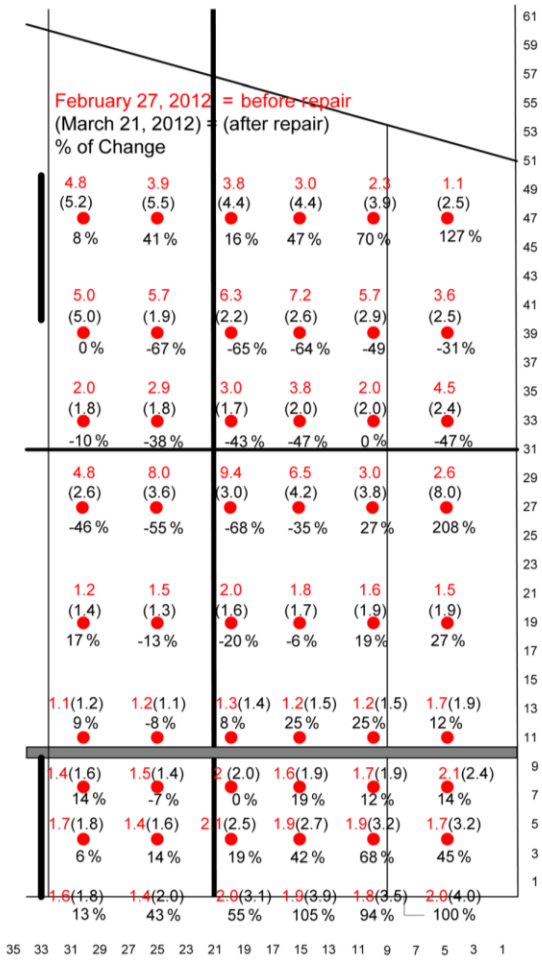


Figure 2-24. Comparison of the FWD deflections before and after the polyurethane-foam injection (IH 35) (Chen and Yi 2015)

3) Monitoring and Measurement:

- Elevation measurements are monitored at various station locations using laser level monitors throughout the injection process to assist in controlling the lift.
- After the treatment, profile measurements are collected using high speed laser profiler to evaluate the ride quality and the effectiveness of the injection.

4) Performance Analysis:

- The roughness of the pavement is quantified by summing areas bound by the deviation plot (see **Figure 2-25**). This method is used to assess the improvement in pavement smoothness and the reduction in localized roughness after the treatment.
- The results from the FWD test are used to demonstrate the effectiveness of the treatment in stabilizing the bridge approaches.

5) Long-term Monitoring:

- Regular profile measurements are collected several times over a year to monitor the long-term effectiveness of the treatment.

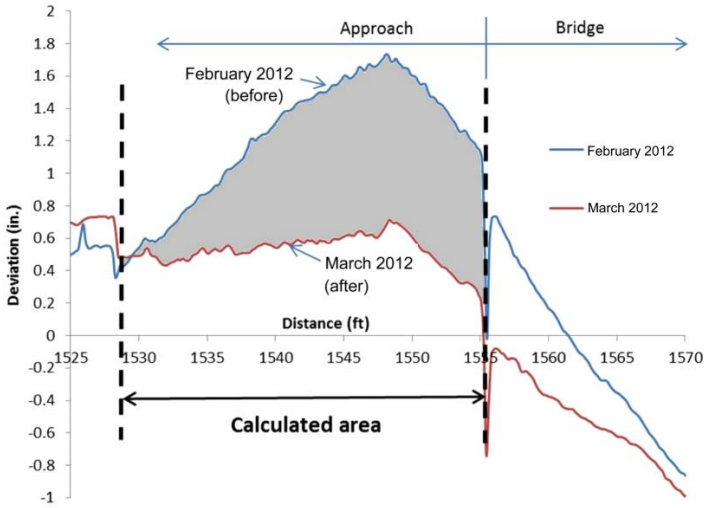


Figure 2-25. Reduction of roughness (shaded area) in deviation plot before and after polyurethane-foam injection (Chen and Yi 2015)

In summary, the field investigation for approach slab condition assessment involves a combination of elevation surveys, surface profiling, settlement measurements, slab deflection measurements, and the analysis of deviation curves to determine the localized roughness.

2.3.4.1.2 Study by Puppala et al. (2011)

Puppala et al. (2011) conducted a series of field tests to assess the condition of bridge approaches, and the following sections summarize their findings.

(a) SH 6 north of Quanah in the Childress District:

An overview of the test section SH 6 north of Quanah is shown in **Figure 2-26**.

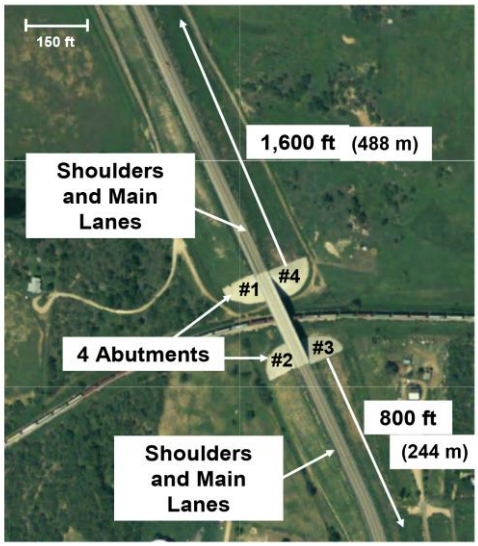


Figure 2-26. Test section along SH 6 (Puppala et al. 2011)

The methods and tools used to obtain field test data and assessment of the embankment condition are summarized as follows:

1) Ground Penetrating Radar (GPR) System:

- A GPR system was used to evaluate bridge approaches and embankments to detect potential voids or anomalies below the surface.
- Different antennas (1.6 GHz, 400 MHz, and 200 MHz) were used to cover different penetration depths, identify pavement interfaces, and detect utilities or anomalies at different depths.
- Test Setup:
    - Line scans with low (200 MHz) and high (1.6 GHz) frequency antennas were obtained along the center of the shoulder and main lanes in both directions.

        - Four line scans with the high-frequency antenna were obtained on each of the four embankment slopes to evaluate the presence and extent of anomalies and voids under selected slabs.

- Analysis of Line Scans:

    - Typical line scans obtained with the high-frequency GPR antenna indicated the structure of the approach slab, such as the hot mix asphalt (HMA) layer on top of a concrete slab, including the thickness of the HMA and the location of steel rebar reinforcement.

    - Areas of discontinuity and different layers within the subgrade were also highlighted.

    - Anomalies potentially indicating voids or areas of concern were observed in certain sections of the slabs.

2) Potential Void Volume Estimation:

- Detailed GPR scans were evaluated to estimate suspected voids under approach slabs. The estimated void areas were then used to calculate void volumes.

- Void volumes were calculated for both shoulders and lanes, as well as for the concrete slabs on each slope.

3) Proposed Mitigation Techniques:

- Based on the estimated void volumes, the use of geofoam blocks and flowable fill were proposed as mitigation techniques.

(b) IH 410 in San Antonio:

Sectional views of the west and east approach slabs of the test site are presented in **Figure 2-27**.



Figure 2-27. Sectional views of the west and east approach slabs of IH 410 in San Antonio (Puppala et al. 2011)

The test procedure and tools used to assess the condition of embankments are summarized as follows:

- GPR tests were conducted at IH 410 and a coring plan was established from the GPR data.
- Six core samples were collected from each approach slab area.
- At selected core locations (five on west approach area and four on east approach area), dynamic cone penetrometer (DCP) tests were performed.
- GPR line scans revealed several layers of the pavement structure, anomalies adjacent to the approach slab, and the locations of transverse reinforcement.
- Core samples provided detailed views of the approach slabs' condition, revealing cracks, voids, and stripped asphalt in certain cores.
- The GPR depth estimations were generally consistent with the ground-truth data obtained from the cores.
- DCP tests identified different soil layers and interfaces, providing additional insights into the subgrade conditions. The detailed coring and GPR lines plan for the IH 410 bridge approach in San Antonio are provided in **Figure 2-28**.

- Based on GPR and core data, void volume was estimated. The use of flowable fills was proposed as a suitable mitigation method. However, it was not implemented due to the uncertainty in the long-term performance of the approach slabs after repairing using the proposed technique.

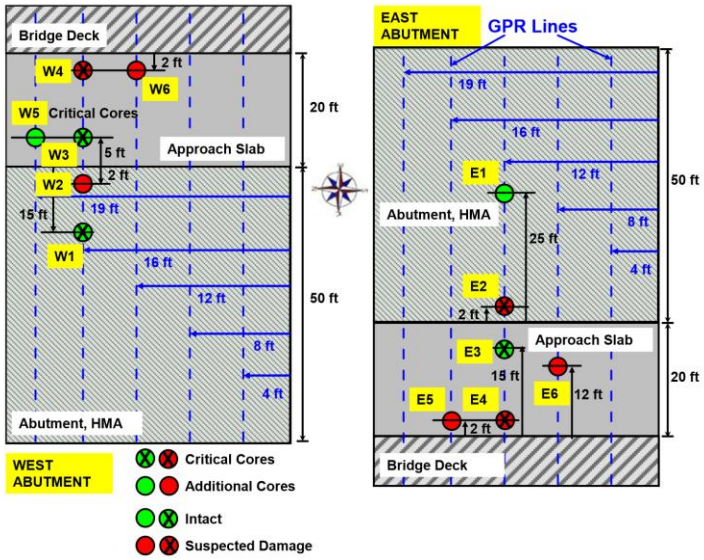


Figure 2-28. Testing layout of IH 410 in San Antonio (Puppala et al. 2011)

2.3.4.2 Other states

2.3.4.2.1 Iowa

The study by ElBatanouny et al. (2018) focuses on evaluating the effectiveness of revised standards by the Iowa DOT to mitigate the formation of bumps at bridge approaches.

The study employed several nondestructive evaluation techniques:

- Visual Inspection: Assessing the condition of bridge components, including approach pavement surfaces, expansion joints, slab panels, barriers, abutment wings, berm slopes, and subdrain outlets.
- Borescope Inspections: Employing a camera to investigate and confirm the presence of voids through access ports and cores.
- Ground Penetrating Radar (GPR): Determining the extent of voids beneath the approach panels.
- Surveying: Measuring the elevation profiles of the approach slabs and calculating the Bridge Approach Performance Index (BI).

Using the evaluation techniques, the following detailed field investigations were performed:

- Visual Inspection:

    - Documented the condition of surfaces of the bridge approach pavement, roadway shoulder, abutment wings, abutment footing face under the bridge, subdrain outlets for abutment backfill drainage, berm slope erosion, and joint type and condition. An example of documentation of visual inspection is presented in **Table 2-13**.

    - Used an in-house annotation program to annotate digital inspection data and photographs onto PDFs.

Table 2-13. Example of documentation from visual inspection (ElBatanouny et al. 2018)

Approach		**East**	**West**
Joints	Abutment	2.75 to 3.5 inches in width Heavily deteriorated; sealant is cracked and pieces can be pulled out by hand Raveling and spalling present Vegetation at shoulders and median	3-inch width Vegetation present
	First CD	0.5-inch width Sealed	Minor raveling
	Second CD	0.5-inch width Sealed	----------
	EF	2.75-inch width Sealant has cracked Vegetation present Minimal raveling and spalling Crack present at longitudinal joint	3.25-inch width Vegetation present
	DW or RT	0.5-inch width Sealant has mostly failed	----------
	Contraction	0.5-inch width Sealant has mostly failed	----------
Shoulder		Ended after third slab Crack present in shoulder of westbound lane of the first slab	----------
Barrier		North: gap is present and erosion has occurred behind the barrier South: joint partially intact	Joints between barriers and deck failed Erosion has occurred behind both barriers
Berm slope		Vegetation present	No erosion under bridge
Subdrain outlets		North drain partially blocked by vegetation	----------

- Borescope (Snake Camera) Surveys:
    - Utilized in bridges where Iowa DOT incorporated access ports at the wing walls.
    - Enabled visual data collection inside the access ports to assess if settlement of the backfill had occurred and to investigate the extent of voiding under the slabs.
- Elevation Surveys:
    - A robotic total station was used to collect elevation survey data of selected portions of the approach slab for each bridge.
    - The data helped determine if settlement of the approach slab had occurred relative to the bridge.
    - The Bridge Approach Performance Index (BI) was calculated using this data to assess the condition of bridge approaches.
- Ground Penetrating Radar (GPR) Testing:
    - Conducted on each approach slab to assess abutment backfill settlement resulting in voiding beneath the approach (see **Figure 2-29**).
    - A SIR4000 GPR control unit with a 2.6 GHz dipole antenna was used for scanning.
    - Discrete scans were collected on the top surface of the approach slabs at a spacing of 2 feet on center.
    - Post-processing and analyses of the collected GPR scans were completed using specific software, with a focus on identifying areas where potential voiding under the slab exists.



Figure 2-29. GPR scanning in progress on an approach slab (ElBatanouny et al. 2018)

- Coring:
    - Concrete cores were drilled at select locations where GPR data was collected to visually confirm the presence of voids (see **Figure 2-30(a)**). In addition, borescope inspections corroborated these findings (see **Figure 2-30(b)**).



(a) (b)

Figure 2-30. Photos showing the presence of voids beneath the bridge approach slab: (a) view of core drop (1/4 in) indicating presence of minor void under the slab and (b) view of void from borescope (ElBatanouny et al. 2018)

The study utilized a comprehensive assessment approach for bridge components, assigning condition ratings from good (minor distress) to poor (end of service life), primarily through visual inspections. Notable variation between designed and actual joint widths indicated the need for maintenance and potential design changes. Based on these observations, the study makes several recommendations, including developing maintenance plans for deteriorated joints, cautious interpretation of data from access ports, incorporating GPR testing in future inspections, considering various abutment designs, and modifying designs to mitigate void formation and water ingress.

2.3.4.2.2 Louisiana

Abu-Farsakh and Chen (2014) conducted a research study at the Bayou Courtableau Bridge in Louisiana, aiming to evaluate, validate, and verify the new bridge approach slab design method they previously proposed. The west approach slab was designed using the proposed new method with slab thickness of 16 in, while the east approach slab was designed using the traditional method with slab thickness of 12 in. The pavement end side of the approach slab was supported by a 4.0-ft-wide sleeper slab with the soil underneath it reinforced by six layers of geogrid placed at a vertical spacing of 12 in. Although the study by Abu-Farsakh and Chen (2014) involves the evaluation of performance of new BASs, it included monitoring of embankment settlement after the construction and, therefore, was included in our literature review.

The study employed following testing methods, instrumentation, and procedures:

- A comprehensive subsurface characterization program: Moisture content, density, Atterberg limits, particle size analysis, 1-D consolidation tests, UU tests, K_0-CU tests, and cone penetration tests (CPT) were performed to investigate the soil properties of the bridge site.

- Foil Strain Gages: These were used to monitor strain changes within the approach slabs and geogrid layers.

- Pressure Cells: Installed beneath the approach slabs and strip footings to measure contact stress between the slab and embankment soil and within the reinforced soil foundation.

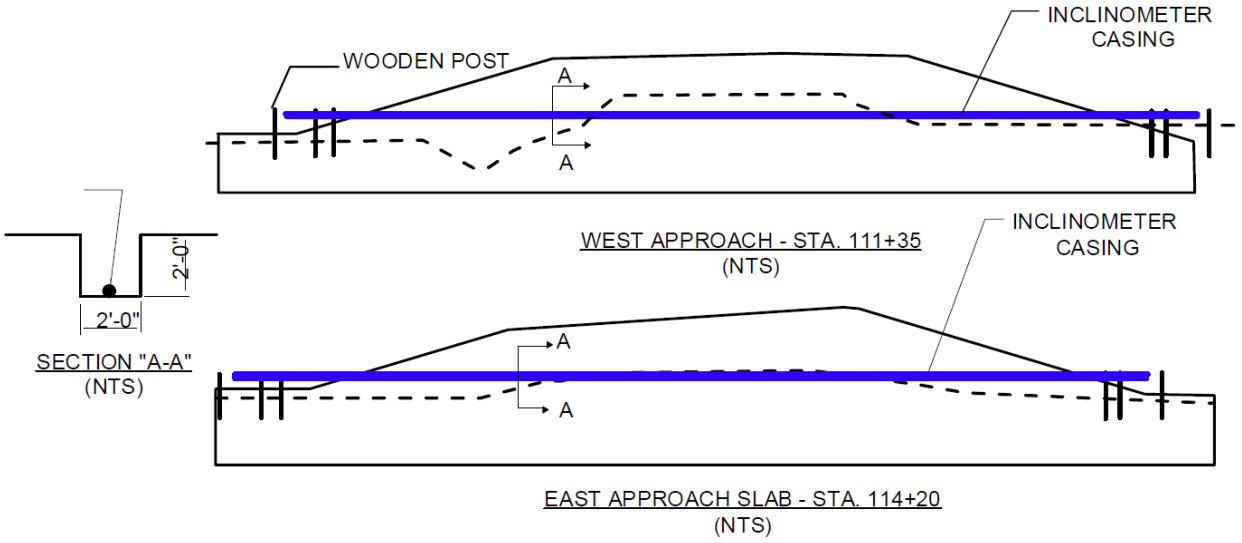
- “Sister Bar” Strain Gages: Deployed within the concrete of the west approach slab to evaluate internal stresses.

- Horizontal Inclinometer: Installed at each embankment side underneath the middle of the approach slab to monitor the profile of consolidation settlement of subsurface soil (see **Figure 2-31**).

- Static Load Tests: Two tests were conducted on both the east and west approach slabs. The first test occurred before the bridge opened to traffic, and the second took place about a year and a half later. A 20-ton large CPT truck was strategically placed on the slab to apply

dead loads during these tests. The instrumentations were installed along the center line of the lane.

- Data Collection: Sensor readings were taken at the beginning of each load test to serve as reference points. Only load-associated responses were reported and analyzed.
- Contact Stress Measurement: This involved measuring the stress between the approach slab and embankment soil under different loading conditions.
- Settlement Profiles: Settlement profiles were measured from the horizontal inclinometers after the completion of the approach slab to assess the embankment behavior.



(a)



(b)

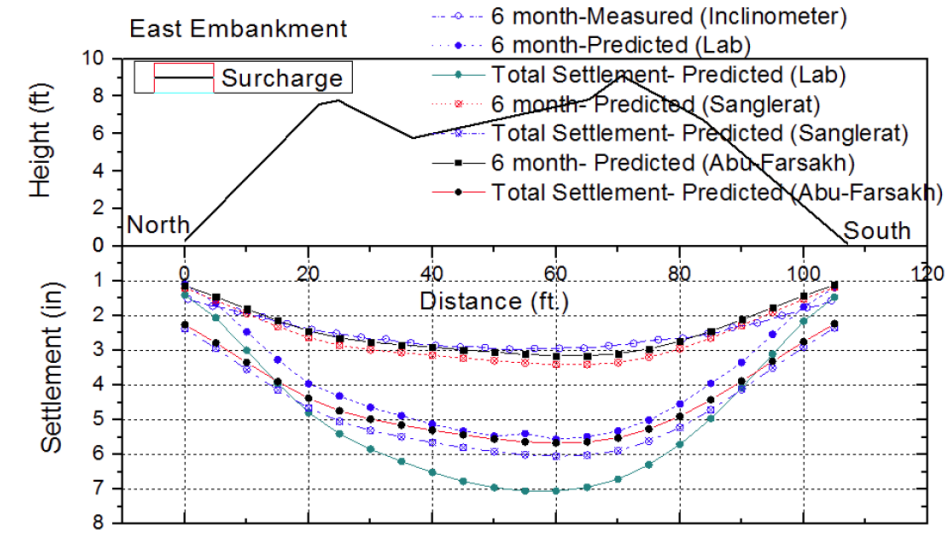
Figure 2-31. (a) Installation plan of horizontal inclinometers and (b) installation of horizontal inclinometer casing and return pipe (Abu-Farsakh and Chen 2014)

The evaluation of the embankment and approach slab performance was based on various parameters:

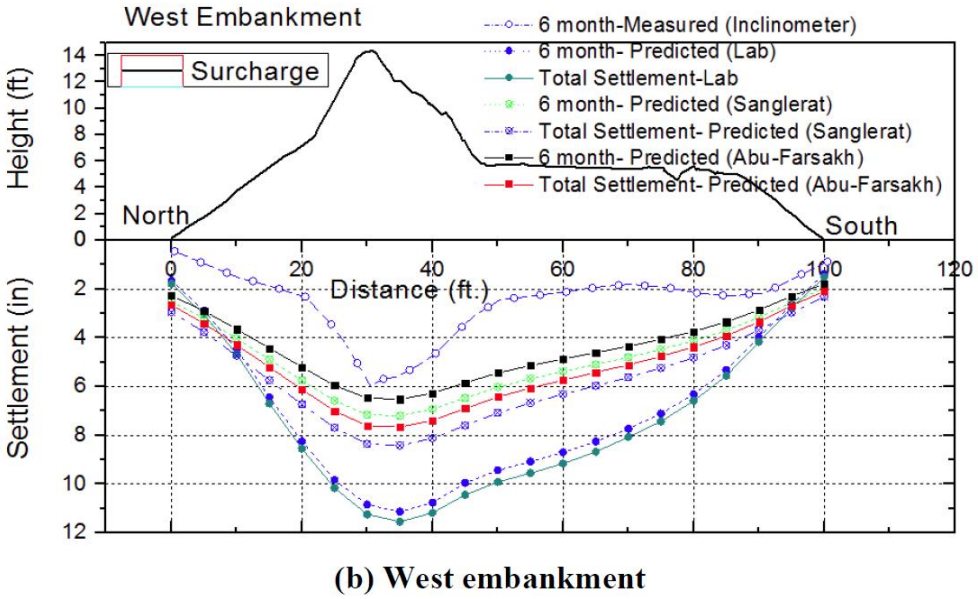
- Contact Pressure Analysis: This assessed the interaction between the slab and the underlying soil, providing insights into the support and contact loss over time.
- Settlement Monitoring: Settlement measurement using strain gauges and inclinometers enabled continuous monitoring the deformation behavior of the embankment soil after construction. Abu-Farsakh and Chen (2014) predicted settlement of foundation soil using the results from CPT performed during site characterization and compared their predictions with the measured value, which is presented in **Figure 2-32**.
- Strain Measurement: Internal strain distributions within the approach slab and along the geogrid were analyzed to assess the structural response of the slab and the reinforced soil foundation to loading simulated by static load testing in the field.
- IRI Profiles: The IRI was used to evaluate the ride quality of the bridge approach. The average 25-ft continuous IRI profiles demonstrated much better performance of the new

approach slab system (west approach slab) compared to the traditional design method (east approach slab).

- The authors attributed the improved performance of the new approach slab system on the west approach slab to increasing slab rigidity, EI, and using geosynthetics to reinforce the soil below the sleeper slab.



(a) East embankment



(b) West embankment

Figure 2-32. Comparison of settlement prediction (Abu-Farsakh and Chen 2014)

2.3.4.2.3 Oklahoma

Miller et al. (2013) critically examined the design and construction methods in Oklahoma to uncover the causes and potential solutions to the problems in BAS and nearby pavement structures in roadway embankments. The study involved extensive fieldwork, including field reconnaissance investigations of 30 bridges at 22 locations and detailed subsurface investigations at five sites. This study employed a range of methods and tools for evaluating embankment conditions as part of its Level I and Level II investigations. A high-level summary of the study is presented below.

(a) Level I Investigations

- Visual Inspection:
    - Utilized visual observation to evaluate surface conditions, drainage, abutment status, and voids.
    - Identified substantial voids beneath approach slabs, abutments, and slope walls, and examined erosion paths and recorded them in photographs.
- Manual Measurements:
    - Involved measuring vertical and horizontal differences between the approach slab and the bridge deck.
    - Measured the depth of visible voids beneath the roadway slab using rulers and tape measures.
- Underdrain Design and Site Behavior Analysis:
    - Analyzed various underdrain designs observed at the bridges.
    - Examined standard underdrain designs, identifying potential design flaws.
    - Assessed severity of erosion under abutments and the performance of underdrain systems using visual inspection.
    - Combined field observations with design, construction, and maintenance records for trend analysis.

(b) Level II Investigations

- Background Documentation Collection:
    - Obtained bridge design, construction, and maintenance records from ODOT.
    - Utilized ODOT's Geographical Resource Internet Portal Lite (GRIP Lite) for additional site details.

- Subsurface Drilling and Sampling:
    - Performed using a truck-mounted drilling rig and air rotary method.
    - Collected split spoon and Shelby tube samples, primarily in cohesive layers, both on and off the embankments.
    - Focused on analyzing soil properties and profiles.
    - SPT:
        - Conducted on and off embankment locations, with 3 to 5 tests per embankment (*e.g.*, see **Figure 2-33**).
        - Split-spoon sampler used via a truck-mounted air rotary drilling method.
        - The number of blows recorded every depth of multiples of 3 feet, with penetration depths ranging from 15 to 30 feet.

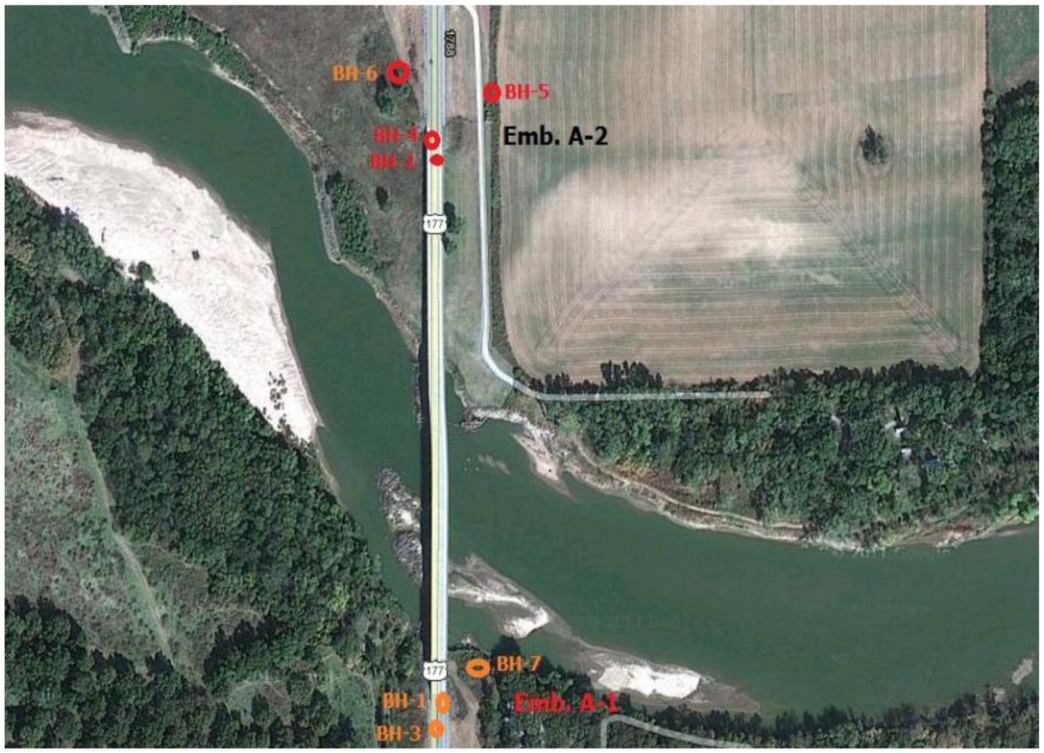
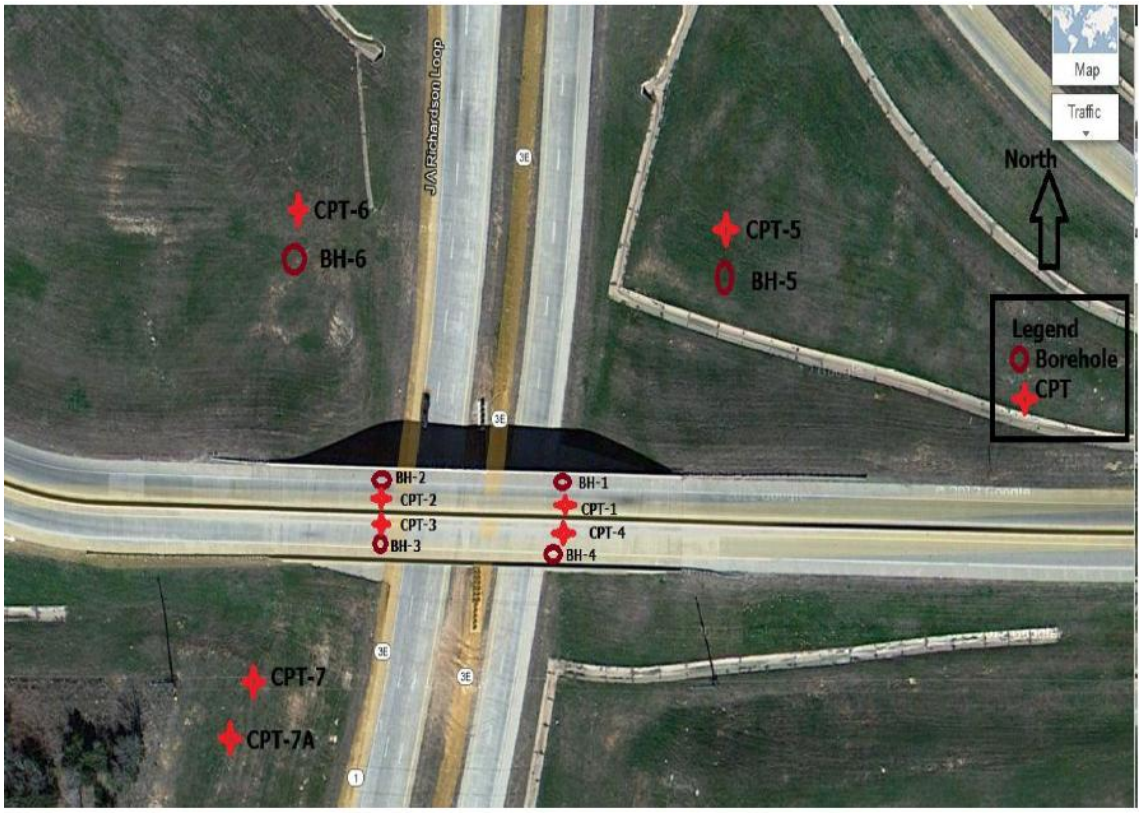


Figure 2-33. Borehole locations for US-177 over Salt Fork in Oklahoma (Miller et al. 2013)

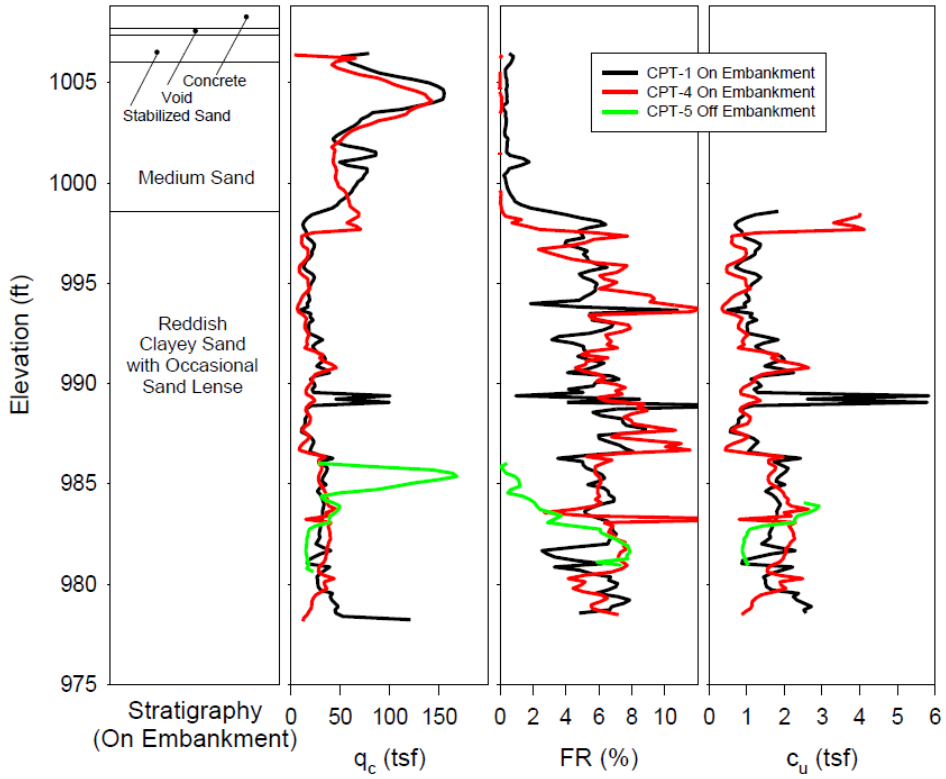
- Laboratory Testing:

- Included Atterberg limit, grain-size distribution, and oedometer tests on cohesive soils.
- Conducted to classify the soil and describe behavior related to approach slab movement.
- Determined over-consolidation ratios, compression index, and recompression index of clay layers.

- Cone Penetration Testing:
  - Conducted at a minimum of three locations on and off the embankment to a depth of 30 to 60 feet.
  - Measured tip resistance, sleeve friction, and pore water pressure (piezocone).
  - Conducted to delineate the stratigraphy at the test sites and to determine parameters for the settlement analysis.



(a)



(b)

Figure 2-34. (a) CPT and borehole locations for SH-1 over SH-99 in Oklahoma and (b) CPT results for East Embankment for SH-1 over SH-99 (Miller et al. 2013)

- Ground Penetrating Radar (GPR) Assessment:
    - Employed a portable GPR unit to detect voids beneath approach slabs using 400MHz and 1.3GHz antennas.
    - Data points collected at intervals of 1.9 inches to 4.7 inches, with the specific interval depending on the antenna frequency.
    - Line spacing maintained at 50 feet.
    - Recommended higher frequency antennas (1-1.6GHz) for better resolution and characterization of voids.
    - Analyzed GPR data to identify evidence of voids and refine detection methods.
- Settlement Analysis:
    - Settlement properties assessed based on the oedometer test results, embankment geometry and soil profiles assuming uniform soil layer.

    - Determined the proportion of total settlement attributable to virgin compression and recompression.

- Data Analysis and Database Development:

    - Identified problems related to design and construction factors.

    - Stored data in a database for statistical analysis to identify trends and relationships between bridge approach settlement and observed distresses.

Based on their observations, Miller et al. (2013) reported that most of the sites investigated had significant problems with drainage and erosion. They were particularly concerned about the loss of soil from beneath the BASs and formation of voids. They strongly suggested "a complete rethinking of design of surface and sub-drainage systems to efficiently remove water from beneath pavements and backfill while diminishing or eliminating the erosive power of the water." Miller et al. (2013) also reported that pavement surface joint seals were largely compromised and argued that "the subsurface drainage must be designed with the expectation that water will enter the joints."

In addition to erosion, they also noted the significant potential for consolidation settlement of foundation soils below embankments. Using the soil properties determined from subsurface exploration and laboratory testing performed on four embankments, they estimated the consolidation of the foundation soil to be between 5 to 11 inches, which are certainly problematic for approach slabs (Miller et al. 2013).

2.3.4.2.4 Florida

Lu et al. (2018) provided a comprehensive methodology for evaluating bridge approach/departure pavement conditions in Florida in their study. Their research involved assessment of the extent of the bridge approach settlement problem, then reviewing existing rehabilitation criteria, and finally, formulating a guideline for selecting optimum rehabilitation strategy.

To assess and identify distresses in bridge approach and departure asphalt pavements, the study utilized a combination of FDOT highway video log images and high-resolution pavement condition survey data from the FDOT State Materials Office. Video logs provided visual crack ratings, while the survey data, recorded for each 5.3-ft segment of highway, offered rut ratings, IRI, and ride quality measurements. The study focused on a detailed analysis of pavement conditions every 0.001 mile (= 5.28 ft), revealing trends in cracking, smoothness, and rutting, and provided a comparison between approach and departure pavements. This approach emphasized the importance of using high-resolution data and diverse data sources for accurate condition assessment of highway embankments.

The evaluation procedure for assessing pavement distresses based on FDOT video log images can be summarized in the following steps:

1) Locate the beginning mile post of the bridge and divide the area into six segments (three each for approach and departure sides).

2) Segment the survey area into five longitudinal sections, including wheel path and outside wheel path areas as shown in **Figure 2-35**.

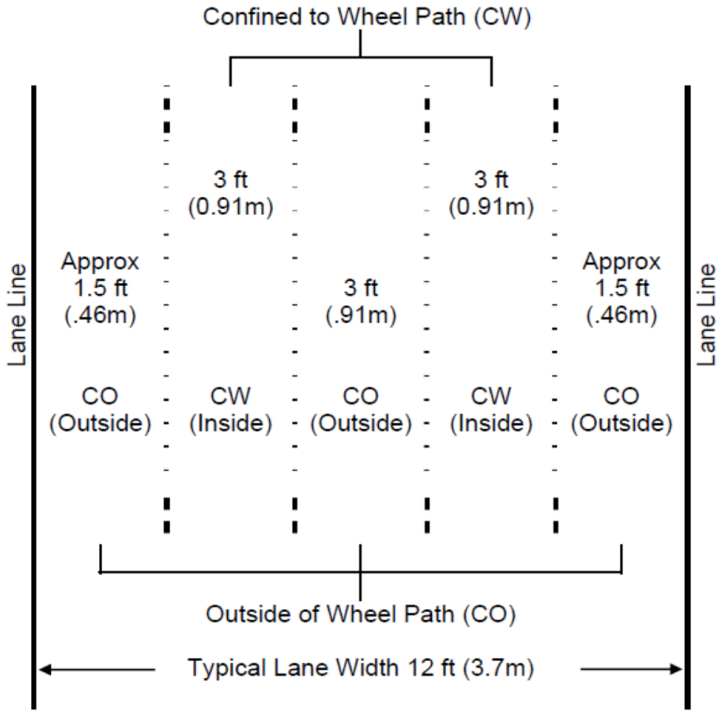


Figure 2-35. Typical wheel path designation in a lane (Lu et al., 2018)

3) Visually record five types of pavement distresses in each segment, such as various types of cracking, raveling, and patching. The distress types based on the characteristics of surface condition are summarized in **Table 2-14**.

Table 2-14. Crack characterization based on surface condition (Lu et al., 2018)

Distress Type	**Description**
1B Cracking	Hairline cracks ≤ ⅛ inch wide, may have slight spalling and branching
II Cracking	Cracks > ⅛ inch and ≤ ¼ inch wide, moderate spalling or severe branching, includes alligator cracking
III Cracking	Cracks > ¼ inch wide, extending longitudinally or transversely, open to base or underlying material
Raveling	Wearing away of pavement surface due to dislodging of aggregate particles
Patching	Area replaced with new material after original construction, indicating repaired defects

4) Choose a 26 ft lane section 0.3 - 0.5 mi away from the bridge as a control for comparison.

5) Use the distress data to calculate a crack rating (CR) for each segment, averaging the ratings for segments to represent the condition of the approach and departure pavements.

The procedure to evaluate pavement distresses based on condition data includes the following steps:

1) Identify Starting Points: Locate the beginning and ending mile posts of each bridge, selecting four segments for both approach and departure sides, each 95 ft in length.

2) Extract Condition Data: Gather rut depth, IRI, and ride number information for each segment and control section.

3) Compute Ratings:

    - Rut Rating: Deduct a value from 10 based on the rut depth. A rating of 10 indicates minimal rutting.

    - Ride Rating: Convert from IRI on a scale of 0 (very rough) to 10 (very smooth). A rating ≤ 6 indicates a rough pavement.

    - IRI Rating: Values < 95 in/mi suggest good riding quality.

Table 2-15. Pavement condition evaluation based on condition rating (Lu et al., 2018)

Rating Type	**Data Used**	**Scale**	**Interpretation**
Rut Rating	Rut depth	0-10	10 = minor rutting
Ride Rating	IRI	0-10	≤ 6 = rough pavement
IRI Rating	IRI	-	< 95 in/mi = good quality

Lu et al. (2018) also analyzed GPR data using various intervals, namely 100 ft, 50 ft, and 5.28 ft, and recommended the GPR analysis with data point spacing of 6 ft.

Based on the analysis of Florida Interstate highway bridge approach/departure asphalt pavement data, a rating system for bridge approach/departure asphalt pavement is proposed, as presented in **Figure 2-36**:

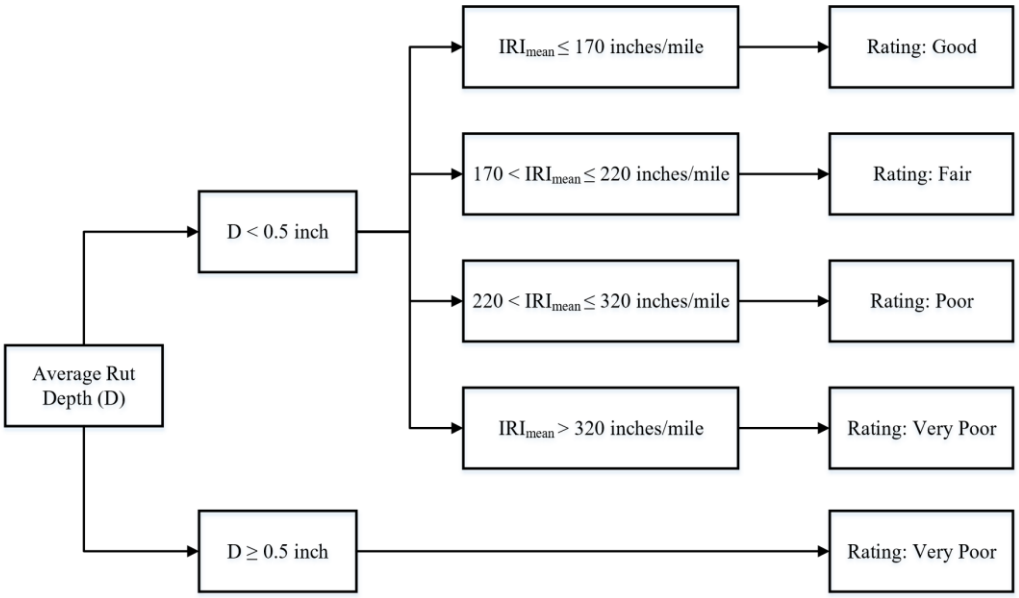


Figure 2-36. Proposed rating system for bridge approach/departure asphalt pavement (Lu et al. 2018)

Lu et al. (2018) further provided a detailed rehabilitation strategy selection procedure, which can be summarized as follows:

- Pavement Condition Survey and Evaluation: Identify a 200 ft section from the bridge approach slab end. Calculate average crack rating, rut depth, and IRI for both the bridge approach section and a control section.

- Detailed Data Collection: Collect detailed data from the pavement condition survey and Roadway Characteristics Inventory (RCI) database, including traffic volumes, speed limits, lane widths, and base materials.

- Select Rehabilitation Techniques: Based on the pavement's current structure, select techniques like structural overlay or complete reconstruction to address issues like rutting and cracking.

- Form Rehabilitation Strategies: Develop alternatives with varying design periods (8, 15, 20, 30 years) and calculate required structural numbers for each. Use traffic level data and FDOT guidelines for this step. The required structural number (SNR) is a weighted thickness representing the required strength of the pavement structure, which can be calculated according to the AASHTO pavement design guide published in 1993 (AASHTO, 1993).

- Life-Cycle Cost Analysis (LCCA): Conduct LCCA considering the analysis period, discount rate, agency costs (including construction and follow-up costs), and user costs to find the most economical option.

- Choose Rehabilitation Strategy: Compare the alternatives in terms of agency cost, frequency of rehabilitation, construction duration, and structural number improvement. Select the strategy that offers the best balance between cost-effectiveness and reduced traffic disruptions.

The rehabilitation strategy selection procedure for bridge approach/departure asphalt pavements is presented in **Figure 2-37**.

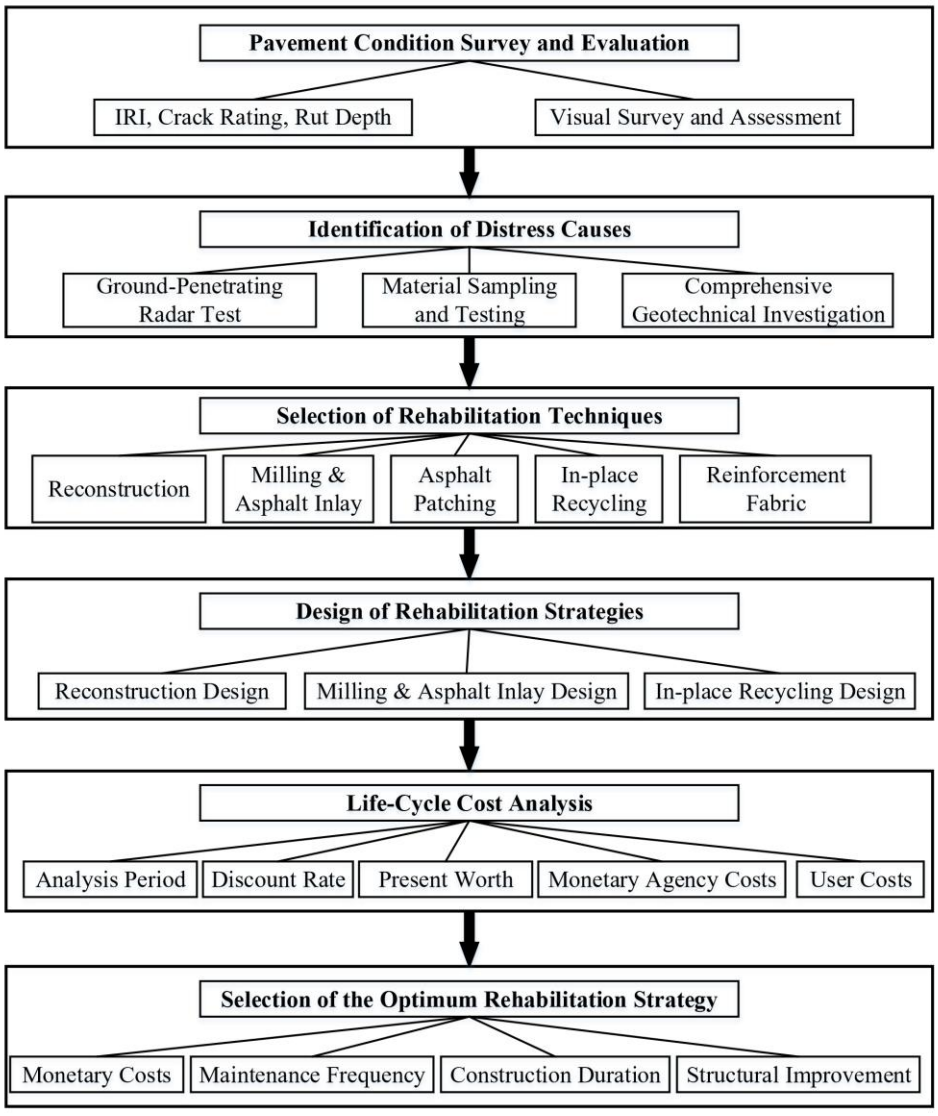


Figure 2-37. Rehabilitation strategy selection procedure for bridge approach/departure asphalt pavements (Lu et al., 2018)

2.3.4.2.5 Missouri

MoDOT (2004) investigates the use of the FWD for detecting voids under bridge approach slabs, highlighting its advantages over traditional proof rolling methods. The FWD's effectiveness in identifying large voids and evaluating support at bridge approach slabs was assessed across 27 bridges in Missouri.

The field evaluation procedure is summarized below:

- Bridge Selection: Selected 27 bridges across Lawrence, Jasper, and MacDonald counties for FWD testing.
- Visual survey: Surveyed the condition of bridge approach slab visually and prepared 'Bridge Approach Slab Condition Sheet' (*e.g.*, see **Figure 2-38**)
- Testing Procedure: Followed 1993 AASHTO pavement design guide protocol; tested three to four slabs on each bridge side.
- Load Levels: Conducted tests at approximately 9,000, 12,000, and 16,000 pounds.
- Data Analysis: Analyzed over 200 joints; plotted load vs. deflection graphs and determined x-axis intercepts to identify undersealing candidates (*e.g.*, see **Figure 2-39**).

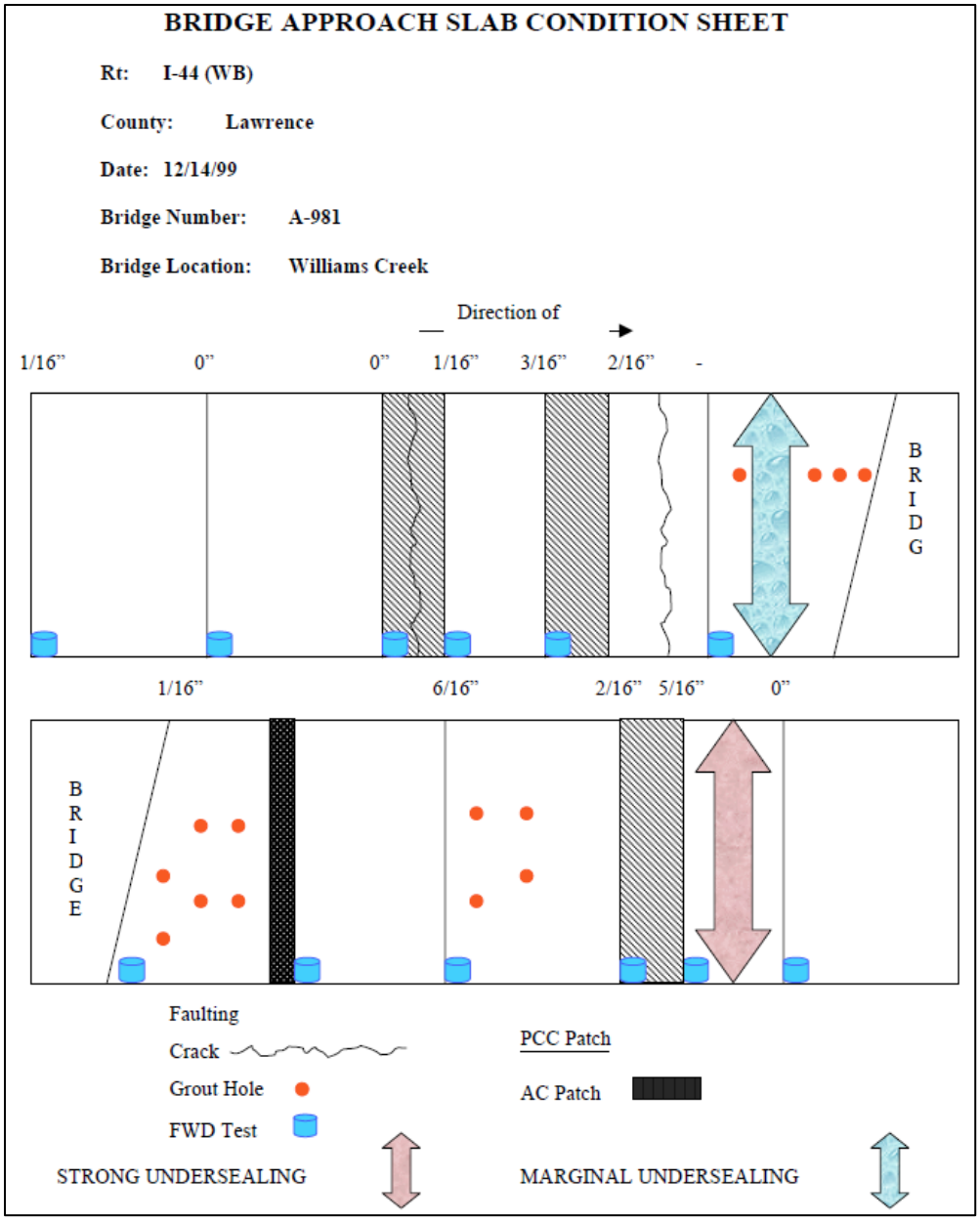


Figure 2-38. An example of Bridge Approach Slab Condition Sheet (MoDOT, 2004)

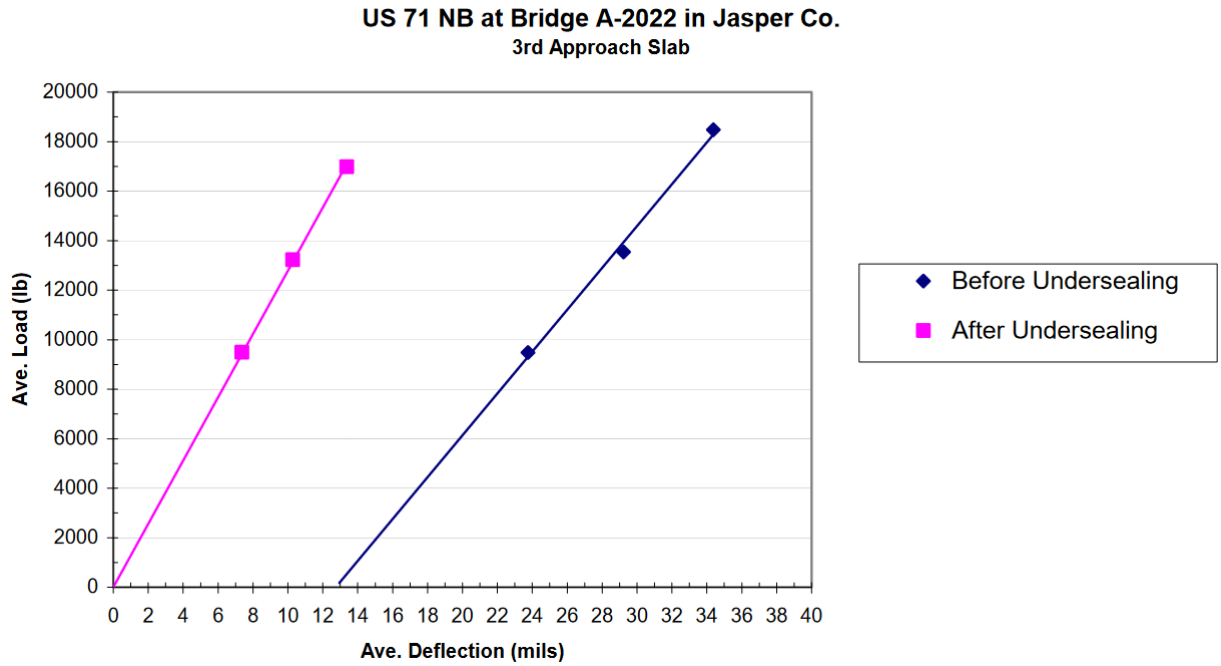


Figure 2-39. Projected x-intercept average deflection (mils) before and after undersealing (MoDOT, 2004)

Table 2-16. Criteria for maintenance (MoDOT 2004)

Maintenance Criteria	**Deflection axis intercept (mils)**
No Undersealing	0 – 3
Marginal Candidates	3 - 7
Strong Candidates	≥ 7

MoDOT used the criteria presented in **Table 2-16** to select joints for undersealing with polyurethane, showcasing FWD's practical application in maintenance decision-making.

2.3.5 Synthesis and Summary

The literature review indicates that no single evaluation method is sufficient to characterize the condition of bridge approach systems in roadway embankment areas. Visual inspection and ride-quality data are useful for identifying surface distress, but they do not directly identify the underlying support condition. Methods such as FWD, GPR, coring, DCP, CPT, and laboratory testing provide complementary information and are most useful when interpreted together. These findings support the need for a staged evaluation framework that connects observed distress to probable distress mechanisms before repair strategies are selected.

2.3.5.1 Typical testing tools used for evaluating in-service roadway embankment

2.3.5.1.1 Nondestructive testing

(a) Falling Weight Deflectometer (FWD)

An FWD is a non-destructive testing device that drops a calibrated weight onto a load plate and measures pavement's surface deformation, simulating a dynamic stress and a pavement deflection caused by a fast-moving truck. FWD testing is widely used among various state DOTs (Alavi et al. 2008). Our literature review reveals that many DOTs, including TxDOT, have reported to have included FWD in their field-testing program for BAS and approach pavements. MoDOT (2004) demonstrated the efficacy of FWD to detect void underneath the bridge approach slab by using the AASHTO 'rapid void detection procedure' (AASHTO, 1993). The widespread use of FWDs among state highway agencies, as well as their non-destructive nature, underscores their popularity and efficacy in evaluating in-service bridge approach pavements while minimizing traffic interruptions.

In practice, FWD tests are conducted at specific locations across a bridge approach to collect data on the pavement's response to loading. Tests are often repeated at several locations with intervals or numbers of drops determined by the specific goals of the assessment. In the assessment of bridge approach slabs, the FWD testing follows a structured protocol. Initially, comprehensive documentation from prior assessments is reviewed. The FWD tests are then systematically conducted at predetermined points along the bridge approach slabs, including the outer wheel path and centerline, with particular focus on areas near bridge abutments or joints. Immediate post-construction testing followed by regular evaluations over a certain period to track the evolution of the pavement's condition, especially when the approach slab is rehabilitated. Typically, a uniformly distributed tests per section is performed, spaced at 10- to 16-ft intervals to create a detailed deflection profile of the approach slab. Generally, a standard drop weight of 9000 lb is used, applied through a 1-ft diameter loading plate, to simulate the stress exerted by vehicular traffic. Key measurements such as peak deflection and the deflection basin shape are recorded at multiple points from the load center to capture the pavement's response. Analysis involves back-calculating subgrade moduli and other deflection parameters, providing insights into the structural integrity and pinpointing any distress. Any anomalies or surface distresses encountered during testing are carefully documented, noting their potential impact on the FWD data. This meticulous approach ensures a thorough understanding of the pavement's performance and the effectiveness of maintenance treatments.

Table 2-17 summarizes studies that have utilized FWD to assess the conditions of the BAS and nearby pavement in roadway embankments.

Table 2-17. Studies that have utilized FWD to assess the conditions of the BAS and nearby pavement in roadway embankments

Reference	Test Locations	Test Frequency	Interval/number	Analysis parameters
Meles et al. (2016)	Outer wheel path and center line of the road	Immediately after construction then monthly for 4 next months	5 m intervals; six test points per section	Backcalculated Subgrade Moduli, Deflection basin parameters
Chen and Yi (2015)	IH 35 AT HILLSBORO; Approach slabs of the right and middle lanes in the northbound direction; Test points uniformly distributed all over Departure slab	Before and after the polyurethanefoam injection treatment	48 per section uniformly distributed	
	US HIGHWAY 385 OVER US 87, AMARILLO; The northbound approach slab; Test points uniformly distributed all over Departure slab	Before and after the polyurethanefoam injection treatment	40 per section uniformly distributed	
Phares et al. (2011)	Conducted on both approaches, or departure slabs, in some cases, for each bridge; down the center line of the driving lane	-	5-ft and 25-ft spacing for approach slab and pavement respectively, along center line of lane; and before and after the joints.	

Reference	Test Locations	Test Frequency	Interval/number	Analysis parameters
Bakeer et al. (2005)	Approach slab and departure slab	-	Approach side of BAS joint, then at 2-4 m spacing, tested upto 10 m away from approach-pavement joint.	
MODOT et al. (2004)	Approach slab and departure slab	-	Corner loading for each joint, discontinuities	
Das et al. (1999)	Approach slab and departure slab	-	Approach side of BAS joint, then at 2-4 m spacing, tested upto 10 m away from approach-pavement joint.	

(b) Ground Penetrating Radar (GPR)

A GPR is a non-intrusive geophysical device that uses radar pulses to image the subsurface and widely used for assessing the condition of bridge approach slabs by identifying the depth of concrete slab, presence of voids, and any anomalies in the ground. A study by Puppala et al. (2011) verified that the GPR can be used to identify voids based on the GPR depth estimations that were generally consistent with the ground-truth data obtained from the cores. The use of GPR in the assessment of bridge approach slabs and roadway embankments is well-documented and widely recognized by various DOTs, including TxDOT, as a valuable and effective non-destructive testing method (Azari 2016; Luna et al. 2004; Puppala et al., 2011; ElBatanouny et al. 2018).

GPR testing protocols in the evaluation of bridge approach slabs involve positioning the GPR equipment to scan various extents of pavement, ranging from directly on the slab to several feet away from bridge abutments. Line spacing during scans can vary from 2 to 4 feet, ensuring comprehensive coverage, while data point spacing recommendations range from 1.9 inches to 6 feet for optimal resolution. Antenna frequencies used in these assessments typically span from 200 MHz for deeper penetration to 2.6 GHz for higher resolution imaging, aiding in the identification of subsurface voids and anomalies. The interpretation of GPR data facilitates the determination of pavement thickness, void detection, and the location of subsurface interfaces. Puppala et al. (2011) suggests the use of multi-frequency antennas to capture a broader range of subsurface detail.

A summary of details of GPR testing conducted for evaluations of bridge approach and nearby pavement from various studies is given in **Table 2-18**.

Table 2-18. A summary of GPR testing procedure from various studies conducted for evaluations of bridge approach and nearby pavement

Source	Location/extent	Line Spacing	Data Point Spacing	Antenna Frequency	Interpretation	Remarks/Additional info
Lu et al. (2018)	Approach/Departure slab + pavement within 200 ft away from BAS	-	100-5.28ft (6 ft recommended)		Used to calculate average asphalt thickness in BAS	GPR data set is available from the FDOT SMO.
ElBatanouny et al. (2018)	Several unreinforced pavement panels and the reinforced approach slab panels adjacent to the bridge, shoulders within the concrete areas included in the approach system	2-4 ft	2 ft	2.6 GHz	Identifying Void	-
Miller et al. (2013)	BAS and approach pavement 10-15 ft past end of BAS	15 ft (50 cm)	1.9" to 4.7"	1-1.6 GHz, 400 MHz, and 200 MHz	Void Detection	A higher frequency antenna (1-1.6GHz) is recommended for better resolution and characterization of the voids
Puppala et al. (2011)	along the center of the shoulder and main lanes in both directions; 800 ft - 1600 ft past end of the bridge; one high frequency antenna per	4 ft	-	1.6 GHz, 400 MHz, and 200 MHz	Interface location; void detection; suspected void area calculation	The three antennas were used to cover different penetration depths, identify precisely pavement interfaces, and also detect the presence of

Source	Location/extent	Line Spacing	Data Point Spacing	Antenna Frequency	Interpretation	Remarks/Additional info
	four embankment slope (total 4)					utilities or anomalies at different depths.
Chen and Scullion (2007)	1 line per lane	-	-	1 GHz	Anomalies detection; Void detection;	The noncontact GPR unit is normally operated at highway speeds (60 mph), transmits 50 pulses/ s, and can effectively penetrate to a depth of 2 - 2.5 ft.
Ha et al. (2002)	1 in outer lane of approach slab + pavement upto 10 ft away from end of BAS	-	-	-	Void Detection; continuity of natural subsurface conditions and features	-

(c) Surface profile measurement

There are various methods to determine the vertical profile of the bridge approaches. The severity of bumps is evaluated by using different roughness measurements such as IRI, localized roughness, Bridge Approach Performance Index (BI), rolling edge, etc. There are several methods commonly used by state DOTs and researchers to determine the IRI, BI, or any other roughness or smoothness index. Some of the most common methods are given below.

- *Profilometers*
    - Profilometers are the most common type of device used to measure pavement roughness. They typically consist of a series of wheels or sensors that measure the elevation of the pavement surface at regular intervals. The data collected from the profilometer is then used to calculate the IRI or other roughness/smoothness indices.
    - Profilometers can be classified as either contact or non-contact profilometers. Contact profilometers use wheels or sensors that come into direct contact with the pavement surface. Non-contact profilometers use lasers or other sensors to measure the elevation of the pavement surface.
- *Inertial profilers*
    - Inertial profilers are a newer type of device used to measure pavement roughness. They use accelerometers and gyroscopes to measure the vertical motion of the vehicle while it is traveling over the pavement. The data collected from the inertial profiler is then used to calculate the IRI or other roughness/smoothness indices.
    - Inertial profilers have a number of advantages over traditional profilometers. They are faster, more efficient, and can operate at higher speeds. The inertial profiler data are analyzed commonly by using a software for calibrating inertial profilers and analyzing profile data (Henderson 2016).
- *Laser scanners/LiDAR*
    - Laser scanners can be used to create a 3D model of the pavement surface. This 3D model can then be used to calculate the IRI or other roughness/smoothness indices. Laser scanners are typically used to measure pavement roughness on large areas, such as highways and runways. They are also used to measure the roughness of pavements that are difficult to access with traditional profilometers.
- *Total Station*
    - A total station is an electronic surveying instrument that combines the functions of a theodolite, electronic distance meter (EDM), and on-board computer. It is used to measure horizontal and vertical angles, as well as distances, with high precision.

Total stations are widely used in surveying, construction, and mining. ElBatanouny et al. (2018) used a robotic total station to gather elevation survey data for approach slabs. Surface elevations of bridge approaches were surveyed along three longitudinal lines in each lane, with only approach lane surveyed at each end. The elevation measurements were referenced to the bridge joint, and the depression of the slab was calculated by assuming a linear profile from the bridge joint's elevation to the roadway-end of the approach slab.

- *String line method:*

    - Chen and Yi (2015) used string lines for measuring settlement in the pavement. This technique provided a cost-effective and quick method for assessing vertical settlement in bridge approach slabs especially when the traffic control is a big concern.

Some of the recent studies adopting various tools for determining the surface profile of bridge approach or pavement are summarized in **Table 2-19**.

Table 2-19. A summary of surface profile measurements

Reference	Method used	Measurement	Interval	Interpretation	Remarks
Wang et al. (2023)	Sub-mm 3D laser imaging	Profile Data; sub-mm 2D/3D images, right-of-way images	-	Roughness (IRI) and Surface Distress	Data collected by using Pave3D 8K system equipped in a high speed (60mi/hr) van.
Mishra et al. (2021)	Inertial Profiler	Profile Data	24.9 mm	Roughness (IRI, RSE)	
Lu et al. (2018)	FDOT SMO Pavement Condition Unit	Profile Data and rut depth	5.3 ft	Roughness (IRI) and Surface Distress (RD)	
Henderson et al. (2016)	FHWA LTPP Profiler	Profile Data	0.012in (0.5 mm)	Roughness (IRI, RSE)	
Chen et al. (2016); Abu-Farsakh et al. (2014)	Inertial Profiler	Profile Data	-	Roughness (IRI)	Three repeated profile testing runs performed for reliability
Chen and Yi (2015)	High-speed laser profiler	Profile data	-	Roughness (IRI, deviation plot)	
	String line	Settlement Measurement	10 ft	Settlement	

(d) Visual inspections and historical information review

Visual inspection is the most common and cost-effective method for evaluating the surface of bridge approach slabs and highway embankments, enabling the identification of visible distress indicators such as cracking, faulting, and differential movement. Jayawickrama et al. (2005) notes that, in Texas, the state of practice for repair strategies is different from District to District, and these repairs are typically based on visual surveys and IRI values.

In a notable extension of visual inspection techniques, Lu et al. (2018) employed Florida Department of Transportation (FDOT) video log images to assess surface distress conditions in asphalt pavements of bridge approach and departure areas. While visual inspection serves as a valuable initial screening tool, additional investigation may become necessary when observable signs of distress, such as cracking, patching, and raveling, are detected.

Furthermore, advances in the examination of subsurface drainage systems, particularly edge drains, have introduced the use of small-diameter optical tube video cameras, substantially enhancing the assessment and maintenance of drainage systems. The innovative use of video inspection methods in Iowa during the early 1990s laid the foundation for more effective evaluation of drainage systems (Jayawickrama et al. 2005). ElBatanouny et al. (2018) employed a borescope, or snake camera, to visually inspect access ports for signs of backfill settlement and to investigate voiding beneath slabs, verifying findings from GPR testing and core samples.

When conducting a visual inspection of a bridge approach slab and highway embankment, it is often looked at following signs of distress (Phares et al. 2011):

- Distresses in the pavement
- Faulting of the pavement
- Differential movement between the pavement and the abutment
- Erosion of the embankment fill materials
- Seepage of water
- Presence of vegetation in joints and embankment faces
- Presence of voids
- Faulting of joints
- Deterioration of joints

Phares et. al. (2011) highlights the significance of visual inspection as an effective method for assessing and addressing problems related to bumps on bridges. The study suggests that after identifying discomfort issues caused by a bridge, a visual investigation should be undertaken to understand the underlying causes and determine appropriate remedies. Phares et. al. (2011) further stated that visual inspection can be an effective method of evaluating bridge bumps, especially when used in conjunction with other methods, such as nondestructive testing.

2.3.5.1.2 Destructive testing

(a) Cone Penetration Test (CPT)

A Cone Penetration Test (CPT) is an in-situ testing method used to determine the geotechnical engineering properties of soils and delineate soil stratigraphy. The test involves pushing an instrumented cone into the ground at a controlled rate, typically at 20 mm/s, and recording the resistance experienced by the cone tip and shaft, including penetration resistance and sleeve friction.

The mechanism of CPT involves the following steps:

- A cone penetrometer is pushed vertically into the ground at a controlled rate.
- The instrumented cone measures penetration resistance at the tip and friction in the shaft during penetration.
- Data are recorded at regular intervals during penetration to delineate soil stratigraphy and determine geotechnical properties such as soil type, density, and strength.

Ha et al. (2002) investigated settlement at bridge approach slab expansion joint, conducted in cooperation with TxDOT, utilized the CPT to assess the soil conditions near the abutment and embankment fill, highlighting the importance of subsurface evaluation for maintaining the integrity of bridge approach slabs. While specific official guides on CPT for evaluating in-service highway embankment conditions were not found, the widespread use of CPT in research and field investigations (Abu-Farsakh, 2014; Chen, 2016; Miller, 2013; Bakeer, 2005; Luna, 2004; Das, 1999) conducted in cooperation with various state DOTs underscores its prevalence and importance in assessing the subsurface conditions of highway embankments.

For an assessment of the condition of highway embankments and bridge approach slabs, the depth of penetration typically ranged from 30 to 80 ft. However, the choice of penetration depth was not discussed in the literature. The frequency of testing varies, but commonly one or more per embankment is generally conducted to ensure comprehensive soil profiling. Critical measurements taken during CPT include cone resistance, sleeve resistance, pore pressure, and friction ratio. TxDOT's application of CPT in the study by Ha et al. (2002) involved conducting two tests per embankment or approach slab, providing data on tip resistance, local friction, and pore pressure, which are essential for assessing strength of soils and predicting settlements. The data derived from CPT feeds into computational models for settlement prediction, as observed in the case of Luna et al. (2004), where CPT data, complemented by seismic velocity measurements were used in informed PLAXIS-based settlement predictions. A summary of CPT tests conducted to evaluate the conditions of roadway embankments is given in **Table 2-20**.

Table 2-20. A summary of CPTs conducted to evaluate the conditions of roadway embankments

References	Location	Frequency/number	Depth of penetration	Interpretation	Notes
Abu-Farsakh and Chen (2014)	on roadway embankment	1 per embankment	98 - 115 ft (30 - 35 m)	Settlement calculation of bridge embankments	Zhang and Tumay CPT classification method (1999) used to profile subsurface soils.
Miller et al. (2013)	on roadway embankment and off roadway embankment	3-4 per embankment on average	30 - 60 ft (9 - 18 m)	Predicts total settlements, shear strengths	Erosion and soil consolidation issues identified.
Luna et al (2004)	Off roadway	1 per embankment	14.5 – 65 ft (4.5 - 20 m)	Settlement prediction in PLAXIS	Uses CPT, SPT, and Shelby Tube data for settlement prediction
Ha et al. (2002); Seo et al. (2003);	Outer lane of Approach slab and Embankment pavement	2 per embankment/approach	20 - 35 ft (6 – 11 m)	Assesses bearing capacity and settlement	Evaluates soil engineering parameters
Das et al. (1999)	Median	1 per embankment	80 ft (24 m)	Settlement and soil classification	-

(b) Dynamic Cone Penetrometer (DCP)

A DCP test provides a measure of a material's resistance to penetration. The DCP test is performed by driving a 20-mm-diameter metal cone into the soil by hammering it with an 8-kg weight dropped from a height of 575 mm. The DCP test has been widely used to determine the California bearing ratio (CBR) or modulus of the subgrade due to its rapid setup and simplicity. Results from the DCP tests can be used not only for the quality assessment of newly prepared subgrade but also for in-service roadways when adopting maintenance strategies. For example, if the results of DCP tests performed for in-service roadways indicate the high quality of the subgrade, maintenance measures can include simply treating the surface pavement layer. However, if the DCP investigations show the poor quality of the subgrade, then extensive stabilization measures or the replacement of the subgrade may be needed.

One of the limitations of the DCP is that the maximum investigation depths of DCP tests are typically limited to about 10 ft due to the bending of the driving shaft. This depth is not sufficiently deep to assess the conditions of backfill materials for the entire height of the roadway embankments. Nonetheless, DCPs are commonly used for assessment of conditions of backfill soils in the bridge approach area, sometimes to check if voids exist or not, as summarized in **Table 2-21**.

Table 2-21. A summary of DCP tests conducted to evaluate the conditions of roadway embankments

Reference	Location	Numbers/ Frequency	Penetration depth	Interpretation	Notes
Puppala et al. (2011)	Approach slab and roadway pavement on top of embankment	5 per approach	2.5 - 5 ft (30-60 in)	Soil Modulus	-
Chen and Scullion (2007)	Approach slab and roadway pavement on top of embankment	Eight DCP tests conducted at two trenches and six additional DCP tests	3.3 ft (40 in)	Pavement Layer Moduli	The DCP is often used in conjunction with the FWD to determine the layer thicknesses, to estimate layer stiffness, and to validate the presence of weak layers.

(c) Standard Penetration Test (SPT) and Soil Sampling

An SPT is widely used in-situ testing tools to characterize subsurface conditions. Because soil samples can be collected using the split-spoon sampler during the testing, SPTs have been used to assess backfill conditions in roadway embankment area and to collect soil samples. Miller et al. (2013) conducted SPT on the embankment soil, and, similarly, Jayawickrama et al. (2005) performed SPT in the bridge approach area.

To collect higher quality soil samples, Shelby tube sampler can be used instead of a split-spoon sampler after drilling a borehole. Miller et al. (2013) drilled embankments boreholes near the abutment, while off-the-embankment boreholes were located as close to the embankment as possible. The standard Shelby tube method was used to obtain nominal 3-inch diameter thin-walled tube samples for cohesive soil layers.

(d) Laboratory tests

Laboratory testing is essential for evaluating in-service highway embankment conditions, offering insights into soil behavior and parameters required for settlement estimations. Miller et al. (2013) implemented Atterberg limits, grain-size distribution, and oedometer tests on cohesive soils in their Level-II investigation plan. For embankments over 20 feet high, double oedometer tests on cohesive fill materials were conducted (Miller et al., 2013). Puppala et al. (2011) carried out an extensive suite of laboratory tests following TxDOT and ASTM standards on embankment fill materials. These tests included particle size analysis, Atterberg limit test, and one-dimensional consolidation test, among others.

Most common tests for the evaluation of condition of highway embankment are:

- Moisture content
- Atterberg limits
- Particle size analysis
- 1-D consolidation tests

(e) Pavement coring

After performing FWD or GPR, coring through pavement structure is often performed at locations where poor slab performance is observed and at control location. The purposes of coring are to assess the quality of concrete material and to verify the existence of any voids and pavement structure configurations. Furthermore, the cored hole serves as an access hole for CPT or DCP tests. Our literature review suggests that coring of pavement structures is routinely performed for evaluations of conditions of BASs and nearby pavement structures.

2.4 Review of repair and soil improvement methods

2.4.1 Classification of soil improvement methods

Soil improvement, sometimes referred to as ground improvement, is often a necessary measure that needs to be undertaken for a project. Depending on the needs of the project, soil can either be utilized as is, substituted, or enhanced (Medina-Martinez et al., 2023). Ground improvement encompasses both the substitution and enhancement categories and has the overall goal of improving or enhancing certain engineering properties of soil, such as shear strength, compressibility, permeability, and shrink/swell potential (Nicholson, 2014).

While a general literature review was done on all types of ground improvement methods, it was determined that to better fit the needs of this research project, the focus should be on methods that would work best post-construction. Although there are many methods of ground improvement, this section aims to provide an overview of the current practices most relevant to the repair of in-service highway embankments.

From the literature review, it was found there is no one universal way to categorize soil improvements. For the purposes of this report, we have adopted the three methods of soil improvements presented by Verma et al. (2021): (a) mechanical, (b) chemical, and (c) biological. From these categories, various subcategories can be identified including, physiochemical, biochemical, geosynthetics, and hydraulics (Nicholson, 2014; Roshan et al., 2022; Verma et al., 2021; Zada et al., 2023).

The mechanical category includes techniques such as densification, compaction, and consolidation (Nicholson, 2014). These methods are the most common and involve physically altering the soil using loading (Verma et al., 2021). Chemical soil improvement techniques change the chemical composition of the soil and involves the addition of admixtures and grouts to the soil (Verma et al., 2021). Polyacrylamide and polyurethane have been identified as two chemical stabilizers that are applicable in the repair of highway pavements and slopes and the sealing of cracks, but more commonly used chemical admixtures/stabilizers are cement and lime (Verma et al., 2021). The biological category includes biochemical reactions via microbially induced calcite precipitation, the introduction of microorganisms to the soil, and live plants being utilized as structural element (Umar et al., 2016; Verma et al., 2021). Broadly, the advantages of mechanical stabilization over chemical are that it is simpler, cheaper, and better for the environment; however mechanical methods alone are often insufficient for sites with expansive soils (Zada et al., 2023). Some organizations such as the International Society for Soil Mechanics and Geotechnical Engineering (ISSMGE) use a more complex categorization method based on whether the soil is cohesive and whether admixtures were used (Roshan et al., 2022).

Most of these ground improvement methods must be done before or during construction. For the repair of roadway embankments, the most useful solution might be a ground improvement method that can be done post-construction. Methods such as mud-jacking, grouting, and injection are the most common solutions. It has been argued that when working on a completed project, “grouting methods may be one of the only feasible solutions” (Nicholson, 2014).

2.4.2 Common methods used to repair roadway embankment/BAS

As of 2011, the current state of practice for bridge approach settlement mitigation/repair in Texas, as reported by TxDOT districts, includes HMA overlays, slab replacement, mud/slab jacking, grouting, and urethane foam injection (Puppala et al., 2011). These methods have also been identified as the repair techniques for bridge approach slabs in other states, including ODOT and Iowa DOT's bridge maintenance manuals, as well as by the US Federal Highway Administration (Al-Eis & LaBarca, 2007; FHWA, 2015; Iowa DOT, 2016; ODOT, 2023). These manuals also identify the cutting of pressure relief joints as a common maintenance measure, although this is usually in response to the age of the slab, temperature changes, or daily traffic, and not to underlying soil issues (FHWA, 2015). Additionally, although not exclusive to bridge approach slabs, a survey of 25 US state DOTs' concrete pavement slab leveling methods further validates these techniques as being the current state of practice (Onyango et al., 2018). As can be seen in the **Figure 2-40**, the top methods include mud-jacking, HMA overlay, polyurethane, and slab replacement.

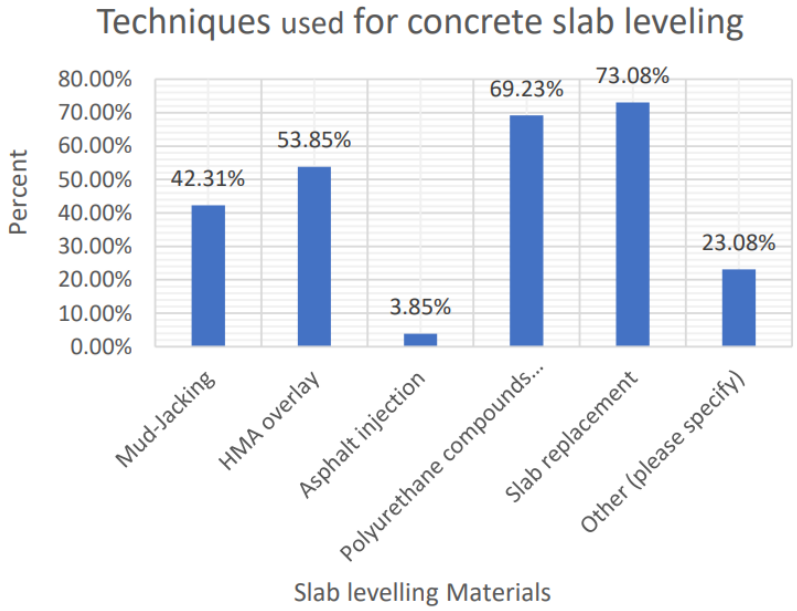


Figure 2-40. Techniques used for concrete slab leveling (Onyango et al. 2018)

2.4.2.1 HMA Overlay

2.4.2.1.1 Definitions of method/technique

A hot-mix asphalt (HMA) overlay is a very common method to address the difference in elevation between the approach slab and bridge, but it does not treat the cause of slab settlement (Jayawickrama et al. 2005). This technique entails placing an overlay of asphalt on top of the existing slab. An HMA overlay improves ride quality, but since it does not address the cause of the problem, it is often done in combination with a method that does address the source of settlement such as grouting or injection. When an overlay is used for the improvement of ride

quality, it is usually a non-structural overlay (Stevenson 2021a). If this method is done alone, or with another technique, the expectation is that the overlay will likely need to be done many times or until the settlement is finished (Jayawickrama et al. 2005). It is possible that the additional weight of the overlay will increase the settlement, and this is why an HMA overlay is not often recommended if there are voids under the BAS (FHWA 2015; Ghorbanpoor et al. 2007). Even so, depending on the project, repeatedly doing HMA overlays could still be the most cost effective solution (Jayawickrama et al. 2005).

Many US states have experience with these asphalt overlays and have their own mix designs in their specifications (FHWA 2015). The reason that HMA overlays are so common is because they are cheap, quick, and inexpensive (FHWA 2015). Since this method is generally regarded as either a temporary fix, finishing technique, or is done in conjunction with another repair method, HMA overlay project specific case studies were not included for this section.

FHWA (2015) identifies the typical thickness of HMA as 1.5 – 6 inches, depending on the differential settlement. There are three main types of thin HMA overlays that can be useful for maintenance: dense graded, gap graded, and open graded (Wilson et al. 2015) .

2.4.2.1.2 Summary of performance

HMA overlays improve ride quality but do not address the causes of slab settlement. They can perform well in the short term, but since they do not treat the causes of typical BAS problems (namely settlement), this method must often be done repeatedly and in combination with a method that does address the root causes of settlement. Even though its performance in the long term is not good, many US states do this as a temporary differential elevation remediation, since it is a quick and relatively inexpensive solution.

2.4.2.2 Full/Partial depth repair or Replacement

2.4.2.2.1 Definitions of method/technique

Full depth slab repair/replacements are also a common method of repair, although this technique is often the most expensive method and can take the longest amount of time to complete as compared with other methods (Al-Eis & LaBarca, 2007). The expected benefits of full depth repair include improved ride quality and improved structural integrity (Chen & Won, 2008). This technique involves removing some or all of an approach slab, and can be done with full depth patching, a concrete pour, or precast panel (Jayawickrama et al., 2005). One of the reasons a full depth repair (FDR) is done is to fix slabs that have support problems caused by settlement or base failure. The overall goal is to only repair the areas that are damaged and leave the undamaged sections of slab alone. The damaged concrete in FDR can be removed either by lifting out the damaged section or by breaking up the damaged slab in place (Jayawickrama et al., 2005). Lifting is usually the preferred method as it does not damage the subbase, and is less likely to damage the surrounding concrete (Jayawickrama et al., 2005). If needed, the base or subbase can be recompacted after the concrete is removed.

While other repair methods are usually rated more cost effective, replacement can become the more cost-effective strategy if the slab has severe damages (Onyango et al., 2018). Severe damages can be described as the BAS being faulted, broken, or settled so much that slab jacking cannot fix the slab (Ghorbanpoor et al., 2007). Some US states perform FDR automatically if a certain percentage of the slab is found to be distressed (Krauss et al., 2009). **Table 2-22** below summarizes some of these criteria.

Table 2-22. Automatic FDR criteria (Krauss et al., 2009)

State	FDR Criteria
California	> 20% of deck area has subsurface distress
Virgina	> 25% of deck is spalling or delaminating
Illinois	> 35% of deck needs patching
Connecticut, Massachusetts, Kansas	> 50% of deck in poor condition

In Texas, there has been some variability with the success of FDR, with "a substantial portion" having continued distress and needing more repairs (Ryu et al., 2012). Also, it is not uncommon for the surrounding slabs to the repaired section to undergo new distresses (Chen et al., 2009). A successful implementation of a FDR should last between 10 and 20 years (Darter, 2017).

The most important factors for good performance in FDRs are the base support, the structural reinforcement, and the load transfer between slabs (Darter, 2017). The correct anchoring of dowel bars is necessary for sufficient load transfer efficiency between slabs. This is why FDR is often done in combination with a method designed to improve the pavement, such as dowel bar retrofitting (DBR) or cross-stitching (Darter, 2017). Descriptions of these techniques are discussed in a later section.

Partial depth repair (PDR) is different from full depth in that it involves removing only the top third to half of the slab, and it can be done much faster and more inexpensively (Chen et al., 2011). Much like HMA overlay, PDR is also not going to fix any issues underneath the slab, but it can improve ride quality. PDR performance appears to be extremely variable, and when done correctly it is expected to have a life of 10 – 15 years (Darter, 2017). However, if anything is done incorrectly it can last less than 5 years (Darter, 2017).

If the entire approach is extremely damaged, the reconstruction method can be utilized where the approach slab is fully or partially replaced with a new slab (Jayawickrama et al., 2005). Although costly, this can be a good alternative since the "root causes" of why the bridge approach slab fail can be directly addressed (Jayawickrama et al., 2005). The reconstruction may involve soil improvement, such as soil replacement with better embankment materials, compaction, or consolidation (Roshan et al., 2022). Additionally, better subsurface drainage system could be implemented during the reconstruction (Jayawickrama et al., 2005).

2.4.2.2.2 State DOT specifications

For Texas, full depth replacement with an in-situ pour entails cutting through the full depth of the slab at the repair boundaries, drilling 12 inches into the surrounding slabs and epoxy grouting the

tie bars in place, and then adding the transverse and longitudinal steel before finishing with new concrete (Ryu et al., 2012). Other US states have slightly different methods, and some example specifications are listed in **Table 2-23** and **Table 2-24.**

Table 2-23. State DOTs' specifications about FDR (Darter, 2017)

State	Specification
California	Section 41-9: Individual Slab Replacement, ISR (2015) Concrete Pavement Guide
Georgia	GA 452, 504, 609
Minnesota	MnDOT 2302 SP
Missouri	MoDOT Standard Specification 613.10. MoDOT Standard Drawing 613 (Sheet #1)
Utah	UDOT: PCC 3055 Precast: SP 02757S, PB4, 2753
Washington	Standard Plan A-60.10-03. WSDOT 5-01 Cement Concrete Pavement Rehab.

Table 2-24. PDR State DOTs' specifications on PDR (Darter, 2017)

State	Specification/Documents
Minnesota	MnDOT 2302 Special Provision MnDOT 2302 Special Provision and 3105
California	Section 41-1: Spall Repair (Polyester Concrete) Section 41-4: Spall repair (fast-setting concrete for pre-overlay repair, anticipated life <5 years) California "Concrete Pavement Guide"
Georgia	GA 451, 435
Missouri	MoDOT 613.20. Standard Drawing 613 (Sheet #2)
Washington	WSDOT 5-01 Cement Concrete Pavement Rehabilitation
Utah	UDOT 2751 Partial Depth (cementitious material). UDOT 2751S Partial Depth (Hot Applied Proprietary Flexible Material).

2.4.2.2.3 Project-specific case studies

Fewer case studies on full and partial depth repairs, specifically on bridge approach slabs or embankments, were found during the literature review versus other methods. For this reason, the project specific case studies shared below mostly involve non-embankment highways and frontage roads. The reviewed reports and their results are presented from oldest to most recent.

(a) Case studies on FDR

In 2008, a study examined the performance of polyurethane foam injection, dowel bar retrofit (DBR), and full depth repair (FDR), on 6 Texas highways that had issues relating to settlement, poor base support, poor load transfer between slabs, slab pumping, and degradation of steel

reinforcement (Chen & Won, 2008). The relevant polyurethane foam injection and dowel bar retro fit portions of this study will be reviewed in later sections.

Several sections of pavement on SH73 were repaired in the early 1990's, and four experimental sections were repaired using FDR and/or a dowel bar retrofit (Chen & Won, 2008). Ten years later, the sections that did not undergo these repairs demonstrated significant reflective cracking; whereas the experimental sections demonstrated only minor cracking. It was also noted that joints with the dowel bar retrofit deflected significantly less than joints that did not have this repair.

A section of SH342 was experiencing longitudinal cracking in, or adjacent to, FDR repairs (Chen & Won, 2008). It was found that the base and subgrade support was insufficient, and this condition contributed to some slab settling. It was noted that FDR should result in a very robust repair; since the full depth of the slab is replaced and the subgrade and base can be optimized. However, depending on the size of the FDR area, it can be difficult to properly prepare the base because the area is so confined. Also, subgrade and base conditions adjacent to the FDR may be substandard, and this can affect the quality and life of the replacement section.

In a case study in Wichita Falls, TX and Amarillo, TX, it was found that an important factor in an effective FDR is being able to restore the "continuity of reinforcement at repair joints". In these two locations the tie bars were grouted with epoxy and yet both locations had poor performance (Ryu et al., 2013).

(b) Case studies on PDR

Chen et al. (2011) reviewed case studies for three Texas locations on the use of PDR on JCP and CRCP. These test sections were monitored for 10 years, and it was found that PDR was successful in improving IRI or keeping it the same as it was before the repair. PDR was also found to be successful in keeping the test sections' distress scores from decreasing significantly (a lower distress score indicating a section was worsening). Overall, PDR was considered to be an effective method and more cost effective than FDR when pavement distresses were not too deep into the concrete.

A case study on the effectiveness of PDR was conducted in Wisconsin in 2012 (Battaglia et al., 2012). Three test sections repairing joints and cracks were evaluated over a 12-year period. Spalling and deterioration were observed in the test sections, and one section had to be reconstructed before the monitoring period was over. It was noted that in Wisconsin, about 50% of PDR projects have undergone distress. As a result of this case study, one district in Wisconsin stopped the use of PDR and has replaced it with the HMA overlay technique.

2.4.2.2.4 Summary on performance

A survey of TxDOT districts found that, for bridge approach settlement, slab replacement was perceived as being a well-designed method, but ineffective (Puppala et al., 2011). In Texas, there has been some variability with the success of FDR, with "a substantial portion" having continued distress and needing more repairs (Ryu et al., 2012). It seems that for FDR to be a viable solution,

the subgrade and base must be in good condition not only in the area of damage, but also under adjacent pavement slabs (Chen & Won, 2008). If this is not addressed, it can lead to a poor performance of the FDR process and surrounding slabs can undergo distresses (Chen et al., 2009).

FDRs seem to have increased chances of success when paired with another method such as a dowel bar retrofit. Full depth slab repair/replacements are a common method of repair for bridge approach slabs, although this technique is often the most expensive method and can take the longest amount of time to complete as compared with other methods (Al-Eis & LaBarca, 2007). While other repair methods are usually rated more cost effective, if the slab has severe damage, FDR can become the more cost-effective strategy (Onyango et al., 2018). Benefits include improved ride quality and improved structural integrity (Chen & Won, 2008).

Texas seems to have good experience with PDR; whereas other states have found varying levels of success with PDR. If done correctly, PDR can last 10-15 years. However, it does not address underlying slab problems.

2.4.2.3 Slab stabilization and slab jacking

Slab jacking involves the raising of a settled slab and can be accomplished by implementing grouting or expanding foam injection beneath the slab. It can be used to solve leveling issues, pumping at joints, increase ride quality, fill voids, and help prevent additional settlement (Jayawickrama et al., 2005; Puppala et al., 2011). This method was traditionally done with a mud grout but is now much more commonly done with either cementitious grout or an injected polyurethane foam.

Slab stabilization (also called undersealing) differs from slab jacking in that it is not intended to raise the slab, but rather only to reduce future settlement and provide uniform support for the slab. This is most commonly done with a cement-based grout, but it can also be done with polyurethane injection (Jayawickrama et al., 2005; Vennapusa et al., 2016).**Table 2-25** summarizes the repair methods discussed thus far.

Table 2-25. Treatment types and applicability (Fortunatus, 2018)

Treatment	Description	Applicability
Slab stabilization	Involves injection of flowable materials underneath a concrete slab through drilled holes to fill the voids	Sections likely to face loss of support, for example, areas showing early sign of pumping or mid-slab cracking
Slab Jacking	Lifting a settled slab to its original profile by injection of cement grouts or expansive polyurethane materials through drilled holes	Localized areas with depression or settlements
Partial-depth repair	Removal of small, shallow-top deteriorated areas (1/3 to 1/2) of concrete slab and replace with cementitious or polymeric material	Low to moderate spalled and cracked areas, localized areas with scaling and joint defects
Full depth repair	Total replacement of deteriorated concrete slab by casting in place a new slab or installing a pre-casted one	Slabs with distresses such as longitudinal cracking, transverse cracking, joint spalling, blowups, punch outs, corner breaks etc.

2.4.2.4 Grouting

2.4.2.4.1 Definitions of method/technique

Grouting is defined as, "the injection of a flowable materials into the ground (usually) under pressure" (Nicholson, 2014). Cementitious grouting is one of the most common materials used in slab jacking and slab stabilization (Vennapusa et al., 2016). Many states use cementitious grouting as a ground improvement method for roads, and it is most commonly used to fix problems with a project after construction (Nicholson, 2014). **Figure 2-41** highlights some of the applications of grouting, which includes the repair of bridge approach slabs.

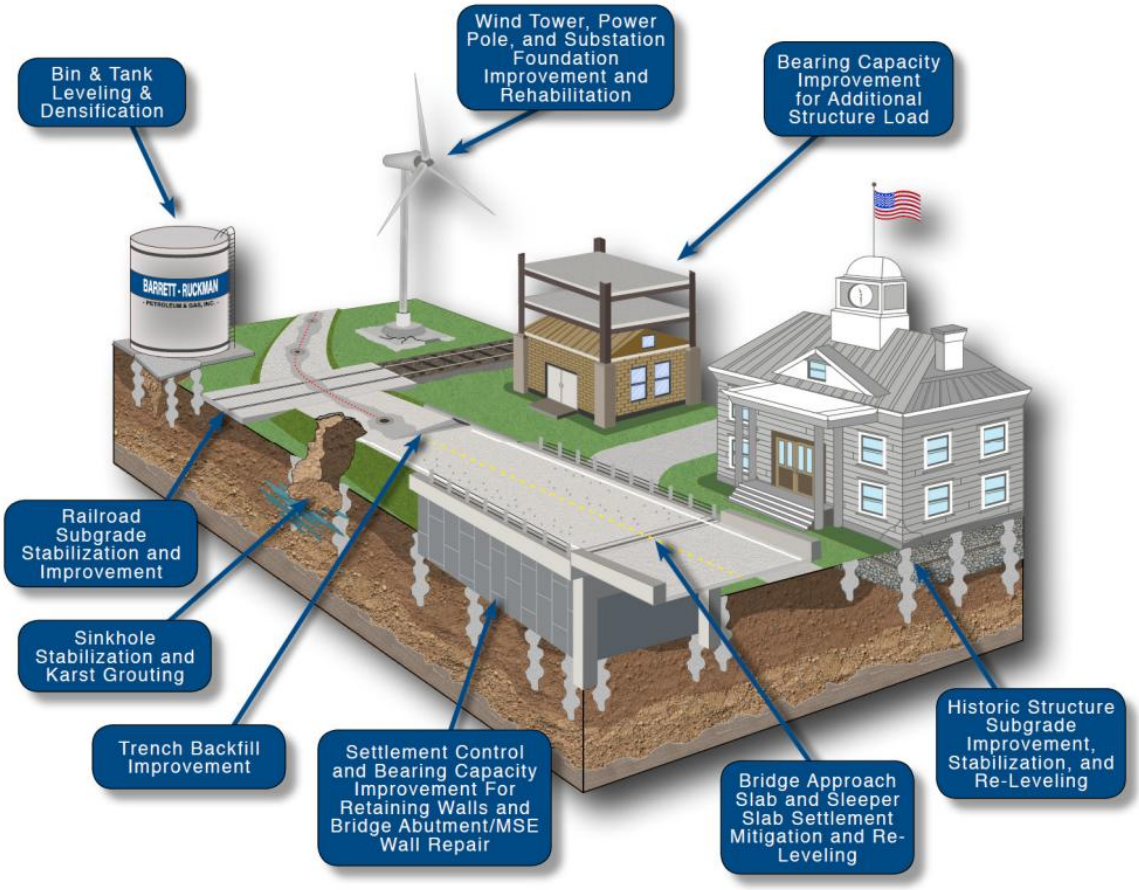


Figure 2-41. Grouting applications (Szynakiewicz, 2016)

There are three main types of grouting materials: Particulate grouts, chemical grouts, and compaction grouts (Nicholson, 2014). Particulate grouts are cementitious as they include suspended solids. Chemical grouts are full solutions, with polyurethane being one such example. Lastly, compaction grouts are usually made up of a thick concrete mix.

There are five main types of grouting: slurry, chemical, compaction, jet, and fracture grouting, as shown in **Figure 2-42** (Nicholson, 2014). Slurry grouting, also known as intrusion, because it follows the path of the voids and pre-existing formations, is usually used on gravels and sands. Chemical grouting permeates pores and voids. Compaction grouting, sometimes called mud/slab jacking, displaces loose sands to create "grout bulbs". Expanding polyurethane foam is sometimes considered a type of compaction grouting. Jet grouting uses high pressure to inject the grout to erode the soil and create uniform columns. Unlike other grouting types, jet grouting can be used for all soil particle sizes. Fracture grouting uses high pressure injections to create connected grout filled fractures, and for soft soils, this method can create a heave to fix settlement problems. In addition to the end goal of grouting, depending on the makeup of the soil, certain grouting methods are more effective than others. **Figure 2-43** shows a suggested method depending on the gradation of the soil (Nicholson, 2014).

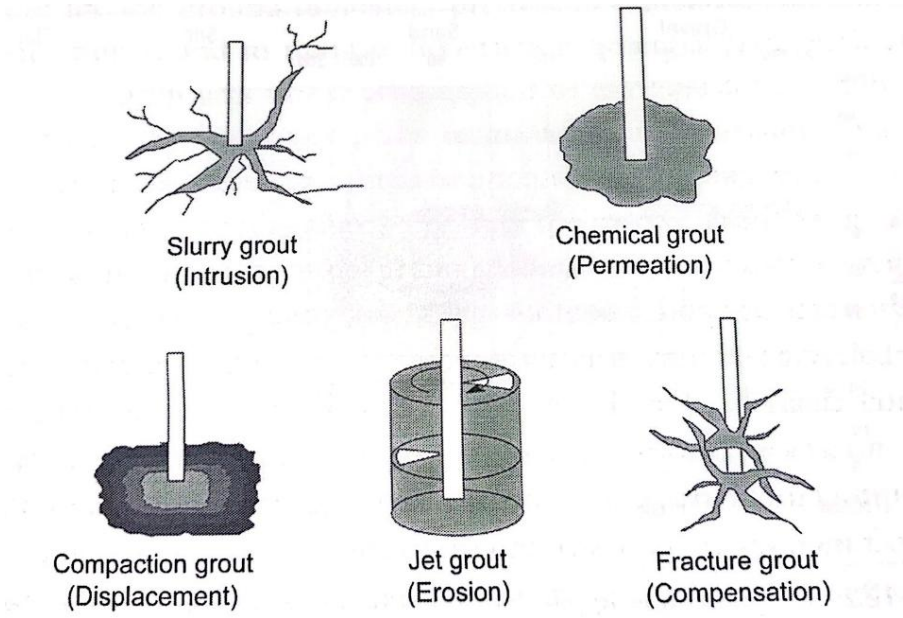


Figure 2-42. Grouting types (Nicholson, 2014)

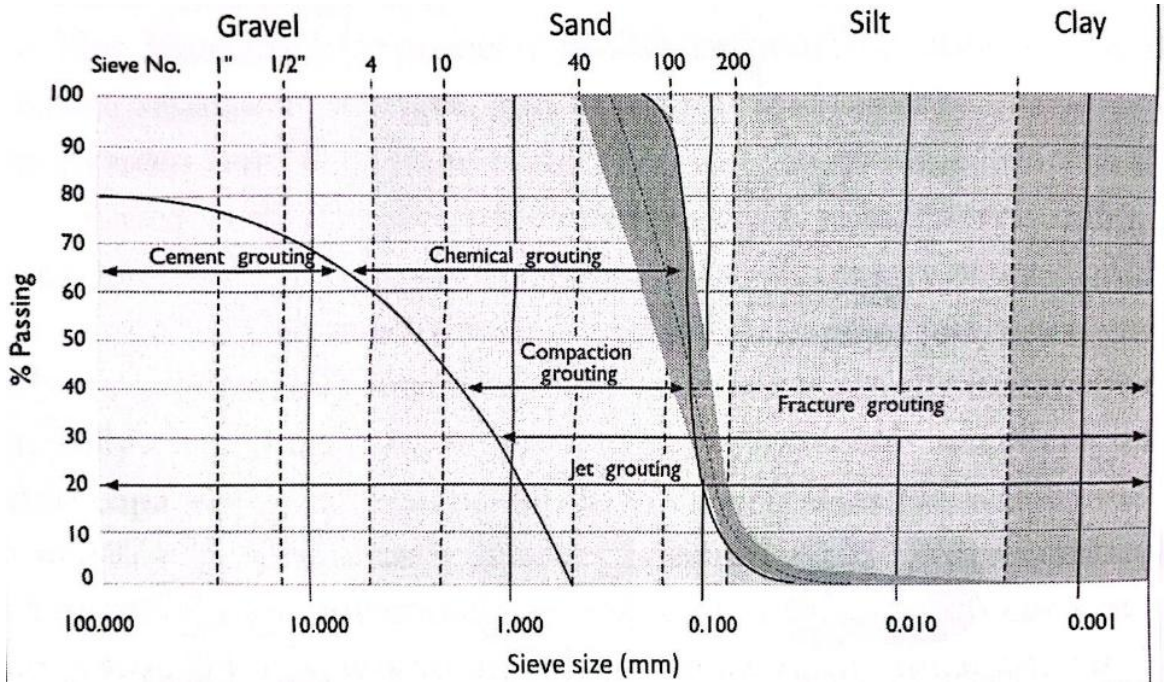


Figure 2-43. Grouting methods and gradation relationship (Nicholson, 2014)

Grouting bonds together soil particles and densifies the soil, reduces settlement, increases soil bearing capacity and, prevents water seepage, pumping, and liquefaction (Roshan et al., 2022; Szynakiewicz, 2016). Unlike the methods of overlays and FDR, grouting treats the causes of settlement (Szynakiewicz, 2016). Another benefit of grouting is that it can be done post-

construction as a repair method with “limited intrusion” (Szynakiewicz, 2016). It has also been found that compaction grouting at a deeper depth removes water from the soil and makes the soil denser (Szynakiewicz, 2016).

The general process of using cementitious grouting for slab jacking is as follows. Injection holes are drilled methodically so that the grout can be allowed to uniformly distribute across the area of the slab (Jayawickrama et al., 2005). Grouting typically starts at the lowest elevation, and important factors to consider when choosing the locations of the grouting injection holes include the area of the slab, desired lifting height, the condition of the subgrade, joints, and cracks in the slab (Jayawickrama et al., 2005). Once the injection holes have been drilled, the injection pipe is inserted, and the grout is pumped under the slab (Jayawickrama et al., 2005). It is important for the slab to be raised slowly at 0.25 inch increments so that voids can be filled, and the slab does not crack or undergo nonuniform pressures (Jayawickrama et al., 2005). **Figure 2-44** and **Figure 2-45** below show the compaction grouting process and a typical grouting layout for a bridge embankment, respectively.

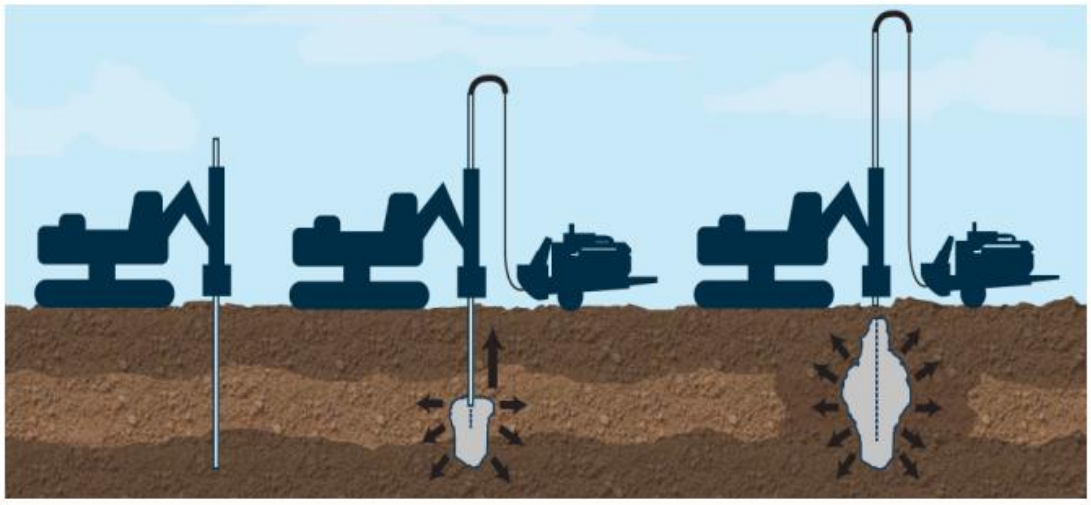


Figure 2-44. Compaction grouting process (Szynakiewicz, 2016)

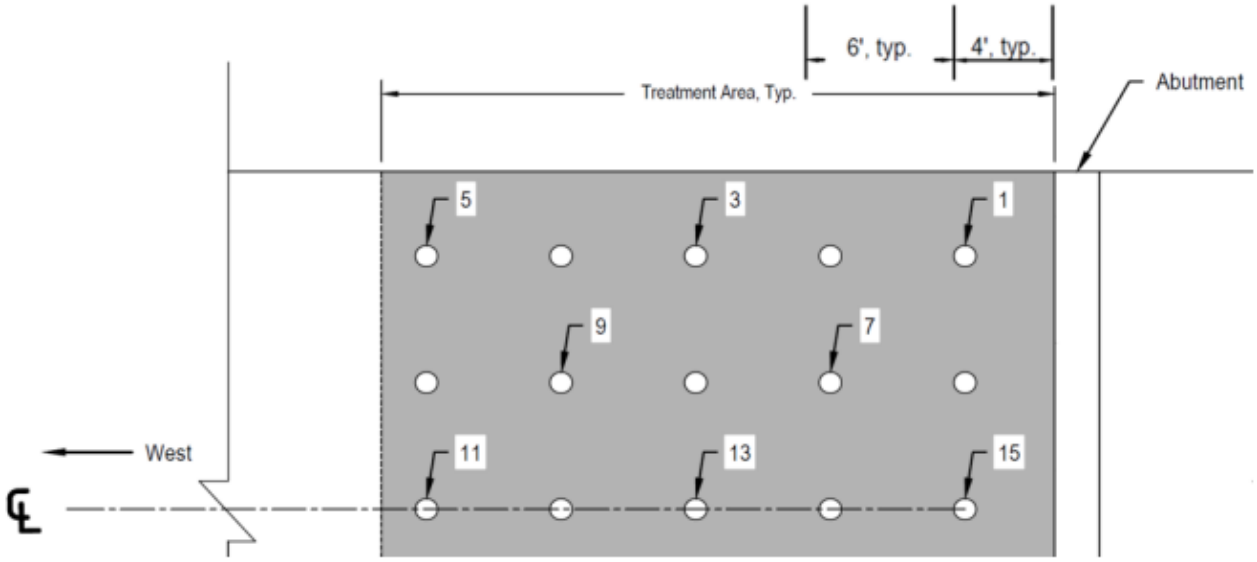


Figure 2-45. Common grouting pattern layout for bridge embankment (Szynakiewicz, 2016)

2.4.2.4.2 State DOT specifications

From the reviewed literature, at least 13 states were identified as having specifications for using cementitious grouting for slab jacking and/or slab stabilization, including Kentucky, Missouri, Minnesota, North Dakota, Oklahoma, Oregon, Texas, Alabama, Iowa, Louisiana, California, South Dakota, Utah, Pennsylvania, Kansas, and New Jersey (Puppala et al., 2011; Vennapusa et al., 2016). All of these states utilize various admixtures and additives in their mix designs, but all share the components of both Portland cement and fly ash. For these states, slab movement, when grouting, is restricted to between 0.825 – 6 mm (Vennapusa et al., 2016). **Table 2-26** summarizes some of these DOTs' specifications.

Table 2-26. State DOTs' specifications on cementitious grout (Vennapusa et al., 2016)

State	Reference	Application	Materials	Mix design	Requirements	Slab movement	Testing	Traffic delay
AL	ALDOT (2012b)	Slab jacking	Type I or III PC, $CaCl_2$, FA, air entraining Additives or chemical admixtures, LD, FS	The following mix design proportions (by volume) are specified: 80%FA + 20%PC 50%LD + 30%FA + 20%PC 80%LD + 20%PC 20%FS + 50%FA + 20%PC	PP: ≤ 1.5 MPa ET: 18–25 s	±6 mm of the final grade	A 4.5-m-long straight edge is used to verify that the final grade is within ±6 mm	Minimum of 3 h. For Type III cement, delay should be greater than the initial set time
	ALDOT (2012a)	Slab stabilization		50%FS + 30%LD + 20%PC	PP: ≤ 1.5 MPa ET: 14–22 s	≤ 1 mm	A rubber-tire 90 kN single-axle load is used to check if slab movement under loading <0.8 mm. Increase in IRI values after stabilization should be <10 mm/km	

State	Reference	Application	Materials	Mix design	Requirements	Slab movement	Testing	Traffic delay
CA	Caltrans (2010a)	Slab stabilization	PC, class C/F FA, chemical admixtures and $CaCl_2$ (optional)	2.4–2.7 parts FA to 1 part PC by weight	7-day CS: ≥ 5.2 MPa ET: 10–16 s PP: ≤ 1.0 MPa	≤ 1.3 mm	Not specified	
	Caltrans (2010b)	Slab jacking			ET: 16–26 s PP: ≤ 1.4 MPa	±3 mm of the final grade		
IA	Iowa DOT (2012)	Slab stabilization	Type I PC, class C FA	One part by volume of Type I PC and three parts by volume of class C FA	ET: 10–16 s Initial PP: ≤ 0.15 MPa PP: ≤ 0.05 MPa	≤ 2.5 mm	Not specified	Delay time should be greater than the initial set time (6 h at 4°C and 4 h at 10°C)
KS	KDOT (2015)	Slab stabilization	Type I or II PC, FA, air entraining or chemical admixtures (optional)	≥ 25% by volume of PC and ≥ 50% by volume of FA	ET: 9–15 s 7-day CS: ≥ 4.1 MPa PP: sustained 1.0 MPa	≤ 3.2 mm	FWD test is used to determine the effectiveness of the undersealing operation through voids under the slabs	Not specified

State	Reference	Application	Materials	Mix design	Requirements	Slab movement	Testing	Traffic delay
LA	Louisiana DOTD (2006)	Slab stabilization and slab jacking	Type I PC, FA, Powdered ammonium sulphonate	One part PC and three parts FA by volume and powdered ammonium lignin sulphonate at 0.5–1.5% by weight of PC	ET: 12–18 s for undersealing and 15–26 s for slab jacking PP: $\leq$ 1.4 MPa	$\pm$3 mm of the final grade	Not specified	At least 1 h after pumping operations
MO	MoDOT (1999)	Slab stabilization	Type I, II or III PC, FA	$\geq$ one part PC by volume to three parts FA	7-day CS: $\geq$ 4.1 MPa ET: 10–16 s Initial PP: 1.380 MPaPP: $\leq$ 0.69 MPa (0.205–0.345 MPa)	$\leq$ 3 mm	FWD test is used for void detection and undersealing verification. Requires $\Delta_A \leq$ 0.38 mm or $(\Delta_A - \Delta_L) \leq$ 0.25 mm	Three hours after the end of pumping operations, and after all drill holes are plugged
NJ	NJDOT (2007a, b)	Slab stabilization	Type I, II, III PC, FA chemical admixtures	One part PC to three parts FA. Use admixtures if needed	7-day CS: $\geq$ 4.1 MPa ET: 9–16 s PP: $\leq$ 0.4 MPa	$\leq$ 2.5 mm	Deflection test is needed to verify if the deflection value is less than 0.25 mm	At least 1 h after initial set
OK	OKDOT (2009)	Slab stabilization	PC, FA, air/chemical /corrosion-inhibiting/la	A mix design showing the CS, ET, VC, and initial set time needs to	7-day CS: $\geq$ 5.5 MPa ET: 10–16 s	0.825–0.925 mm	A standard Benkelman Beam is used to monitor	Three calendar days or directed

State	Reference	Application	Materials	Mix design	Requirements	Slab movement	Testing	Traffic delay
			tex emulsion admixtures	be reviewed and approval by the Engineer	Pumping head: 1.54 m^3/h		excessive lifting of pavement or rising of the adjacent shoulders	by the Resident Engineer
PA	Penn DOT (2011)	Slab stabilization	PC, pozzolan (class C/F/FA, ground granulated blast furnace slag, silica fume)	One part PC to three parts of pozzolan by volume and admixtures if required	7-day CS: ≥ 4.8 MPa ET: 10–15 s PP: ≤ 1.4 MPa VC: –2.5–10% Initial set time: 1–6 h	≤ 1.3 mm	A vehicle having a dual-tire single-axle with an 80 kN single-axle load is used to detect if slab corner deflection ≤ 0.5 mm and joint efficiency ≥ 65%	At least 12 h after completing grouting operations
SD	SDDOT (2004b)	Slab stabilization	Type I or II PC, class C FA	One part PC to three parts FA	7-day CS: ≥ 4.1 MPa ET: 9–15 s PP: ≤ 0.4 MPa	≤ 3 mm	FWD test or a single-axle truck needs to be used to determine if the deflection is in excess of 0.25 mm	Not specified

State	Reference	Application	Materials	Mix design	Requirements	Slab movement	Testing	Traffic delay
SD	SDDOT (2004a)	Slab jacking			7-day CS: ≥ 4.1 MPa Initial ET: 9–15 s ET: 16–36 s PP: ≤ 1.4 MPa	±6 mm of the final grade	A laser leveling unit is used to ensure if the concrete is raised to an even plane and to the required elevation	
UT	UDOT (2012)	Slab jacking	Hydraulic cement, fine aggregate, other ingredients	Packaged dry, hydraulic-cement grout (non-shrink) by manufacturer	7-day CS: ≥ 24 MPa 28-day CS: ≥ 34 MPa Early age VC: ≤ 4% Hardened VC: ≤ 0.3%	±3.2 mm of the final grade	Not specified	

Note: *CS = compressive strength; ET = efflux time; FA = fly ash; FS = fine sand; LD = limestone dust; PC = portland cement; PP = pumping pressure; Δ_A = average of three normalized deflections on approach side; Δ_L = average of three normalized deflections on leave side.*

2.4.2.4.3 Project-specific case studies

Many studies have been conducted on the effectiveness of cementitious grouting as a ground improvement method and to lift pavement slabs on roads and bridges with varied results. Some relevant reports and their results are presented from oldest to most recent in this section.

In 2000, a review of case studies in Illinois that evaluated the effects of using cementitious compaction grouting to reduced voids and improve the soil of a highway bridge and a highway embankment was published (Scherer & Gay, 2000). The first site reviewed was on an Illinois interstate highway bridge. The bridge was built on silty clay and loose sand in a high-risk seismic zone prior to seismic design requirements being established in the state. Compaction grouting was determined as the most economical method to achieve the overall goal of reducing liquefaction potential by densifying the sand under bridge. While grouting, the project was monitored with optical, water, and laser levels and pressure gauges. The results of this ground improvement method were that the standard penetration test N values were increased over required value of 25, showing grouting effectiveness in making soil denser. **Figure 2-46** show the pre and post grouting N values.

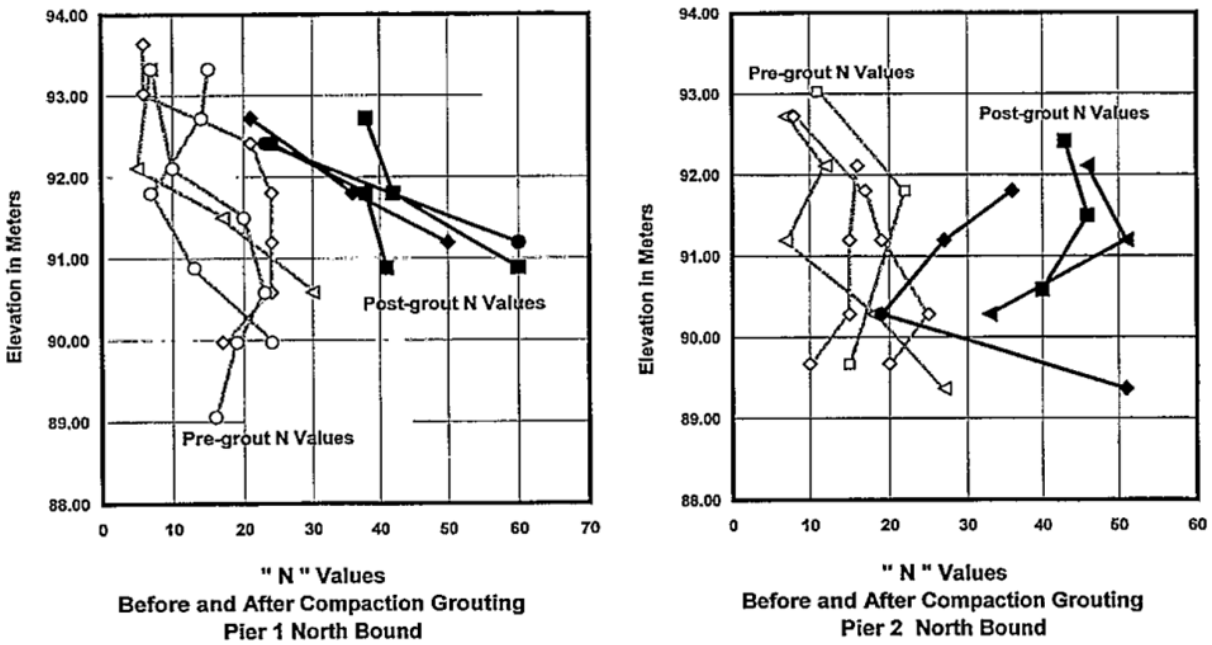


Figure 2-46. Compaction Grouting SPT Results (Scherer & Gay, 2000)

The second site reviewed was a highway embankment on I-88, which is a four lane divided highway, that had two small tunnels installed beneath the embankment (Scherer & Gay, 2000). The goal of the cementitious compaction grouting was to fill voids and densify the loose soil under the highway embankment created by the pipeline constriction. This project was completed in 3

phases, the first phase being taking initial soil borings to understand the soil properties. This was done in both the undisturbed areas and the area near the pipelines. Second, compaction grouting and void filling was done "within zone of influence of pipeline" (Scherer & Gay, 2000). Lastly, post-construction borings near pipeline were taken to confirm effectiveness of treatment. The final outcome of the repair was that the standard penetration Test N values were increased, indicating success in soil densification, and no voids were found.

In 2007, the Iowa DOT conducted a field study on 74 bridges across Iowa to understand why bridge approach slabs tend to have poor performance (White et al., 2007). Researchers reviewed both slabs in good and substandard conditions. They further identified HMA overlays, slab replacement, and slab stabilization with cementitious grouting as common maintenance methods in Iowa. Based on the examinations made in the field, the researchers concluded that neither the HMA overlay method, or the cementitious grouting method were ideal for long term use as they were not able to "prevent further settlement or further loss of backfill material by erosion" (White et al., 2007).

In 2016, a case study comparing the use of polyurethane foam and cementitious grout for slab stabilization on sections of US Highway 422 in Pennsylvania was published (Vennapusa et al., 2016). The highway test sections were Portland cement concrete (PCC) pavement on an open graded aggregate subbase. It was determined from observed cracking and faulting that the subbase was not providing enough support for the slab. The overall goals of the slab stabilization were to fill voids, reduce loading deflections, and improve load transfer efficiency (LTE) on joints/cracks (Vennapusa et al., 2016). It was found that for both methods LTE was improved, and LTE using polyurethane was able to be increased even further after conducting a dowel bar retrofit on the selected pavement sections (Vennapusa et al., 2016). Deflections near cracks were improved with the polyurethane foam method, and near joints with the cementitious grouting method (Vennapusa et al., 2016). Differential settlement was reduced between 2-5 mm with polyurethane foam and between 1-2 mm with cementitious grout (Vennapusa et al., 2016).

2.4.2.4.4 Summary on performance

It was found that cementitious grouting for slab jacking and stabilization generally works well in the short term, but long-term results are more varied. If the repair performs poorly, further settlement can occur and voids can reform. Cementitious grout is currently the most commonly used solution for slab jacking and slab stabilization, but high-density polyurethane (HDP) foam use is increasing (Vennapusa et al., 2016). Both methods can be done post-construction as a repair method with "limited intrusion" to surrounding pavements or structures (Szynakiewicz, 2016). Cement grouting is considered harder to control than polyurethane injection, and it also weighs more, meaning it can eventually contribute to future settlement (Jayawickrama et al., 2005). Some of the benefits of cementitious grouting include denser soil, reduced settlement, increased soil bearing capacity, and the prevention of water seepage, pumping, and liquefaction (Roshan et al., 2022; Szynakiewicz, 2016). Unlike the previously discussed methods of overlays and FDR, grouting treats the causes of settlement (Szynakiewicz, 2016).

2.4.2.5 Polyurethane foam injection

2.4.2.5.1 Definitions of method/technique

Polyurethane foam is an increasingly popular method of soil densification as well as raising and undersealing concrete bridge approach slabs (Vennapusa et al., 2016). Like cementitious grouting, many US states use polyurethane as a post-construction ground improvement method. This technique involves injecting an expanding foam beneath pavement slabs. As the foam expands, it fills voids, makes the surrounding soils denser, and improves the bearing capacity of the subgrade (Soltesz, 2002). The most popular type of injectable polyurethane used in the US by state DOTs is called URETEK (Onyango et al., 2018). URETEK polyurethane foam is high density polyurethane (HDP), which refers to foams with densities of 56 – 240 kg/m^3 (Vennapusa et al., 2016). The URETEK method of polyurethane injection involves injecting the polyurethane into drilled 5/8 inch diameter holes through the pavement and into the subbase (Jayawickrama et al., 2005). The rate at which the polyurethane is injected is what determines the amount of rise (Soltesz, 2002). This method is very quick to complete as it only takes 15 minutes for it to reach 90% of its strength (Jayawickrama et al., 2005). Other relevant facts about polyurethane foam injection include that it can expand to 20 times its liquid volume, lift at a force of 8000 psf, has a final compressive strength of 90 psi, and can fill voids larger than 0.125 in (Jayawickrama et al., 2005; Soltesz, 2002). Compared to other methods like cementitious grouting, polyurethane injection requires less time, equipment, and labor (Vennapusa et al., 2016). Additionally, since the polyurethane foam is lighter than cementitious grout, it "should cause less weight-induced settling" (Soltesz, 2002).

Poor base and subbase conditions are an issue that seems to impact all of the repair methods discussed in this chapter. Some US DOTs use URETEK's deep injection method, which can reach over 30 feet below the surface to stabilize soils and fill voids (Jayawickrama et al., 2005). **Figure 2-47** and **Figure 2-48** depict the method of polyurethane foam injection.

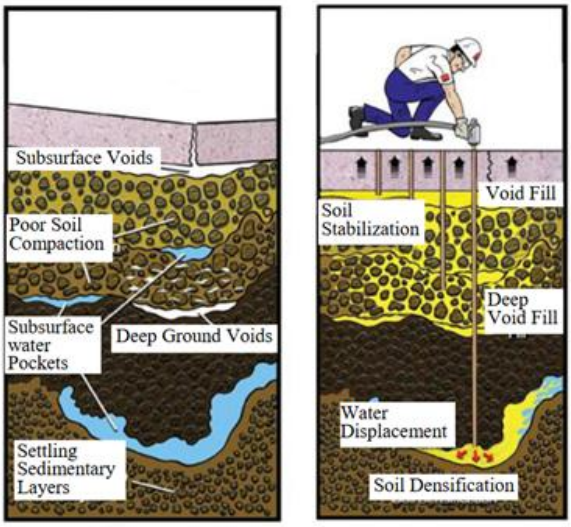


Figure 2-47. Illustrations of polyurethane injection (Ellis, 2015)

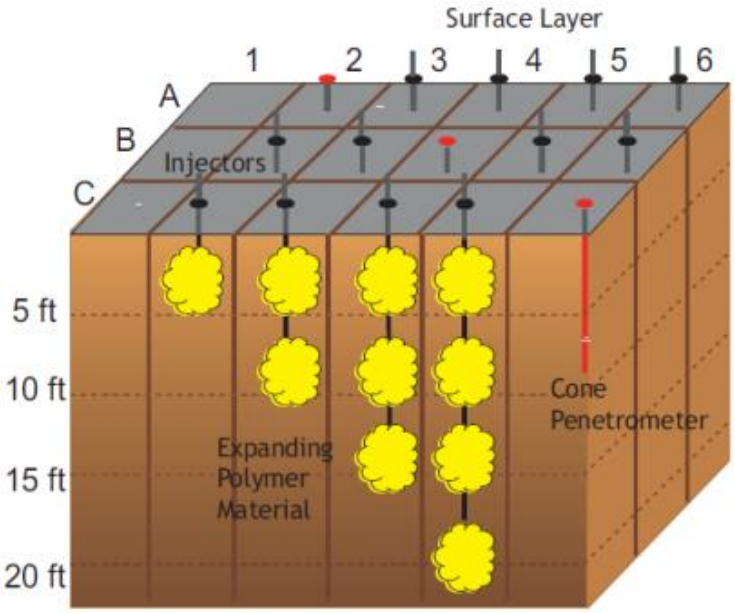


Figure 2-48. An example of layout for injecting polyurethane (Ellis, 2015)

2.4.2.5.2 State DOT specifications

Currently, TxDOT has the Special Specifications of 3025 and 3086 that call for high density polyurethane (HDP) in conducting soil densification and slab raising (TxDOT, 2014a, 2014b). From the literature review, at least seven other states were identified in calling for the use of high density polyurethane resin (HDP) in their specifications for slab jacking (Vennapusa et al., 2016). These states include Missouri, New Jersey, North Carolina, Ohio, Pennsylvania, South Dakota, and Utah, with both Missouri and New Jersey also allowing HDP to be used for slab stabilization. Among these seven states' specifications, slab movement is restricted to between 1.3 – 6.4 mm of final grade, and either FWD, deflection testing, or laser leveling is used to verify results (Vennapusa et al., 2016). The table below provides more detail on these specifications.

Table 2-27. State DOTs' specifications on high density polyurethane (HDP) (Vennapusa et al., 2016)

State	Reference	Application	Requirements	Slab movement	Testing	Traffic delay
MO	MoDOT (2009b)	Slab stabilization	Density: $\geq 64 \pm 8$ kg/m^3 CS: ≥ 0.55 MPa TS: ≥ 0.62 MPa VC: $\leq 5\%$	≤ 3 mm	FWD test is used for void detection and undersealing verification. $\Delta_L \leq 0.38$ mm or $(\Delta_A - \Delta_L) \leq 0.25$ mm	At least 30 min after ceasing pumping operations
MO	MoDOT (2009a)	Slab jacking	CR: $\leq$ 15 min for 90% CS	≤ 3 mm of the final grade		Three hours after the end of pumping operations, and after all drill holes are plugged
NJ	NJDOT (2007a, b)	Slab stabilization and slab jacking	Density: 90.5-94.5 kg/m^3 CS: $0.45 - 0.66$ MPa TS: $0.48 - 0.69$ MPa VC: $5 - 11\%$ for humid 28-day, -0.1 to -0.9% for 5-day freezing SS: $0.28 - 0.59$ MPa Close cell %: $85 - 95\%$ CR: $\leq$15 min for 90% CS	≤ 2.5 mm for undersealing and ± 6.4 mm of the final grade for slab jacking	Deflection test is needed to verify if the deflection value is less than 0.25 mm	At least 1 h after initial set
NC	NCDOT (2008)	Slab jacking	Density: 48 - 67.3 kg/m^3 CS: ≥ 0.28 MPa	± 6.4 mm of the final grade	A tight string line is used to monitor and verify elevations for slab lengths of 15.24 m or less	Not specified

OH	Ohio DOT (2007)	Slab jacking	Density: $\geq$ 48 kg/m^3 TS: $\geq$ 0.28 MPa CS: $\geq$ 0.28 MPa VC: $-0.6 - 4\%$ Water absorption: $\leq$ 2.0% volume	$\pm$5 mm of the final grade	Use a tight string or laser level to monitor and verify elevations	Not specified
PA	Penn DOT (2010)	Slab jacking	Density: $\geq$ 64 kg/m^3 CS: $\geq$ 0.41 MPa TS: $\geq$ 0.48 MPa SS: $\geq$ 0.28 MPa Close cell content: $\geq$ 80%	$\pm$1.3 mm of the final grade	Deflection test is performed to check if slab corner deflection $\leq$ 0.5 mm and joint efficiency $\geq$ 80% at least 24 h after injection	At least 30 min after injection
SD	SDDOT (2004a)	Slab jacking	Free rise density: 48 $-$ 51 kg/m^3 CS: $\geq$ 0.28 MPa CR: $\leq$15 min for 90% CS	$\pm$6 mm of the final grade	A laser leveling unit is used to ensure if the concrete is raised to an even plane and to the required elevation	Not specified
UT	UDOT (2012)	Slab jacking	Density: 60.9-68.9 kg/m^3 TS: $\geq$ 0.55 MPa Elongation: $\leq$ 5.1% CS: $\geq$ 0.41 MPa CR: $\leq$15 min for 100% CS	$\pm$3.2 mm of the final grade	Not specified	

Note: *CS = compressive strength; ET = efflux time; FA = fly ash; FS = fine sand; LD = limestone dust; PC = Portland cement; PP = pumping pressure; Δ_A = average of three normalized deflections on approach side; Δ_L = average of three normalized deflections on leave side.*

2.4.2.5.3 Project-specific case studies

Despite the widespread use of polyurethane foam for pavement remediation, there have been some questions concerning the long-term performance of polyurethane foam injections.

In a 2008 study that examined the performance of polyurethane foam injection, dowel bar retrofit (DBR), and full depth repair (FDR), the researchers determined that polyurethane foam, in and of itself, is not necessarily a reliable method of achieving a long term solution for the repair of a pavement with issues such as settlement, broken or cracked slabs, and slab pumping (Chen & Won, 2008). The relevant FDR portions of this study have already been reviewed in Section 2.4.2.2. This paper looked at case studies on 6 Texas highways that had issues relating to settlement, poor base support, poor load transfer between slabs, slab pumping, and degradation of steel reinforcement.

A section of US75 was having substantial settlement due to poor base support, and polyurethane was injected to raise the slab (Chen & Won, 2008). The slab was successfully raised to the desired level, but upon reviewing the slab 20 months later, multiple new cracks were found, and the slab had demonstrated settling. The researchers theorized the foam injection process created un-even support under the slab, and this contributed to the cracking. The use of dowels and the method of slot stitching was then used to repair this section again, which will be discussed in a later section.

A section of US82 was also experiencing cracking and settlement (Chen & Won, 2008). This section had been treated with polyurethane foam injection for settlement five years ago. Examining the slab, the researchers found that the base and subgrade were extremely weak, and voids existed between the foam and the JCP slab. With less than a five-year life span for the original repair, it was determined that in this case, the foam injection was not very effective.

In 1997, a section US59 was repaired with polyurethane foam injection for settlement issues (Chen & Won, 2008). In 2005, this same section of road was once again repaired with foam injection. During this second repair, it was discovered that the strength of the base was substandard. After the second repair, core sample were taken from the affected slab, and it was found that that this slab had been injected at least four times to counter settlement problems.

These three repairs are examples of poor performance in polyurethane and indicate that polyurethane foam injection alone is not necessarily adequate as a long-term solution in situations where the subgrade and/or base provide substandard support for the slab. It should be noted that all three of the methods (polyurethane, DBR, and full depth repair) attempted to repair the highways failed at preventing future settlement when the subgrade and base were in poor condition.

Despite the results that showed some questions concerning the long-term performance, many other case studies have seen effective results using polyurethane foam injections. In a 2016 survey of US state DOTs, in which 25 states responded, it was found that 76% of respondents “currently use or have used polyurethane material for slab lifting “, and 90% of the respondents who have used the material would recommend this process (Onyango et al., 2018). The survey also found that the most common brand of polyurethane used by the US states DOTs is URETEK (used by 69%) and

that 94% of survey participants indicated that projects which used polyurethane as a repair method did not go over budget (Onyango et al., 2018). Additionally, it was noted that cracking/settlement occurred on the slabs between 1-10 years after polyurethane was used for the repair.

Several states have conducted studies on the effectiveness of polyurethane foam, specifically URETEK, as a ground improvement method and to lift pavement slabs on roads and bridges with varied results. In 1995, the Michigan DOT conducted a study on the use of URETEK to raise and underseal concrete slabs on open graded bases for 3 sections of I-75 (Opland & Barnhart, 1995). The sites were chosen due to severe pavement cracking and failure, and URETEK was chosen as a cost-effective method to stabilize the slabs. To determine if the procedure was successful, FWD, pavement elevations, and ride quality were measured before and after the injections were done. After the procedure was finished the outcome initially appeared to be positive, with raised pavement elevations, increased base stability for areas of severe cracking, and improved LTE at the joints. However, after a one-year monitoring period, the ride quality and LTE at joints and cracks were found to be at pre-injection state conditions. It is important to note that a bordering pavement slab that was not injected underwent a differential frost heave, which was found to probably be the result of the insulating effect the foam had on the base of the treated slabs. After these conclusions, the report recommended URETEK as a repair alternative for dense graded aggregate bases but not open graded bases.

In 2002, the Oregon DOT conducted a study on the use of URETEK to raise the slab and improve settlement of the I-205 Glenn Jackson Bridge exit ramp (Soltesz, 2002). The settlement was due to voids created by water in subgrade being pumped out by traffic loading. After the polyurethane injections, it was found that the slabs were raised to the set goal of 3.5 – 4 inches. The project was monitored for two years to understand long-term stability using 12 surveying caps drilled into the slab to monitor vertical displacement. Elevation measurements were taken at 3, 6, 12, 18, and 24 months after injection. During the monitoring period, minor settling occurred with the majority during the first 3 months, but continued during entire 2-year monitoring period (maximum settlement was 0.413 in). However, this did not impact the ride quality. The compressive strength of the polyurethane foam stayed consistent over the monitoring period. This report argued any method of slab jacking can have settlement, but the injected polyurethane allows for better lifting control and “should produce a higher percentage of successfully raised slabs, than injected grout” (Soltesz, 2002). A follow-up report done a year after found that while the visual inspections showed no changes, the measured elevations found settlement of 0 to 1.9 mm/yr (continued settlement but rate is decreasing) (Heintz, 2003). **Figure 2-49** below shows how the slab joint appeared after injection.



Figure 2-49. Slab joint before and after polyurethane slab jacking (Soltesz, 2002)

In 2004, the LaDOTD and the Louisiana Transportation Research Center (LTRC) investigated the use of URETEK on repairing CRCP, JCP, and bridge approach slabs (Gaspard & Morvant, 2004). Testing methods included FWD, Dynaflect, and a high speed and a walking profiler. FWD was found to be accurate in finding voids with the exception of "0-10 feet from the bridge end on approach slabs" (Gaspard & Morvant, 2004). By using these tests, a fairly accurate estimate of material needed was determined, and equations to estimate the amount of material needed were developed and tested. One section of CRCP, one section of JCP, and two bridge approach slabs were lifted and monitored for several years. For the CRCP and bridge approach slabs, the slabs were raised 2 inches, the IRI improved, and core samples taken showed dense polyurethane inside. For the JCP, the core sample showed soft to dense polyurethane inside, which was noted as possibly "problematic" (Gaspard & Morvant, 2004). For the JCP section, it was also found that the polyurethane filled voids but provided very little support to the joints. After 4 years, the bridge approach slabs had not undergone any additional faulting or needed any new repairs (Al-Eis & LaBarca, 2007). The guidelines provided for rehabilitation on CRCP and the bridge approach slabs include injecting the foam in a 3 – 4 ft grid pattern through the pavement and into the subgrade 20 ft before and after the settlement for CRCP and 2-2.5 ft from the bridge end for the approach slabs. Polyurethane foam injections are only recommended in case of emergency for JCP slabs, and only on CRCP and bridge approach slabs that are not failed or severely distressed (Gaspard & Morvant, 2004). However, it should be noted that URETEK has previously been used successfully on JCP in some Louisiana districts (Gaspard & Morvant, 2004).

In 2007, the WisDOT conducted a study to investigate how well the URETEK method of pavement lifting worked on Portland cement concrete (PCC), especially the bridge approach slabs (Al-Eis & LaBarca, 2007). The study reviewed the results of pavement lifting at two testing sites, I-39 and USH 12, with regular follow-ups up to 5.5 years after remediation. At both sites, the slabs were raised to the required elevations (with a 0.25 - 0.5 inch tolerance), and the safety and ride quality of the roads were found to be improved. Some minor transverse cracks were identified but were thought to be a result of the injection process. At both sites the amount of polyurethane foam needed was greatly underestimated, with the sites needing 2 to 5 times the amount initially

estimated. This underestimation was likely due to a lack of sufficient subsurface investigations prior to the repairs. The report suggested using ground penetrating radar (GPR) to determine the amount of subsurface voids and improve the polyurethane quantity estimate. For these case studies, it was noted that the polyurethane cost was expected to be lower than it was, but insufficient testing beforehand caused an inaccurate estimate of the voids, and this created a significant increase in the amount of foam needed to complete the projects. I-39 had larger amounts of unexpected voids than USH 12, so the foam injection was much more costly and less cost effective.

Some case studies have found increased success with using polyurethane injections combined with dowel retrofit. In 2014, a study was conducted on a sections of jointed PCC pavement highway in Pennsylvania that had undergone HDP foam injection and, in some sections, also patching and a dowel retrofit a year after (Vennapusa & White, 2015). The section of road was on an open graded aggregate subbase layer with the issues of mid-panel cracking and faulting. After the repairs, it was found that the ride quality slightly worsened, the pavement slabs raised an average of 6 mm, which was found to minimize faulting at cracks, and there was significant improvement near cracks (but not near joints) regarding deflection and load transfer efficiency. The LTE near cracks improved from 15% to 45% after HDP and then to 86% after dowel retrofit (Vennapusa & White, 2015).

In 2015, the Vermont Agency of Transportation used URETEK to repair a section of bituminous pavement on I-89 that had undergone severe settlement (Ellis, 2015). The goal was not to lift the pavement back to its original elevation, but rather to conduct subsurface stabilization. Prior to injection, the subsurface testing methods used to determine the necessary volume of polyurethane needed were ground penetrating radar (GPR), capacitively-coupled resistivity (CCR), falling weight deflectometer (FWD), and cone penetrometer testing (CPT) (Ellis, 2015). Six years occurred between these tests and the injection repair. Additional testing using dynamic cone penetration (DCP) was done as a part of the injection process. The injection consisted of 378 drilled holes, with foam injections occurring between 7 and 19 ft below the surface. Over two times the expected amount of polymer was used for repair, and for this reason, the report advised avoiding delays between site evaluation and construction. The results found that after 1 year the rate of settlement was reduced and no new repairs were needed (Ellis, 2015).

In 2018, a case study was done on a section of JPCP on I-24 and I-75 in Tennessee to determine the effectiveness of the polyurethane foam repair, specifically by studying the transverse joint faulting of the sections before and after HDP use (Fortunatus, 2018). Unlike many other case studies reviewed, the brand of polyurethane foam used was PolyLevel. The repaired pavement sections were monitored from 1 to 29 months post repair with an inertial profiler. The results of the study found that the injections maintained the condition of the road before the repair and “did neither improve nor retrogress” (Fortunatus, 2018). The study recommended that if a slab is in poor/bad condition to not use HDP, but on good/fair sections it can be used to extend pavement life. A “poor” road condition was defined as transverse joint faulting of more than 3.8 mm or an IRI larger than 2.70 m/km.

2.4.2.5.4 Summary on performance

As can be seen in the literature, performance of polyurethane foam injection varied from state to state, and sometimes project to project. It seems that a common issue is incorrectly estimating the amount of foam needed, and this can adversely affect the final cost of the improvements. This indicates that subsurface testing prior to conducting the repair is extremely important. The states of Louisiana and Texas both noted issues with repairing JCP with the polyurethane foam (Chen et al., 2009; Gaspard & Morvant, 2004). JCPs have larger joints than CRCP which can allow for water to penetrate more easily, and this can lead to voids and erosion. Although questions have been raised as to its long-term effectiveness, many states have found success with its use. Several sources seem to point to polyurethane injections as a method that can be used to extend the life of a project, since this process can help maintain the quality of the project for an extended period of time with reduced time expenditure. In an Oregon DOT survey, it was found that polyurethane foam has been used on many projects to keep a road in poor condition functioning until it could be replaced at a later date (Heintz, 2003).

2.4.2.6 Miscellaneous repair methods: dowel bar retrofit, slot stitching, and cross stitching

2.4.2.6.1 Definitions of method/technique

Sometimes found in cases studies was a combination of one or more of the previously discussed repair methods with dowel bar retrofit (DBR), slot stitching, and/or cross-stitching. While not considered as soil improvement methods, in cases studies it was found that these methods could amplify the success of a repair by improving the load transfer efficiency (LTE) between cracks and joints (Chen & Won, 2008; Vennapusa & White, 2015). Cross stitching and slot stitching are similar to DBR in that steel reinforcement bars are embedded in pavement slabs to stabilize joints and cracks. Case studies where the methods of dowel bar retrofit and slot stitching were utilized in conjunction with the repair techniques mentioned in the previous sections can be found in the polyurethane and FDR “Project-specific case studies” sections. The methods of dowel bar retrofits, slot stitching, and cross stitching are defined below.

In Texas, for the DBR process, parallel diamond saw blades are used to cut parallel slots in the surface of the slab and across and perpendicular to the joint (Stevenson, 2021b). The material between the slots, also called fins, is removed and the slot is then cleaned (Stevenson, 2021b). The slots should be cut to a depth so that the center of the dowel diameter lies at the same depth as the center of the slab. The dowel bars are then put in place, and joints are sealed with silicon. Finally, the slots are filled with a high strength concrete mixture. **Figure 2-50** and **Figure 2-51** show the slots before the dowels are inserted and a plan and profile view of a DBR for the state of Washington.



Figure 2-50. Dowel bar retrofit in progress (Stevenson, 2021b)

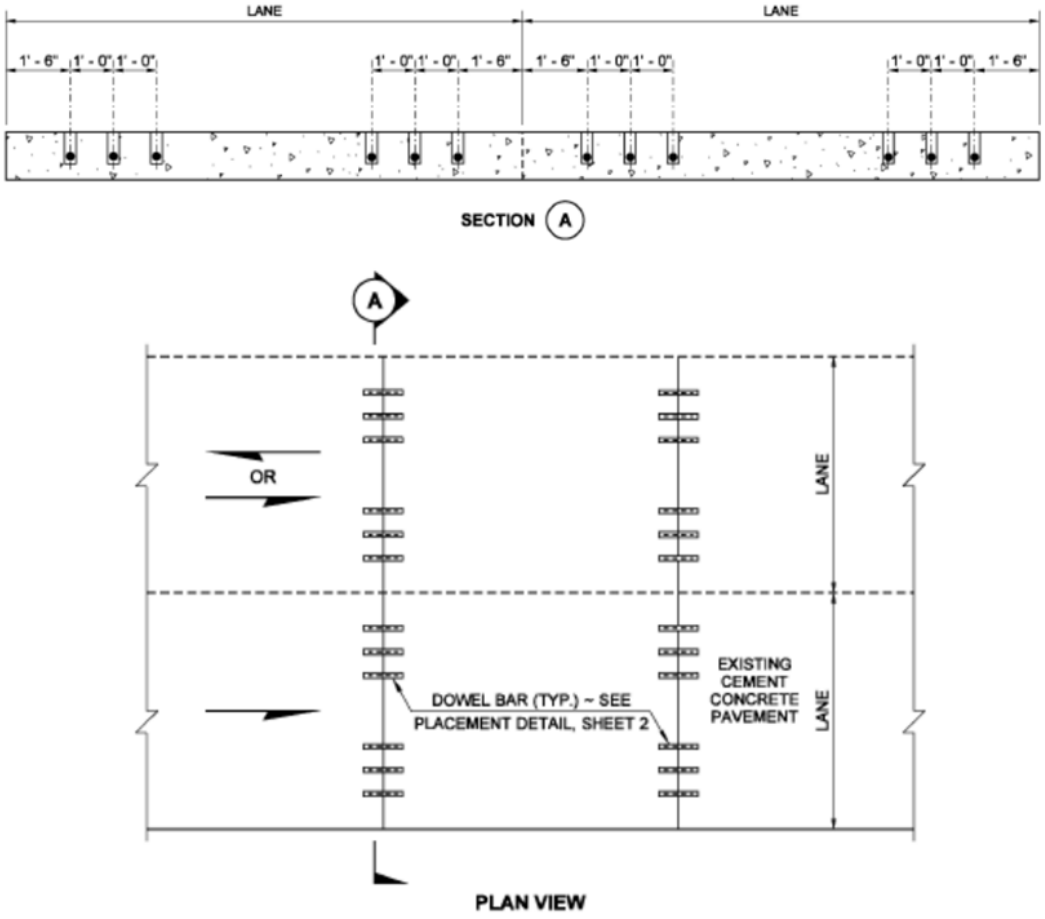


Figure 2-51. Washington state example of dowel bar retrofit (Darter, 2017)

The procedure of slot stitching is similar to the DBR method. Slot stitching is used to repair longitudinal cracks and joints (Fortunatus, 2018). Slot stitching starts when slots are cut perpendicular to joints or cracks (Jayawickrama et al., 2005). Once the slot is cut, it is cleaned of debris, and deformed steel tie bars are positioned in the slot. High strength concrete is then used to fill the slots to finish the repair (Jayawickrama et al., 2005).

Cross stitching is a process used to tie together two vertical surfaces of a crack or joint. This process is also utilized to provide or increase LTE values across joints or cracks (Fortunatus, 2018). In this process, holes are drilled at a 35-45° angle across a joint, intersecting the joint at about the midpoint of the slab thickness (Jayawickrama et al., 2005). The drilled holes alternate from one side of the joint to the other, and are spaced 2 - 3 feet apart (Jayawickrama et al., 2005). Once the holes are drilled, they are cleaned and filled with epoxy. A steel bar is then inserted into the hole so that the end is about one inch below the pavement surface (Jayawickrama et al., 2005). **Figure 2-52** shows a cross-sectional view of a cross-stitching repair.

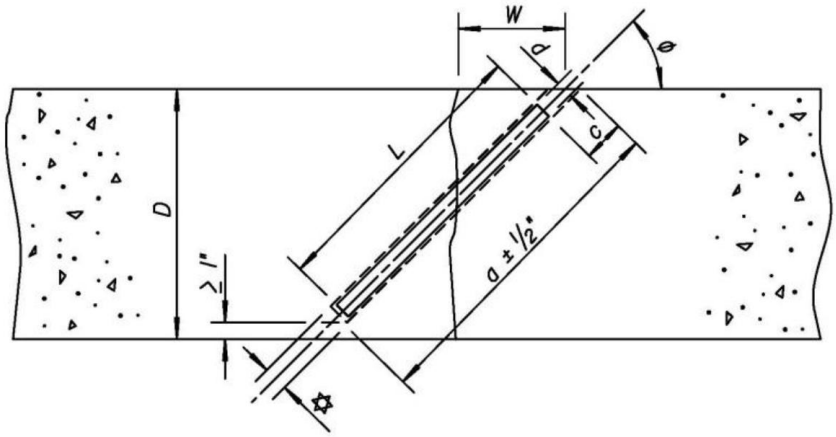


Figure 2-52. An example of cross stitching: section view (Darter, 2017)

Applicability of dowel bar retrofits, cross stitching, and slot stitching are summarized in **Table 2-28**.

Table 2-28. Applicability of dowel bar retrofits, cross stitching, and slot stitching (Fortunatus, 2018)

Treatment	Description	Applicability
Dowel bar retrofit	Restoration of load transfer of slabs by placement of dowel bars across joints or cracks	Slabs with poor load transfer efficiency due to lack of bars, poor aggregate interlocks or support erosion
Cross stitching	Involves maintaining load transfer across non-working longitudinal cracks that are in good condition by preventing horizontal and vertical movements	Longitudinal joints likely to faults, sections showing indication of slab migration and weak aggregate interlocks
Slot stitching	Involves repairing of longitudinal cracks and joints that develop as a result of dowel bar retrofit treatment by using deformed tie bars	Segments with longitudinal cracks due to dowel bar retrofit treatment

2.4.2.6.2 State DOT specifications

From the 2014 specifications, TxDOT has the special specification of 3039 for dowel bar retrofit; and from the 2004 specifications, TxDOT has the special specifications of 3013 for cross-stitching. Other related special specifications were for single-use on specific projects. Some US state specifications for dowel bar retrofits and cross-stitching can be found in **Table 2-29** and **Table 2-30**, respectively. At least 19 US states use some method of slot-stitching or cross-stitching (American Concrete Pavement Association 2001).

Table 2-29. State DOTs' specifications for dowel bar retrofit (Darter, 2017)

State	Specification/Documents
Washington	WSDOT 5-01 Cement Concrete Pavement Rehabilitation Standard Plan A-60.10-03 "Dowel Bar Retrofit: Do's and Don'ts" WSDOT (2009)
Minnesota	MnDOT 2302 SP. Concrete Pavement Rehabilitation Best Practices Manual, MN Local Road Research Board, 2006.
California	Section 40-1, SSP 41-.02, RSP P10 Dowel Bar Retrofit, Revised Standard Plan P7 SSP 41-8. Dowel Bar Retrofit SSP 41-8.03L SSP 41-8.01D(6) "Evaluating Load Transfer Restoration," Karl Smith, Raul Alarcon, July 2002, California DOT
Missouri	MoDOT Standard Specification 613.40 MoDOT Standard Drawing 613 (Sheet #4)
Utah	UDOT Standard 2754

Table 2-30. State DOT's specifications for cross-stitching (Darter, 2017)

State	Specification	Comments
Kansas	Kansas DOT 15-08003 Tiebar Insertion (Cross-Stitching)	Reinforcement content varies with application: longitudinal joints (0.15%), longitudinal cracks (0.18%), transverse cracks (0.37%). Typical Kansas longitudinal tiebar reinforcement = 0.34%.
Minnesota	Information sheet only: "Stitching Longitudinal Pavement Cracks."	Percent area of rebar typically is 0.13%.
Missouri	Standard Specification 613.50. Standard Drawing 613 (Sheet #3)	Percent area of rebar is 0.18%.
Utah	ACPA guidelines for cross-stitching.	Percent area of rebar is 0.18%.

2.4.2.6.3 Project-specific case studies

The first case study reviewed for both polyurethane foam injection and full-depth repair involved a review of 6 Texas highway sections repaired with polyurethane foam injection, FDR, dowel retrofit, or some combination of the three (Chen & Won, 2008). In the US287 section, only a dowel retrofit was used to make the repair for heavy faulting. The faulted joints had low load transfer efficiencies, and this was determined to be the result of potential base erosion and the fact that neither dowel bars or cement or asphalt stabilized bases were used in the initial construction. The strength of the existing concrete was found to be good, so rather than replacing the slab, the DBR method was chosen. Three years after the repair, the section of highway was still found to be in excellent condition.

On the US75 highway, both polyurethane and FDR were previously utilized to repair the pavement for settlement and pumping related problems (Chen & Won, 2008). Unfortunately, these remediation efforts did not provide satisfactory long-term results. Another paper, published a year after this one, examining the same US75 highway, has indicated the importance of good tie-bar design for achieving and maintaining good LTE and preventing further settlement (Chen et al., 2009). This paper involved the analysis of 14 sections of JCP on US75. By analyzing core samples taken from the sections, which included sections of tie-bars, it was determined that settlement was most pronounced in the areas where the strength of the tie-bars was most seriously degraded. From this, the researchers were also able to determine that the pavement had an insufficient tie bar design. Short of replacing all the affected slabs, there was no practical way of improving the overall condition of the base support to improve the LTE values, so it was determined that the use of slot-stitching between adjacent slabs, plus the filling of voids with a low-pressure slurry of cement and fly ash, was the best approach to achieving the higher LTE values and preventing future settlement.

These examples, as well as the examples in the polyurethane and FDR case study sections that also used one of the techniques found in this section, demonstrate that DBR, cross-stitching, and slot-

stitching can provide long term benefits to pavement durability and ride quality, but will not fix poor base or subgrade issues.

2.4.2.6.4 Summary on performance

While not a soil improvement method, combining a dowl bar retrofit or similar technique with one or more of the other BAS repair methods discussed previously can improve the overall quality of a repair and create a more successful outcome. The use of DBR appears to be a commonly used repair method in the state of Texas and is specified in the DOTs' manuals for other US states. As previously mentioned from various case studies, the benefits of DBR include better LTE between slabs, improved ride quality, and prevention of slab faulting (except in instances where the slab has poor base support). In that last case, combining DBR with a soil improvement method can be beneficial to the repair.

2.4.2.7 Synthesis and summary

Among TxDOT districts, a survey of five slab maintenance methods (HMA overlays, slab replacement, mud/slab jacking, grouting, and urethane foam injection) found that all of these techniques' "feasibility" were either effective or proven as shown in **Table 2-31** (Puppala et al., 2011). Urethane foam injection was deemed to be the most effective in overall performance, with slab replacement, mud/slab jacking, and grouting being perceived as ineffective. In terms of cost, TxDOT districts ranked polyurethane foam injection the most expensive, HMA overlay and slab jacking the cheapest, and slab replacement and grouting as having a moderate cost. In two case studies conducted by WisDOT, it was found that polyurethane foam was the median price option, and slab replacement the most expensive as shown in **Table 2-32** (Al-Eis & LaBarca, 2007). A survey of 25 US state DOTs found that that polyurethane was the most cost-effective method of repair, unless the slab had severe damage, in which case slab replacement was the most cost effective (Onyango et al., 2018). In regards to time to complete each technique, it was found that polyurethane foam injection can be completed the quickest, slab replacement requires the longest duration, and HMA overlay and slab jacking fall in between and both take about the same amount of time (Al-Eis & LaBarca, 2007).

Table 2-31. TxDOT District-wide survey on mitigation techniques for bridge approach settlement (Puppala et al., 2011)

New or Maintenance Measure	Mitigation method	Technique Feasibility (a)			Construction Requirements (b)			Cost Considerations (c)			Overall Performance			Is this method recommended for present research?
		Infeasible	Effective but unproven	Proven, well design method	Low	Medium	High	Low	Medium	High	Not proven	Ineffective	Effective	
Maintenance Measures	HMA overlay			✓		✓		✓			✓			×
	Mud/ Slab jacking		✓		✓			✓				✓		✓
	Slab replacement			✓		✓			✓			✓		×
	Grouting			✓	✓				✓			✓		✓
	Urethane foam injection		✓		✓					✓			✓	✓

Table 2-32. Cost comparison of slab faulting repair methods (Al-Eis & LaBarca, 2007)

Location	Method	Total Cost	Cost per yd²	Days to Complete
I-39 (80 yd²)	URETEK	$19,440	$243	0.75
	Slab Replacement	$34,000	$425	3
	HMA Overlay	$3,630	$45	1
	Mud-jacking	$3,000	$38	1
USH 14 (53.3 yd²)	URETEK	$6,260	$117	0.5
	Slab Replacement	$22,670	$425	3
	HMA Overlay	$3,375	$63	1
	Mud-jacking	$3,000	$56	1

Based on the findings of this literature review, out of all of the current practices for ground improvements used for highways embankments, there is no single perfect option when choosing a remediation technique. Generally, all of these methods were found to work well in the short term, but long-term performance seems to be variable. Factors such as time, cost, and effectiveness must be considered, as well as the individual needs of each project.

Given these methods for ground improvement, there are a few recommendations found in the literature as to when each technique should be utilized (Jayawickrama et al., 2005). Generally, an asphalt overlay can be used to correct ride quality problems from differential settlement when there is not a soil erosion issue. It is important to note that this method alone will likely require repeated application since it does not address the root causes of the settlement and, therefore, will not fix the issue. Slab stabilization and undersealing is best used for minor void developments, and slab jacking (either polyurethane or cementitious) should be used for slab settlement due to large voids. Slab jacking and stabilization can also be done with asphalt, but this appears to be a much less popular/successful material. If just a section of the approach slab has severe damage, a full or partial depth slab replacement can be done. If the tie bar design or load transfer between the joints or cracks is found to be insufficient, a dowel bar retrofit can be done to enhance the LTE. Finally, if the slab damage is so significant that the other repair techniques are deemed not cost effective, a reconstruction might need to be done.

Chapter 3 Survey of Current TxDOT District Practice

This chapter presents results of the survey conducted to identify (i) the current state of the practice for evaluation of in-service roadway embankments and (ii) the current state of the practice for soil improvements and repair methods related to roadway embankments in Texas. The draft survey questionnaire was first submitted to the TxDOT Project Monitoring Committee (PMC) members for their review and then later finalized based on the feedback from the PMC members. A printable format of the final survey questionnaire is presented in Appendix A.

The survey was distributed to all TxDOT districts, and the Research Team used *Google Form* as an online platform to conduct the survey. To distribute the survey, an invitational email along with the online link to the survey was sent to survey respondents. In addition, to provide a preview of the questionnaire, a PDF file of the survey questionnaire was attached to the distribution email.

3.1 Survey Questionnaire

The questionnaire starts with a brief description of the research project, purpose of the survey, and instructions on how to complete the survey. It then collects the contact information of the survey respondents.

Part 1 of the survey questionnaire aims to collect information about the current practice for evaluation of bridge approach slabs and nearby pavement section in roadway embankments/retaining walls such as:

- Common distress types
- Timing of appearance of distresses after completion of the construction
- Methods to identify sections that need repairs
- Specific criterion used for making decisions for repairs
- Typical activities conducted to evaluate the conditions of bridge approach slabs and nearby pavement section in embankment/retaining walls
- Typical activities conducted to evaluate the conditions of the embankment fills
- Properties of embankment fills that need to be determined to assess their conditions
- Major contributing factors to the distresses

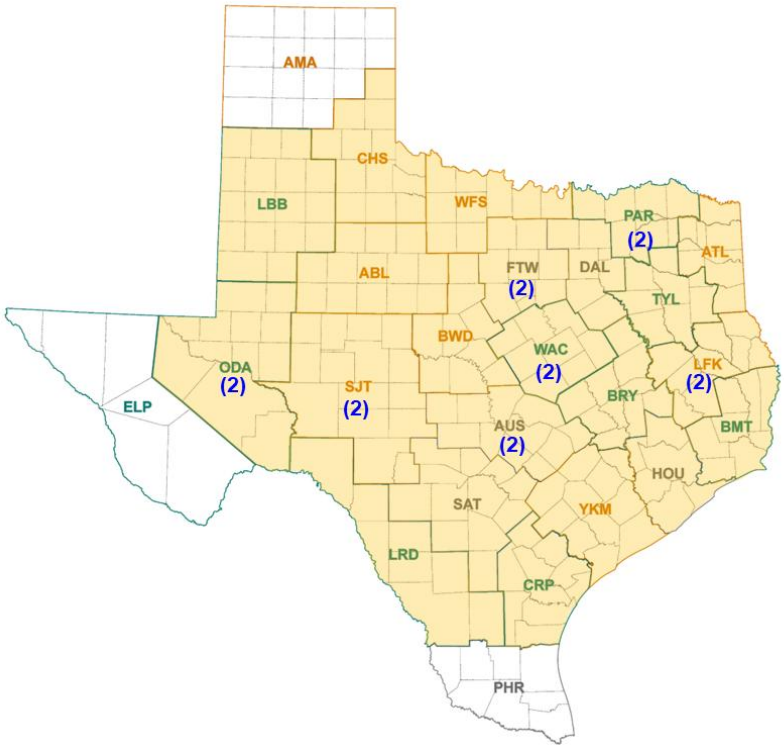
Part 2 of the questionnaire aims to collect information about the current repair practice such as:

- Common repair/maintenance measures taken
- Typical frequency of performing repairs on a previously repaired section
- Distressed sections that need a new investigation
- Sections that were previously repaired and have been performing well since then

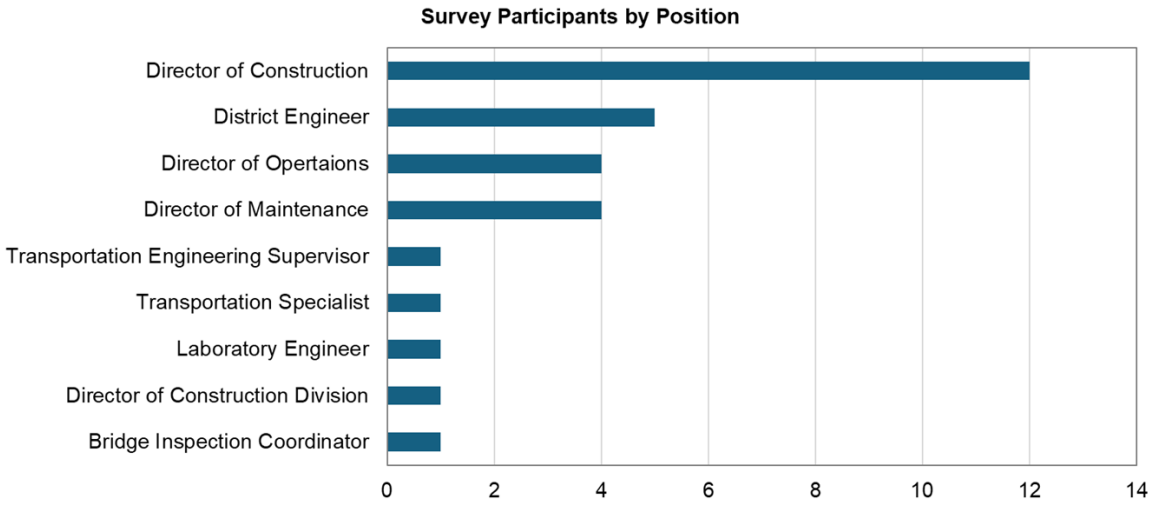
Part 3 seeks for recommendations for (i) fill materials used for embankment/retaining walls, (ii) construction practices, and (iii) repair practices to improve performance of bridge approach slabs and nearby pavement section in embankments/retaining walls.

3.2 Survey Responses

In total, 30 responses were collected from the survey. **Figure 2-5(a)** shows the districts that responded to the survey questionnaire in light yellow (the number in the parentheses indicate that two responses were provided from these districts), and **Figure 2-5(b)** presents professional positions of survey participants.



(a)



(b)

Figure 3-1. Summary of survey responses: (a) districts responded (the number in the parentheses indicate that two responses were provided from these districts) and (b) survey participants by position.

The locations of survey respondents cover 22 out of 25 TxDOT districts. As shown in **Figure 2-5(a)**, the Austin, Fort Worth, Lufkin, Odessa, Paris, San Angelo, and Waco Districts have provided two responses each. All other responding districts provided one response each. Most of the survey respondents were among directors of construction, district engineers, directors of operations, and directors of maintenance.

3.2.1 Question 1: Common distress types

Survey Question 1 asks "*What are the common problems you encountered at the bridge approach slabs (BAS) and nearby pavement structures in embankments/retaining walls? Check all that apply*," and **Figure 3-2** summarizes collected information about the common distress types.

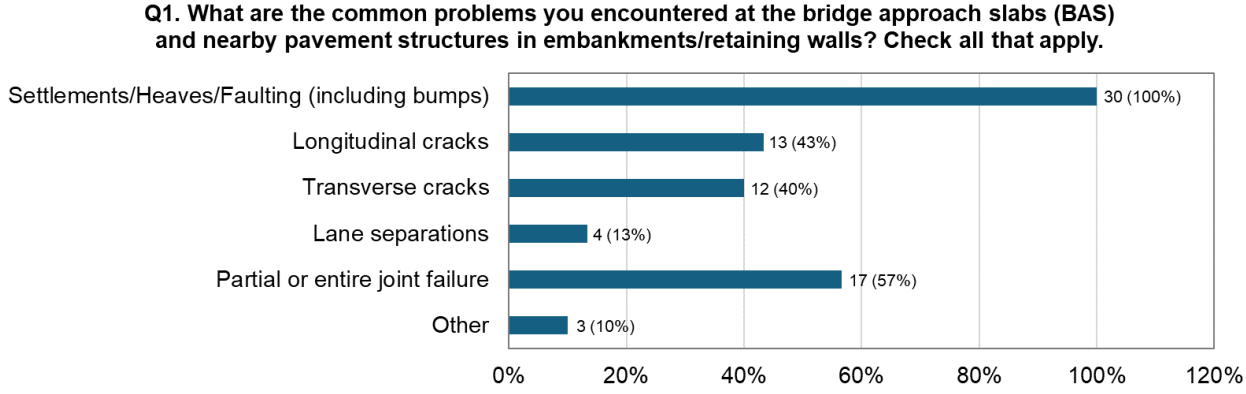


Figure 3-2. Summary of survey responses to common distress types (Question 1).

Figure 3-2 suggests that 'Settlements/Heaves/Faulting (including bumps)' is the most common distress type (100%) observed at the BAS and nearby pavement structure in embankments/retaining walls, followed by 'Partial or entire joint failure' (57%), 'Longitudinal cracks' (43%), and 'Transverse cracks' (40%). **Table 3-1** presents the survey response to Question 1 by districts.

Table 3-1. Survey response to Question 1 by districts

Distress type	Response by district
Settlements/Heaves/Faulting (including bumps)	22 (Abilene, Atlanta, Austin, Beaumont, Brownwood, Bryan, Childress, Corpus Christi, Dallas, Fort Worth, Houston, Laredo, Lubbock, Lufkin, Odessa, Paris, San Angelo, San Antonio, Tyler, Waco, Wichita Falls, and Yoakum)
Longitudinal cracks	10 (Austin, Beaumont, Bryan, Corpus Christi, Dallas, Fort Worth, Lufkin, Odessa, Paris, and Waco)
Transverse cracks	10 (Austin, Beaumont, Corpus Christi, Fort Worth, Houston, Lufkin, Paris, San Angelo, Tyler, and Waco)
Lane separations	4 (Beaumont, Fort Worth, San Antonio, and Tyler)
Partial or entire joint failure	14 (Abilene, Atlanta, Beaumont, Bryan, Dallas, Fort Worth, Houston, Lubbock, Lufkin, Odessa, Paris, San Angelo, Tyler, and Waco)
Other	3 (Austin: "Retaining wall issues"; Bryan: "Severe erosion at shoulder drain due to poor drainage off the pavement into should[er] [d]rain (if present)"; Fort Worth: "Separation of wingwalls")

3.2.2 Question 2: Timing of distress appearance

Survey Question 2 asks "*When do you typically start noticing/observing problems in bridge approach slabs or nearby pavement structures in embankments/retaining walls*," and **Figure 3-3** summarizes collected information about the timing of distress appearance.

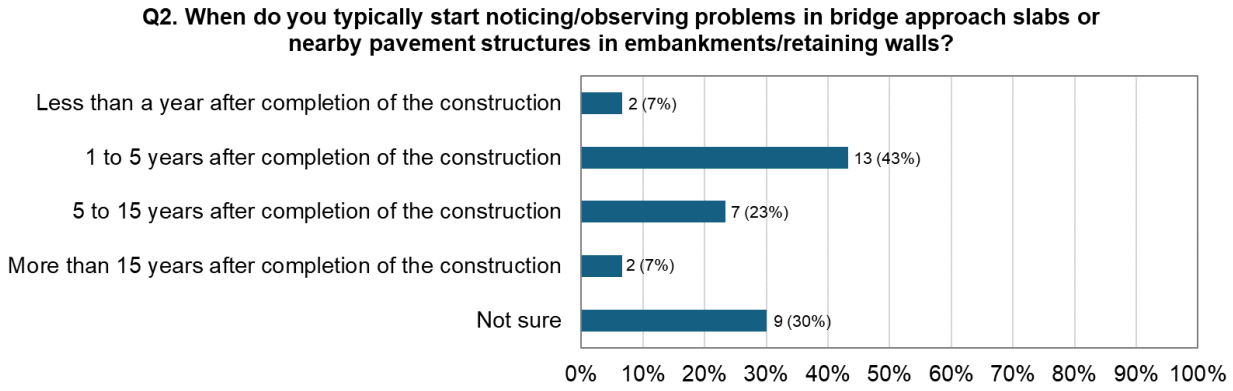


Figure 3-3. Summary of survey responses to timing of distress appearance (Question 2).

Figure 3-3 shows that 1 to 5 years after completion of the construction is the most common response (43%), followed by 5 to 15 years after completion of the construction (23%). It should be noted that 50% of the respondents indicated that they started observing problems in less than 5 years. Issues related to very long-term behavior (more than 15 years) seem to be not common (7%). **Table 3-2** presents the survey response to Question 2 by districts.

Table 3-2. Survey response to Question 2 by districts

Timing of distress appearance	Response by district
Less than a year	2 (Corpus Cristi and Odessa)
1 to 5 years	12 (Abilene, Atlanta, Beaumont, Bryan, Childress, Fort Worth, Laredo, Odessa, San Angelo, Tyler, Waco, and Wichita Falls)
5 to 15 yeas	7 (Austin, Dallas, Houston, Lubbock, Odessa, San Antonio, and Waco)
More than 15 years	2 (Lufkin and Odessa)

3.2.3 Question 3: Methods to identify sections that need repairs

Survey Question 3 asks "*How do you identify bridge approach slabs and nearby pavement sections in embankments/retaining walls that need repair? Check all that apply*," and **Figure 3-4** summarizes collected information about the methods used to identify sections that need repair.

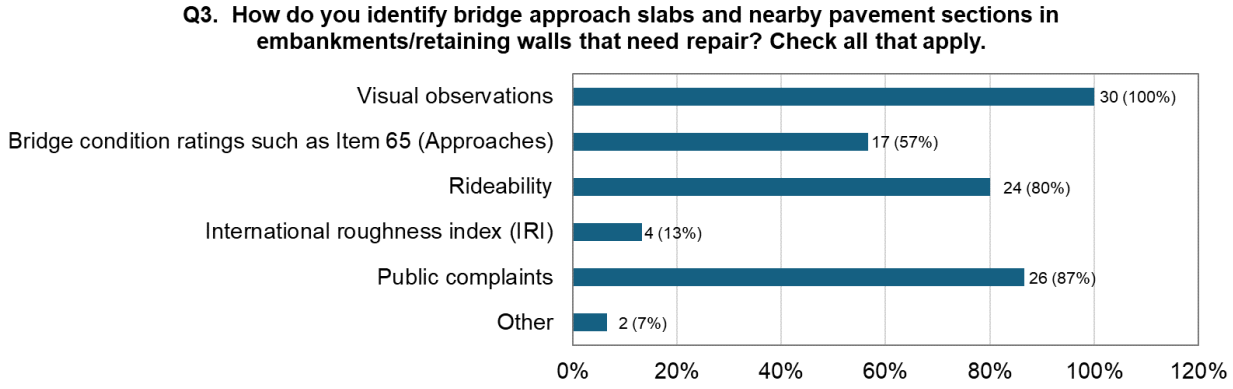


Figure 3-4. Summary of survey responses to methods to identify sections that need repairs (Question 3).

Figure 3-4 suggests that 'Visual observations' (100%), 'Public complaints' (87%), and 'Rideability' (80%) are the most common methods used by districts to identify sections that need repair. Two responses that indicated 'Other' were "MNT supervisors & district staff observing the issue" and "Field survey." **Table 3-3** presents the survey response to Question 3 by districts.

Table 3-3. Survey response to Question 3 by districts

Identification method	Response by district
Visual observations	22 (Abilene, Atlanta, Austin, Beaumont, Brownwood, Bryan, Childress, Corpus Christi, Dallas, Fort Worth, Houston, Laredo, Lubbock, Lufkin, Odessa, Paris, San Angelo, San Antonio, Tyler, Waco, Wichita Falls, and Yoakum)
Bridge condition ratings such as Item 65 (Approaches)	14 (Atlanta, Austin, Brownwood, Bryan, Corpus Christi, Fort Worth, Houston, Lubbock, Lufkin, Odessa, Paris, San Angelo, Tyler, and Waco)
Rideability	20 (Abilene, Amarillo, Atlanta, Austin, Beaumont, Bryan, Childress, Corpus Christi, Dallas, Fort Worth, Houston, Laredo, Lufkin, Odessa, Paris, San Angelo, Tyler, Waco, Wichita Falls, and Yoakum)
International roughness index (IRI)	3 (Austin, Odessa, and San Angelo)
Public complaints	21 (Abilene, Atlanta, Austin, Beaumont, Brownwood, Bryan, Corpus Christi, Dallas, Fort Worth, Houston, Laredo, Lubbock, Lufkin, Odessa, Paris, San Angelo, San Antonio, Tyler, Waco, Wichita Falls, and Yoakum)
Other	2 (Bryan: "Field survey" and Lufkin: "MNT supervisors & district staff observing the issue")

3.2.4 Question 4: Specific criterion used for making decisions for repairs

Survey Question 4 asks "*Do you have any specific criterion when making decisions for repair of bridge approach slabs and nearby pavement sections in embankments/retaining walls?*" If respondents indicated "Yes," they were then asked to specify the criterion. **Figure 3-5** summarizes the collected responses.

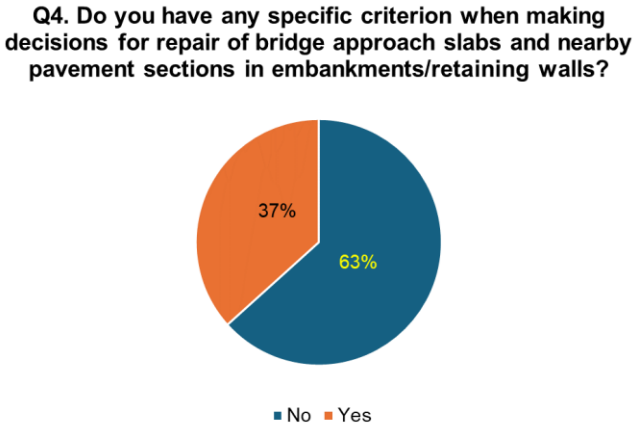


Figure 3-5. Summary of survey responses to specific criterion used for making decisions for repairs (Question 4).

As shown in **Figure 3-5**, 63% of respondents indicated that they did not have a specific criterion used for making decisions for repairs. The specific criteria from respondents who replied "Yes" to Question 4 are given below:

- "It is maintenance, we restore what was originally there with minor upgrades if possible." [Bryan]
- "Take photos, notify AE, AAE, design engr. And take them to site for visual observation and further direction" [Fort Worth]
- "If the relief joints have failed or if the cracks in the slab need to be sealed/repaired." [Fort Worth]
- "Structural integrity, safety, traffic volume and type, geotechnical conditions, and cost." [Houston]
- "We look at the past three routine inspection reports and see the change on the approach slab condition, then depending on the issue we propose repair." [Lubbock]
- "Further evaluation" [Odessa]
- "We look at the extent of erosion to determine the repairs needed. We have used the flowable fill to fill in the larger voids. We also form and pour concrete bag mix to address smaller areas to patch." [Odessa]
- "Consult w/ BRG division" [San Angelo]
- "As soon as there is a noticeable difference in the elevation of the adjacent pavement, corrections are made with a plan of action for a permanent solution if a temporary one is initially installed." [Waco]

3.2.5 Question 5: Typical activities conducted to evaluate the condition of BAS and nearby pavement structures

Survey Question 5 asks "*What activities do you conduct to evaluate the conditions of the bridge approach slabs and nearby pavement section in embankments/retaining walls? Check all that apply.*" **Figure 3-6** summarizes the collected responses.

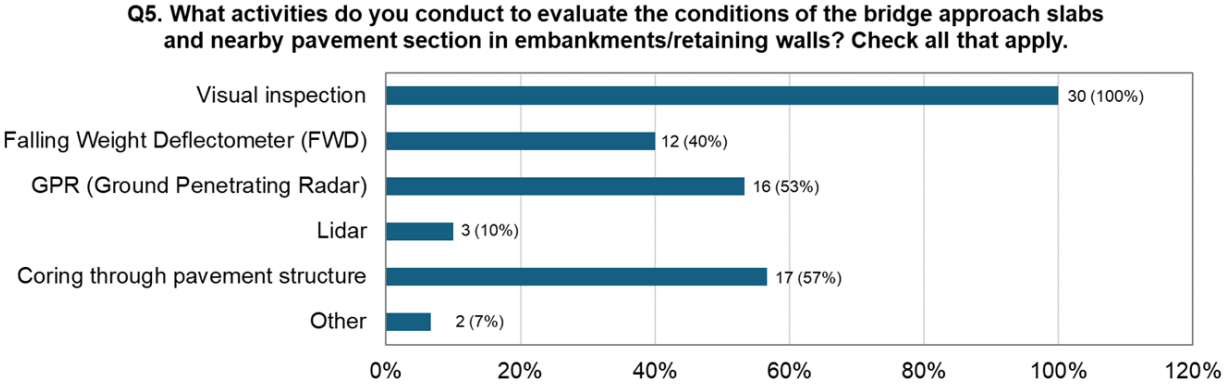


Figure 3-6. Summary of survey responses to typical activities conducted for condition evaluation of BAS and nearby pavement structures (Question 5).

Figure 3-6 shows that 100% of respondents indicated that they conducted 'Visual inspection,' followed by 'Coring through pavement structure' (57%), 'Ground Penetrating Radar' (53%), and 'Falling Weight Deflectometer' (40%) to evaluate the condition of BAS and nearby pavement structures. The two 'Other' responses were "Field survey" and "Measurement of movements of structural elements." **Table 3-4** below presents the survey response to Question 5 by districts.

Table 3-4. Survey response to Question 5 by districts

Investigation activity	Response by district
Visual inspection	22 (Abilene, Atlanta, Austin, Beaumont, Brownwood, Bryan, Childress, Corpus Christi, Dallas, Fort Worth, Houston, Laredo, Lubbock, Lufkin, Odessa, Paris, San Angelo, San Antonio, Tyler, Waco, Wichita Falls, and Yoakum)
Falling Weight Deflectometer (FWD)	10 (Austin, Brownwood, Bryan, Childress, Houston, Laredo, Odessa, Paris, San Antonio, and Waco)
GPR (Ground Penetrating Radar)	12 (Austin, Beaumont, Brownwood, Bryan, Childress, Houston, Odessa, Paris, San Angelo, San Antonio, Tyler, and Waco)
Lidar	3 (Bryan, Houston, and Odessa)
Coring through pavement structure	15 (Abilene, Austin, Brownwood, Bryan, Childress, Houston, Laredo, Lubbock, Lufkin, Odessa, Paris, San Angelo, San Antonio, Waco, Wichita Falls)
Other	2 (Austin: "Measurement of movements of structural elements" and Bryan: "Field survey")

3.2.6 Question 6: Typical activities conducted for condition evaluation of in-service embankment fills

Survey Question 6 asks "*What activities do you conduct to evaluate the conditions of the embankment fills that are already in service? Check all that apply.*" **Figure 3-7** summarizes the collected responses.

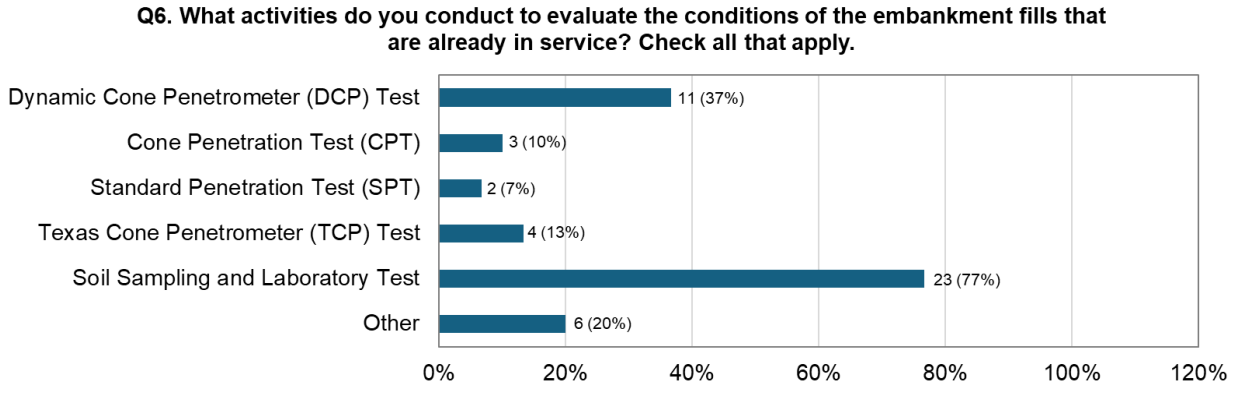


Figure 3-7. Summary of survey responses to specific criterion used for conducted for condition evaluation of in-service embankment fills (Question 6).

Most of the respondents (77%) indicated that they conducted 'Soil Sampling and Laboratory Test,' followed by 'Dynamic Cone Penetrometer Test (37%)' for the condition evaluation of embankment fills. The six 'Other' responses were:

- "None" [Abilene]
- "Normally not done to my knowledge" [Austin]
- "Field evaluation of in-situ soils if excavation/core is present and results are time-sensitive." [Bryan]
- "Unknown" [Fort Worth]
- "None" [Lubbock]
- "Not sure" [No information on District]

It should be noted that five out of six respondents who said 'Other' indicated that either no activities are conducted or they are unsure whether any activities are conducted to evaluate the conditions of in-service embankment fills. **Table 3-5** presents the survey response to Question 6 by districts.

Table 3-5. Survey response to Question 6 by districts

Investigation activity	**Response by district**
Dynamic Cone Penetrometer (DCP) Test	10 (Austin, Brownwood, Bryan, Corpus Christi, Houston, Laredo, Odessa, San Angelo, Waco, and Wichita Falls)
Cone Penetration Test (CPT)	2 (Bryan and Odessa)
Standard Penetration Test (SPT)	2 (Houston and Paris)
Texas Cone Penetrometer (TCP) Test	4 (Beaumont, Houston, Odessa, and Waco)
Soil Sampling and Laboratory Test	19 (Atlanta, Beaumont, Brownwood, Bryan, Childress, Corpus Christi, Dallas, Fort Worth, Houston, Laredo, Lufkin, Odessa, Paris, San Angelo, San Antonio, Tyler, Waco, Wichita Falls, and Yoakum)
Other	5 (Abilene, Ausin, Bryan, Fort Worth, and Lubbock)

3.2.7 Question 7: Properties of embankment fills that need to be determined to assess their conditions

Survey Question 7 asks "*What are the main properties that you want to determine for in-service embankment fills when assessing their conditions? Check up to 2 items.*" **Figure 3-8** summarizes the collected responses.

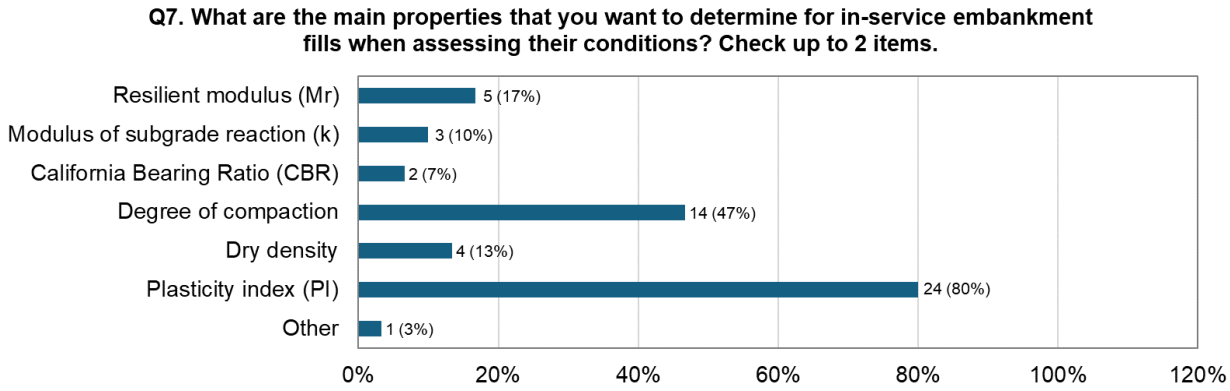


Figure 3-8. Summary of survey responses to properties of embankment fills that need to be determined to assess their conditions (Question 7).

Most of the respondents indicated that they wanted to determine 'Plasticity Index' (80%) of in-service embankment fills, followed by 'Degree of compaction' (47%), and 'Resilient modulus' (17%). The one 'Other' response was 'Not sure.' **Table 3-6** presents the survey response to Question 5 by districts.

Table 3-6. Survey response to Question 7 by districts

Backfill property	**Response by district**
Resilient modulus (M_r)	5 (Atlanta, Corpus Christi, Waco, Wichita Falls, and San Angelo)
Modulus of subgrade reaction (k)	3 (Austin, Waco, and Paris)
California Bearing Ratio (CBR)	2 (Brownwood and Corpus Christi)
Degree of compaction	22 (Abilene, Atlanta, Austin, Beaumont, Brownwood, Bryan, Childress, Corpus Christi, Dallas, Fort Worth, Houston, Laredo, Lubbock, Lufkin, Odessa, Paris, San Angelo, San Antonio, Tyler, Waco, Wichita Falls, and Yoakum)
Dry density	4 (Abilene, Bryan, Fort Worth, and Waco)
Plasticity index (PI)	19 (Abilene, Atlanta, Austin, Beaumont, Brownwood, Bryan, Dallas, Fort Worth, Houston, Laredo, Lubbock, Lufkin, Odessa, Paris, San Angelo, San Antonio, Tyler, Waco, and Yoakum)

3.2.8 Question 8: Major contributing factors to the distresses

Survey Question 8 asks "*In your opinion, what would be the major factors contributing to the distresses of bridge approach slabs and nearby pavement in embankments/retaining walls? Check up to 3 items.*" **Figure 3-9** summarizes the collected responses.

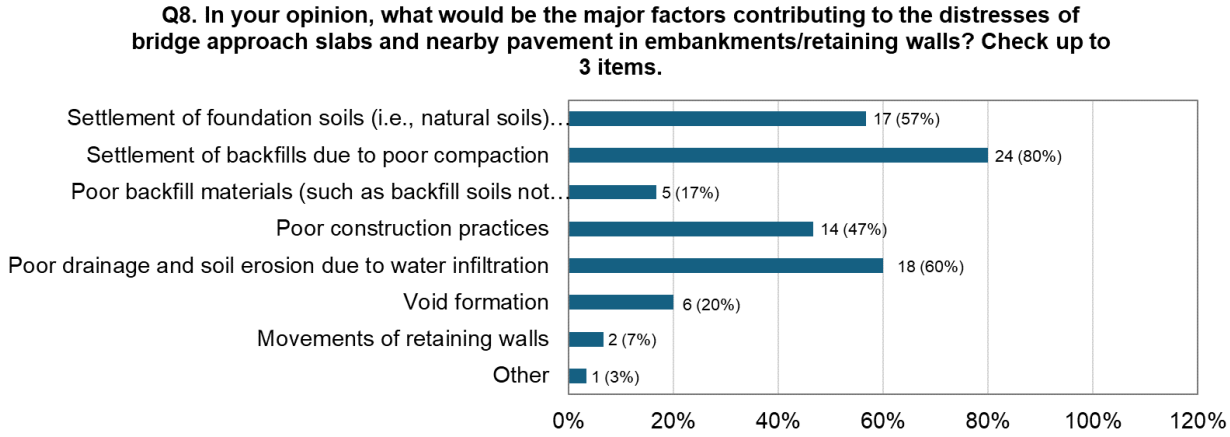


Figure 3-9. Summary of survey responses to major contributing factors to the distresses (Question 8).

Most of the respondents were of the opinion that 'Settlement of backfills due to poor compaction' was the major contributing factor to the distresses of bridge approach slabs and nearby pavement in embankments/retaining walls (80%), followed by 'Poor drainage and soil erosion due to water infiltration' (60%), 'Settlement of foundation soils (i.e., natural soils) beneath the embankment/retaining wall' (57%), and 'Poor construction practices' (47%). Furthermore, 20% of the respondents indicated the 'Void formation' as the major factor. Considering that the void formation is often the result of washout of fill materials due to water infiltration, the distresses associated with water infiltration (poor drainage and soil erosion due to water infiltration and void formation) consists of 80% the response.

Table 3-7 presents the survey response to Question 8 by districts.

Table 3-7. Survey response to Question 8 by districts

Contributing factor	Response by district
Settlement of foundation soils (i.e., natural soils) beneath the embankment/retaining wall	13 (Austin, Childress, Corpus Christi, Dallas, Fort Worth, Houston, Laredo, Lufkin, Odessa, Paris, San Angelo, Waco, and Wichita Falls)
Settlement of backfills due to poor compaction	18 (Abilene, Atlanta, Austin, Beaumont, Brownwood, Corpus Christi, Dallas, Fort Worth, Houston, Lubbock, Lufkin, Odessa, Paris, San Angelo, Tyler, Waco, Wichita Falls, and Yoakum)
Poor backfill materials (such as backfill soils not meeting specifications)	5 (Austin, Beaumont, Bryan, Paris, and San Antonio)
Poor construction practices	12 (Abilene, Atlanta, Beaumont, Corpus Christi, Fort Worth, Lufkin, Odessa, San Angelo, San Antonio, Tyler, Waco, and Yoakum)
Poor drainage and soil erosion due to water infiltration	16 (Abilene, Austin, Brownwood, Bryan, Childress, Fort Worth, Houston, Laredo, Lubbock, Lufkin, Odessa, Paris, San Angelo, Tyler, Waco, and Wichita Falls)
Void formation	6 (Atlanta, Bryan, Childress, Dallas, Fort Worth, and San Antonio)
Movements of retaining walls	1 (Lubbock)
Other	1 (Yoakum: "Poor construction practices - Not using approach slabs")

3.2.9 Question 9: Common maintenance measures taken

Survey Question 9 asks "*Please check the most common repair/maintenance measures taken in your District for bridge approach slabs and nearby pavement in embankments/retaining walls. Check up to 2 items.*" **Figure 3-10** summarizes the collected responses.

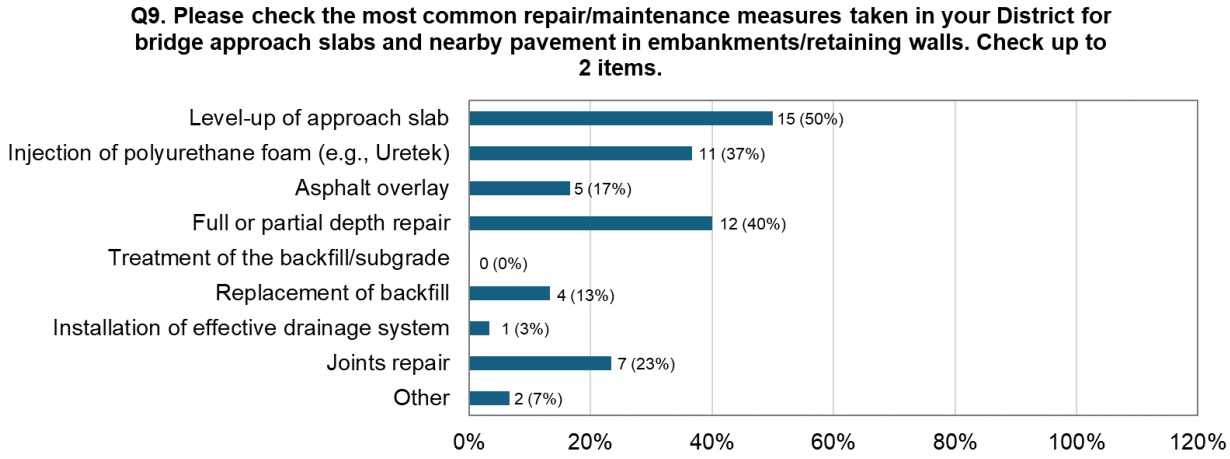


Figure 3-10. Summary of survey responses to common maintenance measures taken (Question 9).

The most common maintenance measure taken is 'Level-up of approach slab' (50%), followed by 'Full or partial depth repair' (40%), 'Injection of polyurethane foam' (37%), and 'Joints repair' (23%). **Table 3-8** presents the survey response to Question 9 by districts.

Table 3-8. Survey response to Question 9 by districts

Maintenace method	Response by District
Level-up of approach slab	14 (Abilene, Atlanta, Austin, Brownwood, Childress, Corpus Christi, Dallas, Laredo, Lufkin, Paris, San Angelo, San Antonio, Tyler, and Yoakum)
Injection of polyurethane foam (e.g., Uretek)	9 (Abilene, Austin, Beaumont, Bryan, Fort Worth, Houston, Lubbock, Waco, and Wichita Falls)
Asphalt overlay	5 (Austin, Corpus Christi, Odessa, San Antonio, and Waco)
Full or partial depth repair	11 (Atlanta, Childress, Dallas, Fort Worth, Houston, Lubbock, Lufkin, Paris, San Angelo, Wichita Falls, and Yoakum)
Treatment of the backfill/subgrade	0
Replacement of backfill	3 (Brownwood, Paris, and San Angelo)
Installation of effective drainage system	1 (Waco)
Joints repair	6 (Beaumont, Bryan, Fort Worth, Lufkin, Odessa, and Tyler)
Other	2 (Laredo and Odessa)

3.2.10 Question 10: Typical frequency of performing repairs

Survey Question 10 asks "*What is the typical frequency of performing repairs on a previously repaired section of bridge approach slabs and nearby pavement in embankments/retaining walls?*" **Figure 3-11** summarizes the collected responses.

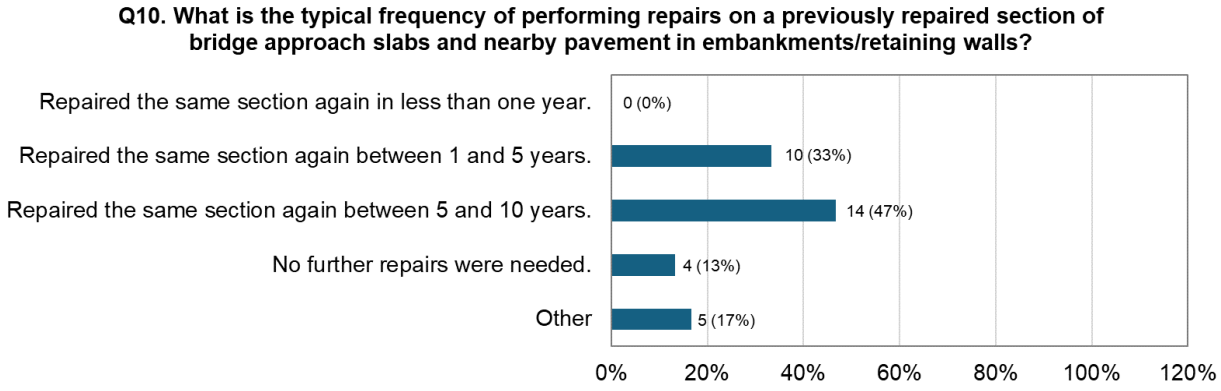


Figure 3-11. Summary of survey responses to typical frequency of performing repairs (Question 10).

About half of the respondents (47%) indicated that they repaired the same section again between 5 and 10 years after the previous repair, and 33% of the respondents indicated between 1 and 5 years. The survey results revealed that about 80% of the respondents had to repair the previously repaired sections in less than 10 years. The 'Other' responses were:

- "Level up - Repair every few years; Full depth repair - No further repairs." [Yoakum]
- "Level up can be frequent (every couple years). Uretek holds pretty well." [Austin]
- "Unknown" [Fort Worth]
- "Once voids and undermining is corrected, repairs hold up." [Odessa]

Table 3-9 below presents the survey response to Question 10 by districts.

Table 3-9. Survey response to Question 10 by districts

Repair frequency	**Response by district**
Repaired the same section again in less than one year.	0
Repaired the same section again between 1 and 5 years.	9 (Abilene, Brownwood, Dallas, Lubbock, Odessa, Paris, San Angelo, Waco, and Wichita Falls)
Repaired the same section again between 5 and 10 years.	13 (Atlanta, Austin, Bryan, Childress, Corpus Christi, Fort Worth, Houston, Lufkin, Paris, San Antonio, Tyler, Waco, and Wichita Falls)
No further repairs were needed.	4 (Beaumont, Laredo, Odessa, and San Angelo)
Other	3 (Austin: "Level up can be frequent (every couple years). Uretek holds pretty well."; Fort Worth: "Unknown"; Odessa: "Once voids and undermining is corrected, repairs hold up."; and Yoakum: "Level up - Repair every few years; Full depth repair - No further repairs.")

3.2.11 Question 11: Potential sections for new investigation

Survey Question 11 asks "*Do you have any distressed bridge approach slabs and nearby pavement sections in embankments/retaining walls that you would like the Research Team to investigate?*" If clicked "Yes," they were asked to provide approximate GPS locations of the section. A total of 10 sections were submitted from nine districts, and **Table 3-10** summarizes these sections. **Figure 3-12** shows locations of the 10 potential sections for new investigations.

Table 3-10. Potential sections for new investigation from survey Question 11

District	Highway	GPS coordinates	Remarks
Austin	SH71	30.227295, -97.776627	BAS settlement
Beaumont	US96	30.68295961, -93.89593947	Longitudinal Cracks
Dallas	US175 Ramp	32.6911, -96.6304	BAS settlement; Longitudinal cracks
Dallas	SH34	32.7514, -96.2609	BAS settlement
Fort Worth	US67	32.3863, -97.350268	Longitudinal cracks
Odessa	LP250	32.04191, -102.09603	Longitudinal and transverse cracks; BAS settlement
San Angelo	IH10	30.717432, -101.807956	Longitudinal crack; BAS settlement
San Angelo	FM1223	31.430991, -100.431393	Longitudinal cracks
San Antonio	IH10 Ramp	29.4315671, -98.5003482	BAS settlement; Longitudinal cracks
Waco	IH35	31.805507, -97.099671	Longitudinal cracks

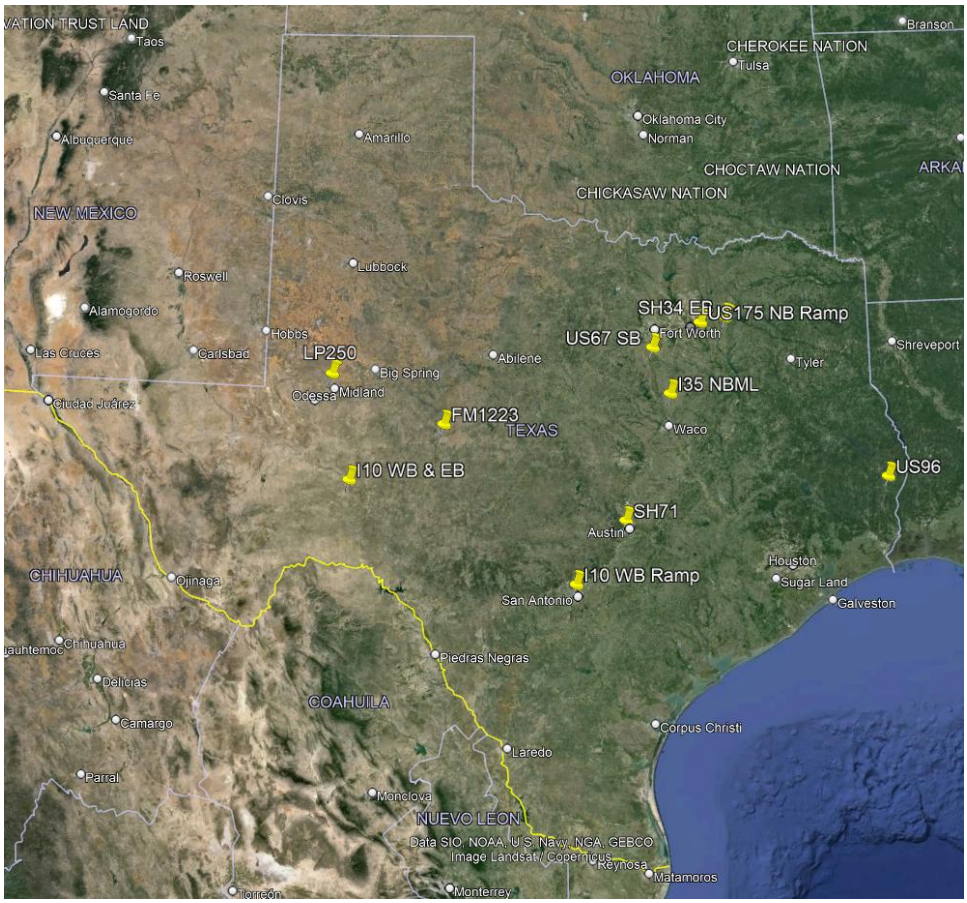


Figure 3-12. Locations of potential sections for new investigation, collected from survey Question 11.

3.2.12 Question 12: Sections that have been performing well after repair

Survey Question 12 asks "*Do you have any bridge approach slabs and nearby pavement sections in embankments/retaining walls that you previously repaired and have been performing well since then?*" If clicked "Yes," they were asked to provide approximate GPS locations of the section. A total of six sections were submitted from five districts, and **Table 3-11** summarizes these sections. **Figure 3-13** shows the locations of the six sections.

Table 3-11. Sections that have been performing well after repair from survey Question 12

District	Highway	GPS coordinates	Remarks
Childress	SH6	34.31033333, -99.7389138	
Fort Worth	US121	32.832923, -97.201484	
Houston	BW8	29.604814, -95.208025	
Laredo	IH69	27.601374, -99.517187	
Lubbock	IH29	34.1751944, -101.7506806	BASs at both southbound and northbound
Yoakum	SH35	28.629234, -96.633371	

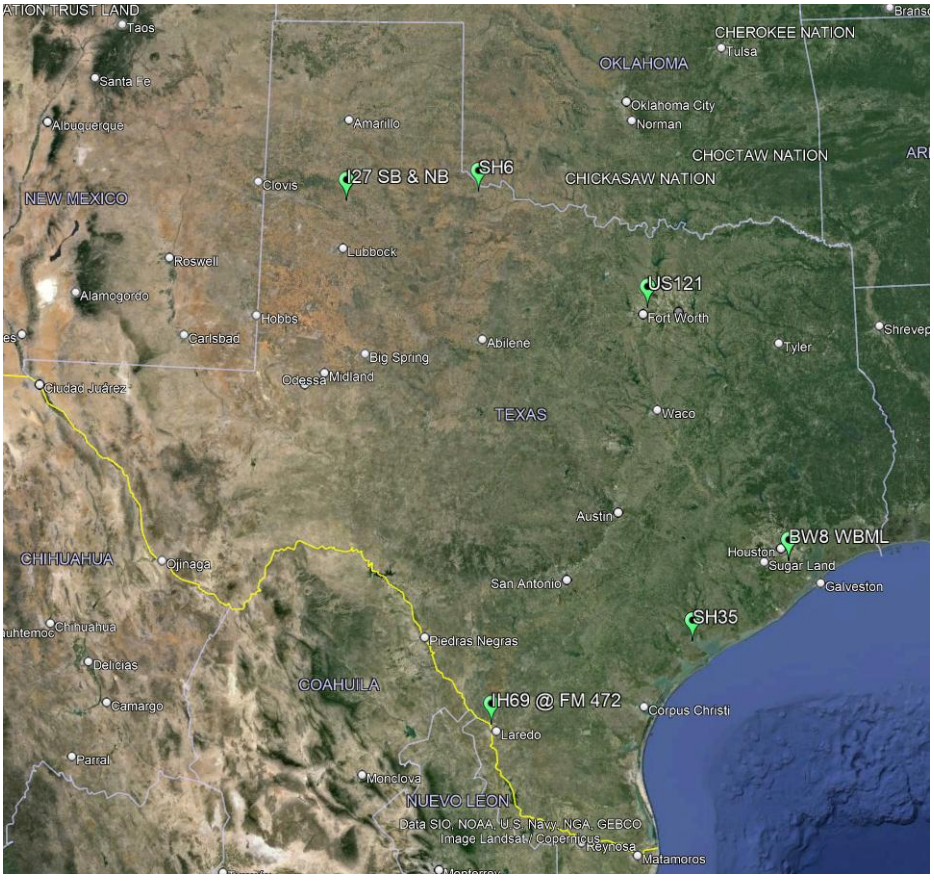


Figure 3-13. Locations of sections that have been performing well after repair, collected from survey Question 12.

The 16 sections (10 sections for potential new investigation and six sections that were previously repaired) provided by survey respondents are carefully reviewed in Chapter 4. In doing so, the Research Team has compiled comprehensive data including plan sets, construction records, historical imagery, and previous testing data, if exists, for each potential field section and then selected field test sections that encompass various types of distresses.

3.2.13 Question 13: Recommendations for fill materials for embankments/retaining walls or for construction practices

Survey Question 13 asks "*Do you have any specific recommendations (a) for fill materials for embankments/retaining walls or (b) for construction practices to further improve performance of bridge approach slabs and nearby pavement structures in embankments/retaining walls?*" Responses to Question 13 are provided below:

- "We have used flowable fill behind the abutment to help with settlement, but it has failed as well." [Abilene]
- "Embankment TY-C1. PI and gradation controlled." [Austin]
- "Use a cement stabilized sand with the CSB TxDOT Standard that is stair stepped." [Beaumont]
- "Increased testing of materials by TxDOT to confirm contractor testing and testing layers to ensure proper compaction as the area is built up." [Bryan]
- "Cement stabilized backfill or some sort of self-leveling/self compacting material." [Corpus Christi]
- "Specify select backfill material. Design/construct drainage at bridge ends." [Dallas]
- "Good select material and compaction." [Fort Worth]
- "Select materials that are stable and durable, especially in areas where there is a potential for erosion or settlement. Proper compaction. Install proper drainage systems. Ensure that embankments/retaining walls are properly designed and constructed. Regular inspection and maintenance." [Houston]
- "The spec is very vague for backfill for retaining walls, we should have standard materials." [Lufkin]
- "We are ensuring the sleeper slab is constructed as per the Cement Stabilized Abutment Backfill (CSAB) standard. We also ensure the flashing is installed between the abutment and riprap. We also ensure the approved joint sealant is applied in between the riprap, wingwall, and approach slab. We also ensure the sealed expansion joint (SEJ) is properly installed. We also limit the PI of all embankment between 6 and 15 to eliminate having blow sand material in our headers." [Odessa]
- "a) rock placement behind retaining walls. b) cement stabilized backfill behind abutments." [Paris]
- "Compacting at abutment, typically rollers stop short so need to compact with other methods near abutment. Maybe flowable fill for backfill." [San Angelo]
- "Deep flowable backfill during original construction has worked well for us." [Tyler]

- "Assure adequate drainage, ground improvement of existing ground before building large head banks and or walls to limit settlement, assess need for above standard proctor compactions for lower layers of deeper fills e.g. modified proctor to limit future settlement in larger (deeper) headers." [Waco]
- "Cement stabilized backfill works best for us, when constructed correctly." [Waco]
- "Flowable fill or cement stabilized sand." [Wichita Falls]
- "Type DS stone material in lieu of embankment." [Yoakum]

3.2.14 Question 14: Recommendations for repair practices

Survey Question 14 asks "*Do you have any specific recommendations for repair practices to further improve performance of bridge approach slabs and nearby pavement structures in embankments/retaining walls?*" Responses to Question 14 are provided below:

- "Replace approach slab." [Austin]
- "Depends on the issue." [Beaumont]
- "It seems to make more sense for us to remove settling material and replace with good material that is well compacted." [Brownwood]
- "Flowable fill is best for voids greater than 1 CF when the void is accessible from the surface. Perform forensic testing before any foam injection. The foam messes up future testing and measurements. Backfilling of cores more than 3-ft deep, within 50-ft of bridge abutments should be cement stabilized or flowable fill. Deep cores should be flowable fill. Consider drilling through abutment cap to pump flowable fill or foam injection to leave pavement structure in place." [Bryan]
- "Need good seal on MSE wall joints to prevent soil from leaching out." [Childress]
- "Use milling and overlay techniques. Pump in flowable backfill to avoid cracking the approach slab. Provide proper drainage." [Houston]
- "Our most common repair has been filling in the large voids with flowable fill. We have been successful using this repair method. We also plan to repour our approach slab and backfill underneath the full length of the approach slab." [Odessa]
- "Keep up with bridge joint maintenance." [San Angelo]
- "Do not overlay with HMAC if at all avoidable, makes it harder to monitor and evaluate, and can trap water." [Waco]
- "Foam injection works really well." [Waco]
- "Include an underdrain and/or proper drainage as well as improved stabilized material for backfill." [Wichita Falls]
- "Full-depth (12") TY B hot mix repair." [Yoakum]

3.3 Synthesis of Survey Responses

3.3.1 Current practice for evaluation of bridge approach slabs and nearby pavement section in roadway embankments/retaining walls

According to the survey results, a differential movement between BAS and bridge or between BAS and pavement, such as settlements, heaves, faulting, and bumps, was the most common distress type (100%). Failures of joints (57%), longitudinal cracks (43%), and transverse cracks (40%) were also commonly observed distress types. 50% of the respondents indicated that they started observing these distresses in less than 5 years after completion of the construction.

To identify a roadway embankment section that needs a repair, all districts mainly relied on visual observations (100%) as well as public complaints (87%), and rideability (80%). 63% of the respondents indicated that they did not have specific criteria when making decisions for repairs. 37% of the respondents reported that they had specific criteria for repair such as failure of relief joints, structural integrity of BAS and pavement structures, safety, traffic volume and type, geotechnical conditions, cost, past inspection reports, extent of erosion, and noticeable difference in elevation of the adjacent pavement.

To evaluate the conditions of BAS and nearby pavement structures, a visual inspection was the most common method (100%), followed by coring through pavement structure (57%), ground penetrating radar (53%), and FWD (40%). On the other hand, activities related to the evaluation of conditions of embankment fills were very limited. Although 77% of the respondents indicated that they took samples of fill materials and conducted laboratory tests, the survey results revealed that in-situ testing that can provide stiffness/strength of fill materials were not commonly done. 37% of the respondents indicated that they performed DCP tests, followed by 13% TCP tests, 10% CPTs, and 7% SPTs. 17% of the respondents indicated that either no activities were conducted or they were unsure whether any activities were conducted to evaluate the conditions of in-service embankment fills. When asked about the material properties of in-service embankment fills that they want to determine to evaluate the embankment condition, most of the respondents wanted to determine plasticity index (80%) of fills, followed by relative compaction (47%) and resilient modulus (17%).

Most of the respondents believed that settlement of backfills due to poor compaction was the major contributing factor to the distresses of bridge approach slabs and nearby pavement in embankments/retaining walls (80%), followed by poor drainage and soil erosion due to water infiltration' (60%), settlement of foundation soils (*i.e.*, natural soils) beneath the embankment/retaining wall (57%), poor construction practices (47%), and void formation (20%). Considering that the void formation is often caused by fill materials being washout due to water infiltration, the distresses associated with water infiltration (poor drainage and soil erosion due to water infiltration and void formation) consists of 80% the response.

3.3.2 Current practice for repair of bridge approach slabs and nearby pavement section in roadway embankments/retaining walls

The most common measure taken to repair/maintain the BAS and nearby pavement structures in roadway embankments was level-up of approach slab (50%), followed by full or partial depth repair (40%). Injection of polyurethane foam (37%) and joints repair (23%) were also commonly performed. When asked about the repair frequency, 80% of the respondents indicated that they had to repair the same section again in less than 10 years after the previous repair was completed (33% between 1 and 5 years and 47% between 5 and 10 years). Both Austin and Yoakum Districts indicated that level-up of approach slabs had to be done every few years.

3.3.3 Recommendations to improve performance of bridge approach slabs and nearby pavement section in embankments/retaining walls

Survey respondents were asked to provide any recommendations for fill materials for embankments/retaining walls or for construction practices to improve performance of bridge approach slabs and nearby pavement section in embankments/retaining walls. A total of 17 responses from 16 districts were provided, and the synthesis of the responses is presented below:

- Eight districts (Beaumont, Corpus Christi, Odessa, Paris, San Angelo, Tyler, Waco, and Wichita Falls) recommended the use of cement stabilized backfill or flowable fill at BAS. However, Abilene District noted that the flowable fill was not effective in reducing settlement.
- Eight districts (Austin, Dallas, Fort Worth, Houston, Lufkin, Odessa, Paris, and Yoakum) recommended to use more erosion-resistance fill materials or to improve TxDOT specification on fill materials. Odessa District noted that they "limit the PI of all embankment between 6 and 15."
- Five districts (Bryan, Fort Worth, Houston, San Angelo, and Waco) recommended better compaction or proper compaction control of fill materials.
- Three districts (Dallas, Houston, and Waco) emphasized the installation of adequate drainage system.
- Odessa District recommended to properly install and maintain the sealed expansion joint.
- Waco District recommended to perform ground improvement of existing ground before construction.

In response to question seeking for recommendations for repair practices, a total of 12 responses from 11 districts were provided, and the synthesis of the responses is presented below:

- Three districts (Bryan, Houston, and Odessa) recommended the use of flowable fill to fill in large voids rather than foam injection to avoid cracking, whereas Waco District noted a satisfactory performance of foam injection. Bryan District recommended to perform forensic evaluation before any foam injection because "the foam messes up future testing and measurements."

- Both Houston and Wichita Falls recommended to provide proper drainage system. Particularly, Wichita Falls District recommended including an underdrain.
- Another response (Childress District) related to water infiltration was the need for "good seal on MSE wall joints to prevent soil from leaching out." San Angelo District also recommended to "keep up with bridge joint maintenance."
- Waco District recommended to avoid the use of HMAC because it "makes it difficult to monitor and evaluate and can trap water." On the other hand, Houston District recommended milling and overlay techniques.
- Both Brownwood and Wichita Falls Districts recommended to remove settling material and replace it with improved material.
- Yoakum District recommended "full-depth (12") TY B hot mix repair."

Chapter 4 Selection of Test Sections

This chapter presents the details of potential field test sections (*i.e.*, candidate sections for field testing) and selected final test sections. For each potential field test section, comprehensive data including plan sets, construction records, maintenance history, if available, and Google historical imagery were compiled. The Research Team also conducted site visits for sections that needed further details. The Research Team then carefully reviewed the collected data to identify distress types and severities of distresses. After the review, final test sections were selected to encompass various types of distresses (or potentially different causes of poor performance) as well as various types of embankment configurations.

4.1 Potential field test sections

The research team initially identified 11 potential field test sections at the time of proposal writing based on the Research Team's previous experience. The potential sections identified in the proposal stage are named P-X-# (P-alphabet-number) format in this chapter, and their locations are shown in **Figure 4-1**.

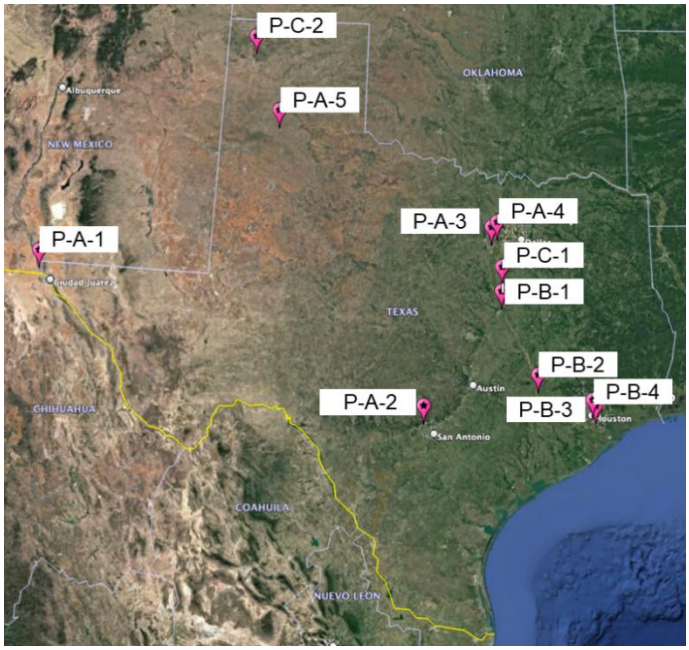
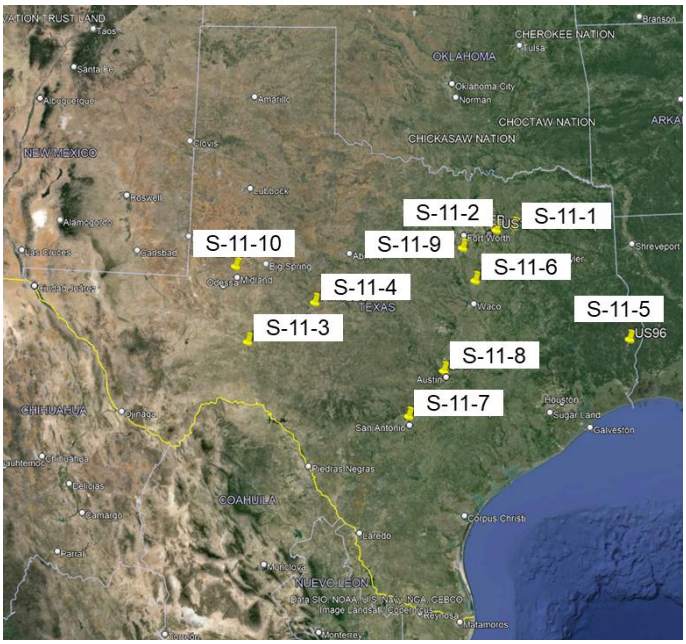


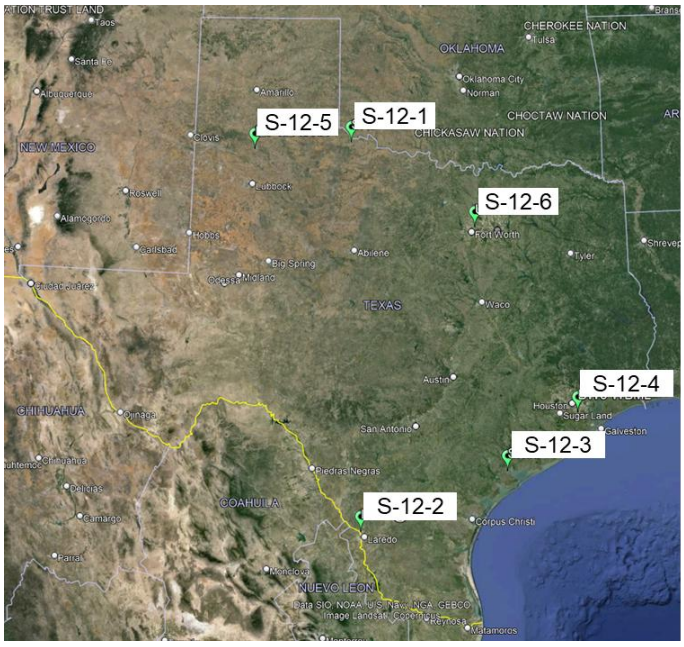
Figure 4-1. Location of potential test sections identified at the time of proposal writing

Additionally, in Chapter 3 of this project, the Research Team asked the survey respondents to provide (a) potential sections for new investigation (Survey Question 11 in Chapter 3) and (b) sections that have been performing well after repair (Survey Question 12 in Chapter 3). In response to the survey Question 11, TxDOT districts provided 10 potential sections for new investigation, and these sections are named S-11-# format in this chapter. Similarly, in response to the survey

Question 12, TxDOT districts provided six sections, and these sections are named S-12-# format in this chapter. The locations of the potential sections obtained from the survey are shown in **Figure 4-2**.



(a)



(b)

Figure 4-2. Locations of potential test sections identified from survey in response to (a) Question 11 (new section) and (b) Question 12 (sections that have been performing well after repair).

In addition to the sections that were identified in the proposal and via survey, the Research Team identified four extra sections that could be beneficial to this project. These sections are named E-# format. Furthermore, during the review of potential test sections provided via the survey, the Research Team noticed that one section identified in the proposal (P-B-3) and another section provided from the survey (S-12-4) are the identical section, leading to a total of 30 potential field test sections. **Table 4-1** below summarizes key information of all 30 sections.

Table 4-1. A summary of potential field test sections

Section ID	District	Highway	GPS Coordinate	Year completed	Pavement type	Embank. type	Embank. height at BAS	Pavement/BAS condition	Distress Type
(i) Sections identified in the proposal									
P-A-1	El Paso	SH-178	31°52'45.8"N 106°36'20.2"W	2000	Rigid - CRCP	MSE Wall - MSE Wall	27'	Very Poor	Longitudinal cracks; Lateral movement of wall
P-A-2	San Antonio	SL-1604	29°35'14.5"N 98°37'39.6"W	1992	Flex - ACP	MSE Wall - MSE Wall & Slope - Slope	16'	Fair	Rutting in approach pavement
P-A-3	Fort Worth	IH-20	32°39'51.0"N 97°19'52.2"W	1992	Rigid - CRCP	Retaining Wall - Slope	17'	Very Poor	Settlement; Longitudinal crack
P-A-4	Fort Worth	IH-820	32°45'13.4"N 97°13'00.4"W	1991	Rigid - CRCP	MSE Wall - MSE Wall	16'	Very Poor	Excessive settlement

P-A-5	Lubbock	IH-27	34°34'34.0"N 101°47'37.8"W	1988	Rigid - CRCP	Slope - Slope	32'	Very Poor	Longitudinal crack; Concrete pavement delamination and spalling
P-B-1	Waco	IH-35	31°33'58.2"N 97°06'57.9"W	2019	Rigid - CRCP	MSE Wall - Slope	35'	Very Poor	Voids in BAS; Longitudinal cracks and faulting
P-B-2	Bryan	US-290	30°08'36.1"N 96°21'51.4"W	2013	Rigid - CRCP	MSE Wall - MSE Wall	34'	Very Poor	Longitudinal crack; Settlement
P-B-3 (S-12-4)	Houston	BW-8	29°36'17.3"N 95°12'28.9"W	1997	Rigid - CRCP	MSE Wall - Slope	20'	Very Poor	Settlement; Lane separations; MSE wall movement
P-B-4	Houston	SH-225	29°42'37.1"N 95°16'02.0"W	1970	Rigid - CRCP	Slope - Slope	32'	Very Poor	Settlement; Lane Separation; Loss of materials in joints
P-C-1	Waco	IH-35	31°58'57.2"N 97°06'35.1"W	2012	Rigid - CRCP	Slope - Slope	29'	Poor	Settlement; Longitudinal cracks

P-C-2	Amarillo	US-385	35°52'38.1"N 102°23'27.8"W	1999	Flex - ACP	Slope - Slope	28'	Poor	Settlement; Longitudinal cracks
(ii) Sections identified from the survey in Chapter 3									
S-11-1	Dallas	US-175 Ramp	32°41'28.0"N 96°37'49.4"W	1971	Rigid - CRCP	Slope - Slope	22'	Very Poor	Settlement; Longitudinal cracks
S-11-2	Dallas	TX-34	32°45'11.6"N 96°15'32.7"W	2009	Rigid - CRCP	Slope - Slope	11'	Poor	Settlement; Longitudinal cracks
S-11-3	Sheffield	IH-10	30°43'02.8"N 101°48'28.6"W	1980	Flex - ACP	Slope - Slope	17'	Poor	Settlement; Longitudinal cracks
S-11-4	San Angelo	FM-1223	31°25'51.6"N 100°25'53.0"W	1983	Flex - ACP	Slope - Slope	22'	Poor	Longitudinal cracks
S-11-5	Beaumont	US-96	30°40'58.7"N 93°53'45.4"W	2007	Rigid - CRCP	Slope - Slope	10'	Poor	Longitudinal cracks; Settlement
S-11-6	Waco	IH-35	31°48'19.8"N 97°05'58.8"W	2016	Rigid - CRCP	MSE Wall - MSE Wall	28'	Poor	Longitudinal cracks; Settlement

S-11-7	San Antonio	IH-10 Ramp	29°25'53.6"N 98°30'01.3"W	1994	Rigid - CRCP	MSE Wall - MSE Wall	16'	Poor	Longitudinal cracks; Spalling
S-11-8	Austin	US-290	30°13'38.3"N 97°46'35.9"W	1996	Flex - ACP	MSE Wall - MSE Wall	33'	Very Poor	Longitudinal cracks; Settlement; Wall Movement
S-11-9	Fort Worth	US-67	32°23'10.7"N 97°21'01.0"W	2019	Flex - ACP	Slope - Slope	12'	Fair	Longitudinal cracks; Settlement
S-11-10	Odessa	SL-250	32°02'30.9"N 102°05'45.7"W	1997	Flex - ACP	Stepped Wall - Stepped Wall	21'	Fair	Settlement; Longitudinal cracks
S-12-1	Childress	SH-6	34°18'37.2"N 99°44'20.1"W	2015	Flex - ACP	Slope - Slope	36'	Very Poor	Longitudinal cracks
S-12-2	Laredo	IH-69	27°36'04.1"N 99°31'03.6"W	2023	Rigid - CRCP	MSE Wall - MSE Wall	28'	Fair	Settlement; Longitudinal crack; Void under BAS
S-12-3	Yoakum	SH-35	28°37'45.2"N 96°38'00.1"W		Flex - ACP	Natural Ground -		Fair	Longitudinal crack

						Natural Ground			
S-12-4 (P-B-3)	Houston	BW-8	29°36'17.3"N 95°12'28.9"W	1997	Rigid - CRCP	MSE Wall - Slope	20'	Very Poor	Settlement; Lane separations; MSE wall movement
S-12-5	Lubbock	IH-27	34°10'30.8"N 101°45'01.5"W		Rigid - CRCP	MSE Wall - MSE Wall		Fair	New construction rather than repair
S-12-6	Fort Worth	SH-121	32°49'58.5"N 97°12'05.3"W		Rigid - CRCP	MSE Wall - MSE Wall		Very Poor	Settlement; Diagonal cracks; Lateral movement in MSE Wall
(iii) Extra sections identified									
E-1	Lubbock	IH-27	33°38'35.6"N 101°50'08.8"W	1978	Rigid - CRCP	Slope - Slope	31'	Very Poor	Longitudinal crack; Spalling: Settlement (Lane separation in the past)
E-2	San Antonio	IH-10	29°29'41.4"N 98°32'51.3"W	2009	Rigid - CRCP	MSE Wall -	35'	Very Poor	Excessive settlement; Lane

						MSE Wall			separation; Voids
E-3	College station	SH-47	30°35'40.3"N 96°23'30.2"W	2014	Flex - ACP	MSE Wall - MSE Wall	30 ft (west wall); 14 ft (east wall)	Poor	Settlement
E-4	Hillsboro	IH-35	32°00'59.5"N 97°05'45.3"W	2002	Rigid - CRCP	MSE Wall - Slope	23 ft	Very poor	Longitudinal cracks; Lateral movement of wall

As shown in **Table 4-1**, the 30 potential sections represent a range of embankment configurations, pavement structures, and distresses. Twelve sections have sloped embankments on both sides, 17 include a retaining wall on one or both sides. For sections with available information, the embankment height at the bridge approach slabs (BAS) ranges from approximately 10 ft to 36 ft. The potential sections include 20 concrete-pavement sections and 10 asphalt-pavement sections. Observed distresses include settlement, longitudinal crack, wall movements, voids, faulting, lane separation, and surface distresses like spalling and map-cracks. Among these, settlement and longitudinal cracking were the most common distress types near the BAS and adjacent pavement. Section S-12-3 does not include a BAS and appears to be constructed on natural ground or on an embankment of negligible height; therefore, it was considered less representative of the embankment conditions evaluated in this study.

The following sections summarize details of each potential section.

4.1.1 Section ID: P-A-1

4.1.1.1 Overview

Section P-A-1 consists of bridge approach slabs (BAS) and nearby pavement structures of the roadway embankment on SH 178 eastbound main lane (EBML) near Rio Grande River in El Paso, Texas. Pavement type is a continuously reinforced concrete pavement (CRCP), and the construction was completed in 2000. Detailed description and the location of Section P-A-1 is shown in **Table 4-2** and **Figure 4-3** respectively.

Table 4-2. Detailed descriptions of Section P-A-1

Attribute	Information	Notes
District & Highway	El Paso, SH-178	
CSJ	3592-01-005	
County	El Paso	
Reference Marker	RM 11+0.51	
GPS Coordinates	31°52'44.0"N 106°36'10.5"W	
Date Work Begin	02/13/1998	
Date Completed	12/15/2000	
Pavement Type	CRCP	
BAS Thickness	13-in	
Base Type	18-in Flexible Base (Type A)	
Subgrade Type	Density Control Type A	
Drainage Type	Box culvert with reinforced concrete pipe	
Embankment Height at BAS	~27-ft	
Distress Observed (Severity)	Longitudinal cracks (Severe)	

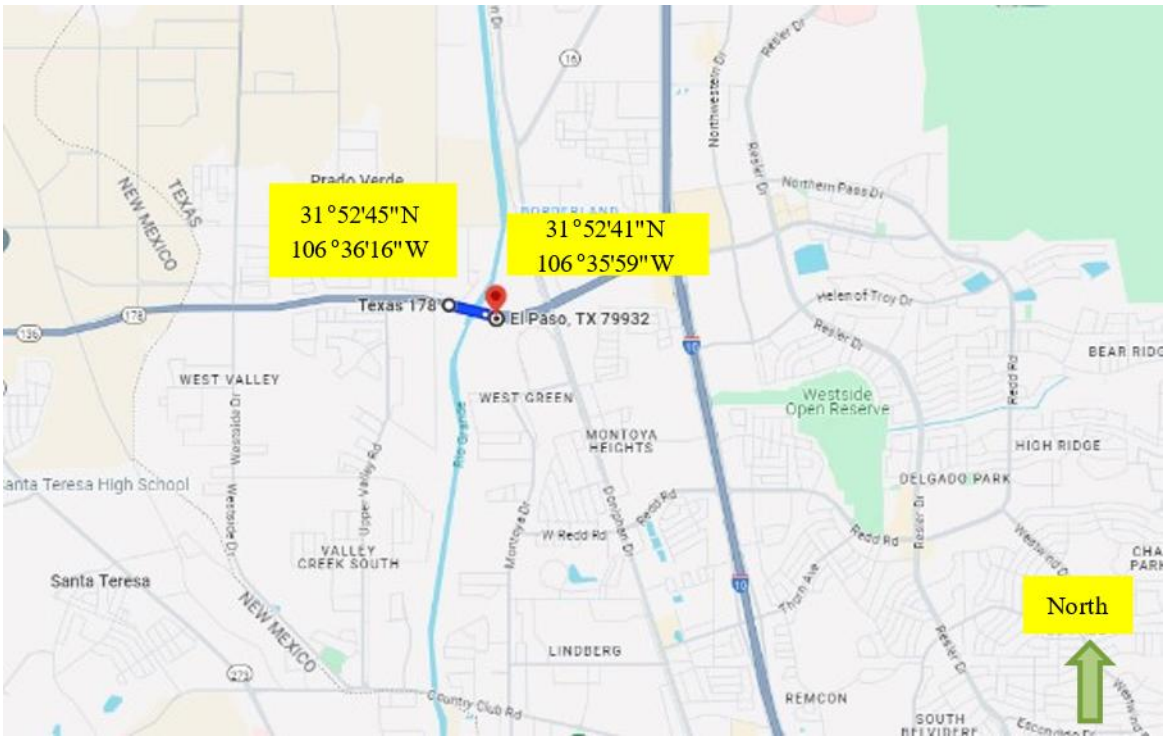


Figure 4-3. Location of Section P-A-1

4.1.1.2 Distress types

The embankment type at the location of BAS was a mechanically stabilized earth (MSE) wall, both eastbound and westbound, and the adjacent pavement structures were supported on sloped side embankment. A longitudinal crack is the major distress type observed in Section P-A-1 (see **Figure 4-4(a)** and **Figure 4-4(b)**), and the embankment appeared to exhibit lateral movement as indicated by the misalignment of the traffic rails as shown in **Figure 4-4(c)**.



(a) (b)



(c)

Figure 4-4. Observed distresses at Section P-A-1: (a) a longitudinal crack on the leave side of the subject section, (b) a longitudinal crack on the approach side of the subject section, and (c) misalignment of the traffic rail in approach side BAS.

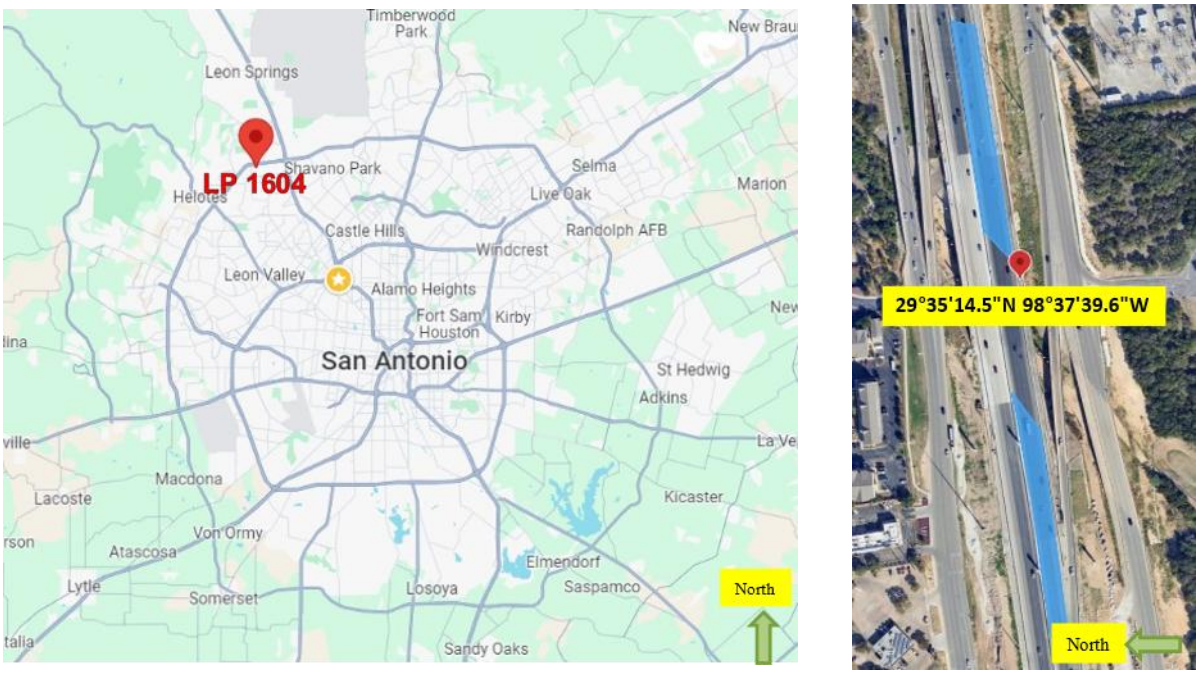
4.1.2 Section ID: P-A-2

4.1.2.1 Overview

Section P-A-2 is located on eastbound main lane of LP-1604 in San Antonio, Texas. Pavement type is an asphalt concrete pavement (ACP) with sloped side embankment on approach side and MSE wall embankment on leave side. The construction was completed in 1992. Detailed descriptions of Section P-A-2 is given in **Table 4-3**, and the location is shown in **Figure 4-5**.

Table 4-3. Detailed descriptions of Section P-A-2

Attribute	Information	Notes
District & Highway	San Antonio, LP-1604	
CSJ	2452-02-042	
County	Bexar	
Reference Marker	RM 279+0.45	
GPS Coordinates	29°35'14.5"N 98°37'39.6"W	
Date Work Begin	10/25/1990	
Date Completed	04/16/1992	
Pavement Type	1 ½-in ACP TY D	
BAS Thickness	NA	
Base Type	4-in Asphalt Stabilized Base (Gr. 4) +6-in Flex Base (TY A GR. 1)	
Subgrade Type	Embankment Ordinary Compaction TY B	
Drainage Type	Inlets & Side Drain/ Ditch	
Embankment Height at BAS	~16-ft	MSE Wall - MSE Wall in leave (east) & Slope – Slope in approach (west)
Distress Observed (Severity)	Rutting (Minor)	



(a) (b)

Figure 4-5. (a) Site location and (b) location of Section P-A-2

4.1.2.2 Distress types

Section P-A-2 has minor rutting in the pavement as illustrated in **Figure 4-6**. In addition, the Google historical imagery suggests poor performance of MSE wall at Section P-A-2 in the past, and repair work was undergoing (see **Figure 4-6(c)** and **Figure 4-6(d)**) at the time of Task 4. The pavement does not have any other significant distresses.



(a) (b)





(c) (d)

Figure 4-6. Observed distresses at section P-A-2: (a) rutting of ACP on EBML approach side, (b) rutting of ACP on EBML leave side, (c) Google historical image that suggests poor performance of MSE wall and (d) repair in progress.

4.1.3 Section ID: P-A-3

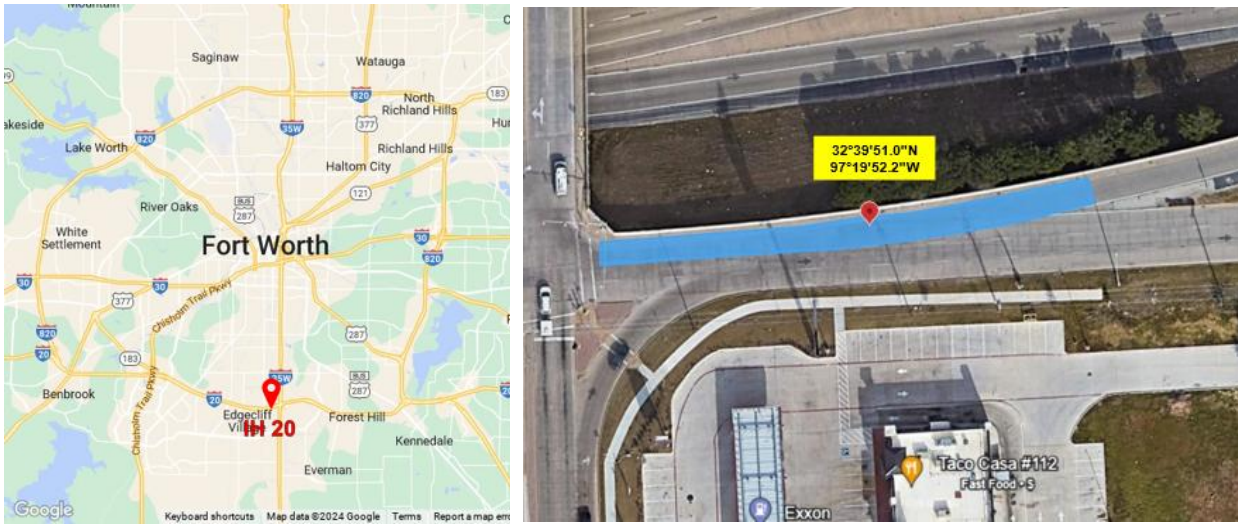
4.1.3.1 Overview

Section P-A-3 covers the pavement structure for the roadway embankment on the eastbound frontage road (EBFR) of IH-20 in Fort Worth, Texas. The pavement type is a continuously reinforced concrete pavement (CRCP), and the construction was completed in 1992. Plan sets for the construction of nearby sections were identified, but those for the subject section were not available.

Table 4-4 presents detailed descriptions of the subject section, and the location of Section P-A-3 is shown in **Figure 4-7**. The area of interest is approximately 430 ft away from the bridge approach slab.

Table 4-4. Detailed descriptions of Section P-A-3

Attribute	Information	Notes
District & Highway	Fort Worth & IH-20	
CSJ	0008-12-047	
County	Tarrant County	
Reference Marker	RM 29+0.5	
GPS Coordinates	32°39'51.0"N 97°19'52.2"W	
Date Work Begin	10/10/1988	
Date Completed	4/12/1992	
Pavement Type	No plan set available for the subject section.	
BAS Thickness	No plan set available for the subject section.	
Base Type	No plan set available for the subject section.	
Subgrade Type	No plan set available for the subject section.	
Drainage Type	No plan set available for the subject section.	
Embankment Height at BAS	No plan set available for the subject section.	
Distress Observed (Severity)	Settlement and Longitudinal crack (Severe)	

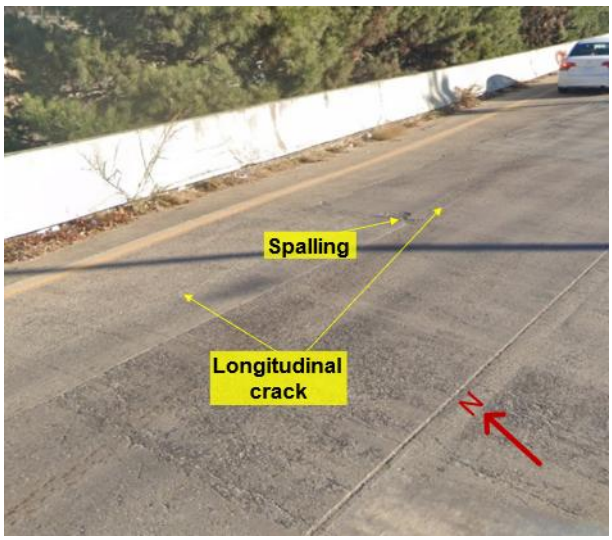


(a) (b)

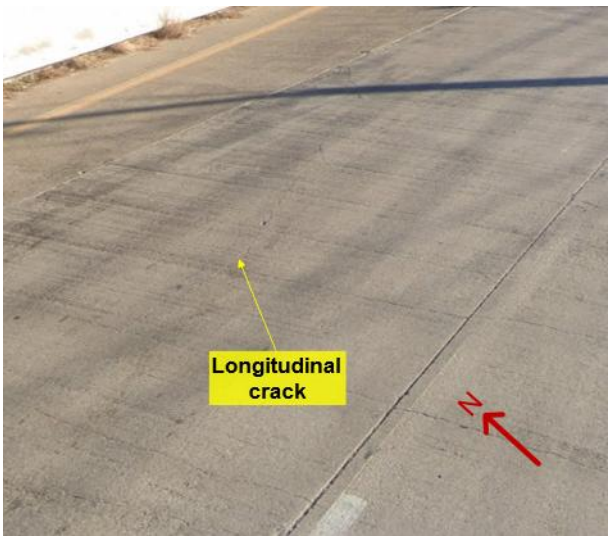
Figure 4-7. (a) Site location and (b) location of Section P-A-3

4.1.3.2 Distress types

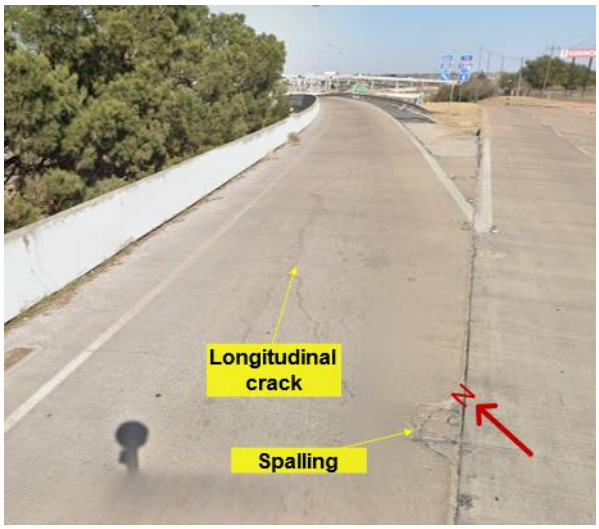
The embankment is supported by a retaining wall on the north side and the south side is built on top of gently sloping ground. Longitudinal cracks and settlement were the major distress types observed at Section P-A-3 as illustrated in **Figure 4-8**.


Spalling
Longitudinal crack
N

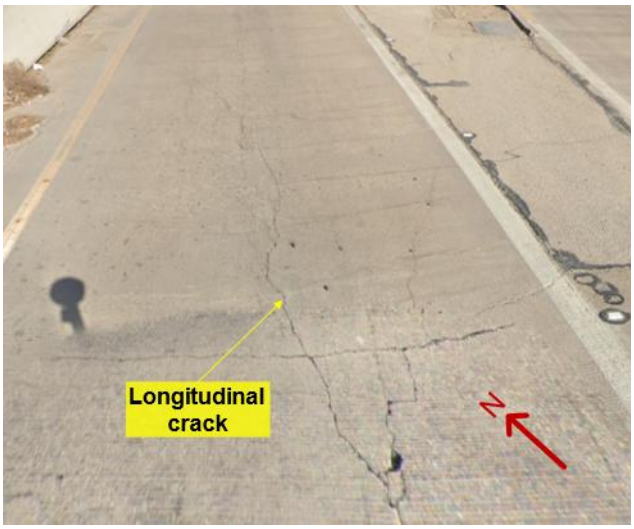
(a)


Longitudinal crack
N

(b)


Longitudinal crack
Spalling
N

(c)


Longitudinal crack
N

(d)



(e)

Figure 4-8. Observed distresses at Section P-A-3: (a) initiation of longitudinal crack on the leave side of the subject section with signs of spalling, (b) propagation of longitudinal crack on the subject section, (c) initiation of another longitudinal crack on the leave side of the subject section with signs of spalling, (d) propagation of longitudinal crack, and (e) settlement of pavement and separation from railing.

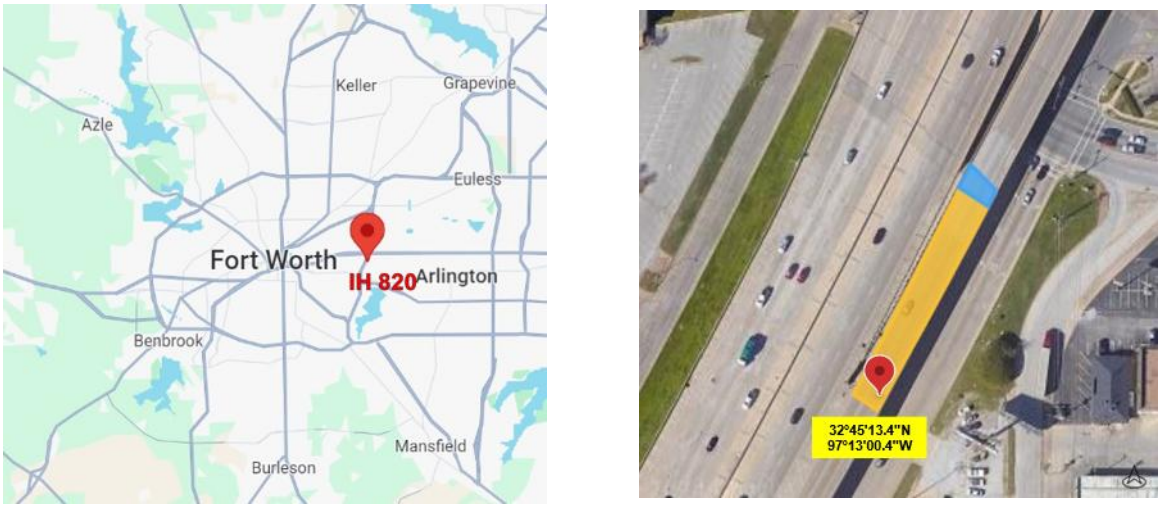
4.1.4 Section ID: P-A-4

4.1.4.1 Overview

Section P-A-4 pertains to the pavement structure for the roadway embankment on the north bound exit ramp (NBER) of IH-820 in Fort Worth, Texas. The pavement type is a continuously reinforced concrete pavement (CRCP), and the construction was completed in 1991. The embankment is supported by mechanically stabilized earth (MSE) wall on the east and west sides. The detailed description and location of Section P-A-4 are presented in **Table 4-5** and **Figure 4-9**, respectively.

Table 4-5. Detailed descriptions of Section P-A-4

Attribute	Information	Notes
District & Highway	Fort Worth & IH-820	
CSJ	0008-13-107	
County	Tarrant County	
Reference Marker	RM 29+0.5	
GPS Coordinates	32°45'13.4"N 97°13'00.4"W	
Date Work Begin	1/3/1989	
Date Completed	02/22/1991	
Pavement Type	CRCP 12-in	
BAS Thickness	10.5-in	
Base Type	2-in ACP TY. G, GR. 1	
Subgrade Type	8-in Lime Treated Subgrade	
Drainage Type	Grating Inlets	
Embankment Height at BAS	~16-ft	
Distress Observed (Severity)	Settlement (Severe); Stripping of Asphalt overlay at joints	



(a) (b)

Figure 4-9. (a) Site location of P-A-4 and (b) location of Section P-A-4

4.1.4.2 Distress types

Longitudinal crack and settlement in the BAS are the major distress observed in the section as seen in **Figure 4-10.** It appears that the pavement on top of embankment fill material settled as can be indicated by the separation of guard rails from the approach pavement as shown in **Figure 4-10.**

(a). Google historical imagery indicates that the section had multiple repair attempts through asphalt overlays to address this issue, but the excessive settlement problem still persists. Additionally, the section also exhibited spalling/stripping of asphalt overlay at expansion joint as presented in **Figure 4-10. (c)**.



(a)



(b)



(c)

Figure 4-10. Observed distresses at section P-A-4 (Google Street view image, March 2022): (a) settlement and longitudinal crack in BAS, (b) overlay in the BAS and approaching road, and (c) spalling in the BAS joint.

4.1.5 Section ID: P-A-5

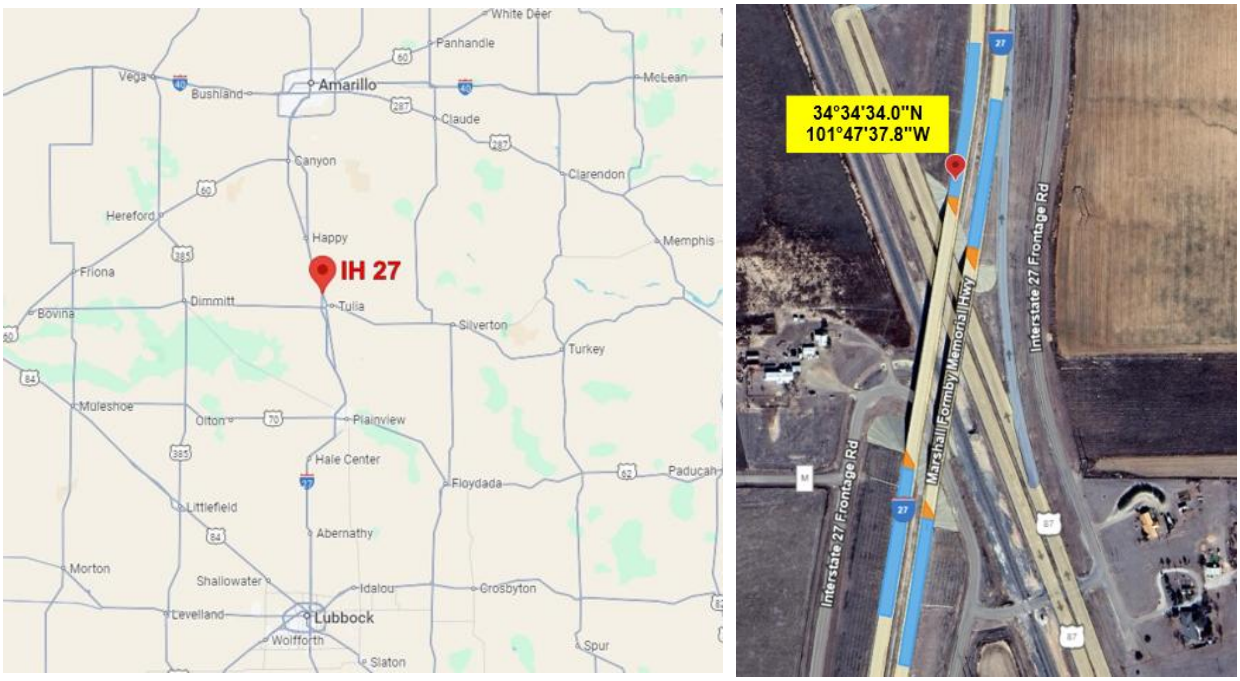
4.1.5.1 Overview

Section P-A-5 covers the bridge approach slab and the adjacent continuously reinforced concrete pavement (CRCP) on the south bound and north bound main lanes of IH-27 in Lubbock, Texas. The embankment has slopes on both sides. The construction of the section was completed in 1988.

Table 4-6 presents detailed descriptions of the subject section, and **Figure 4-11** shows the location of Section P-A-5.

Table 4-6. Detailed descriptions of Section P-A-5

Attribute	Information	Notes
District & Highway	Lubbock & IH-27	
CSJ	0067-02-031	
County	Swisher County	
Reference Marker	RM 77 + 0.90	
GPS Coordinates	34°34'34.0"N 101°47'37.8"W	
Date Work Begin	4/10/1985	
Date Completed	6/24/1988	
Pavement Type	CRCP (9-in Thk.)	
BAS Thickness	9-in	20-ft Skewed
Base Type	6-in ASB + 6-in Flex Base (DC) (TY. F, GR. 4, CL. 2)	
Subgrade Type	2-ft Emb. Matl. With PI Less Than 25	AGGR. (GR. 4)
Drainage Type	Side Drain / Ditch (Conc. RIPRAP)	
Embankment Height at BAS	~32-ft	Slope - Slope
Distress Observed (Severity)	Longitudinal crack, repair-joint deterioration and spalling (Severe)	



(a) (b)

Figure 4-11. (a) Site location and (b) location of Section P-A-5.

4.1.5.2 Distress types

Severe longitudinal cracks, spalling and repair-joint deterioration are the major distresses observed in the section, especially on the south bound main lane as shown in **Figure 4-12**. Multiple patchworks can be observed via Google Street View imagery.

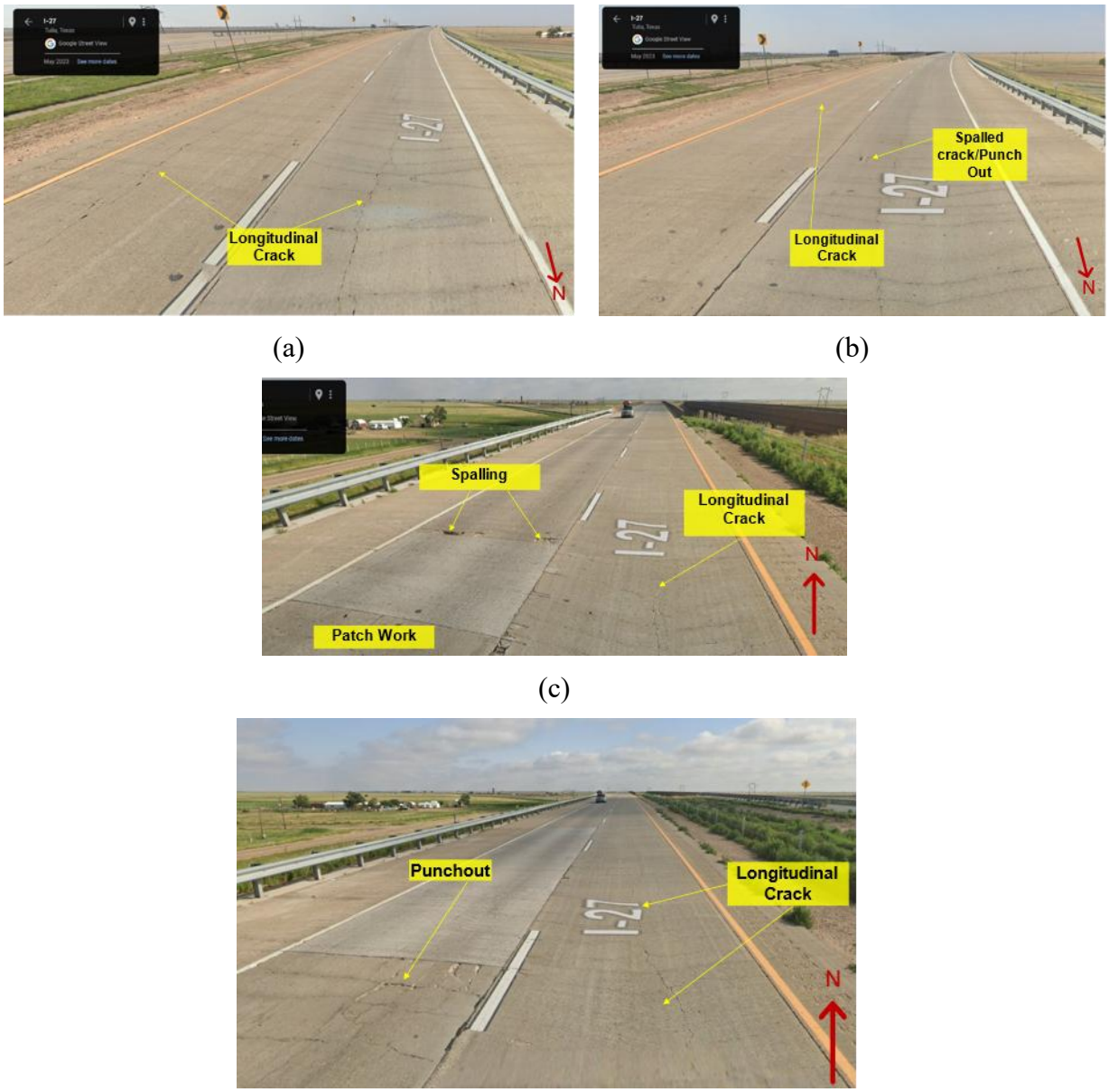


Figure 4-12. Observed distresses at Section P-A-5 (Google street view image, May 2023): (a) longitudinal crack on the approach side of SBML, (b) propagation of longitudinal crack with signs of spalling/punchout, (c) longitudinal crack with spalling and patchwork, and (d) repair-joint deterioration and longitudinal crack on the leave side of SBML.

4.1.6 Section ID: P-B-1

4.1.6.1 Overview

Section P-B-1 consists of bridge approach slabs (BAS) and nearby pavement structures of the roadway embankment on IH-35 northbound frontage road (NBFR) in Waco, Texas. Pavement type is a continuously reinforced concrete pavement (CRCP), and the construction was completed in 2019. Field evaluations of Section P-B-1 were previously conducted by TxDOT in August 2022 and by the Research Team & TxDOT in January 2023. **Table 4-7** presents detailed descriptions of the subject section, and location of Section P-B-1 is shown in **Figure 2-5.**

Table 4-7. Detailed descriptions of Section P-B-1

Attribute	Information	Notes
District & Highway	Waco, IH-35 NBFR	
CSJ	0015-01-229	
County	McLennan County	
Reference Marker	RM 335+0.867 to RM 336+0.694	
GPS Coordinates	31.566172, -97.116072	
Date Work Begin	03/09/2015	
Date Completed	08/06/2019	
Pavement Type	CRCP	
BAS Thickness	15-in (Main Lane) / 9-in (Frontage Road)	
Base Type	4-in TY-D HMA	
Subgrade Type	8-in LTS (6% Lime)	
Drainage Type	Curb & Inlets	
Embankment Height at BAS	35-ft	MSE wall - Slope
Distress Observed (Severity)	Longitudinal cracks, faulting and voids (Severe)	

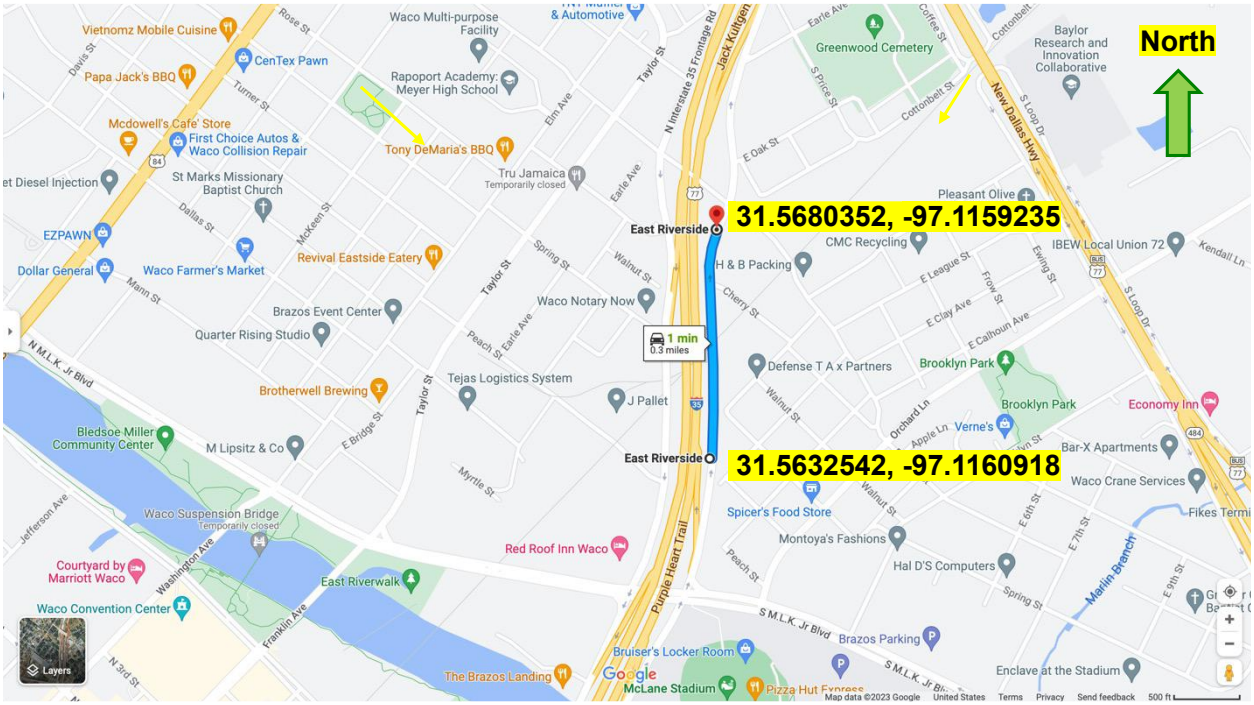
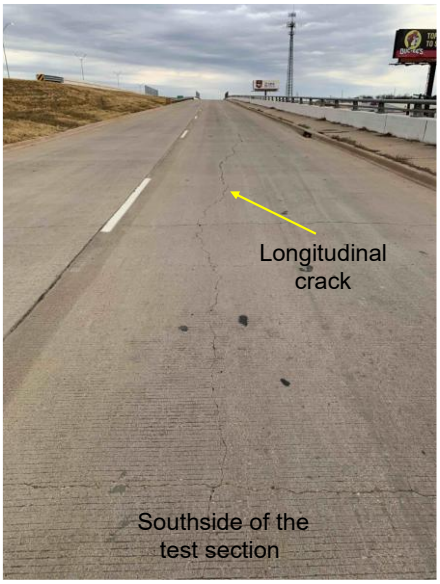


Figure 4-13. Location of Section P-B-1

4.1.6.2 Distress types

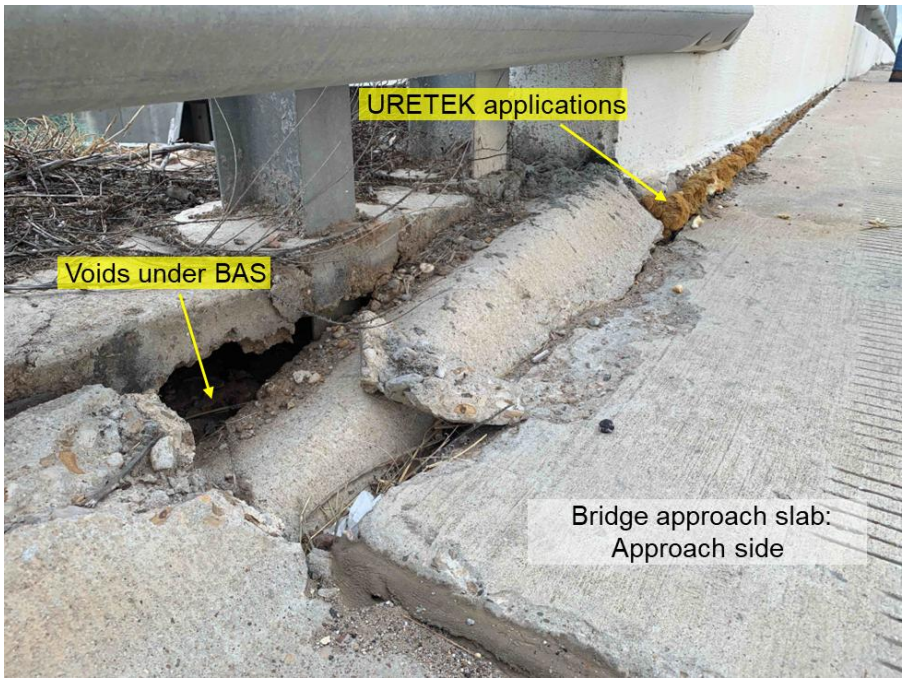
The east and west sides of the entire roadway embankment, including frontage roads and main lanes, was a mechanically-stabilized earth (MSE) wall. However, the east side of the subject section on the northbound frontage road was an MSE wall, whereas the west side was a gently sloped embankment between the main lane and frontage road. Voids in the approach side of BAS and severe longitudinal cracks nearby both approach and leave sides of the BASs were observed; faulting was also observed. The high-density polyurethane foam (HDPF) observed near the BASs indicates past repair attempts. Photos showing various distresses are presented in **Figure 4-14**. The main distress type observed in Section P-B-1 is a longitudinal crack, and its severity is very high.


Longitudinal crack
Southside of the test section

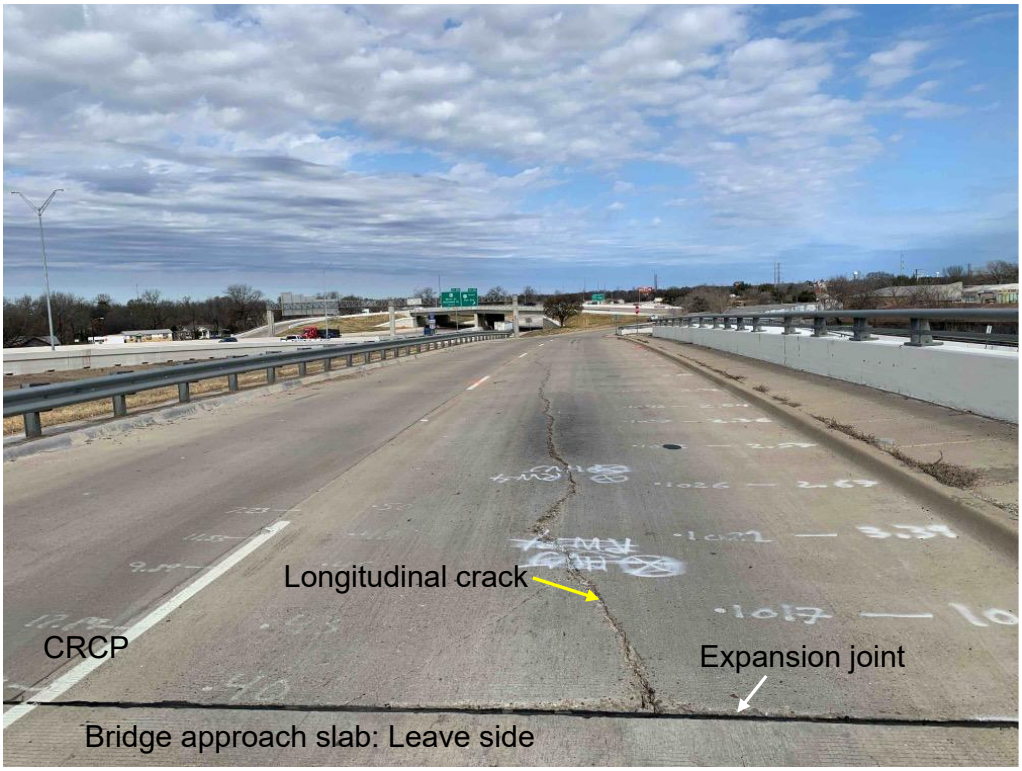
(a)


Faulting

(b)


URETEK applications
Voids under BAS
Bridge approach slab:
Approach side

(c)



(d)

Figure 4-14. Observed distresses at Section P-B-1: (a) a longitudinal crack on the southside of the subject section, (b) faulting between inside lane and edge (c), voids under the approach side of BAS and signs of HDPF applications in the past, and (d) a severe longitudinal crack in CRCP nearby the leave side of BAS

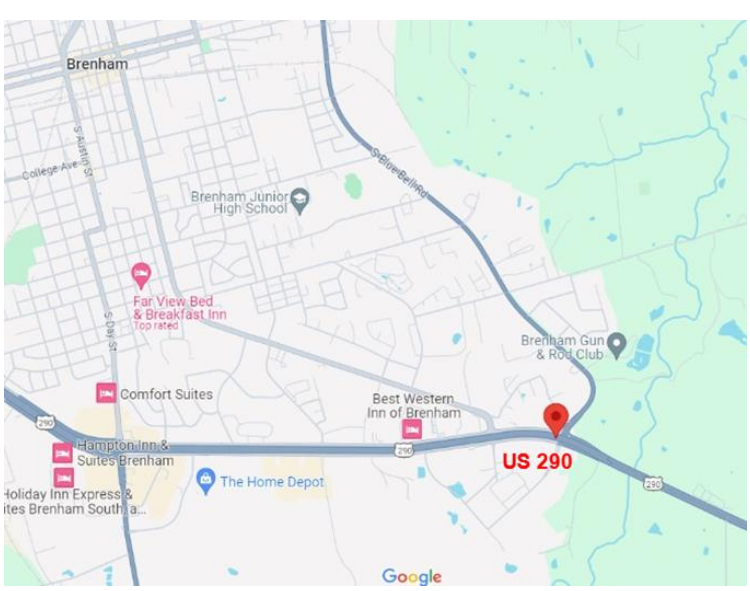
4.1.7 Section ID: P-B-2

4.1.7.1 Overview

Section P-B-2 encompasses the bridge approach slab and the adjacent pavement structure on the east bound and west bound main lanes of US-290 in Brenham, Texas. The embankment has MSE walls both on north and south sides. The construction of the section was completed in 2013. Field evaluations of Section P-B-2 were previously conducted by TxDOT prior to the beginning of this research project. Additional field evaluations were conducted by TTU in February 2024 and May 2024 during a repair process. **Table 4-8** presents detailed descriptions of Section P-B-2, and **Figure 4-15** shows the location of the subject section.

Table 4-8. Detailed descriptions of Section P-B-2

Attribute	Information	Notes
District & Highway	Brenham/ Bryan & US-290	
CSJ	0186-06-066	
County	Washington County	
Reference Marker	RM 672+1.622 MI to RM 676+1.074 MI	
GPS Coordinates	30°08'36.1"N 96°21'51.4"W	
Date Work Begin	04/25/2011	
Date Completed	12/17/2013	
Pavement Type	CRCP 11.5-in	
BAS Thickness	13-in	
Base Type	1-in TY D ACP + 6-in Cement TRT Base W/ Prime	
Subgrade Type	8-in TRT SUBGR	
Drainage Type	Inlets @ Median	
Embankment Height at BAS	34-ft	MSE Wall - MSE Wall
Distress Observed (Severity)	Longitudinal crack and Settlement (Severe)	



(a)



(b)

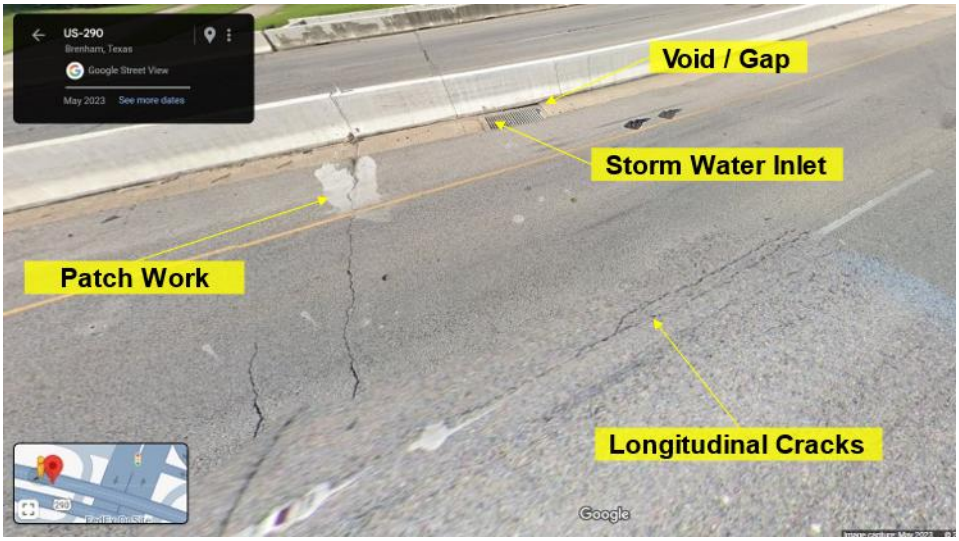
Figure 4-15. (a) Site location and (b) location of Section P-B-2

4.1.7.2 Distress types

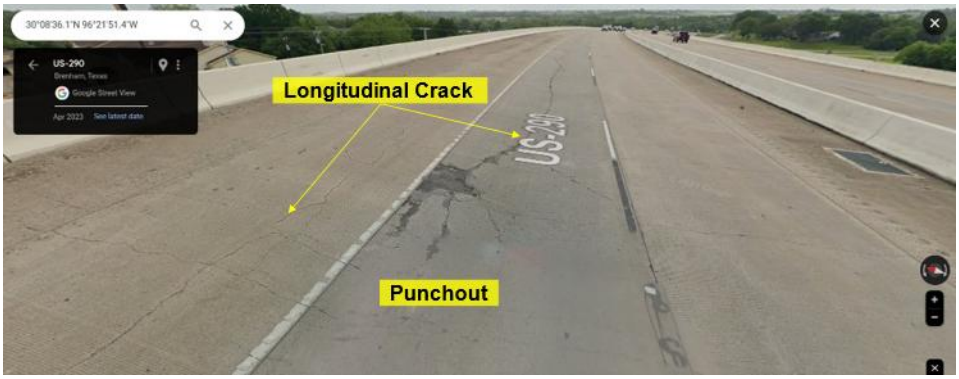
Figure 4-16. presents the distresses in Section P-B-2 before the major repair process was conducted in 2024. There were severe settlements in the BAS and the approach pavement as seen in **Figure 4-16.**(a). The settlement of pavement was more significant near drainage inlet as seen in **Figure 4-16.**(b). The section also included severe longitudinal cracks and spalling in the pavement as shown in **Figure 4-16.** Further, it can be observed from Google Street View images that there have been attempts to match the level of BAS with that of pavement through asphalt overlays; patch work were also done to address the spalling in the past.



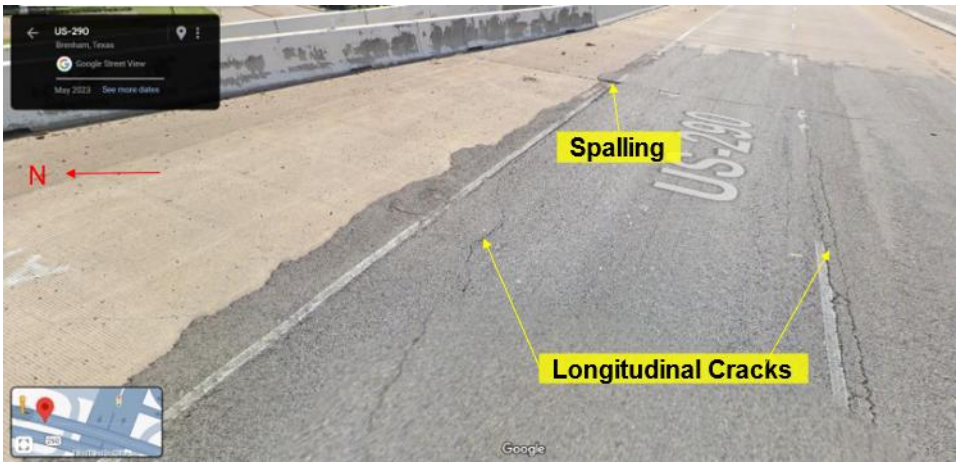
(a)



(b)



(c)



(d)

Figure 4-16. Observed distresses at section P-B-2 (Google street view image, May 2023): (a) settlement in BAS on Westbound main lane leave side, (b) pavement condition near drainage inlet, (c) longitudinal crack with punchout on the westbound main lane leave side, and (d) longitudinal crack and spalling in the BAS overlay.

4.1.8 Section ID: P-B-4

4.1.8.1 Overview

Section P-B-4 encompasses the bridge approach slab and the adjacent pavement structure on the east bound entry ramp of US 225 in Huston, Texas. The construction of the section was completed in 1970. The embankment has sloped side and concrete riprap. **Table 4-9** presents detailed descriptions of the subject section. **Figure 4-17** shows the location of Section P-B-4.

Table 4-9. Detailed descriptions of Section P-B-4

Attribute	Information	Notes
District & Highway	Houston & SH-225	
CSJ	0271-15-008	
County	Harris County	
Reference Marker		
GPS Coordinates	29°42'37.1"N 95°16'02.0"W	
Date Work Begin		
Date Completed	1970	
Pavement Type	CRCP (CL C) 8" + CSB 7" @ Edges	
BAS Thickness	NA	
Base Type	Cement Stabilized Base 6-in	
Subgrade Type	Compacted Embankment (DC) 6-in	
Drainage Type	Side Slope	
Embankment Height at BAS	~32-ft	Slope - Slope
Distress Observed (Severity)	Settlement, Lane Separation, and Joint damage (Severe)	



(a) (b)

Figure 4-17. (a) Site location and (b) location of Section P-B-4

4.1.8.2 Distress types

Section P-B-4 experienced substantial settlement in the BAS, and separation of shoulder and pavement was observed with signs of material loss from the joint as shown in **Figure 4-18(a)** and **Figure 4-18(b)**. According to the Google Street view images, a full depth repair was carried out in 2023 as shown in **Figure 4-19**.



(a)



(b)

Figure 4-18. Observed distresses at Section P-B-4 (Google street view image, Feb 2022): (a) Settlement in BAS and separation of shoulder and pavement and (b) separation of shoulder and pavement with loss of material from the joint.



Figure 4-19. New BAS and CRCP of Section P-B-4 after repair (June 2024).

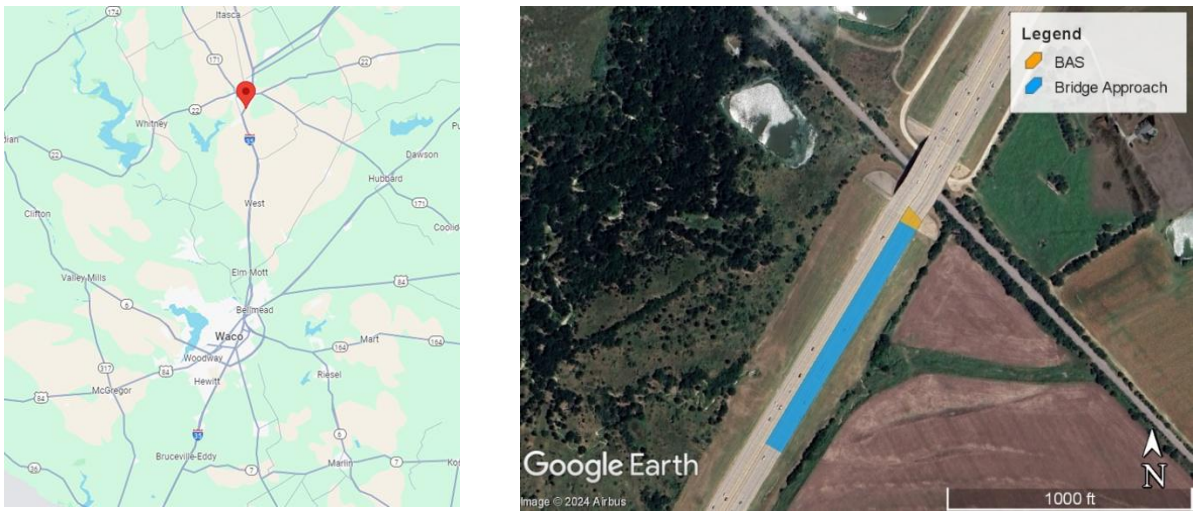
4.1.9 Section ID: P-C-1

4.1.9.1 Overview

Section P-C-1 includes the bridge approach slab and the adjacent pavement structure on the northbound main lane of IH-35 in Waco, Texas, on the approach side which was completed in 2012. This section includes 13-inch BAS and 14-inch CRCP nearby pavement structure with 4-inch Type-B HMA base atop 18-inch lime treated subgrade. The embankment features slopes on both sides. **Table 4-10** presents detailed descriptions of the subject section, and location of Section P-C-1 is shown in **Figure 4-20**.

Table 4-10. Detailed Description of P-C-1

Attribute	Information	Notes
District & Highway	Waco & IH 0035	
CSJ	0014-24-049	
County	Hill County	
Reference Marker	RM 364 + 0.110 to RM 368 + 0.316	
Project Limits	SH 81 to FM 286, ETC	
GPS Coordinates	31°58'57.2"N 97°06'35.1"W	
Date Work Begin	2/13/2006	
Date Completed	7/25/2012	
Pavement Type	14-in CRCP	
BAS Thickness	13-in	BAS-C (Skewed)
Shoulder Type	14-in CRCP	
Base Type	HMAC TY B 4-in	
Subgrade Type	18-in LTS on Existing Pavement	
Drainage Type	Side Drain	
Embankment Height at BAS	~29-ft	Slope - Slope
Distress Observed (Severity)	Settlement (Moderate)	



(a) (b)

Figure 4-20. (a) Site location and (b) location of Section P-C-1

4.1.9.2 Distress types

The major distress type for Section P-C-1 is the settlement of northbound approach BAS. This section was previously studied by Chen and Yi (2015), and they focused on the approach slabs of the right and middle lanes in the northbound direction, which had been exposed to heavy traffic for approximately then five years. No visible voids or other distress were observed alongside the bridge and riprap area at that time. However, the approach slabs experienced the maximum settlement of 2.5 inches through stringline measurement. The settlement on BAS is still present based on Google Streetview images as shown in **Figure 4-21**.



Figure 4-21. Settlement of P-C-1 northbound approach BAS

4.1.9.3 Repair history

In March 2012, a polyurethane-foam injection was conducted to address settlement issues at the bridge approach, as detailed by Chen and Yi (2015). Following the polyurethane-foam injection, string line measurements showed a significant reduction in settlement, with the maximum value reduced to 6.4 mm (0.25 inches), according to Chen and Yi (2015). Additionally, FWD tests were conducted at 48 locations before and after the treatment. The results indicated a reduction in deflection by more than 40% at 10 of these locations, demonstrating the effectiveness of the foam injection, as reported by Chen and Yi (2015).

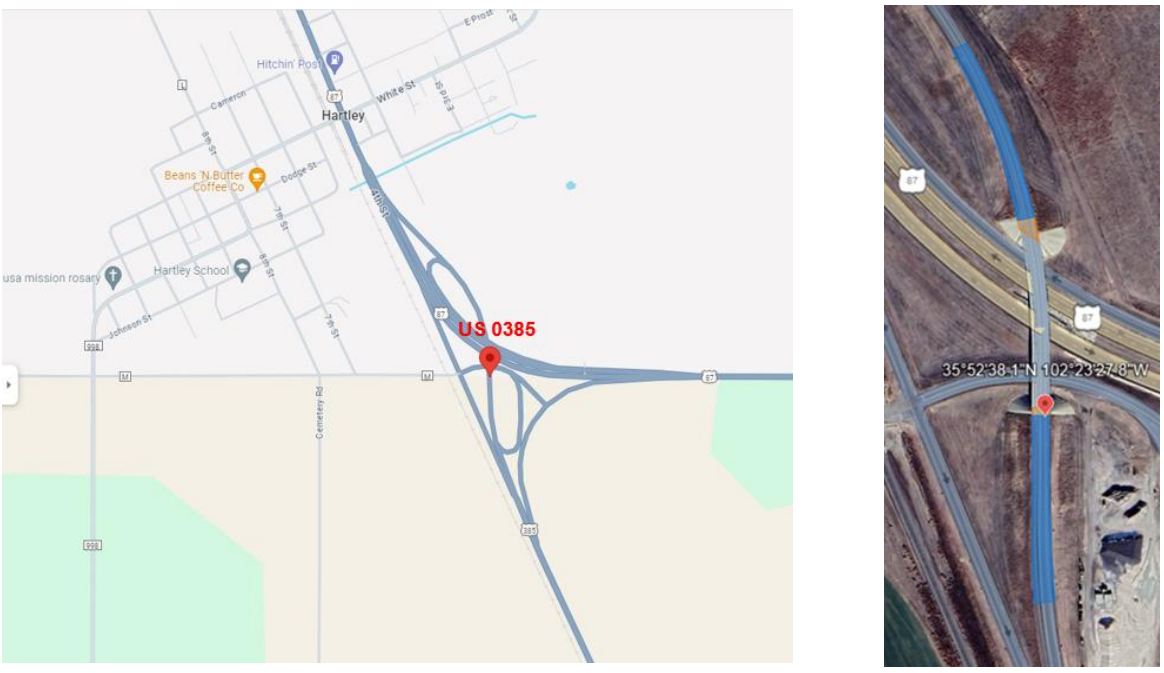
4.1.10 Section ID: P-C-2

4.1.10.1 Overview

Section P-C-2 encompasses the bridge approach slab and adjacent pavement structure on the northbound and southbound main lanes of US 385 in Amarillo, Texas, which was completed in 1999. This section includes 13-inch BAS and TY-D ACP pavement structure atop 6-inch fly ash treated subgrade. The embankment features slopes on both sides. **Table 4-11** presents detailed descriptions of the subject section, and location of Section P-C-2 is shown in **Figure 4-22**.

Table 4-11. Detailed descriptions of Section P-C-2

Attribute	Information	Notes
District & Highway	Amarillo & US-385	
CSJ	0041-01-033	
County	Hartley County	
Reference Marker	RM 46 + 0.46	
GPS Coordinates	35°52'38.1"N 102°23'27.8"W	
Date Work Begin	6/30/1998	
Date Completed	11/24/1999	
Pavement Type	1-in ACP TY D	
BAS Thickness	13-in	BAS-94
Base Type	12-in Fly Ash Treat Salvage Flex Base	
Subgrade Type	6-in Fly Ash Treat	
Drainage Type	Side Slope	
Embankment Height at BAS	~28-ft	Slope - Slope
Distress Observed (Severity)	Settlement @ BAS (Minor) and Longitudinal Cracks (Moderate)	



(a) (b)

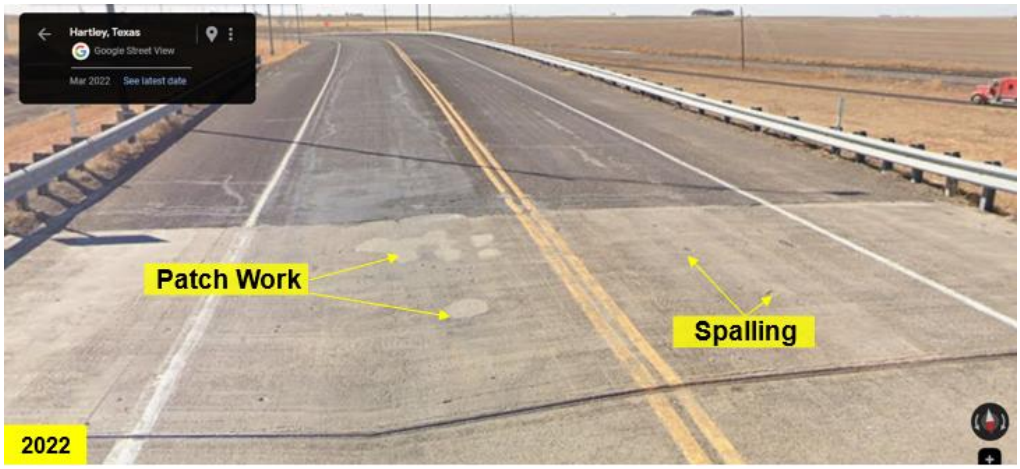
Figure 4-22. (a) Site location and (b) location of Section P-C-2

4.1.10.2 Distress types

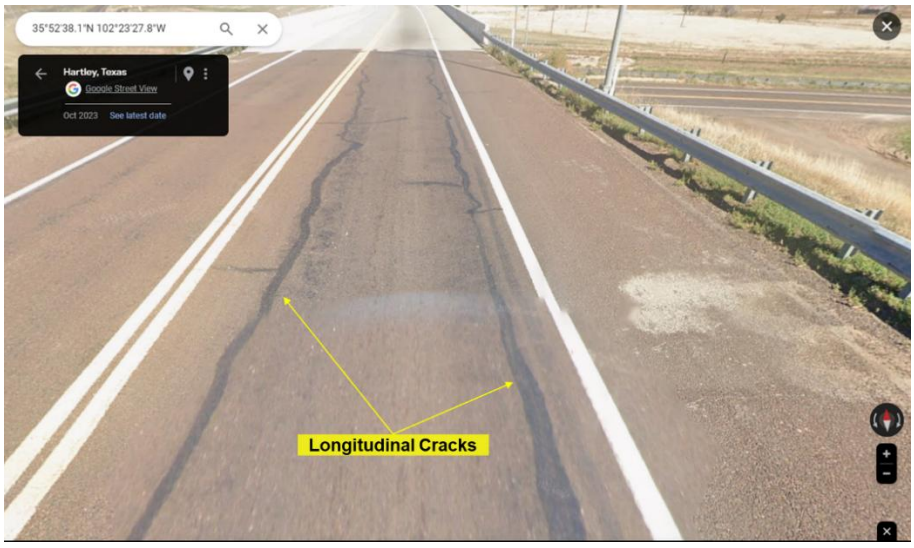
The BAS in this section has bumps, spalling and longitudinal cracks as shown in **Figure 4-23**. The pavement has substantial longitudinal cracks, especially in the north bound main lane, and minor spalling. According to Chen and Yi (2015), field evaluation of Section P-C-2 was conducted in 2010 and voids were observed beneath the BAS. Flowable fill was used to fill the void in 2010, and polyurethane-foam injection was conducted to lift the settled slab. Asphalt overlay was also done to level the pavement with BAS in 2010. Google historical images suggest that asphalt overlay was done again between 2013 and 2018 and later in 2022. Even after the multiple asphalt overlays, longitudinal cracks and spalling in the pavement are still observed.


Hartley, Texas
Google Street View
Oct 2023 See more dates
Spalling
Bump
N
2023

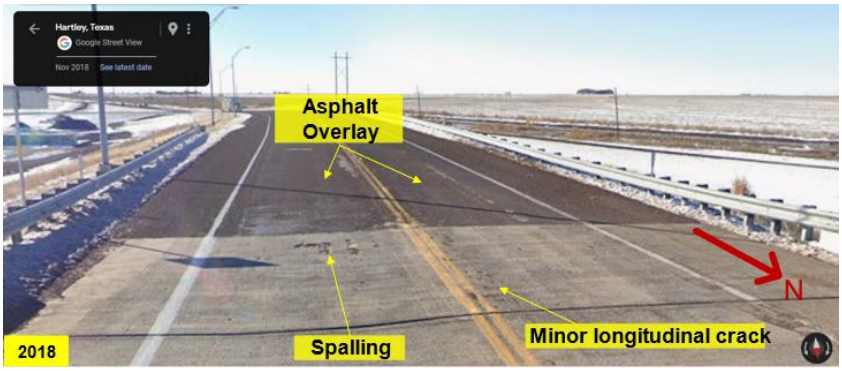
(a)


Hartley, Texas
Google Street View
Mar 2022 See latest date
Patch Work
Spalling
2022

(b)


35°52'38.1"N 102°23'27.8"W
Hartley, Texas
Google Street View
Oct 2023 See latest date
Longitudinal Cracks

(c)



(d)

Figure 4-23. Observed distresses at Section P-C-2 (Google Street View images): (a) minor bumps and spalling in the BAS, (b) patch work and spalling in the BAS, (c) longitudinal crack in the pavement, and (d) spalling and minor longitudinal crack in the BAS and asphalt overlay in the pavement

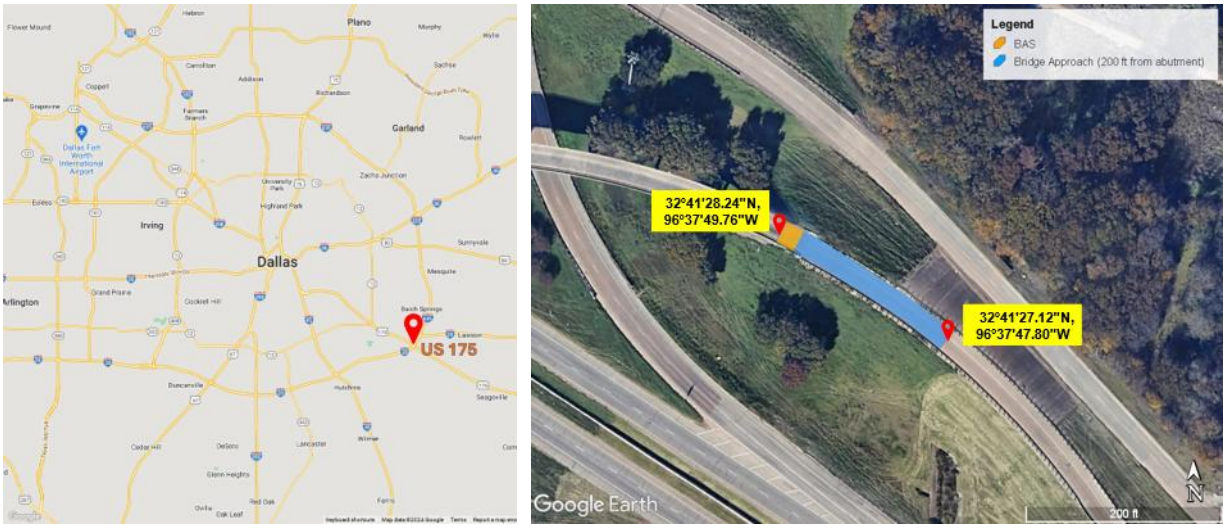
4.1.11 Section ID: S-11-1

4.1.11.1 Overview

Section S-11-1 encompasses a bridge approach slab and the adjacent pavement structure on the northbound ramp of US-175 in the Dallas district. This section, constructed in 1971, features an 8-inch continuously reinforced concrete pavement (CRCP). The embankment features slopes on both sides. **Table 4-12** and **Figure 4-24** provide a detailed descriptions and location of Section S-11-1, respectively.

Table 4-12. Detailed description of Section S-11-1

Attribute	Information	Notes
District & Highway	Dallas & US-175	
CSJ	2374-03-005	
County	Dallas	
Reference Marker	RM 600+0.3	
GPS Coordinates	32°41'28.0"N 96°37'49.4"W	
Date Work Begin	6/5/1967	
Date Completed	12/29/1971	
Pavement Type	CRCP 8-in	
BAS Thickness	9-in	
Base Type	6-in Soil Cement Base	
Subgrade Type	12-in Density control type C with top 6-in stabilized 4% Lime	
Drainage Type	Box Culvert and Pipe Culvert	
Embankment Height at BAS	22-in	
Distress Observed (Severity)	Longitudinal cracks (Moderate) and BAS settlement (Severe)	

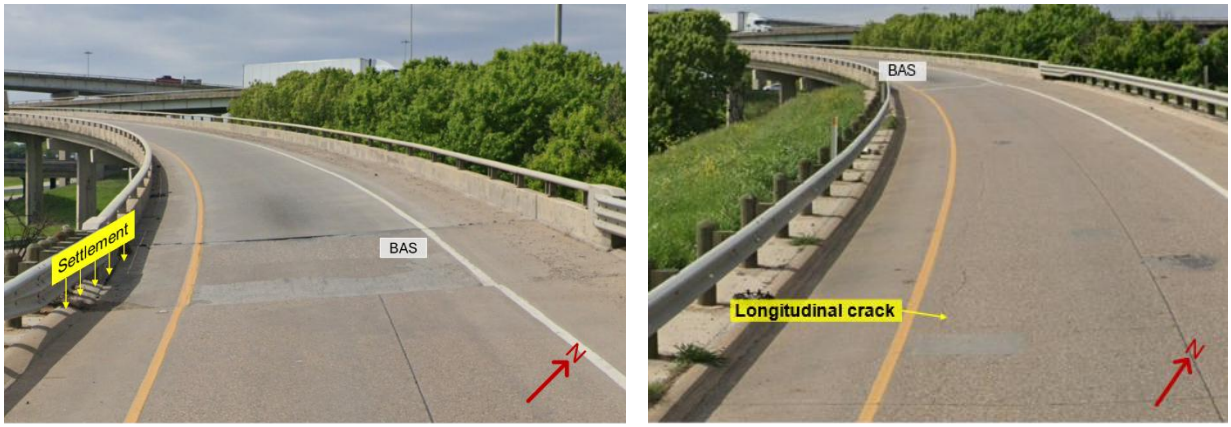


(a) (b)

Figure 4-24. (a) Site location and (b) location of Section S-11-1

4.1.11.2 Distress types

Severe settlement of bridge approach slab (BAS) and longitudinal crack in the adjacent pavement are the major distresses observed in Section S-11-1, as depicted in **Figure 4-25. Figure 4-25(a)** suggests that there have been attempts to address the settlement issue through overlays. However, recent imagery from Google Street View confirms that the settlement issue has not yet been fully resolved.



(a) (b)

Figure 4-25. Observed distresses at Section S-11-1: (a) severe settlement in bridge approach slab and (b) longitudinal cracks in the adjacent pavement (Google Street View images of March 2023).

4.1.12 Section ID: S-11-2

4.1.12.1 Overview

Located on SH34 in Terrell, Texas, Section S-11-2 comprises two bridges, each with approaches in both the northbound and southbound directions, totaling eight bridge approach slabs (BAS) and nearby pavement sections (see **Figure 4-26**). This section was constructed in 2009, featuring a 10-inch continuously reinforced concrete pavement (CRCP) for the nearby pavement and 13-inch bridge approach slabs. Section S-11-2 is subdivided into Section 1 and Section 2. The embankments are stabilized with slopes on both sides. The detailed description of Section S-11-2 is presented in **Table 4-13**.

Table 4-13. Detailed description of site S-11-2

Attribute	Information	Notes
District & Highway	Dallas, SH-34	
CSJ	0173-05-018	
County	Kaufman	
Reference Marker	RM 308 + 2.06	
GPS Coordinates	32°45'05.0"N 96°15'39.2"W	
Date Work Begin	8/21/2006	
Date Completed	7/29/2009	
Pavement Type	CRCP 10-in	
BAS Thickness	13-in	
Base Type	6-in Type B HMA	
Subgrade Type	12-in select material	
Drainage Type	Box culvert with reinforced concrete pipe and/or riprap ditch	
Embankment Height at BAS	11-ft	
Distress Observed (Severity)	BAS settlement and Longitudinal crack (Moderate)	



(a) (b)

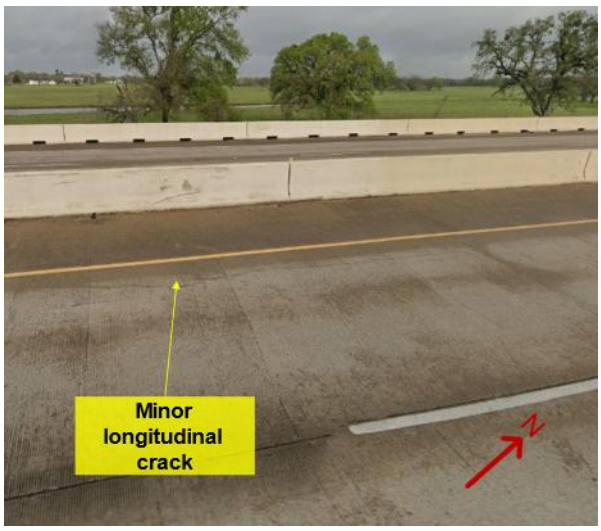
Figure 4-26. (a) Site location and (b) location of Section S-11-2

4.1.12.2 Distress types

A detailed review of Google Street View revealed excessive settlements at both the northbound approach and southbound leave bridge approach slabs (BAS) of Section 1, as depicted in **Figure 4-27(a)** and **Figure 4-27(b)**. Additionally, a longitudinal crack was observed in the nearby pavement of the northbound leave of Section 1 (**Figure 4-27(c)**). On the other hand, no significant distresses were observed in the northbound leave BAS of Section 1, the southbound approach BAS of Section 1, or in entire Section 2.



(a) (b)



(c)

Figure 4-27. Observed distresses at Section S-11-2: (a) settlement (bump) at the northbound approach bridge approach slab (BAS), (b) settlement (bump) at the southbound leave BAS, and (c) minor longitudinal crack in the nearby pavement of the northbound leave in Section 1 (Google Street View images of March 2023).

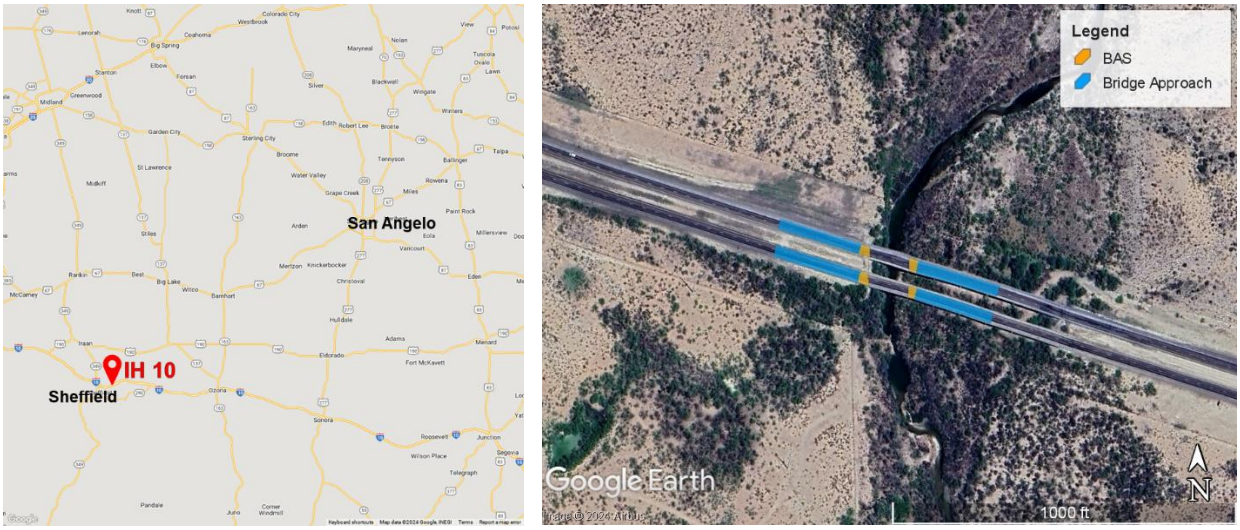
4.1.13 Section ID: S-11-3

4.1.13.1 Overview

Section S-11-3 is located on IH 10 in San Angelo, over the Pecos River, in Texas. It was constructed in 1980. It includes a 3-inch asphalt concrete pavement (ACP) atop a 15-inch type-A, grade-4 density-controlled flex base and a 9-inch-thick bridge approach slab (BAS). Further details and location of Section S-11-3 are presented in **Table 4-14** and **Figure 4-28**, respectively.

Table 4-14. Detailed description of Section S-11-3

Attribute	Information	Notes
District & Highway	San Angelo & IH-10	
CSJ	0140-13-003	
County	Crockett	
Reference Marker	RM 327+0.98	
GPS Coordinates	30°43'02.8"N 101°48'28.6"W	
Date Work Begin	11/11/1977	
Date Completed	03/09/1980	
Pavement Type	3-in ACP	
BAS Thickness	BAS-75 (MOD) 9-in Thick. 20-ft Long (Skewed)	
Base Type	15-in Flex Base (DEL) (DEN CON) (TY A GR 4 CL 1)	
Subgrade Type	Embankment Item 132 (Density 98 Min)	
Drainage Type	Slope (6:1 on Edges & 8:1 on Median)	
Embankment Height at BAS	17-ft	
Distress Observed (Severity)	BAS settlement (Minor); Longitudinal cracks (Moderate)	



(a) (b)

Figure 4-28. (a) Site location and (b) location of Section S-11-3

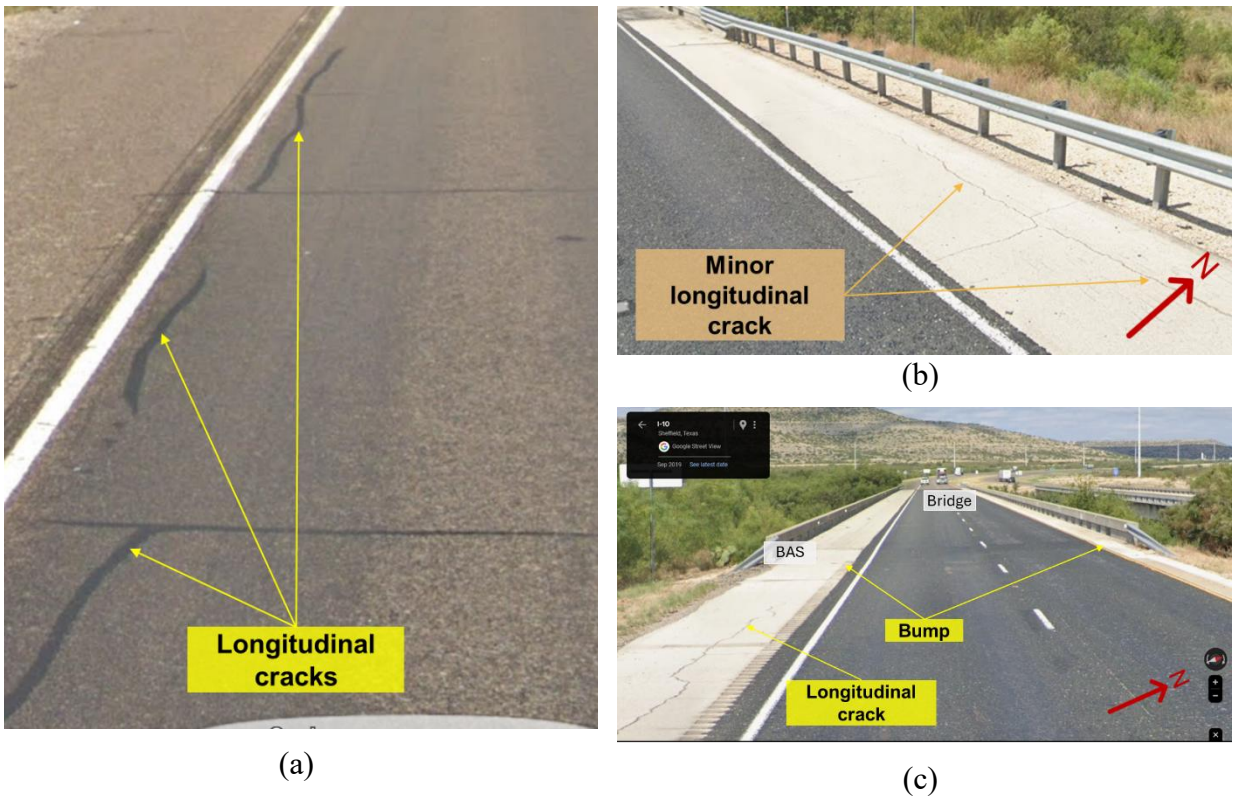
4.1.13.2 Distress types

The current condition of this section includes a settlement (bump) at the bridge approach slab (BAS) and occasional longitudinal cracks in the nearby pavement, as shown in **Figure 4-29** and **Figure 4-30**. Both the westbound approach and eastbound leave sides exhibit longitudinal cracks in the shoulder, shown in **Figure 4-30(b)** and **Figure 4-30(c)**, respectively. Similarly, minor bumps/settlements in the BAS on the westbound approach and eastbound leave sides are visible in **Figure 4-29(b)** and **Figure 4-30(c)**. A review of Google Street View images indicates multiple repair attempts with asphalt overlays, specifically between 2008 and 2011, and again in 2019, as illustrated in **Figure 4-29**.



(a) (b)

Figure 4-29. Observed distresses in WB approach side at Section S-11-3: minor bumps based on Google Street View images of (a) Sep 2019 and (b) July 2022.



(a) (b) (c)

Figure 4-30. Observed distresses in EB leave side at Section S-11-3: (a) longitudinal cracks on EB Approach Side, May 2024, (b) longitudinal cracks on WB Approach Side shoulder, and (c) bump and longitudinal crack (Google Street View images of Sep 2019)

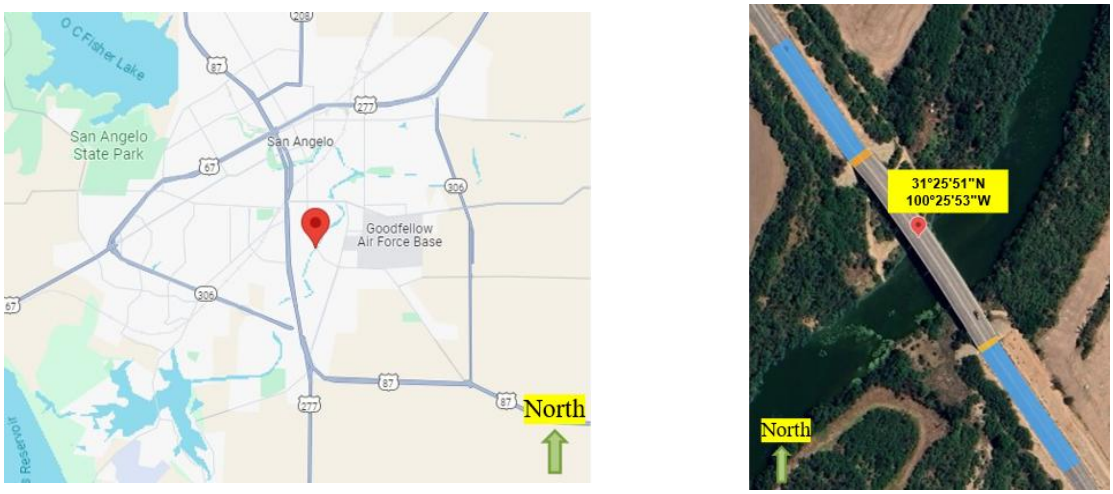
4.1.14 Section ID: S-11-4

4.1.14.1 Overview

Section S-11-4 consists of the bridge approach slab and adjacent pavement structure on the northbound and southbound main lanes of FM 1223 in San Angelo, Texas, which was completed in 1983. **Table 4-15** and **Figure 4-31** provide detailed descriptions of Section S-11-4 and the location, respectively. The embankment features sloped sides for stability on both sides.

Table 4-15. Detailed descriptions of Section S-11-4

Attribute	Information	Notes
District & Highway	San Angelo & FM 1223	
CSJ	0070-01-042	
County	Tom Green	
Reference Marker	RM 361+22	
Project Limits	Approx. 0.41 Mi. S. of Ave. N in San Angelo to 0.5 Mi. South	
GPS Coordinates	31°25'51.6"N 100°25'53.0"W	
Date Work Begin	11/23/1981	
Date Completed	05/27/1983	
Pavement Type	ACP 1 1/2"	
BAS Thickness	9-in BAS-75 (North Side) & 9-in BAS-75 (MOD) (South Side)	
Shoulder Type		Curb on both sides provided
Base Type	10 ½-in Flex Base (DEL) (Den Con) (TY. A GR4 CL3)	
Subgrade Type	Borr. (DEL) (Den Con) (TY. C CL3)	
Drainage Type	Shoulder Drain	
Embankment Height at BAS	~22-ft	Slope-slope
Distress Observed (Severity)	Longitudinal crack (Moderate)	

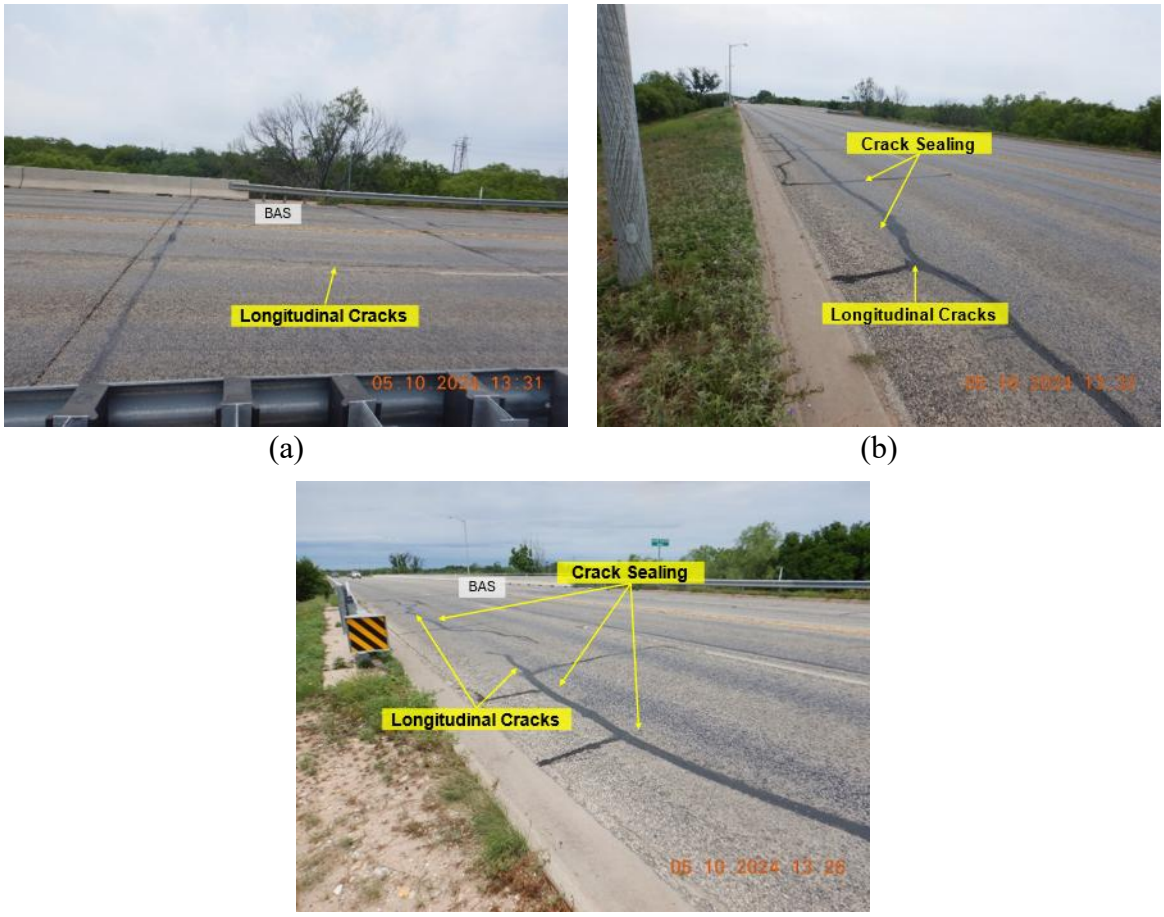


(a) (b)

Figure 4-31. (a) Site location and (b) location of Section S-11-4

4.1.14.2 Distress types

The main distresses observed in the BAS and pavement were moderate longitudinal cracks and transverse cracks as presented in **Figure 4-32**. Repair attempts were previously made to seal the crack as shown in **Figure 4-32**.



(a) (b)

(c)

Figure 4-32. Observed distresses at Section S-11-4: (a) longitudinal crack in BAS, (b) longitudinal cracks in pavement with crack sealing, and (c) longitudinal cracks in pavement and BAS with crack sealing.

4.1.15 Section ID: S-11-5

4.1.15.1 Overview

Section S-11-5 encompasses the bridge approach slab and the adjacent pavement structure on the northbound and southbound main lanes of US 96 in Beaumont, Texas, which was completed in

2007. The embankment features slopes on both sides. **Table 4-16** and **Figure 4-33.** provide detailed descriptions of Section S-11-5 and the location, respectively.

Table 4-16. Detailed descriptions of Section S-11-5

Attribute	**Information**	**Notes**
District & Highway	Beaumont US-96	
CSJ	0065 - 02 - 045	
County	Jasper	
Reference Marker	RM 410 + 1.38	
GPS Coordinates	30°40'58.7"N 93°53'45.4"W	
Date Work Begin	12/13/2004	
Date Completed	10/25/2007	
Pavement Type	Concrete Pavement (CRCP)	
BAS Thickness	12-in (Main Lane & Shoulder)	
Base Type	1 ¼-in ASB (GR 4) + 10-in ASB (GR 1)	
Subgrade Type	6-in Lime Treated	
Drainage Type	Side Ditch	
Embankment Height at BAS	~10-ft	Slope-Slope
Distress Observed (Severity)	Longitudinal crack; Settlement (Moderate)	



(a)



(b)

Figure 4-33. (a) Site location and (b) location of Section S-11-5

4.1.15.2 Distress types

Longitudinal cracks and settlements are main distress types observed in the BAS on both southbound approach and leave sides as shown in **Figure 4-34.** The pavement does not have any other significant distress. Also, most of the potential sections presented in **Table 4-1** have an embankment height at BAS taller than 15 ft, whereas that for Section S-11-5 is only about 10 ft.



(a) (b)

Figure 4-34. Observed distresses at Section S-11-5: longitudinal cracks in BAS (a) on SB leave side and (b) SB approach Side

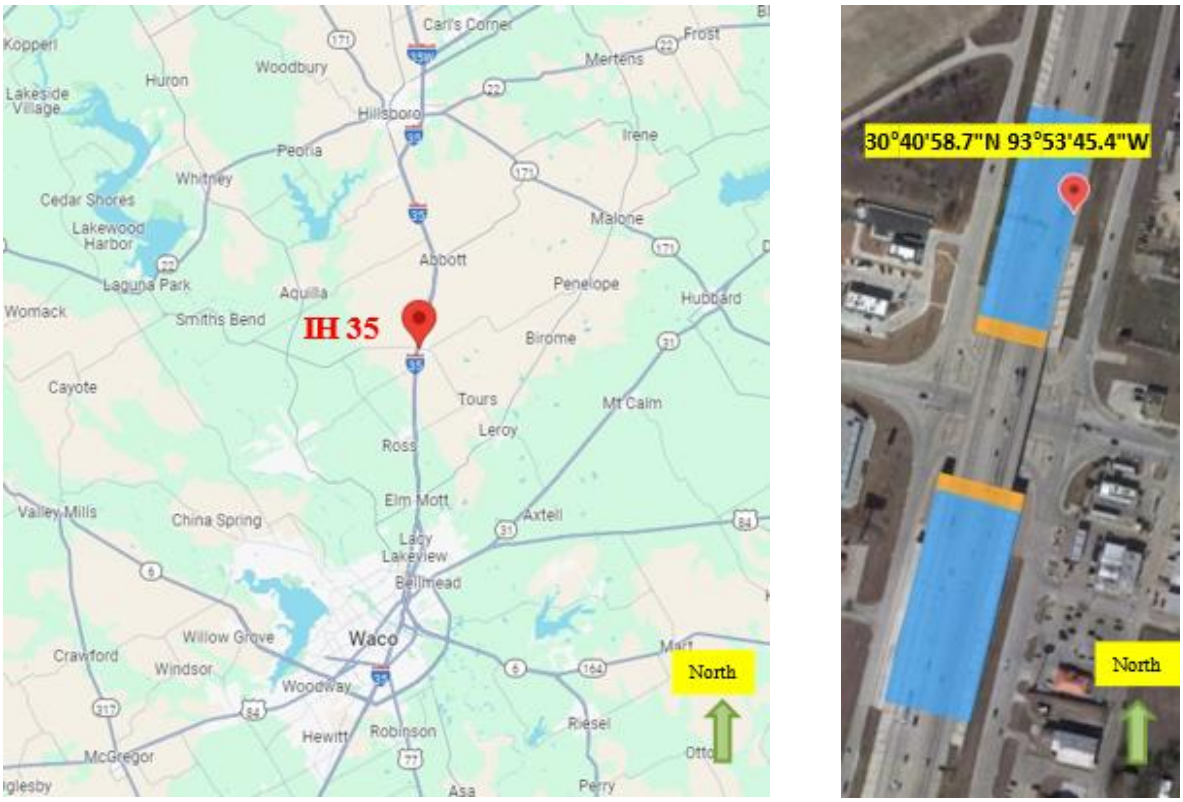
4.1.16 Section ID: S-11-6

4.1.16.1 Overview

Section S-11-6 is located on IH-35 in West, Texas. This section consists of a CRCP pavement and a BAS on an MSE wall embankment. The construction of this section was completed in 2016. and **Figure 4-35.** provide the detailed descriptions and location of Section S-11-6, respectively.

Table 4-17. Detailed descriptions of Section S-11-6

Attribute	**Information**	**Notes**
District & Highway	Waco & IH-35	
CSJ	0014-07-082	
County	McLennan	
Reference Marker	RM 353+0.11	
GPS Coordinates	31°48'19.8"N 97°05'58.8"W	
Date Work Begin	10/17/2011	
Date Completed	5/13/2016	
Pavement Type	CRCP 13-in	
BAS Thickness	13-in	
Shoulder Type	CRCP 13-in	
Base Type	1-in TY D HMA (PG 64-22) + 6-in CTB (4.5% Cement) (Road Mixed)	
Subgrade Type	8-in LTS	
Drainage Type	Prefabricated Drainage Panel	
Embankment Height at BAS	~28-ft	
Distress Observed (Severity)	Longitudinal cracks and Settlement (Moderate)	

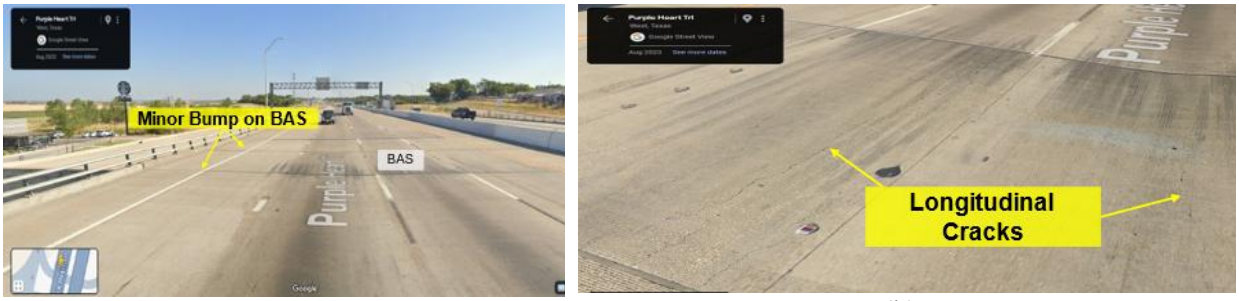


(a) (b)

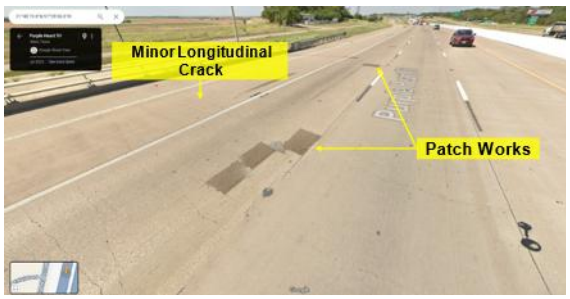
Figure 4-35. (a) Site location and (b) location of Section S-11-6

4.1.16.2 Distress types

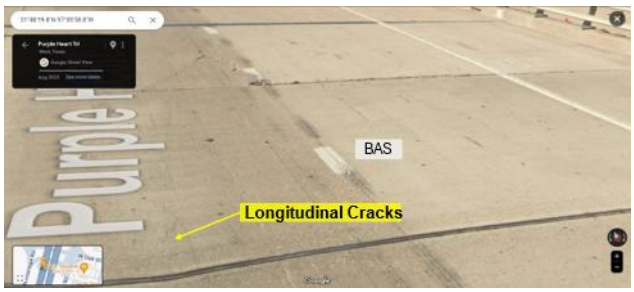
Longitudinal cracks and settlements (bumps) are main distress types observed in the BAS on both SB approach and leave side as shown in **Figure 4-36**. Particularly, leave side of southbound of Section S-11-6 shows lateral movement of MSE wall and repair attempts in the past as evidenced by the presence of an additional buttress wall (see **Figure 4-36(e)**).



(a) (b)



(c)



(d)

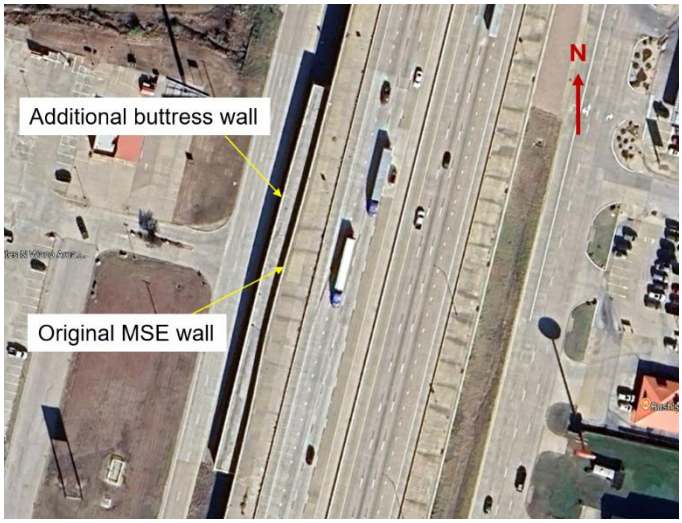


Figure 4-36. Observed distresses at Section S-11-6: (a) settlement (bump) in BAS in SB approach side, (b) longitudinal crack in BAS in SB approach side, (c) longitudinal crack and patchwork in SB approach side, (d) longitudinal crack in BAS in SB leave side, and (e) lateral movement of MSE wall in SB leave side.

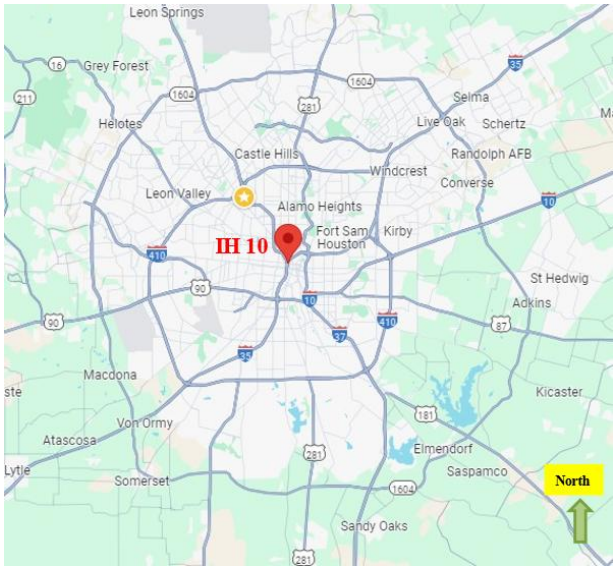
4.1.17 Section ID: S-11-7

4.1.17.1 Overview

Section S-11-7 encompasses a pavement structure on the northbound entry ramp of IH 10 in San Antonio, Texas. This section, constructed in 1994, features a 12-inch continuously reinforced concrete pavement (CRCP) but does not have a BAS. The embankment features MSE wall on both sides. **Table 4-18** and **Figure 4-37.** provide detailed descriptions of Section S-11-7 and the location respectively.

Table 4-18. Detailed descriptions of Section S-11-7

Attribute	Information	Notes
District & Highway	San Antonio & Connection IH 10	
CSJ	0017-10-145	
County	Bexar	
Reference Marker	RM 156 + 0.29	
Project Limits	From Poplar St. to IH 0035	
GPS Coordinates	29°25'53.6"N 98°30'01.3"W	
Date Work Begin	8/11/1990	
Date Completed	2/5/1994	
Pavement Type	CRCP 12"	
BAS Thickness	NA	
Shoulder Type	CRCP 12"	
Base Type	6" ASB (GR 4)	
Subgrade Type		
Drainage Type	CTB & Inlet	
Embankment Height	~16'	MSE Wall - MSE Wall
Distress Observed (Severity)	Longitudinal cracks and Spalling (Moderate)	



(a)

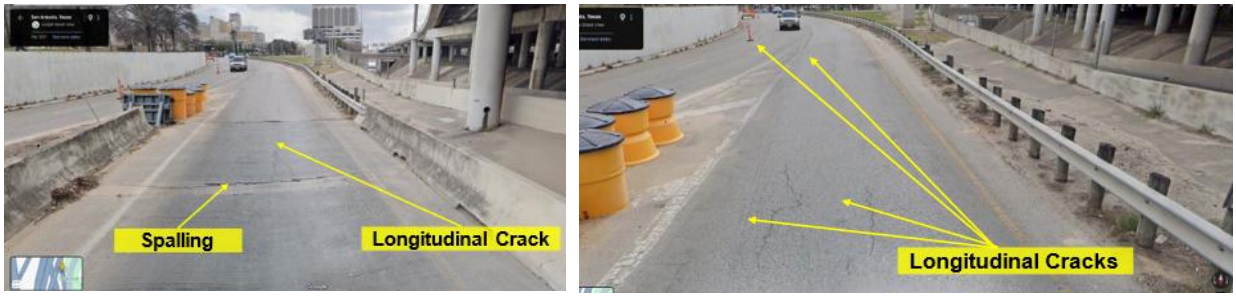


(b)

Figure 4-37. (a) Site location and (b) location of Section S-11-7

4.1.17.2 Distress types

Main distress types observed in Section S-11-7 are longitudinal cracks and spalling at the start of embankment as shown in **Figure 4-38**. The pavement in the embankment does not appear to have any other significant distress.



(a) (b)

Figure 4-38. Observed distresses at Section S-11-7: (a) spalling and longitudinal crack in the pavement and (b) longitudinal crack in the pavement.

4.1.18 Section ID: S-11-8

4.1.18.1 Overview

Section S-11-8, located on the frontage road of US 290 in Austin, Texas, over the Mopac railroad, was constructed in 1996. Unlike other typical sections considered in this research project, it does not have a bridge approach slab. The pavement structure comprises a 2-inch-thick Type C asphalt concrete pavement (ACP) layered over a 4-inch Type B ACP, which rests atop a 7-inch type-A asphalt stabilized base (ASB). The embankment features MSE walls on both sides. Detailed descriptions and the location of this section can be found in **Table 4-19** and **Figure 4-39**, respectively.

Table 4-19. Detailed description of site S-11-8

Attribute	Information	Notes
District & Highway	Austin & US-290	
CSJ	0113-13-067	
County	Travis	
Reference Marker	RM 575+0.61	
GPS Coordinates	30°13'38.3"N 97°46'35.9"W	
Date Work Begin	9/24/1992	
Date Completed	10/31/1996	
Pavement Type	ACP 2-in TY. C (PV-35 Min.)	
BAS Thickness	-	
Shoulder Type	-	
Base Type	ACP 2-in TY. C + ACP 4-in TY. B	
Subbase Type	ASB 7-in TY. A	
Subgrade Type	OC TY. C	
Drainage Type	Curb & Gutter (TY. 11)	
Embankment Height	~33-ft	MSE Wall – MSE Wall
Distress Observed (Severity)	Longitudinal cracks, settlement, and wall movement (Severe)	

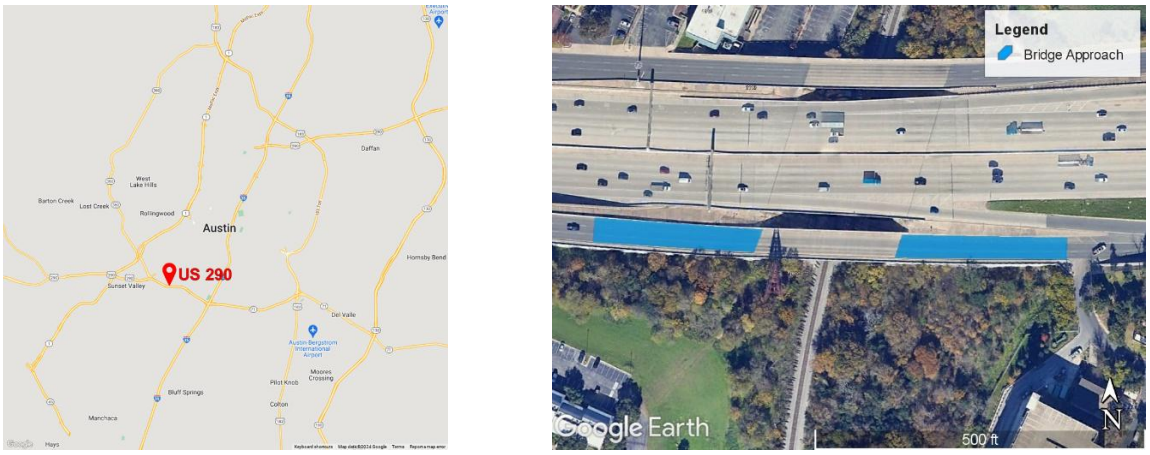
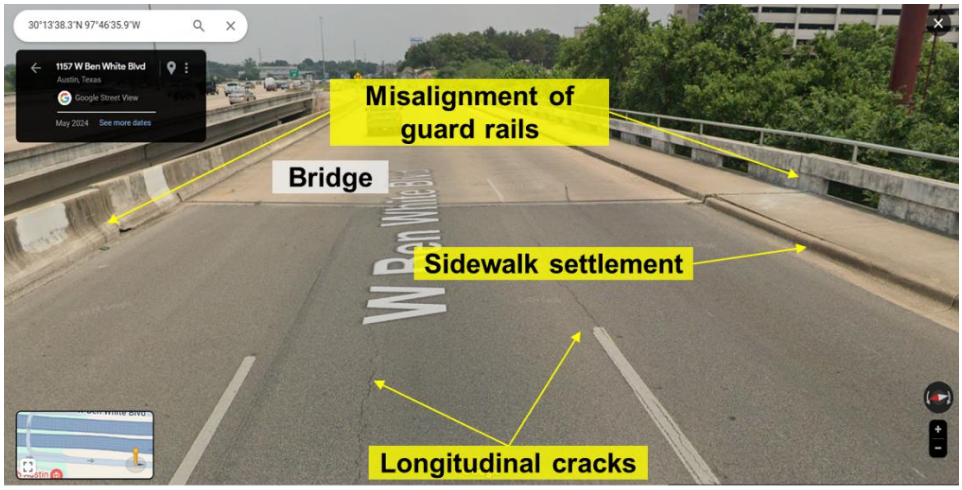


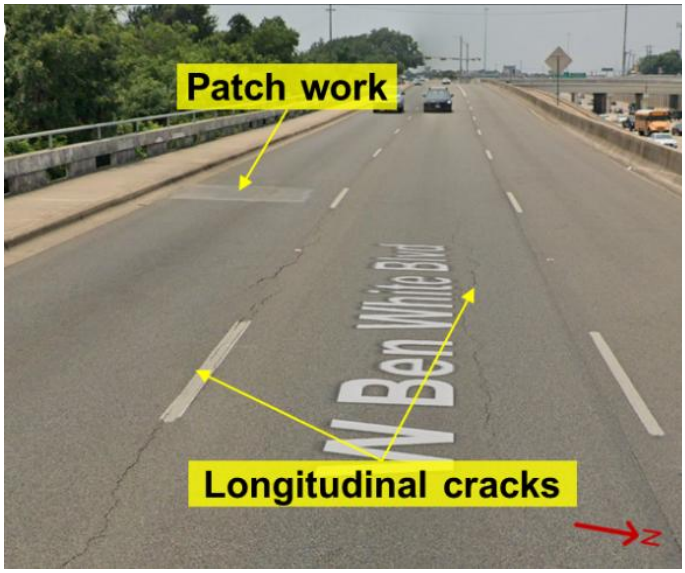
Figure 4-39. (a) Site location and (b) location of Section S-11-8

4.1.18.2 Distress types

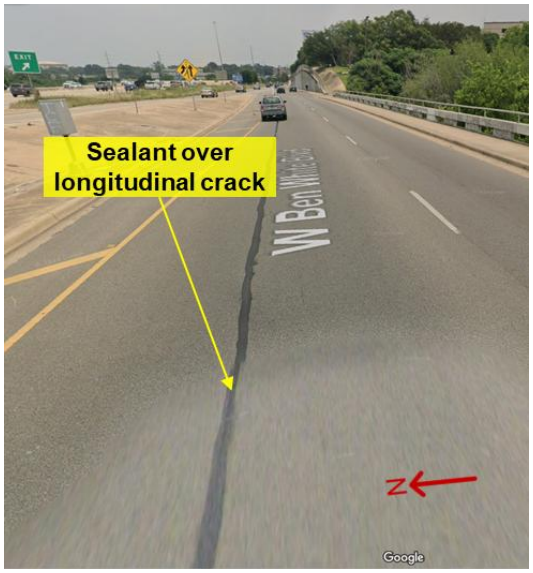
Section S-11-8 exhibits severe longitudinal cracks as its primary distress type. Misalignment of guard rails on the eastbound frontage road approach side suggests movement in the embankment, as shown in **Figure 4-40(a)**. It can also be observed that the longitudinal crack has been treated with sealant over it.



(a)



(b)



(c)

Figure 4-40. (a) EB Frontage Road Approach Side (May 2024), (b) EB Frontage Road Approach Side (May 2024), and (c) EB Frontage Road Leave Side (May 2024).

Past repair efforts involved an asphalt overlay, and the persistence of these cracks post-overlay is presented in **Figure 4-41**.



(a) (b)

Figure 4-41. Google Street View images of (a) EB Leave side pavement before asphalt overlay in Feb 2020, (b) EB Leave side pavement after asphalt overlay in May 2024.

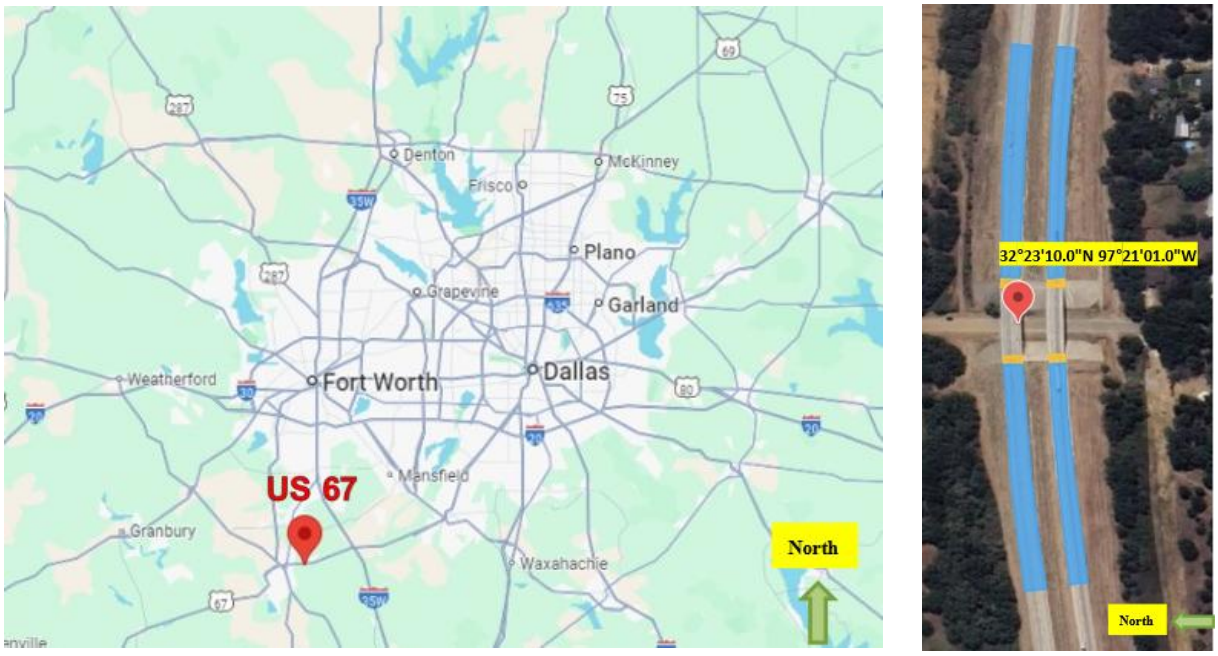
4.1.19 Section ID: S-11-9

4.1.19.1 Overview

Section S-11-9 consists of a BAS and a nearby pavement structure of US 67 in Fort Worth, Texas. The section has eastbound and westbound main lanes supported on a side sloped embankment. This section was constructed in 2019, and pavement structure is ACP. **Table 4-20** and **Figure 4-42** provide the detailed descriptions and the location of Section S-11-9, respectively.

Table 4-20. Detailed descriptions of Section S-11-9

Attribute	Information	Notes
District & Highway	Fort Worth & US-67	
CSJ	0259-06-001	
County	Johnson County	
Reference Marker	RM 450+0.20	
GPS Coordinates	32°23'10.7"N 97°21'01.0"W	
Date Work Begin	4/30/2014	
Date Completed	5/15/2019	
Pavement Type	½-in Hot Mix (Type D) + ½-in Hot Mix (Type B)	
BAS Thickness	13-in	
Base Type	Prime Base+6" Flex Base	
Subgrade Type	8-in Lime Treated Subgrade + Prime Subgrade	
Drainage Type	Box Culvert	
Embankment Height at BAS	~12-ft	Slope - Slope
Distress Observed (Severity)	Longitudinal cracks & BAS Settlement (Minor)	



(a) (b)

Figure 4-42. (a) Site location and (b) location of Section S-11-9

4.1.19.2 Distress types

The section has minor longitudinal cracks in BAS and nearby pavement in both eastbound and westbound approach/leave side as shown in **Figure 4-43.(a), (b), and (d). Figure 4-43.(e)** further indicates a settlement (bump) in west bound bridge approach slabs.



(a)



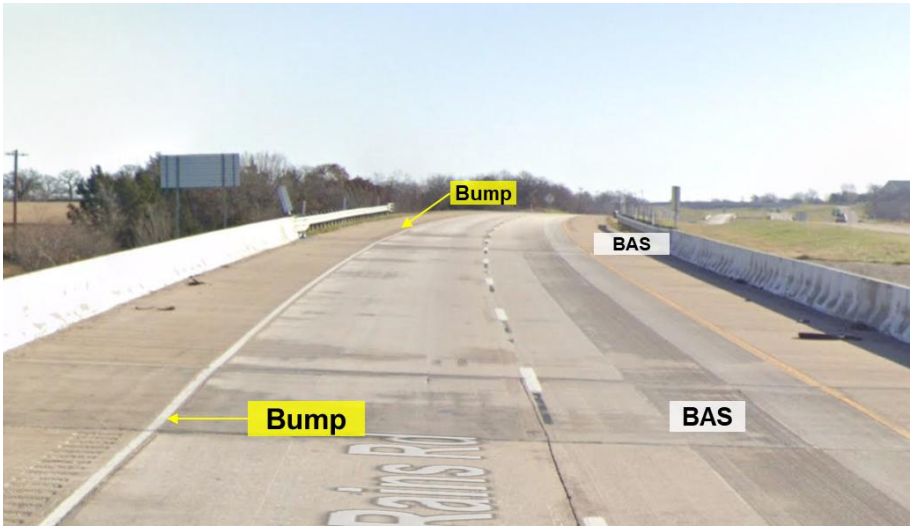
(b)



(c)



(d)



(e)

Figure 4-43. Observed distresses at Section S-11-9: (a) longitudinal crack in BAS on WBML approach side, (b) longitudinal crack in BAS on WBML leave side, (c) diagonal crack on WBML leave side, and (d) longitudinal crack on EBML approach side, and (e) settlement (bump) in westbound BAS

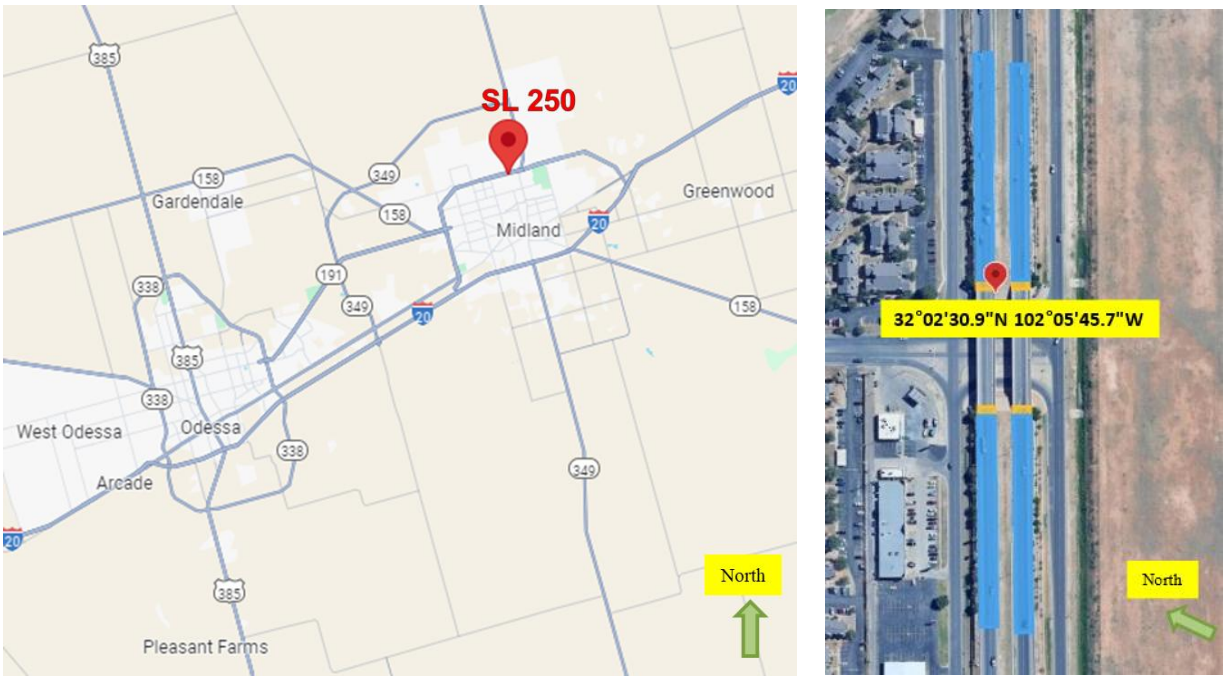
4.1.20 Section ID: S-11-10

4.1.20.1 Overview

Section S-11-10 consists of bridge approach slabs (BAS) and nearby pavement structures of the roadway embankment on SL-250 eastbound and westbound main lanes in Odessa, Texas. Pavement type is an asphalt concrete pavement (ACP) built on MSE wall embankment, and the construction was completed in 1997. Detailed descriptions of Section S-11-10 is given in **Table 4-21**, and the location is shown in **Figure 4-44.**.

Table 4-21. Detailed descriptions of Section S-11-10

Attribute	**Information**	**Notes**
District & Highway	Odessa, SL-250	
CSJ	1188-02-052	
County	Midland	
Reference Marker	RM 279+0.45	
GPS Coordinates	32°02'30.9"N 102°05'45.7"W	
Date Work Begin	10/30/1996	
Date Completed	12/8/1997	
Pavement Type	Asphalt Concrete Pavement	
BAS Thickness	13-in	
Shoulder Type	Asphalt Concrete Pavement	
Base Type	Flex Base 14-in	
Subgrade Type	Embankment DC TY A CL 3	
Drainage Type	Shoulder Drain	
Embankment Height at BAS	~21-in	Stepped Wall - Stepped Wall
Distress Observed (Severity)	Longitudinal Cracks and Settlement (Minor)	



(a) (b)

Figure 4-44. (a) Site location and (b) location of Section S-11-10

4.1.20.2 Distress Types

The section has minor longitudinal and diagonal cracks and asphalt overlay in BAS as presented in **Figure 4-45.** The pavement does not have any other significant distress.



(a) (b)



(c) (d)

Figure 4-45. Observed distresses at Section S-11-10: (a) longitudinal crack in BAS on EBML leave side, (b) diagonal crack in BAS on WBML leave side, (c) longitudinal crack and settlement in BAS on WBML approach side, and (d) longitudinal crack and settlement in BAS on EBML approach side.

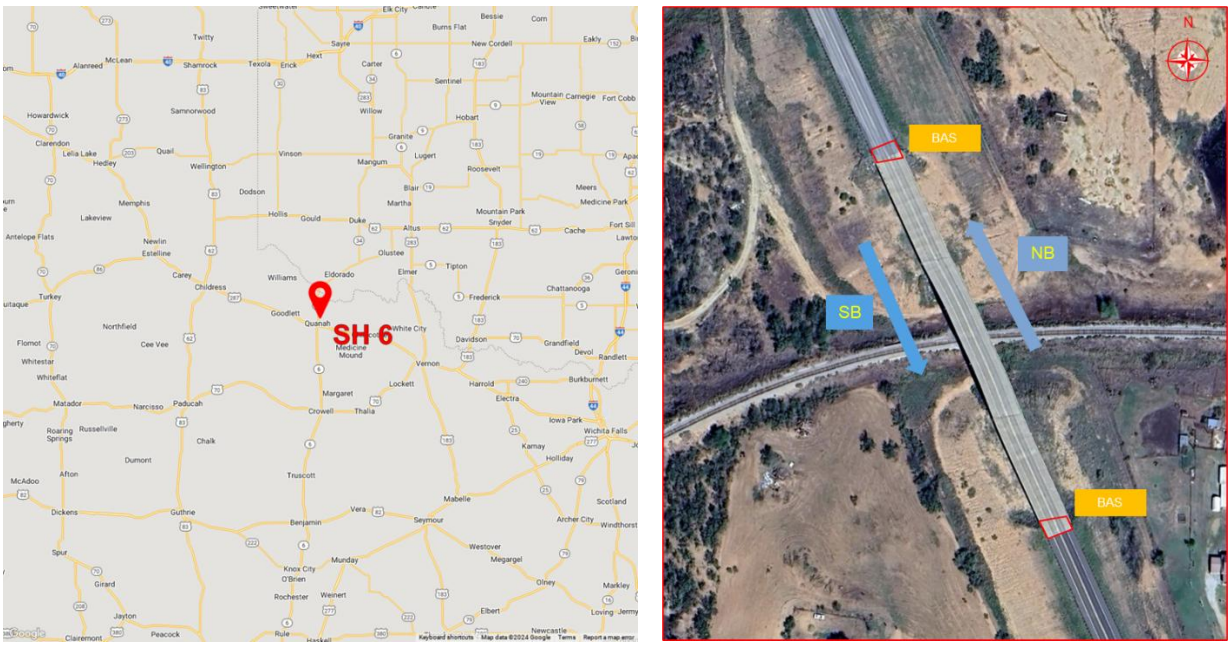
4.1.21 Section ID: S-12-1

4.1.21.1 Overview

Section S-12-1 consists of a bridge approach slab (BAS) and nearby pavement on SH6 northbound and southbound main lanes in Quanah, Texas. The pavement type is Asphalt Concrete Pavement (ACP) of Type-D 3" + ACP of type-B 4". The embankment is supported on both sides by a slope, and the construction was completed in 2006. The detailed descriptions and location of Section S-12-1 are presented in **Table 4-22** and in **Figure 4-46**, respectively.

Table 4-22. Detailed Description of S-12-1

Attribute	Information	Notes
District & Highway	Childress, SH-6	
CSJ	0097-02-024	
County	Hardeman	
Reference Marker	RM 165 + 0.20	
GPS Coordinates	34°18'37.2"N 99°44'20.1"W	
Date Work Begin (as-built)	09/07/2004	
Date Completed	03/20/2006	
Pavement Type (approach)	TY-D ACP 3-in + TY-B ACP 4-in	
Base Type	TY-B ACP 4-in	
Subgrade Type	3% Lime Treated Subgrade 8-in	
Drainage Type	Side Drain	
Embankment height at BAS	36-ft	
Repair History	Full depth repair/reconstruction	
Distresses Observed (Severity)	Longitudinal cracks (Severe)	

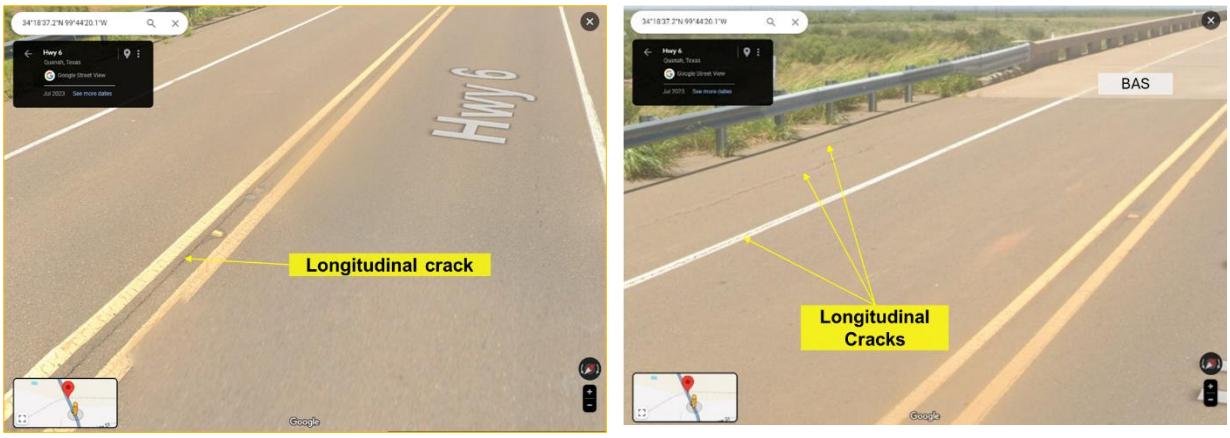


(a) (b)

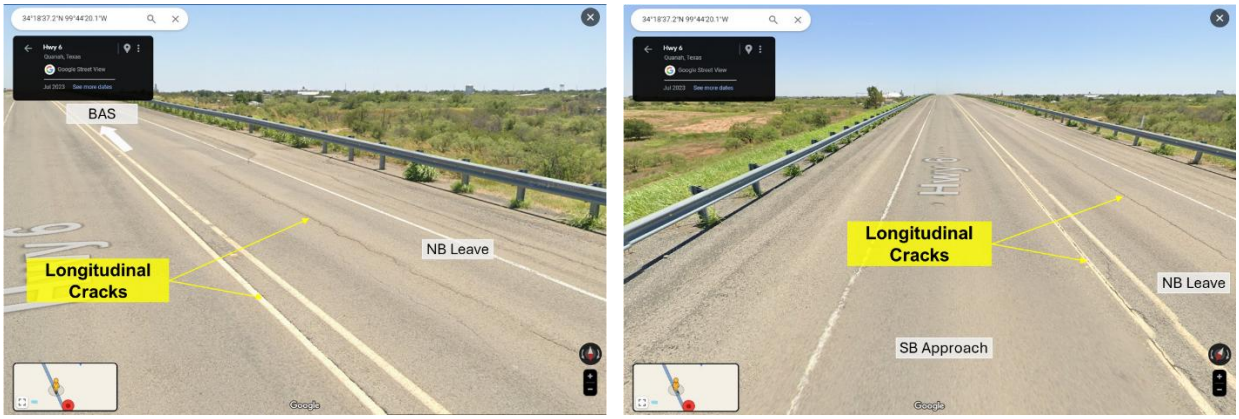
Figure 4-46. (a) Site location and (b) location of Section S-12-1

4.1.21.2 Distress Types

The bridge approach slab currently shows no signs of major issues. However, the adjacent pavement section exhibited longitudinal cracks over an asphalt overlay in both the northbound and southbound lanes, as shown in **Figure 4-47**. Some of these cracks align with the location of what should be a construction joint, which may indicate the presence of lane separation.



(a) (b)



(c) (d)

Figure 4-47. Distress observed at Section S-12-1: longitudinal cracks in (a) northbound approach, (b) southbound leave, (c) northbound leave, and (d) southbound approach

4.1.21.3 Repair History

An email communication with TxDOT revealed that the initial primary issue with this section was the instability and movement of the abutment. Following an extensive investigation, TxDOT decided to remove portions of the embankment, extend the girder length, and relevel the section with a 2 to 4-inch asphalt overlay. As a result, the bridge approach slab was replaced. The construction history of this section is depicted in **Figure 4-48**. Google satellite images clearly show that by March 2015, the embankment had been partially excavated, and additional girders were installed between that time and August 2019.



Figure 4-48. Google satellite images showing construction history and condition of Section S-12-1

4.1.22 Section ID: S-12-2

4.1.22.1 Overview

Section S-12-2 encompasses the bridge approach slabs (BAS) and adjacent pavement structures along the northbound lanes of IH 69W in Laredo, Texas. The section features a pavement structure composed of 12-inch Continuously Reinforced Concrete Pavement (CRCP). Beneath the CRCP lies a 4-inch asphalt concrete pavement (ACP) base, transitioning to a 4-inch dense-graded hot-mix asphalt (HMA) at the edges. The subgrade consists of 8 inches of lime-treated soil (LTS), which shifts to a 6-inch flexible base at the edges. The height of embankment supporting this section is approximately 28 feet, with MSE walls on both sides. The detailed attributes and location of Section S-12-2 are presented in **Table 4-23** and in **Figure 4-49**, respectively.

Table 4-23. Detailed description of Section S-12-2

Attribute	Information	Notes
District & Highway	Laredo & IH-69W	
CSJ	0086-14-084	
County	Webb County	
Reference Marker	RM 1-1 to RM 1+0.735	
GPS Coordinates	27°36'04.1"N 99°31'03.6"W	
Date Work Begin	11/9/2020	
Date Completed	4/20/2023	
Pavement Type	CRCP (12-in Thk.)	At Edges: 13-in CRCP
BAS Thickness	13-in	
Base Type	4-in ACP (TY A)	At Edges: 4-in D-GR HMS TY-B
Subgrade Type	8-in LTS	At Edges: 6-in FL BS (CMP in PLC) (TYA GR1-2)
Drainage Type	Single Slope Traffic Rail (W/ Drain Slots) With Side Drain and Inlet	
Embankment Height at BAS	~28-ft	MSE Wall - MSE Wall
Distress Observed (Severity)	Settlement & Longitudinal crack (Minor)	

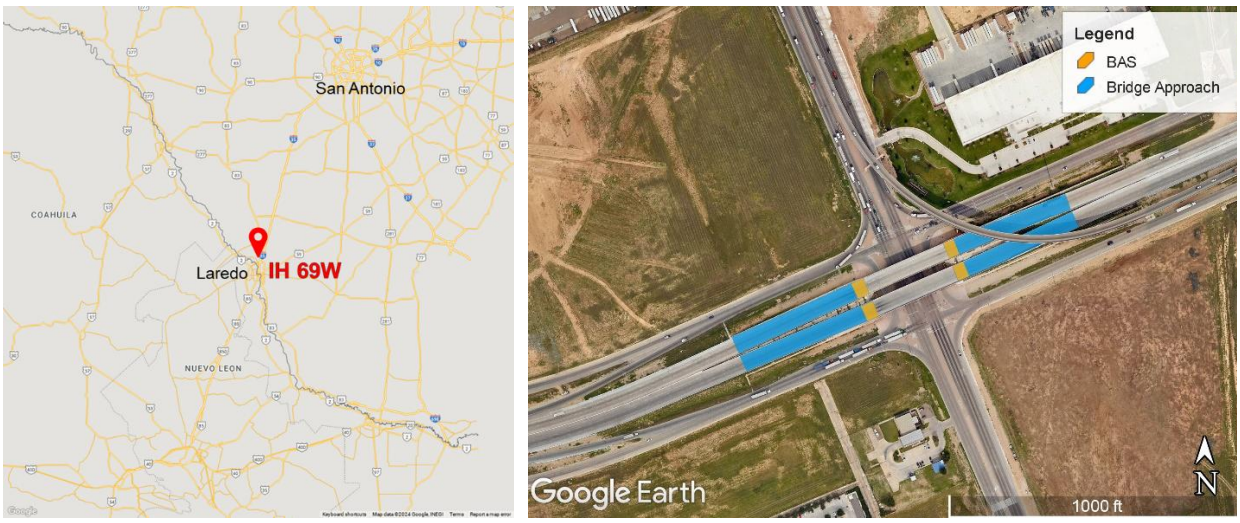


Figure 4-49. (a) Site location and (b) location of Section S-12-2

4.1.22.2 Distress types

The primary issue identified in this section is the settlement of the bridge approach slab (BAS) at both the northbound and southbound approaches and leaves. While no visible distress was observed on the approaches via Google Earth imagery, a significant void was discovered beneath the approach slab in 2021 by TxDOT, as shown in **Figure 4-50**. This information was provided to us through an email by TxDOT, including the accompanying photo. Although the void was filled using flowable fill as a repair method, recent reviews of Google Street View imagery (post-repair) suggest that the settlement issue may not have been fully resolved (see **Figure 4-51**). Additionally, a longitudinal crack has been observed in the BAS on the northbound exit side, indicating ongoing distress (**Figure 4-51 (c)**).



Figure 4-50. Void discovered beneath the bridge approach slab on October 4, 2021, as identified by TxDOT (*Source: Email communication with TxDOT*)

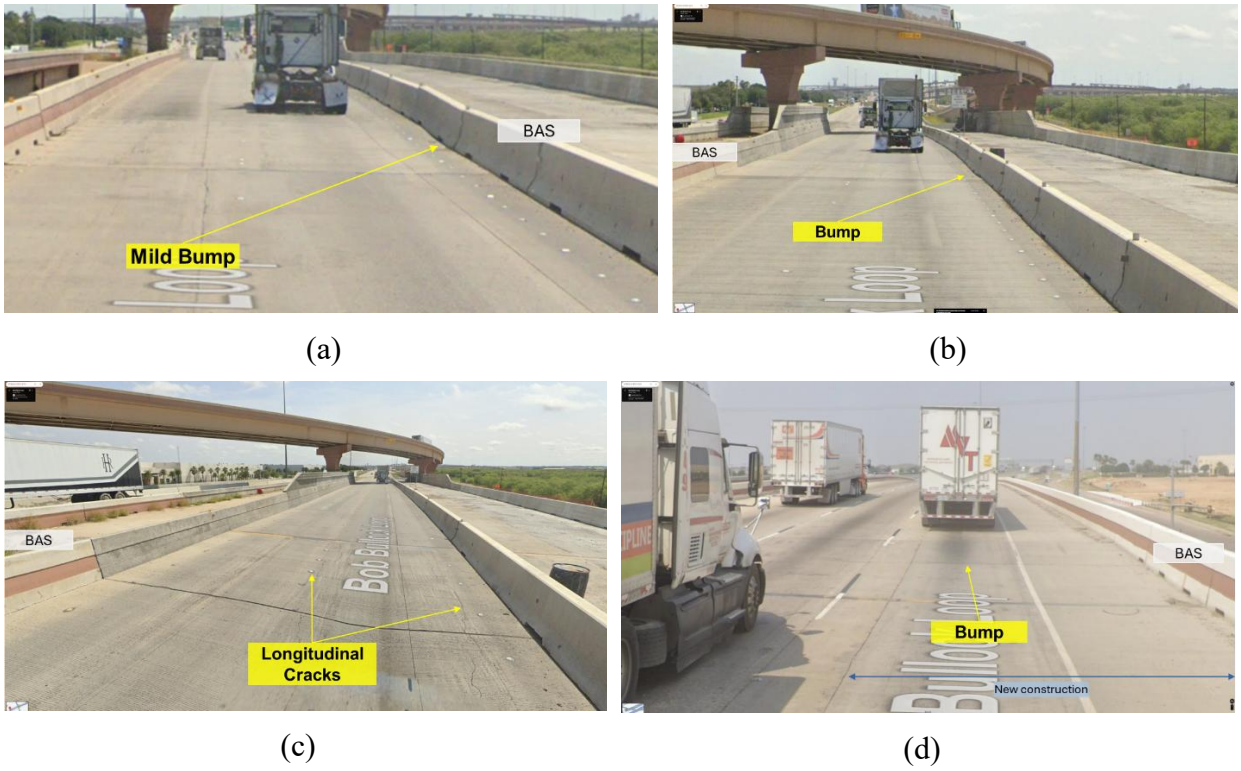


Figure 4-51. Google Street View images of (a) NB Approach side pavement (May 2022), (b) NB leave side pavement (May 2022), (c) longitudinal crack observed in NB Leave side pavement (May 2022), and (d) SB approach side pavement (May 2024)

4.1.22.3 Repair history

During a bridge widening project in the summer of 2021, a void beneath the approach slab was discovered by contractors. Following guidance from TxDOT, the contractor filled the void with flowable fill. This involved coring holes directly above the approach slab to inject the fill material. The work was executed on-site, directed by field conditions, without the generation of new plans.

4.1.23 Section ID: S-12-3

4.1.23.1 Overview

Section S-12-3 consists of bridge approach pavements of SH-35 highway in Port Lavaca, Texas. This section does not have a bridge approach slab, and the pavement appeared to be constructed on a natural ground, not on an elevated embankment (or on an embankment with very short height), making it less relevant to roadway embankments that we are considering in this research project. The Research Team were not able to obtain further details on Section S-12-3 at the time of this report writing.

4.1.23.2 Distress types

The major distresses for this section are continual settlement of abutment (per communication with TxDOT) and longitudinal crack in the nearby pavement indicated by Google Street View images as shown in **Figure 4-52**. To address this issue, TxDOT has been performing frequent overlays with a major full depth repair (12") with TY-B hot mix asphalt in 2019.

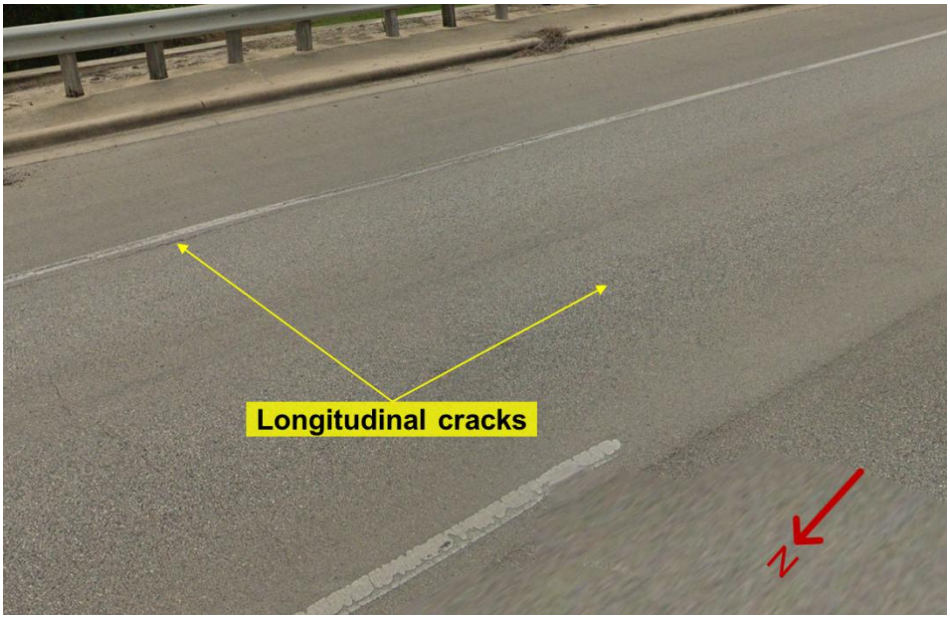


Figure 4-52. Longitudinal crack in approach pavement (March 2023).

4.1.24 Section ID: S-12-4 (P-B-3)

4.1.24.1 Overview

Section S-12-4 consists of bridge approach slabs (BAS) and adjacent pavement structures on the westbound main lanes of BW-8 in Houston, Texas. The pavement structure consists of 12-inch CRCP, 1-inch asphalt stabilized base (ASB), a 6-inch permeable cement treated base (PCTB), and a 6-inch lime treated subgrade (LTS). The westbound side of the embankment is MSE wall, and eastbound side is 4:1 slope. The Research Team & TxDOT conducted field evaluations of this section in February 2023. The detailed descriptions and location of Section S-12-4 are presented in **Figure 4-53** and in **Table 4-24**, respectively.

Table 4-24. Detailed description of Section S-12-4

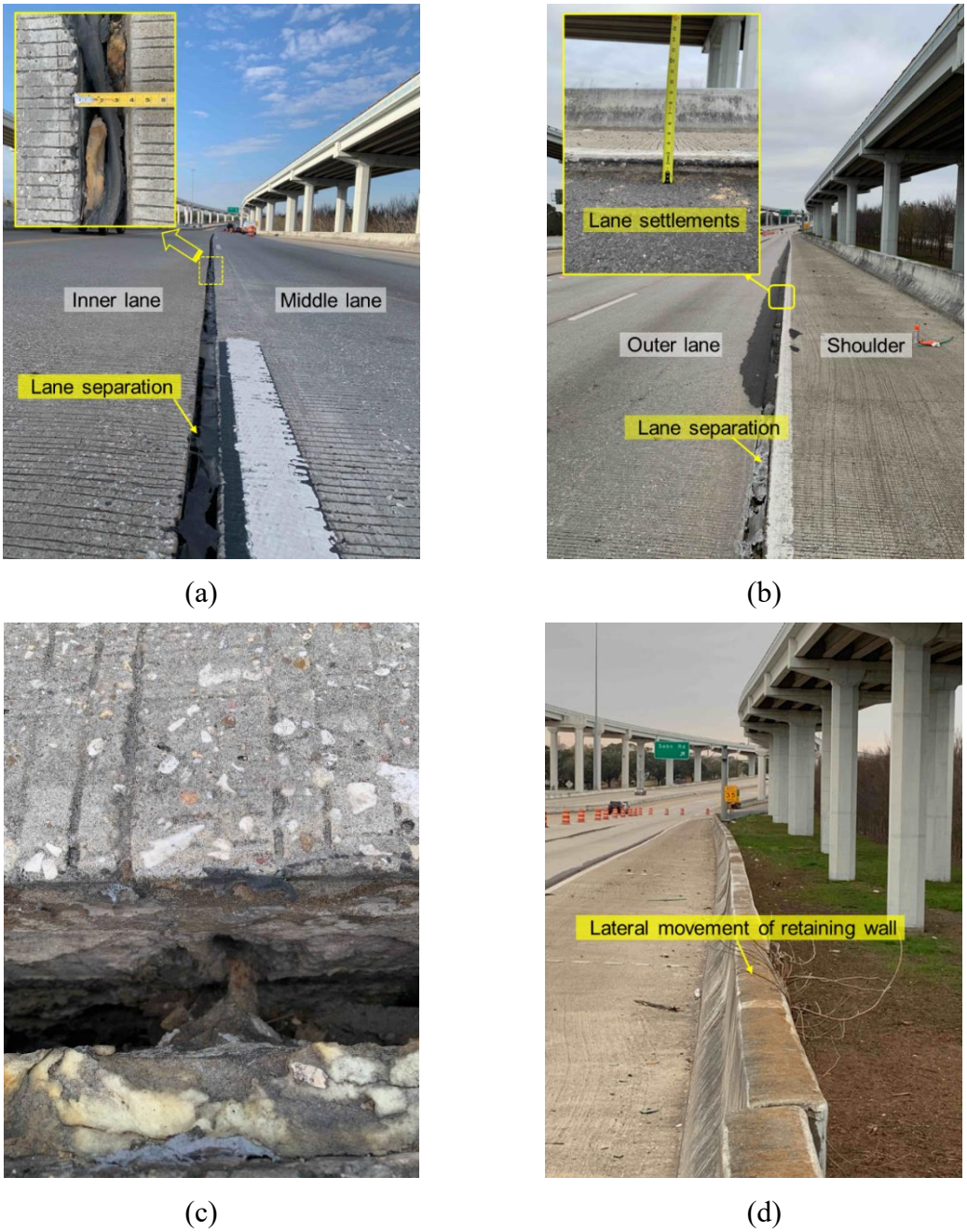
Attribute	Information	Notes
District & Highway	Houston, BW-8 WB	
CSJ	0500-03-429	L = 0.74 miles
County	Harris County	
Reference Marker	RM 758+0.288 to RM 758+0.395	
GPS Coordinates	From 29.6048608, -95.2080190 to 29.6038540, -95.2094106	
Date Work Begin	06/03/1996	
Date Completed	11/01/1997	
Pavement Type	Rigid – CRCP	
Slab thickness	12-in (Main Lane and Shoulder)	
Base Type	1-in ASB (GR 4) + 6" CTB	
Subgrade Type	6-in LTS	
Drainage Type	Curb & Inlets	
Embankment Height at BAS	~20-ft	MSE Wall - Slope
Distress Observed (Severity)	Settlement; Lane separations; MSE wall movement (Severe)	



Figure 4-53. Location of Section S-12-4

4.1.24.2 Distress types

The onsite evaluation of Section S-12-4 (P-B-3) conducted by TxDOT and the Research Team in February 2023 identified lane separation, settlement, and movement of retaining wall as the major distresses. **Figure 4-54** illustrates these observed distresses. Lane separation was particularly severe, as wide as 5 inches, and led to a tie-bar failure between lanes (see **Figure 4-54(c)**).



(a) (b)

(c) (d)

Figure 4-54. Distress observed at Section S-12-4 (P-B-3): (a) lane Separation between main lanes, (b) lane Separation ranges between main lane and shoulder as well as lane settlement, (c) tie-bar failure, and (d) MSE wall movement

4.1.24.3 Repair history

Core samples of a pavement structure taken during the field evaluation showed a layer of polyurethane foam beneath the concrete, suggesting that the base materials were washed out, creating a significant void, and the polyurethane foam was used to fill the void in the past prior to the field evaluations. However, due to the significance of MSE wall movement and lane separations, the repair strategy adopted by TxDOT after the field evaluation was to remove the materials from the outside shoulder to middle lane and reconstruct the MSE wall. The reconstruction of MSE wall and main lanes were completed in 2023.

4.1.25 Section ID: S-12-5

4.1.25.1 Overview

Section S-12-5 encompasses a bridge approach slab and nearby pavement structure on IH 27 that crosses FM 3466 in Lubbock, Texas. In 2014, the original east-west bridge along FM 3466 was decommissioned and replaced with a new north-south bridge along IH 27. This section is a new construction rather than "repair" activities. Accordingly, this section was not considered for further study.

4.1.26 Section ID: S-12-6

4.1.26.1 Overview

Section S-12-6 consists of a bridge approach slab (BAS) and nearby pavement of TX 183 northbound ramp in Fort Worth, Texas. The pavement type is CRCP. The embankment is supported on both sides by MSE walls. **Figure 4-55** shows the location of section S-12-6.



(a) (b)

Figure 4-55. (a) Site location and (b) location of Section S-12-6.

4.1.26.2 Distress types

The bridge approach slab did not exhibit any major distresses. However, the nearby approach pavement includes distresses such as settlement, diagonal cracks at the depressed pavement, and some PCC patches to address distresses including spalling and punchouts, as shown in **Figure 4-56**.



(a) (b)

Figure 4-56. Distress observed at Section S-12-6: (a) settlement at approach pavement and (b) diagonal crack and PCC patch.

4.1.26.3 Repair history

As shown in **Figure 4-56(b)**, issues such as spalling and joint distresses have been mitigated with PCC patches. The Research Team contacted the survey respondent to get further details on the repair history but could not obtain such information at the time of report preparation.

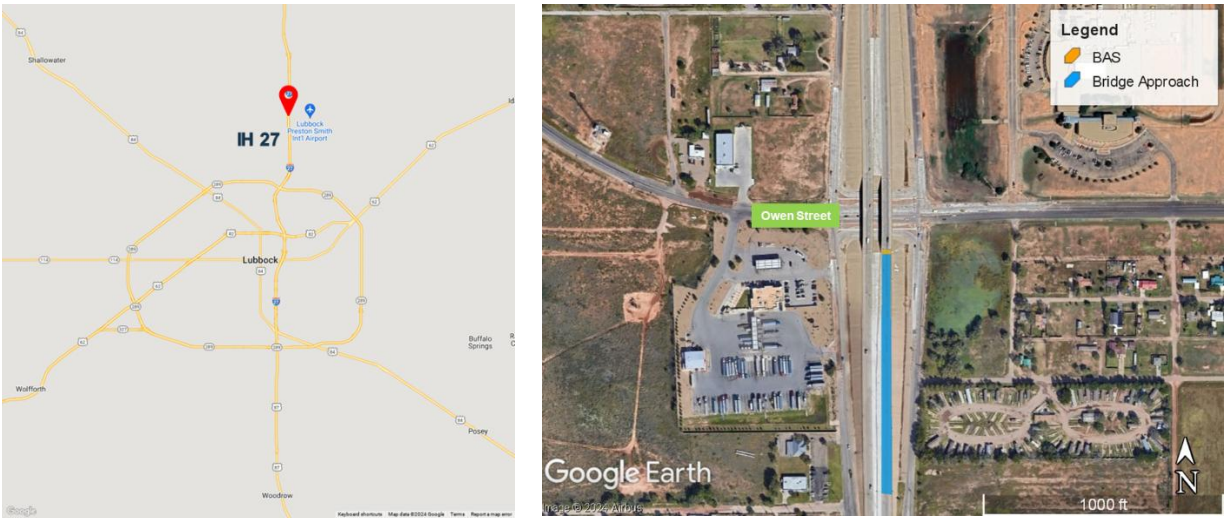
4.1.27 Section ID: E-1

4.1.27.1 Overview

Section E-1 is the northbound approach road and bridge approach slab (BAS) of IH-27 across Owen Street in Lubbock, Texas. This section consists of CRCP and features an embankment with slope protection. The Research Team conducted a reconnaissance visit to this site. **Figure 4-57** and **Table 4-25** provides an overview of the location of Section E-1.

Table 4-25. Detailed description of Section E-1

Attribute	Information	Notes
District & Highway	Lubbock & IH-27 NB	
CSJ	0067-07-054/059	*Note: Pavement Details 0067-07-059
County	Lubbock County	
Reference Marker	RM 8 + 0.38	
GPS Coordinates	33°38'35.6"N 101°50'08.8"W	
Date Work Began	10/7/1975	*10/18/1978
Date Completed	8/7/1978	*05/13/1981
Pavement Type	CRCP 9-in	*0067-07-059
BAS Thickness	NA	
Shoulder Type	CRCP 9-in	
Base Type	4-in ASB	
Subgrade Type	Dens. Contr.	Prep. SUBGR (Dens. Contr.) Item 1006
Drainage Type	Side Ditch @ Median & Side Slope @ Edges & Culverts	
Embankment Height at BAS	~31-ft	Slope - Slope
Repair History	Full Depth Repair	
Distress Observed (Severity)	BAS settlement (Moderate); Longitudinal cracks (Severe)	



(a) (b)

Figure 4-57. (a) Site location and (b) location of Section E-1

4.1.27.2 Distress types

Section E-1 is noted for having undergone previous repairs due to lane separation. **Figure 4-58** shows a photograph of the lane separation issue as it appeared during the 2003 repair process. Following the repair, no further lane settlement issues have been observed. However, the section still exhibits some distresses, such as longitudinal cracks, BAS settlement, spalling, and punchouts, as illustrated in **Figure 4-59**.



Figure 4-58. Lane separation observed in the approach pavement pre-repair, 2003 (Photo courtesy of Dr. Moon Won)

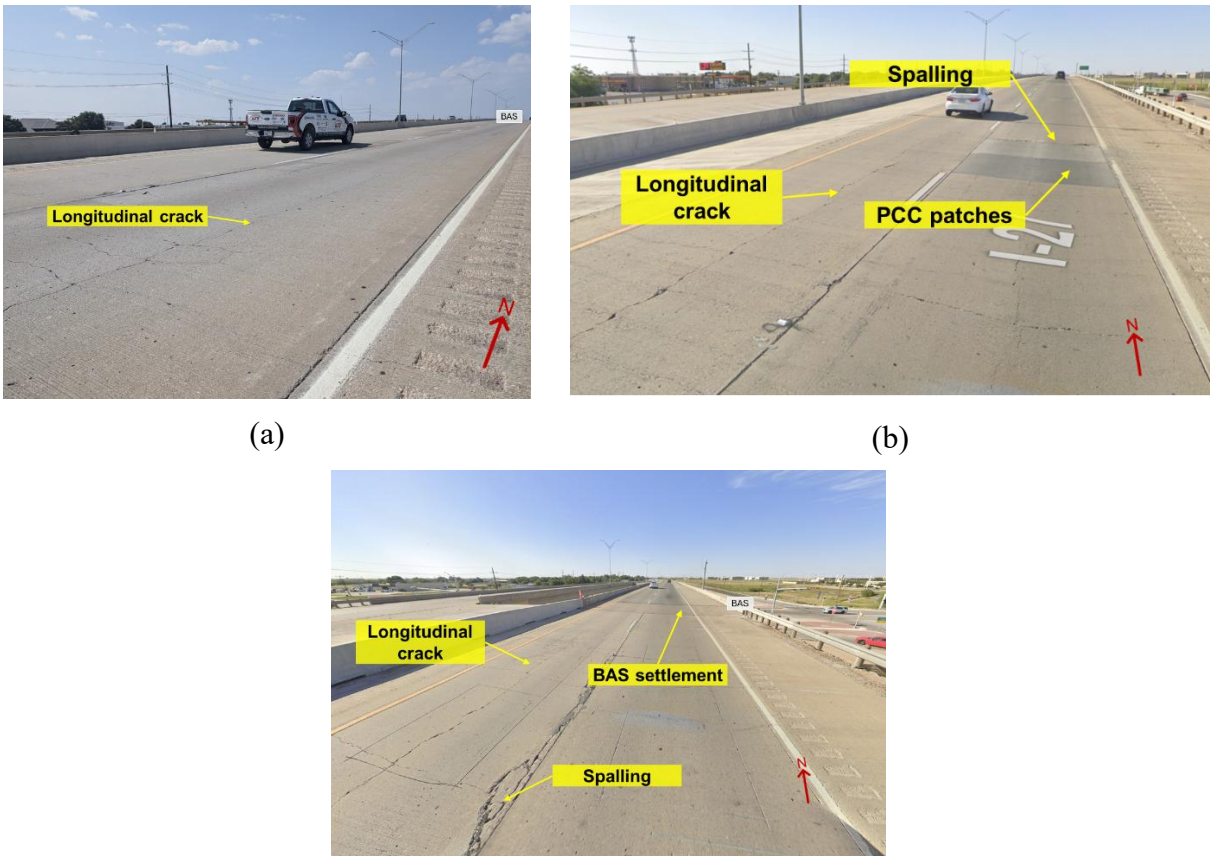


Figure 4-59. Distress observed at Section E-1 (a) longitudinal crack, (b) PCC Patches, (c) spalling in NB approach pavement and (d) settlement in BAS.

4.1.28 Section ID: E-2

4.1.28.1 Overview

Section E-2 consists of bridge approach slabs (BAS) and nearby pavement structures of the roadway embankment on IH 10 main lanes (both eastbound and westbound) in San Antonio, Texas. Pavement type is a continuously reinforced concrete pavement (CRCP) and the construction was completed in 2009. Field evaluations of Section E-2 were previously conducted by TxDOT in November 2023, and the Research Team were present during the evaluation and assisted various testing. **Table 4-26** presents detailed descriptions of the subject section, and location of Section E-2 is shown in **Figure 4-60**.

Table 4-26. Detailed descriptions of Section E-2

Attribute	Information	Notes
District & Highway	San Antonio, IH-10 Main Lanes	Eastbound and westbound
CSJ	0072-12-159	
County	Bexar County	
Reference Marker	RM 564.236	
GPS Coordinates	29.494832, -98.547583	
Date Work Begin	09/23/2002	
Date Completed	03/09/2009	
Pavement Type	Rigid – CRCP (13-in)	
BAS Thickness	13-in	
Shoulder Type	Tied Concrete	
Base Type	10-in HMA (Type A)	
Subgrade Type	Embankment materials - Type B	
Drainage Type	Curb & Inlets	
Embankment Height at BAS	35 ft	MSE wall – MSE wall
Distress Observed (Severity)	Excessive settlement, lane separation, and voids (Severe)	

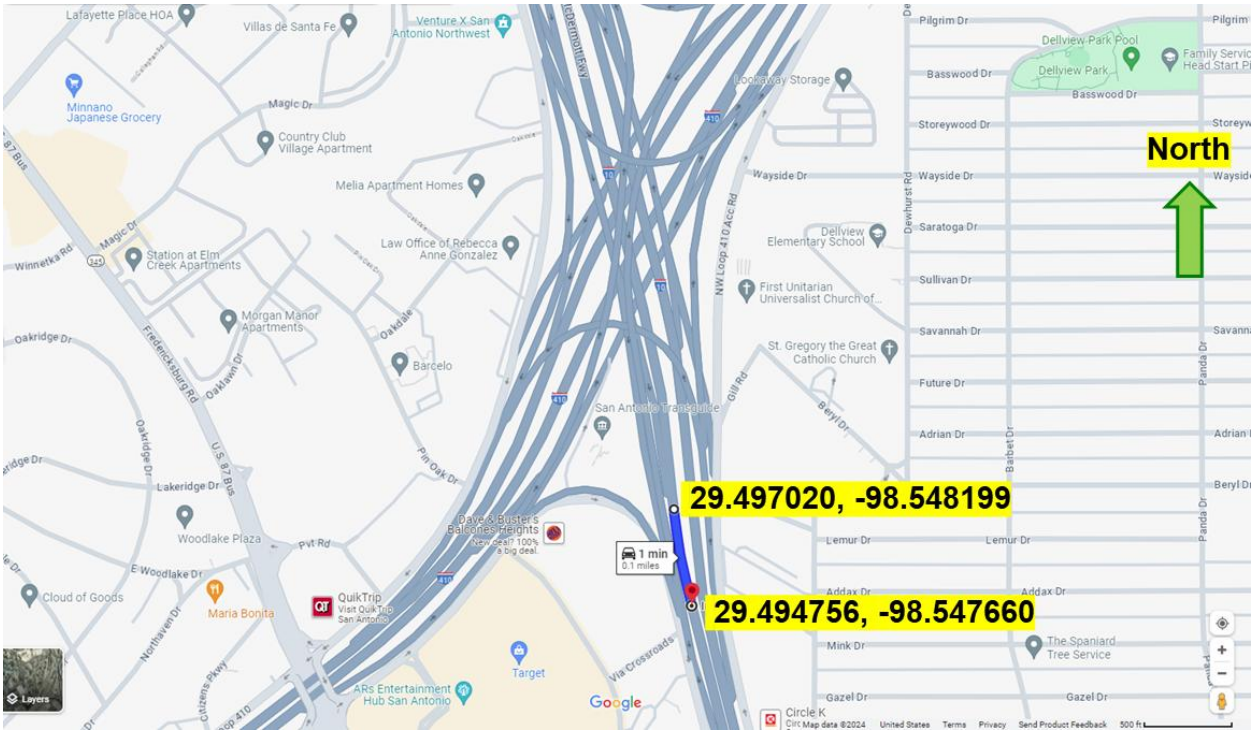


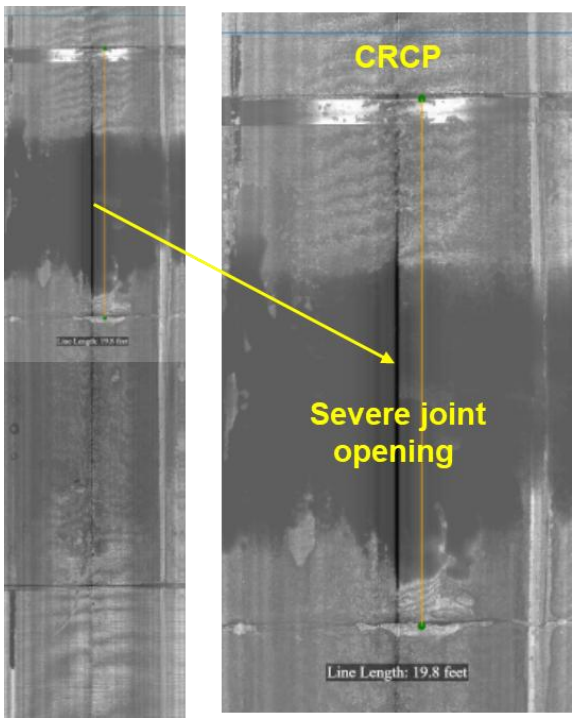
Figure 4-60. Location of Section E-2 (IH 10 main lanes in San Antonio, TX)

4.1.28.2 Distress types

The east and west sides of the subject roadway embankment are mechanically stabilized earth (MSE) walls. Excessive settlements have been observed in the BAS area over the past years, and large voids (as thick as 7 inches) were identified via coring during the field evaluations, as shown in **Figure 4-61(a)**. Also, severe longitudinal joint opening was observed (see **Figure 4-61(b)**). The main distress type observed in Section E-2 is a settlement and a lane separation, and their severities are very high.



(a)



(b)

Figure 4-61. Observed distresses at Section E-2: (a) 7-inch-thick void beneath the bridge approach slab (BAS) and (b) severe joint opening between the outside two lanes of westbound (Image source: TxDOT)

4.1.29 Section ID: E-3

4.1.29.1 Overview

Section E-3 consists of bridge approach slabs (BAS) and nearby pavement structures of the roadway embankment on SH-47 main lanes (both Northbound and southbound) in College station, Texas. Pavement type is an asphalt concrete pavement and construction was completed in 2014. **Table 4-27** presents detailed descriptions of the section, and location of Section E-3 is shown in **Figure 4-60**.

Table 4-27. Detailed descriptions of Section E-3

Attribute	Information	Notes
District & Highway	Bryan & SH-47	Northbound and southbound
CSJ	3138-02-010	
County	Brazos County	
Reference Marker	From RM 416 + 0.885 to RM 418 + 0.515	
GPS Coordinates	30°35'40.3"N 96°23'30.2"W	
Date Work Begin	2/9/2012	
Date Completed	8/7/2014	
Pavement Type	2-in TY C ACP PG64-22 SAC-A + 2-in TY C ACP PG64-22 + One Course Surface Treatment	
BAS Thickness	13-in BAS-A (MOD)	
Shoulder Type	ACP	
Base Type	6-in Flex Base	
Subgrade Type	8-in Stabilized Subgrade	
Drainage Type	Side Ditches & Curbs	
Embankment Height at BAS	30-ft (West Side), 14.5-ft (East Side)	MSE wall – MSE wall
Distress Observed (Severity)	Settlement (Major)	

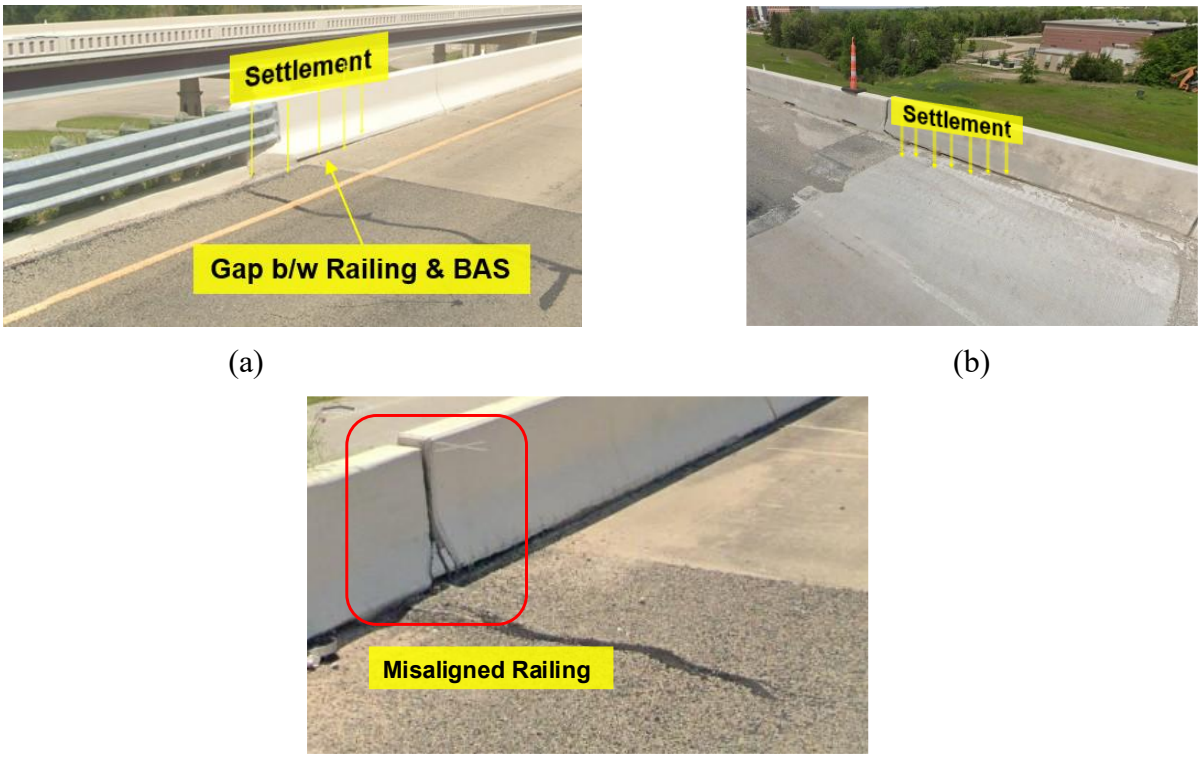


(a) (b)

Figure 4-62. Location of Section E-3 (SH-47 main lanes College station, TX)

4.1.29.2 Distress types

The major distresses identified during detailed review of Google Street View survey were settlement and misaligned railing as shown in **Figure 4-63**. A visible gap was seen between the railing and the pavement at SB approach and NB leave side BAS due to settlement of BAS as shown in **Figure 4-63**.



(a) (b)

(c)

Figure 4-63. Observed distresses at Section E-3: (a)Settlement at SB approach and (b) Settlement at NB leave (c) Misaligned railing at SB approach.

4.1.30 Section ID: E-4

4.1.30.1 Overview

Section E-4 is the on the southbound departure ramp of IH 35 at Exit 368A (Whitney/Corsicana) in Hillsboro, Texas, as shown in **Figure 4-64**. The ramp connects the IH 35 main lanes to the IH 35 frontage road. This section consists of CRCP and features an embankment with MSE wall on one side and slope on another side. The Research Team conducted a reconnaissance visit to this site. **Table 4-28** provides description of Section E-4.

Table 4-28. Detailed description of Section E-4

Attribute	Information	Notes
District & Highway	Waco & IH-35 Southbound Exit 368A Ramp (IH-35 Main-lanes to IH-35 Frontage)	
CSJ	0014-24-045	
County	Hill County	
Station	Sta. 6+060 to Sta 6+660	
CSJ Project Limits	South of FM 3267 to North of FM 286 in Hillsboro, TX	
GPS Coordinates	32°01'00.1"N 97°05'45.2"W to 32°00'52.2"N 97°05'45.6"W	
Date Work Begin	8/20/1999	
Date Completed	9/12/2002	
Pavement Type	CRCP 12.8-in	325 mm
BAS Dimension	12.8-in X 20-ft (T X L)	325 mm
Shoulder Type	CRCP 12.8-in	
Base Type	4-in ACP TY. B, GR. 1	100 mm
Subgrade Type	6-in Lime Treated Subgrade	150 mm
Drainage Type	-	
Embankment Height	~23-ft	
Distress Observed	MSE wall bulging, Departure slab settlement, Faulting, Lane Separation	



(a) (b)

Figure 4-64. (a) Site location and (b) location of Section E-4

4.1.30.2 Distress types

The major distresses observed in Section E-4 were bulging of MSE wall, settlement of departure BAS, faulting and lane separation along longitudinal joint between the pavement and gore area. Repair was performed in 2021 by undersealing and adding an additional support for MSE wall. **Figure 4-65** shows settlement, lane separation, faulting, lateral bulging of MSE wall panel and diagonal crack.



Figure 4-65. Distress observed at Section E-4 (a) settlement of departure BAS (b) lateral separation and faulting between gore area and ramp (c) MSE wall panel bulge (d) diagonal/halfmoon crack.

4.2 Final field test sections

From the 30 total potential sections, the Research Team selected 11 final test sections to be investigated in this project. In the selection process, the Research Team considered the types of observed distresses, severities of the distresses, and embankment configurations. The main goal

was to review the 30 sections holistically and select final test sections in such a way that they encompass various types of severe distresses (or potentially different causes of poor performance) as well as various types of embankment configurations. Locations of the final 11 sections are presented in **Figure 4-66**.

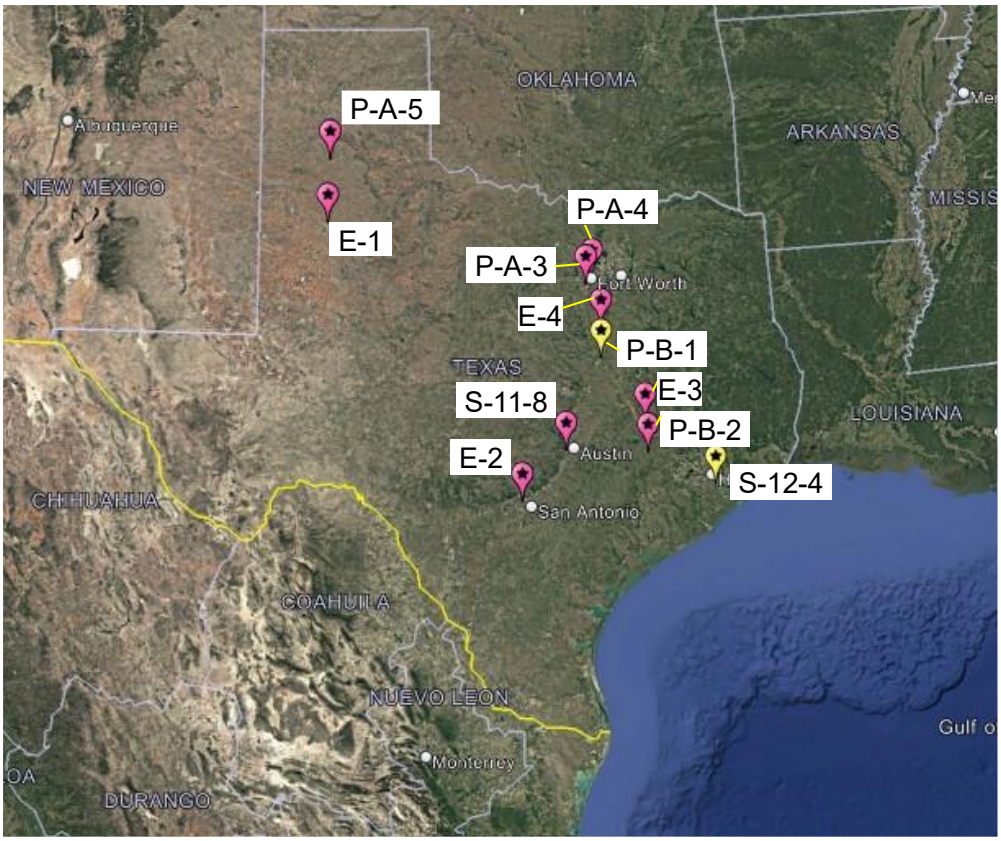


Figure 4-66. Locations of final sections selected for this project

The final selected section can be subdivided into two categories: (1) sections that require new field investigations (a total of 9 sections) and (2) sections that were previously investigated and require detailed data analyses (a total of 2 sections). **Table 4-29** summarizes details of final selected sections.

Table 4-29. Summary of final test sections selected

Section ID	District	Highway	GPS Coordinate	Year completed	Pavement type	Embank-ment type	Embankment height at BAS	Major distress types/Repair history
(1) Sections where new field evaluations are required								
P-A-3	Fort Worth	IH-20	32°39'51.0"N 97°19'52.2"W	1991	CRCP	WS	17 ft	Excessive settlements; Longitudinal cracks
P-A-4	Fort Worth	IH-820	32°45'13.4"N 97°13'00.4"W	1989	CRCP	WW	19 ft	Excessive settlement
P-A-5	Lubbock	IH-27	34°34'34.0"N 101°47'37.8"W	1988	CRCP	SS	32 ft	Longitudinal cracks; Spalling
P-B-2	Bryan	US-290	30°08'36.1"N 96°21'51.4"W	2013	CRCP	WW	34 ft	Excessive settlement; Longitudinal cracks (Full-depth repair)
S-11-8	Austin	US-290	30°13'38.3"N 97°46'35.9"W	1996	ACP	WW	33 ft	Settlement; Longitudinal crack
E-1	Lubbock	IH-27	33°38'35.6"N 101°50'08.8"W	1978	CRCP	SS	31 ft	Longitudinal crack; Settlement (Lane separation in the past)
E-2	San Antonio	IH-10	29°29'41.4"N 98°32'51.3"W	2009	CRCP	WW	35 ft	Excessive settlement, lane separation, and voids
E-3	College station	SH-47	30°35'40.3"N 96°23'30.2"W	2014	ACP	WW	30 ft (west wall); 14 ft (east wall)	Settlement
E-4	Hillsboro	IH-35	32°00'59.5"N 97°05'45.3"W	2002	CRCP	WS	23 ft	Longitudinal cracks; Lateral movement of wall
(2) Sections that were previously investigated and included in this project for detailed data analyses								
P-B-1	Waco	IH-35	31°33'58.2"N 97°06'57.9"W	2019	CRCP	WS	35 ft	Severe longitudinal cracks

S-12-4 (P-B-3)	Houston	BW-8	29°36'17.3"N 95°12'28.9"W	1997	CRCP	WS	20 ft	Excessive settlements; lane separation; and faulting; movement of MSE wall

Note: 'WW' stands for Wall-Wall, 'SS' stands for Slope-Slope, and 'WS' stands for Wall-Slope.

As shown in **Table 4-29**, two sections out of 11 sections are embankments with slopes on both sides and the remaining 9 sections have a retaining wall on one side or both. Embankment heights at the location of bridge approach slabs (BAS) vary from 17 ft to 35 ft, with 9 sections at least 20 ft or taller. Regarding the pavement structures, 9 sections are CRCP, and 2 sections are ACP. The selected final sections encompass various distress types such as settlement, longitudinal crack, lane separation, wall movement, and void formation near the bridge approach slabs.

Chapter 5 Field Investigations

The final field test sections described in Chapter 4 were selected to represent the range of distress types, embankment configurations, and pavement structures observed across TxDOT districts. This chapter documents the field investigation program conducted at those sections, discuss testing results, identify potential distress mechanisms, and propose repair strategies.

5.1 Section E-2: IH-10 in San Antonio

5.1.1 Overview

Section E-2 is the BAS and nearby pavement on eastbound and westbound main lanes of IH-10 in San Antonio, Texas, built on roadway embankments with MSE walls on both sides. Location of Section E-2 is shown in **Figure 5-1**. The pavement type of Section E-2 is a 13-in-thick continuously reinforced concrete pavement (CRCP) with a 10-in-thick hot mix asphalt (HMA) base. According to plan sets, Type B material was used as the embankment non-select fills below the base layer. Section E-2 has shown excessive settlements over the years, and hot mix asphalt overlays have been regularly performed to cope with the excessive settlements. Field evaluations of Section E-2 were conducted on November 14 (eastbound) and November 15 (westbound), 2023, by the TxDOT MNT division with assistance from the Research Team. **Figure 5-2** and **Table 5-1** show the typical section and detailed descriptions of Section E-2, respectively.

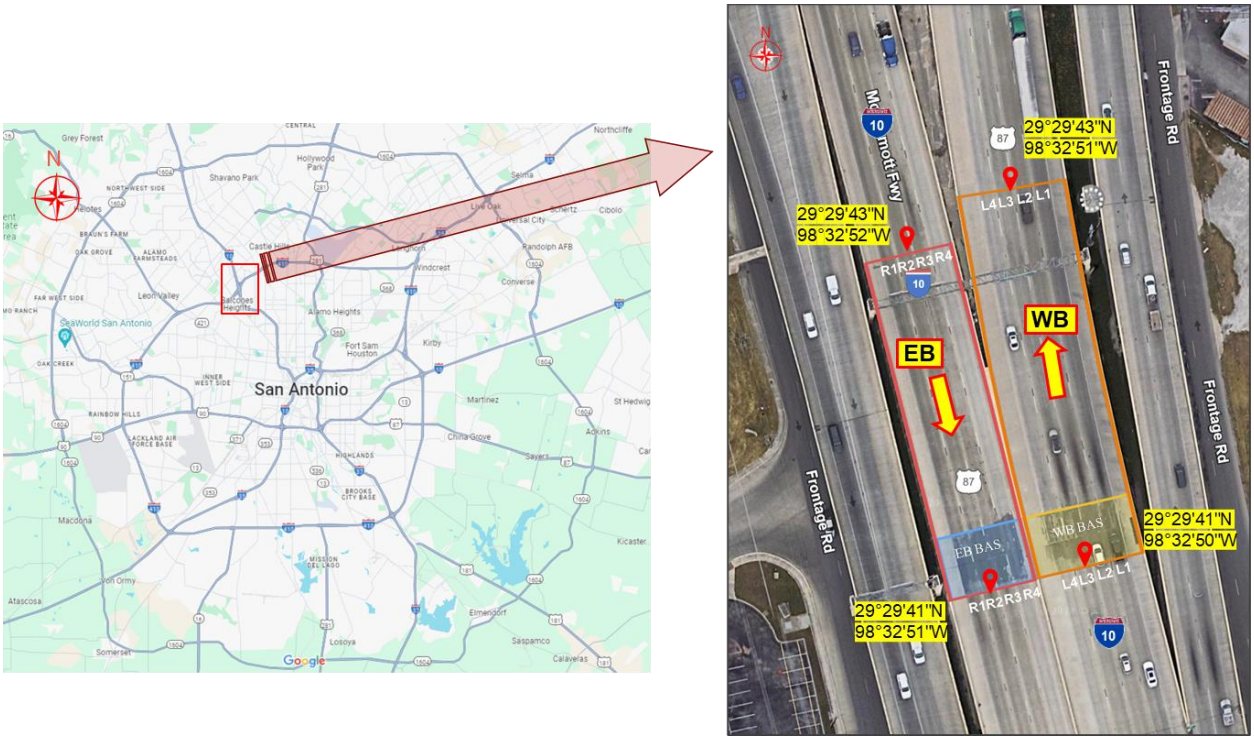


Figure 5-1. Location of Section E-2 on IH-10 in San Antonio, Texas

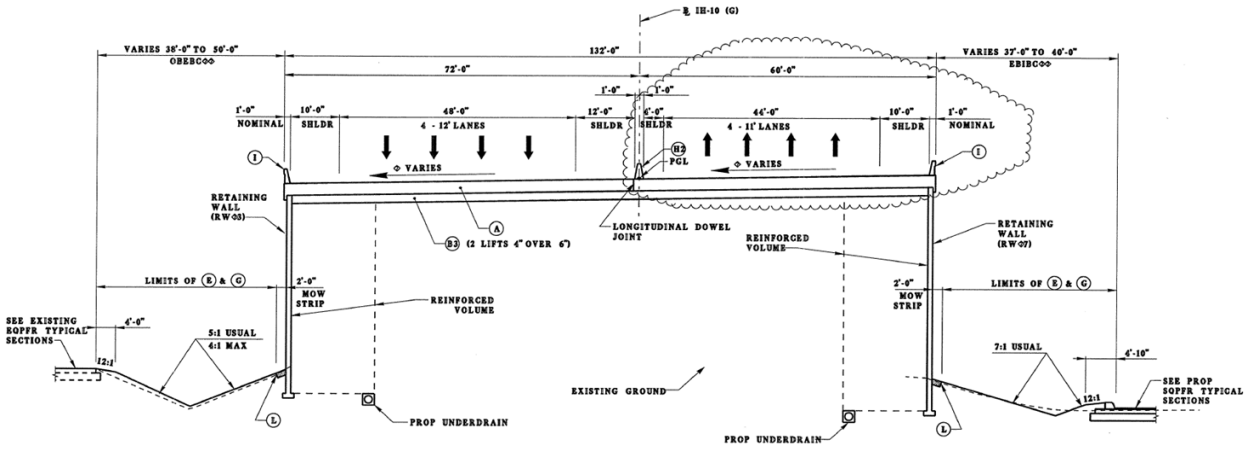


Figure 5-2. Typical section of Section E-2 on IH-10 in San Antonio, Texas

Table 5-1. Detailed descriptions of Section E-2 on IH-10 in San Antonio, Texas

Attribute	Information	Notes
District & Highway	San Antonio, IH-10 Mainlanes	Eastbound and westbound
CSJ	0072-12-159	
County	Bexar County	
Reference Marker	RM 564.236	
GPS Coordinates	29.494832, -98.547583	
Date Work Begin	09/23/2002	
Date Completed	03/09/2009	
Pavement Type	Rigid – CRCP (13")	
BAS Thickness	13"	
Shoulder Type	Tied Concrete	
Base Type	10" HMA (Type A)	
Subgrade Type	Embankment materials - Type B	
Drainage Type	Curb & Inlets	
Embankment Height at BAS	35 ft	MSE wall – MSE wall

5.1.2 Falling Weight Deflectometer (FWD) tests

FWD tests were conducted on the inside two lanes (R3 and R4) of eastbound and the inside two lanes (L3 and L4) and inside shoulder (IS) of westbound for structural evaluation of the pavement system. The spacing between FWD drop locations was 20 ft on CRCP and 2 ft on BAS. **Figure 5-3** below shows the FWD drop locations as performed in the project site.

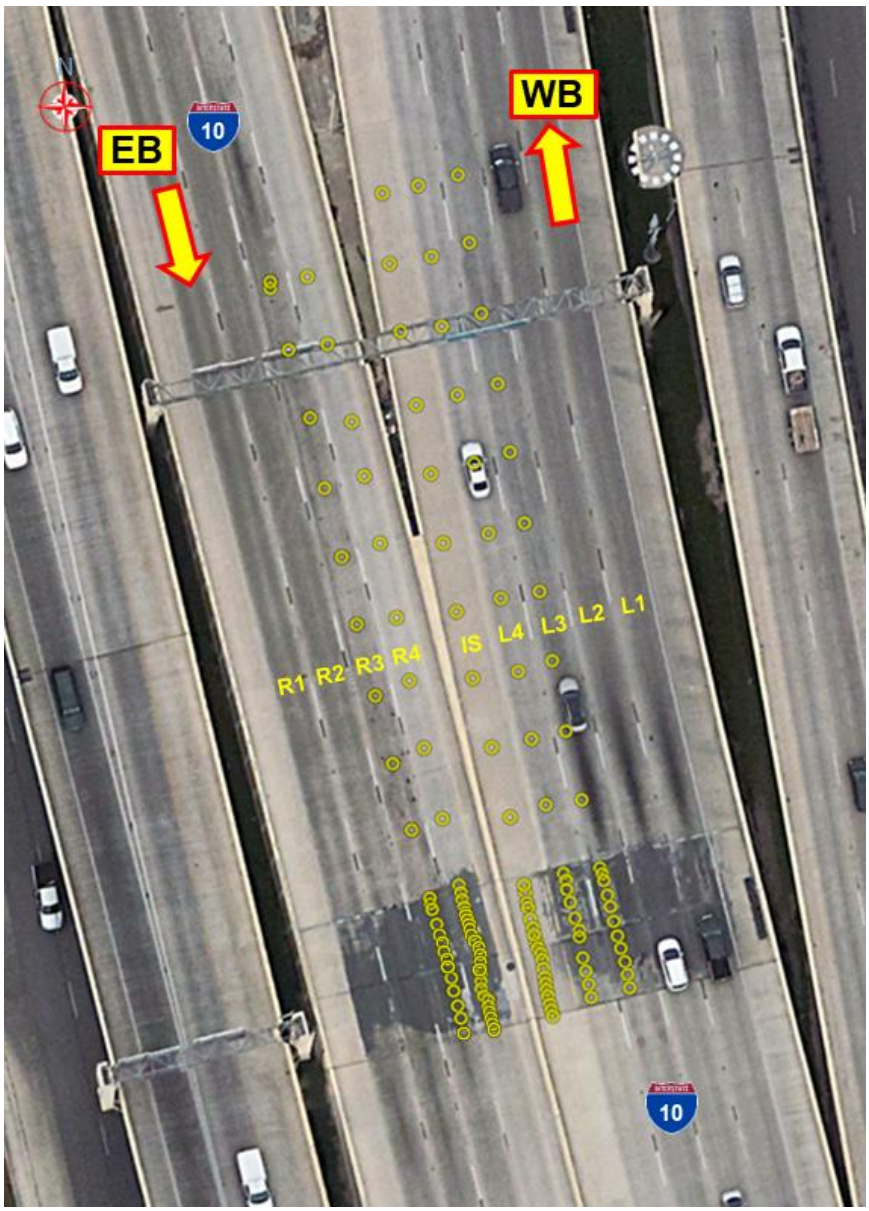


Figure 5-3. FWD drop location of Section E-2 on IH 10 in San Antonio, Texas

Eastbound

Figure 5-4 below presents FWD deflections normalized to a 9,000-lb load versus DMI for the inside two lanes (R3 and R4) of eastbound mainlanes. For the CRCP section (DMI 0 to DMI 200 ft), the deflection values were generally less than 2 mils except at DMI 38 ft in the R3 lane. In the BAS section (DMI 200 ft to 240 ft), the deflection values were generally greater than those in the CRCP section.



Figure 5-4. FWD testing location and deflections measured in the middle (R3) and inside (R4) lanes of eastbound main lanes

Westbound

Figure 5-5 presents the normalized FWD deflections versus DMI for the inside lane (L4), middle lane (L3), inside shoulder (IS) of westbound main lanes. For the inside and middle lanes in the CRCP section (DMI 0 to DMI 200 ft), the deflection values were less than 2 mils but at BAS section (DMI 200 ft to 240 ft) the deflection values were much greater than those from the CRCP section, exceeding 6 mils at several locations. Similarly, for the inside shoulder, higher deflection values were observed at BAS section than at CRCP section, except the high deflection value at DMI of 140 ft.

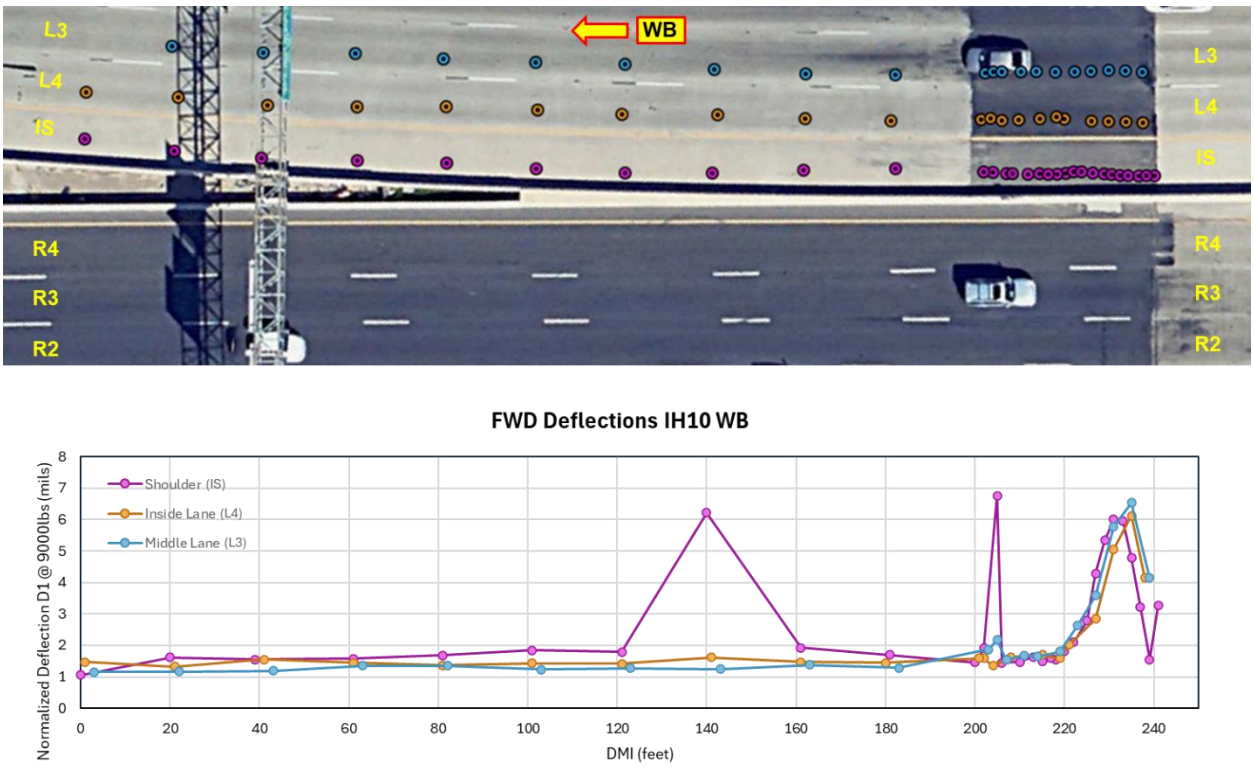


Figure 5-5. FWD testing location and deflections measured at inside lane (L4), middle lane (L3), and inside shoulder (IS) of westbound

5.1.3 Coring

Four concrete cores samples (C1, C2, C3, and C6) were taken in the vicinity of the areas where high FWD deflections were observed. As a control, two additional core samples (C4 and C5) were taken where low FWD deflection were observed. The locations of the six core samples are presented in **Figure 5-6**, as well as images of the core samples taken.

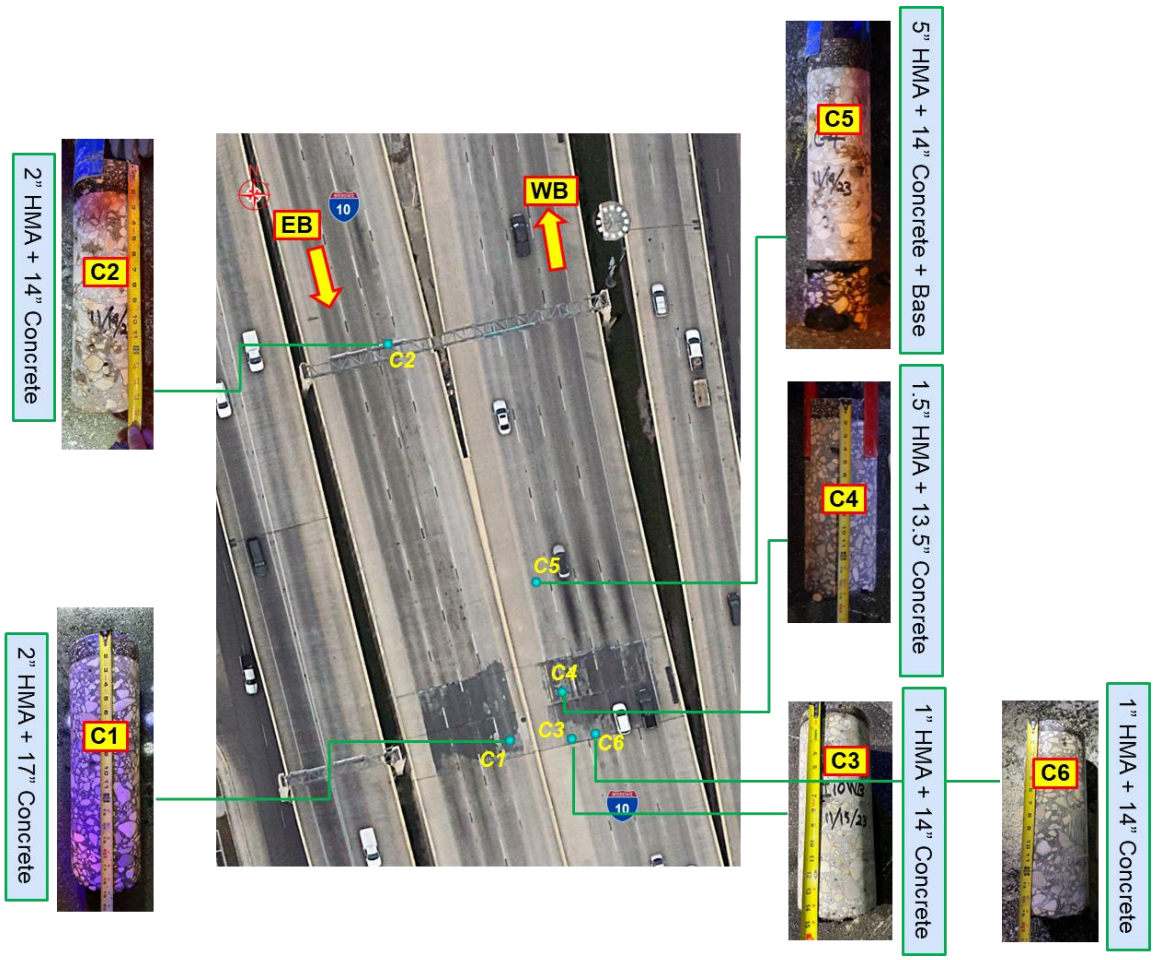
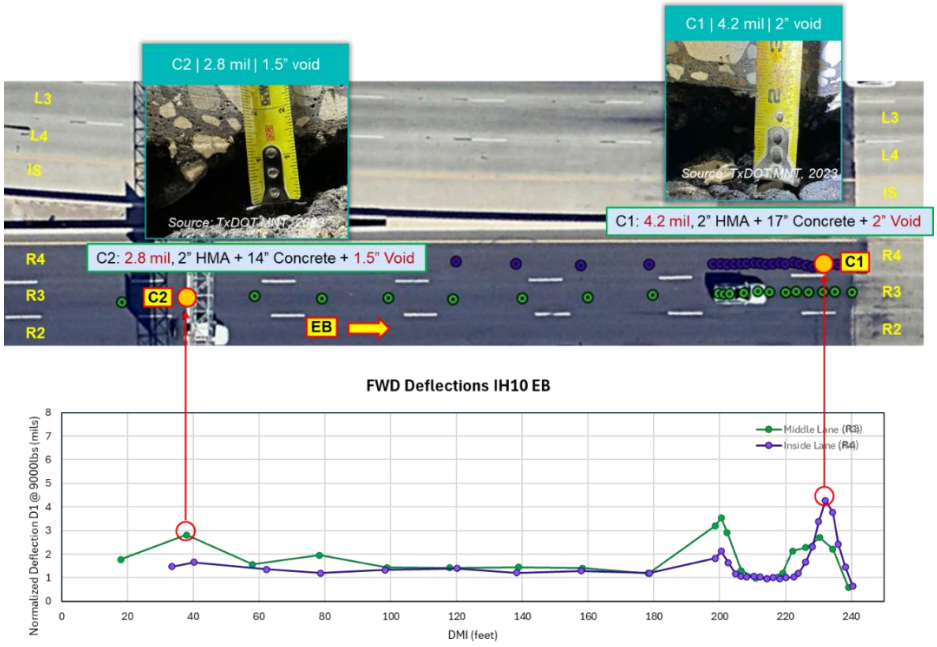
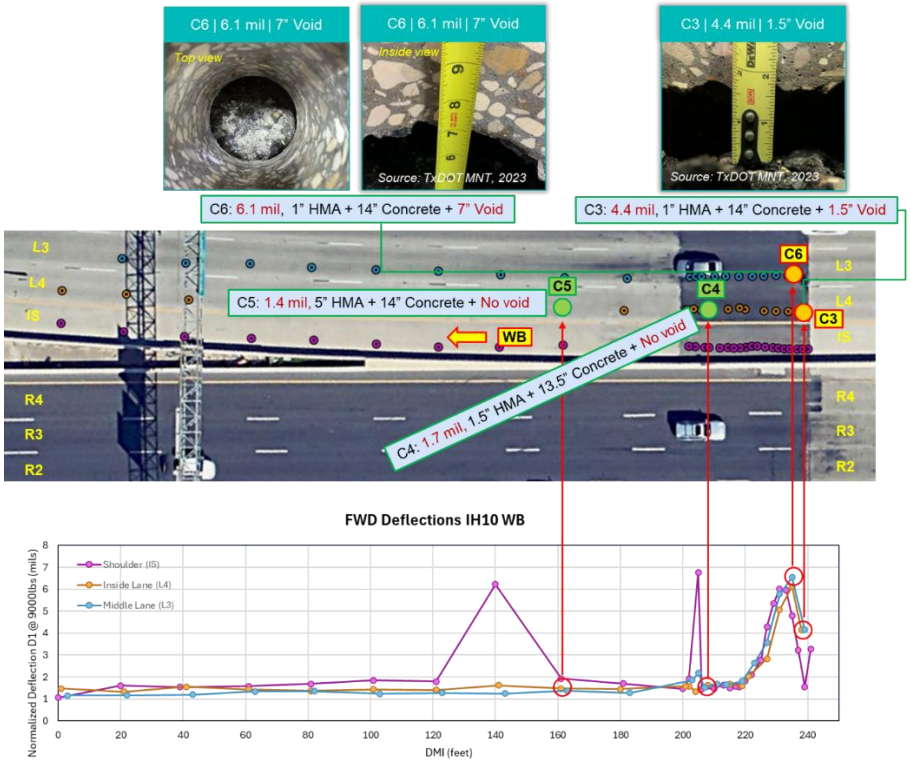


Figure 5-6. Coring locations and images of core samples

All six core samples had a HMA layer above the concrete with the thickness of the HMA layer ranging from 1 to 5 in, indicating the previous repair attempts via HMA overlays. Out of the six core samples, none of them exhibited any signs of poor concrete material quality. However, at the bottom of the cored hole, voids were observed from the four locations where high FWD deflection values were recorded. **Figure 5-7(a)** and **Figure 5-7(b)** show the photos of void thickness measurement at the cored holes in relation to FWD deflection at eastbound and westbound, respectively.



(a)



(b)

Figure 5-7. Void thickness measured from coring operations in relation to FWD deflection: (a) eastbound and (b) westbound main lanes

As presented in **Figure 5-7**, voids with the thicknesses ranging from 1.5 to 7 in were observed beneath the concrete at four core locations (C1, C2, C3, and C6) where high FWD deflections were observed. On the other hand, no voids were observed at the two control locations (C4 and C5). **Table 5-2** summarizes the thickness of voids as well as FWD deflections at each core location.

Table 5-2. Summary of void thickness measured at core holes

Core location	Latitude	Longitude	Pavement structure	FWD deflection (mil)	Void thickness (in)
C1	29.4947910	-98.5476169	2" HMA + 17" Concrete	4.2	**2**
C2	29.4952972	-98.5477949	2" HMA + 14" Concrete	2.8	**2**
C3	29.4947931	-98.5475251	1" HMA + 14" Concrete	4.1	1.5
C4	29.4948549	-98.5475394	1.5" HMA + 13.5" Concrete	1.7	0
C5	29.4949943	-98.5475782	5" HMA + 14" Concrete	1.4	0
C6	29.4948110	-98.5474926	1" HMA + 14" Concrete	6.1	**7**

5.1.4 Dynamic Cone Penetrometer (DCP) tests and Cone Penetration Tests (CPT)

To estimate backfill/subgrade conditions of the embankment in the test section, DCP tests were conducted at each core location. To access the subgrade material for further testing activities, additional drilling was performed through the bottom of the cored hole. The DCP cone was then inserted through this drilled hole to perform the DCP test.

Results from DCP tests are usually interpreted from the cumulative DCP blow counts vs. depth curves to determine the resilient moduli of soils. The slope of the cumulative DCP blow counts vs. depth curve represents a penetration rate (*i.e.*, penetration depth per blow), and the steeper slope indicates a greater penetration rate or lower modulus of soil. Webster et al. (1992) proposed the following equation to estimate the soil modulus (M_r) of soil from the penetration rate of DCP:

$$M_r[ksi] = 2.55\left(\frac{292}{PR^{1.12}}\right)^{0.64} \quad (1)$$

where PR = penetration rate in mm/blow. The cumulative DCP blow counts vs. depth curves from all six DCP tests are presented in **Figure 5-8**.

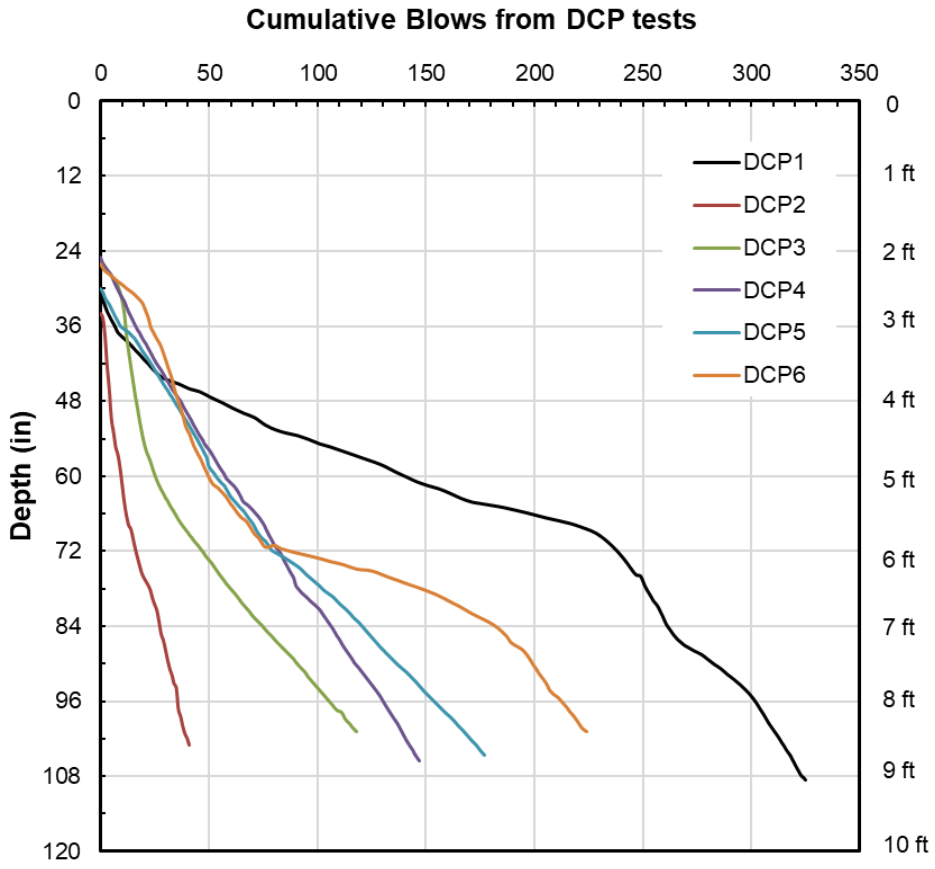


Figure 5-8. Results from DCP tests: Cumulative blow counts vs. Penetration depth below the pavement surface

The moduli (M_r) of embankment soils at each DCP test location were estimated using Eq. (1), and the results are presented in **Figure 5-9**. At control locations (DCP4 and DCP5), M_r values were greater than 10 ksi for the entire investigation depth (about 9 ft) and no voids were observed beneath the concrete. However, at other locations (DCP1, DCP2, DCP3, and DCP6), soil layers with M_r values less than 10 ksi were observed (DCP2 and DCP3) and/or voids existed beneath the concrete.

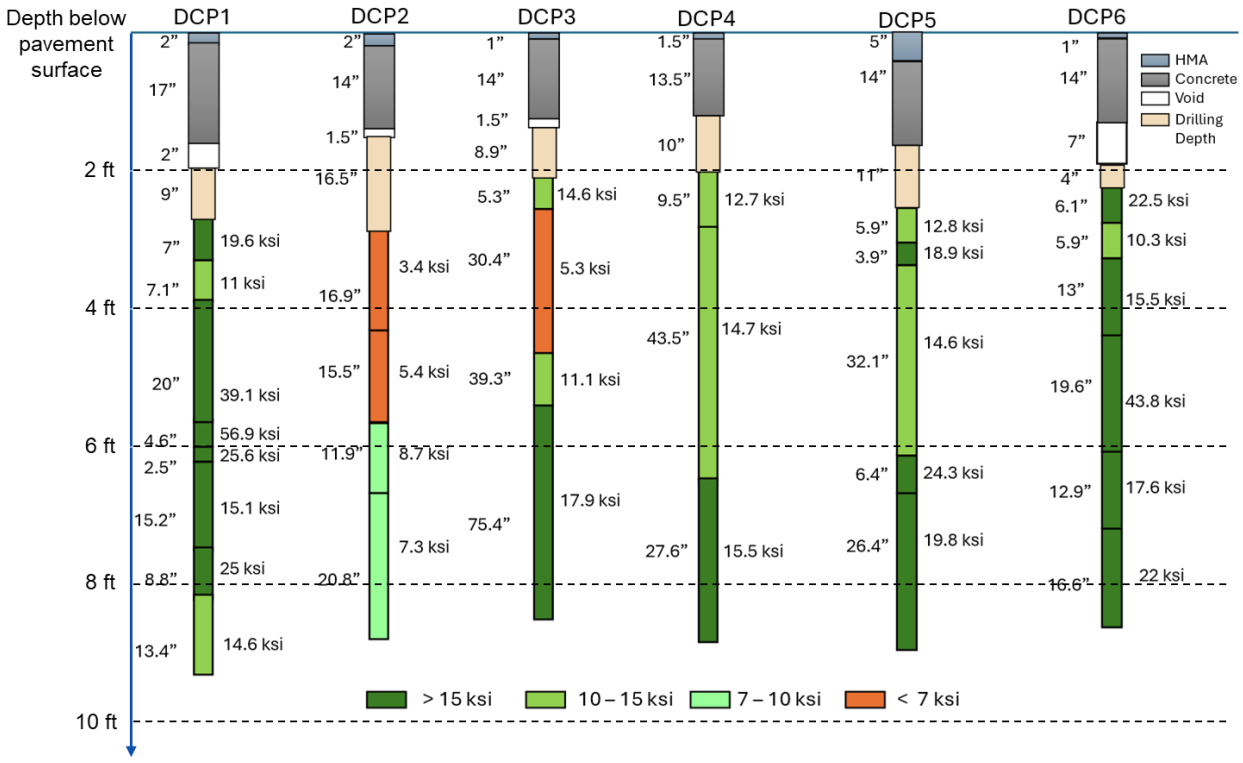


Figure 5-9. Resilient modulus determined from DCP tests (Notes: DCP4 and DCP5 are controls; the color scheme for M_r value is for illustrative purposes only.)

To characterize soil conditions for the entire embankment height, six CPTs were conducted at locations 1 through 6 near the corresponding DCP tests, typically within 2 ft of each other. The maximum CPT investigation depth was 32.7 ft below the pavement surface at location CPT2. **Figure 5-10** presents the cone tip resistance (in tsf) at all six CPT locations. Overall, the cone tip resistance was less than 30 tsf, except for CPT1.

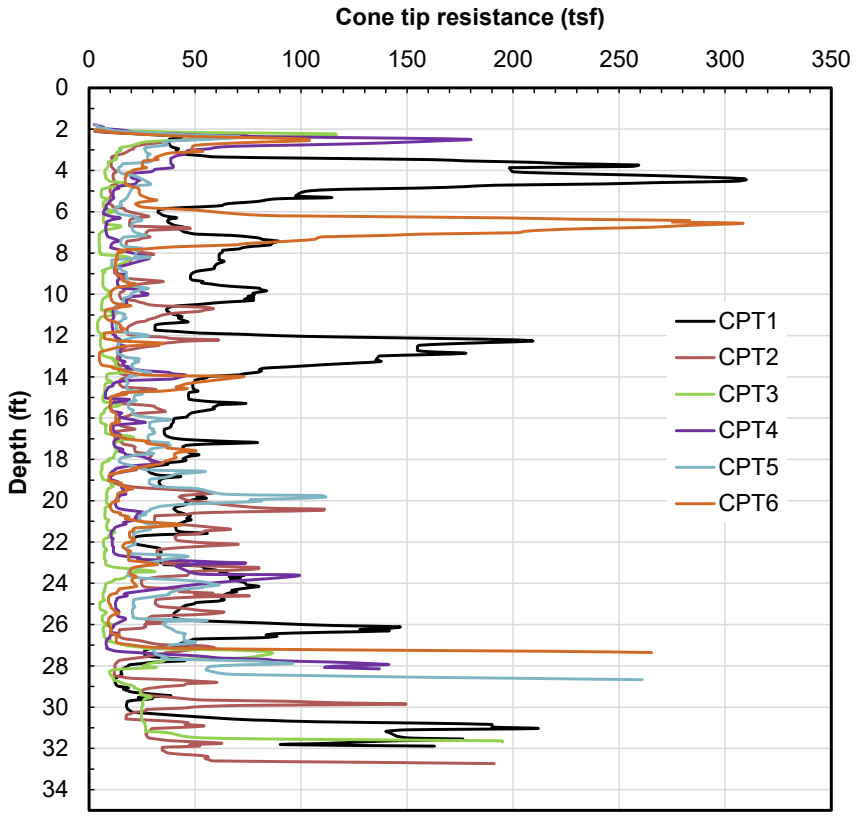


Figure 5-10. Cone tip resistance measured from CPTs

The soil behavior types of the embankment backfill interpreted from the CPTs are presented in **Figure 5-11** which indicate that the embankment soils are likely clayey soils. The soil behavior type charts further suggest that soils are coarser at shallow depths (3' – 5') than at deeper depths. Particularly, at CPT6, where a 7" void was observed beneath the BAS, the CPT results suggest that the soil behavior types are sands or sand mixture to a depth of about 8 ft; whereas below 8 ft, the soil behavior type is a predominantly clay. Also, the results from CPT1, where 2" void was observed beneath the CRCP, indicate the presence of sandy soils to a depth of about 15' below the pavement surface. The fact that the backfill soils are coarser at shallow depths and become finer at deeper depths suggests that the embankment fill might have lost fines over time, potentially due to washout caused by water infiltration at the shallow depths.

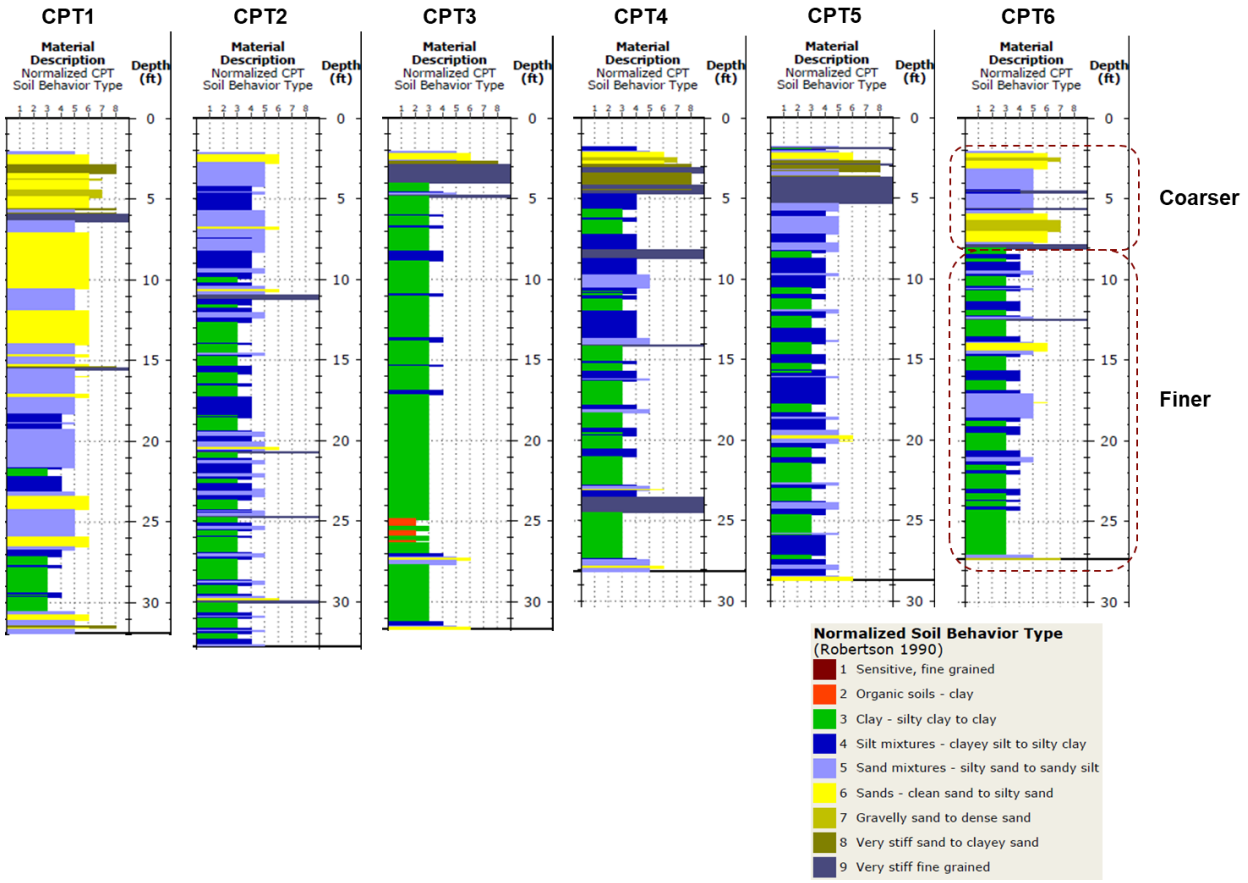


Figure 5-11. Soil behavior types estimated from CPT results

To empirically determine soil moduli M_r of the embankment fill soils using the CPT results, the resilient moduli from the DCP tests were compared to the average CPT cone resistances for the corresponding soil layers. A regression analysis, as shown in **Figure 5-12**, was then performed to establish a site-specific correlation between them. It should be noted that the CPT tip resistances greater than 50 tsf were excluded from the regression analysis to focus on characterization of soft soils.

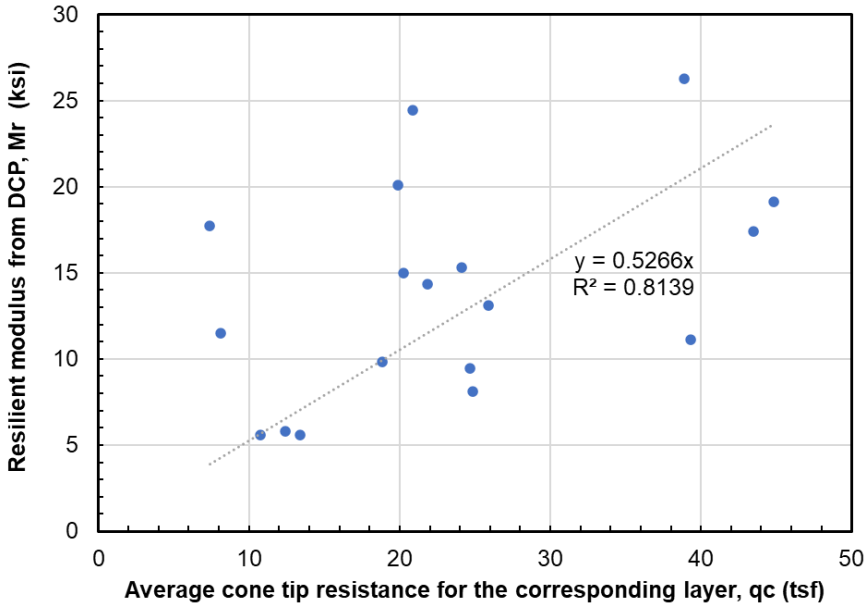
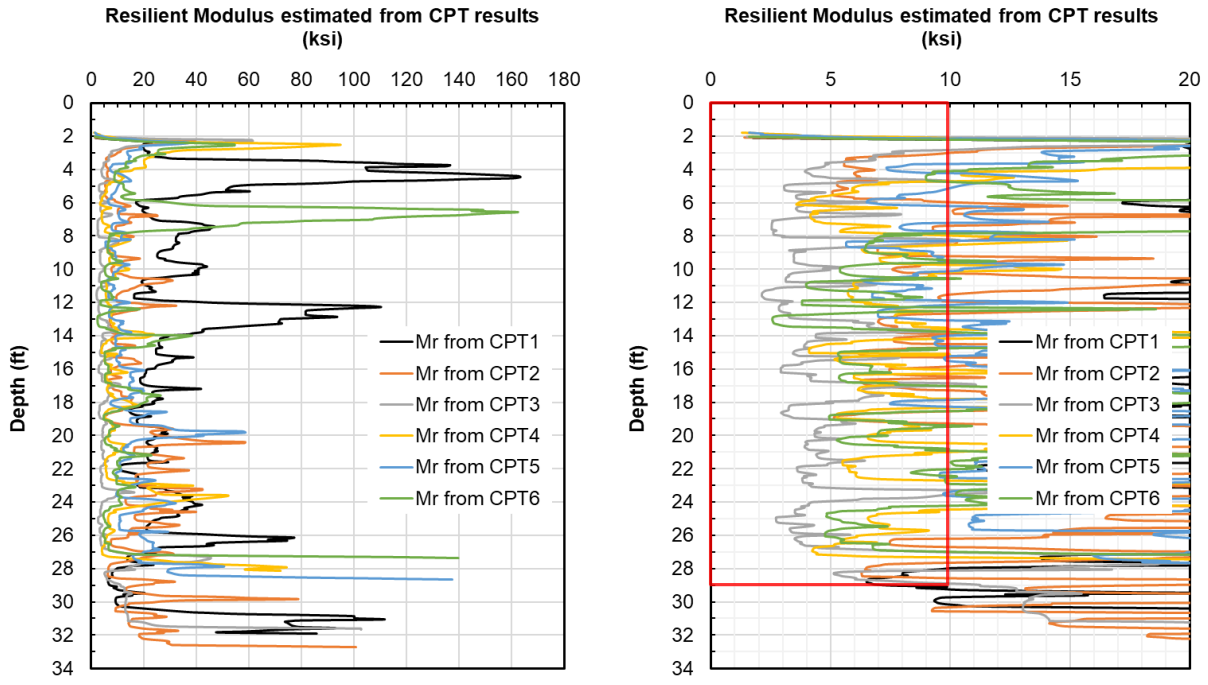


Figure 5-12. Correlation between resilient moduli from DCP tests and average cone resistances from CPTs for the corresponding layers (Note: For information purpose only)

The M_r values of embankment fill soils were then determined using the established correlation from the cone resistance measurements for the entire CPT investigation depths. **Figure 5-13** presents the M_r values estimated from CPT results, showing that the M_r values of embankment backfill soils are overall less than 10 ksi to a depth of 29 ft, except for CPT1 and CPT5, suggesting the poor conditions of backfill soils.

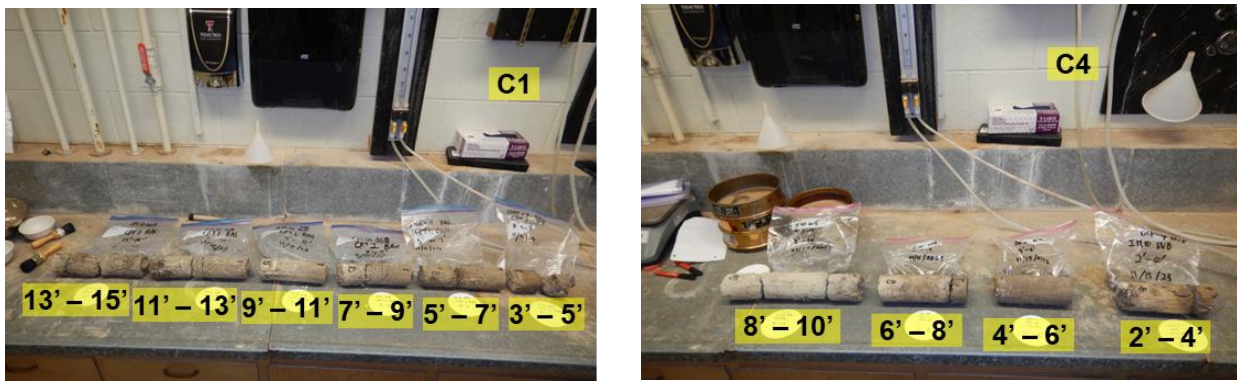


(a) (b)

Figure 5-13. Resilient moduli of embankment backfill soils estimated from CPT results: (a) whole data and (b) zoomed-in view (Note: For information purpose only)

5.1.5 Soil sampling

The CPT rig was equipped with soil sampling equipment, and the Shelby tube was used to collect soil samples at the locations of C1 (from 3' to 15') and C4 (from 2' to 10'). **Figure 5-14** shows the photos of soil sample taken from the two holes.



(a) (b)

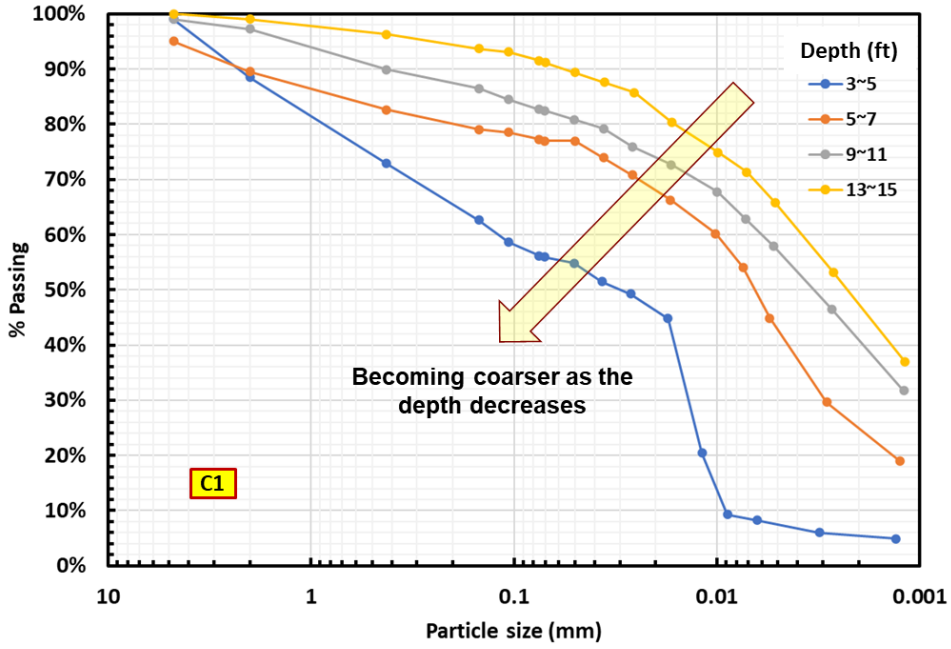
Figure 5-14. Photos of soil sample taken from the locations of (a) C1 and (b) C4

A series of laboratory tests conducted on the collected soil samples classified the embankment fills as low-plastic clay (CL), with LL ranging between 27 and 48 and PI ranging between 10 and 28 per the USCS. The water contents of the collected soil samples ranged between about 11% and 24%. **Table 5-3** summarizes the results of the laboratory tests conducted on the soil samples.

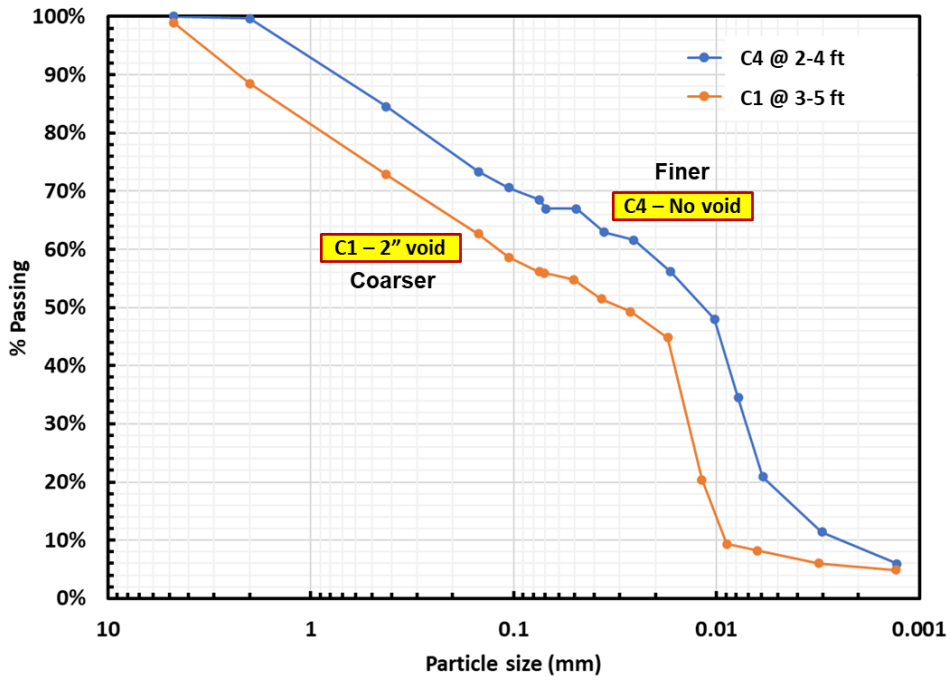
Table 5-3. Summary of laboratory test results.

Sample and sampling depth		**Moisture Content**	**Atterberg limits**			**USCS Classification**	**% Passing No. 200 sieve**
			LL	**PL**	**PI**		
C1	3’ – 5’	11.2%	27	17	10	CL	56.1%
	5’ – 7’	22.2%	38	19	19	CL	77.2%
	7’ – 9’	23.1%	40	16	24	CL	-
	9’ – 11’	21.7%	40	16	24	CL	82.7%
	11’ – 13’	24.3%	42	14	28	CL	-
	13’-15’	22.3%	43	20	23	CL	91.5%
C4	2’ – 4’	15.6%	29	18	11	CL	68.5%
	4’ – 6’	23.4%	41	14	27	CL	67.6%
	6’ – 8’	17.2%	42	18	24	CL	-
	8’ – 10’	21.4%	48	21	27	CL	88.2%

Particle size distribution curves obtained from C1 sample at various depths are presented in **Figure 5-15(a)**. Both the CPT results and laboratory particle size analysis confirm that fill material is significantly coarser at the shallow depth. For example, the percentage passing No. 200 sieve was about 56% at a depth of 3’ to 5’ but increased to about 92% at 13’ to 15’. **Figure 5-15(b)** shows the comparison of particle size distribution curves between C1 (where 2” void was observed beneath the BAS) and C4 (where no void was observed) at similar depth. **Figure 5-15(b)** indicates that the backfill soils were coarser at the location of C1 than at C4, and this observation suggests that the formation of void at C1 might have been caused by the washout of fines due to water infiltration and ensuing volume decrease. **Figure 5-16** conceptually illustrates this process.



(a)



(b)

Figure 5-15. Particle size distribution curves: (a) soil samples taken from C1 at various depths and (b) comparison between C1 and C4 at similar depth

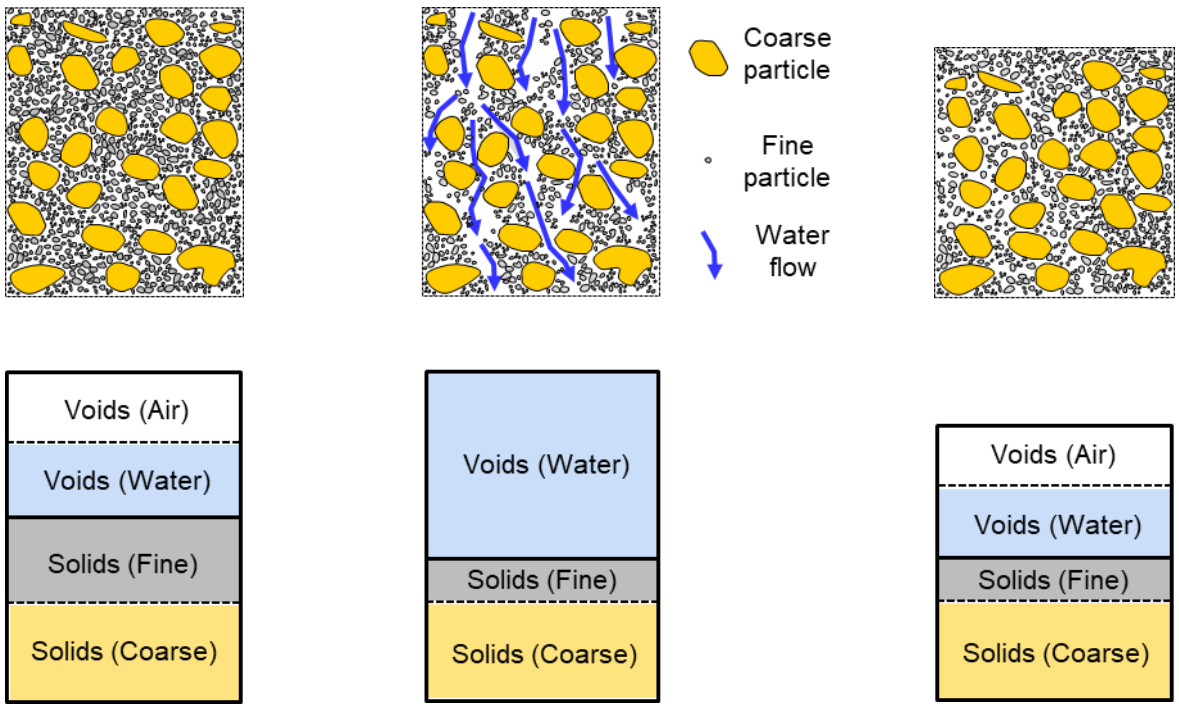


Figure 5-16. Conceptual illustration of washout of fines due to water infiltration and ensuing volume decrease: (a) initial soil composition, (b) washout of fines due to water infiltration, and (c) decrease in volume after washout

5.1.6 Potential Distress Mechanisms

Based on field observations and test results, the observed distresses for Section E-2 are attributed to a combination of compression of fill materials and subsequent material washout caused by water infiltration. This process can be described in two primary stages as shown in **Figure 5-17** and **Figure 5-18**. First, DCP tests indicated that the fill materials were poorly-compacted or had weakened because of material washout over time, particularly in areas exhibiting high FWD deflections (**Figure 5-17**). Specifically, resilient moduli values less than 10 ksi were observed in the soil layers beneath the pavement where distresses were evident. Under continuous traffic loads, the lack of adequate slab support led to differential settlement and the formation of voids beneath the BAS.

The formation of the voids and the deterioration of pavement joints facilitated water infiltration into the embankment. Laboratory particle size analysis provided strong evidence of material washout. The embankment fills were found to be significantly coarser at shallow depths compared to deeper depths. This suggests that as water flowed through the embankment, fine particles were washed out from the upper layers, causing a decrease in soil volume and further exacerbating the voids beneath the BAS (see **Figure 5-18**).

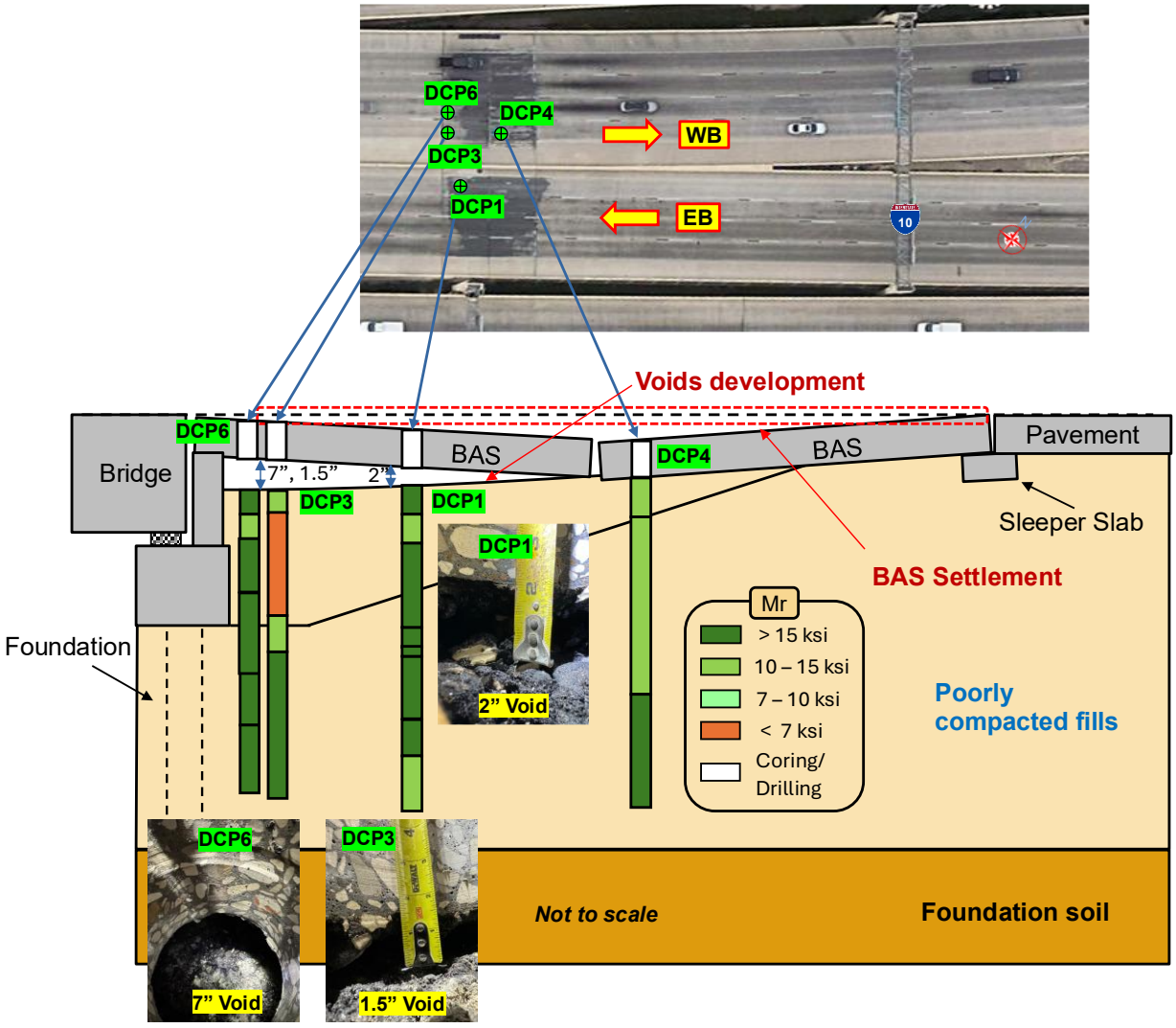


Figure 5-17. Distress mechanism of void formation and BAS settlement in Section E-2 (Note: the color scheme for M_r value is for illustrative purposes only.)

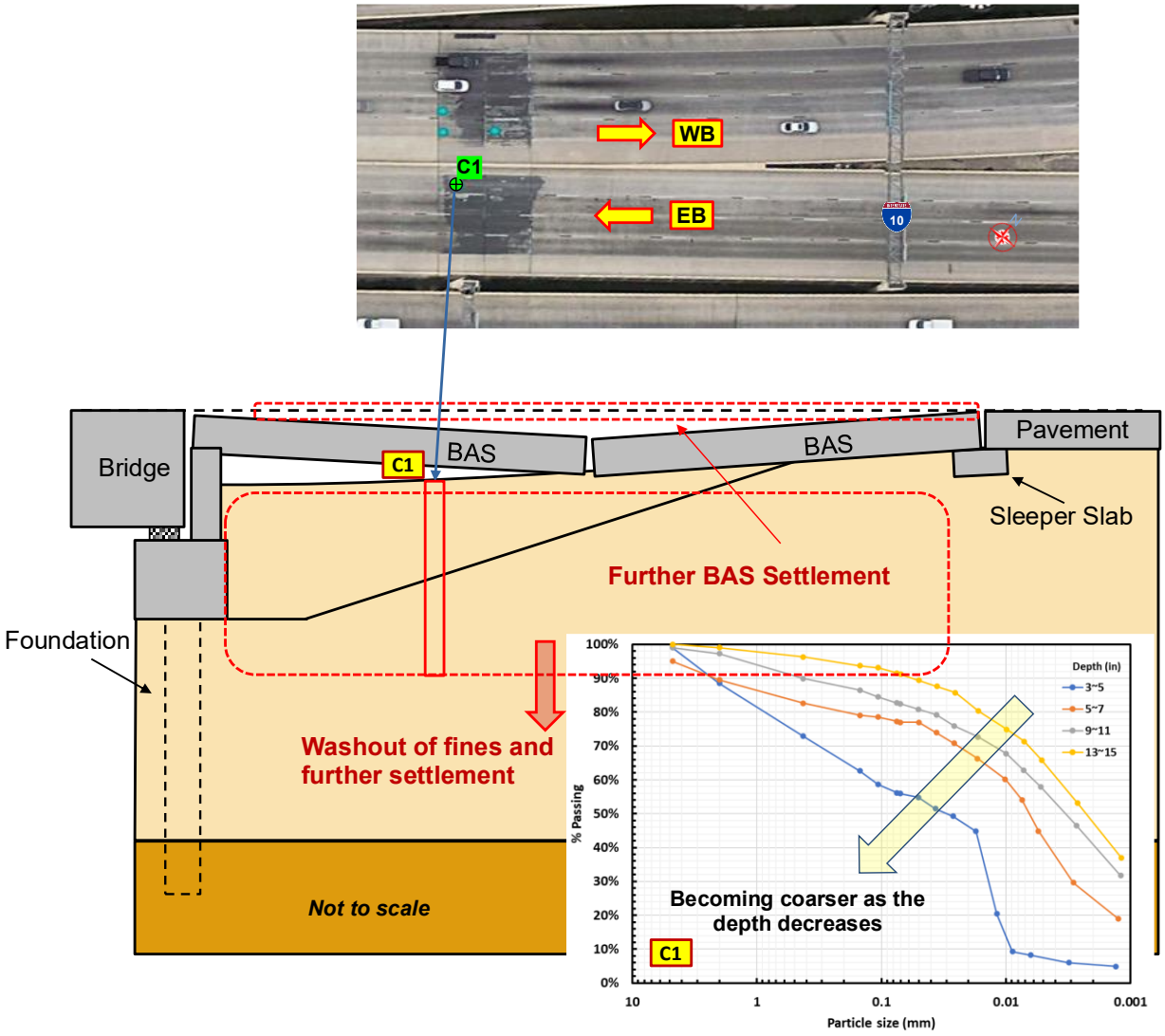


Figure 5-18. Potential distress mechanism of material washout in Section E-2

5.1.7 Repair Recommendation

Field investigations indicated that the distresses observed in Section E-2 such as settlement of bridge approach slab (BAS), void formation, and material washout can be attributed to the compression of embankment fill and water infiltration.

Significant voids (up to 7 inches) were detected in the westbound lanes, requiring immediate attention. To restore pavement-base contact, it is recommended to inject flowable fill (TxDOT Item 401) using the existing investigation core holes. These holes currently contain the original concrete cores covered by temporary HMA cold mix patches as shown in **Figure 5-19**. To prepare for injection, the cold mix and the underlying concrete cores must be removed. The recommended

flowable fill injection location is shown in **Figure 5-20**. During the injection process, MSE wall panel joints, coping, and riprap must be monitored to detect any material loss or blowout.



(a) (b)

Figure 5-19. Existing investigation (a) core hole temporarily patched with (b) HMA cold mix.

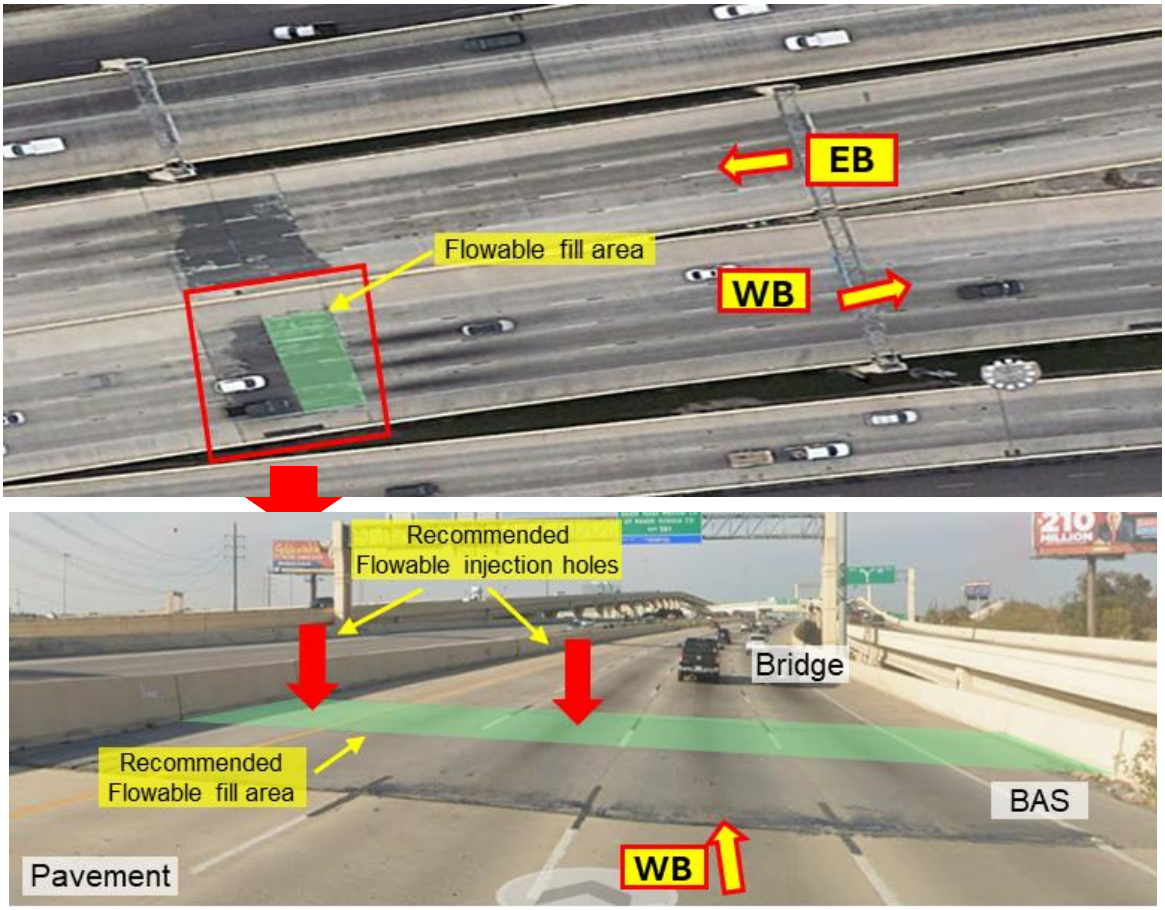


Figure 5-20. Recommended flowable fill injection locations

Regarding the westbound outside two lanes and shoulder, two rehabilitation options are recommended to address the condition without immediate reconstruction. Option 1 is to implement a continued hot mix asphalt (HMA) overlay to maintain BAS serviceability. Option 2 is undersealing (SS 3025) for the BAS area and soil densification with HDPF (SS 3086) for the CRCP sections. Following repairs, annual FWD testing should be conducted to monitor pavement structural performance over time. Also, any deteriorated joints or openings should be sealed to prevent the infiltration of water.

5.2 Section E-3: SH-47 in College Station

5.2.1 Overview

Section E-3 comprises the BAS and nearby pavement on southbound and northbound main lanes of SH-47 in College Station, Texas, built on roadway embankments with MSE walls on both sides. The location of Section E-3 is shown in **Figure 5-21**. The pavement structure consists of a 4-in-thick asphalt concrete pavement (ACP), a 6-in-thick flex base, and an 8-in cement-treated subgrade. According to plan sets, Type A material was used as non-select embankment fill, and Type BS material was used as select fill for the MSE wall. Due to historic settlement issues, HMA overlays have been regularly applied as a repair measure. Field evaluations were conducted by the TxDOT MNT Division and the Research Team on October 9 (Southbound) and October 10 (Northbound), 2024. **Figure 5-22** and **Table 5-4** show the typical section and detailed descriptions of Section E-3, respectively.

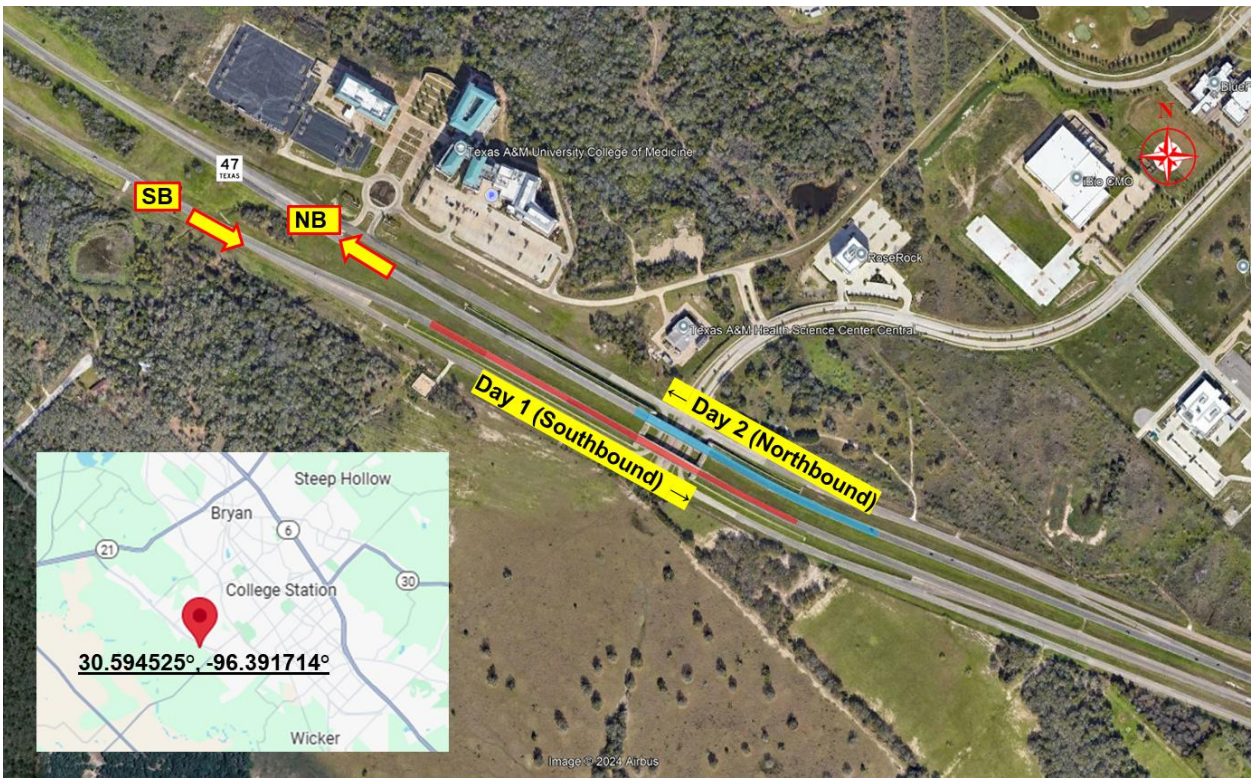


Figure 5-21. Location of Section E-3 on SH-47 in College Station, Texas

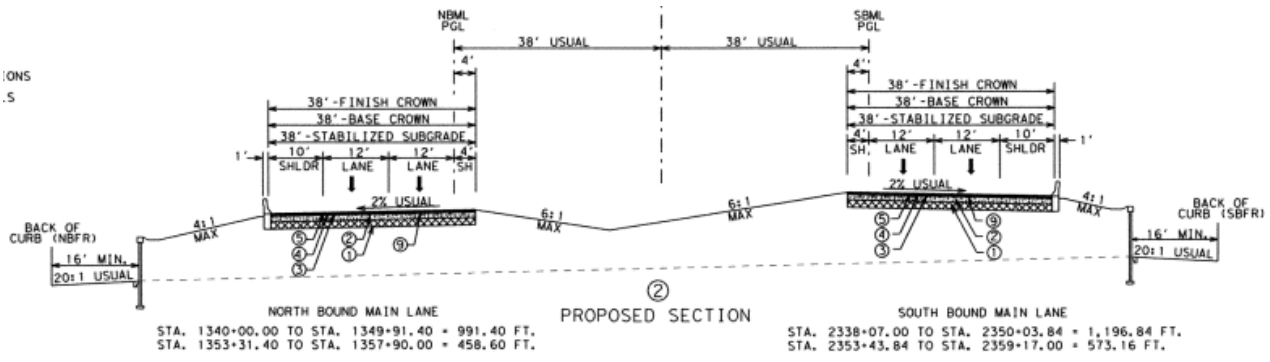


Figure 5-22. Typical section of Section E-3 on SH-47 in College Station, Texas

Table 5-4. Detailed descriptions of Section E-3 on SH-47 in College Station, Texas

Attribute	Information	Notes
District & Highway	Bryan & SH-47 main lanes	Southbound and Northbound
CSJ	3138-02-010	
County	Brazos County	
Reference Marker	From RM 416 + 0.885 to RM 418 + 0.515	
GPS Coordinates	30°35'40.3"N 96°23'30.2"W	
Date Work Begin	2/9/2012	
Date Completed	8/7/2014	
Pavement Type	2-in TY C ACP PG64-22 SAC-A + 2-in TY C ACP PG64-22 + One Course Surface Treatment	
BAS Thickness	13-in BAS-A (MOD)	
Shoulder Type	ACP	
Base Type	6-in Flex Base	
Subgrade Type	8-in Cement Treated Subgrade	
Drainage Type	Side Ditches & Curbs	
Embankment Height at BAS	30-ft @ Begin Bridge (West Side) 14.5-ft @ End Bridge (East Side)	MSE wall – MSE wall

5.2.2 Falling Weight Deflectometer (FWD) tests

For the southbound main lanes, FWD tests were conducted on the inside and outside lanes to evaluate the structural performance of the pavement. In the northbound main lanes, testing was extended to the inside lane, outside lane, and outside shoulder. FWD drop intervals ranged from 20 to 50 ft on the regular pavement and were reduced to 2 ft at BAS. FWD deflections were evaluated at a normalized 9,000-lb load.

Southbound

Figure 5-23 below presents FWD drop locations and deflections versus DMI from the southbound inside and outside lanes. The pavement section is located from DMI 0 to DMI 900 ft and DMI 1240 ft to 1800 ft, while the BAS section spans from DMI 900 ft to 920 ft and DMI 1220 ft to 1240 ft. The deflection values range from approximately 2 to 33 mils, with the outside lane generally exhibiting higher deflections than the inside lane. Furthermore, BAS and nearby pavement on the west side (approach side) of the bridge exhibited higher deflections than those on the east side (leave side).

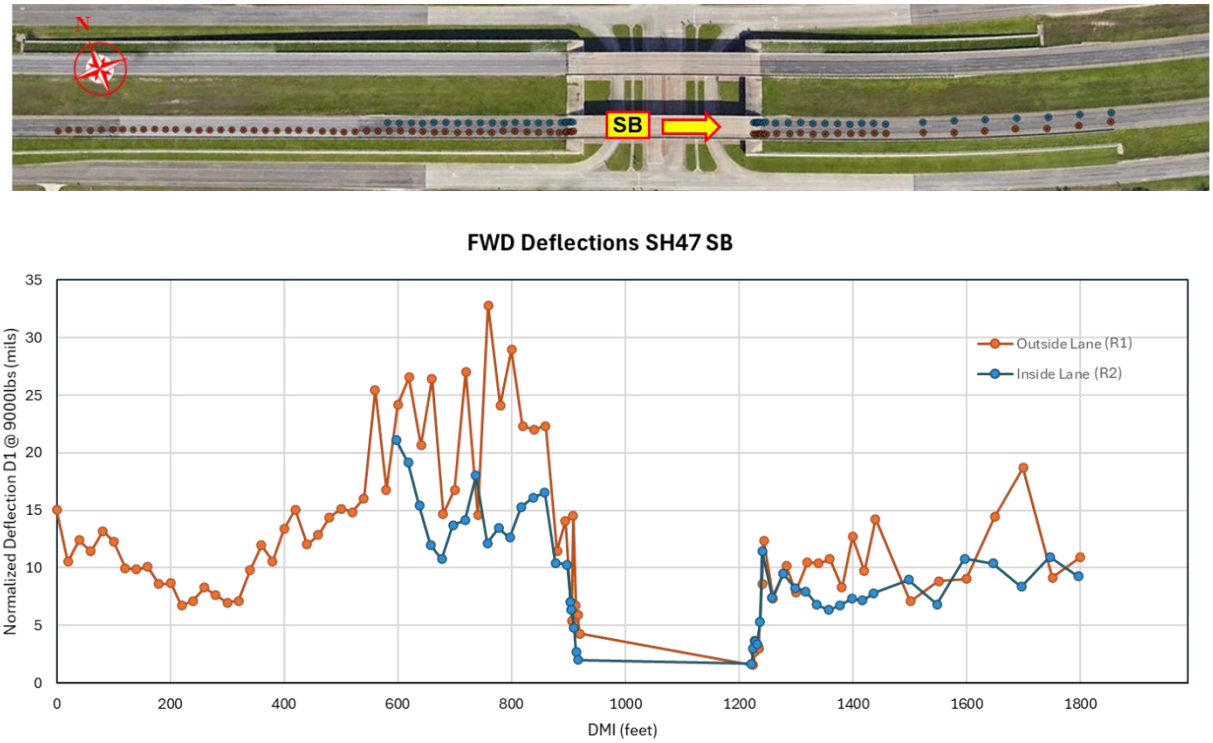


Figure 5-23. FWD testing location and deflections measured at inside and outside lanes of southbound

Northbound

Figure 5-24 presents FWD drop locations and deflections versus DMI for northbound the inside lane, outside lane, and outside shoulder. In the northbound main lanes, the deflection values range from approximately 1 to 24 mils. The BAS and adjacent pavement on the west side (leave side) of the bridge showed greater deflections than those on the east side (approach side).

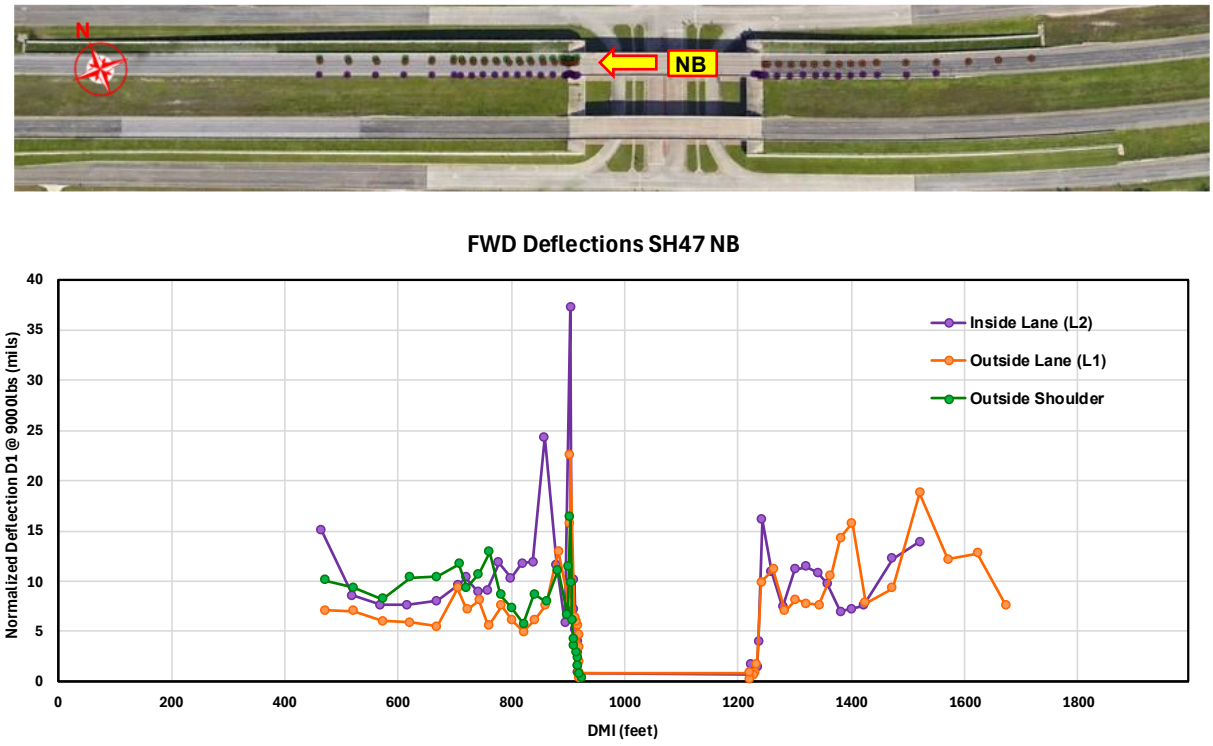
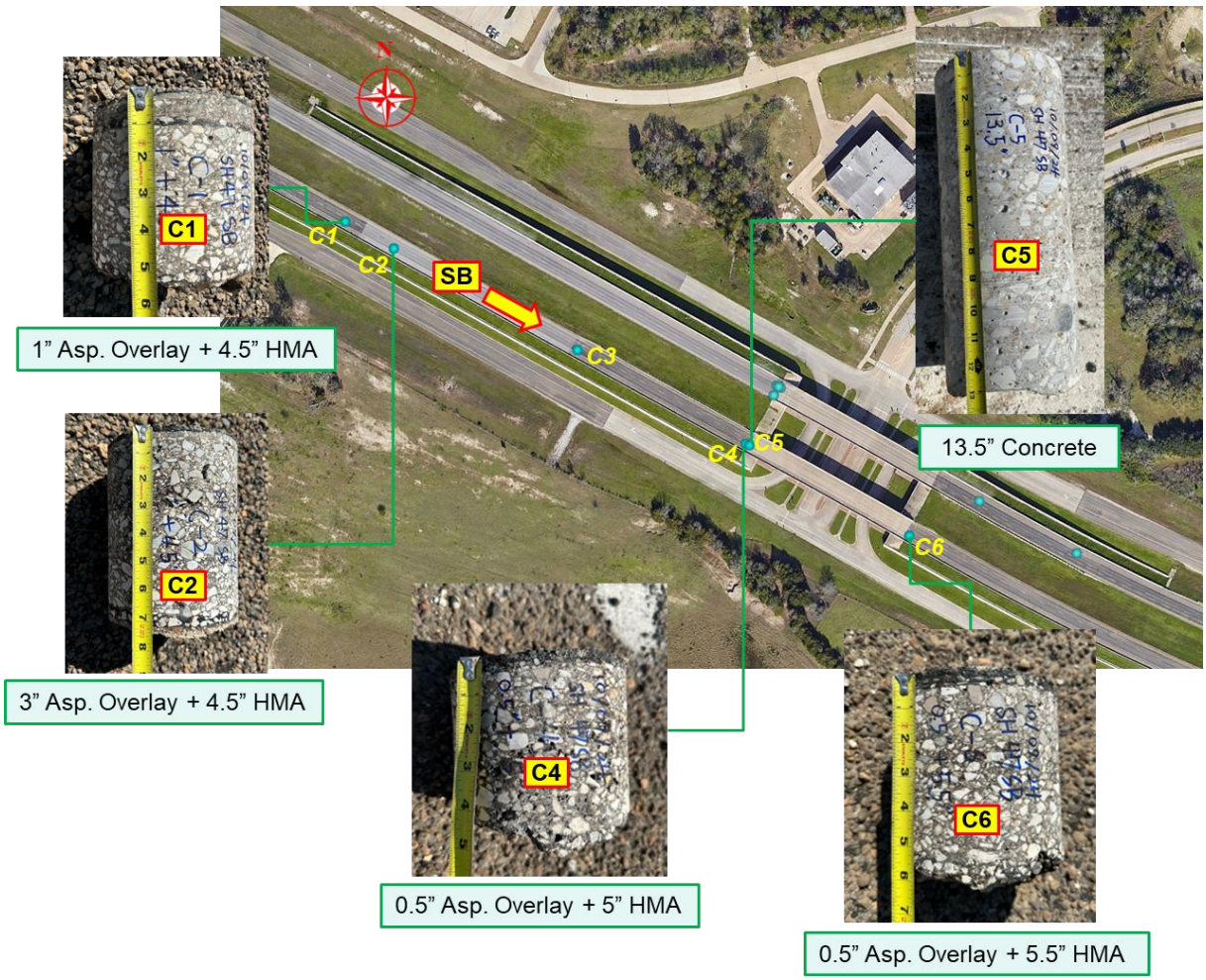


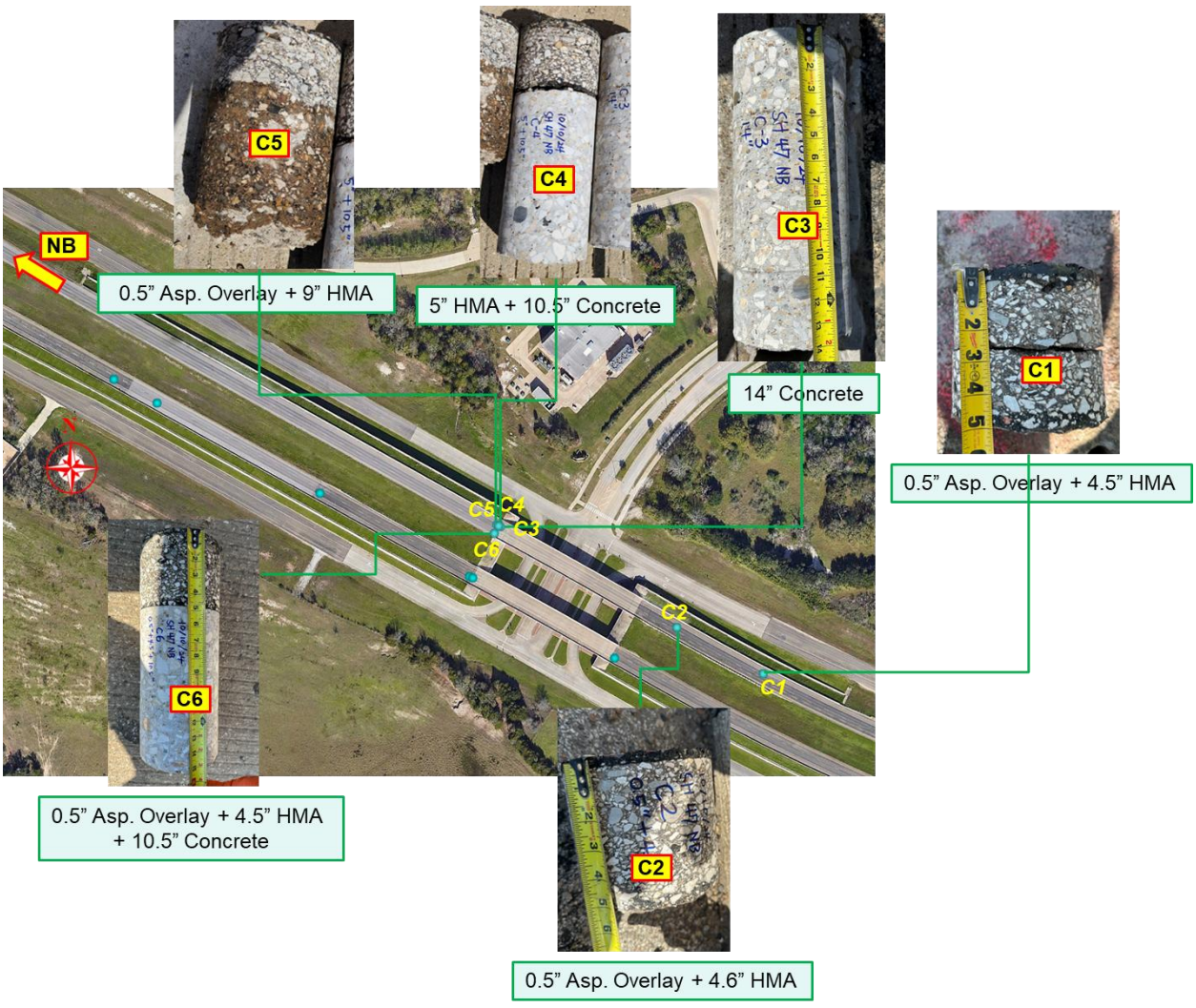
Figure 5-24. FWD testing location and deflections measured at inside lane, outside lane, and outside shoulder of northbound.

5.2.3 Coring

Six core samples (C1 through C6) were taken from the southbound, and additional six core samples were taken from the northbound lanes. **Figure 5-25**(a) and **Figure 5-25**(b) present the locations and images of the cores from southbound and northbound lanes, respectively. All core samples from pavement section had an asphalt overlay atop the original ACP, with the thickness ranging from 0.5 to 3 inches due to previous repair attempts.


C1
C2
C3
C4
C5
C6
SB
1” Asp. Overlay + 4.5” HMA
3” Asp. Overlay + 4.5” HMA
0.5” Asp. Overlay + 5” HMA
13.5” Concrete
0.5” Asp. Overlay + 5.5” HMA

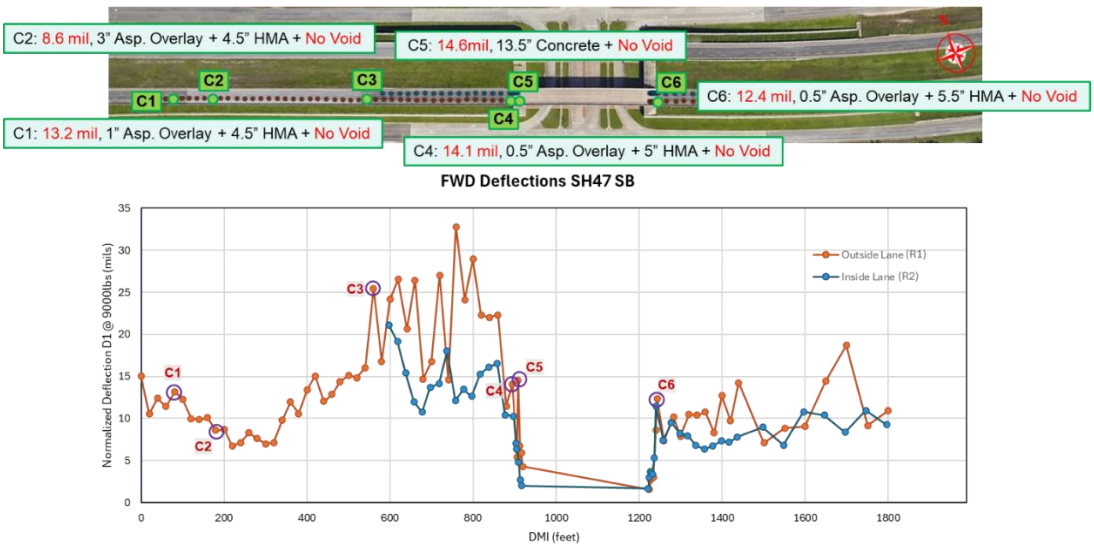
(a)



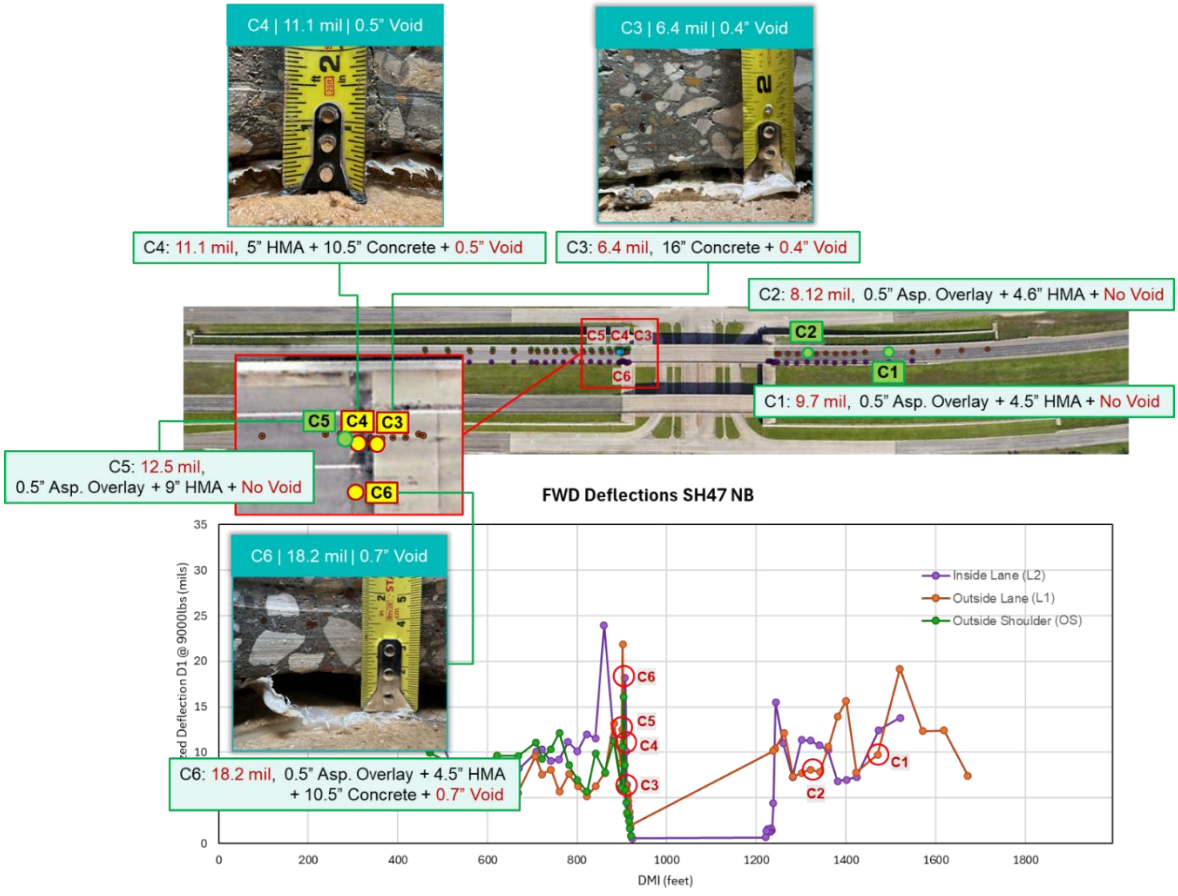
(b)

Figure 5-25. Coring locations and images of core samples: (a) southbound and (b) northbound

In the southbound lanes, no voids were observed at the bottom of the cored holes. However, in the northbound lanes, voids were detected at three locations (C3, C4, and C6) within the BAS area. Void thicknesses measured approximately 0.4, 0.5, and 0.7 inches for C3, C4, and C6, respectively. **Figure 5-26(a)** and **Figure 5-26(b)** show the photos of these void measurements in relation to FWD deflections in the southbound and northbound lanes, respectively.



(a)

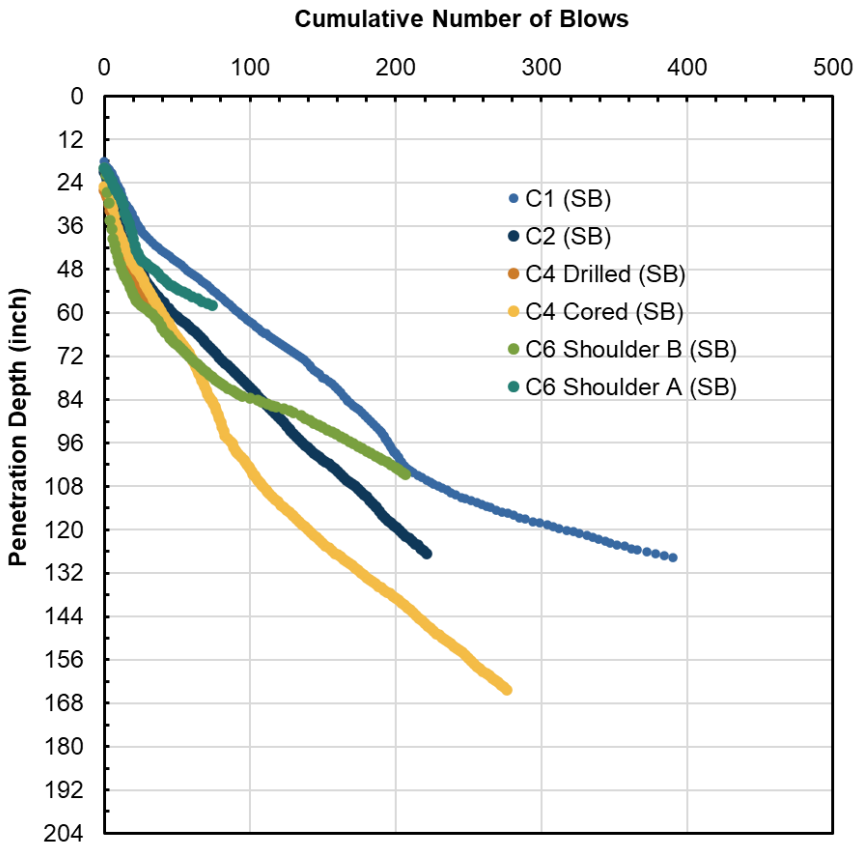


(b)

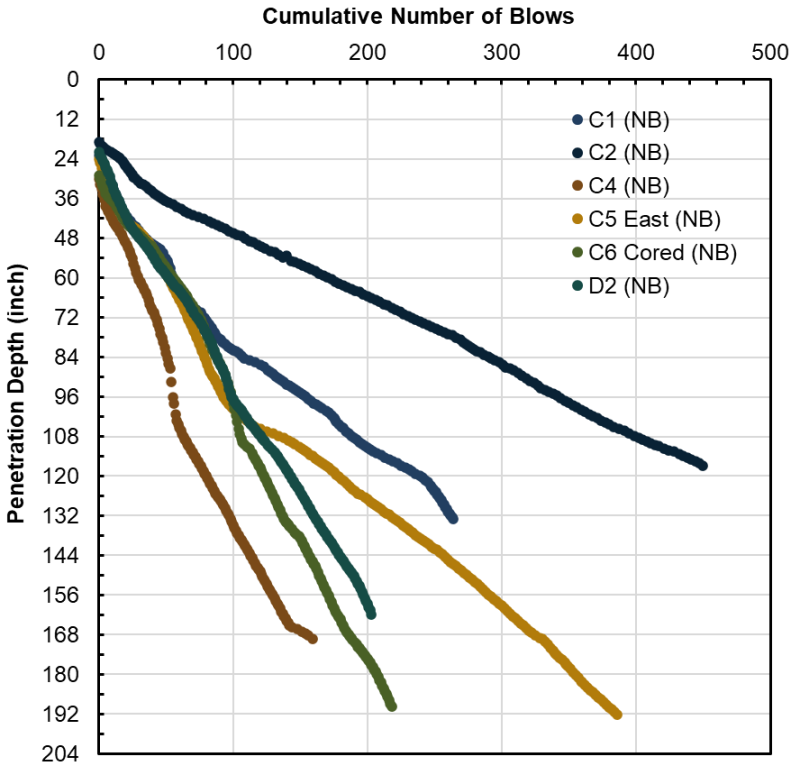
Figure 5-26. Void thickness measured from coring operations in relation to FWD deflection: (a) southbound and (b) northbound

5.2.4 Dynamic Cone Penetrometer (DCP) tests

To evaluate the embankment fill and subgrade conditions, DCP tests were conducted at each core location in both the southbound and northbound lanes. To access the untreated subgrade material, additional drilling was performed through the bottom of the cored hole. **Figure 5-27** presents the cumulative DCP blow counts versus depth for all 12 tests (six in each traffic direction).



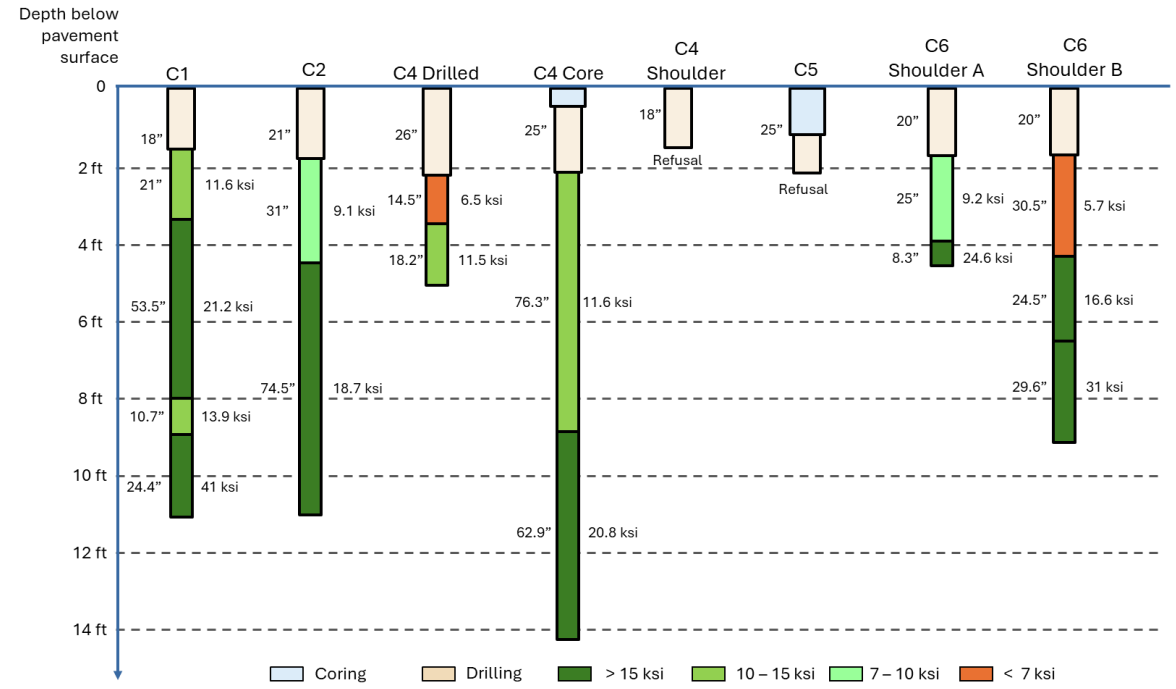
(a)



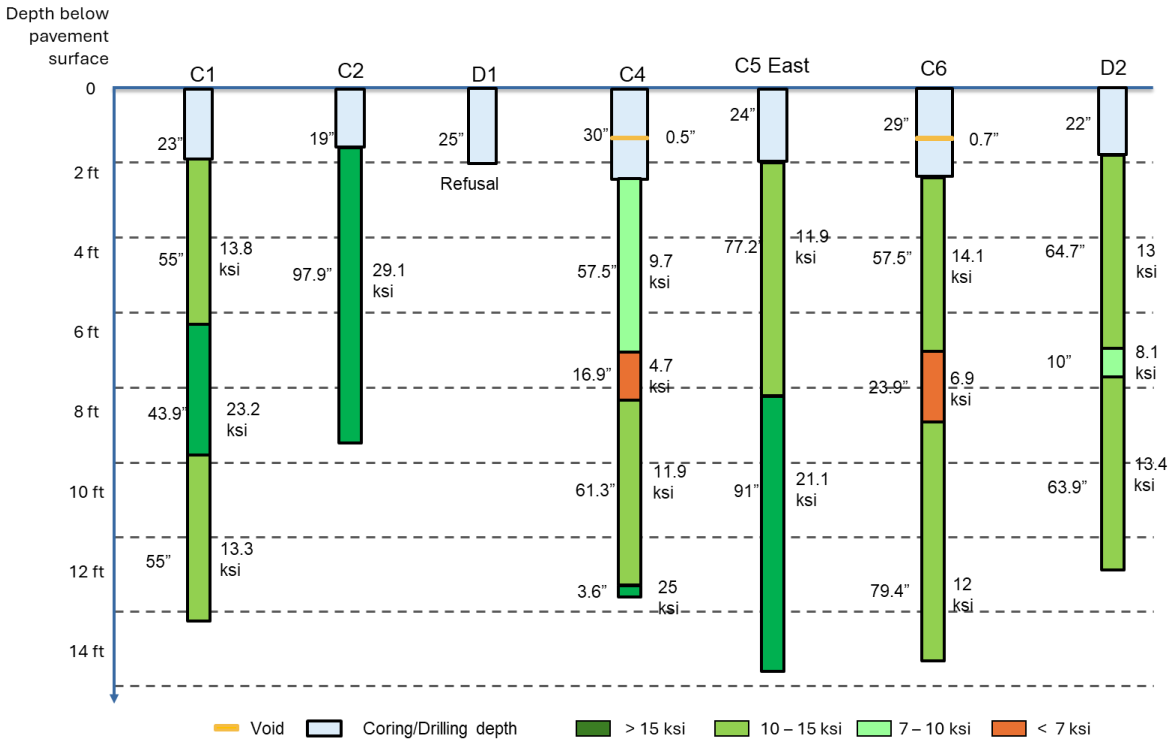
(b)

Figure 5-27. Cumulative DCP blow counts vs. penetration depth below the pavement surface: (a) southbound and (b) northbound

The resilient moduli (M_r) of embankment soils at each DCP test location were estimated using Eq. (1), and the results are presented in **Figure 5-28(a)** and **Figure 5-28(b)** for the southbound and northbound lanes, respectively. In the southbound, the DCP tests performed at locations C2, C4 and C6 showed M_r values less than 10 ksi. In the northbound, locations C4 and C6 (both at BAS) showed M_r values less than 10 ksi.



(a)



(b)

Figure 5-28. Resilient modulus determined from DCP tests: (a) southbound and (b) northbound lanes (Note: the color scheme for M_r value is for illustrative purposes only.)

5.2.5 Potential Distress Mechanism

The major distresses identified were settlement/bumps at the BAS, misaligned railing and void development under BAS. The embankment and abutment backfill soils are susceptible to post-construction compression due to dynamic traffic loading, long-term consolidation, and construction-related variability in compaction.

The embankment at this location is supported by an MSE wall, above which a soil slope was constructed to support the pavement structure. The DCP results showed that the embankment fills had variability in their stiffness, with weaker layers identified at C4 and C6. Settlement of the embankment fill due to the presence of the weaker layers led to a gradual loss of support beneath the BAS. The end of the BAS resting on the sleeper slab and embankment fill settled more than the other end supported by the abutment that remained relatively fixed. This differential movement and the compression of the fill materials resulted in the formation of voids beneath the BAS and localized settlement of the slab (see **Figure 5-29**).

Unlike CRCP, which tends to bridge localized loss of support and redistribute stresses over a larger area, the ACP readily conforms to changes in subgrade support. As voids formed beneath the BAS and adjacent embankment fill compressed, the ACP deformed downward into these unsupported zones, producing localized undulations.

When the supporting soil mass beneath the pavement and the BAS settles, the compression is rarely uniform. The sloped embankment fill placed above the MSE wall is supported primarily by the slope geometry, and not by any rigid structural elements. As this sloped soil mass undergoes settlement or lateral displacement, it may experience non-uniform vertical compression, particularly where material washout or erosion occurs due to water infiltration into the slope face. These processes can lead to uneven support conditions beneath the BAS, resulting in localized vertical displacement and rotation of the slab. The railing segment supported by the BAS follows this rotation, while the bridge railing remains relatively stable, producing the observed vertical offset and misalignment between the BAS railing and the bridge railing. This is illustrated in **Figure 5-30(a).** Furthermore**,** Google Street View image presented in **Figure 5-30(b)** shows that fill materials had been washed out of the southbound departure MSE wall.

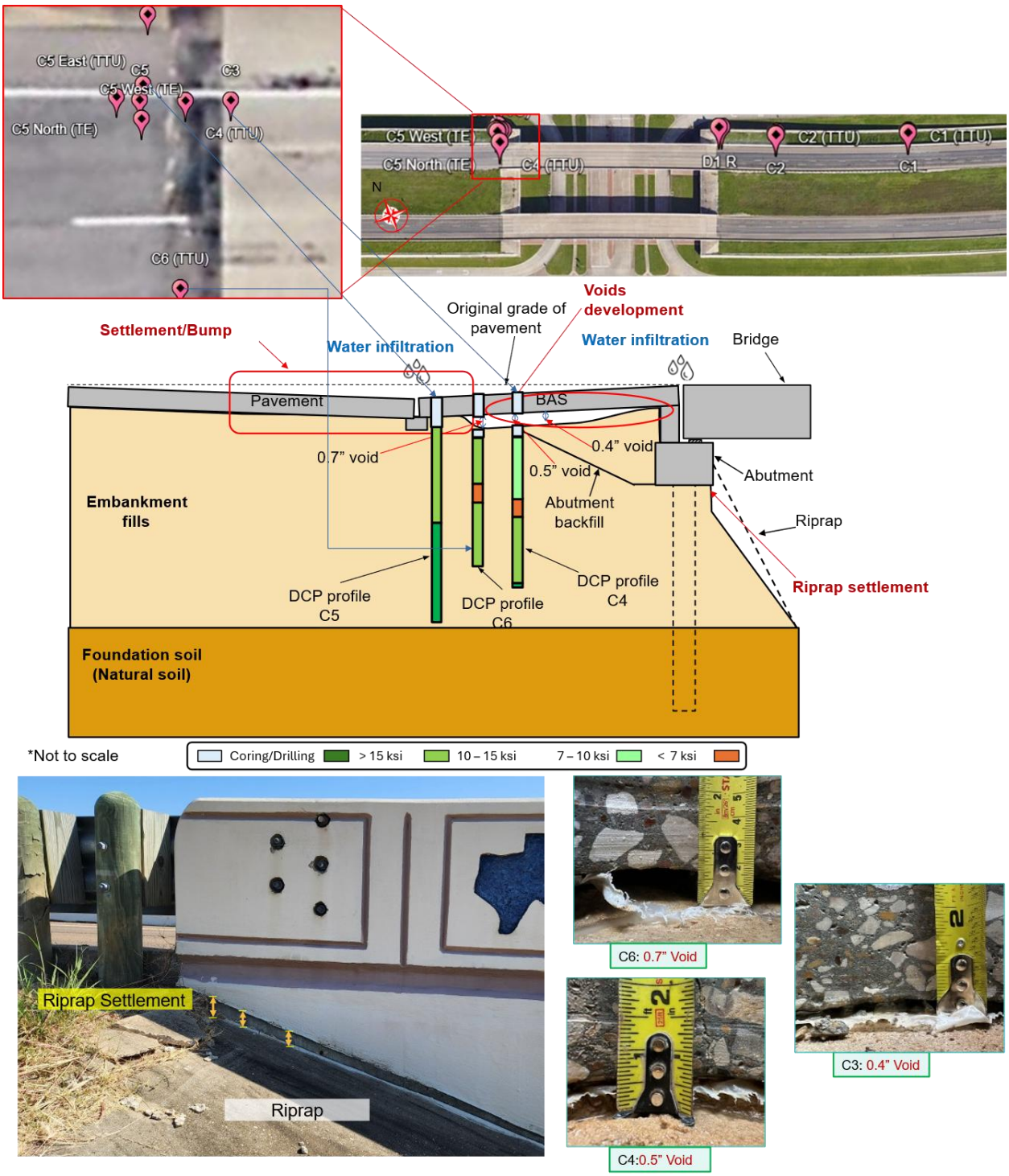
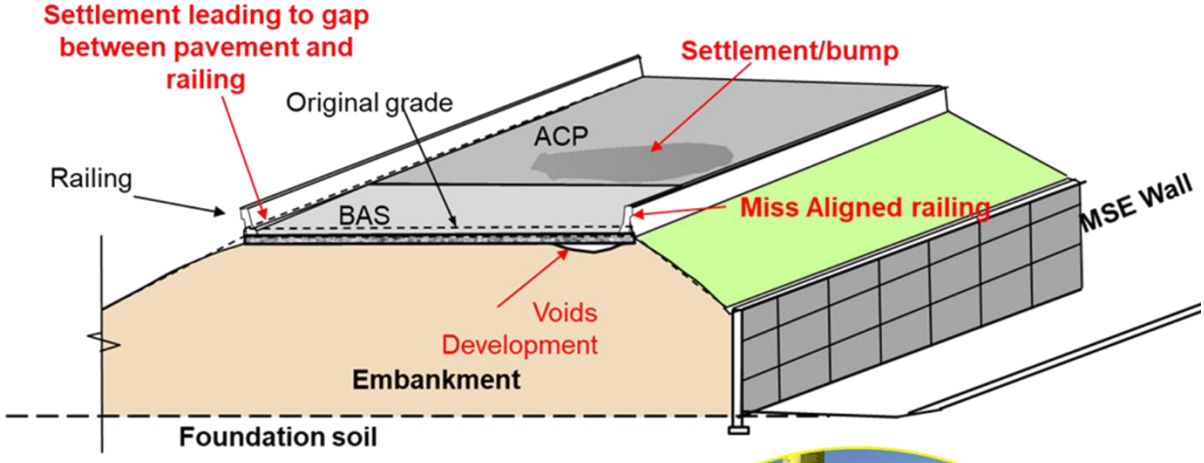


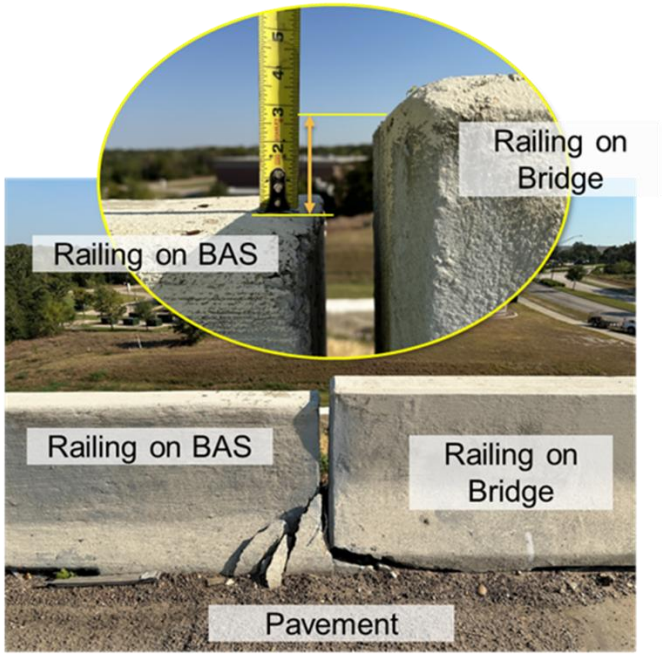
Figure 5-29. Illustration showing void development under BAS and settlement/bump on BAS and nearby pavement due to the settlement of embankment soil and water infiltration (Note: the color scheme for M_r value is for illustrative purposes only)





*Not to scale





(a)



(b)

Figure 5-30. (a) Illustration showing the probable distresses mechanism in the embankment in SH 47, College Station and (b) fill materials washed out of MSE wall (Google Street View from April 2021)

5.2.6 Repair Recommendations:

The required cement-stabilized backfill was missing at the SH 47 SB Approach BAS, leaving a weak sandy support layer between 2.0 and 3.5 feet in depth. The primary recommendation is a full-depth reconstruction to a depth of 5 feet to establish a stable support condition. High-density polyurethane foam injection (slab lifting) is not recommended for this section since the settlement was caused by weak subgrade support and slab jacking without firm support from underlying materials may often be only a temporary solution. If immediate reconstruction is not feasible, periodic HMA overlays should be used as a temporary measure to maintain ride quality.

The SH 47 NB Departure has weak embankment soils at a deeper depth (7–9 feet) and an 0.7-inch void beneath the slab. The recommended repair option is a full-depth reconstruction of BAS to a 3-foot depth. Furthermore, to mitigate a potential continued settlement, soil densification with HDPF (per TxDOT SS 3086) is also recommended to improve the weak layer at a depth of 7 to 9 ft. **Figure 5-31(a)** shows the primary repair recommendation for SB approach and NB departure BAS areas.



Figure 5-31. Repair recommendations for SH 47 SB approach and NB departure areas

For the SH 47 SB departure area, distress is primarily driven by washout and erosion along the open slope. To stabilize this, concrete riprap is recommended over the open slope per TxDOT Item 432 to minimize water infiltration and ensuing loss of fines. Additionally, soil densification using HDPF (TxDOT SS 3086) can be performed to a depth of 5 to improve the weak layer observed in the shoulder area. The SH 47 NB approach area was found to be structurally sound and required no maintenance at the time of field testing. **Figure 5-32** shows the repair recommendation for SH 47 SB departure.



Figure 5-32. Repair recommendation for SH 47 SB departure.

5.3 Section P-B-2: US 290 in Brenham

5.3.1 Overview

Section P-B-2 encompasses the bridge approach slab and adjacent pavement structure on the eastbound and westbound main lanes of US 290 in Brenham, Texas. The embankment has MSE walls on both sides. The construction of the section was completed in 2013, and Section P-B-2 has shown excessive settlements since then. Field evaluations of Section P-B-2 were conducted by TxDOT prior to the beginning of this research project, and TxDOT decided to perform a comprehensive full depth repair (FDR) to a depth of 7 ft below the pavement surface after the evaluation. The Research Team visited the site during the full-depth repair process and conducted additional field evaluations on 2/1/2024 – 2/2/2024, 2/20/24 – 2/22/24, and 5/2/2024. **Figure 5-33** and **Table 5-5** show the location and detailed descriptions of Section P-B-2, respectively.

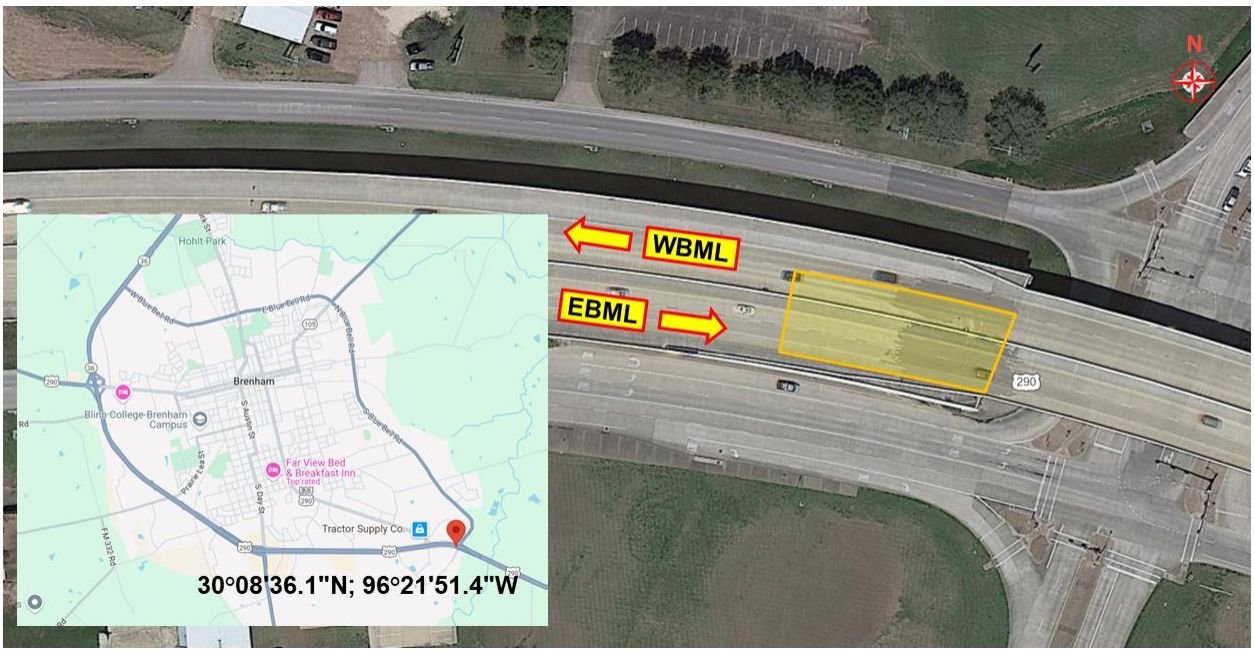


Figure 5-33. Location of Section P-B-2 of US 290 in Brenham, Texas

Table 5-5. Detailed descriptions of Section P-B-2 of US 290 in Brenham, Texas

Attribute	Information	Notes
District & Highway	Brenham/ Bryan & US 0290	
CSJ	0186-06-066	
County	Washington County	
Reference Marker	RM 672+1.622 to RM 676+1.074	
GPS Coordinates	30°08'36.1"N 96°21'51.4"W	
Date Work Begin	04/25/2011	
Date Completed	12/17/2013	
Pavement Type	CRCP 11.5"	
BAS Thickness	13"	
Base Type	1" TY D ACP + 6" Cement Treated Base w/ Prime	
Subgrade Type	8" cement treated subgrade	
Drainage Type	Inlets @ Median	
Embankment Height at BAS	34'	MSE Wall - MSE Wall

5.3.2 Dynamic Cone Penetrometer (DCP) tests

At the time of the first visit to Section P-B-2 by the Research Team on 2/1/2024, a full-depth repair was underway. The pavement structure had been already removed, and the subgrade was directly exposed. The area close to the BAS had been excavated to a depth of 7 ft. The Research Team performed a total of 14 DCP tests (DCP1 through DCP14) on 2/1/2024 and 2/2/2024. DCP1 through DCP5 were performed in the excavated area, and DCP6 through DCP14 were performed in the pavement area further away from the BAS. An additional visit was made on 5/2/2024, and seven additional DCP tests (DCP15 through DCP21) were performed in the pavement area. Locations of the DCP tests performed at Section P-B-2 by the Research Team are shown on **Figure 5-34**.

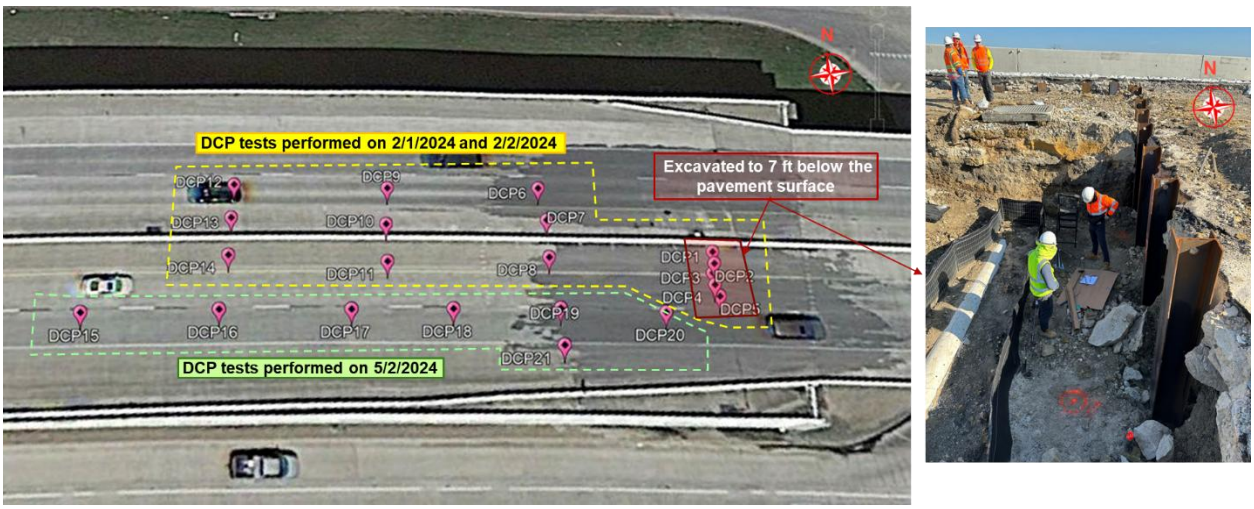


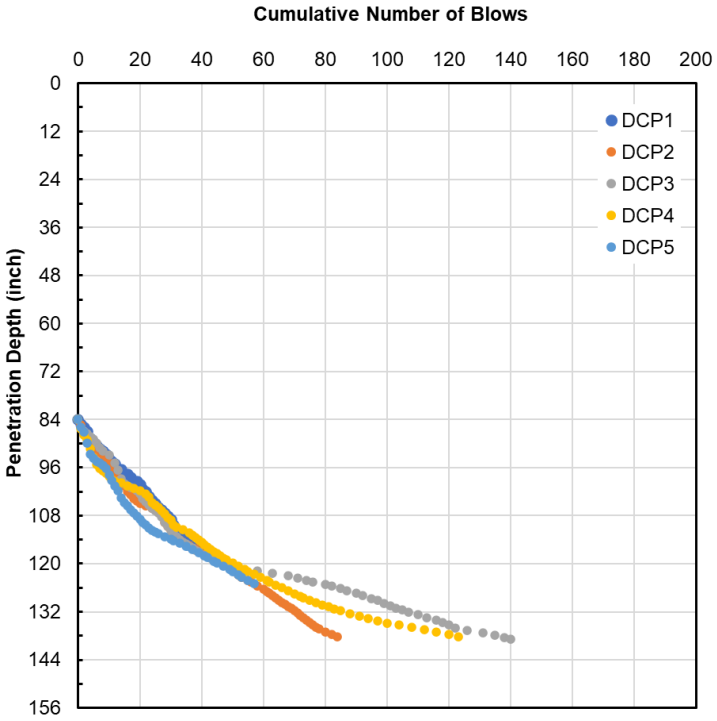
Figure 5-34. Location of DCP tests

The cumulative DCP blow counts vs. depth curves from all 21 DCP tests are presented in **Figure 5-35**. The resilient moduli (M_r) at each DCP test location were estimated using Eq. (1), and the results are presented in **Figure 5-36**.

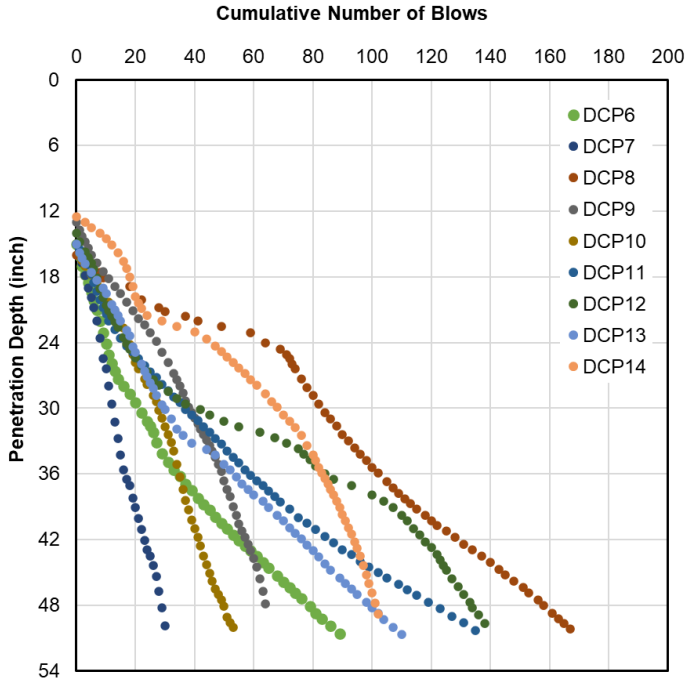
The results from the DCP tests performed on 2/1/2024 and 2/2/2024 indicated that the embankment condition in the pavement area was more favorable than the BAS area. However, there were three DCP locations − DCP7, DCP9, and DCP10 − where M_r values were still less than 20 ksi up to the maximum investigation depth, which was about 4 ft – 4.2 ft below the exposed surface at the time of the testing. Particularly, the M_r value at DCP7 was less than 10 ksi up to the maximum investigation depth of 4.2 ft below the exposed surface. Also, DCP test results indicated that the embankment condition was variable, rather than uniform, across the investigated area.

The results from the additional seven DCP tests performed on 5/2/2024 showed that the embankment condition in the pavement area (DCP15 through DCP18) that was further away from BAS area is overall more favorable than the area near the BAS (i.e., DCP19 and DCP20), similar to what was observed from the tests on 2/1/2024 and 2/2/2024. At DCP19 and DCP20, M_r values less than 7.5 ksi were observed to a depth of about 5 ft.

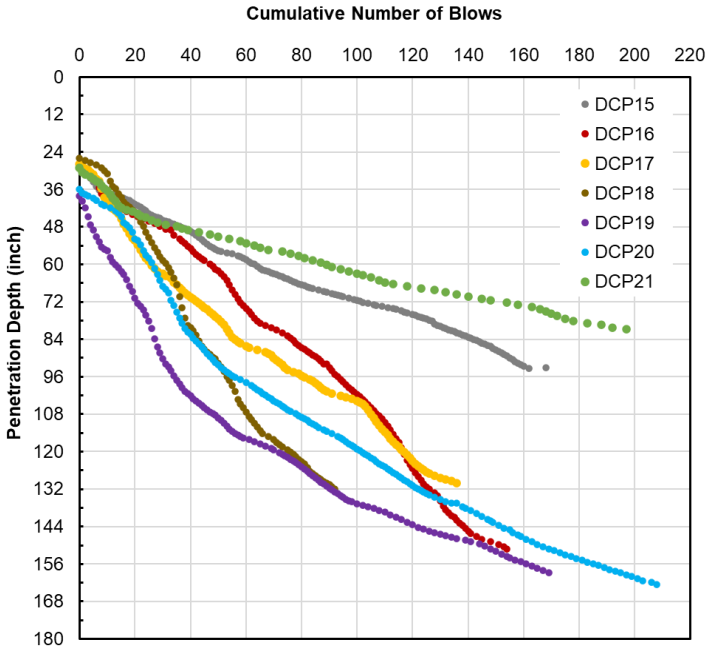
It heavily rained in the morning of 5/2/2024 in Brenham until about 1:15 pm, and the Research Team began conducting DCP tests from 2 pm and finished testing at 8 pm. Therefore, at the time of our investigation, the exposed subgrade was wetter than normal conditions, and DCP the results might have been affected by the wetter conditions. For example, a low M_r value of 6.9 ksi was observed to a depth of about 6 ft at DCP18, and there was standing water in the vicinity of DCP18 due to the heavy rain in the morning (DCP18 was the wettest location among all seven DCP locations).


Cumulative Number of Blows
0
20
40
60
80
100
120
140
160
180
200
Penetration Depth (inch)
0
12
24
36
48
60
72
84
96
108
120
132
144
156
DCP1
DCP2
DCP3
DCP4
DCP5

(a)

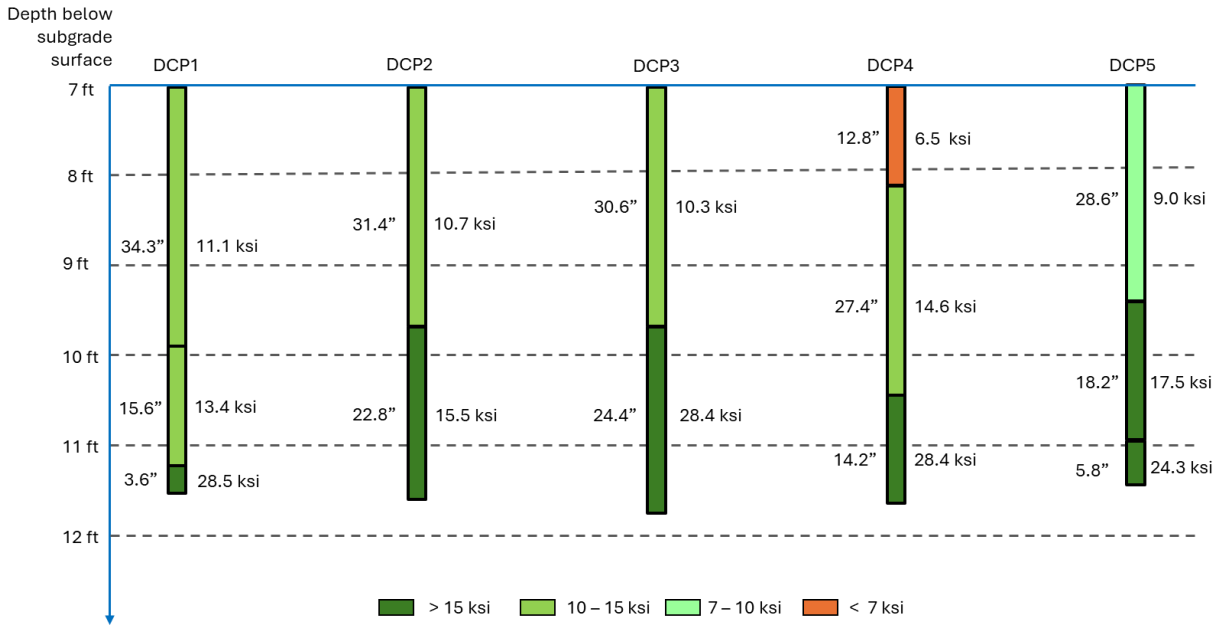

Cumulative Number of Blows
0
20
40
60
80
100
120
140
160
180
200
Penetration Depth (inch)
0
6
12
18
24
30
36
42
48
54
DCP6
DCP7
DCP8
DCP9
DCP10
DCP11
DCP12
DCP13
DCP14

(b)

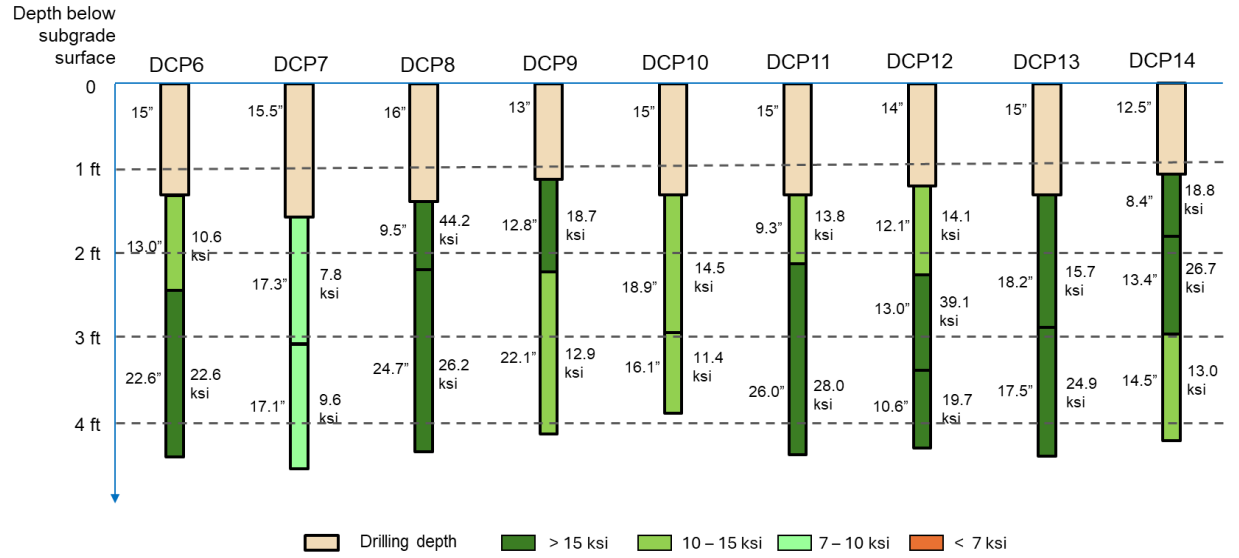


(c)

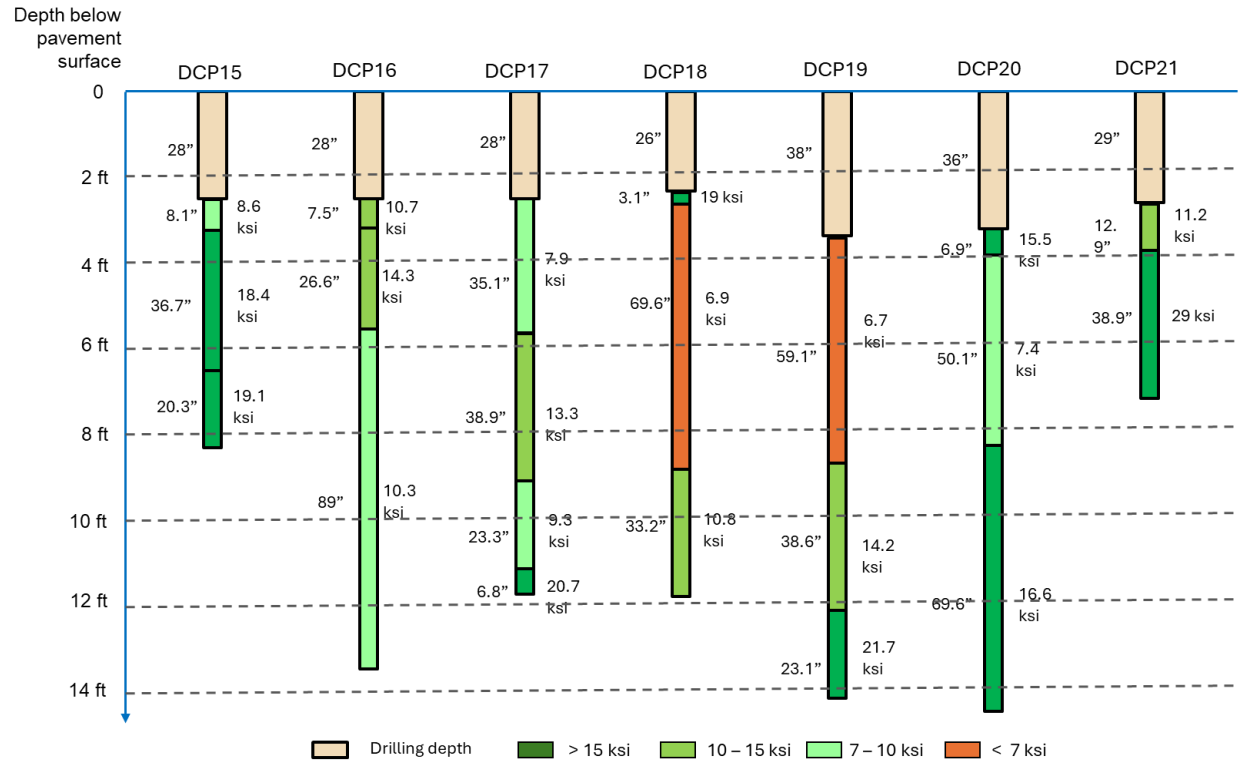
Figure 5-35. Results from DCP tests: (a) DCP1 through DCP5 in the excavated area (BAS area), (b) DCP6 through DCP14 (pavement area), and (c) DCP15 through DCP21 (pavement area)



(a)



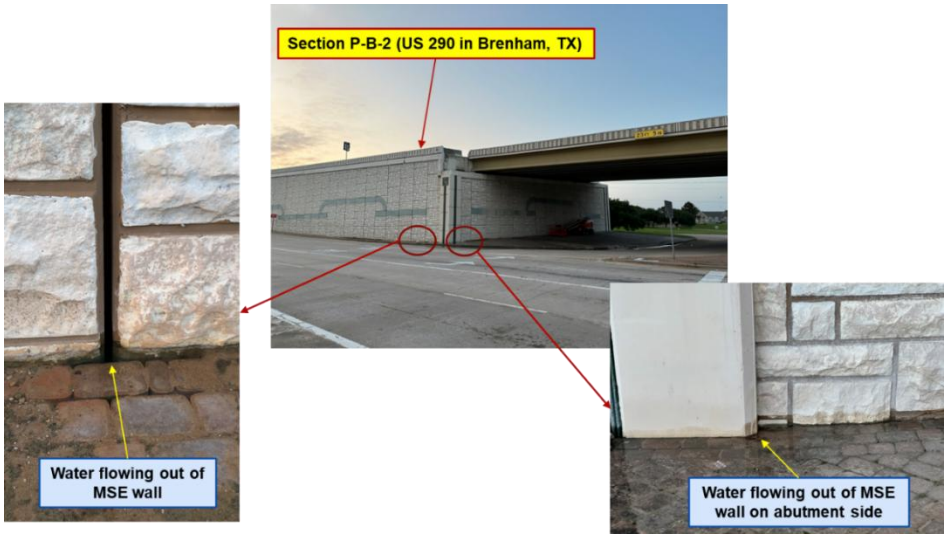
(b)



(c)

Figure 5-36. Resilient modulus determined from DCP tests: (a) DCP1 through DCP5 in the excavated area (BAS area), (b) DCP6 through DCP14 (pavement area), and (c) DCP15 through DCP21 (pavement area) (Note: the color scheme for M_r value is for illustrative purposes only.)

The Research Team conducted a visual survey of the MSE wall supporting the subject section after the rainfall on 5/2/2024. It was observed that water was flowing out of the bottom of the MSE wall on the sides of the frontage road and abutment wall (refer to **Figure 5-38(a)**). Backfill materials washed out due to the water flow were deposited near the MSE wall facing, and **Figure 5-38(b)** and **Figure 5-38(c)** show the washed-out backfill materials on the side of the frontage road and abutment wall, respectively, that had been accumulated over time.



(a)



(b)



(c)

Figure 5-37. Photos showing (a) water flowing out of the MSE wall, (b) backfill materials washed out of the MSE wall on the side of frontage road, and (c) backfill materials washed out of the MSE wall on the side of abutment wall

5.3.3 Injection of polyurethane foam

The Research Team was informed by TxDOT that a loose layer was encountered at a depth of 12 ft during installation of shoring piles for excavation at the subject section. It was decided by TxDOT to densify the loose layer by injecting High Density Polyurethane Foam (HDPF) into it per TxDOT *Special Specification 3086: Soil Densification and Raising Concrete Slabs with High Density Polyurethane Foam (HDPF)*. The Research Team was present during the HDPF injection process during 2/20/24 – 2/22/24 and observed the operations. The contractor, *NORTEX Concrete Lift and Stabilization*, notified the Research Team that about 70 lb of HDPF was injected per tube with a total amount of about 7000 lb for the 108 tubes. The injection process was performed as follows:

(1) Install a 0.5-in-diameter tube with a sacrificial cone to a depth of 12 ft (**Figure 5-38(a)**). After reaching the target depth, break the sacrificial cone by pushing in a smaller rod inside.
(2) Install the 0.5-in-diameter tubes in a grid pattern with 5’ by 5’ spacing. Nine tubes were installed in the transverse direction and 12 tubes were installed in the longitudinal direction (a total of 108 tubes were installed, covering an area of about 50 ft by 65 ft).
(3) Connect an injection gun with the tube and supply two separate chemical components from a truck (see **Figure 5-38(b)**), where the chemical tanks and pumps are stored, to the injection tube via two separate hoses. The two chemicals are mixed in situ and get hardened

as soon as they are mixed. Note that the *TxDOT Special Specification 3086* requires that the mixed material (HDPF) must reach 90% compressive strength within 30 minutes of injection.

(4) Install a rotating laser level and a receiver (see **Figure 5-38(c)**) and monitor the ground movement throughout the injection process.

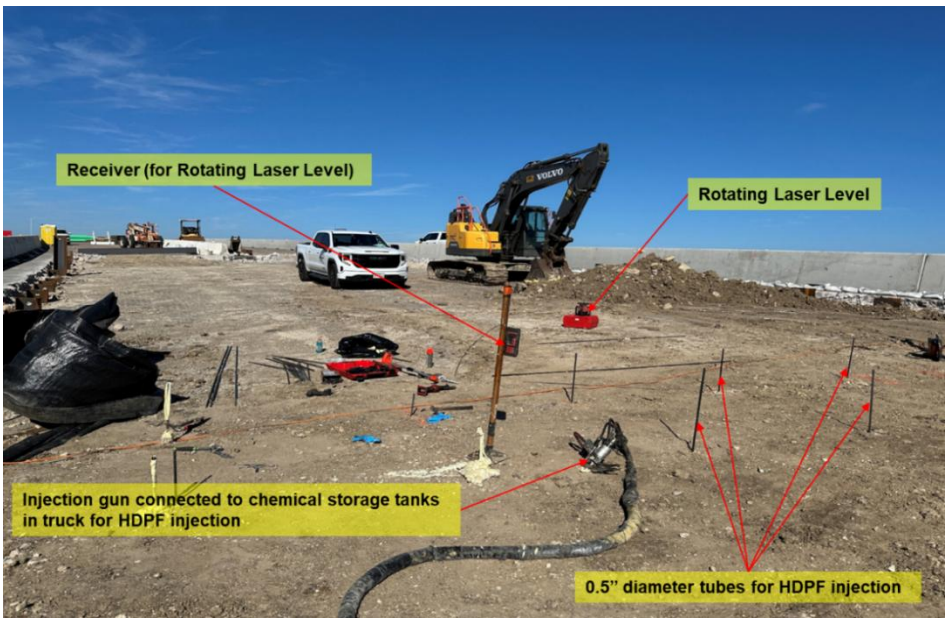
(5) After the injection is completed, remove any excessive polyurethane material after the injection gun is removed from the tube (see **Figure 5-38(d)**).


0.5” diameter tube for HDPF Injection

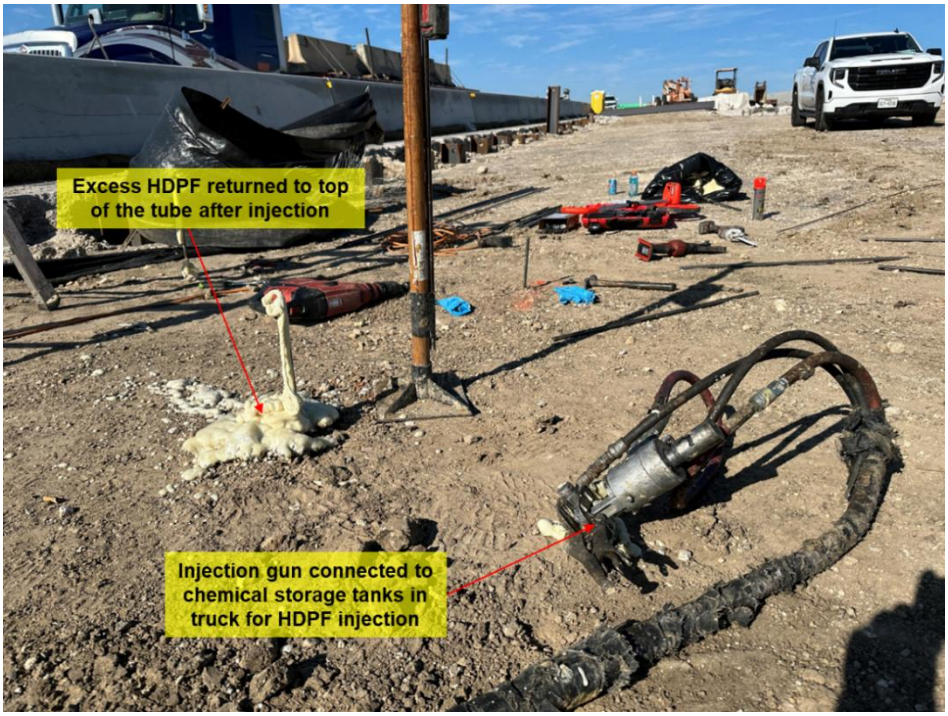
(a)


Truck equipped with pump to inject HDPF by mixing chemical components.

(b)



(c)

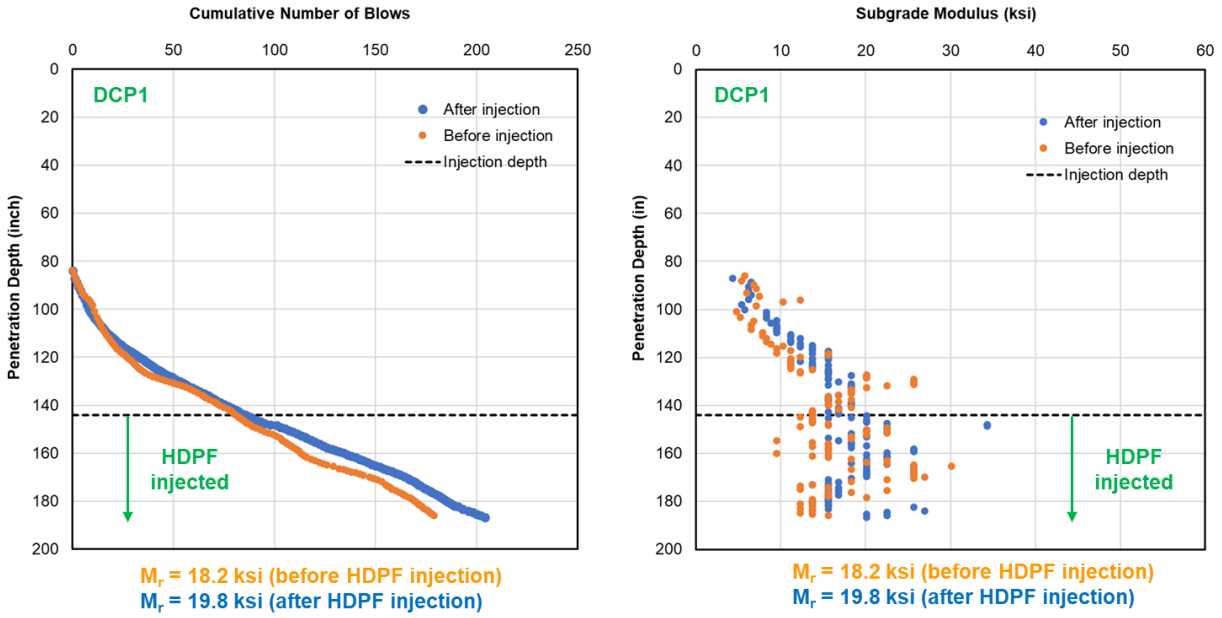


(d)

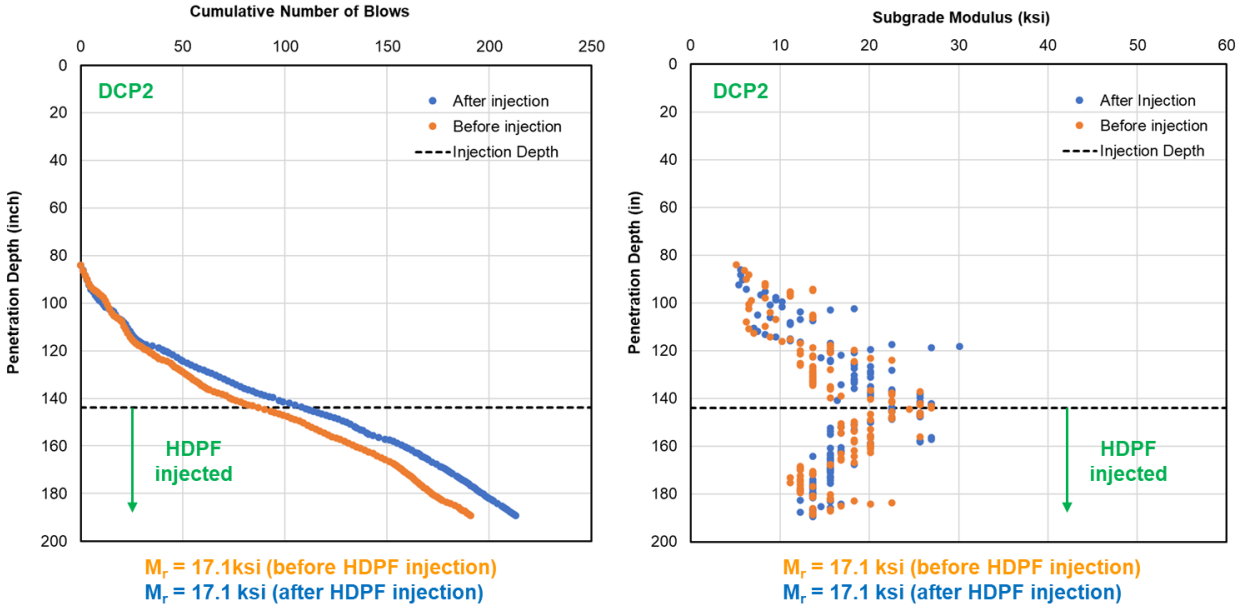
Figure 5-38. Photos showing the injection process of high-density polyurethane foam (HDPF): (a) installation of 0.5-in. diameter injection tubes on a 5-ft by 5-ft grid, (b) connection of an injection gun with the tube to supply HDPF from a truck where the chemical tanks and pumps are stored, (c) monitoring the ground movement throughout the injection process using a rotating laser level and a receiver, and (d) removal of excessive polyurethane material after the injection is completed.

5.3.4 Comparison of Dynamic Cone Penetrometer (DCP) test results before and after injection of polyurethane foam

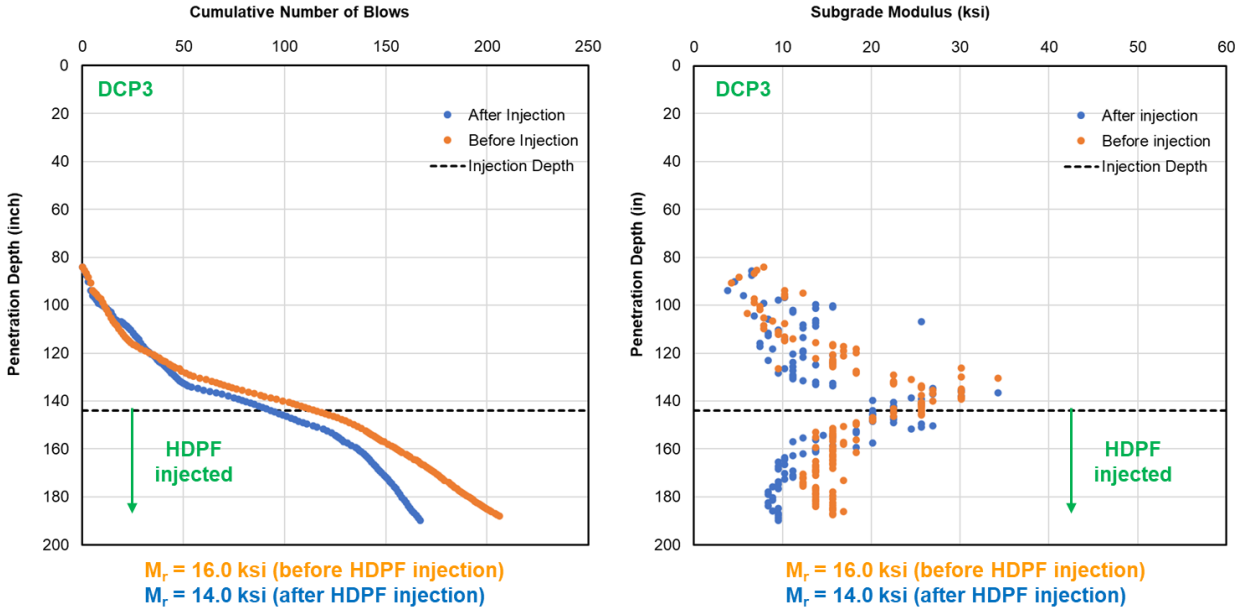
The Research Team conducted DCP tests before and after HDPF injection. Before the injection process began, four DCP tests were performed within 1 ft distance from the location of HDPF injection tube in the excavated area. About 2-3 hours after the injection process was completed, additional four DCP tests were performed within 1 ft distance from the location of HDPF injection tube. **Figure 5-39** shows the results from the DCP tests before and after HDPF injection.



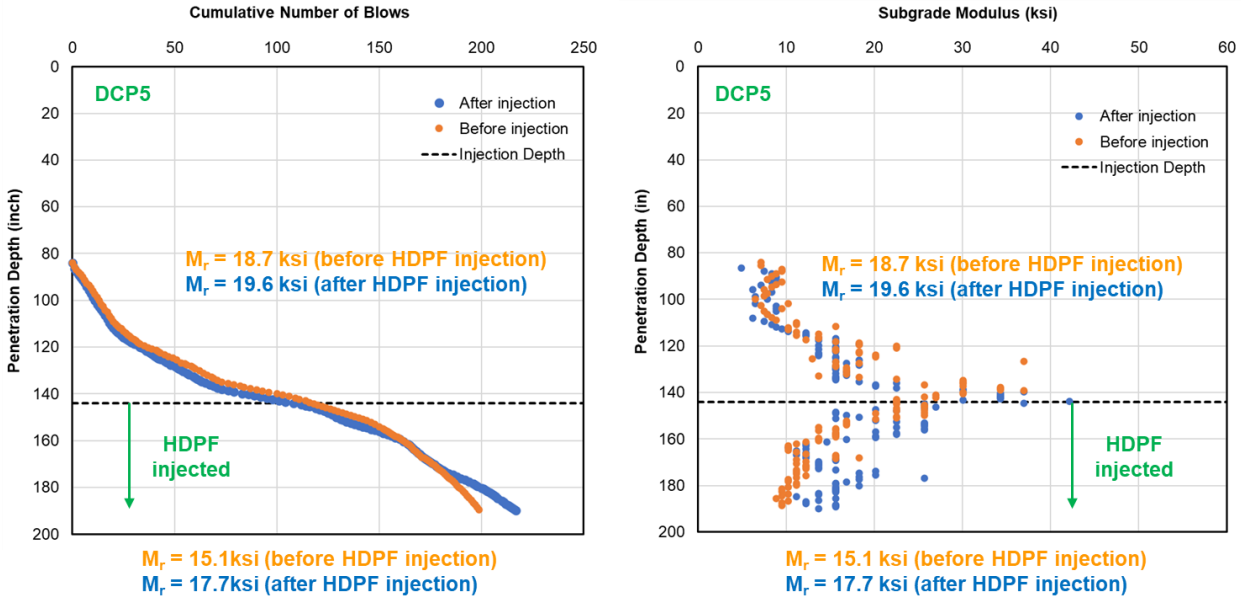
(a)



(b)



(c)



(d)

Figure 5-39. Comparison of DCP test results before and after high-density polyurethane foam (HDPF) injection: (a) DCP1, (b) DCP2, (c) DCP3, and (d) DCP5

The resilient modulus (M_r) was determined using Eq. (1), and the average M_r value below the HDPF injection depth of 12 ft (= 144 in) was computed before and after HDPF injection. **Table 5-6** shows the computed M_r values, and the percent changes before and after HDPF injection range

from -12.5% to 17.2%. HDPF is known to reach 90% of its strength in less than an hour and full strength within 24 hours. Therefore, the M_r values obtained about 2-3 hours after the HDPF injection may not reflect its full strength. Furthermore, since the location of DCP test before and after HDPF injection was about 1 to 2 ft from each other for each injection hole, the initial soil conditions might not have been identical. Therefore, the negative value of -12.5% might be due to the potential differences in the initial soil conditions. Nonetheless, the greatest percent increase is still less than 18%. It appears that the HDPF injection may be effective in increasing the density of backfill soils by filling the voids with polyurethane material but less effective in increasing the strength/stiffness of backfill soils.

Table 5-6. Resilient moduli of backfill soils before and after HDPF injection

Test location	M_r before HDPF injection (ksi)	M_r after HDPF injection (ksi)	Percent change
DCP1	18.2	19.8	8.8%
DCP2	17.1	17.1	0%
DCP3	16.0	14.0	-12.5%
DCP5	15.1	17.7	17.2%

5.3.5 Potential Distress Mechanism

Major distresses included settlement near BAS, material washout, and distinct half-moon shaped cracking in adjacent pavement area. Historical Google Earth imagery confirmed the progression of these distresses, while field investigations during full-depth repair provided physical evidence of the potential distress mechanism.

The potential distress mechanism at the US 290 Brenham site is a compound result of a sequence of compaction issues, widened joints, seal deterioration, and material washout. DCP tests confirmed the presence of weak soil layers with low resilient modulus. As these weak fill materials compressed under overburden and traffic loads, the BAS and nearby pavement section settled. It is likely that this settlement widened the joints and broke the seal at the expansion joint, creating a pathway for water infiltration. This is illustrated in **Figure 5-40**.

Once water infiltrated the embankment, it triggered material washout and internal erosion. The water migrated through the fill and exited via the retaining wall system. Field observations confirmed this process, showing water actively flowing out from the bottom of the MSE wall and the abutment wall, carrying washed-out backfill materials with it (**Figure 5-37** and **Figure 5-40**). This washout process created significant voids beneath the pavement structure, leading to a loss of support. Consequently, differential settlement occurred within the embankment, specifically affecting the region near the BAS and the pavement where the inlet is located. This non-uniform settlement ultimately caused the half-moon crack observed on the surface. This progressive distress mechanism is illustrated in **Figure 5-41**.

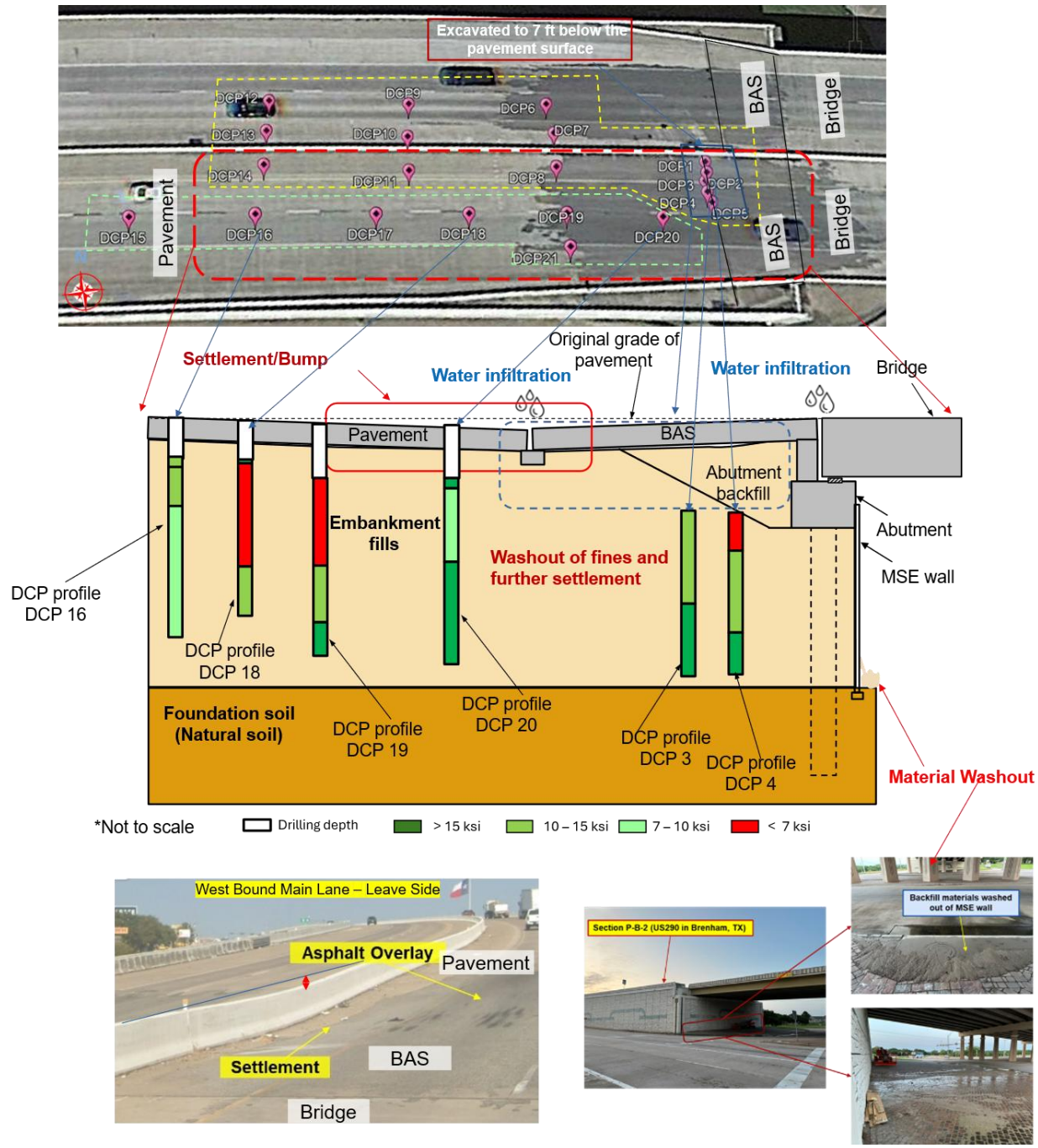


Figure 5-40. Illustration showing settlement of BAS and nearby pavement due to the compression of embankment soil and washout (Note: the color scheme for M_r value is for illustrative purposes only.)

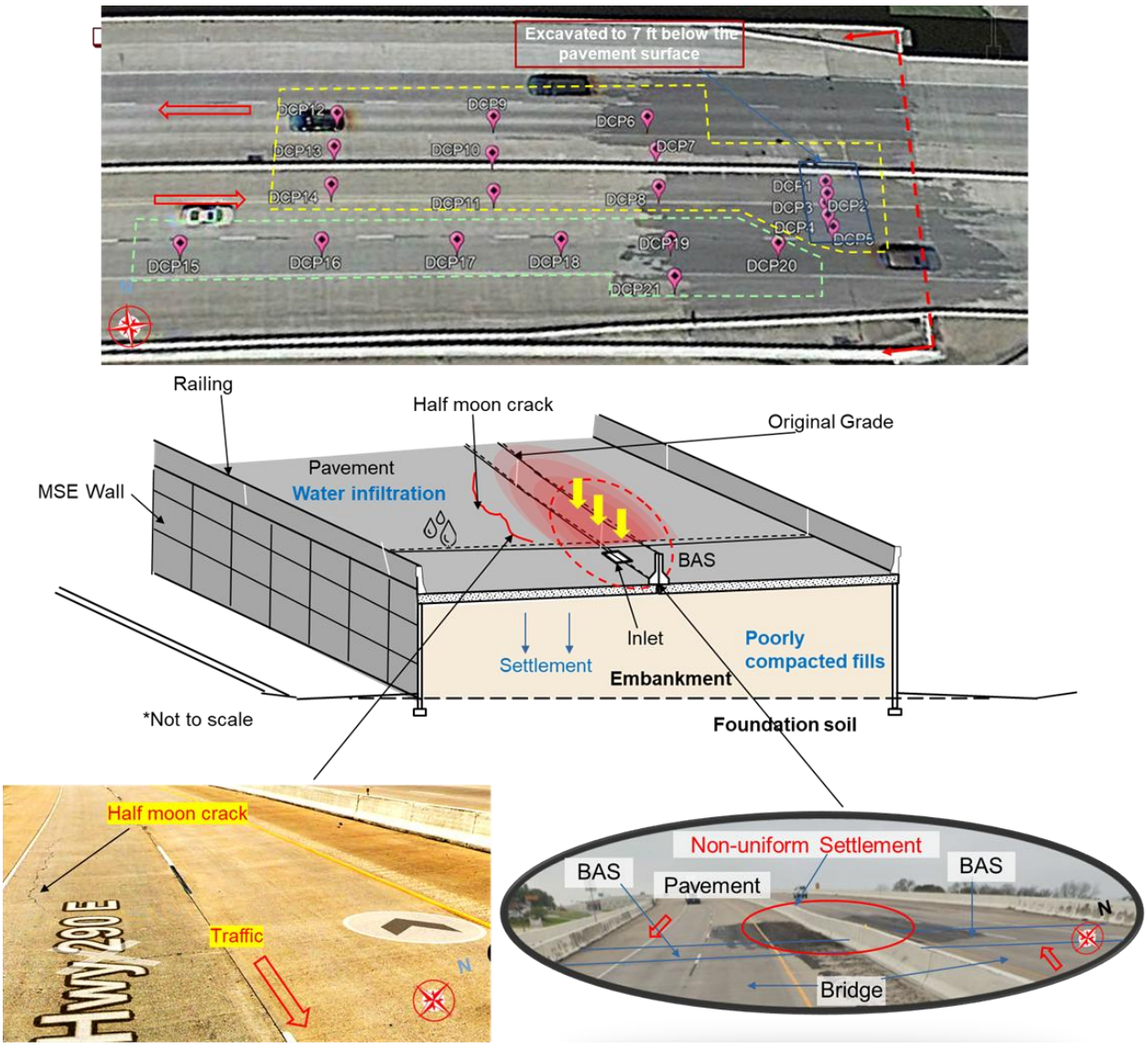
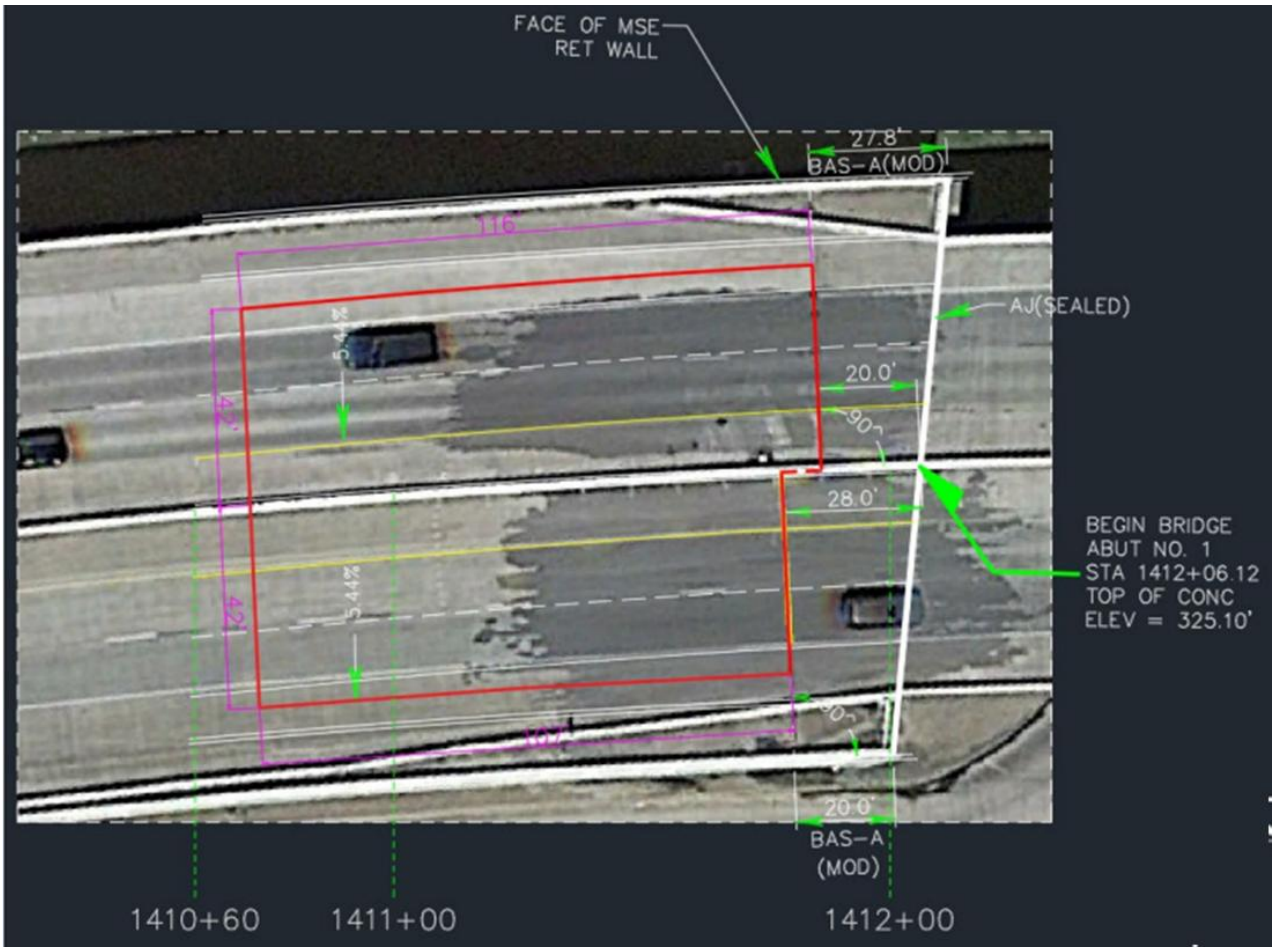


Figure 5-41. Illustration showing the distress mechanism in the embankment in US-290, Brenham.

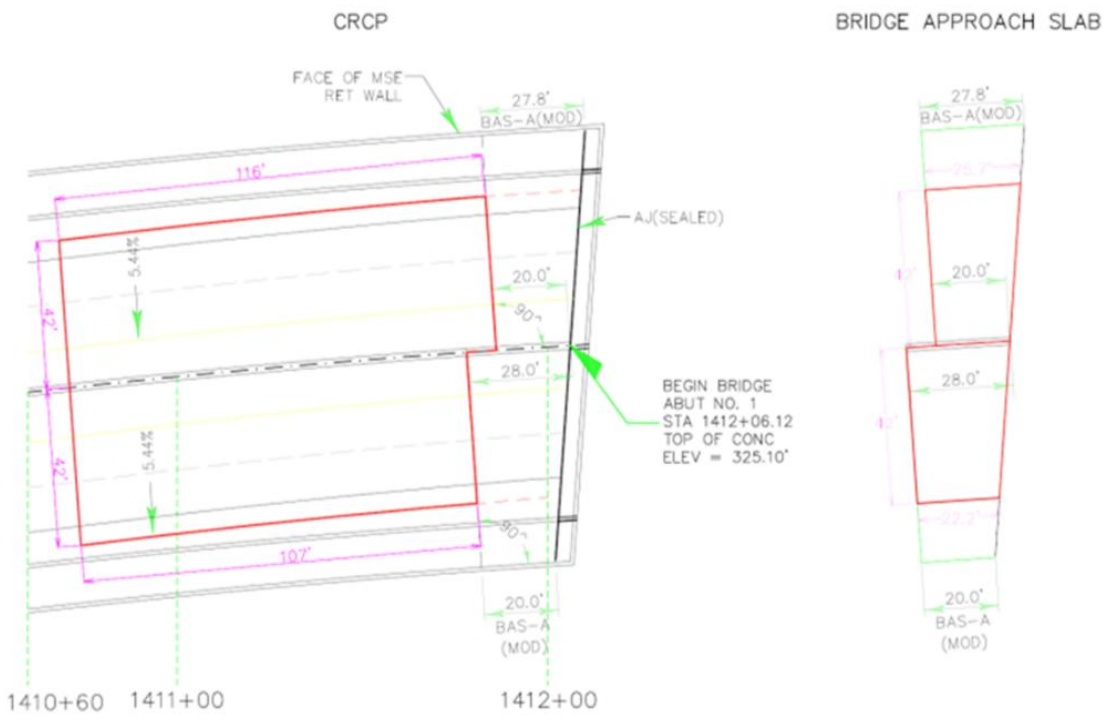
5.3.6 Repair Recommendations

As stated earlier, the repair recommendations were made by TxDOT after their field evaluations prior to the beginning of this research project, and this section summarizes the repair plan. The persistent distresses at the subject section were due to weak subgrade below BAS and CRCP, along with the faulty expansion joints which allowed for the water infiltration further exacerbating the distress by accelerating the settlement due to material washout. To address the distresses, a comprehensive full depth repair was recommended by TxDOT MNT Division. The existing BAS, CRCP, base and the subgrade need to be removed to a depth of 7 ft. The excavated volume must be reconstructed using Cement Stabilized Backfill (CSB) in accordance with Item 276, Class L

specifications, with a minimum 7-day compressive strength of 500 psi. Following the stabilization of the embankment, the Bridge Approach Slab, armor joint, and main lane CRCP must be replaced in accordance with CRCP-120 standards. The extent of full depth repair is shown in **Figure 5-42**.



(a)



(b)

Figure 5-42. Extent of full depth repair (FDR) for US-290, Brenham (provided by TxDOT).

5.4 Section S-11-8: US-290 Frontage Road in Austin

5.4.1 Overview

Section S-11-8 is the approach and departure side pavement on the eastbound frontage road of US-290 at the MOPAC Railroad in Austin, Travis County, TX. The location of Section S-11-8 is shown in **Figure 5-43**. Field evaluations of the pavement and embankment structures were conducted from 2/18/2025 to 2/19/2025 by the Research team.



Figure 5-43. Location of Section S-11-8 of US-290 in Austin, Texas

The roadway pavement structure is built on a roadway embankment with an approximate height of 33 feet. The pavement type is Hot Mix Asphalt concrete (HMA) with multiple overlays. The overall pavement thickness is 15 inches, which includes 2 to 7 inches of overlay thickness. No bridge approach slab (BAS) was observed in this section. According to the plan sets (CSJ 0113–13-067), construction began on 9/24/1992 and was completed on 10/31/1996. **Table 5-7** shows the detailed descriptions of Section S-11-8.

Table 5-7. Detailed descriptions of Section S-11-8 of US 290 in Austin, Texas

Attribute	Information	Notes
District & Highway	Austin, US-290	
CSJ	0113-13-067	
County	Travis County	
Reference Marker	RM 575+0.61	
GPS Coordinates	30°13'38.2"N 97°46'35.9"W	
Date Work Begin	9/24/1992	
Date Completed	10/31/1996	
Pavement Type	ACP TY. C 2-in	(Surface course 2-in TY. C (PV-35 Min.))
BAS Thickness	NA	No BAS
Base Type	ACP 4-in TY. B + ASB 7-in TY. A	
Subgrade Type	Embankment OC (TY C)	
Drainage Type	Slotted Drain connected to Manhole and Conc. Riprap	
Embankment Height at BAS	33-ft	Wall – Wall

The approach side exhibited significant distress, including lateral movement of the railing and sidewalk, settlement of the railing, and severe longitudinal cracks on the asphalt overlaid surface. The observed distresses at approach side are shown in **Figure 5-44**. Additionally, distress related to the MSE wall was identified, including broken coping, dislocated wall panels, settlement and lateral movement of the coping, and bulging of the abutment wall (see **Figure 5-45**). Riprap joint separation and settlement were also noted. In contrast, the departure side was in significantly better condition, exhibiting minimal distress compared to the severe issues observed on the approach.



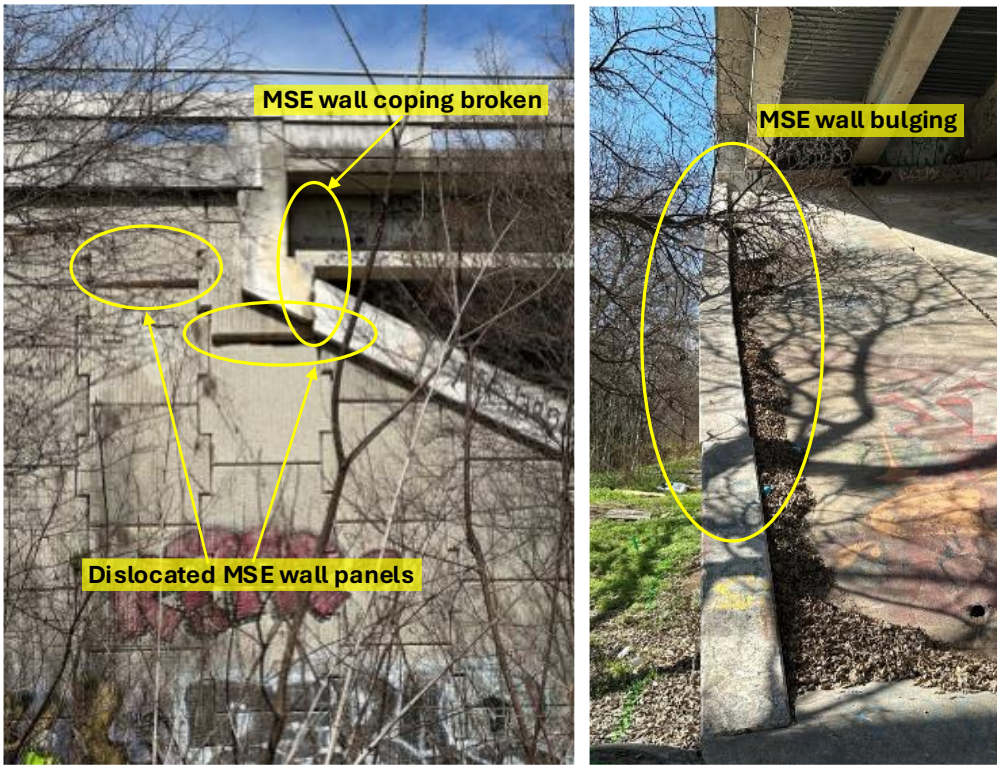
(a)





(b) (c)

Figure 5-44. Observed distresses at bridge approach side in section S-11-8: (a) lateral movement of railing and sidewalk, (b) railing settlement, and (c) longitudinal cracks on pavement surface



(a)



(b)

Figure 5-45. Observed distress (a) on MSE wall panels and (b) on coping and riprap

5.4.2 Falling Weight Deflectometer (FWD) tests

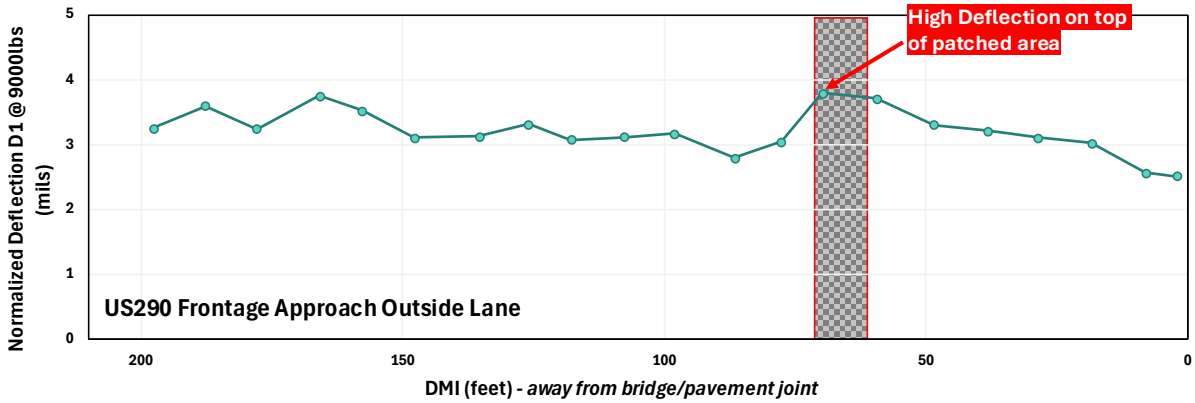
FWD tests were conducted on the inside and outside lanes of the approach side and the outside lane of the departure side. Spacing between FWD drop locations was 10 ft. FWD tests were also performed near the joint between the pavement and the bridge on the approach side. Deflections were normalized to a 9000-lb loading and evaluated. **Figure 5-46** below shows the FWD drop locations.



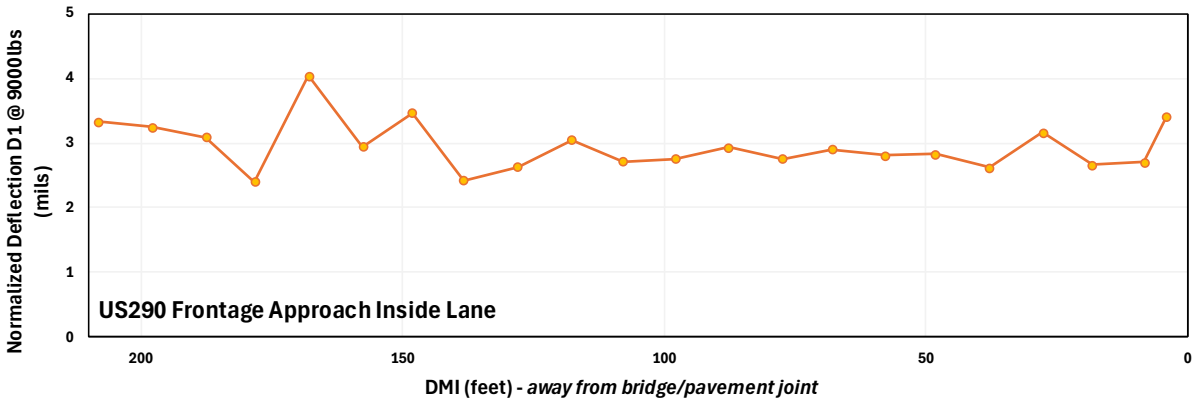
Figure 5-46. FWD testing locations at the approach and departure side

Approach Side

Figure 5-47 presents FWD deflections versus DMI for the outside and inside lanes of the approach side. For the outside lane (**Figure 5-47(a)**), measured deflections from DMI 200 ft to 150 ft were in the range of approximately 3 to 4 mils. From DMI 150 ft to 80 ft, the measured deflections were approximately 3 mils. A higher deflection was observed at DMI 70 ft and 60 ft; this higher deflection resulted from FWD tests being performed around a patchwork area. A decrease in deflection was identified from DMI 60 ft to 0 ft in the outside lane. The measured deflections for the inside lane (**Figure 5-47(b)**) were in the range of 2 to 3 mils, with the exception of the location at DMI 170 ft.



(a)



(b)

Figure 5-47. FWD deflections measured at the approach outside (a) and inside (b) lanes

Departure Side

Figure 5-48 presents the measured deflections of the outside lane of the departure side. The overall deflections were between 2 and 3 mils. A comparison of the deflections from the approach and departure sides indicates no significant difference in terms of structural performance.

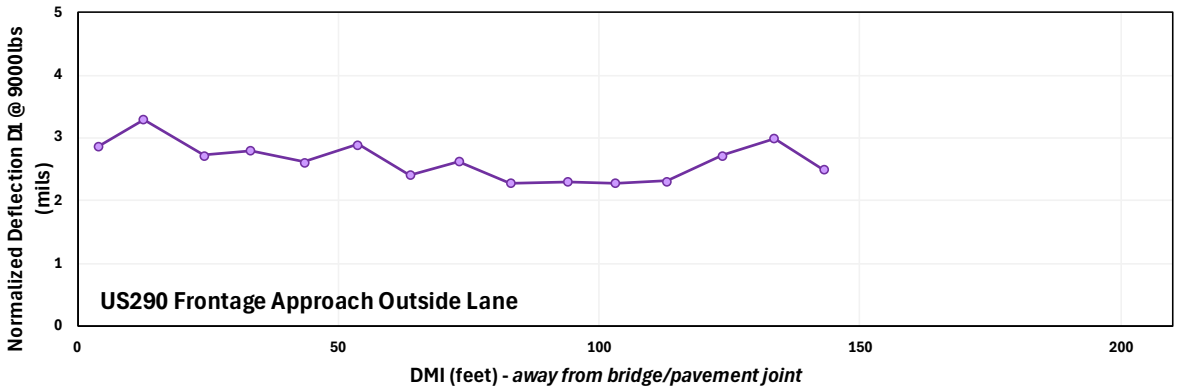


Figure 5-48. FWD deflections measured at the outside lane of departure side

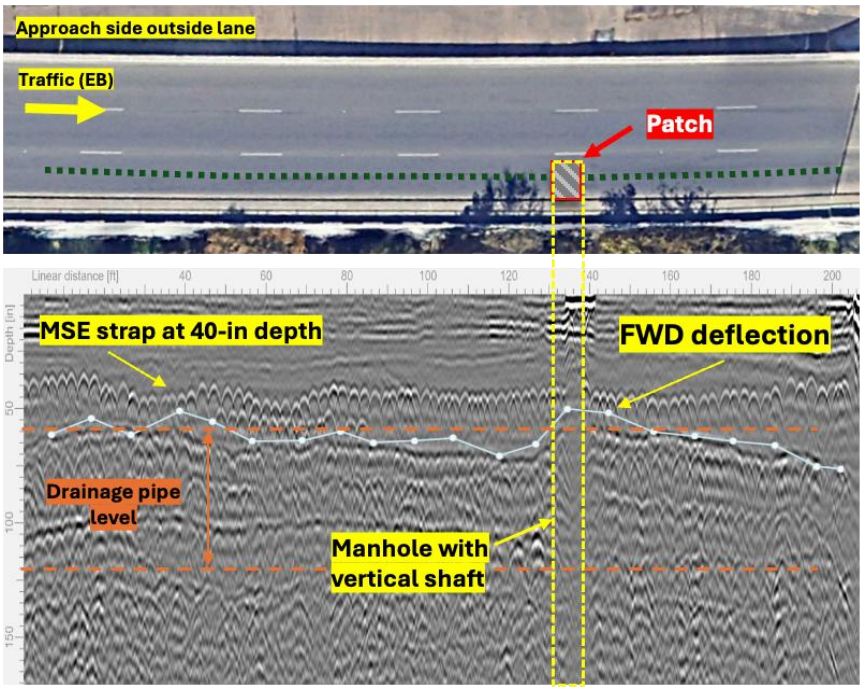
5.4.3 Ground Penetration Radar (GPR) Utility Scan

Ground Penetrating Radar (GPR) surveys were performed across the entire test section with a 2-ft transverse spacing to identify subsurface anomalies. Representative GPR data from the eastbound (EB) approach are presented in **Figure 5-49**.

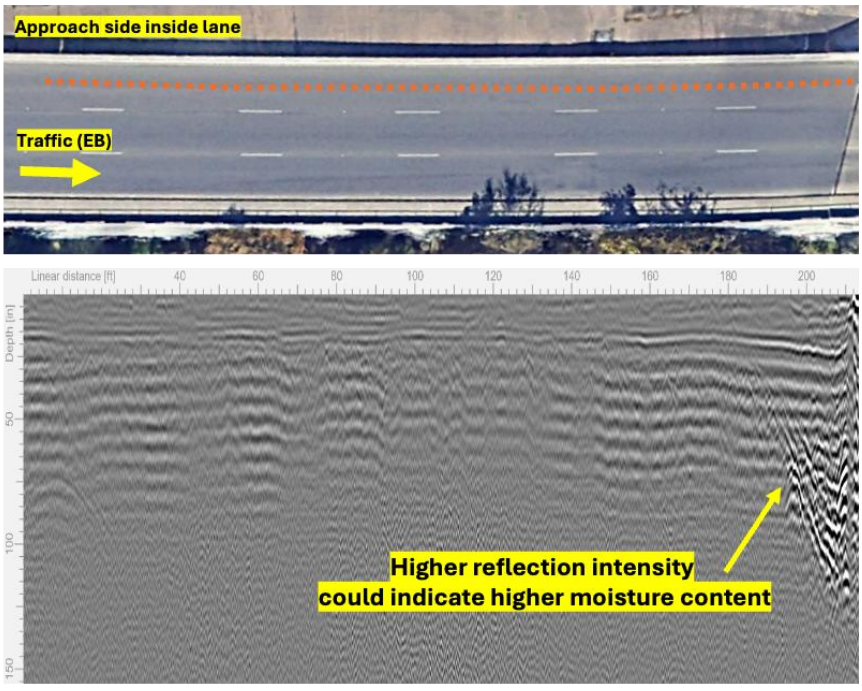
In the outside lane, the GPR profile clearly identified MSE wall reinforcing straps at a depth of approximately 40 inches, appearing as a sequence of uniformly spaced hyperbolic reflections. Other notable features include a strong surface-level reflection between 130 and 140 ft attributed to the presence of a manhole. Additionally, a drainage pipe with a diameter of approximately 3.5 ft, located at a depth of about 6 ft, was delineated and is highlighted by the orange dashed lines in **Figure 5-49**.

Dynamic Cone Penetrometer (DCP) testing conducted in the same area identified low subgrade moduli (M_r = 2–5 ksi), indicating the presence of a weaker soil layer. Interestingly, the FWD deflection profile (shown as a white overlay in **Figure 5-49**) closely follows the upper interface of this soft layer delineated by GPR, demonstrating a strong correspondence between subsurface layer thickness variation and surface deflection response. This alignment between FWD, DCP, and GPR data highlights that the measured FWD deflection in asphalt-surfaced pavements is significantly influenced by the stiffness and thickness of the underlying subgrade.

In the inside lane, high-intensity reflection was detected near the bridge (DMI 180–210 ft), potentially suggesting an area with elevated moisture content. The increased moisture was further verified by laboratory soil tests and lower strength by DCP in this region, which will be discussed in subsequent sections.



(a)



(b)

Figure 5-49. GPR scanned locations and data of approach side for (a) outside lane and (b) inside lane

5.4.4 Coring

Six locations on the approach side and three locations on the departure side were selected for coring. Based on FWD deflections and observed distresses, the approach side was determined to be in worse condition than the departure side; therefore, testing was focused on the approach side. On the approach side, coring locations C2 and C7 were selected due to their proximity to severe longitudinal cracks. Location C6 was selected where the highest FWD deflection was observed, and C9 was selected based on GPR scan results. Two locations (C1 and C8) were selected as controls. The detailed coring locations and images of the core samples are presented in **Figure 5-49**.

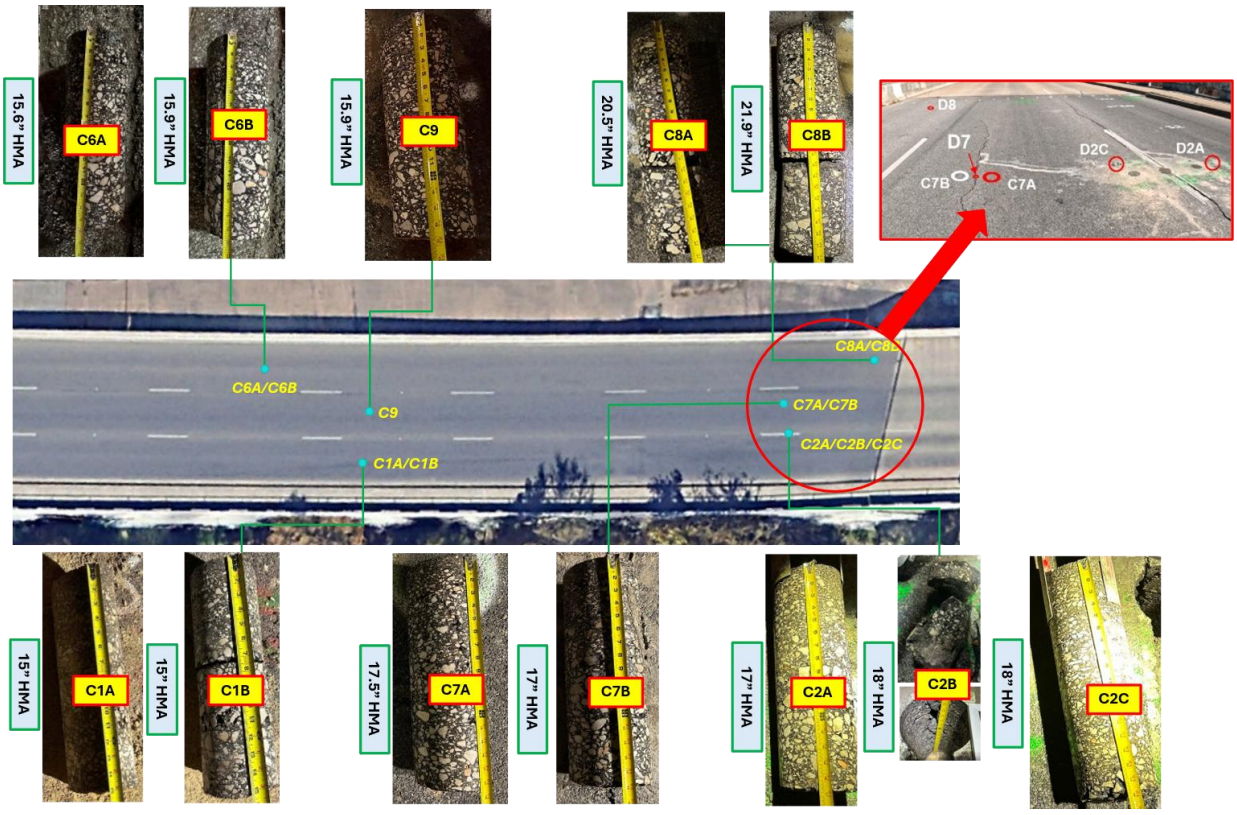


Figure 5-50. Coring Locations and images of core samples

All coring locations consisted of HMA pavement with layer thicknesses ranging from 15 to 21.9 inches, indicating previous repair attempts to address continuous pavement settlement. The HMA thickness was observed to increase toward the bridge.

5.4.5 Dynamic Cone Penetrometer (DCP) tests

To estimate the backfill/subgrade conditions of the embankment, DCP tests were conducted at or near the core locations for the outside and inside lanes of the approach side. To directly access the untreated subgrade soil, auguring was performed beneath the bottom of the cored holes. For DCP tests performed near cored holes, drilling was conducted to penetrate from the pavement surface to the untreated subgrade. A total of eight DCP tests were performed on the approach side; detailed locations are shown in **Figure 5-51**.

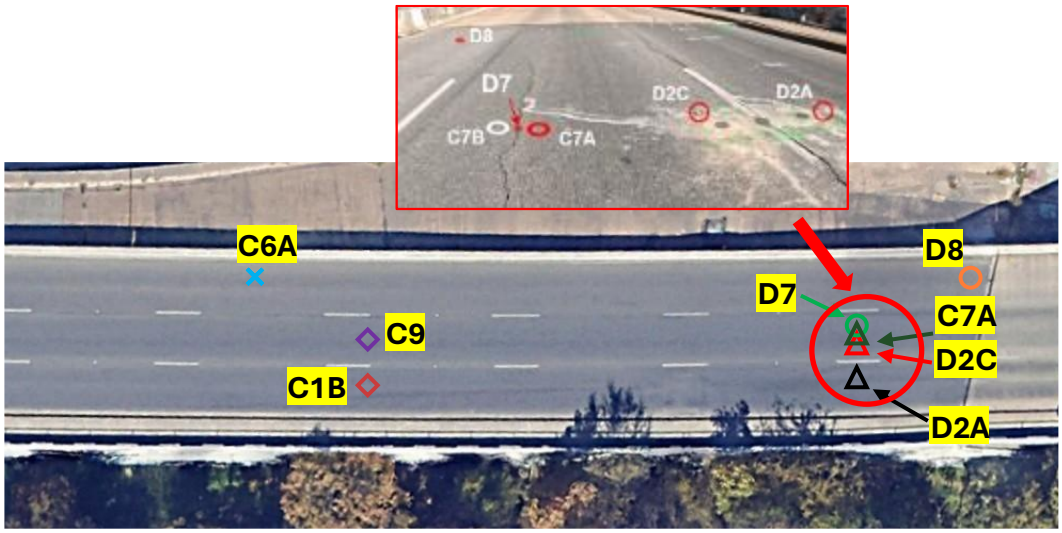
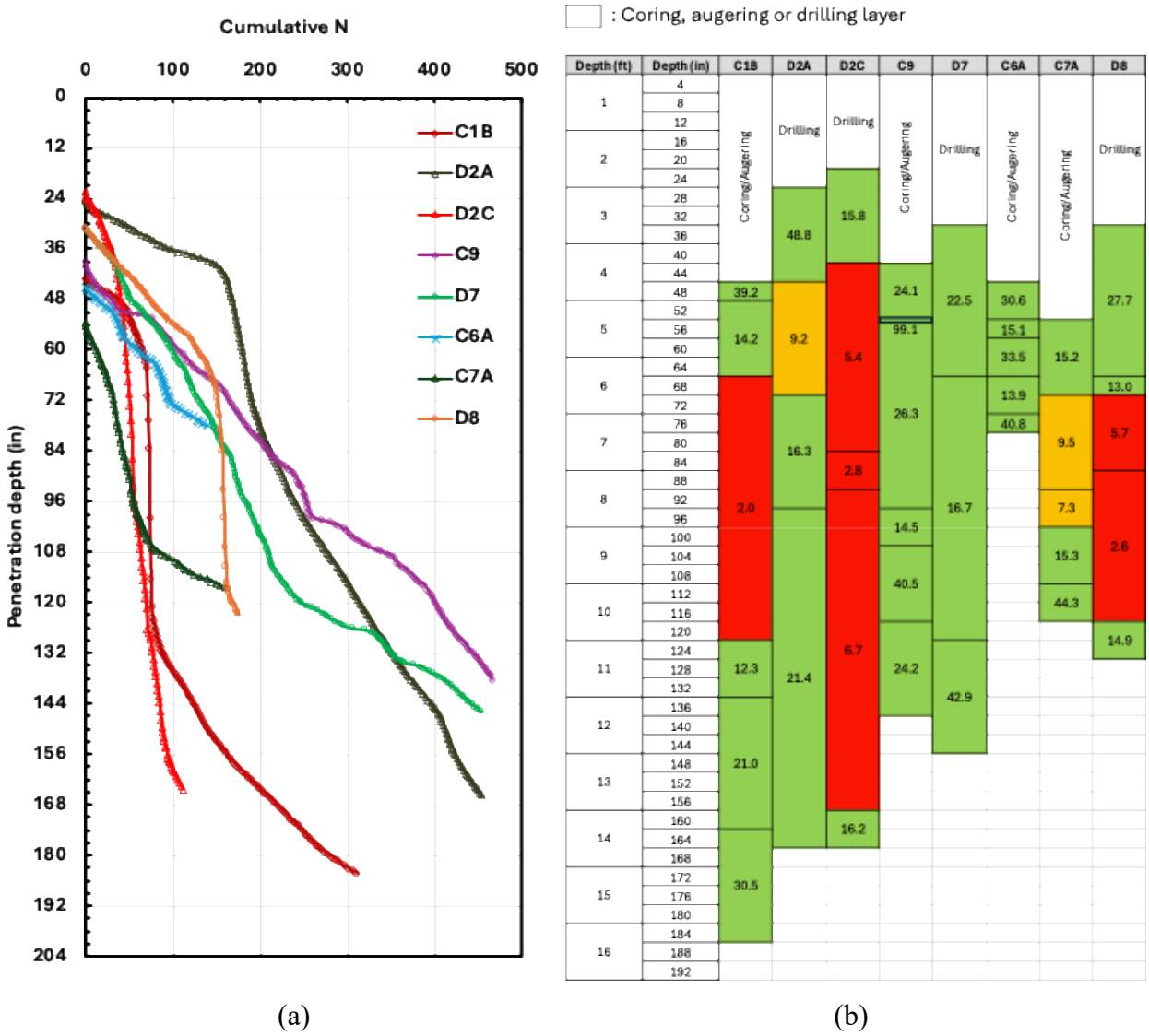


Figure 5-51. Locations of DCP testing

The cumulative DCP blow counts vs. depth relationships from all DCP tests are presented in **Figure 5-52(a)**. The resilient moduli (M_r) of the subgrade soil were evaluated using Eq. (1), and the results are shown in **Figure 5-52(b)**. At locations C1B, D2C, C7A, and D8, the M_r values from DCP tests were lower (less than 7 ksi) than at other locations within the depth range of 5 to 11 ft.



(a) (b)

Figure 5-52. (a) Cumulative DCP blow counts vs. penetration depth below the pavement surface. (b) Resilient modulus (M_r) determined from DCP tests (Note: the color scheme for M_r value is for illustrative purposes only.)

5.4.6 Soil Sampling

Soil samples were collected using a Shelby tube and auger at various depths from locations C1, C2, C3, C6, C7, C8, and C9. For samples taken by Shelby tube sampler (from 5–11 ft at C7B and 5–10 ft at C8A), the Research Team performed pocket penetrometer tests. A series of laboratory tests were performed on the collected samples. Soil classification tests (USCS and AASHTO) were conducted for samples from C1A, C7B, and C8A. Water contents were measured for all collected samples. The results of the pocket penetrometer tests and other lab data are presented in **Table 5-8**.

Table 5-8. Summary of laboratory test results

Sampling Location	Sampling Type (Grab or Shelby tube)	Classification (USCS/AASHTO[GI])	Sampling Depth (ft)	Pocket Penetrometer (tsf)	Moisture Content (%)	Retained on #4 (%)	Passing #200 (%)	PI (%)	LL (%)
C1A	Grab	GC-GM/ A-1-b[0]	1.25-13	-	3.8	53	17	5	17
C2A	Grab	-	1.46-8	-	7.0	-	-	-	-
C2C	Grab	-	1.5-8	-	10.8	-	-	-	-
C6B	Grab	-	1.3-5	-	11.0	-	-	-	-
	Grab	-	5-10	-	15.9	-	-	-	-
C7A	Grab	-	1.46-5	-	15.1	-	-	-	-
C7B	Shelby	SC/ A-2-4[0]	5-7	1.5	17.0	33	32	10	28
	Shelby	SC-SM/ A-2-4[0]	7-8	3.5	16.0	31	32	6	22
	Shelby	GW/ A-1-a[0]	8-10	2.5	14.9	74	3	-	-
	Shelby	SC/ A-2-4[0]	10-11	0	17.4	43	29	10	24
C8A	Grab	CL-ML/ A-4[0]	1.7-5	-	10.3	16	50	5	12
	Shelby	SC-SM/ A-4[0]	5-7	1.5	12.2	31	40	5	18
	Shelby	SC-SM/ A-2-4[0]	7-9	2	12.9	43	27	10	27
	Shelby	SC/A-6[1]	9-10	0	15.4	29	38	13	25
C8B	Grab	-	1.82-5	-	12.7	-	-	-	-
	Grab	-	5-10	-	13.2	-	-	-	-
C9	Shelby	-	1.32-5	-	10.1	-	-	-	-

Figure 5-53 shows the moisture content from sampling locations at various depths. Moisture contents from locations away from the bridge (C6B, C9, C1A) were between about 4% and 15%. In contrast, moisture contents from locations close to the bridge (C8A/C8B, C7A/C7B, C2A/C2C) were in the range of 10–20%. A comparison of water content among C6, C8, C9, and C7 shows that moisture contents were higher at the inside lane (C6 and C8) than the outside lane (C9 and C7). These higher moisture concentrations are consistent with the roadway geometry and surface drainage patterns, which direct runoff toward the inside lane and the bridge interface. At locations C6B, C7A/C7B, and C8A/C8B, water contents at 5 to 10 ft depths were higher than at shallow depths.

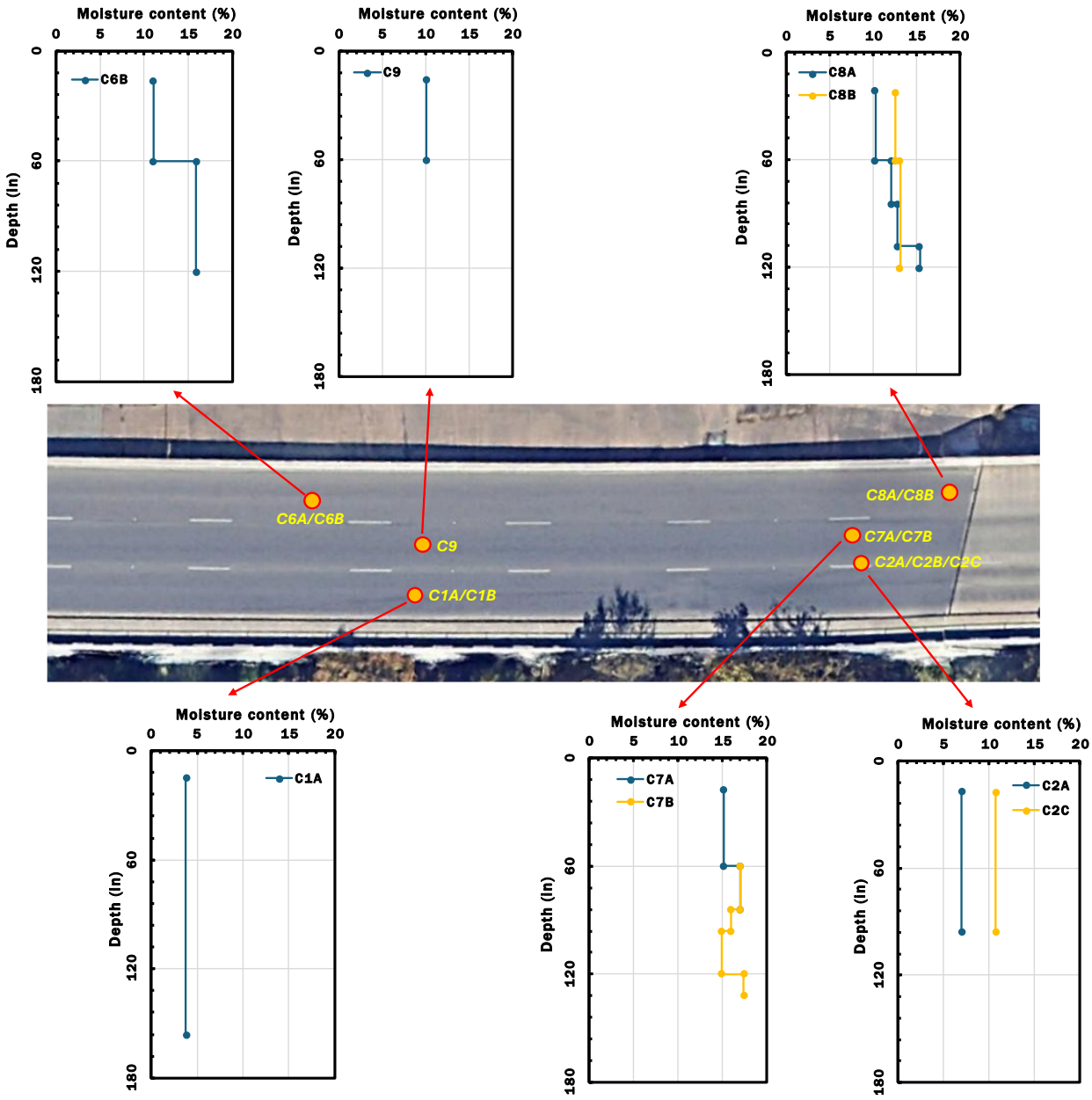
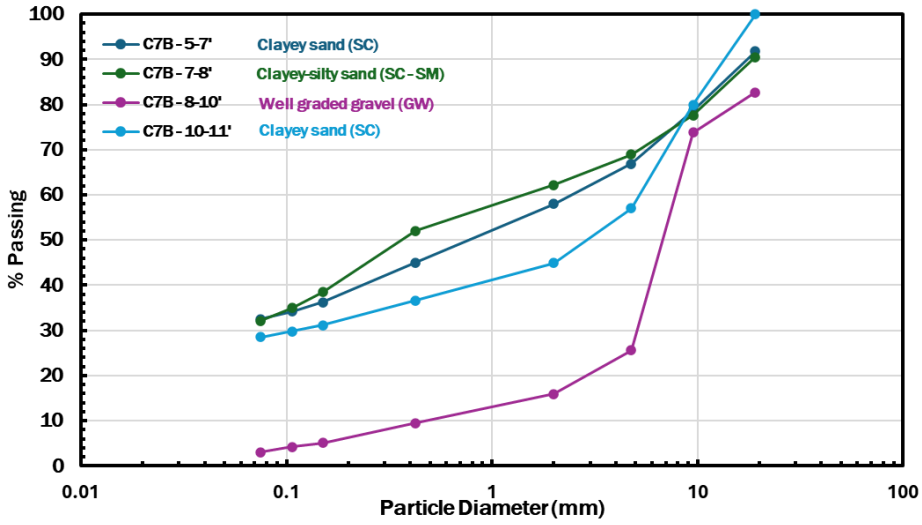


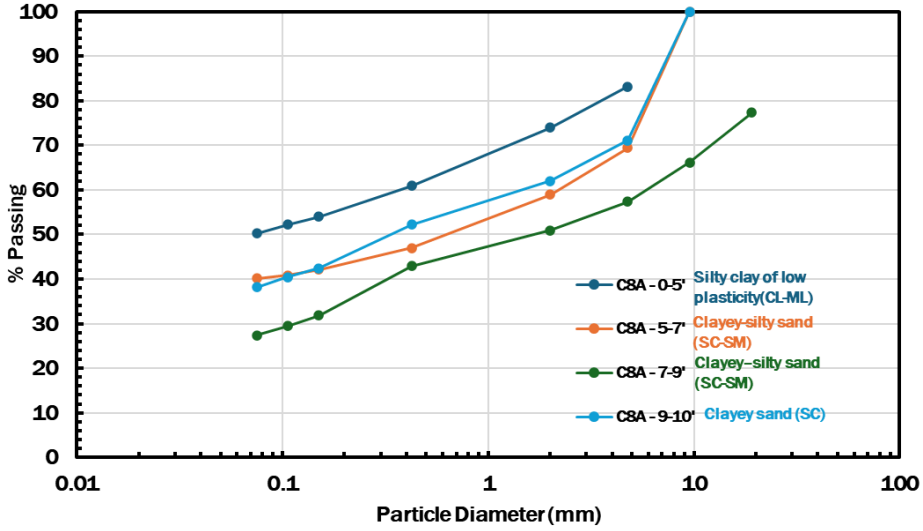
Figure 5-53. Sampling locations and moisture contents with various depths

Particle size distribution curves for samples from C7B and C8A at various depths are presented in **Figure 5-54**. Particle size analysis indicates that the soils at shallow depths (5–7 ft for C7B and 0–5 ft for C8A) were finer than at other depths. At C7B, the percent passing the #200 sieve was 32.5% at 5–7 ft depth but decreased to 3% at 8–10 ft, strongly suggesting washout of fines. Samples collected from deeper depths at both locations (10–11 ft for C7B and 9–10 ft for C8A) were finer than samples from the middle depths. Based on the particle size analysis and water

content data, it is suggested that fine particles in the depth where the drainage pipe is buried have been washed out.



(a)



(b)

Figure 5-54. Particle size distribution curves: (a) soil samples taken from C7B and (b) soil sample from C8A at various depths

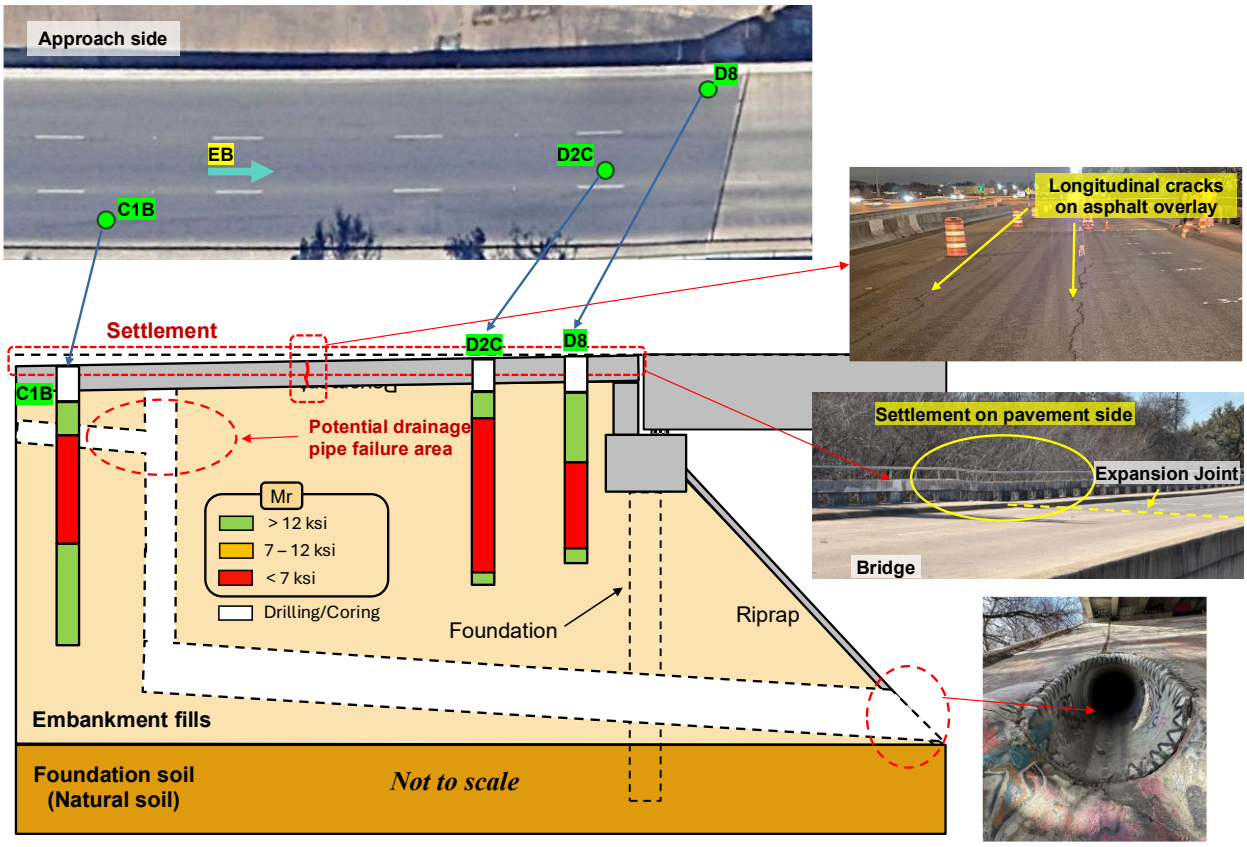
5.4.7 Potential Distress Mechanisms

Based on the field observations and laboratory test results, the observed distresses at Section S-11-8 are primarily attributed to water infiltration and poor compaction of the embankment fill. To

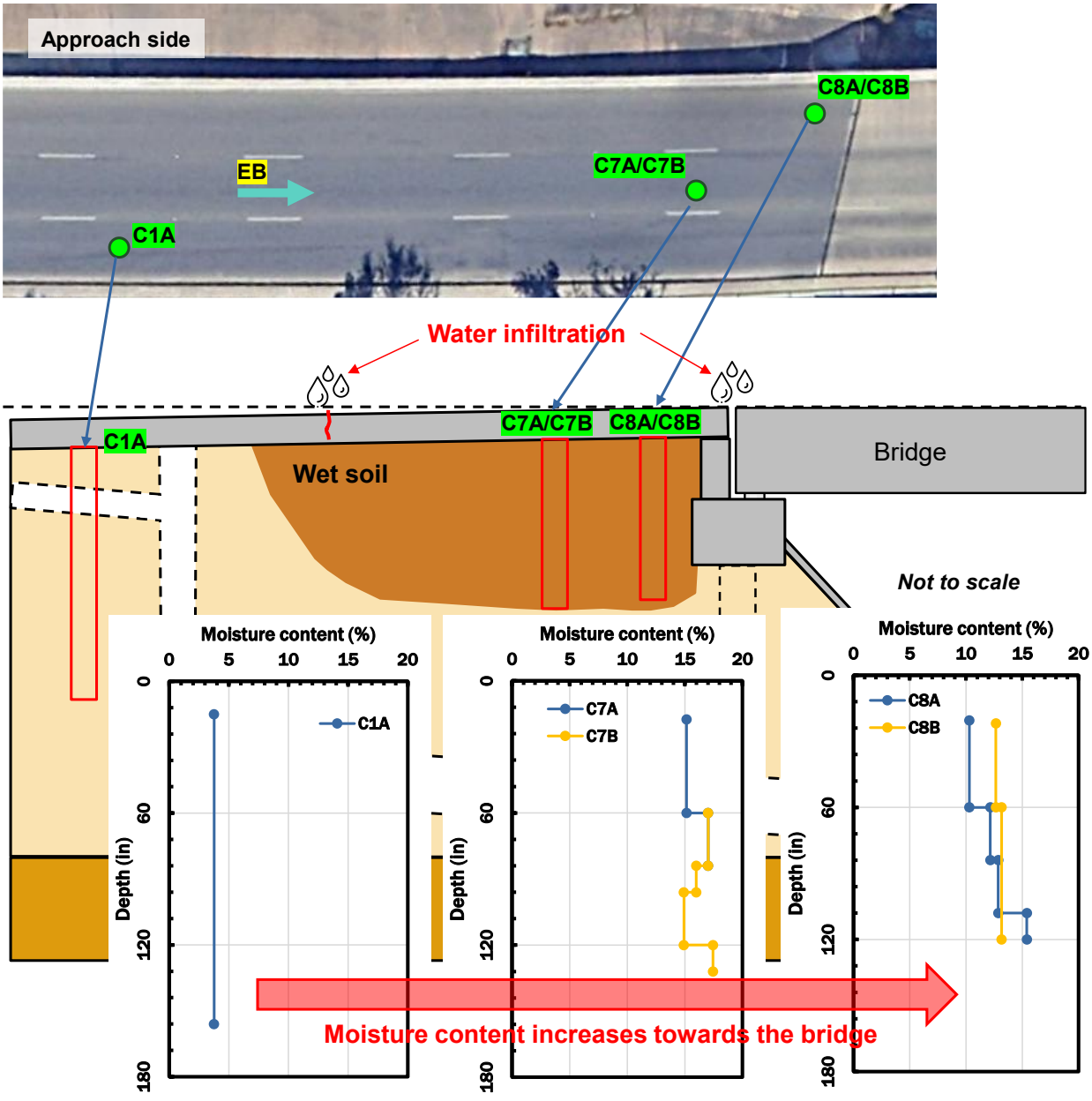
illustrate the distress mechanism, two representative sections were considered (**Figure 5-55** and **Figure 5-56**): **Figure 5-55** illustrates the longitudinal cross-section through the pavement, embankment, and bridge, and **Figure 5-56** shows the transverse section through MSE wall and embankment.

DCP test results indicated significant variability in the embankment fill stiffness, with weak zones (M_r values were less than 7 ksi) identified at depths between 5 and 11 ft as shown in **Figure 5-55(a)**. The drainage system is suspected to be compromised, which prevented effective water discharge from the embankment. This combination of potentially variable compaction and drainage issue likely contributed to the differential settlement and subsequent longitudinal cracking.

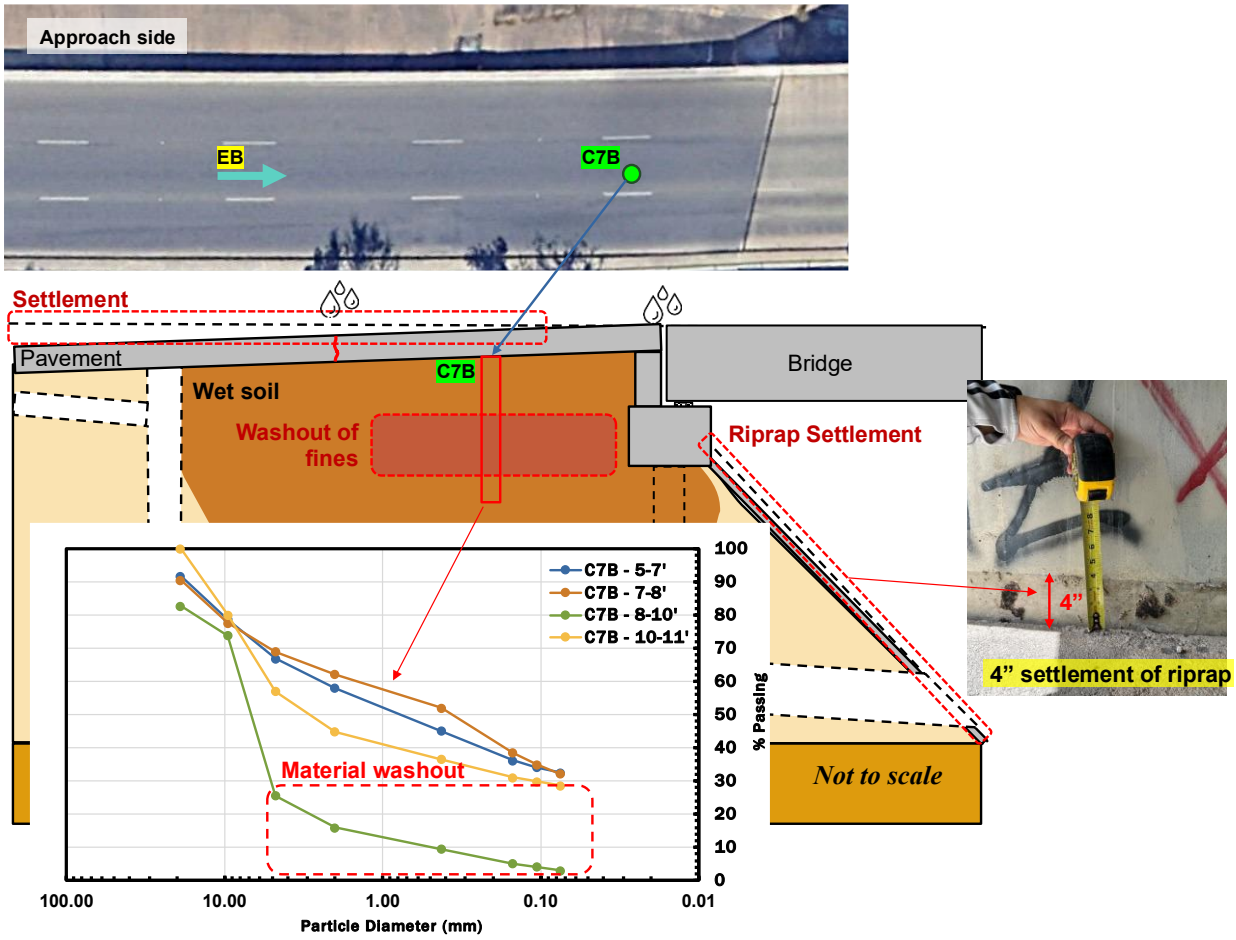
It is likely that water infiltrated into the fill material through the surface cracks and joints. Laboratory tests confirmed that moisture contents were higher in locations closer to the bridge compared to areas further away as shown in **Figure 5-55(b)**. As water continuously flowed through the embankment fill, fine particles migrated and were washed out, evidenced by a reduction in fines passing the No. 200 sieve from 32.5% to 3% at location C7B. This material washout further weakened the soil structure, causing further settlement of the pavement and riprap (**Figure 5-55(c)**).



(a)


Approach side
EB
C1A
C7A/C7B
C8A/C8B
Water infiltration
Wet soil
Bridge
Not to scale
Moisture content (%)
0 5 10 15 20
Depth (in)
0 60 120 180
C1A
C7A
C7B
C8A
C8B
Moisture content increases towards the bridge

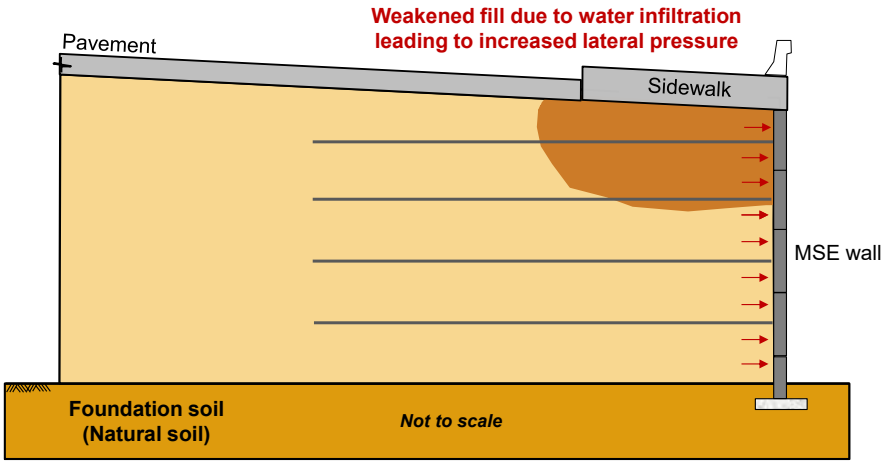
(b)



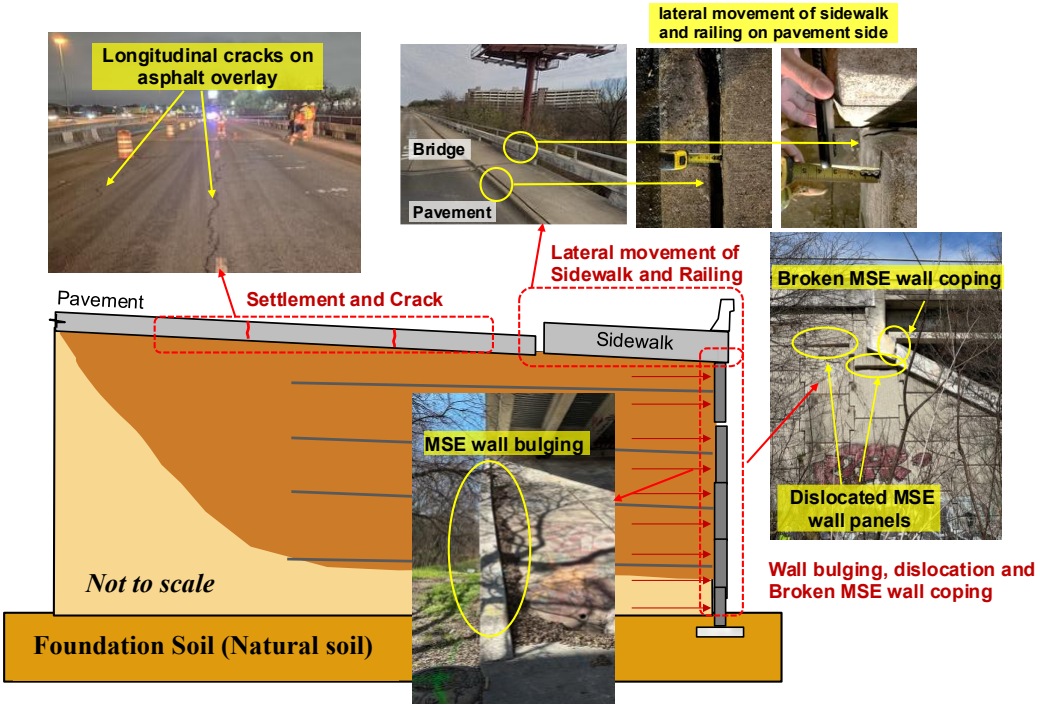
(c)

Figure 5-55. Potential distress mechanism (Note: the color scheme for M_r value is for illustrative purposes only.)

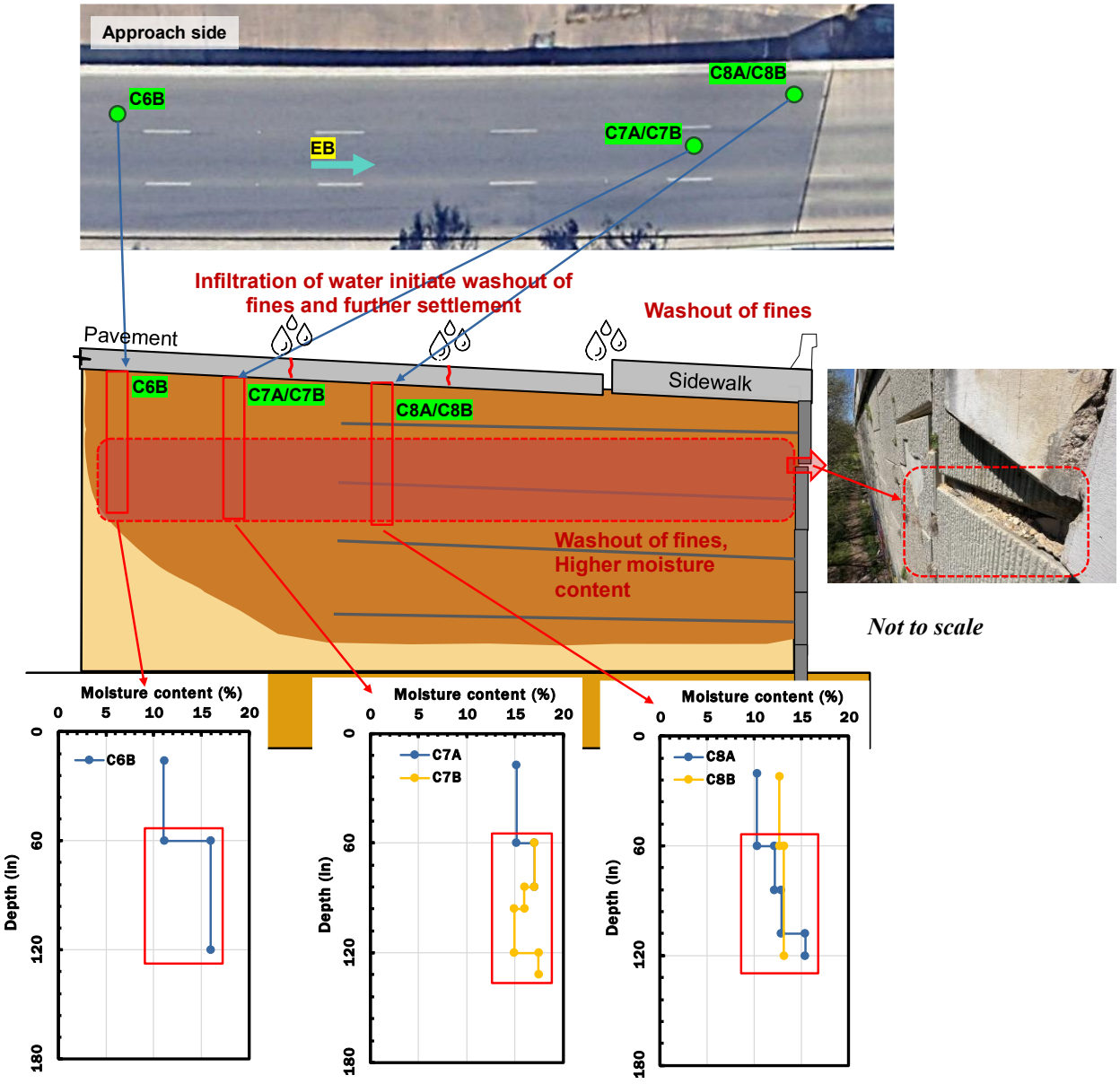
The water infiltration through pavement joints and cracks, as illustrated in **Figure 5-55**, not only weakened the embankment fill but also increased the lateral pressure acting on the MSE wall, as conceptually shown in **Figure 5-56(a)**. The elevated lateral pressure, combined with the reduced shear strength of the saturated soil, resulted in significant instability of the MSE wall, including the bulging of the MSE wall, dislocation of wall panels, and breakage of the wall coping. Furthermore, the lateral movement of the retaining wall structure contributed to the lateral displacement of the sidewalk and railing, as well as the development of severe longitudinal cracks on the pavement surface, as illustrated in **Figure 5-56(b)**. As water continuously infiltrated through the embankment, fine particles migrated from the fill material. This loss of fine particles created voids and further weakened the soil structure, leading to progressive settlement of the pavement and riprap (**Figure 5-56(c)**).


Weakened fill due to water infiltration
leading to increased lateral pressure
Pavement
Sidewalk
MSE wall
Foundation soil
(Natural soil)
Not to scale

(a)


Longitudinal cracks on
asphalt overlay
lateral movement of sidewalk
and railing on pavement side
Bridge
Pavement
Lateral movement of
Sidewalk and Railing
Broken MSE wall coping
Pavement
Settlement and Crack
Sidewalk
MSE wall bulging
Dislocated MSE
wall panels
Not to scale
Wall bulging, dislocation and
Broken MSE wall coping
Foundation Soil (Natural soil)

(b)



(c)

Figure 5-56. Potential distress mechanism for MSE wall

5.4.8 Repair Recommendation

Based on field observations and laboratory analysis, the primary causes of the distresses at Section S-11-8 were identified as water infiltration and likely poor compaction of the embankment backfill. A compromised drainage system prevented effective water discharge, leading to differential settlement and the formation of longitudinal cracks that allowed further water ingress. This continuous water infiltration caused a significant washout of fine particles with increasing lateral

pressure. Consequently, the increased lateral pressure caused bulging of the wall, dislocation of panels, breakage of the coping, and lateral displacement of the sidewalk and railing.

To address these issues, Soil Densification with High-Density Polyurethane Foam (HDPF) according to Special Specification 3086 (TxDOT SS 3086) is recommended as a short-term repair plan. The injection should be targeted at a depth of 7 feet to effectively densify the soft embankment fills located between 5 and 10 feet below the surface. During this process, the construction team must carefully monitor the coping, MSE wall panel joints, and riprap to ensure that the injected foam does not leak. Simultaneously, the drainage system requires inspection and repair, and all cracks on the sidewalk and separations on the riprap must be sealed to minimize water infiltration. Extreme caution is required during these operations to avoid damaging the drainpipe and vertical shaft located beneath the outside lane. A permanent resolution involves the full reconstruction of the MSE wall, which requires replacing the defective embankment materials up to a depth of approximately 15 feet to eliminate the instability source. **Figure 5-57** shows the target repair zone for short-term and long-term plans. Alternatively, the construction of a buttress wall or soldier pile wall is recommended along with the existing MSE structure to mechanically mitigate lateral movement. Regardless of the repair options, it is strongly recommended to perform periodic monitoring of the MSE wall movement and surface settlement.

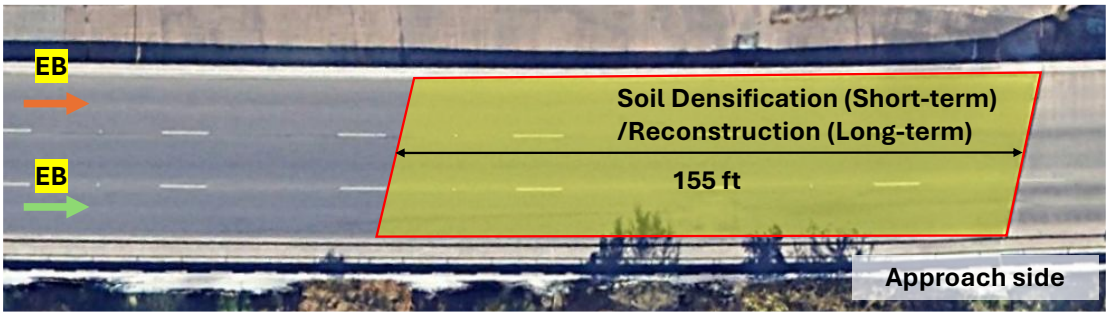


Figure 5-57. Recommended repair area for short-term and long-term plans

5.5 Section P-A-3: IH 20 on-ramp in Fort Worth

5.5.1 Overview

The Bridge Approach Slab (BAS) and the nearby CRCP pavement on on-ramp connecting to IH 20 main lanes in Fort Worth, Tarrant County, Texas, were investigated by the Research Team on 07/21/25 and 07/22/25. This specific segment is referenced by RM 29+0.5, and the location of Section P-A-3 is shown in **Figure 5-58**. The roadway section rests upon an embankment, estimated at approximately 16.5 ft in height at BAS location based on surrounding bridge clearance data. The purpose of the investigation was to evaluate the existing pavement structure and subsurface conditions. **Table 5-9** shows the detailed descriptions of Section P-A-3.

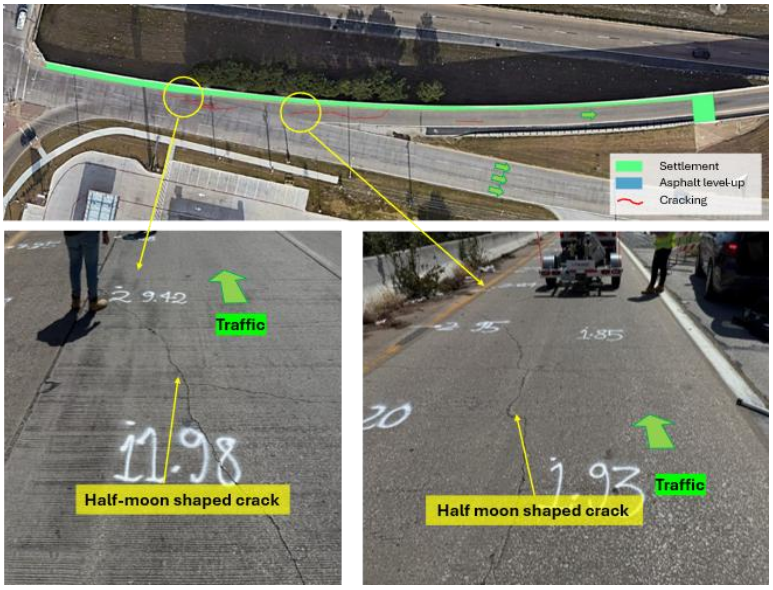


Figure 5-58. Location of Section P-A-3 of IH20 on-ramp in Fort Worth, Texas

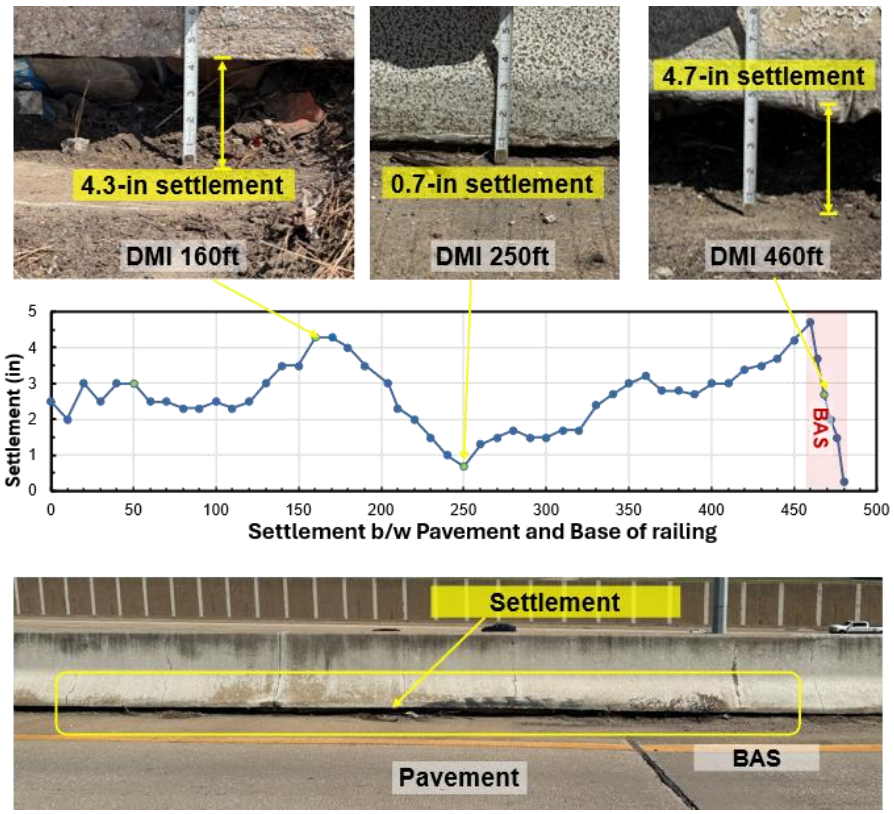
Table 5-9. Detailed descriptions of Section P-A-3

Attribute	Information	Notes
District & Highway	Fort Worth & IH-20	
CSJ	0008-12-047	
County	Tarrant County	
Reference Marker	RM 29+0.5	
GPS Coordinates	32°39'51.0"N 97°19'52.2"W	
Date Work Begin	10/10/1988	
Date Completed	4/12/1992	
Pavement Type	No plan set available for the subject section.	
BAS Thickness	No plan set available for the subject section.	
Base Type	No plan set available for the subject section.	
Subgrade Type	No plan set available for the subject section.	
Drainage Type	No plan set available for the subject section.	
Embankment Height at BAS	16.5 ft	Wall - Slope
Distress Observed (Severity)	Settlement and Longitudinal crack (Severe)	

A visual survey during the field evaluation indicated the presence of severe pavement settlement and BAS settlement and a half-moon shaped cracking within the pavement surface, highlighting substantial structural distress in the area. This section has shown settlement of the pavement and BAS over the years, and HDPF was also found during coring confirming the past repair attempts for settlement issues. Overview of the distress is shown in **Figure 5-59(a)**. The separation between the pavement and the base of railing recorded at 10-ft spacing is presented in the **Figure 5-59(b)**.



(a)



(b)

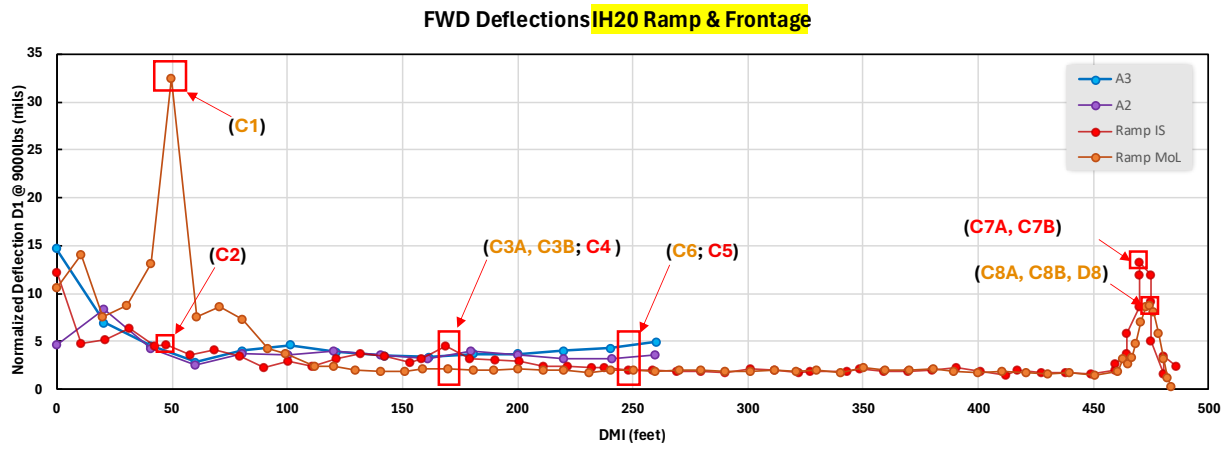
Figure 5-59. Distress observed at IH-20 on-ramp: (a) Half-moon shaped cracking (b) Settlement between pavement and base of railing at different DMI.

5.5.2 Falling Weight Deflectometer

Falling Weight Deflectometer (FWD) tests were conducted along the inside shoulder (Ramp IS) and middle of lane (Ramp MoL) on IH20 On-Ramp and along the middle of lane (A2) and inside lane (A3) on the adjacent frontage road. The spacing between FWD drop locations was approximately 10 ft on the pavement sections, 2 ft on the BAS, and immediately before and after joints. **Figure 5-60(a)** presents the FWD drop locations along with the coring locations marked with blue markers. The location of the construction joint is represented in **Figure 5-60(a)** as a yellow line. The FWD deflections normalized to a target load of 9,000-lb at different DMI along with coring location are presented in **Figure 5-60(b)**.



(a)



(b)

Figure 5-60. (a) FWD testing locations with coring location marked. (b) Deflections measured at the inside shoulder and on middle of lane on the Ramp and middle lane and inside lane of adjacent frontage road at different DMI along with coring location marked.

To put the measured FWD deflections in context, the Research Team proposes to use 'statewide average' as the performance benchmark. Adopted from TxDOT Research Project 0-5445 (Won and Medina, 2008), the statewide average FWD deflection defines the expected behavior of sound CRCP based on slab thickness. As slab thickness increases, surface deflection under a load decreases due to better load distribution. The governing equation for this relationship is:

$$D_0^w = 252.85 \times (t_{slab})^{-2.005} \quad (2)$$

where D_0^w= central deflection normalized with respect to 9000 load from FWD test performed on well-performing CRCP (in mils) and t_{slab} = thickness of CRCP (in inches).

The FWD data along the ramp (Ramp MoL) generally exhibited low and consistent deflections across the CRCP section, remaining near or below the statewide average deflection for the section between DMI 100 and 460 ft after the joint at about DMI 85. However, for the section between DMI 0 and 100 ft, the FWD deflections were generally greater than the statewide average value and a significant spike in deflection (32.5 mils) was recorded at about DMI 50 ft. This peak is associated with a void and HDPF beneath the slab, indicating a loss of support, which was observed

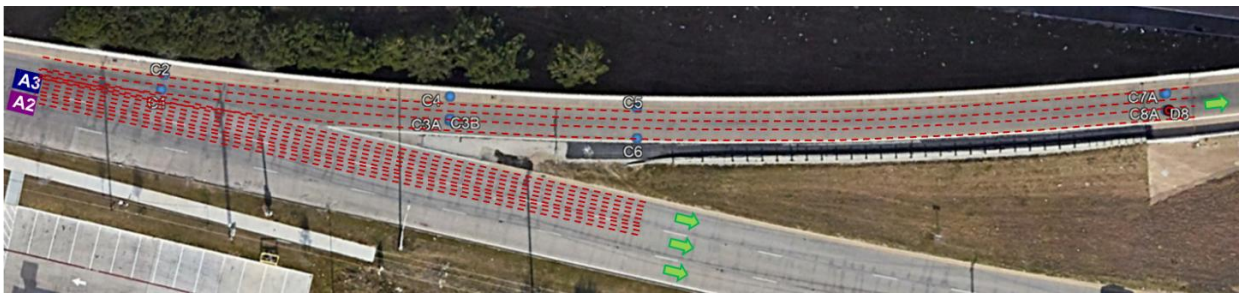
during coring process (more details on coring data are presented in the subsequent sections). High deflections were also observed on the BAS (between DMI 460 and 480) with a peak of 8.7 mils at DMI 470, suggesting potential issues or loss of support at the BAS (1.5" void was observed in the area during coring, which is discussed in a later section).

The Ramp IS showed a similar pattern of low deflections across the CRCP section, remaining near or below the statewide average deflection for the section after the joint (between DMI 100 and 460) with comparatively higher deflection for the section before the joint (between DMI 0 and 100). High deflections were also observed on the BAS with a peak of 13.3 mils at DMI 470 where a void of 4 inches was found during coring.

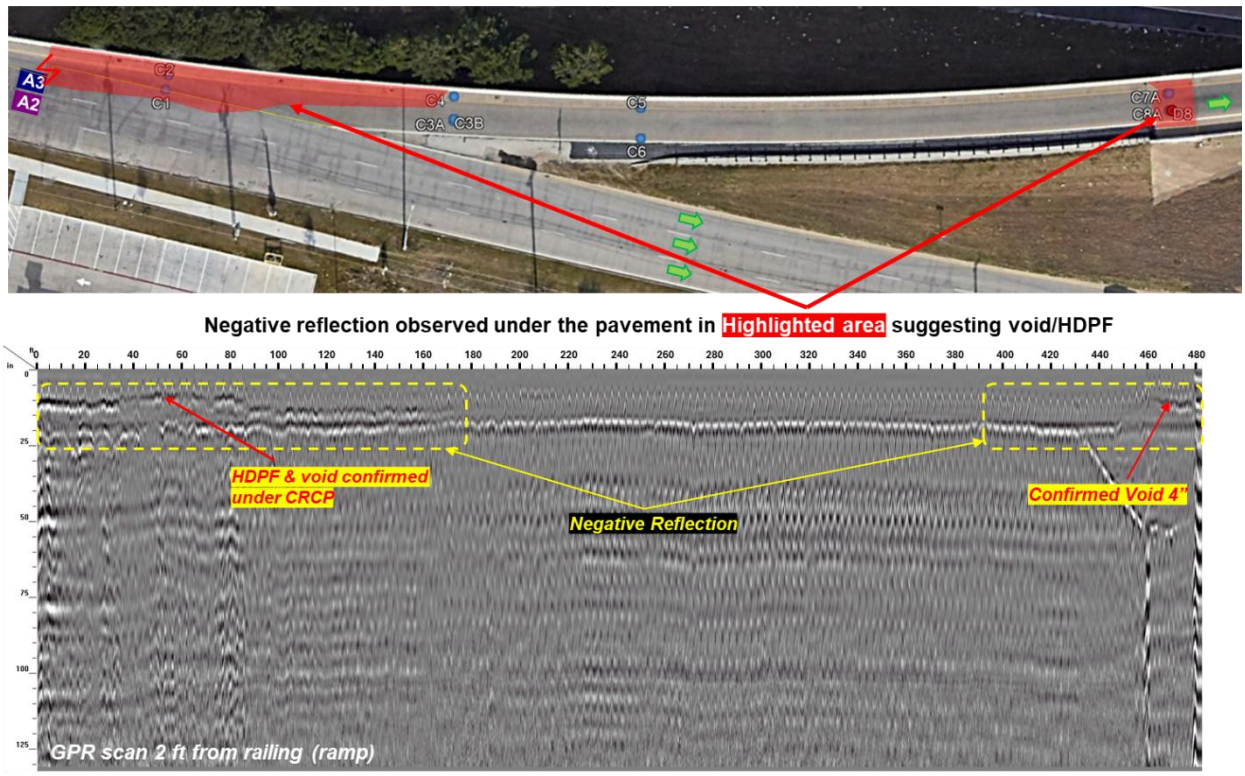
The deflection data from the FWD tests for both the frontage road inside lane (A3) and the frontage road middle lane (A2) show a high value at DMI 0 due to the presence of a joint but rapidly drops and stabilizes, remaining near the statewide average after approximately DMI 50. The deflection values for both lanes of the frontage road indicate that the frontage pavement has good support compared to the ramp pavement.

5.5.3 Ground Penetrating Radar (GPR) Utility Scan

A total of 18 passes were made at 2 ft intervals and calibrated for depth with physical core samples. The GPR scan taken from 2 ft to 10 ft from the railing detected strong negative reflections in key distress areas, which were interpreted as the presence of voids or low-density material and supported by coring results: the GPR anomaly near DMI 50 ft (coring location C2) was confirmed as HDPF below the CRCP, while a major anomaly near DMI 460 and DMI 480 ft (coring location C7B) was validated as a 4-in void. Other scans (4 ft to 10 ft from railing) similarly indicated persistent negative reflections suggesting voids below the pavement at the beginning of the ramp (DMI 0 to DMI 160 ft) and in the BAS (DMI 460 to DMI 480 ft). **Figure 5-61(a)** shows the GPR pass location, **Figure 5-61(b)** shows the visualization of void and GPR scan result at 2 ft from the railing.



(a)



(b)

Figure 5-61. (a) GPR pass location. (b) Visualization of void and HDPF and GPR scan result at 2ft from the railing.

5.5.4 Coring

Ten cores (C1 through C8B) were taken at a total of seven key locations to determine the pavement composition and confirm subsurface anomalies. Coring locations were based on settlement (separation between pavement and base of railing presented in **Figure 5-59(b)**) and the FWD deflection.

Coring confirmed a high degree of variability in the pavement structure, with the CRCP thickness ranging from 8.75 inches to 13.25 inches for the pavement section and 11.25 inches to 11.5 inches for BAS. The pavement on the Frontage Road was found to consist of 8 to 10 inches of CRCP over 5 inches ACP.

Figure 5-62 and **Figure 5-63** show the images of the cores taken and the voids identified from the coring process. The location with the maximum deflection (C1) revealed both a 1-inch void and 1-inch HDPF, confirming a loss of support and prior repair efforts. Furthermore, the high deflections observed on the BAS were directly attributed to loss of support underneath the pavement, with cores at C7A/C7B and C8A/C8B revealing voids up to 4 inches beneath the bridge approach slab. The severe settlement and structural compromise of the ramp pavement likely resulted from voids leading to a loss of foundation support, especially near the construction joints

and the bridge approach area. **Table 5-10** summarizes the thickness of CRCP, HMA, HDPF and void measured at cored locations.

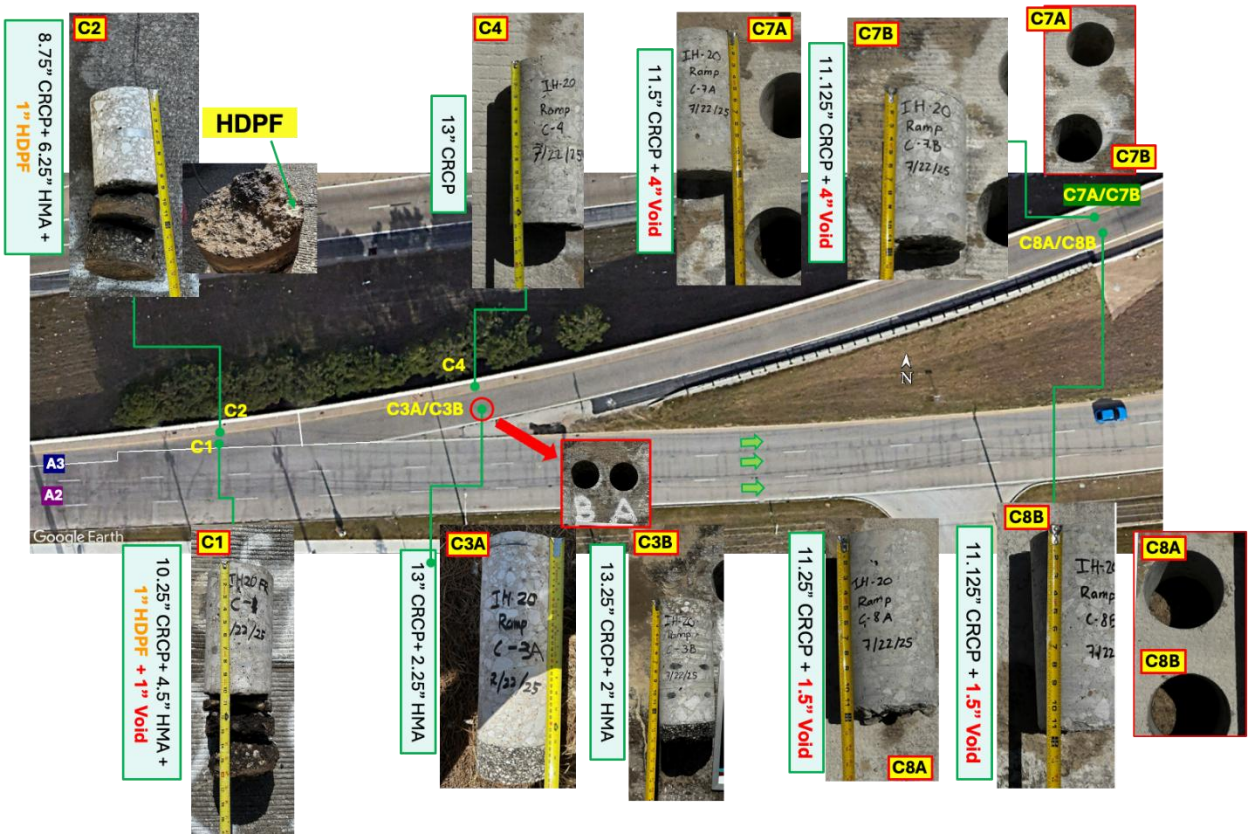


Figure 5-62. Coring location and images of cored samples.

Table 5-10. Summary of measurement at cored locations

Core	C1	C2	C3A	C3B	C4	C7A	C7B	C8A	C8B
CRCP (in)	10.25	8.75	13.00	13.25	13.00	11.50	11.25	11.25	11.25
HMA (in)	5	6.25	2.25	2	*N/A	-	-	-	-
Void (in)	1	-	-	-	-	4	4	1.5	1.5
HDPF (in)	1	1.5	-	-	-	-	-	-	-

* Note: Not able to core through base in C4 due to operation challenges.

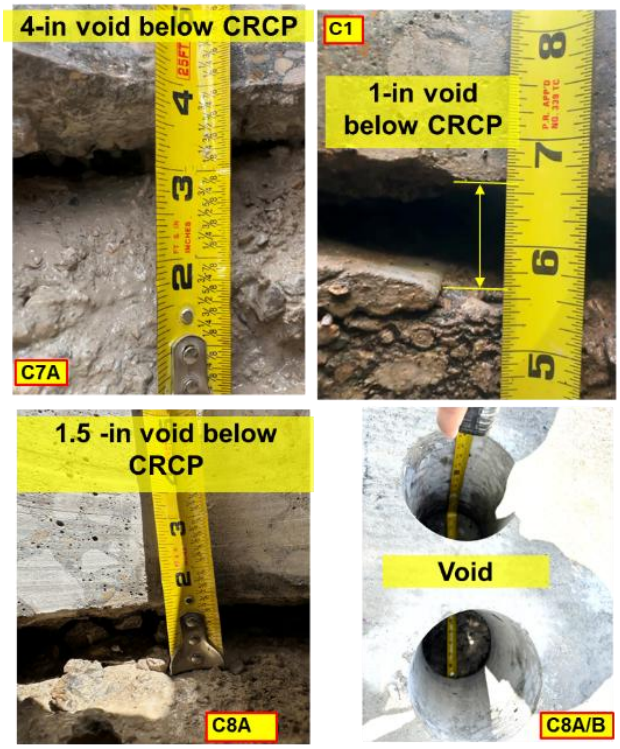


Figure 5-63. Void thickness measured at cored location.

5.5.5 Dynamic Cone Penetration (DCP) tests and CPT Tests

DCP tests were conducted at 8 locations either in cored holes or drilled holes to estimate fill/subgrade conditions of the embankment in the test section. The DCP test locations are presented in **Figure 5-64**. To have direct access to the subgrade material, a further drilling beneath the bottom of the cored hole was performed for some cored holes. The cumulative DCP blow counts vs. depth curves and the estimated M_r from all 8 DCP tests are presented in **Figure 5-65**.



Figure 5-64. Detail DCP locations

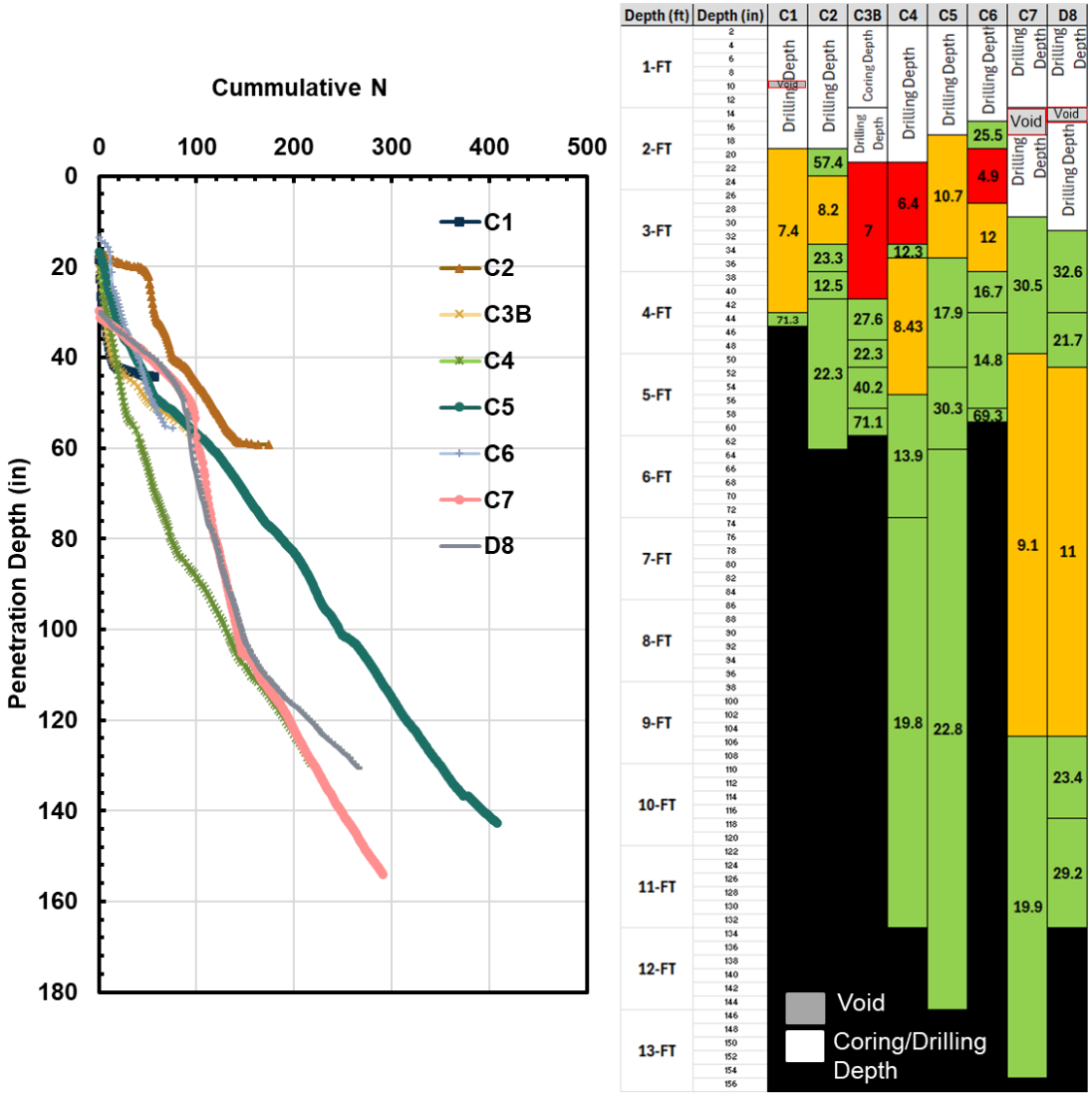


Figure 5-65. Cumulative blow counts vs. penetration depth below the pavement surface and the resilient modulus determined from DCP tests (Note: the color scheme for M_r value is for illustrative purposes only.)

The DCP tests indicate presence of weaker soil layer at shallow depths, with minimum resilient modulus (M_r) values often below 10 ksi. At location C4, where the maximum settlement between the railing and pavement was observed, the overall shallow subgrade condition is notably poor, with the largest cumulative thickness of weak soil, with M_r values 6.4 ksi and 8.4 ksi at depths of 2 to 5 ft. In the BAS area, the DCP locations C7 and D8 both show voids at the pavement bottom and indicate underlying weak material with M_r of 9.1 ksi and 11 ksi respectively, at a depth of 5 ft to 9 ft.

To characterize soil conditions for the entire embankment height, five CPT tests were conducted at cored locations C1, C2, C3A, C7A and C8 (C1, C2 and C3A were refusal) of the corresponding DCP tests, typically within 1 ft of each other as shown in **Figure 5-66**. The maximum CPT investigation depth was 32.7 ft below the pavement surface at C8A location. **Figure 5-67** presents

cone tip resistance at different depths for C7A and C8A. The cone tip resistance value drops around 20 ft at location C8A and stays low, primarily below 12 tsf, suggesting presence of weaker foundation soil. This weaker foundation soil layer could have partially contributed to the long-term settlement.

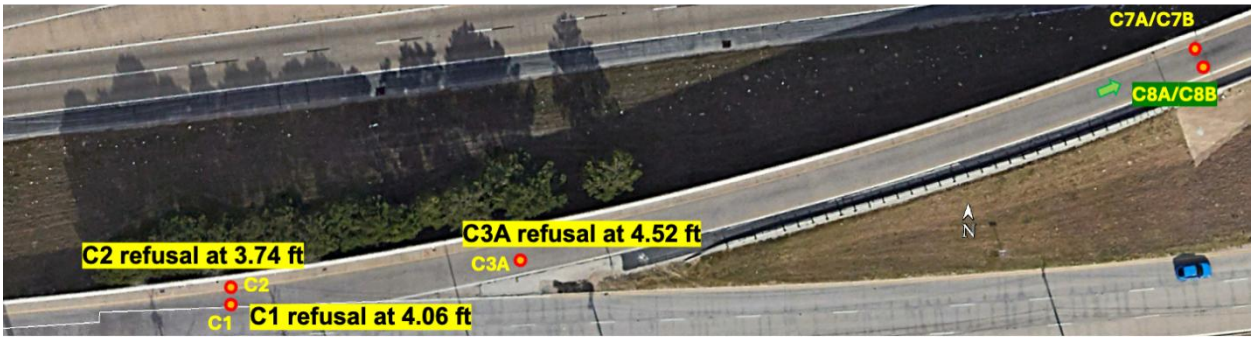


Figure 5-66. Locations of CPTs

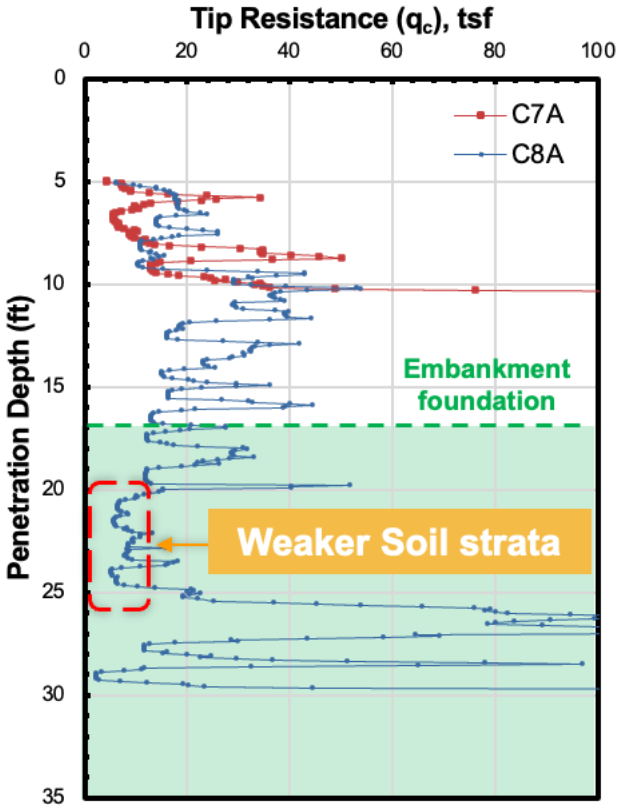


Figure 5-67. CPT cone tip resistance vs. penetration depth below the pavement surface.

5.5.6 Soil sampling

Soil samples were collected from the embankment fills using grab samples at the location C1, C7B and C8A, and using Shelby tube at location C8B. A series of laboratory tests were conducted on these samples to characterize their properties.

Table 5-11 summarizes the results of the laboratory tests conducted on the soil samples.

Table 5-11. Summary of lab test results.

Sampling Location	Sampling Type	Classification (USCS/ AASHTO[GI])	Sampling Depth (ft)	Moisture Content (%)	Retained on #4 (%)	Passing #200 (%)	PI (%)	LL (%)
C1	Grab	CL/A-6[9]	2 - 3	19.7	11	54	20	33
C7B	Grab	CL/A-6[8]	2.5 – 3.5	21.6	16	58	19	32
C8A	Grab	CL/A-6[12]	0 - 4	20.8	9	63	23	38
	Grab	-	4 - 5	20.6	-	-	-	-
C8B	Grab	-	5 - 7	16.7	-	-	-	-
	Shelby	CL/A-6[12]	7 - 8	18.6	9	64	17	29
	Shelby	CL/A-6[12]	8 - 9	21.6	13	70	22	38
	Shelby	-	9 - 10	19.5	-	-	-	-
	Shelby	GC	10 - 11	13.3	35	38	-	-
	Shelby	GC/A-6[4]	11 - 13	15.6	34	45	17	32
	Shelby	CL/A-6[11]	13 - 15	19.4	5	76	15	37

Particle size distribution curves obtained from C7A, C8A and C8B samples at various depths are presented in **Figure 5-68**. The embankment fill material is predominantly classified as CL/A-6 with high fines content and PI values from 15% to 23%. The natural moisture contents for these cohesive soils range between approximately 18.6% and 21.6%. A layer of course-grained material classified as GC (Clayey gravel) was encountered at the depth interval 10-13 ft at C8B. This layer showed a higher percentage of retained gravel on the #4 sieve (34% and 35%) and lower fines content (35% to 45%), compared to soil samples at other depths, potentially suggesting wash out of fines.

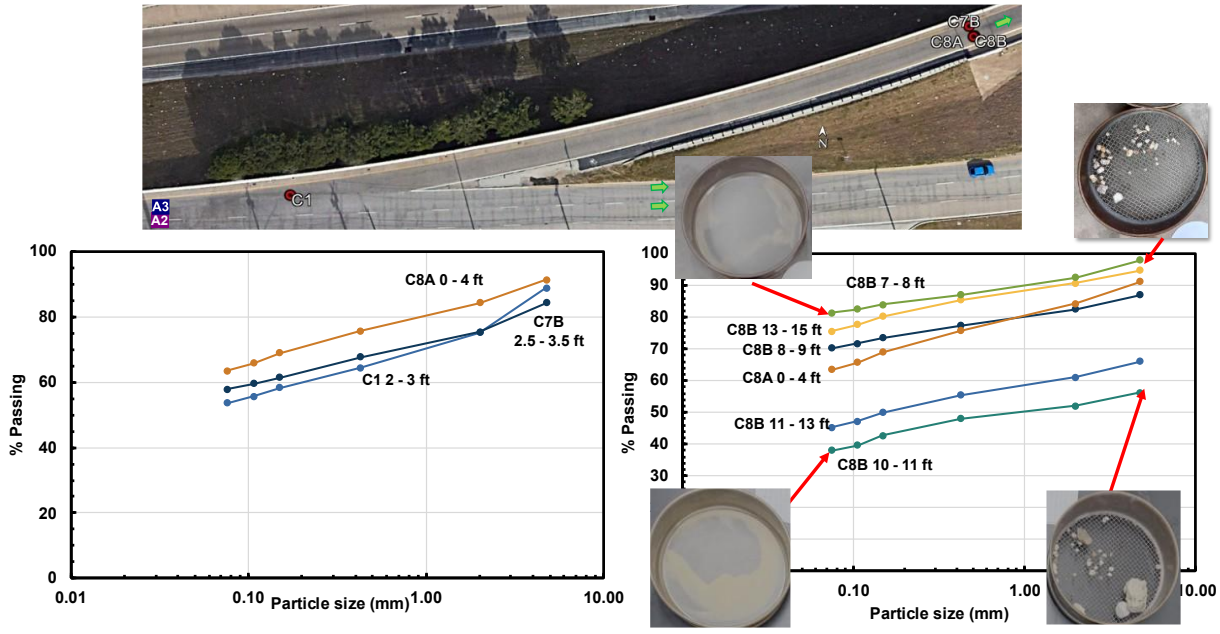


Figure 5-68. Soil sampling location and results from particle size distribution analysis.

5.5.7 Potential Distress Mechanism

The major distress observed was settlement of pavement as manifested by the visible gap between the base of railing and the pavement surface. In addition, voids underneath the BAS and halfmoon shaped crack on the pavement were observed. The observed distress can be attributed to the combined effect of compression of embankment fills and natural soil, water infiltration, and the mechanical response of the continuous pavement structure.

The CPT and DCP tests indicated that the embankment fills and foundation soils were relatively weak. The embankment likely settled over time due to the presence of the weak materials, causing the entire pavement section to sink relative to the traffic railing that is supported by the retaining wall and, thus, creating the persistent vertical gap observed between the railing and the pavement edge along the ramp. The visual representation of this process is presented in **Figure 5-69.**

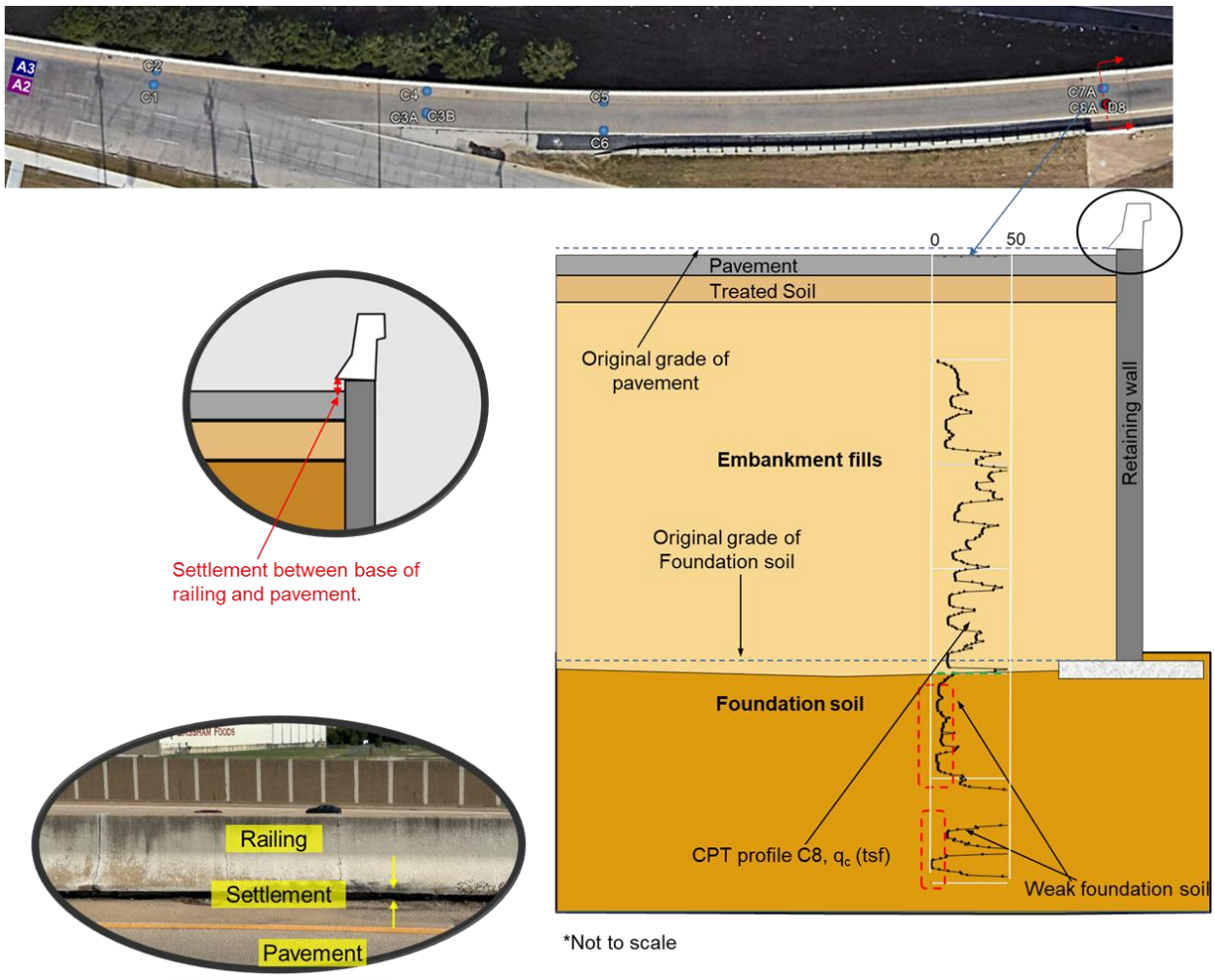


Figure 5-69. Illustration showing formation of gap between base of railing and the pavement due to settlement of embankment soil and foundation soil.

The observed voids beneath the BAS are attributed to the compression of embankment fills and founding soils as well as material washout. While the edge of the bridge approach slab resting on sleeper slab settled along with the fill material, the edge resting on the abutment did not settle as much, as illustrated in **Figure 5-70**. As the settlement increased, the joint between the CRCP and BAS was widened, allowing more water to ingress. The infiltrated water washed the fill materials out through the weep holes which were observed in the field (see **Figure 5-70**). This washout could have led to the development of significant differential void thicknesses along the transverse direction of the approach slab. Field documentation confirmed that the void was more pronounced near the wall, measuring 4 inches in thickness, compared to approximately 2 inches away from the wall.

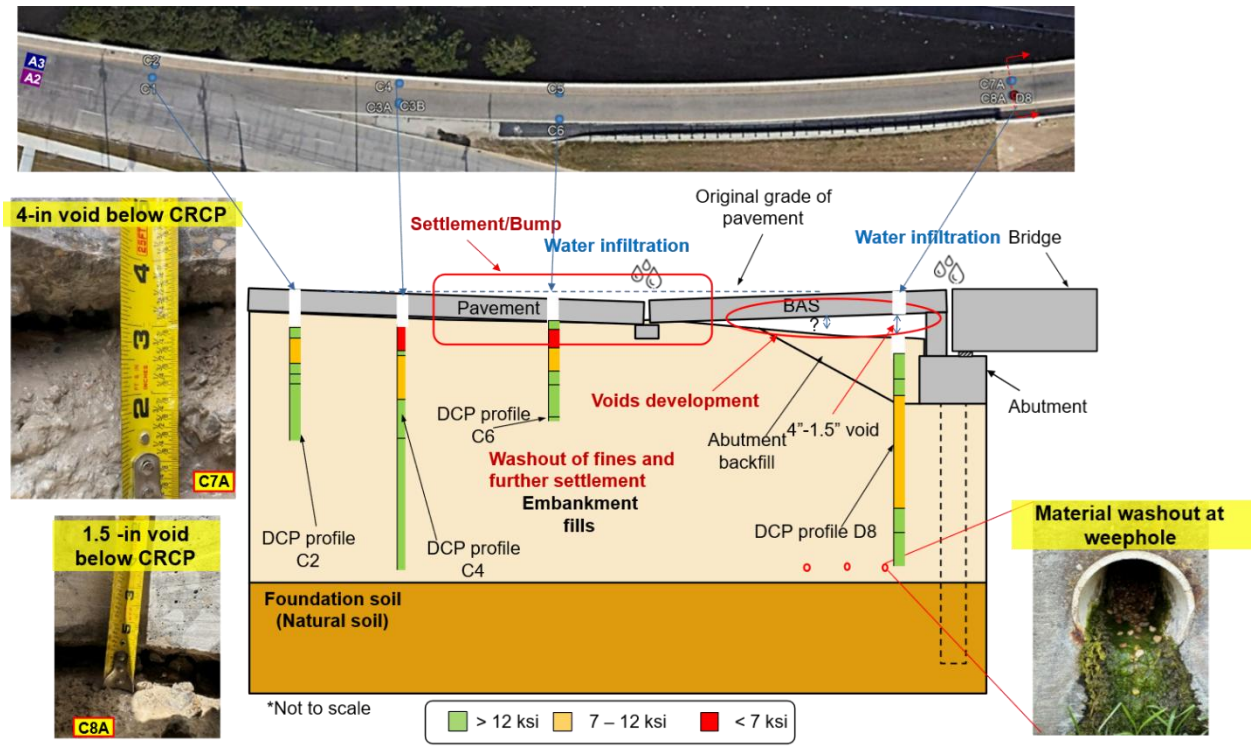


Figure 5-70. Illustration showing Void development under BAS due to the settlement of embankment soil and foundation soil and water infiltration (Note: the color scheme for M_r value is for illustrative purposes only.)

On the other hand, the voids detected beneath the main CRCP section away from the bridge are likely to be resulted from a differential settlement. The outer end (near the wall) of the on-ramp pavement and the base material settled with the embankment. However, the inner end connected to the frontage road through the tie bars at regular spacing acted as a constraint, separating the base material from the pavement base causing void underneath the slab. This uneven settlement and slab rotation is likely to have caused a characteristic "half-moon" crack visible on the frontage road surface. This is shown in **Figure 5-71.**

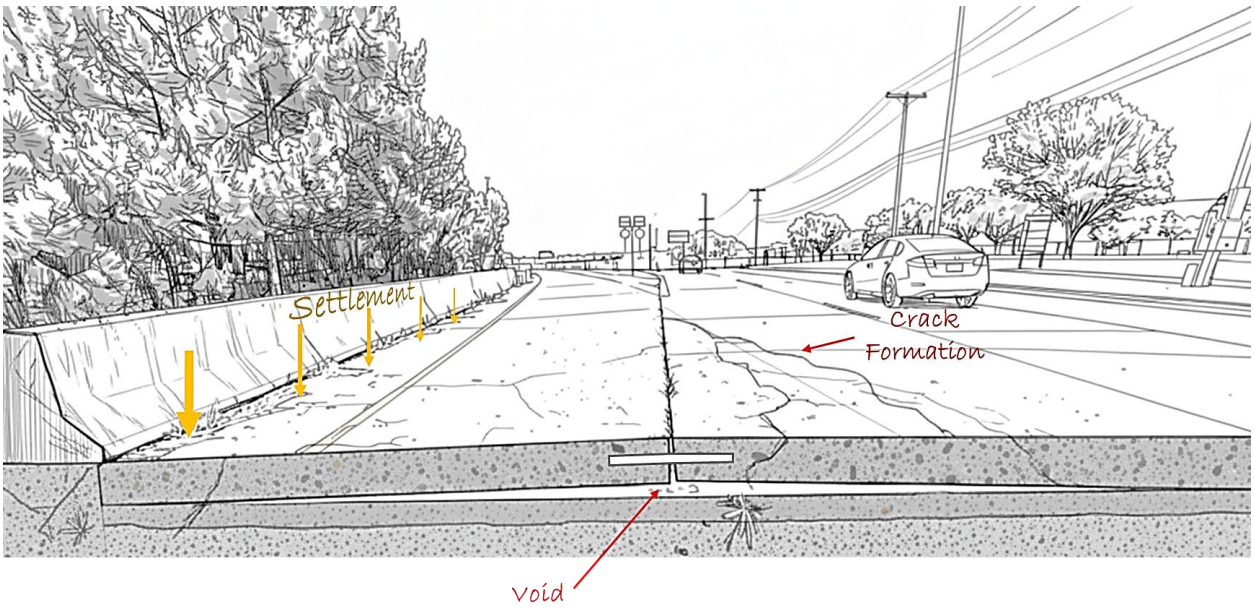


Figure 5-71. Illustration showing void development under CRCP.

5.5.8 Repair Recommendation

The primary distress is driven by weak embankment and foundation soil compression, causing the pavement to settle, while the wall-supported railing remained relatively stationary, and water infiltration and material washout through weep holes. Additionally, settlement at the wall edge while the slab was tied to the frontage road caused rotation and structural "half-moon" cracking in the frontage road.

For the short-term repair, soil densification using High-Density Polyurethane Foam (HDPF) is recommended in accordance with TxDOT Special Specification 3086, as detailed in **Figure 5-72**. This process involves injecting the foam into the embankment fill to a target depth of 4 feet and undersealing BAS. The primary objectives are to fill the existing voids created by washout and to stabilize the loose upper soil layers, thereby minimizing further settlement. Also, all the joints and openings from where water can infiltrate must be repaired and sealed to prevent water from infiltrating.



Figure 5-72. Short term repair recommendation for IH 20, Fort Worth using HDPF.

For long-term permanent rehabilitation, the repair is divided into two distinct zones. In the area highlighted by green in **Figure 5-73**, HDPF injection (SS 3086) should be utilized to a 4-foot depth to densify the soil. Once the underlying soil has been stabilized, the area highlighted in blue in **Figure 5-73** is recommended for a Full-Depth Repair (FDR), TxDOT item 361. This is because the characteristic "half-moon" cracks represent loss of slab support and loss of load transfer, injection alone is considered insufficient for this area. The fractured CRCP must be removed and replaced with new reinforced sections only after the subgrade has been fully densified to provide a stable, non-yielding foundation for the new slabs.



Figure 5-73. Long term repair recommendation for IH 20, Fort Worth Section

5.6 P-A-4: IH 820 on-ramp in Fort Worth

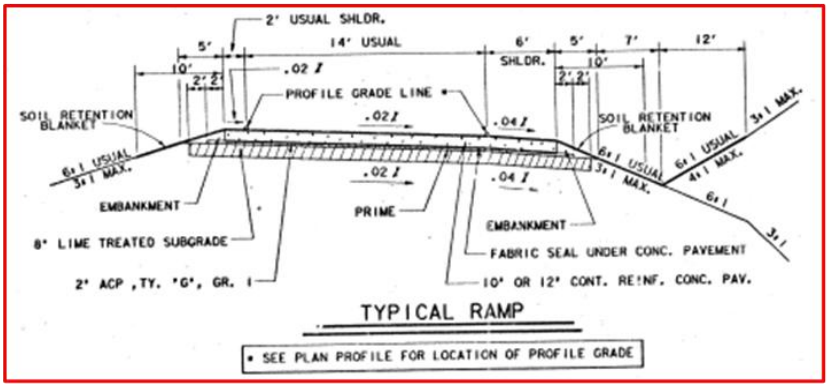
5.6.1 Overview

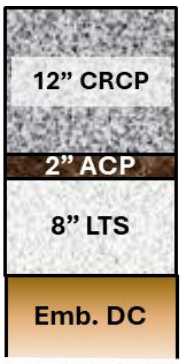
Section P-A-4 encompasses the BAS and adjacent pavement structure on the IH 820 Ramp (Connector A) in Fort Worth, Tarrant County, Texas. This ramp connects IH 820 to IH 30 East and IH 30 West (32°45'13.4"N 97°13'00.4"W). **Figure 5-74** shows the detailed location of P-A-4 investigated on 07/23/25 - 07/24/25 by the Research Team. The roadway rests upon an embankment, approximately 19-feet in height at the BAS and supported by a retaining wall on the east side. According to the plan sets, the project (CSJ 0008-13-107) was constructed between March 1, 1989, and Feb 22, 1991.



Figure 5-74. Location of Section P-A-4 of IH820 On-ramp in Fort Worth, Texas

The pavement system consists of 12-in-thick CRCP with a 2" ACP base and 8" of Lime Treated Subgrade (LTS). The BAS has a thickness of 10.5". Typical section view and pavement structure are shown in **Figure 5-75**, and details of the test section are summarized in **Table 5-12**.





(Pavement structure of Ramp, CSJ 0008-13-107)

Figure 5-75. Typical section view and pavement structure of IH820 Ramp.

Table 5-12. Detailed descriptions of Section P-A-4 IH 820, Fort Worth, Texas.

Attribute	Information	Notes
District & Highway	Fort Worth & Grade Separated Connector 585R (IH820 to IH30WB)	
CSJ	0008-13-107	
County	Tarrant County	
Station	PT 5+60 (Connector A)	
Project Limits	At Interchange with IH 30 (East Bound to North, South Bound to East & West & Final Increment)	
GPS Coordinates	32°45'13.4"N 97°13'00.4"W	
Date Work Begin	1/3/1989	
Date Completed	2/22/1991	
Pavement Type	CRCP 12"	
BAS Thickness	10.5"	
Shoulder Type	CRCP 12"	
Base Type	2" ACP TY. G, GR. 1	
Subgrade Type	8" Lime Treated Subgrade	
Drainage Type	Grating Inlets	
Embankment Height	~19'	@ BAS
Distress Observed (Severity)	Approach Pavement Settlement (Severe); Stripping of Asphalt overlay at joints; Longitudinal crack	

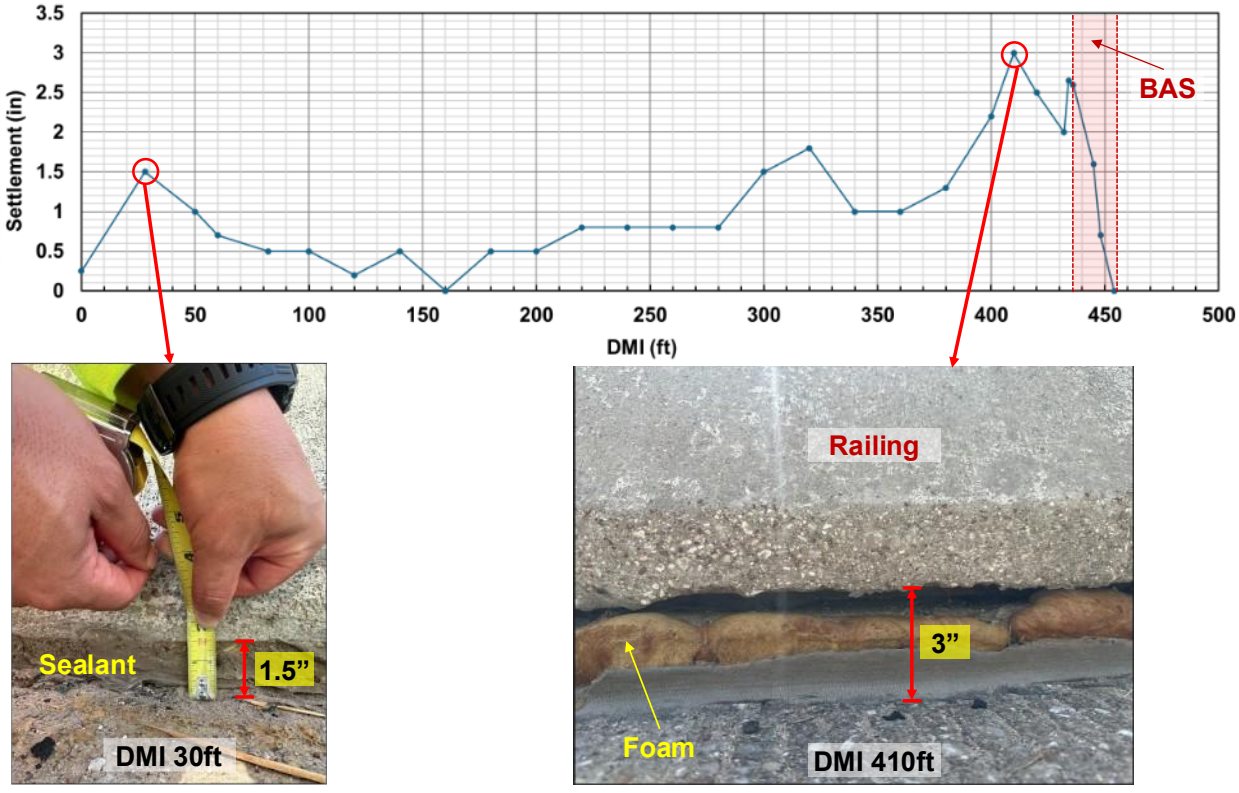
A field investigation indicated the presence of severe pavement settlement and BAS settlement over the structure's service life. Repair attempts were also made in the past to address the settlement between the pavement and the railing, evident from the HMA overlay/level-up in the

BAS and nearby pavement and HDPF found underneath the BAS identified during coring. About 1.75” of lateral movement of BAS railing was also observed (see **Figure 5-76**). Settlement between the base of railing and the pavement/BAS was also recorded every 10 ft and is shown in **Figure 5-77**.

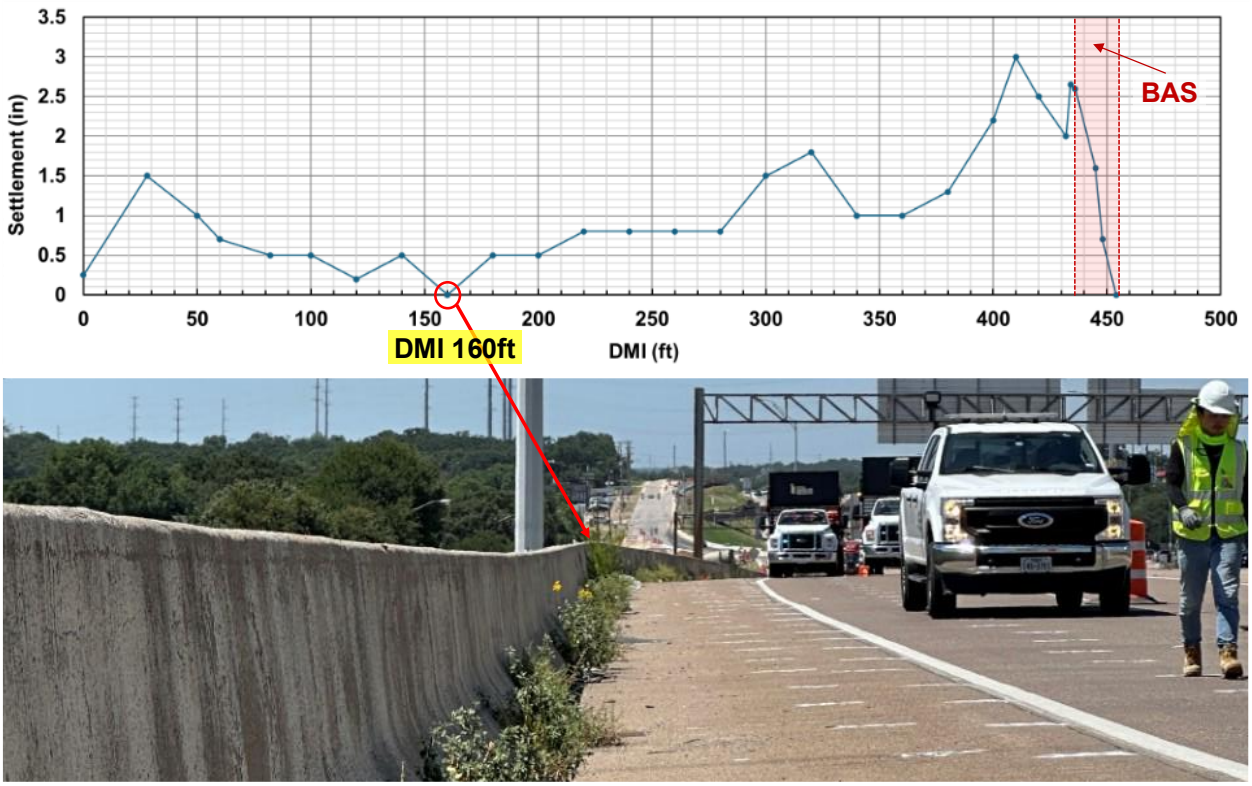


(a) (b)

Figure 5-76. (a) HMA overlay and (b) lateral movement of BAS railing.



(a)



(b)

Figure 5-77. Settlement between base of railing and the pavement with photos taken (a) at DMI 30 and 410 ft and (b) at DMI 160 ft

5.6.2 Falling Weight Deflectometer Test

Falling Weight Deflectometer (FWD) tests were conducted along the outside shoulder (Ramp Shoulder) and middle of lane (Ramp) on IH820 ramp. FWD deflections were normalized to a target load of 9,000-lb. Spacing between FWD drop locations was approximately 10 ft on the pavement sections and 2 ft on the BAS and before and after joints. **Figure 5-78** presents the FWD drop locations and the normalized deflection data along the FWD path.

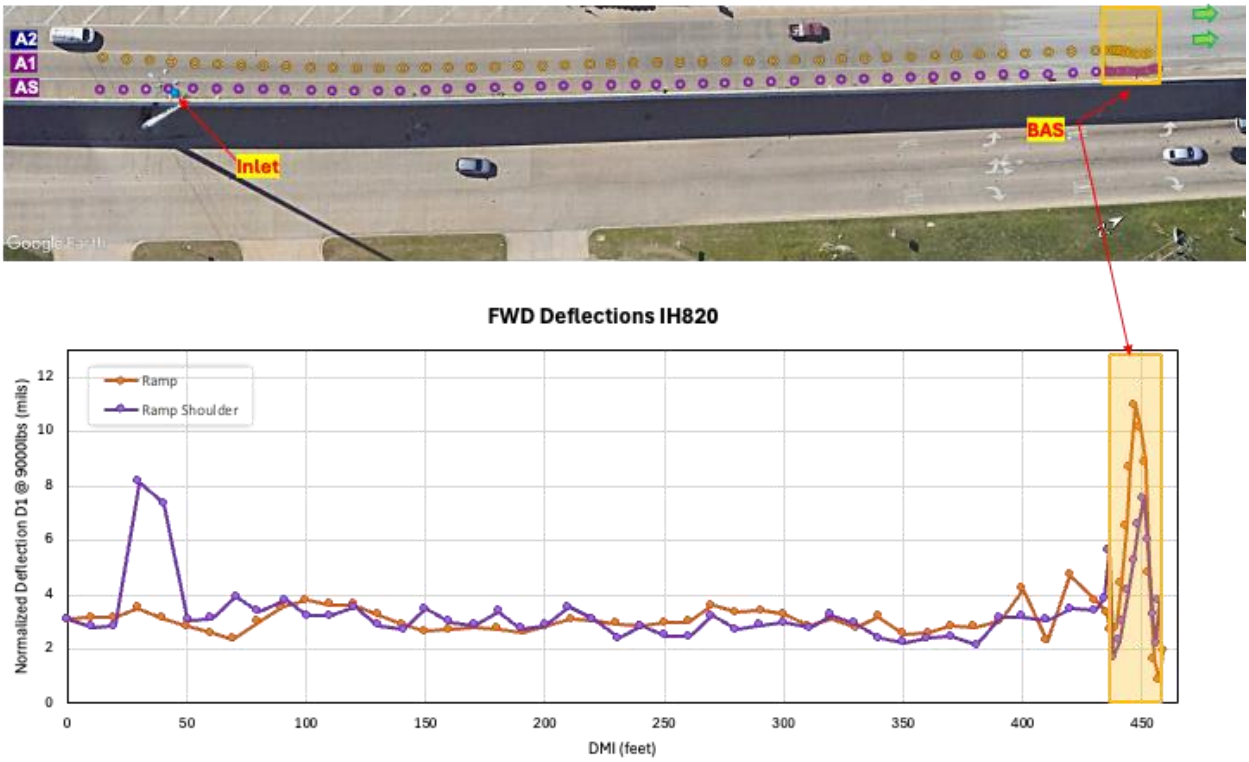


Figure 5-78. FWD testing locations and deflections measured at the outside shoulder (Ramp Shoulder) and middle of the lane (Ramp).

The deflections on the outside shoulder were between 2 mils to 4 mils for the pavement section with a highest value of 7.5 mils in the BAS area. The high deflection in the BAS area is associated with the void and HDPF present below the BAS which was confirmed during coring. The detailed coring information is presented in the subsequent sections. The spike in FWD deflections at around DMI 20 to 50 ft (as high as about 8 mils) correlates with the presence of the nearby drainage inlet.

The ramp showed a similar pattern of low deflections across the CRCP section, between 2 to 4 mils. The FWD deflections increased for the overlayed section and BAS after DMI 400 ft.

5.6.3 Ground Penetrating Radar (GPR) Utility Scan

A total of 8 passes were made at 2 ft intervals and calibrated for depth with physical core samples (more details on coring data are presented in the subsequent sections). The GPR scan taken from 2 ft to 10 ft from the railing detected strong negative reflections from DMI 250 to 400 ft, which were interpreted as the presence of low-density material (supported by coring results as HDPF below the pavement structure). Other scans, at 16 ft from the railing, similarly indicated thicker asphalt overlay and the settlement of subgrade material below the asphalt overlaid section at around DMI 400 ft. **Figure 5-79(a)** and **Figure 5-79(b)** show the GPR pass location and GPR scan results at 2 ft, 10 ft and 16 ft from the railing, respectively.

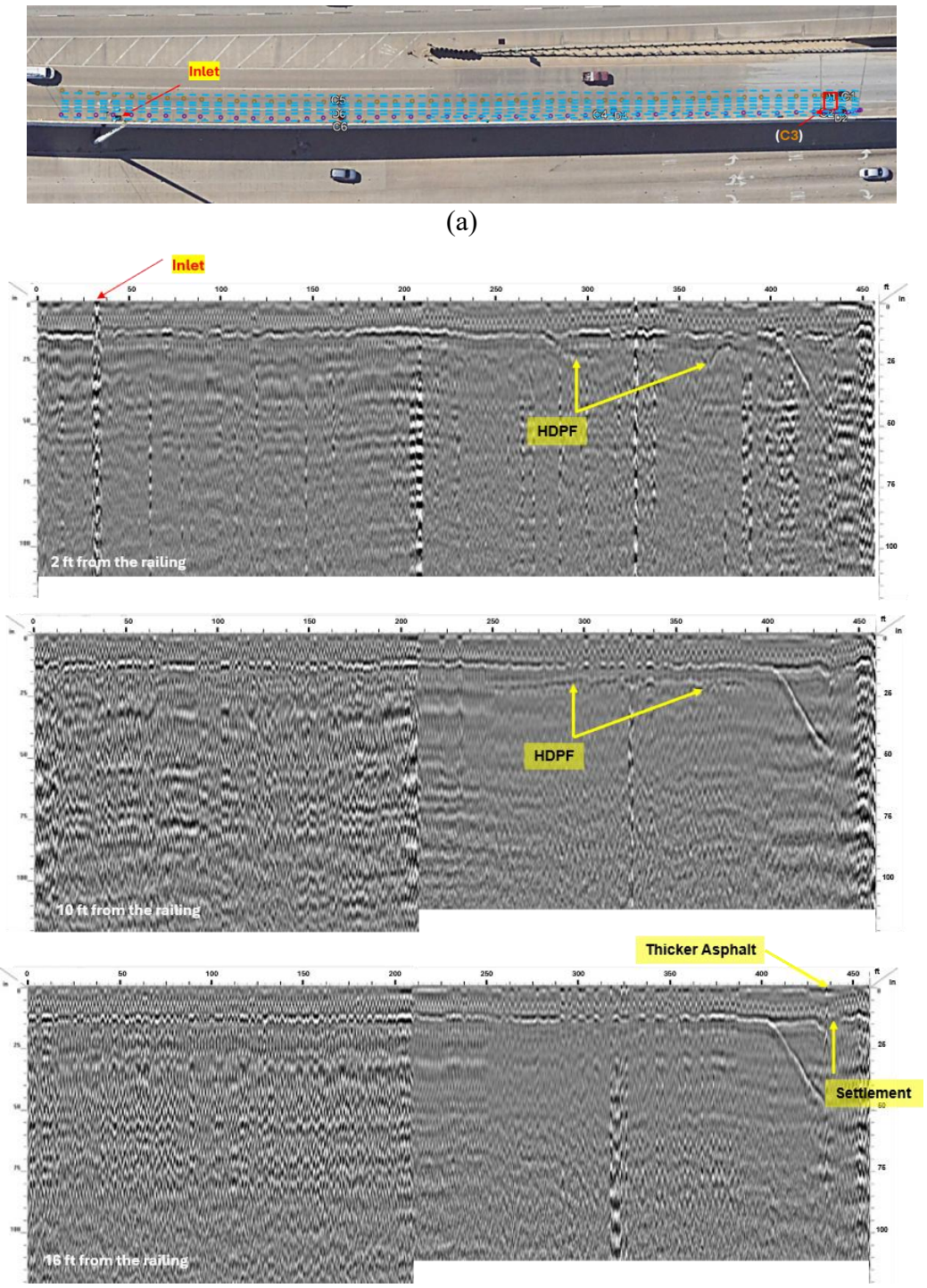


Figure 5-79. (a) GPR paths and (b) GPR results at 2ft, 10ft and 16ft from the railing

5.6.4 Coring

Six cores (C1 through C6) were taken to inspect the pavement structure and confirm subsurface anomalies. Coring locations were based on the observed distress, especially pavement and railing settlement, as well as the FWD deflection. Coring confirmed a variability in the CRCP thickness ranging from 8.75 inches to 13.25 inches for the pavement section and 11.5 inches to 12 inches for BAS.

Figure 5-80 shows the photos of the coring location, individual cores, and the void beneath the CRCP. The coring locations in the BAS area (C1, C2, C3) revealed the presence of 2-inch void from all three locations and HDPF with thickness ranging from 1.25 to 1.75 inches, confirming a loss of support and prior repair efforts. **Table 5-13** summarizes the thickness of CRCP, HMA, HDPF, and void measured at all cored locations.

Table 5-13. Summary of measurement at cored locations.

Core	C1	C2	C3	C4	C5	C6
HMA overlay (in)	2.375	2.75	2.625	-	-	-
CRCP (in)	11.5	11.875	12	12.5	11.5	11.75
HMA (in)	-	-	-	1.25	1.875	2
Void (in)	2	2	2	-	-	-
HDPF (in)	1.75	1.75	1.25	-	-	-

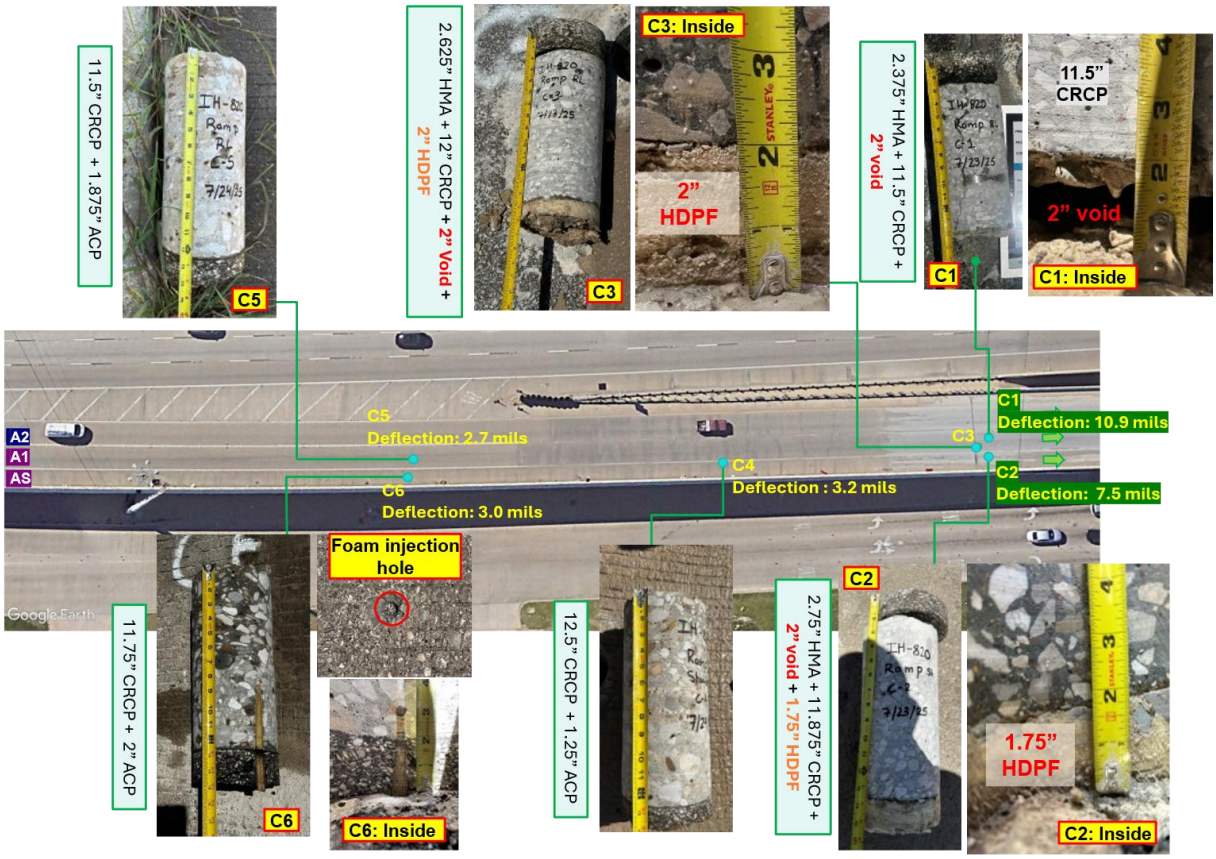


Figure 5-80. Coring location and images of cored samples.

5.6.5 Dynamic Cone Penetration (DCP) tests and CPT Tests

DCP tests were conducted at 6 locations either in cored holes or drilled holes to estimate backfill/subgrade conditions of the embankment in the test section. The layout for location of DCP tests is shown in **Figure 5-81**.

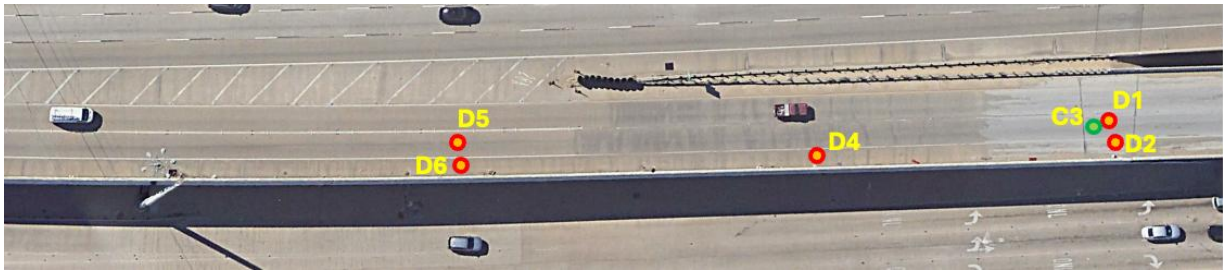


Figure 5-81. Locations of DCP tests.

The cumulative DCP blow counts vs. depth curves from all 6 DCP are presented in **Figure 5-82**, along with the resilient moduli (M_r) of embankment fills at each DCP test location determined

from the DCP tests. D1, D2, C3 were on the BAS and D4, D5 and D6 were on the pavement. All three locations in the BAS area demonstrated a void immediately beneath the pavement structure. The DCP tests D1 and D2 indicate good subgrade material to a depth of 4 ft, and there was a weak soil layer from about 4 to 6 ft. DCP test at location D2 had soil layer with moderate stiffness with M_r of 11.6 ksi from about 7.5 ft to 11 ft. DCP tests at CRCP pavement (D4, D5, and D6) showed weaker soil profile at shallow depth of about 2 ft to 3.5 ft with relatively stiffer soil beneath that. Particularly, D5 showed very weak soil layer from about 2 ft to 5.5 ft with M_r 5.7 ksi.

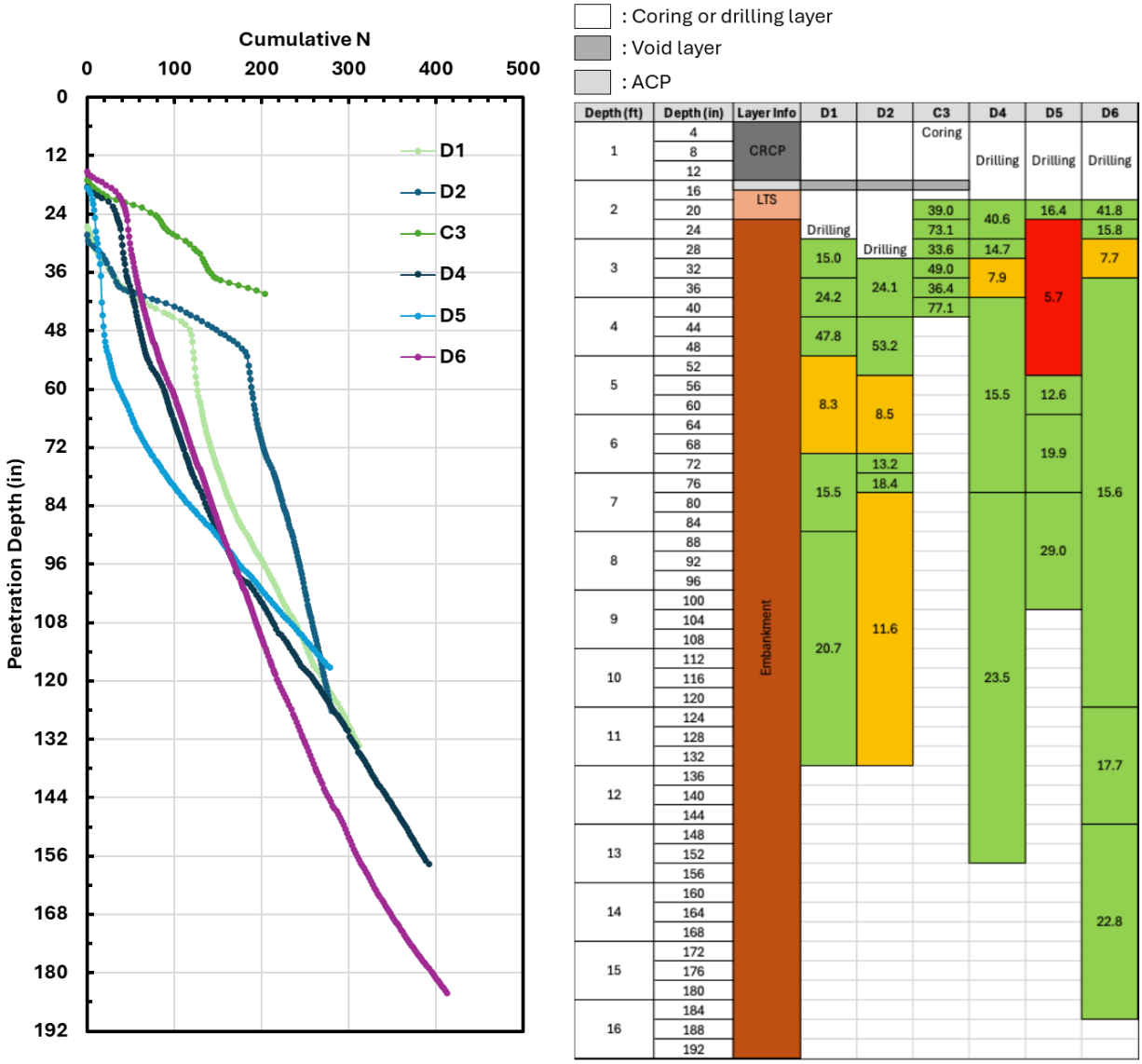


Figure 5-82. DCP Cumulative blow counts vs. penetration depth below the pavement surface and resilient modulus determined from DCP tests

Three CPTs were conducted at cored locations C1, C4 and C5 typically within 1 ft of DCP locations to characterize soil conditions for the entire embankment height. The CPT C1 was located on the BAS, C4 on the shoulder, and C5 on the pavement. The maximum CPT investigation

depth was about 29 ft below the pavement surface at C5 location. **Figure 5-83** presents detailed location of CPT tests.

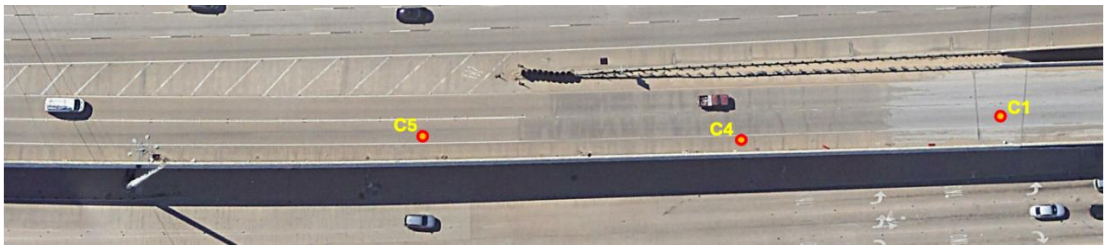
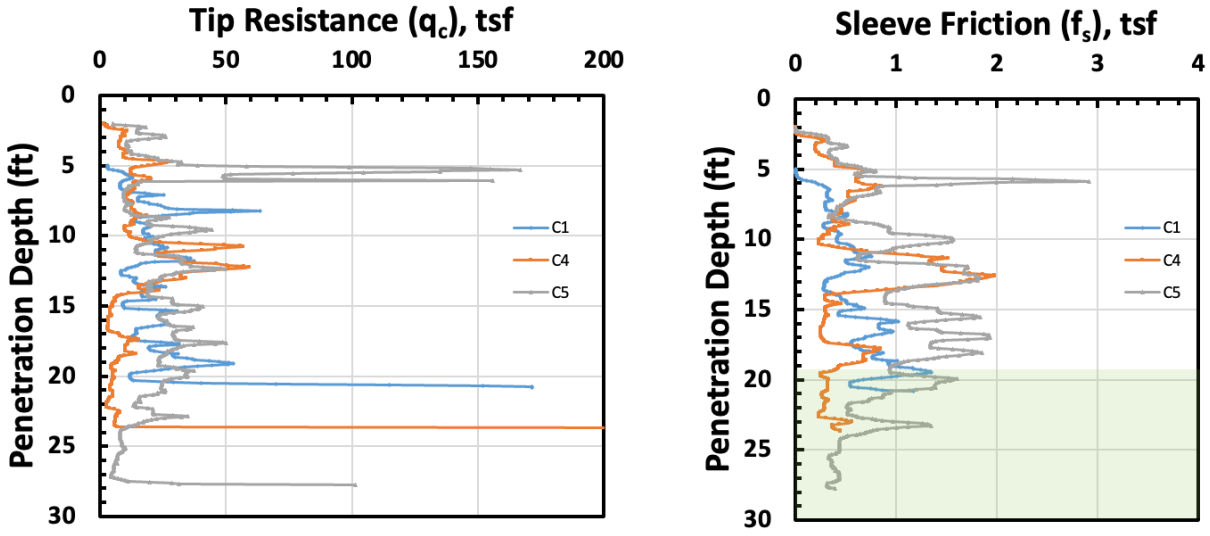


Figure 5-83. Locations of CPTs

Figure 5-84 shows the cone tip resistance (q_c) and sleeve friction (f_s) from C1, C4 and C5. The cone tip resistance value from C4 dropped below 10 tsf at a depth of 19 ft (where the founding soil is located) as well as between 14 to 17 ft. Similarly, q_c from C5 was below 10 tsf after 23 ft. These low q_c values from C4 and C5 suggest the presence of weaker foundation soil which might have partially contributed to the long-term settlement.



(a) (b)

Figure 5-84. Results from CPT: (a) cone tip resistance and (b) sleeve friction vs. penetration depth below the pavement surface.

5.6.6 Soil sampling

Soil samples were collected from the embankment fills using grab samples and Shelby tube at the locations C1, C2, C4 and C5. **Table 5-14** summarizes the results of the laboratory tests conducted on the soil samples.

Table 5-14. Summary of lab test results.

Sampling Location	Sampling Type	Classification (USCS/ AASHTO[GI])	Sampling Depth (ft)	Moisture Content (%)	Retained on #4 (%)	Passing #200 (%)	PI	LL
C1	Grab	CL/A-6[6]	0 - 5	16.8	17	57	17	29
C2	Grab	-	0 - 5	17.0	-	-	18	30
	Shelby	CL/A-6[4]	6 - 8	18.3	9	53	14	25
	Shelby	CL/A-6[3]	8 - 10	17.1	2	50	13	25
	Shelby	CL/A-6[4]	10 - 12	19.4	2	51	15	26
	Shelby	-	12 - 13	18.4	-	-	-	-
	Shelby	CL/A-6[5]	13 - 14	18.0	2	51	17	28
	Shelby	SC/A-6[3]	14 - 15	20.0	16	41	19	29
	Shelby	-	15 - 16	19.7	7	55	-	-
C4	Grab	CL/A-6[5]	0 - 2.5	19.6	8	58	12	32
C5	Grab	-	0 - 2	16.5	-	-	13	31
	Shelby	CL/A-6[10]	2 - 4	16.9	3	71	18	31
	Shelby	CL/A-6[8]	4 - 6	18.9	3	69	16	29
	Shelby	CL/A-6[18]	6 - 8	23.9	6	69	29	43
	Shelby	-	8 - 10	18.5	-	-	-	-
	Shelby	CL/A-6[4]	10 - 12	15.8	2	51	15	25
	Shelby	-	12 - 14	16.6	-	-	-	-

The particle size distribution curves obtained from C1, C2, C4 and C5 samples at various depths are presented in **Figure 5-85(a)**. The embankment fill materials are classified as CL/A-6. These are low-plastic to medium-plastic clays, generally exhibiting LL values ranging from 25 to 43 and PI values ranging from 12 to 29. The natural moisture content ranged from 15.8% to 23.9%. The highest moisture content of 23.9% was observed at C5 (6 to 8 ft depth). The comparison of shallow samples shows that materials closest to the bridge (C1) are generally coarser than the embankment material away from the bridge (C4 and C5).

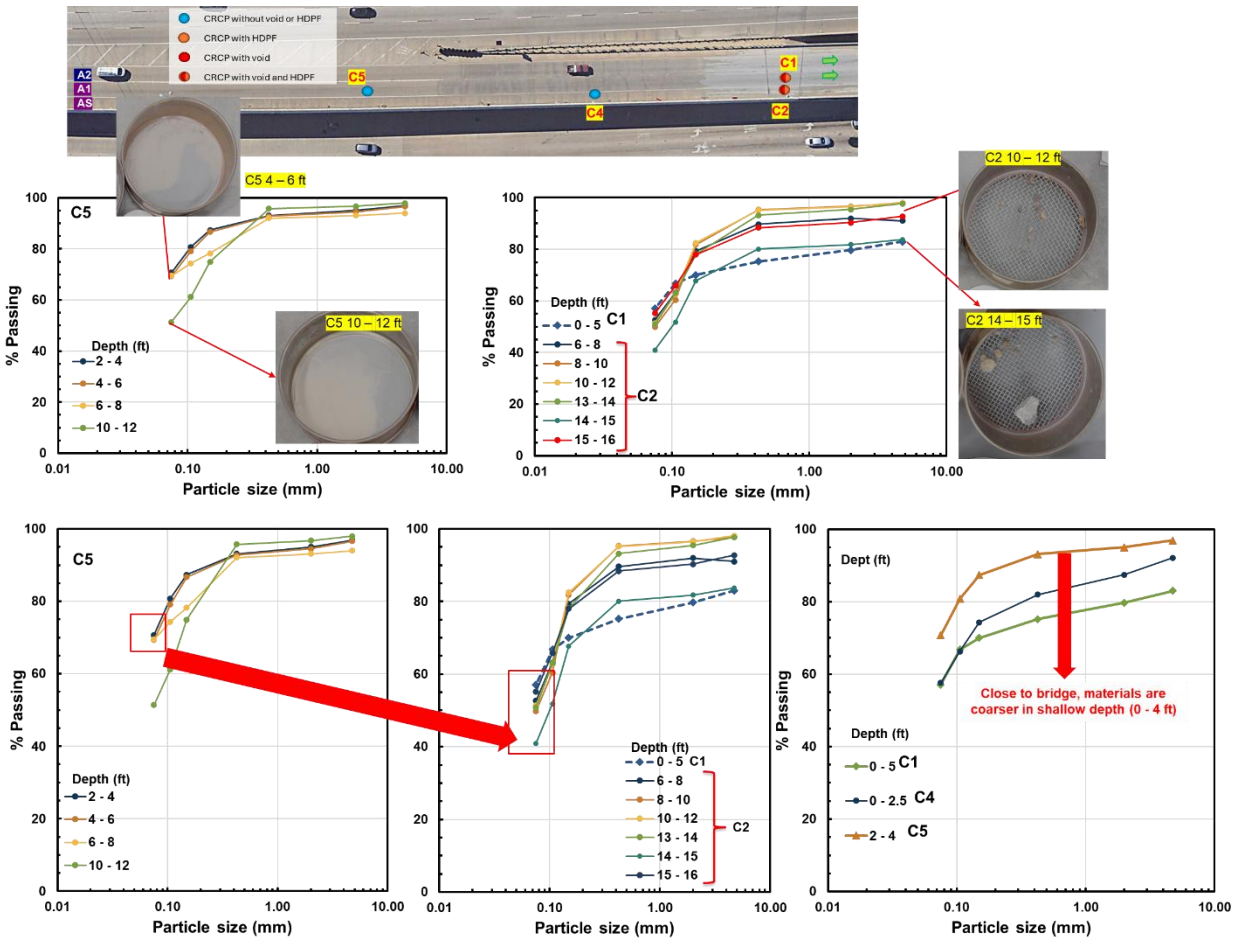


Figure 5-85. Soil sampling location and particle size distribution.

5.6.7 Potential Distress Mechanism

The major distresses observed include settlement of pavement causing a gap between base of railing and pavement, voids underneath BAS, bump/settlement at BAS and nearby pavement and settlement of riprap. These distresses are likely due to the compression of embankment fills and founding soils.

All DCP tests except for D3 indicated the presence of relatively weak layer in the embankment fill materials with M_r values less than 10 ksi. Furthermore, CPT C4 indicated the presence of weak soil layer in the founding soil. These observations suggested that these weak soils underwent settlement over time under traffic loads, and such settlement widened the joint between the CRCP and the BAS, permitting water infiltration. The infiltrated water further weakened the embankment fills and contributed to the settlement. This mechanism is illustrated in **Figure 5-86.**

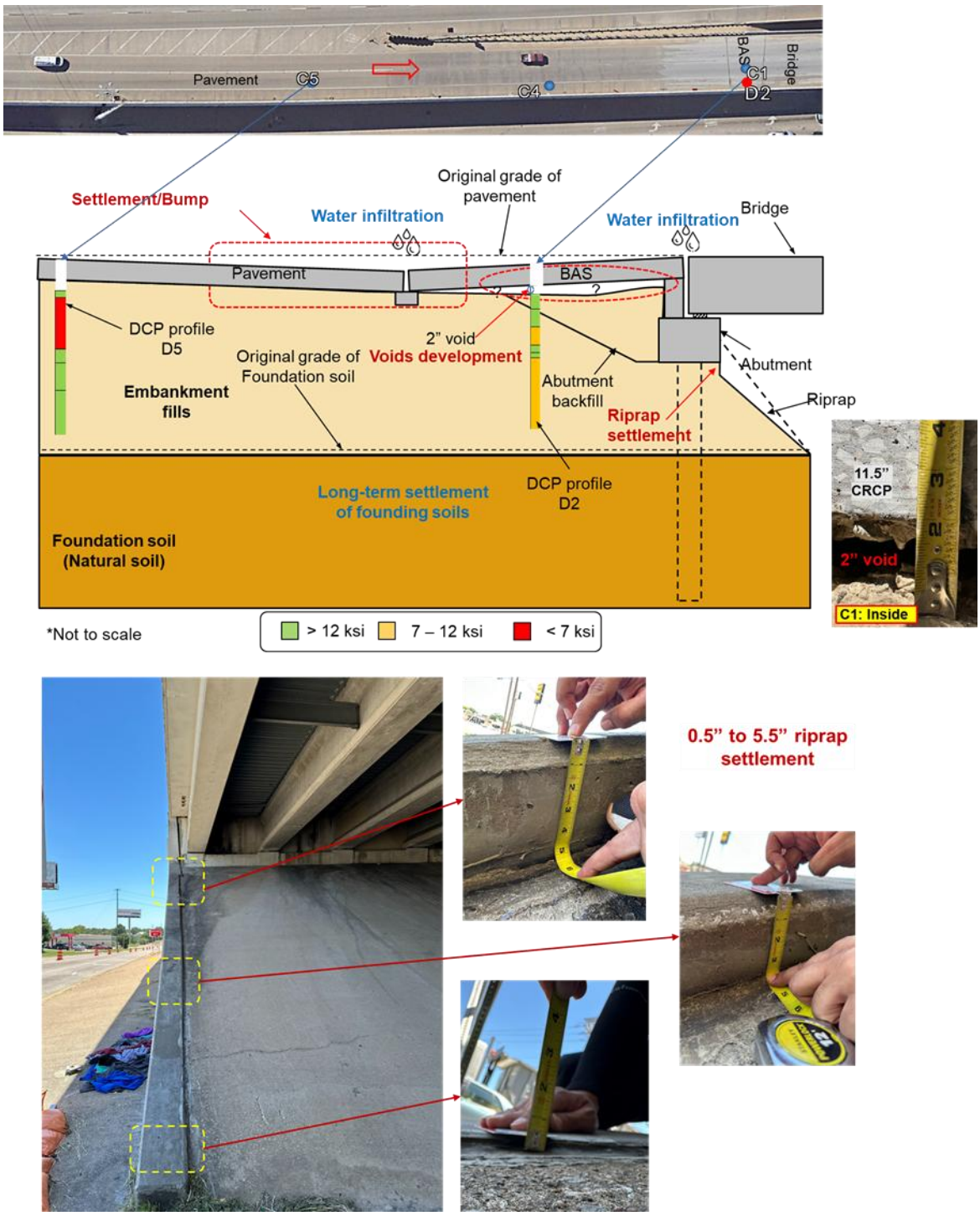
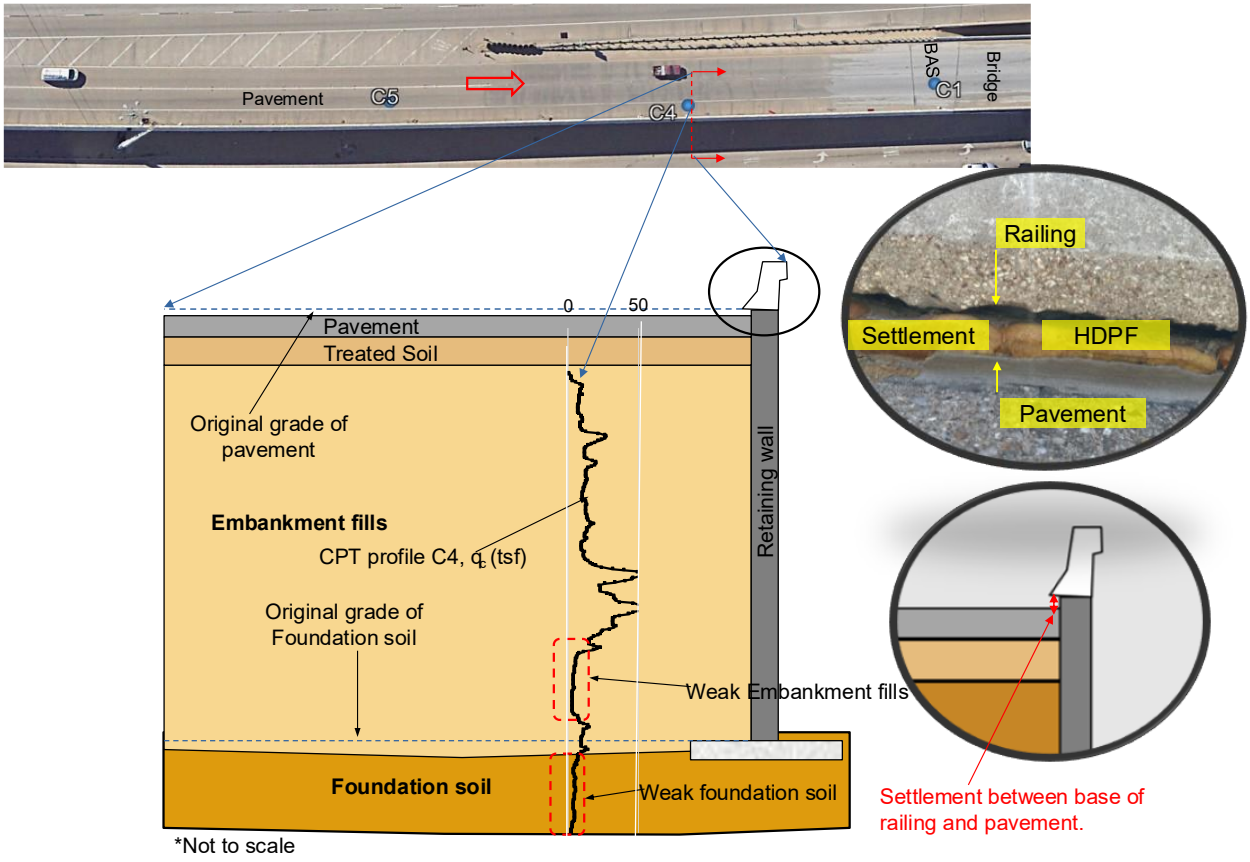
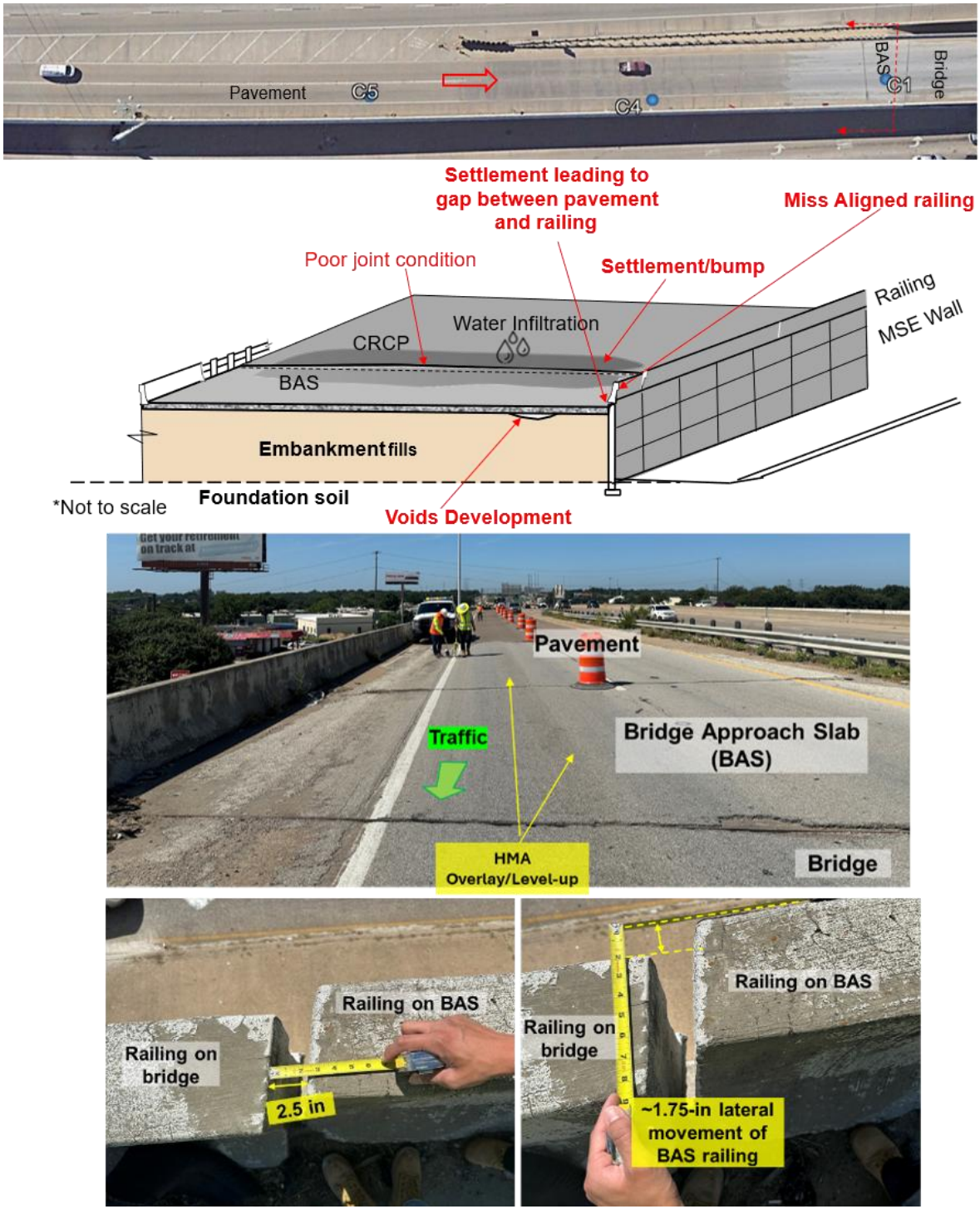


Figure 5-86. Illustration showing void development under BAS, settlement/bump on BAS and nearby pavement, and riprap settlement due to the settlement of embankment soil and water infiltration (Note: the color scheme for M_r value is for illustrative purposes only.)

While the entire pavement section settled along with the embankment, the railing (Rail type T501) supported by the retaining wall did not sink as much, creating the vertical gap observed between the railing and the pavement edge along the ramp, similar to what was observed in IH-20 ramp in Fort Worth (Section P-A-3). Also, the settlement of the embankment fill is rarely uniform, and the non-uniform settlement caused localized rotation and vertical displacement of the railing segment supported by the BAS. On the other hand, the railing segment attached to the bridge remains relatively stationary, leading to the observed misalignment and structural distress at the railing, illustrated in **Figure 5-87(a) and Figure 5-87(b).**



(a)



(b)

Figure 5-87. (a) Illustration showing formation of gap between base of railing and the pavement due to settlement of embankment soil and foundation soil and (b) birds-eye-view illustration of the distresses in the embankment in IH-820, Fort Worth.

5.6.8 Repair Recommendation

The primary distress is potentially driven by compression of weak embankment fills and foundation soils, causing the pavement to settle while the wall-supported railing remained relatively stable, and water infiltration through distressed joints further accelerated the process.

Soil densification is recommended in the shoulder and the BAS area using High-Density Polyurethane Foam (HDPF) in accordance with Special Specification 3086 as shown in **Figure 5-88**. This process involves injecting the foam into the embankment fills to a target depth of 3 feet to fill the existing voids created and to densify the weak upper soil layers, thereby minimizing any further settlement. Also, all the joints and openings from where water can infiltrate must be repaired and sealed to prevent water entry. Continued monitoring of the settlement between the base of railing and pavement, and at BAS-CRCP transition is recommended as well.



Figure 5-88. Repair recommendation for IH 820, Fort Worth, using HDPF and HMA overlay.

5.7 Section E-5: Beltway-8 at IH-45 in Houston, Houston

5.7.1 Overview

The test section is located on the westbound main lanes of Beltway-8 (Sam Houston Tollway) at the interchange with IH-45 South in Houston, Harris County, Texas as shown in **Figure 5-89**. The project limits for the investigation extend from approximately 1,010 feet South of IH 45 to 1,573 feet South of IH 45 (Reference Markers 758+0.288 to 758+0.395). Specific GPS coordinates for the site range from 29°36'17.55"N 95°12'28.41"W to 29°36'13.88"N 95°12'33.70"W.



Figure 5-89. Location of the Beltway-8 test section at IH-45 in Houston.

This field investigation was initiated in response to severe and rapidly progressing pavement distresses that posed immediate safety risks to the traffic. The westbound lanes, supported by an MSE wall, exhibited significant lane separation and faulting. The separation between the lanes created a hazardous gap capable of trapping motorcycle or small vehicle tires, while the vertical faulting presented a dangerous obstacle for lane changes at highway speeds. Additionally, the continued lateral movement of the MSE wall raised a concern about the global stability of the embankment itself.

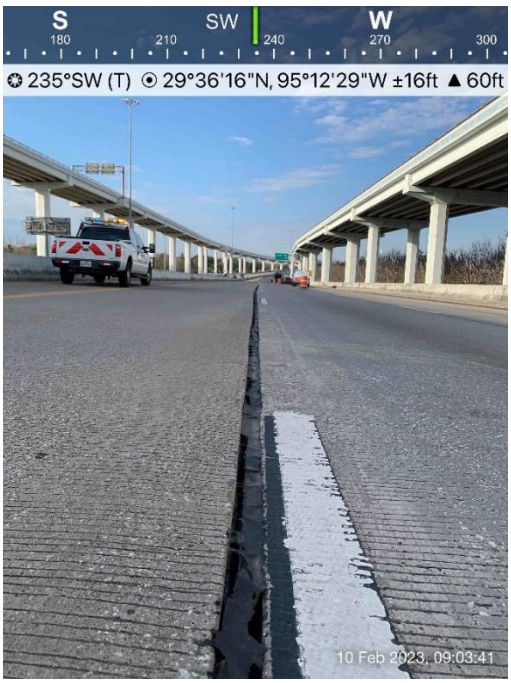
The roadway rests on an embankment that reaches a maximum height of approximately 25 feet near the bridge abutment. The distressed westbound section is retained by the MSE wall, while the eastbound lanes utilize a standard 4:1 sloped embankment. The pavement structure consists of a 12-inch Continuously Reinforced Concrete Pavement (CRCP) over a 1-inch Asphalt Stabilized Base (ASB), supported by a 6-inch Portland Cement Treated Base (PCTB) and a 6-inch Lime

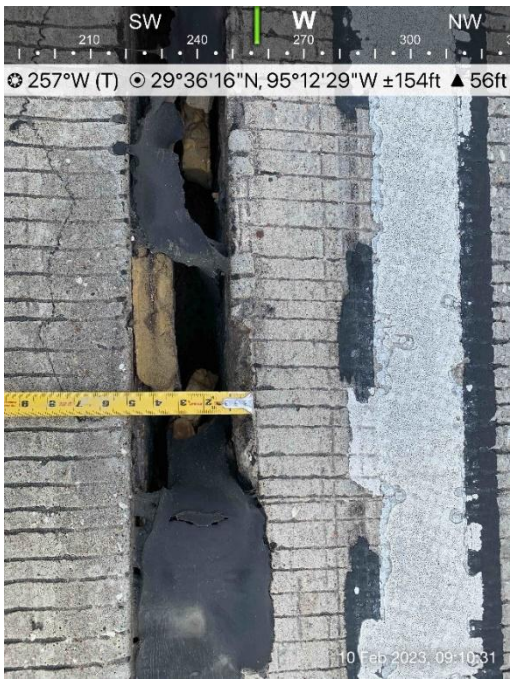
Treated Subgrade (LTS). The original construction occurred between June 1996 and November 1997. The detailed information on this site is presented in **Table 5-15**.

Table 5-15. Detailed descriptions of the Beltway 8 test section at IH 45 in Houston.

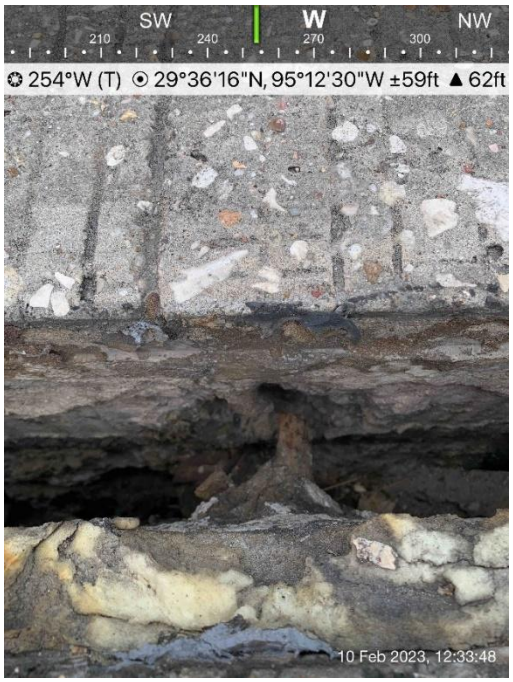
Attribute	Information	Notes
District & Highway	HOU, BW-8 SB	
CSJ	0500-03-429	L = 0.74 miles
County	Harris County	
Reference Marker	RM 758+0.288 to RM 758+0.395	
Project Limits	From 1010-ft South of IH-45 to 1,573-ft South of IH-45	Westbound
GPS Coordinates	From 29.6048608, -95.2080190 to 29.6038540, -95.2094106	
Date Work Begin	06/03/1996	
Date Completed	11/01/1997	
Pavement Type	12-in CRCP	
Shoulder Type	Tied Concrete	T501 Traffic Rail
Base Type	1-in ACP (GR 4) + 6-in CTB	
Subgrade Type	6-in LTS	
Drainage Type	Curb & Inlets	
Embankment Height	~26-ft	
Distresses Observed	Faulting; Lane Settlement; BAS Settlement	

Field evaluations were conducted on February 10–11, 2023. Visual surveys and LiDAR scans quantified the severity of the distress (**Figure 5-90**). A lane separation ranging from 2 to 5 inches was observed between the travel lanes, accompanied by pavement settlement of approximately 4.8 inches. The MSE wall showed significant distress, with recorded lateral movement of 7.2 inches at the bottom and 11.3 inches at the top, along with an outward tilt of approximately 1.4 degrees. A separation of approximately 2.5 inches was also noted at the bridge abutment interface.


S SW W
180 210 240 270 300
235°SW (T) 29°36'16"N, 95°12'29"W ±16ft ▲60ft
10 Feb 2023, 09:03:41


SW W NW
210 240 270 300
257°W (T) 29°36'16"N, 95°12'29"W ±154ft ▲56ft
10 Feb 2023, 09:10:31

(a)


SW W NW
210 240 270 300
254°W (T) 29°36'16"N, 95°12'30"W ±59ft ▲62ft
10 Feb 2023, 12:33:48

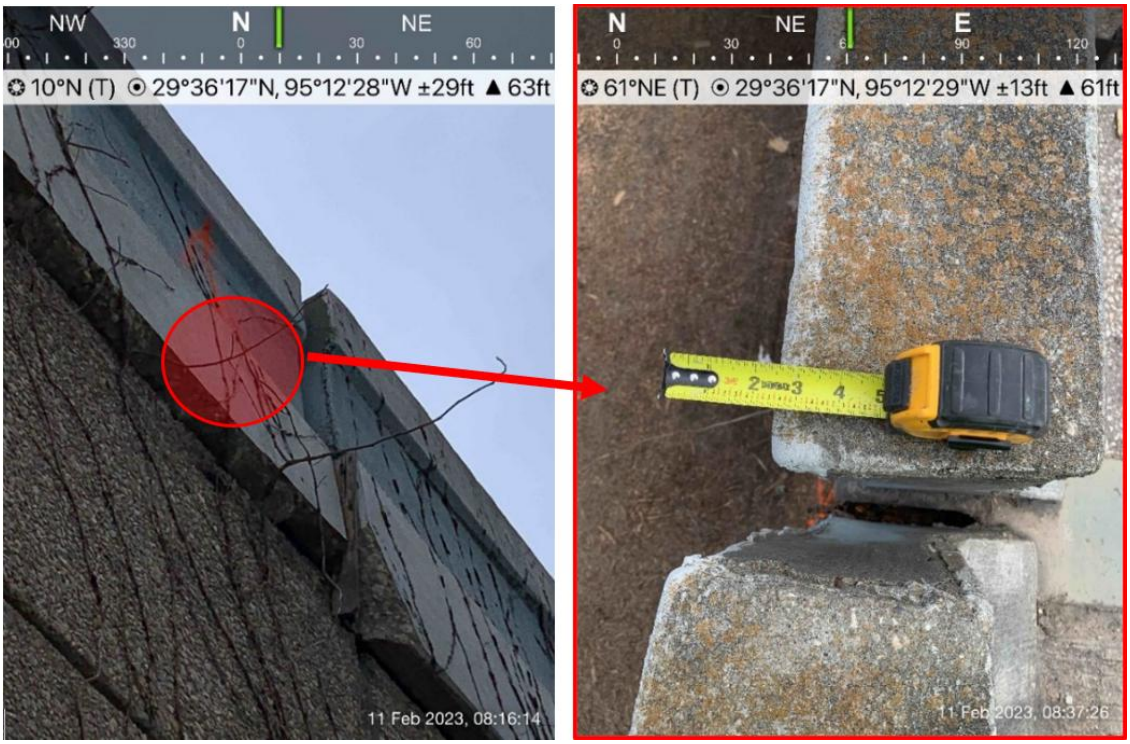
(b)


W NW N
270 300 330 0 30
332°NW (T) 29°36'16"N, 95°12'30"W ±72ft ▲55ft
11 Feb 2023, 08:02:51

(c)



(d)



(e)

Figure 5-90. Observed Distress (a) wide lane separation, (b) tie-bar failure, (c) faulting, (d) abutment Separation, and (e) MSE wall lateral movement.

5.7.2 Falling Weight Deflectometer (FWD) Tests

Falling Weight Deflectometer (FWD) testing was conducted on February 10, 2023, on the inside lane, middle lane, outside lane, and shoulder along the westbound mainlanes. The results presented in **Figure 5-91** revealed a trend in structural response across the roadway width. The inside lane, which is positioned furthest from the MSE wall, exhibited consistently low deflection values, averaging approximately 3.4 mils. This result is consistent with the hypothesis that the embankment support beneath the inside lane remains stiff, intact, and unaffected by the slope instability observed near the wall.

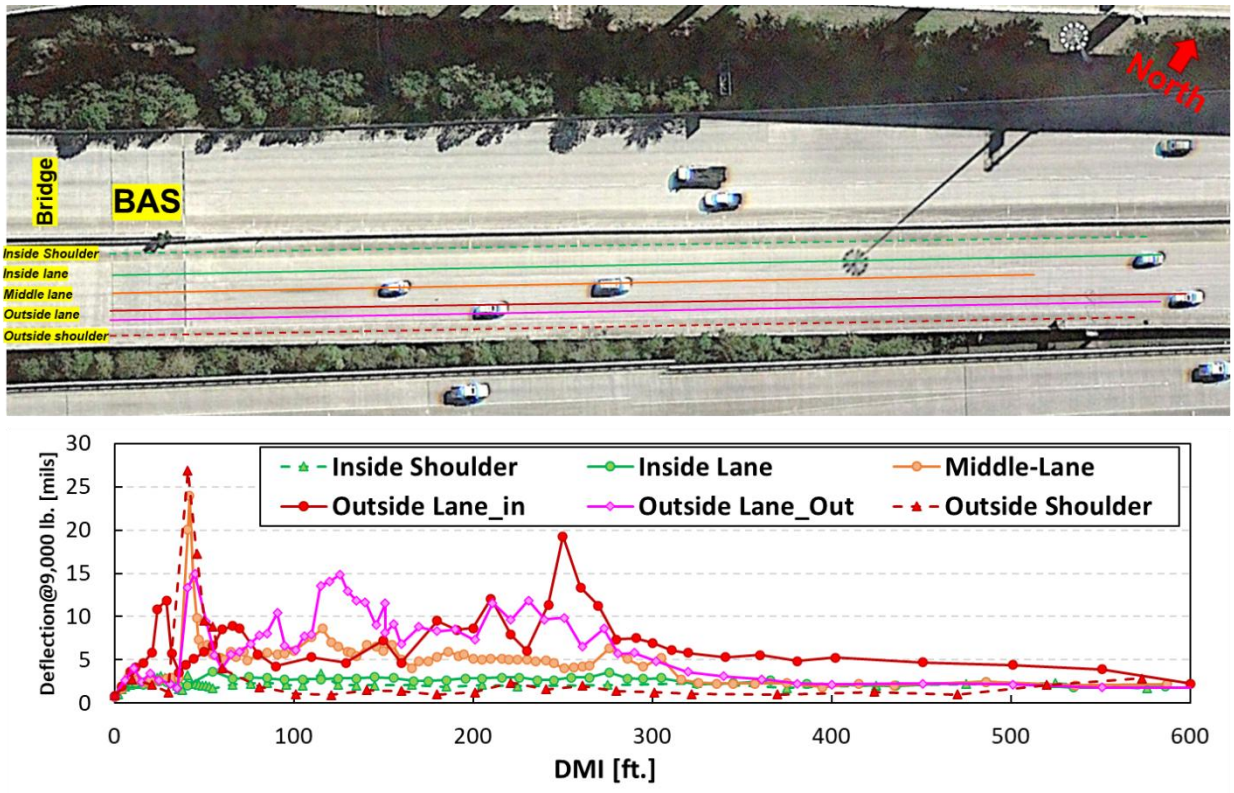


Figure 5-91. Longitudinal FWD deflection profiles (d1) across BW-8 test site at Houston

On the other hand, the middle and outside lanes recorded significantly higher deflections, with averages of 12.3 mils and 17.5 mils, respectively. However, these high deflection values should not be interpreted as a degradation of the concrete slab itself. The excessive deflections in the outer lanes are attributed to a severe loss of foundation support rather than slab failure. The observation from visual investigation and LiDAR survey suggests that the embankment fill has settled or displaced laterally away from the pavement structure. The "stiff" concrete slab is currently bridging over these voids, but without adequate subgrade support, it deflects excessively under load.

5.7.3 Coring

Coring was performed at several locations (**Figure 5-92**) to verify pavement layer thickness, visually inspect the subsurface for voids and repair materials, and facilitate access to the subgrade

for subsequent Dynamic Cone Penetrometer (DCP) and Cone Penetration Test (CPT) testing. The coring locations were distributed across the outside shoulder, outside lane, middle lane, inside lane, and inside shoulder to evaluate the condition of the pavement structure across the entire roadway width.

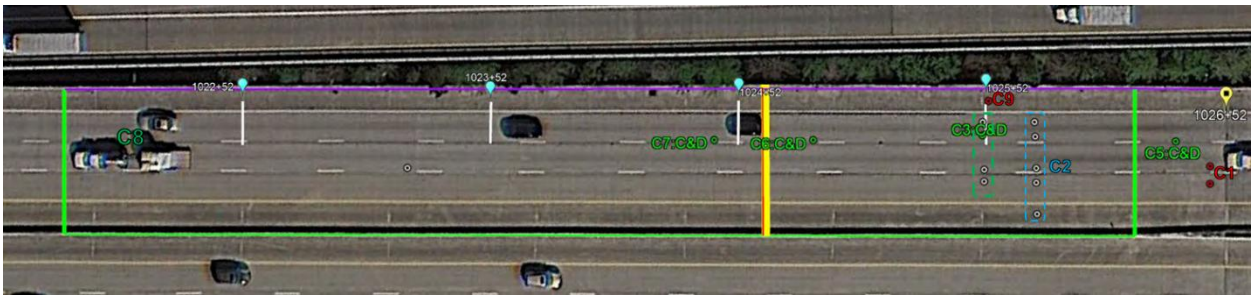


Figure 5-92. Location of cores and drills at BW8 test section in Houston

Visual inspection of the core holes and extracted samples confirmed the presence of subsurface distresses and previous repair attempts. Voids were notably observed in the vicinity of the Bridge Approach Slab (BAS) and along the outside shoulder, correlating with the areas exhibiting large deflections. Additionally, evidence of previous maintenance activities was identified at location C5 (C5) and C2 in middle lane. As shown in **Figure 5-93**, pieces of polyurethane foam were retrieved from the subgrade soils at this location, confirming the use of High-Density Polyurethane Foam (HDPF) injections in prior efforts to address faulting.



(a) (b)

Figure 5-93. Presence of HDPF and void under the slab at location (a) C2 and (b) C5 at BW-8 test site in Houston

5.7.4 Dynamic Cone Penetrometer (DCP) tests and Cone Penetration Test (CPT)

Following the coring operations, 17 dynamic cone penetrometer (DCP) tests and 5 cone penetration tests (CPTs) were conducted to evaluate the stiffness and stability of the underlying pavement layers. The layout and the location of DCP tests and CPTs are presented in **Figure 5-94**.

The DCP tests were performed through the core holes, extending to depths ranging from approximately 81.4 inches (6.8 ft) to 102.7 inches (8.6 ft) below the pavement surface. The primary objective of the DCP testing was to characterize the in-situ modulus of the backfill and subgrade materials.



Lane	C1	C2	C3	C4	C5	C6	C7	C8	C9
Outside Shoulder(OS)									
Outside Lane - Outside (OL_O)		DCP	DCP						
Outside Lane - Inside (OL_I)		DCP	CPT + DCP						
Mid Lane (ML)	DCP	DCP	DCP	DCP	CPT + DCP	CPT + DCP	CPT + DCP	CPT + DCP	DCP
Inside Lane (IL)	DCP	DCP	DCP						
Inside Shoulder (IS)		DCP							

Figure 5-94. Locations of DCP and CPT testing across the pavement width.

During the investigation, three locations (DCP1 ML, DCP1 IL, and DCP9 OS) experienced refusal, likely due to the presence of cement-treated backfill or other hard obstructions. For the remaining 14 locations, the cumulative blow counts were plotted against penetration depth to identify distinct soil layers and variations in stiffness (**Figure 5-95**). Two locations, DCP4 ML and DCP8 OL LWP, were identified as control sections due to the relative lack of distress. These sections yielded weighted average moduli of 15.8 ksi and 17.8 ksi, respectively. In contrast, locations within the distressed areas (e.g., DCP2, DCP3, DCP6, and DCP7) exhibited significantly lower stiffness, with weighted subgrade moduli consistently falling below 10 ksi (**Figure 5-95**).

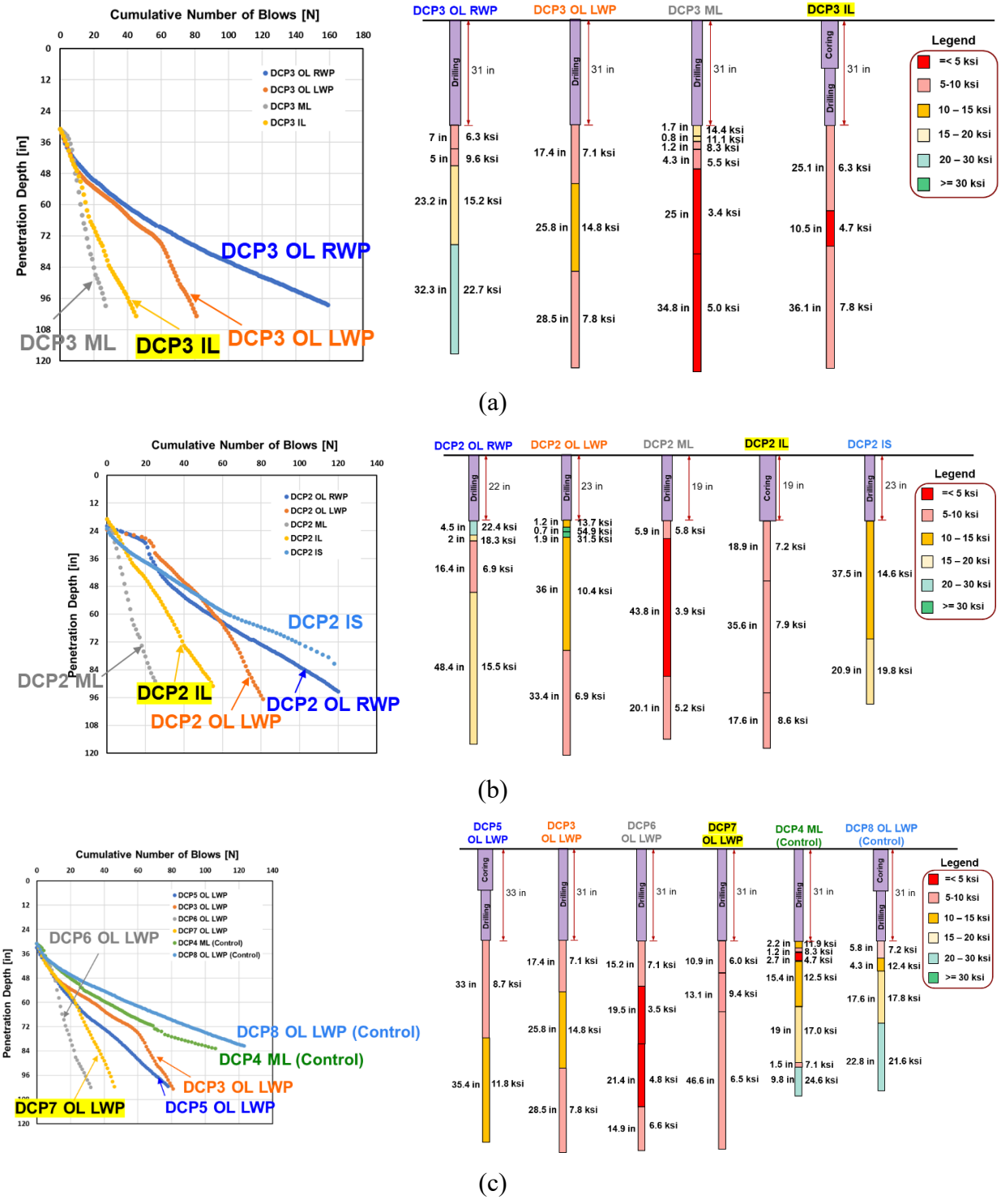


Figure 5-95. Cumulative blow counts and layer M_r vs. penetration depth for select locations, highlighting the contrast between control and distressed sections (Note: the color scheme for M_r value is for illustrative purposes only.)

To characterize the backfill and subgrade materials at depths beyond the limit of the DCP, Cone Penetration Tests (CPT) were conducted at five key locations (Locations 3, 5, 6, 7, and 8). These tests were performed by Terracon Consultants, Inc., within approximately 2 feet of the corresponding DCP locations for data comparability. The CPT logs indicated that the embankment backfill consists predominantly of clayey soils with isolated sandy layers at shallow depths. The cone resistance (q_c) values within the embankment (approx. 2.5 ft to 20 ft depth) were consistently low (< 15 tsf), with CPT8 (control) exhibiting the highest resistance and CPT7 (distressed) the lowest.

To estimate the resilient modulus (M_r) for the full depth of the embankment, a site-specific correlation was established between the DCP and CPT data as presented in **Figure 5-96**. Using regression analysis on paired data from the five overlapping locations ($R^2 = 0.866$), the following relationship was developed:

$$M_r(ksi) = 0.91 q_c(tsf)$$

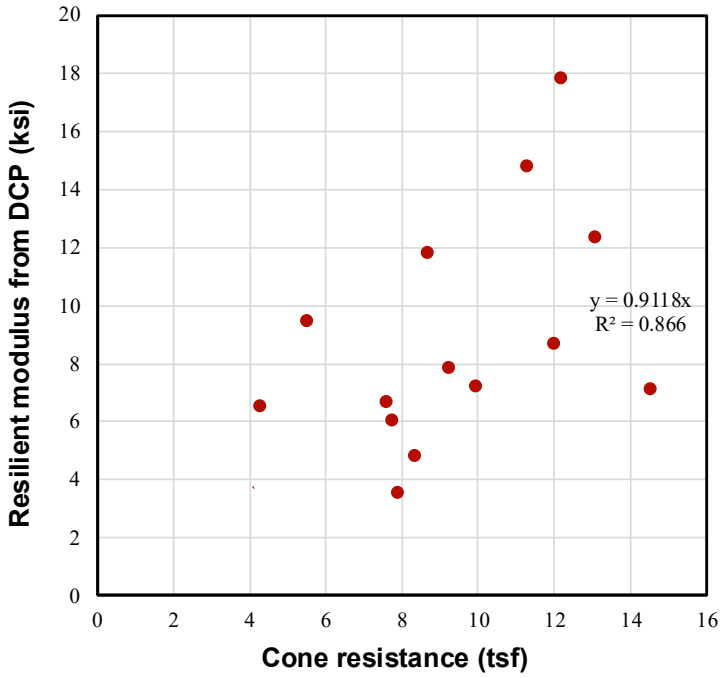


Figure 5-96. Correlation between subgrade moduli from DCP and average cone resistance from CPT (Note: For information purpose only).

The CPT data (**Figure 5-97**) at Location 7 revealed weak founding soils (M_r < 10 ksi) extending well below the embankment. Although this underlying instability may exacerbate the total vertical movement or trigger the ultimate lateral movement, the primary mechanisms driving the surface distress appear to be located within the shallower embankment layers.

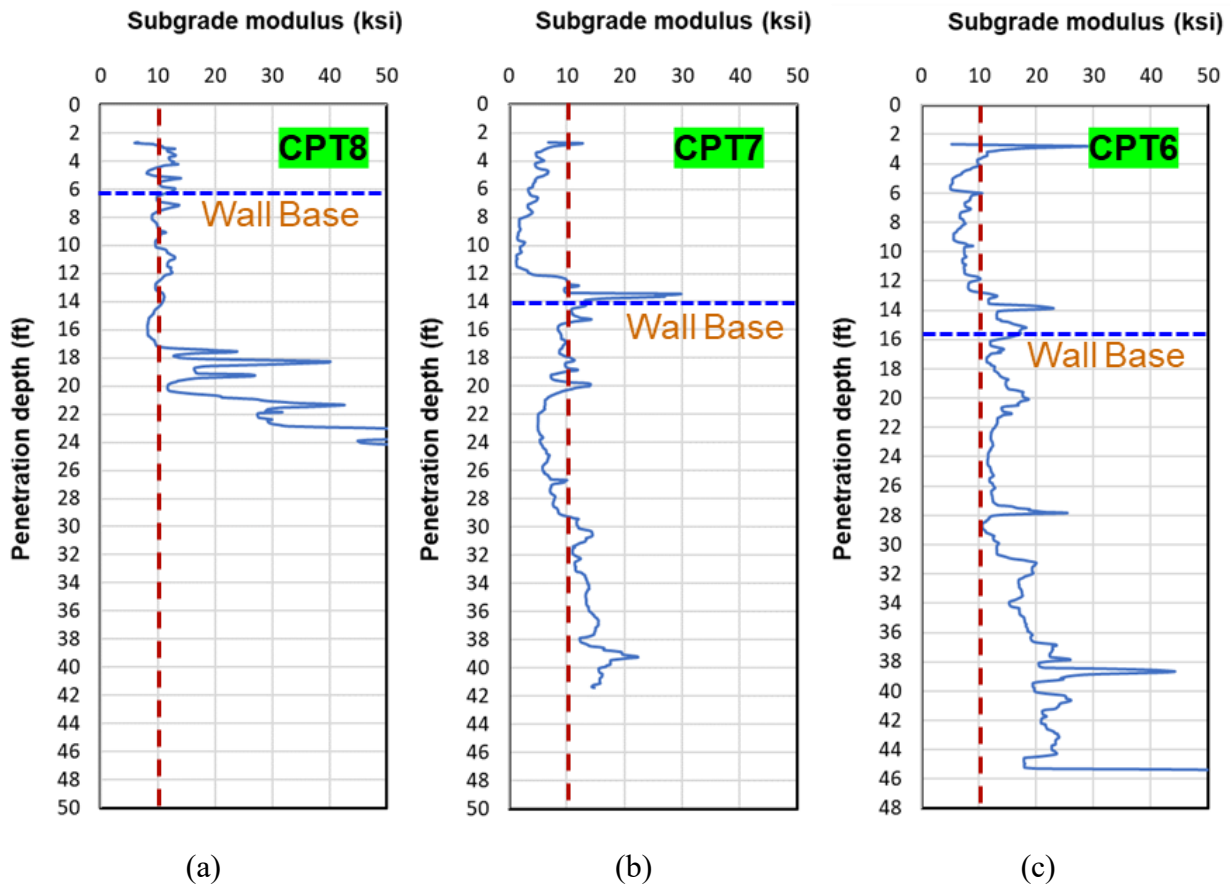


Figure 5-97. Moduli of backfill materials and founding soils determined from CPT data using the site-specific correlation at (a) CPT8, (b) CPT7, and (c) CPT6 (Note: For information purpose only)

5.7.5 Soil Sampling

Soil samples were collected from two locations (Location 2 and Location 5) for detailed laboratory analysis. At Location 2, samples were retrieved using a hand auger through the coring hole, targeting depths between 20 inches and 38 inches below the pavement surface. At Location 5, material was collected from the drill cuttings discharged by the CPT rig's auger bit from depths of approximately 20 to 31 inches. Laboratory tests including particle size distribution (sieve and hydrometer analysis), Atterberg limits, specific gravity, and moisture content determination were performed on these samples.

The particle size distribution curves for the tested samples are presented in **Figure 5-98**. The embankment fill from Location 2 exhibited a high percentage of fines, whereas the sample from Location 5 at presumably abutment fill was predominantly coarse-grained.

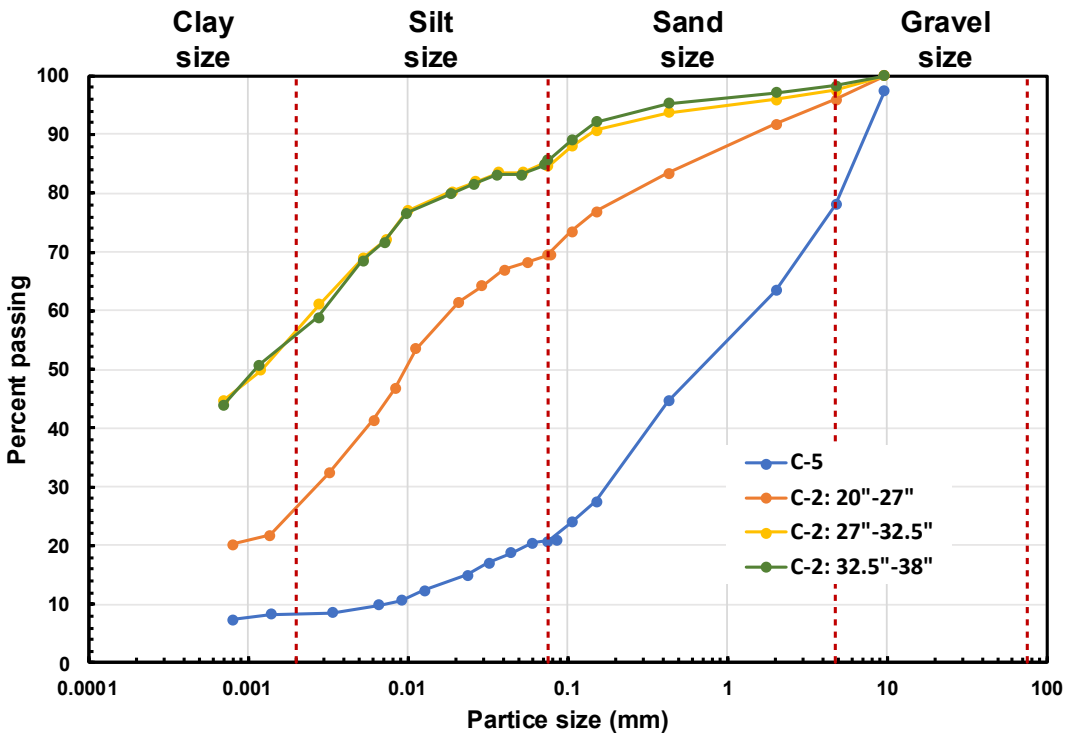


Figure 5-98. Particle size distribution curves determined from wet sieve and hydrometer analysis

Table 5-16 summarizes the laboratory test results and soil classifications. The soil at Location 2 was classified as Fat Clay (CH) according to the Unified Soil Classification System (USCS) and as A-7-6 under the AASHTO system. These soils exhibited high plasticity, with Liquid Limits (LL) ranging from 68 to 74 and Plasticity Indices (PI) between 43 and 48. The natural moisture content for these clay samples was consistent at approximately 35% to 36%.

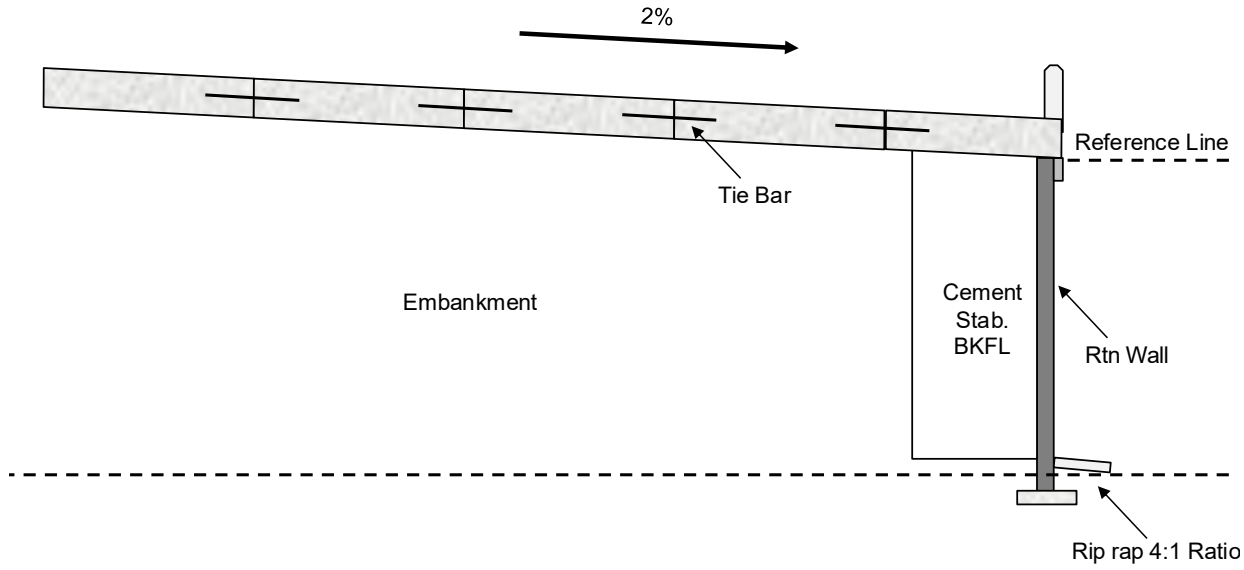
Table 5-16. Summary of laboratory test results for backfill and subgrade soil samples.

Sample	Depth (in)	Classification		Water content (%)	% passing #200	*LL*	*PL*	*PI*	*LI*	G_s
		USCS	AASHTO							
C-2	20 – 27	CH	A-7-6	35	70	68	25	43	0.24	2.69
	27 - 32.5	CH	A-7-6	36	85	74	27	47	0.19	2.70
	32.5 - 38	CH	A-7-6	35	86	74	26	48	0.20	2.70
C-5	-	SM (Silty sand) or SC (Clayey sand)	A – 2	23	21	-	-	-	-	-

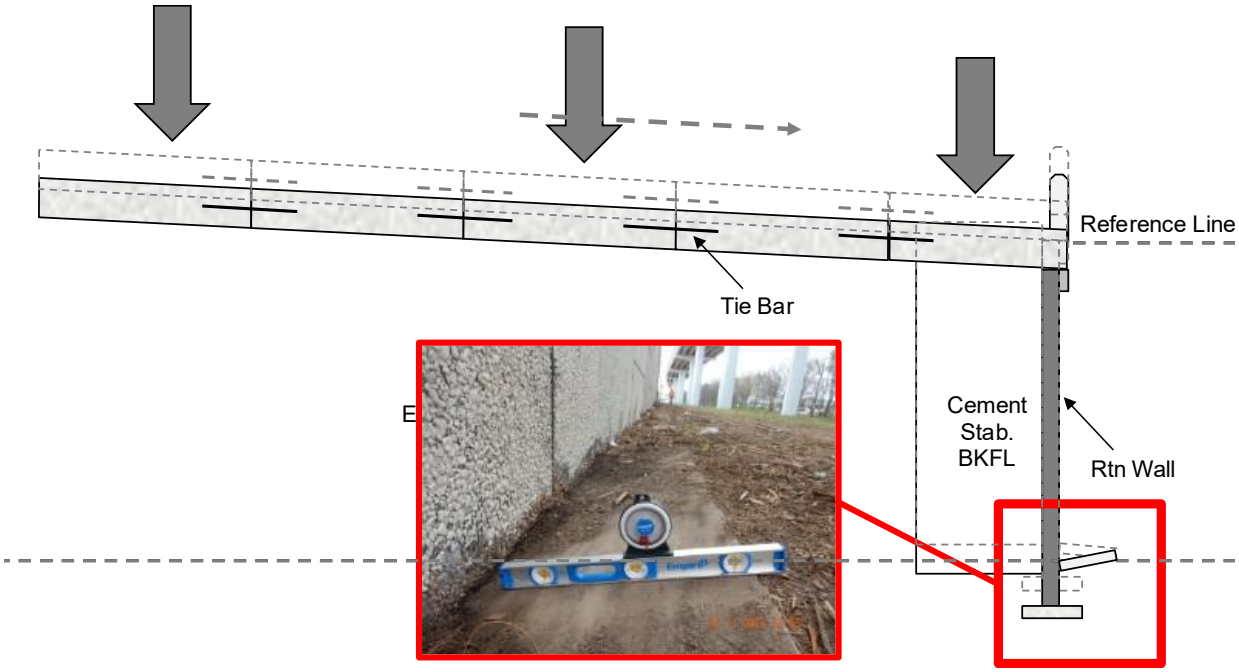
5.7.6 Potential Distress Mechanism

The primary trigger for the distress was identified as weak founding soil, which was confirmed during the CPT investigation. This soil weakness caused the wall to settle, a mechanism clearly by the rotation of concrete riprap at the base of the wall as shown in **Figure 5-99.**

This yielding of founding soil led to global instability and a slight outward rotation of the MSE wall. As the wall rotated away from the roadway centerline, it allowed the retained embankment soil mass to move laterally. This lateral movement of the subgrade imparted significant tensile forces into the pavement structure, specifically at the longitudinal joint between the inside lane and the middle lane. The pavement reinforcement was unable to resist this sustained lateral drift, resulting in the observed lane separation (**Figure 5-100**). Visual inspection of the exposed tie bars revealed distinct "necking". This reduction in cross-sectional area is characteristic of ductile tensile yielding, confirming that the initial failure mode was horizontal tension caused by the shifting soil mass.



(a)



(b)

Figure 5-99. Illustration of (a) original embankment configuration and (b) vertical displacement due to weak founding soil

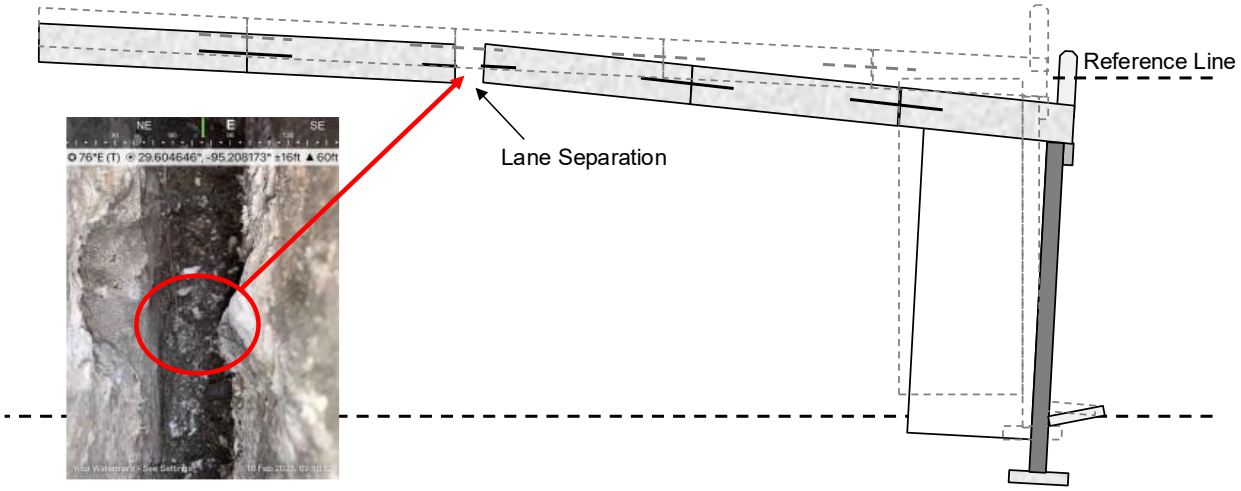


Figure 5-100. Illustration of lane separation triggered by rotation of wall

Once the longitudinal joint separated, it created a direct conduit for surface water to infiltrate the embankment system. Laboratory testing confirmed that the backfill material is a high-plasticity fat clay (CH), which has a high affinity for water retention. The accumulation of water within the embankment increased the pore water pressure, subsequently increasing the lateral earth pressure acting against the MSE wall. This elevated pressure exacerbated the wall's instability, driving further rotation and expanding the voids beneath the pavement due to washout.

With the subgrade support compromised by moisture-induced softening and washout, the tie bars at middle-outside lane joint were subjected to excessive vertical shear stresses they were not designed to withstand. As the tie bars broke, the slabs began to settle differentially (faulting). In contrast to the initial necking, the tie bars in the faulted sections eventually snapped, exhibiting clean shear failures (**Figure 5-101**).

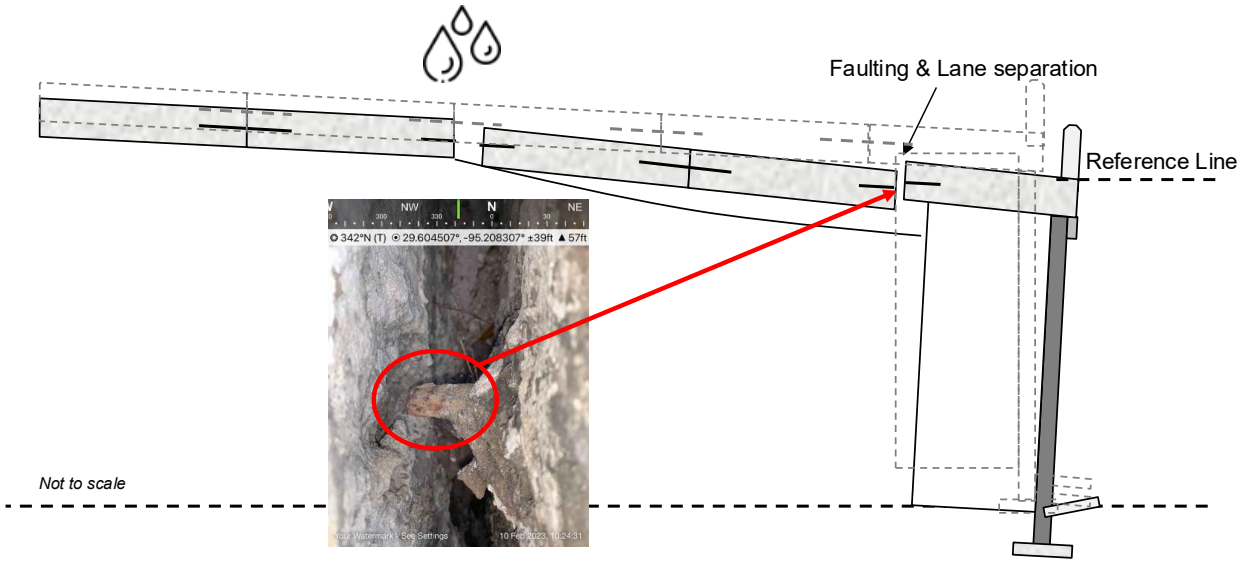


Figure 5-101. Illustration of subsequent void formation and faulting.

5.7.7 Repair Recommendation

The repair recommendations for this site were made by TxDOT MNT division, and this section summarizes the recommendations.

To prevent the rapid progression of joint separation and rainwater infiltration, immediate temporary repairs were recommended before the upcoming rainy season. Previous repair attempts by the TxDOT Area Office using standard filler and sealant were ineffective, with joint separation recurring within eight months. A more durable repair method is required, starting with the removal of the existing filler board and sealant. The voids should be filled with flowable grout (TxDOT Item 401), as illustrated in **Figure 5-102**, and the concrete side faces must be thoroughly cleaned. Subsequently, a fiber-reinforced polymer patching material (TxDOT Item 721) should be applied. Fibrecrete G is recommended for this purpose due to its excellent bonding capabilities and frequent use in the Houston District for CRCP spalling repairs.

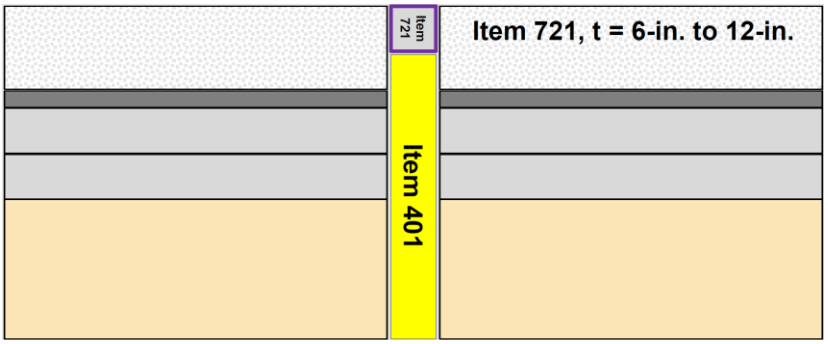


Figure 5-102. Proposed temporary repair plan (TxDOT item 721 & 401) to prevent rainwater infiltration

The long-term effectiveness of the pavement repair is contingent upon the global stability of the MSE retaining wall. Once the global stability of the wall is verified, two long-term, pavement rehabilitation options are proposed based on the desired level of structural intervention.

Option 1 includes repair methods which are based on the structural performance of the pavement as indicated by FWD deflection data in **Figure 5-103**. Full-Depth Repair (FDR) is specified for the zone exhibiting high deflections to replace the structurally deficient pavement and eliminate the existing lane separation. On the other hand, in the section where FWD results indicate acceptable structural support, slot-stitching is proposed to tie the lanes together without replacing the existing slab. The entire repair area then needs to be levelled with an HMA overlay to seal the surface, improve ride quality, and mitigate any BAS bump present at the site.

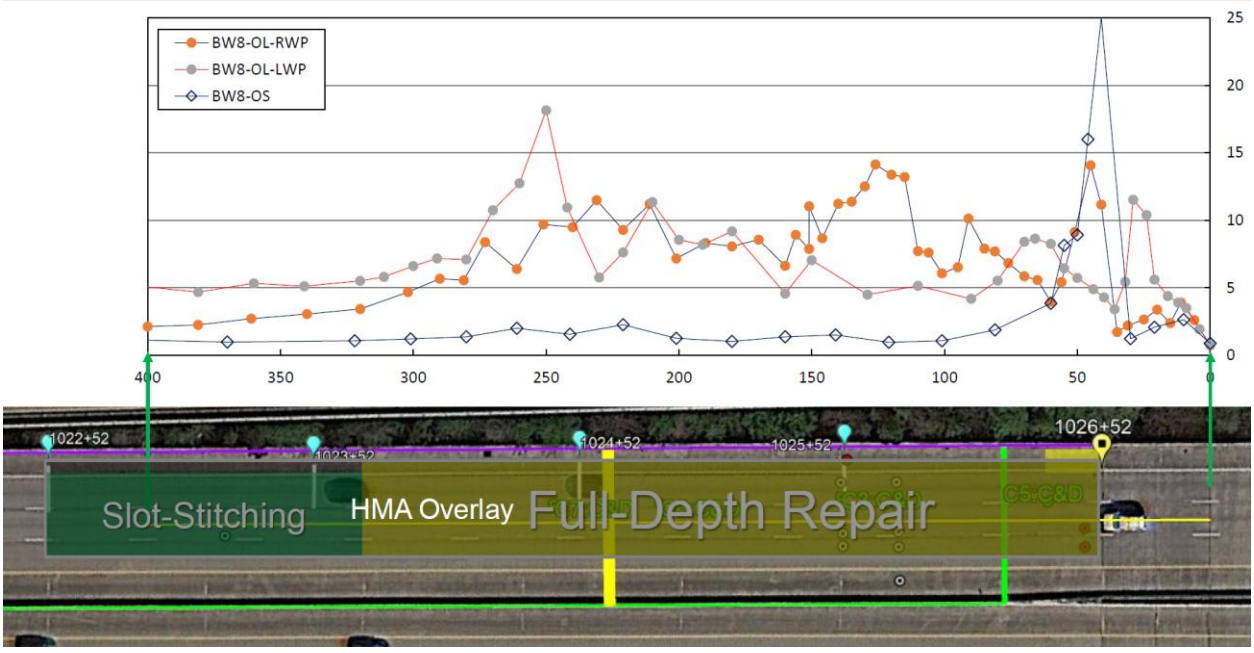


Figure 5-103. Illustration of proposed layout for Repair Option 1 with longitudinal FWD deflection profiles.

Option 2 includes a complete removal of the pavement structure and subgrade to a depth of approximately 14 feet on specified area as detailed in **Figure 5-104**. The embankment would then be reconstructed using special provision to Item 132 Embankment, with recommended modulus greater than 20 ksi, followed by the construction of a new CRCP layer with No. 6 tie bars spaced at 1 foot. It is recommended that the lift will only be accepted if the modulus determined from DCP testing is equal to or greater than 20 ksi. Any material failing to meet this stiffness requirement is recommended to be removed and replaced. While this offers superior structural capacity, it is noted that the required excavation depth may present significant practical challenges during construction.

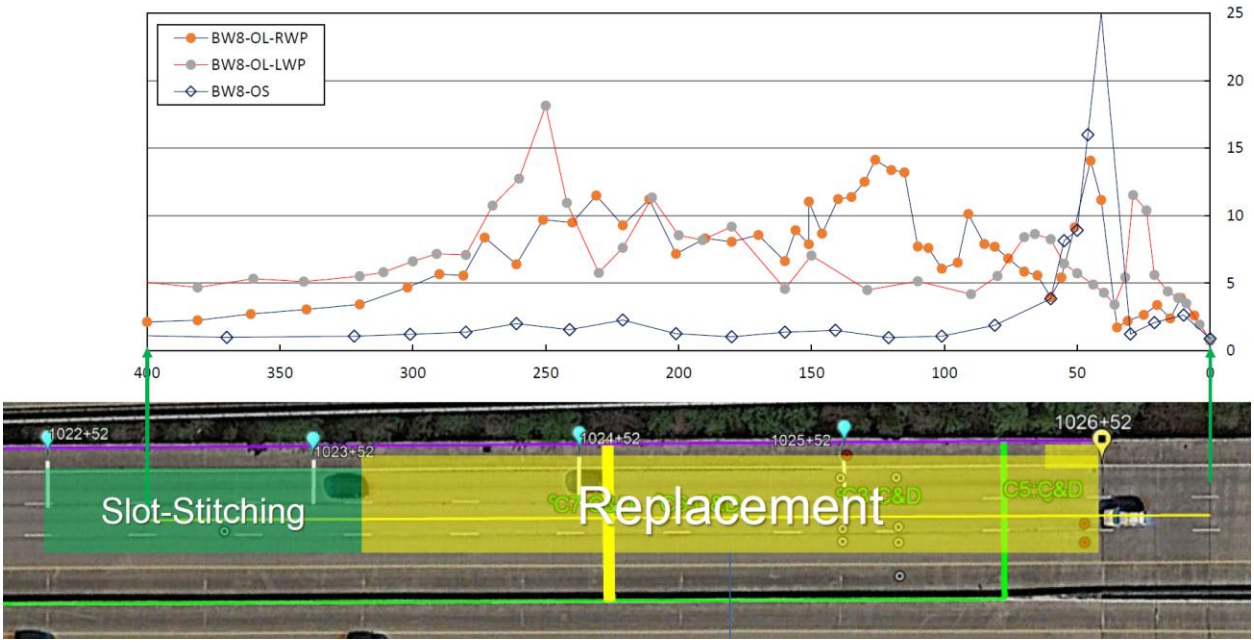


Figure 5-104. Illustration presenting proposed layout for Repair Option 2 with longitudinal FWD deflection profiles.

5.8 Section E-4: IH 35 Exit 368A in Hillsboro, Waco

5.8.1 Overview

The test section is located on the southbound departure ramp of IH 35 at Exit 368A (Whitney/Corsicana) in Hillsboro, Hill County, Texas as shown in **Figure 5-105**. The ramp connects the IH 35 mainlanes to the IH 35 frontage road. The project limits for the investigation extend from Station 6+060 to Station 6+660 (from 32°01'00.1"N 97°05'45.2"W to 32°00'52.2"N 97°05'45.6"W).

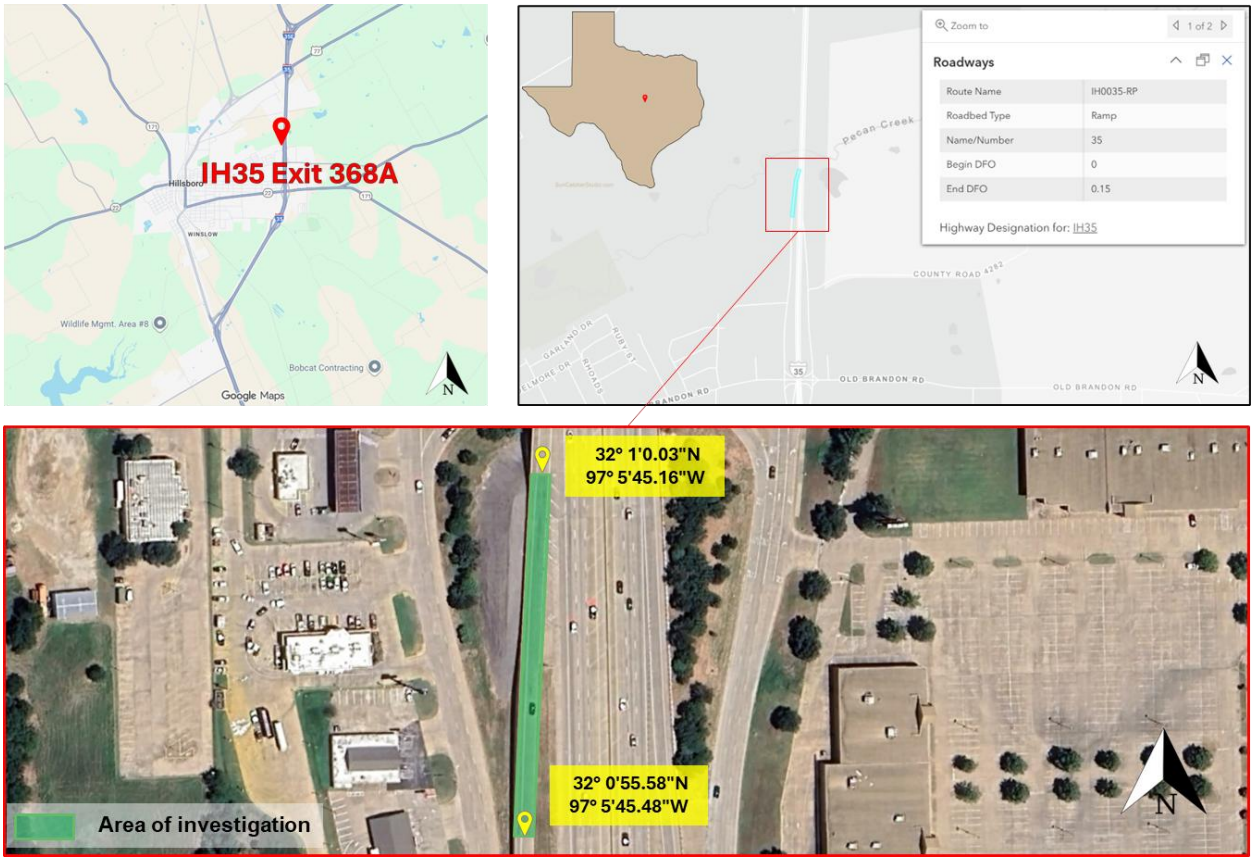


Figure 5-105. Location of the IH 35 Exit 368A test section in Hillsboro, Texas.

The roadway rests on an embankment approximately 23 feet in height. The test section, southbound departure corner, was constructed with a Mechanically Stabilized Earth (MSE) wall, while the other corners utilized sloped embankments as shown in **Figure 5-106**. The pavement structure consists of a 12.8-inch (325 mm) Continuously Reinforced Concrete Pavement (CRCP) over a 4-inch (100 mm) Asphalt Concrete Pavement (ACP) Type B base, supported by a 6-inch (150 mm) Lime Treated Subgrade (LTS). The detailed information on this site is presented in**Table 5-17**:

Table 5-17. Detailed descriptions of IH-35 Exit 368A in Hillsboro, Texas.

Attribute	Information	Notes
District & Highway	Waco & IH-35 Southbound Exit 368A Ramp (IH-35 Main-lanes to IH35 Frontage)	
CSJ	0014-24-045	
County	Hill County	
Station	Sta. 6+060 to Sta 6+660	
CSJ Project Limits	South of FM-3267 to North of FM-286 in Hillsboro, TX	
AOI GPS Coordinates	32°01'00.1"N 97°05'45.2"W to 32°00'52.2"N 97°05'45.6"W	Area of Interest
Date Work Begin	8/20/1999	
Date Completed	9/12/2002	
Pavement Type	CRCP 12.8-in	325 mm
BAS Dimension	12.8-in X 20-ft (T X L)	325 mm
Shoulder Type	CRCP 12.8-in	
Base Type	4-in ACP TY. B, GR. 1	100 mm
Subgrade Type	6-in Lime Treated Subgrade	150 mm
Drainage Type	-	
Embankment Height	~23-ft	
Distress Observed	MSE wall bulging, Departure slab settlement, Faulting, Lane Separation	

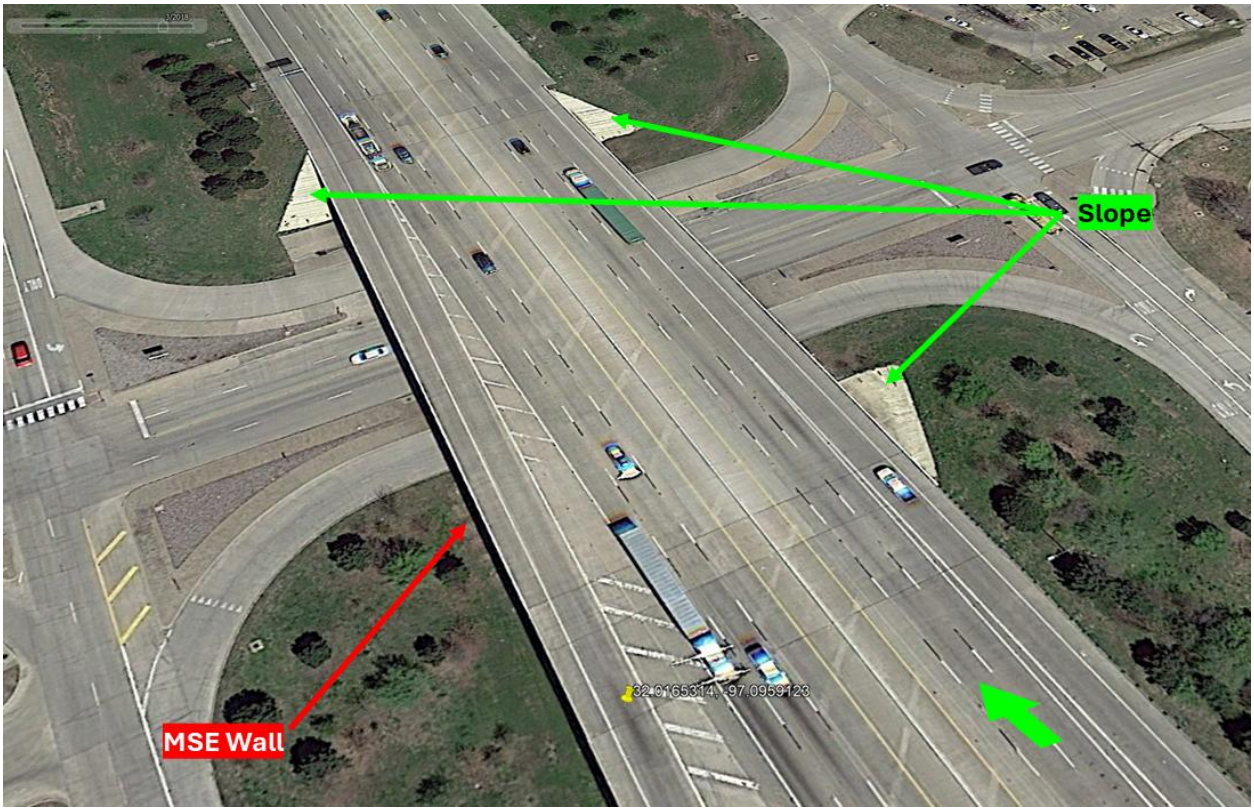


Figure 5-106. Wall configuration of IH 35 Exit 368A test section in Hillsboro, Texas

The original construction work for this specific section occurred between August 1999 and September 2002 as a broader expansion project which added inside lanes and relocated exit ramps (see **Figure 5-107**).

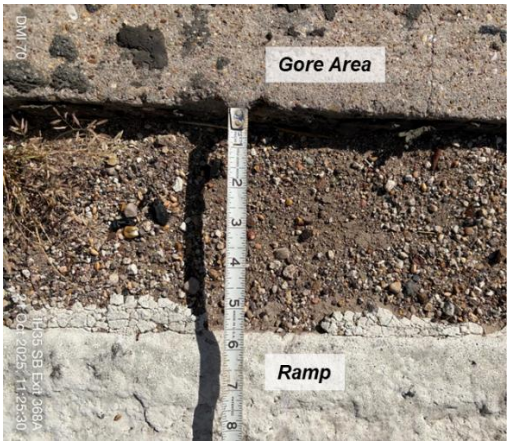


Figure 5-107. Comparison of test section after expansion

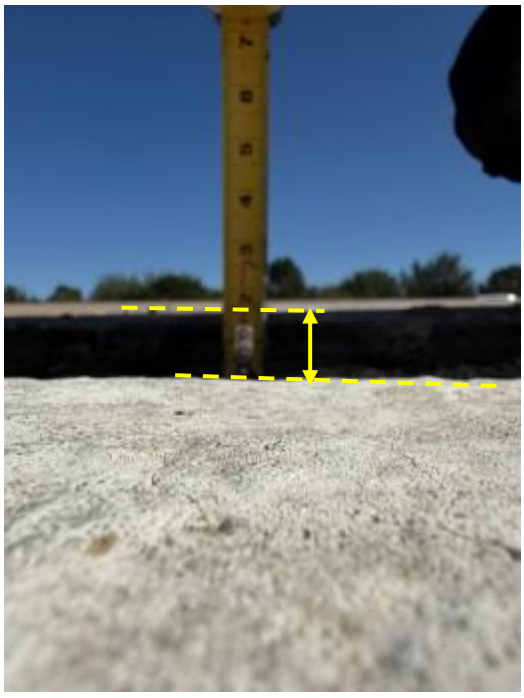
Field evaluations were conducted by the TTU research team on October 21–22, 2025. Visual surveys identified severe and progressing distresses, including settlement of the departure slab, bulging of the MSE wall panels, and faulting and lane separation at longitudinal joint between the pavement and the gore area. A lateral separation of approximately 5.5 inches observed between the pavement and the gore area along with bulging/dislocation of MSE wall panels and diagonal cracks are shown in **Figure 5-108**.



(a)



(b)



(c)



(d)



(e)

Figure 5-108. Observed distresses including (a) settlement of departure slab (b) lateral separation between gore area and ramp (c) faulting between gore area and ramp (d) MSE wall panel bulge (e) diagonal/halfmoon crack.

5.8.2 Falling Weight Deflectometer (FWD) tests

Falling Weight Deflectometer (FWD) testing was conducted along the shoulder, right wheel path, and left wheel path of the ramp pavement. Testing intervals were set at 10 feet for the main pavement section and reduced to 2 feet at the BAS. **Figure 5-109** illustrates the longitudinal deflection profiles (D1) obtained from the FWD tests. The results indicate a strong correlation between deflection magnitude, slab thickness, and the presence of subsurface voids or High-Density Polyurethane Foam (HDPF).

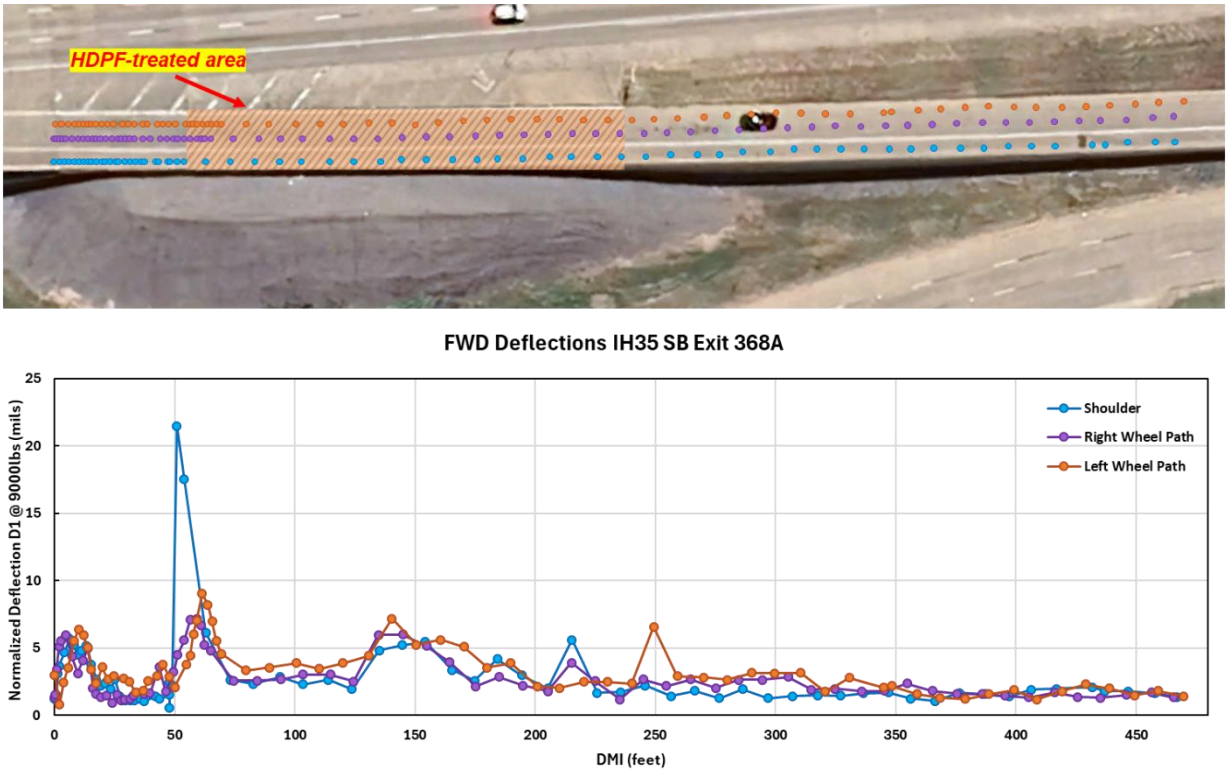


Figure 5-109. Longitudinal FWD deflection profiles (D1) for shoulder and wheel paths across IH35 SB (Exit 368A) test section

As shown in the profiles, the highest deflection of 21.5 mils was recorded at core location C3. This peak is attributed to the presence of a 1-inch void and the FWD drop's proximity to the pavement edge, which likely amplified the deflection magnitude. In other areas, deflections varied: location C1 (2-inch void) exhibited 4.5 mils of deflection, while location C4 (3-inch void) recorded 7.1 mils. In contrast, the control location C7, characterized by no voids, observed a minimal deflection of 1.8 mils.

The influence of slab thickness and slab-support condition on FWD response is further evidenced in the section between DMI 125 and 200 ft, where deflections were slightly elevated (e.g., 7.1 mils at C6 and 6.6 mils at C8). As visualized in the spatial heatmaps in **Figure 5-110**, these elevated deflections correspond to a reduced slab thickness of 10 - 12 inches and the presence of HDPF. **Figure 5-110** integrates these datasets, comparing FWD surface deflections (D0) with CRCP thickness, determined via GPR and verified by coring, and HDPF treatment areas confirmed through field observation.

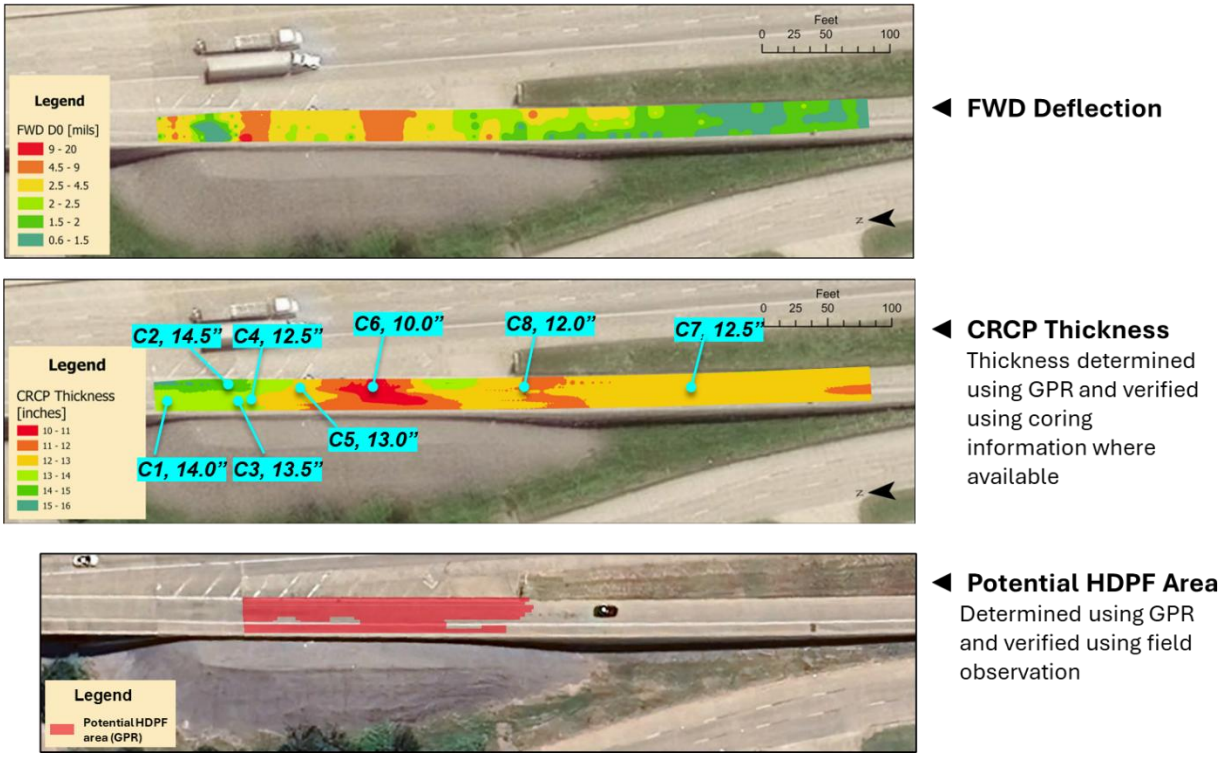


Figure 5-110. Spatial comparison of FWD surface deflections (D0), GPR-derived CRCP thickness with core locations (C1–C8), and potential HDPF injection areas.

5.8.3 Ground Penetration Radar (GPR) Utility Scan

Ground Penetrating Radar (GPR) testing was conducted to assess the subsurface conditions of the pavement and embankment. GPR was extensively used to identify potential voids beneath the pavement slab and to map the extent of High-Density Polyurethane Foam (HDPF) from previous repair efforts. A total of 11 longitudinal GPR passes were performed across the test section. The scans were spaced at 2-foot lateral intervals.

The GPR data revealed distinct subsurface anomalies that correlated with the findings from the coring investigation. Strong reflections indicative of HDPF layers were observed, particularly in the scans taken across DMI 60-250 feet which corresponds to the pavement area where the lane separation and faulting between the pavement and gore area were observed. This indicates the previous attempt to repair the pavement by uplifting the slab using HDPF to address the faulting. GPR Pass 004 shown in **Figure 5-111** exhibited significant continuous negative reflection in the area corresponding to cores C5 and C6, confirming the presence of a thick layer of foam beneath the slab in this region. These results were used to verify the horizontal extent of the previous foam injection repairs, which were concentrated in the area of the slab exhibiting the most severe settlement. The core C2 and C8 had void of 1.25" and 0.25" respectively.

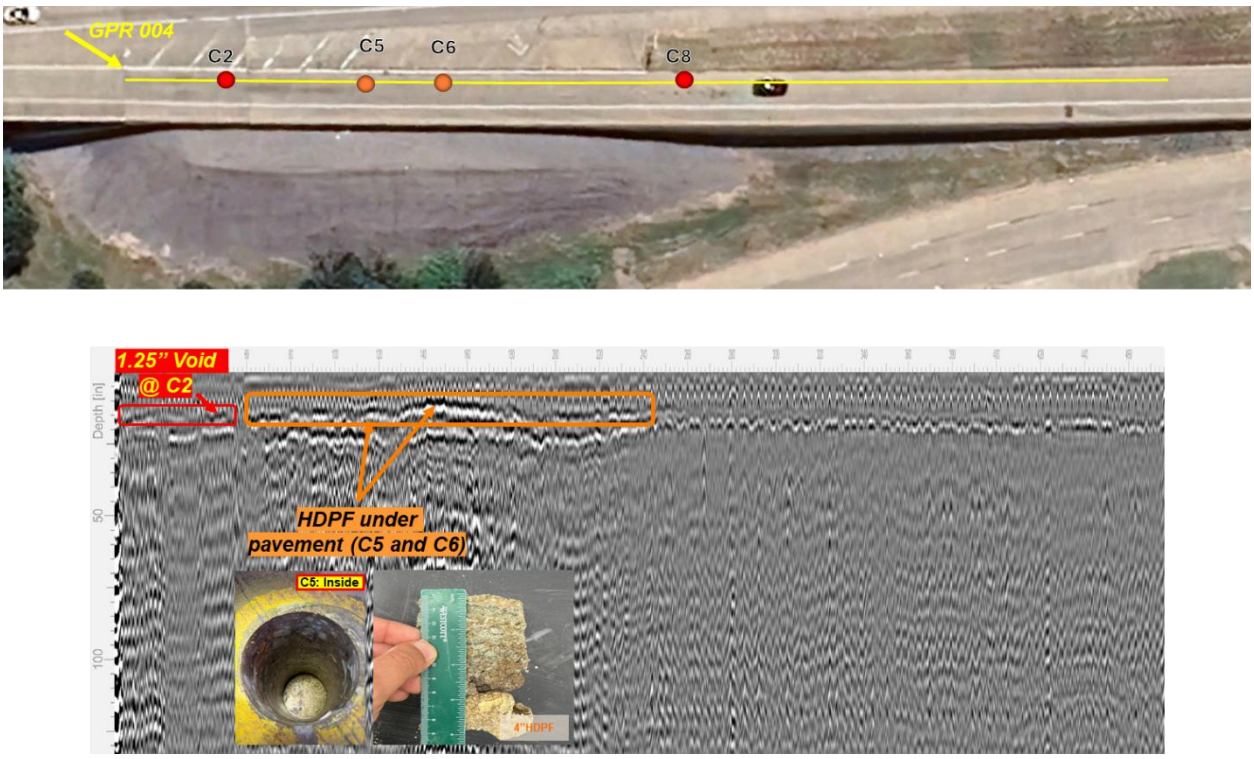


Figure 5-111. GPR scan 4 showing the extent of void and HDPF under pavement

The comprehensive lateral extent of the HDPF, determined by GPR and verified by field observation, presented in **Figure 5-112**.

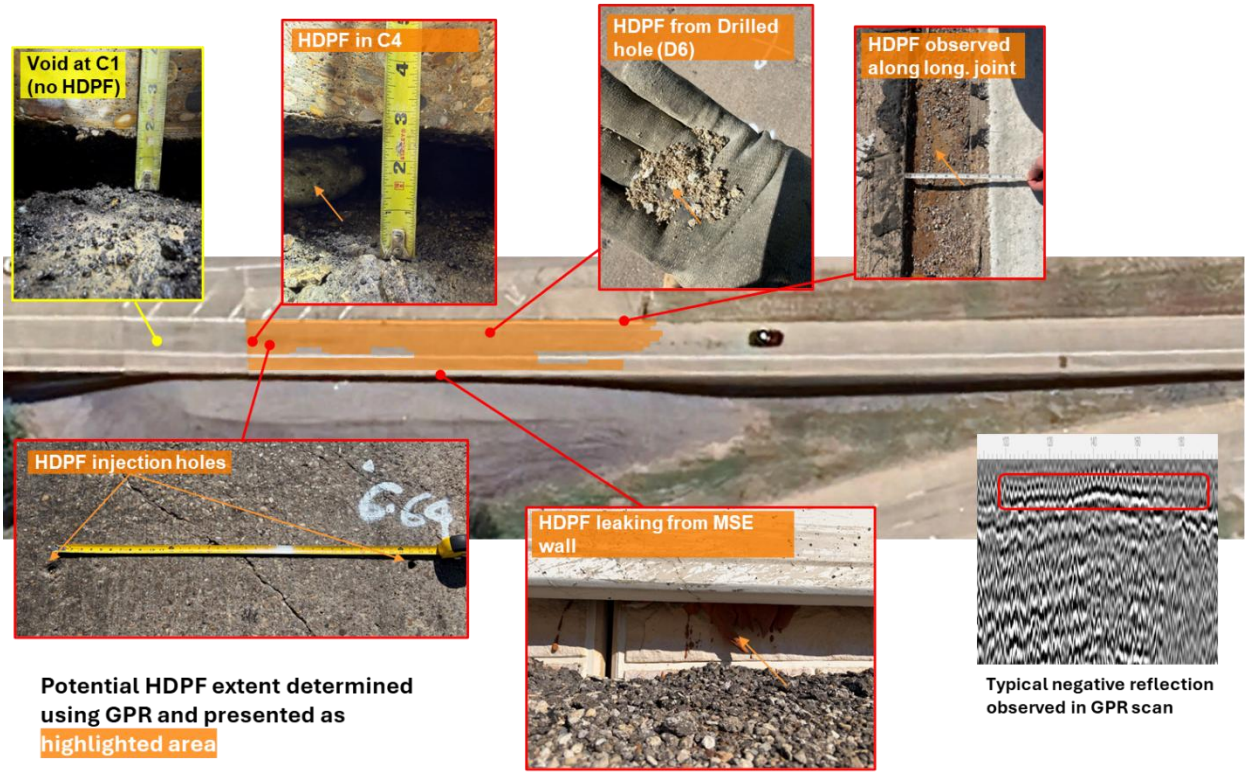


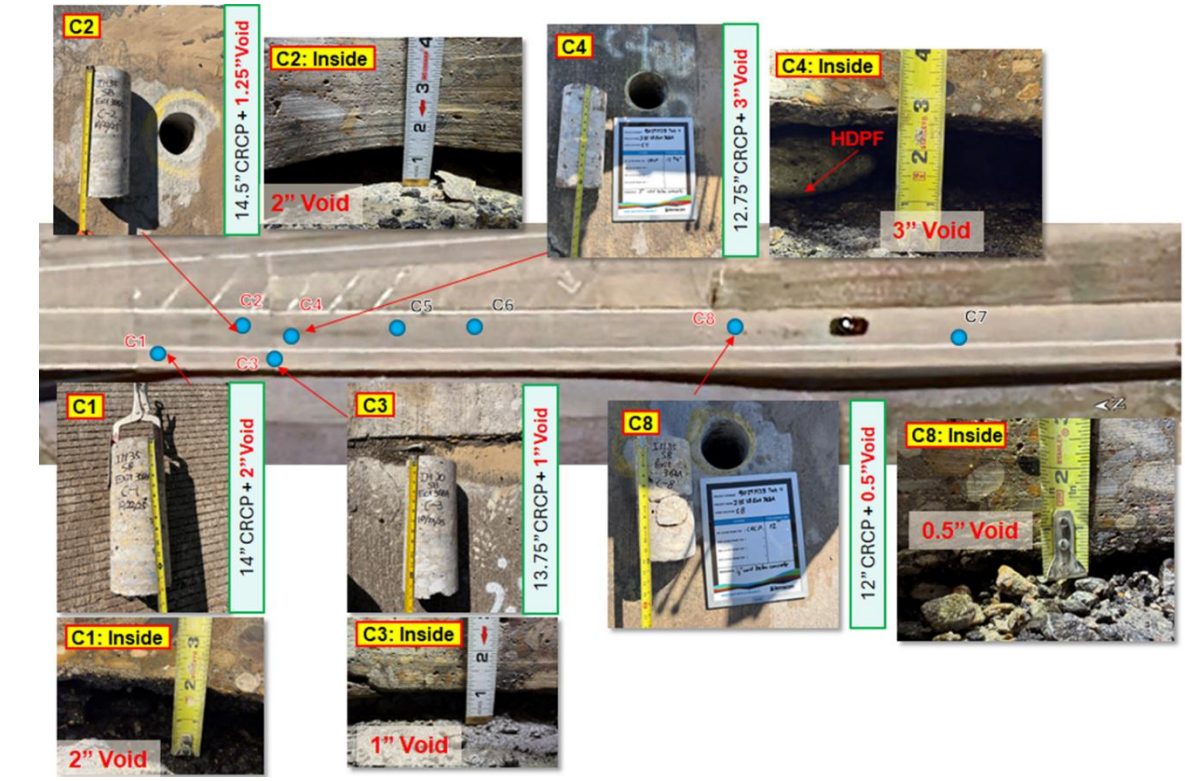
Figure 5-112. Potential HDPF extent determined using GPR and verified using field observation.

5.8.4 Coring

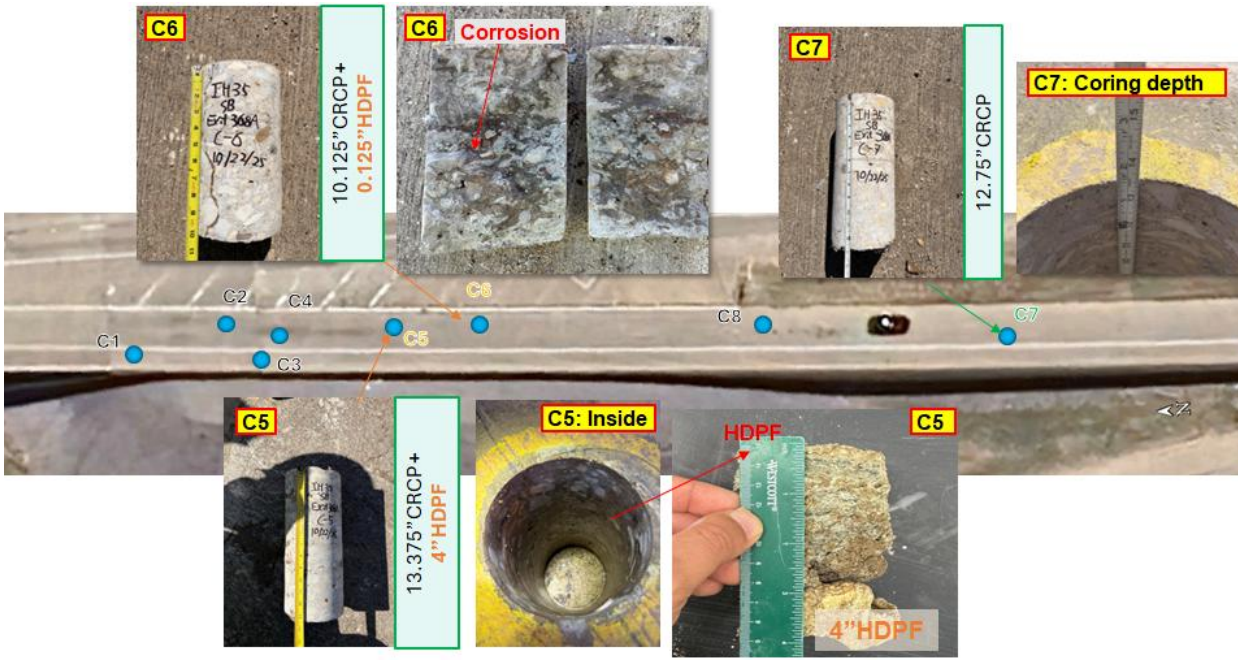
Coring was performed at nine locations (**Figure 5-113**) to verify pavement layer thickness, visually inspect the subsurface for voids and repair materials, and facilitate access to the subgrade for subsequent DCP testing. The cores revealed significant variability in the pavement structure. The CRCP thickness varied across the section, ranging from 10.375 inches (Core C8) to 14.0 inches (Core C1) as summarized in the **Table 5-18**.

Table 5-18. Summary of measurement at cored locations

Core	C1	C2	C3	C4	C5	C6	C7	C8
CRCP (in)	14	14.5	13.75	12.75	13.375	10.125	12.75	12
Void (in)	2	1.25	1	3	-	-	-	0.5
HDPF (in)	-	-	-	-	4	0.125	-	-



(a)



(b)

Figure 5-113. Coring locations and images of core samples

The visual inspection confirmed the presence of substantial voids at multiple locations, especially beneath the BAS, with thicknesses ranging from 0.5 inches to 3.0 inches. Evidence of previous repair efforts was found in cores C5 and C6, where High-Density Polyurethane Foam (HDPF) was observed. Core C5 contained a 4-inch thick layer of HDPF, while Core C6 showed a thinner 0.25-inch layer.

5.8.5 Dynamic Cone Penetrometer (DCP) Test

Deep DCP testing was conducted at nine locations (D1 through D9) to characterize the in-situ strength and stratification of the embankment fill material. The testing was performed through open core holes and drilled holes to depths of approximately 14 feet. The test locations were distributed to complement the wide range of FWD deflections and surface condition conditions in the shoulder, wheel paths, and control areas.

The primary finding from the testing was that the embankment fill generally exhibits high stiffness and significant penetration resistance, contrary to what is typically observed in areas with severe pavement settlement. As illustrated in **Figure 5-114**, the cumulative blow count profiles for the majority of the test locations, including D1, D4, D5, D8, and D9, closely align with or exceed the stiffness of the control section (D7). Notably, this high stiffness was observed even at locations where significant voids were found beneath the pavement (e.g., D4). The presence of a void above a stiff, dense soil layer suggests that the loss of support is likely not due to vertical consolidation or deep-seated soil failure, but rather a result of the soil mass being physically displaced due to the lateral movement of the MSE wall.

Tests conducted at locations with existing High-Density Polyurethane Foam (HDPF) injections (specifically D5 and D6) further support this observation. The subgrade immediately beneath the foam layers exhibited high blow counts, confirming that the previous repairs were filling a void created by separation rather than remediating a soft or unstable foundation. This implies that the subgrade at these locations provided adequate bearing capacity but lacked the necessary confinement to remain in contact with the pavement.

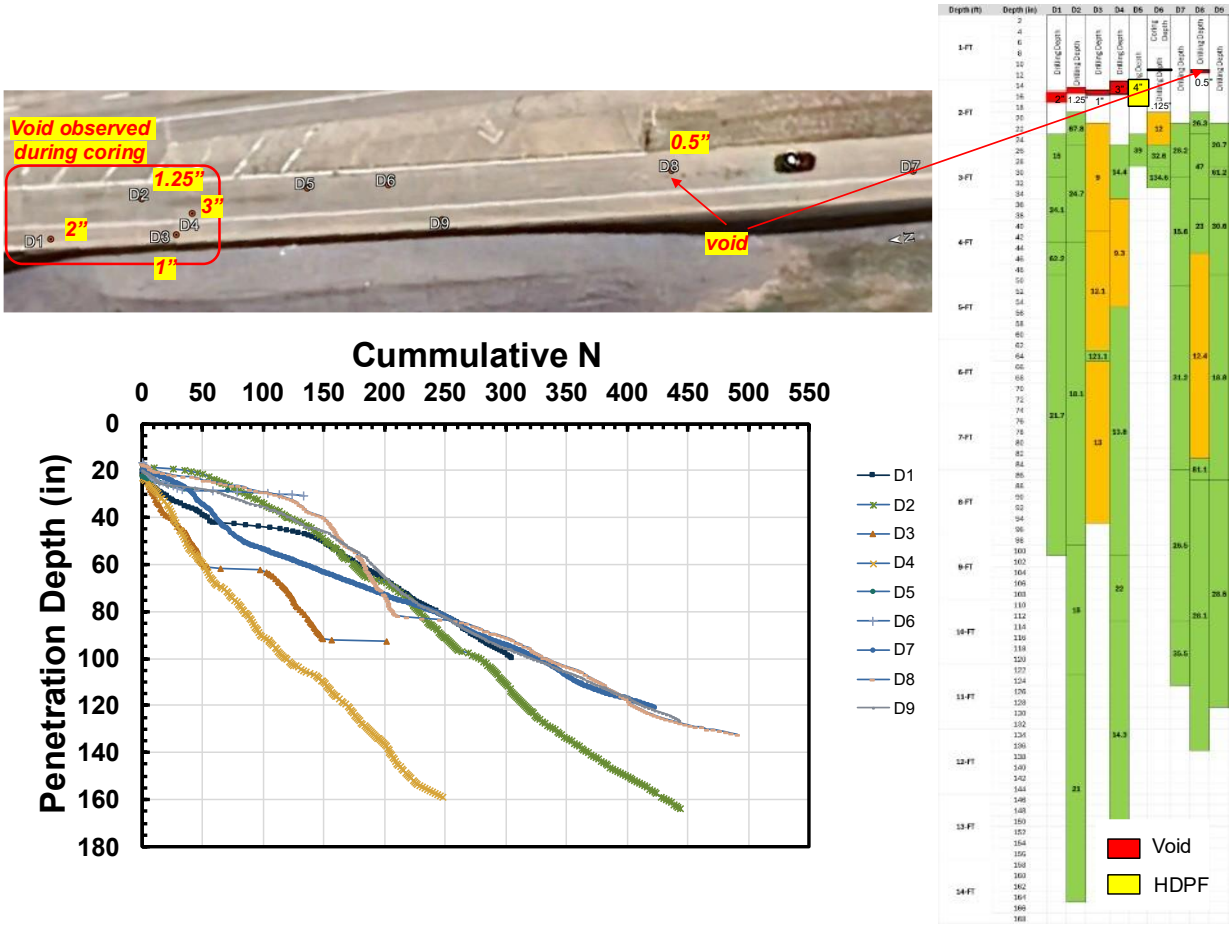


Figure 5-114. Cumulative DCP blow counts and layer M_r values

However, a distinct exception to this trend was observed at Location D3. D3, situated on the shoulder immediately adjacent to the BAS and near the start of the MSE wall flare, exhibited noticeably lower penetration resistance compared to the rest of the site. As shown in **Figure 5-114**, the penetration profile for D3 indicates a zone of weaker, likely saturated soil. This localized weakness correlates with the probable entry point for surface runoff at the BAS joint. The data suggests a mechanism where moisture infiltration at this specific interface softened the soil, potentially creating a "weak link" that compromised lateral stability at the wall interface, while the remainder of the embankment block remained stiff but mobile.

5.8.6 Soil Sampling

To characterize the physical properties of the embankment fill, we collected soil samples from the open core holes immediately after the coring operations. Samples were retrieved using a combination of grab sampling from auger and Shelby tubes, covering depths ranging from the surface down to approximately 10 feet. Detailed laboratory tests were conducted on these fill materials to determine their classification, moisture content, and plasticity.

Table 5-19. Summary of laboratory test results

Sampling Location	Sampling Type	Classification (USCS/AASHTO[GI])	Sampling Depth (ft)	Pocket Penetrometer Reading (tsf)	Moisture Content (%)	Retained on #4 (%)	Passing #200 (%)	PI	LL
C1	Grab	Fine-grained Soil/ Silt-Clay Material	0 - 3	-	16.2	3	70	-	-
	Shelby	GC/A-1-b[0]	3 - 5	4.5+	15.2	62	24	17	31
	Grab/Split Spoon	CL/A-6[3]	5 - 7	-	15.9	17	56	11	27
C2	Shelby	SC/A-6[1]	1 - 3	4.5+	14.5	23	44	11	25
	Shelby	CL/A-4[2]	3 - 5 (Top)	4.5+	17.7	18	52	10	27
	Shelby		3 - 5 (Bottom)	-	17.4				
	Shelby	CL/A-6[8]	5 - 7	3	17.8	15	57	20	32
	Shelby	(GW/GP)-GC/A-1-a[0]	7 - 9	1.5	12.9	51	10	16	28
	Split Spoon	(SM/SC)/A-1-b[0]	9.5 - 11	-	3	20	24	-	-
	Split Spoon	-	11.5 - 13	-	3.4	-	-	-	-
	Split Spoon	(SM/SC)/A-1-b[0]	13.5 - 15	-	4.4	23	18	-	-
C4	Split Spoon	(SM/SC)/ Silt-Clay Material	2.5 - 4	-	12.1	25	40	-	-
	Split Spoon	SC/A-6[2]	4.5 - 6	-	16.7	41	36	12	25
	Split Spoon		6.5 - 8	-	18				
	Split Spoon	(GM/GC)/ Silt-Clay Material	8.5 - 10	-	16.7	34	40	-	-
	Split Spoon	GC/A-2-6[0]	10.5 - 12	-	14.9	46	31	11	27
	Split Spoon	-	12.5 - 14	-	10.8	-	-	-	-
	Split Spoon	-	14.5 - 16	-	6.4	-	-	-	-
	Split Spoon	SP-(SM/SC)/ A-1-a[0]	16.5 - 18	-	3.8	24	10	-	-
	Split Spoon	-	18.5	-	3.8	-	-	-	-
C5	Split Spoon	-	1.5 - 2	-	10.2	-	-	-	-

	Split Spoon	-	2 - 4	-	13.6	-	-	-	-
	Split Spoon	SC/A-4[2]	4.5 - 6	-	17.1	28	48	9	25
	Split Spoon		6.5 - 8	-	16.4				
	Split Spoon	-	8.5 - 10	-	15.4	-	-	-	-
	Split Spoon	-	10.5 - 12	-	9.9	-	-	-	-
	Split Spoon	(SM/SC)/A-1-a[0]	12.5 - 14	-	5.9	25	23	-	-
	Split Spoon	(SM/SC)/A-1-b[0]	14.5 - 16	-	9.8	32	12	-	-
	Split Spoon	CH/A-7-6[51]	16	-	33.7	-	-	43	70

The laboratory analysis, as summarized in **Table 5-19**, classified the embankment material primarily as Clayey Sand (SC) and Lean Clay (CL) according to the Unified Soil Classification System (USCS). Significant proportion of fines, or material passing the No. 200 sieve, were determined from the particle size distribution analysis. High fines content drastically reduces the permeability of the soil. Unlike clean sand or gravel, which allows water to drain freely, the Clayey Sand and Lean Clay found at this site tend to retain moisture. This low hydraulic conductivity can be a significant factor in the observed distress, as it prevents water that enters near the bridge approach from dissipating effectively, leading to the buildup of pore water pressure behind the retaining wall.

5.8.7 Inclinometer Monitoring

TxDOT provided inclinometer monitoring records for a casing installed within the wall-supported embankment at approximately DMI 68 ft, inside the length of the ramp where the pavement and wall distresses are concentrated. An initial baseline reading was taken on December 5, 2019, followed by nine subsequent readings through July 28, 2022, as shown in **Figure 5-115**. Displacements reported here are the change from the December 2019 baseline; positive lateral displacement is directed toward the MSE wall face, and positive longitudinal displacement is directed toward the bridge abutment. In June 2020, during the monitoring period, an additional support berm was placed against the wall face as a temporary stabilization measure. This monitoring record is a direct, dated measurement of ground movement available at the site, and it is a strong piece of evidence for the distress mechanism proposed in the following subsection.

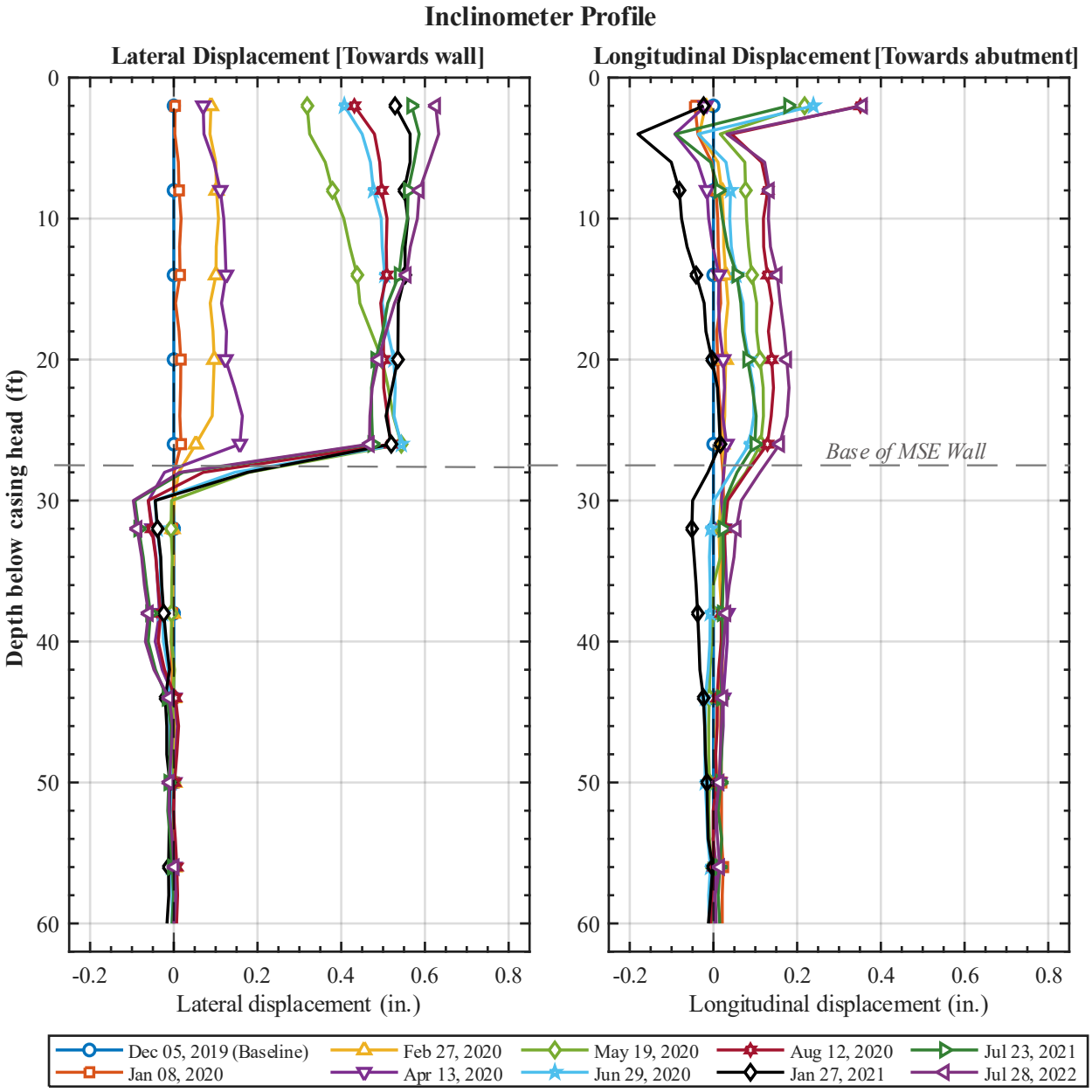


Figure 5-115 Inclinometer displacement profiles with depth by reading date: (a) lateral displacement, positive toward the MSE wall; (b) longitudinal displacement, positive toward the abutment.

Figure 5-116 presents the displacement time-history at five representative depths, grouped by the fill type/location. The three depths lying within the wall-supported embankment, 2 ft (top of wall), 14 ft (mid wall fill), and 26 ft (base of wall fill), all show substantial, systematic outward movement (toward the wall), reaching 0.63, 0.56, and 0.47 inches respectively by the final reading. In contrast, the two depths within the foundation soil below the wall, 36 ft and 50 ft, remained stationary

throughout the entire 32-month record, with displacements never exceeding 0.10 inch and, at 50 ft, remaining within ±0.01 inch of the baseline for the full period.

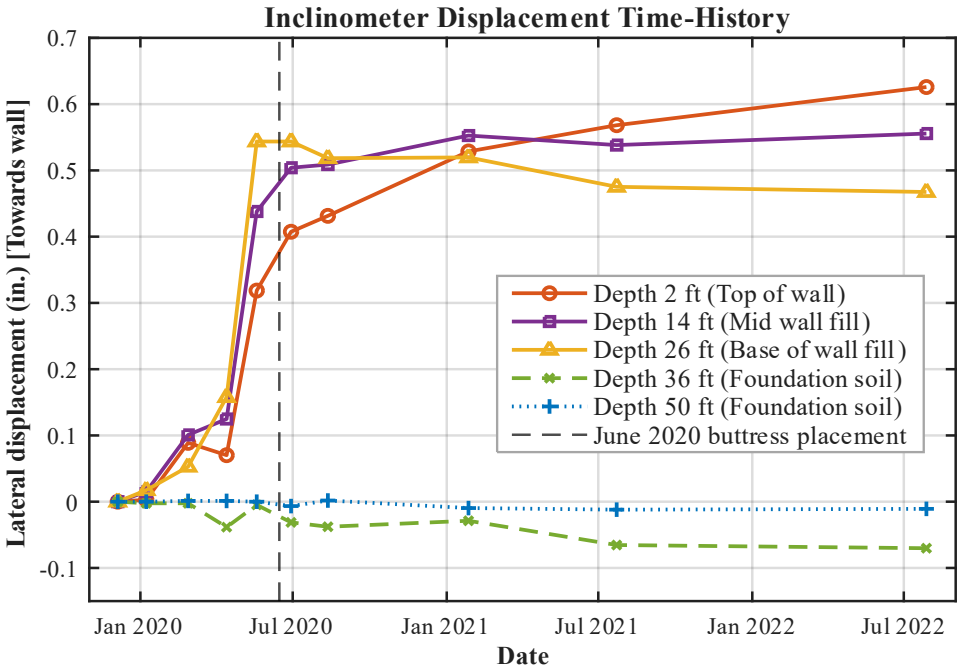


Figure 5-116. Inclinometer displacement time-history at selected depths

Figure 5-117 presents the rate of movement between successive readings and shows the effect of the stabilization berm. Movement was slow through the winter of 2020, then accelerated sharply over the 36-day interval between April 13 and May 19, 2020, reaching 3.9 in/year at a depth of 26 ft and 2.5 in/year at 2 ft. The berm was placed in June 2020, and every subsequent reading shows a significantly lower rate. At 26 ft the rate fell to approximately zero and remained stable. At 2 ft the rate dropped to 0.21 in/year through the winter of 2020–2021, then to 0.08 in/year and 0.06 in/year in the final two intervals measuring to a reduction of roughly 40 times relative to the pre-berm peak.

The berm was effective at minimizing movement at the base of the reinforced fill. Movement of the upper part of the embankment slowed sharply but did not stop entirely. The location of the maximum displacement migrated upward over the monitoring period, from 26 ft in May 2020 to 4 ft by July 2022. The berm restrains the wall near its toe, and the residual movement recorded in the upper profile is consistent with continued, much slower outward leaning of the upper portion of the wall.

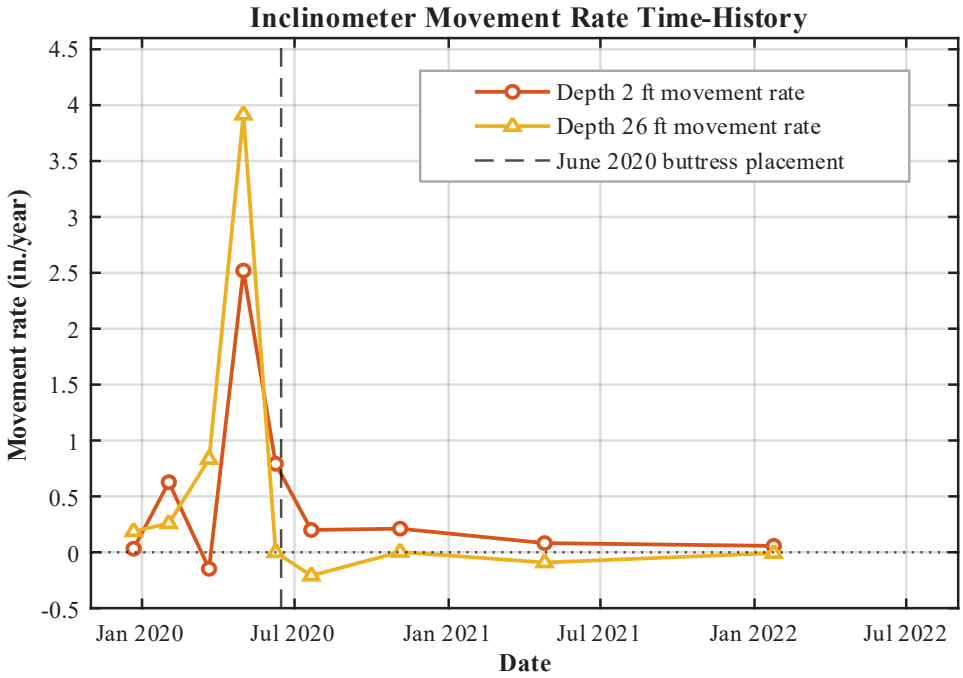


Figure 5-117. Rate of lateral movement between successive inclinometer readings at depths of 2 ft and 26 ft, showing the reduction in rate following the June 2020 buttress placement.

Two limitations should be stated with these results. The record comes from a single casing at one location and describes the movement of the casing and the ground immediately surrounding it, not the translation or rotation of the wall panels themselves, which were not surveyed. In addition, the total lateral movement recorded through July 2022, approximately 0.63-inch, is an order of magnitude smaller than the approximately 5.5-inch lateral separation measured between the ramp pavement and the gore area during the October 2025 field evaluation. These two quantities are not directly comparable: the separation at the longitudinal joint accumulates over the full history of the section and includes translation of the pavement slab itself, whereas the inclinometer records ground movement at one point over a 32-month window that ended more than three years before the field evaluation. Monitoring data after July 2022 was not available at the time of writing this report, so the record cannot establish whether movement resumed.

5.8.8 Potential Distress Mechanism

Based on the synthesis of the visual surveys, FWD data, GPR scans, inclinometer record, and material testing, the following sequence of events appears to be the most plausible explanation for the observed distress. The evidence strongly suggests that the distress is driven by moisture-induced lateral instability rather than a deep-seated foundation issues.

The mechanism likely initiated with surface water infiltrating the embankment through open construction joints, specifically at the joint between the BAS and the main pavement, and the gore

area and the ramp. As moisture accumulated and pore water pressure developed, it likely built up significant hydrostatic pressure against the wall panels.

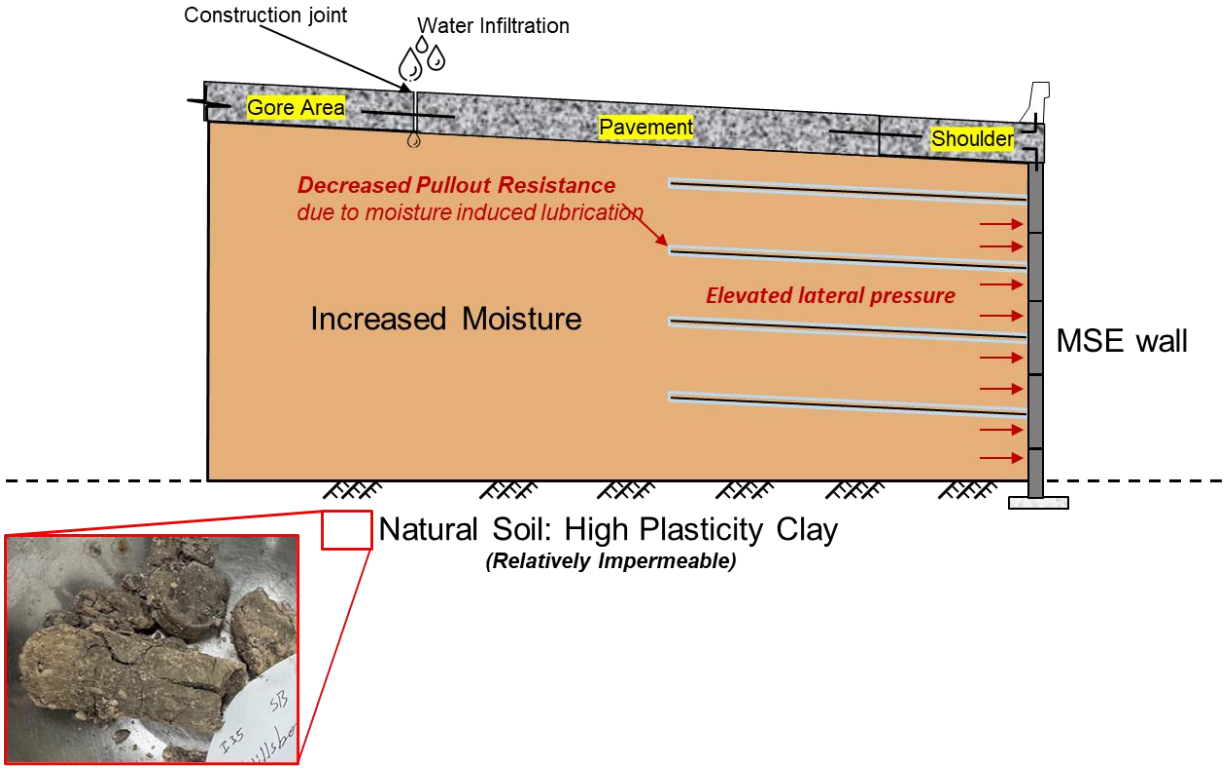
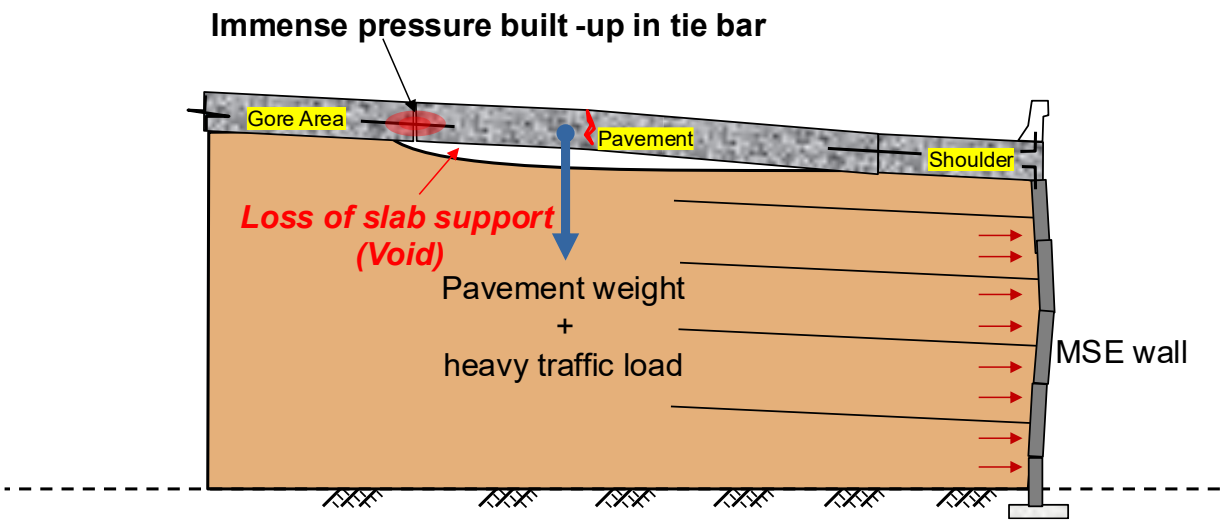
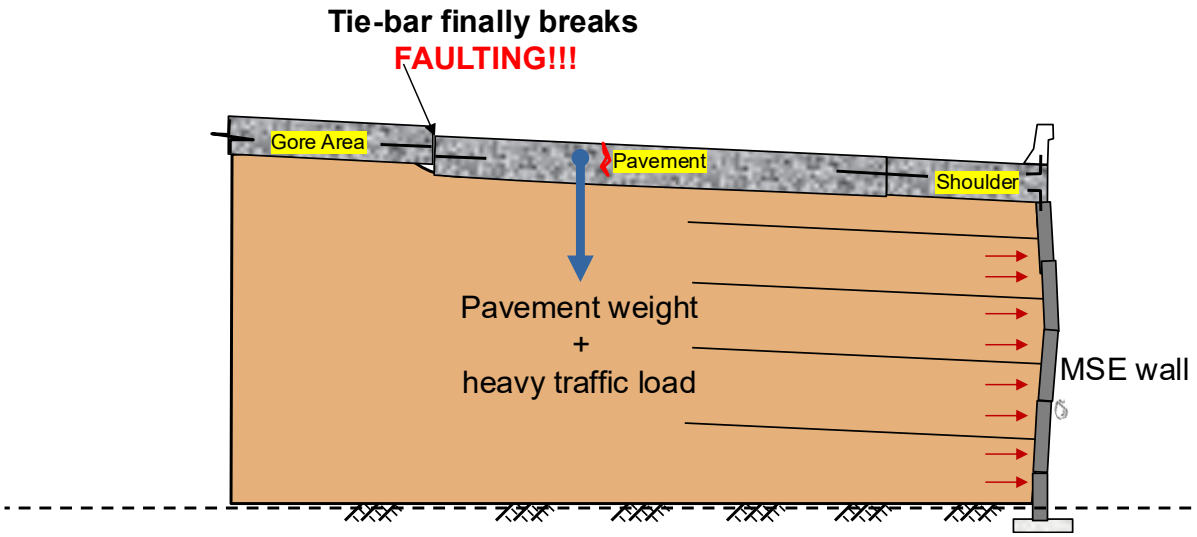


Figure 5-118. Initial phase: Water infiltration leading to elevated lateral pressure and reduced reinforcement friction.

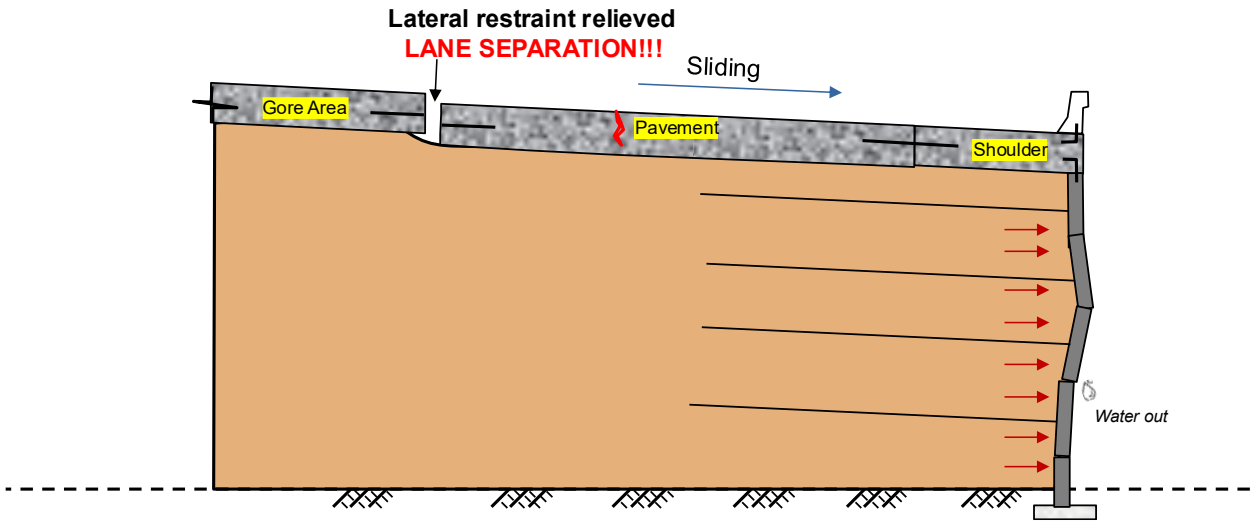
Under this increased lateral pressure, the MSE wall panels began to bulge outward. The soil mass likely displaced laterally along with the moving wall. This lateral displacement of the fill created a separation between the pavement slab and the subgrade, resulting in void formation. With the subgrade moving laterally and receding, the pavement slab lost its vertical support, effectively acting as a cantilever supported largely by the tie bars connecting the ramp slab to the adjacent gore area. The combined weight of the concrete slab and the dynamic loading from heavy traffic placed immense shear and tensile stress on these tie bars. Since these bars are designed primarily to prevent lane drift rather than support the structural weight of the slab, they yielded. Once this lateral restraint was compromised, the pavement followed the movement of the subgrade, sliding laterally with the retaining wall. This movement manifested as the observed faulting and the lane separation between the gore area and the ramp. This separation widens the path for further water infiltration, accelerating the saturation of the embankment and further destabilizing the wall system. **Figure 5-119** illustrates this process.


Immense pressure built -up in tie bar
Gore Area
Pavement
Shoulder
Loss of slab support
(Void)
Pavement weight
+
heavy traffic load
MSE wall

(a)


Tie-bar finally breaks
FAULTING!!!
Gore Area
Pavement
Shoulder
Pavement weight
+
heavy traffic load
MSE wall

(b)



(c)

Figure 5-119. Progress of distress: (a) Lateral subgrade movement creates a void, (b) transferring immense load to the tie bars causing them to yield and fracture, and (c) lane separation and further MSE wall bulging

Additionally, the specific shape and orientation of the observed cracks provide further evidence for this failure sequence. We theorize that the structural failure of the slab occurred in two distinct phases. First, faulting likely occurred at pavement and gore-area joint while the pavement was still fully connected at the approach end of the BAS. This created a condition of non-uniform settlement where the edge of slab dropped into the underlying void while its ends remained restrained. This differential movement resulted in the formation of the distinct halfmoon-shaped crack observed on site.

With the wall continuing to bulge outward and the lateral restraint removed, the pavement slab began to experience significant shear forces. As illustrated in the free-body diagram in **Figure 5-120**, this secondary shear movement generated a series of parallel diagonal cracks perpendicular to the original halfmoon fracture.

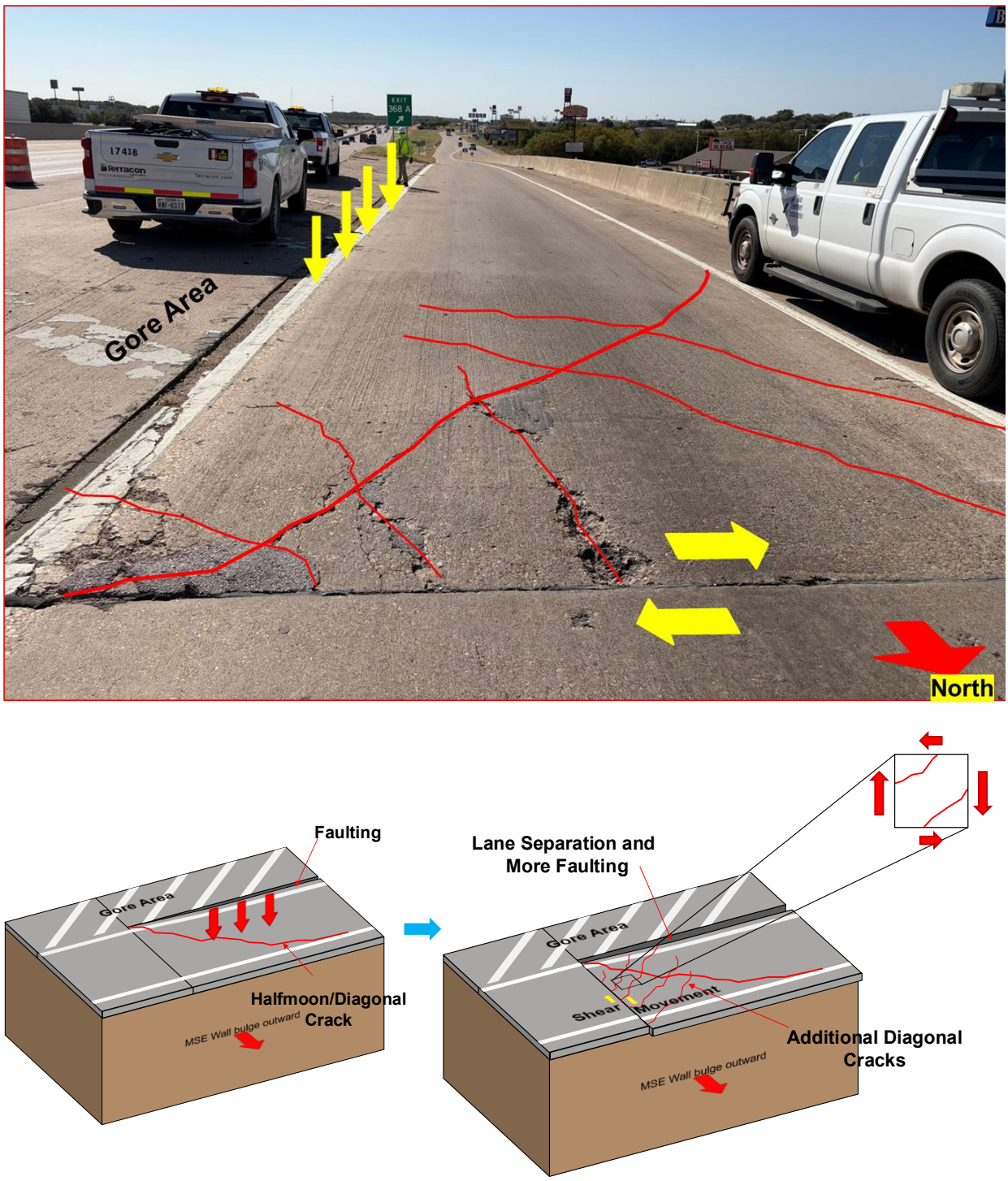


Figure 5-120. Proposed cracking sequence: Initial faulting causes halfmoon cracks, followed by shear movement causing parallel diagonal cracks.

5.8.9 Repair Recommendation

Similar to Section E-5 (Beltway 8), the long-term effectiveness of any pavement repair at this location is contingent upon the global stability of the MSE retaining wall. The existing MSE wall is currently supported by a berm consisting of recycled asphalt to counteract lateral earth pressures and prevent further bulging. Once the global stability of the MSE wall is verified, the following two repair options are proposed:

Option 1 focuses on re-establishing the longitudinal connection between the ramp and the gore area, minimize further water infiltration, and correcting the profile at the Bridge Approach Slab (BAS) by taking the following measures:

- Void Filling: Inject High-Density Polyurethane Foam (HDPF) to fill identified voids beneath the BAS and re-establish slab support.
- Longitudinal Joint Repair: Perform a "cut-and-fill" operation at the longitudinal joint between the ramp and gore area. This involves removing approximately 1.5 feet of concrete on both sides of the joint, installing new tie bars (drilled and epoxied at 2-foot intervals), and pouring new concrete to fill the gap.
- Surface Leveling: Apply an asphalt overlay or level-up course to the BAS and settled slab sections to correct the profile and improve ride quality.



Figure 5-121. Illustration of proposed layout for Repair Option 1 (cut-and-fill/overlay)

Option 2 is to fully restore the pavement's structural capacity. The field investigation revealed that the high FWD deflections in the ramp are largely attributed to reduced slab thickness and the presence of thick HDPF layers beneath the slab from previous repairs, which act as a compressible cushion rather than a rigid slab support. Accordingly, this option involves removing existing CRCP slab and excavating the underlying HDPF layer. A new base layer would then be added to level the grade, providing a stable, uniform foundation for the construction of a new, 13" CRCP slab. As with Option 1, voids under the BAS would be filled with HDPF, and the tie connection at the ramp-gore area would be restored.

It is important to note that continued monitoring of the section is required for both Options 1 and 2. If significant movement or separation recurs, the stability of the MSE wall must be re-evaluated, and more aggressive stabilization measures or reconstruction may become necessary.

5.9 Section E-1: IH 27 in Keuka Street, Lubbock

5.9.1 Overview

The BAS and nearby pavement on the northbound and southbound mainlanes of IH 27 at E Keuka Street in Lubbock, Texas (**Figure 5-122**), was built on a roadway embankment approximately 24 feet in height. Field evaluations of Section E-1 were conducted on August 13 and August 14, 2025, by the Research Team to investigate the subsurface conditions and pavement structure. Outside lane and outside shoulder of both direction road in both approach and departure sides were investigated. The pavement type of this section is a 9-in thick continuously reinforced concrete pavement (CRCP) with a 5 to 6-in. asphalt stabilized base (ASB) as shown in **Figure 5-123**. The bridge approach slab has a thickness of 10 inches. According to the plan sets, the project (CSJ 0067-07-054/059) was constructed between October 18, 1978, and May 13, 1981.

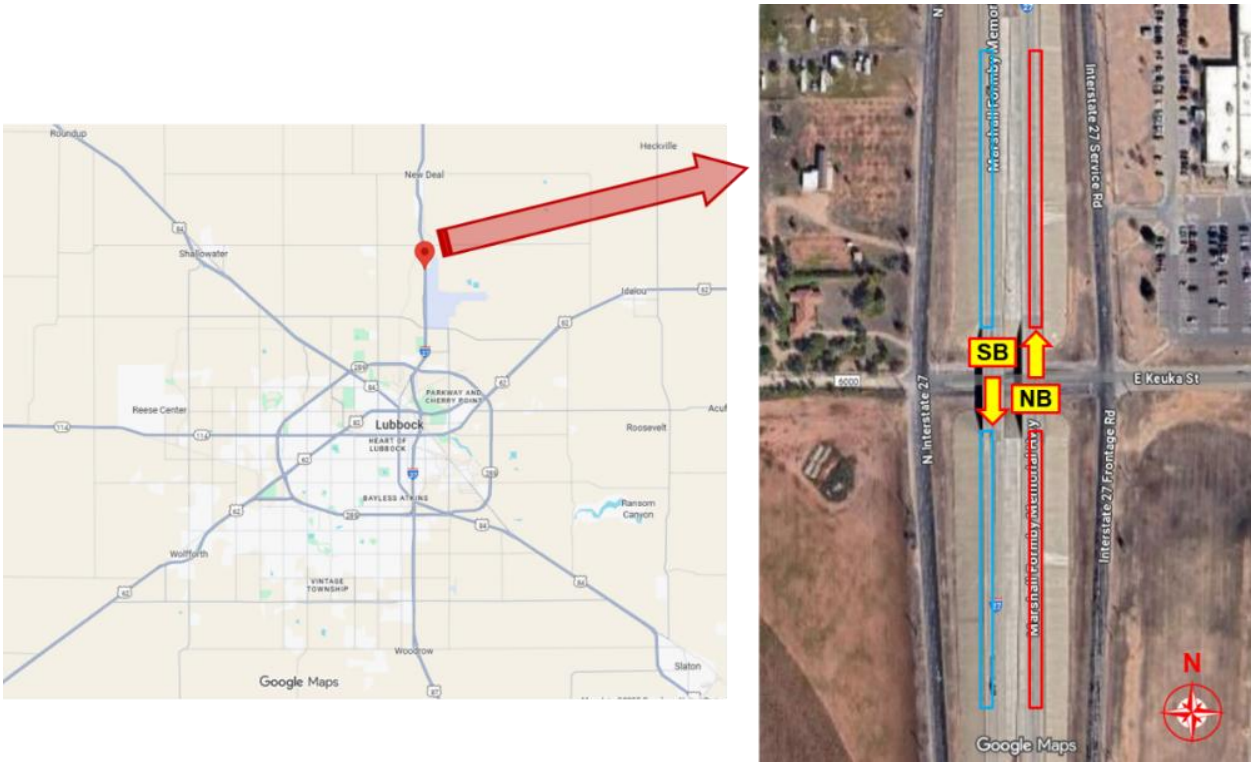


Figure 5-122. Location of Section E-1 on IH-27 in Lubbock, Texas

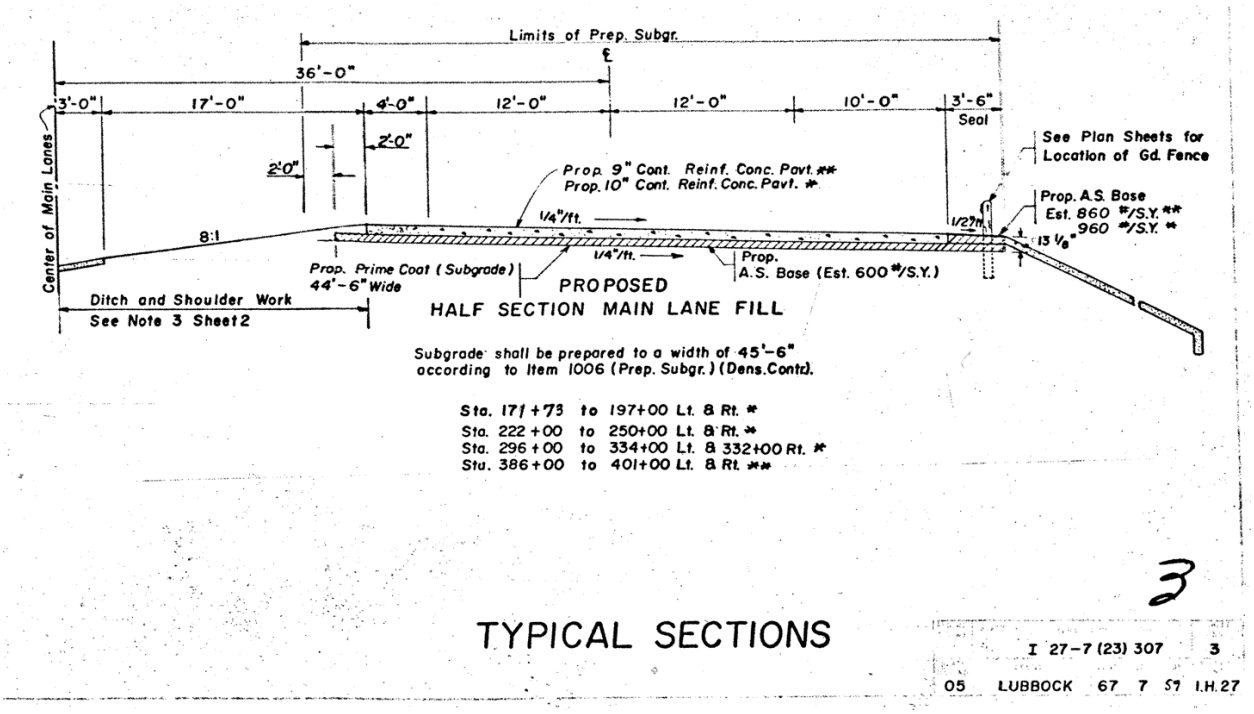


Figure 5-123. Typical section of Section E-1 on IH-27 in Lubbock, Texas

This section has exhibited moderate settlement of the bridge approach slab over the years. A visual survey revealed additional surface distresses, including longitudinal cracking on both northbound and southbound approaches and concrete patches to address lane separation. The pavement was saw-cut approximately 1 to 2 ft on either side of the longitudinal joint where separation occurred in the past, and tie bars were subsequently installed and grouted along both edges to restore load transfer. The current condition of the patch is presented in the **Figure 5-124**.



Figure 5-124. Current condition of patch to address lane separation observed in SB departure

5.9.2 Falling Weight Deflectometer (FWD) tests

FWD tests were conducted on the outside lanes and outside shoulders of both the northbound (NB) and southbound (SB) main lanes. Spacing between FWD drop locations was approximately 10 ft on the pavement sections and 2 ft on the bridge approach slab (BAS). FWD deflections at a 9,000-lb loading were evaluated. **Figure 5-125** presents the FWD drop locations and the collected deflection data along the test section. Consistently lower deflections were observed in the area where anchor lugs were located. The anchor lugs were located at 16 to 17 feet spacing, and 16 feet away from sleeper slab or BAS-pavement joint. A noticeable peak in deflection was observed between the anchor lugs, suggesting the potential presence of voids between the lug structures. This observation is consistent with findings from TxDOT Research Project 0-6326 (Jaiswal *et al.*, 2012), which reported that slab movement causes permanent deformation of embankment soils

adjacent to lug walls. As the lugs move back and forth, the soil does not fully retract, leaving voids behind.

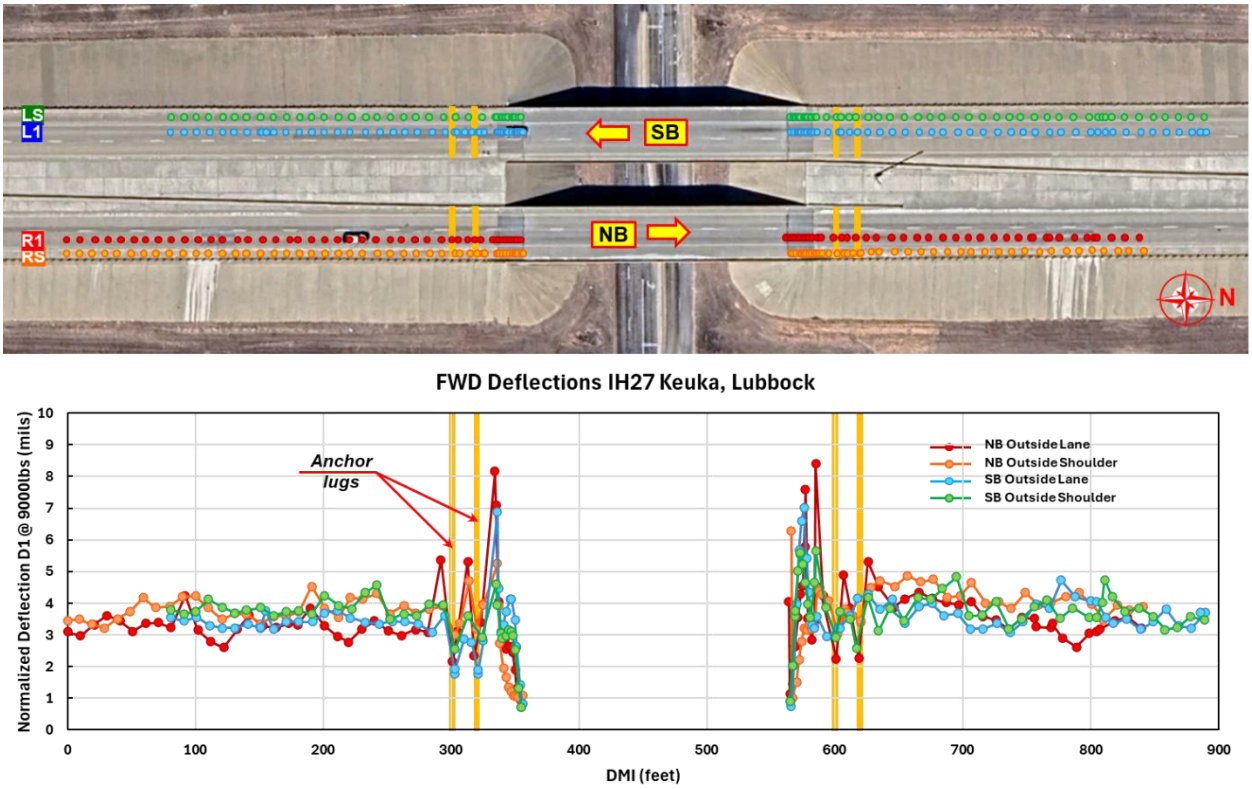


Figure 5-125. FWD testing locations and deflections measured at the outside lanes and shoulders of northbound and southbound main lanes

Northbound

The FWD deflections from the northbound (NB) outside lane and outside shoulder are shown in **Figure 5-126**. For the pavement sections away from the bridge (e.g., DMI 0 to 300 ft and DMI 650 to 900 ft), deflection values for both the outside lane and outside shoulder were generally in the range of 2 to 4 mils. Significantly higher deflections were observed on the bridge approach slab (approx. DMI 330 to 350 ft) and the departure slab (approx. DMI 580 to 600 ft).

The NB outside lane exhibited the highest deflections, with a sharp peak exceeding 8 mils on the sleeper slab area of approach and departure slab. Coring at either side of transverse BAS-pavement joint revealed separation of 0.5 inches between BAS and the sleeper slab which will be discussed in the further section.

The NB outside shoulder followed a similar trend but with lower peak deflections: about 5 mils on the approach slab and 6 mils on the leave slab. Deflections tapered from the sleeper-slab peak to minimal values near the bridge abutment, where the slab was well supported. Coring confirmed

that the BAS in this direction did not include an asphalt base layer and instead rested on a flex base. No voids were observed near the mid-slab region of the BAS.

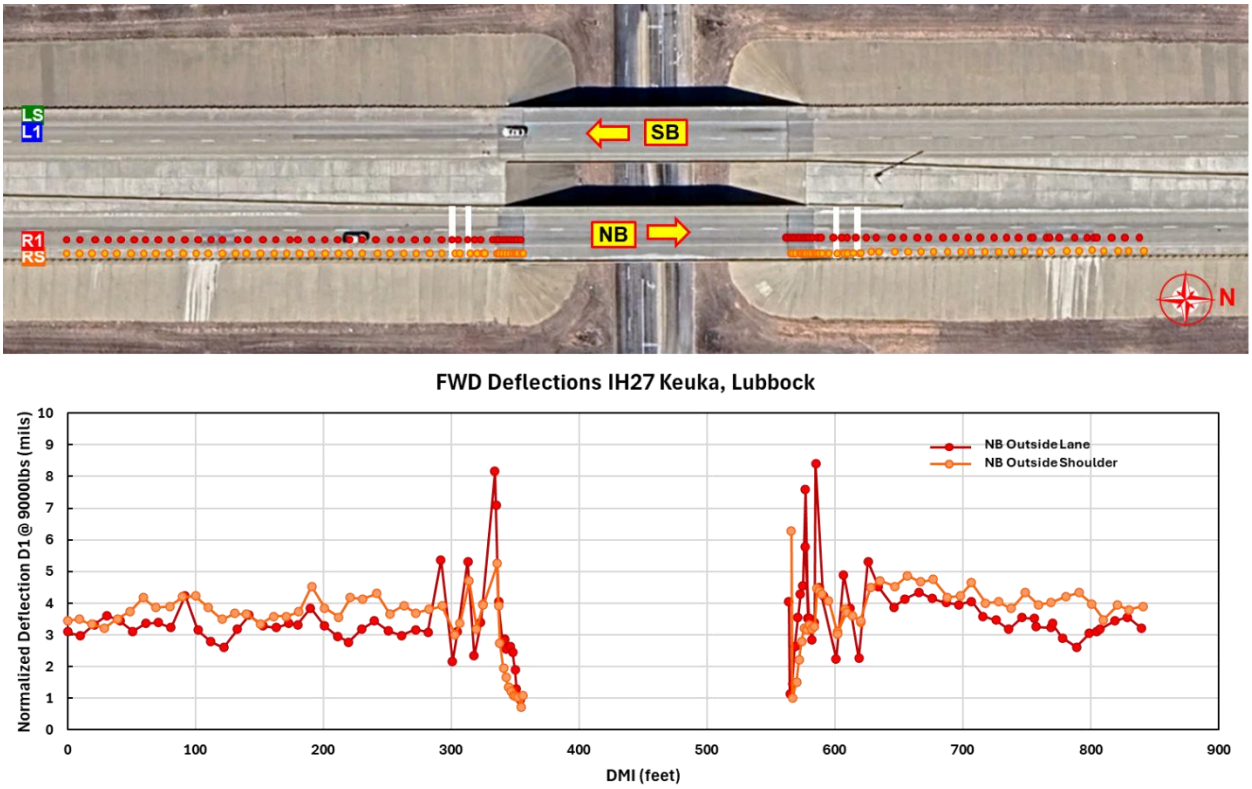


Figure 5-126. FWD testing locations and deflections measured at the outside lanes and shoulders of northbound main lanes

Southbound

Figure 5-127 presents the FWD deflections for the southbound (SB) outside lane and outside shoulder. Similar to the northbound direction, the pavement sections showed relatively low and consistent deflections, typically between 3 and 4 mils. Elevated deflections were recorded on both the approach and departure slabs. The SB outside lane showed peaks of approximately 7 mils on both the approach and departure sides, indicating potential issues at both ends of the bridge. The SB outside shoulder followed a similar pattern to the outside lane, though with slightly lower peak deflections, generally staying below 5.5 mils.

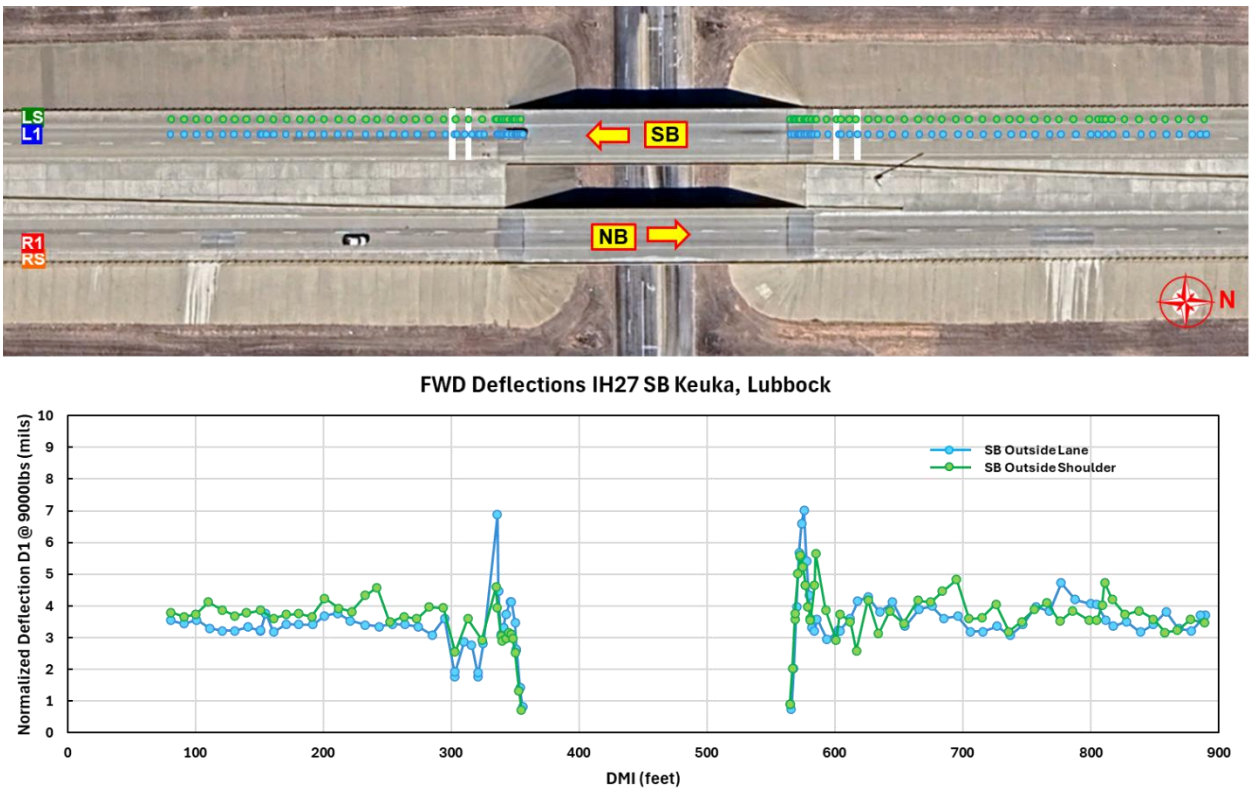


Figure 5-127. FWD testing locations and deflections measured at the outside lanes and shoulders of southbound main lanes

A statistical summary of the deflection data is presented in the box plot in **Figure 5-128**. The plot shows that the median deflection for most sections is consistent, generally falling between 3 and 4 mils. However, the box plot highlights the greater variability and the presence of significant outliers in the northbound direction. Specifically, the northbound approach outside lane ("IH27NB_APP_OUTLN" in **Figure 5-128**) exhibits a wider range of deflections and several high-end outliers, with values reaching up to 8.5 mils. This confirms the presence of localized, poor-performing areas identified in the deflection profile plots and indicates a less uniform structural support compared to the southbound sections.

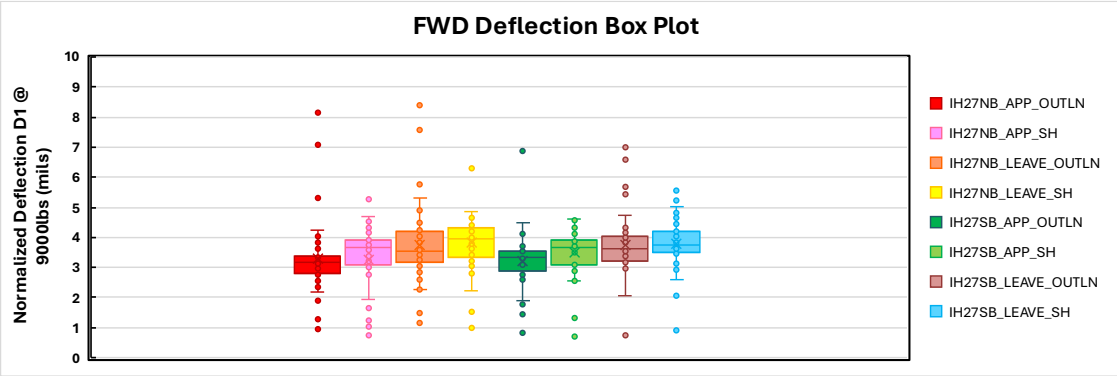
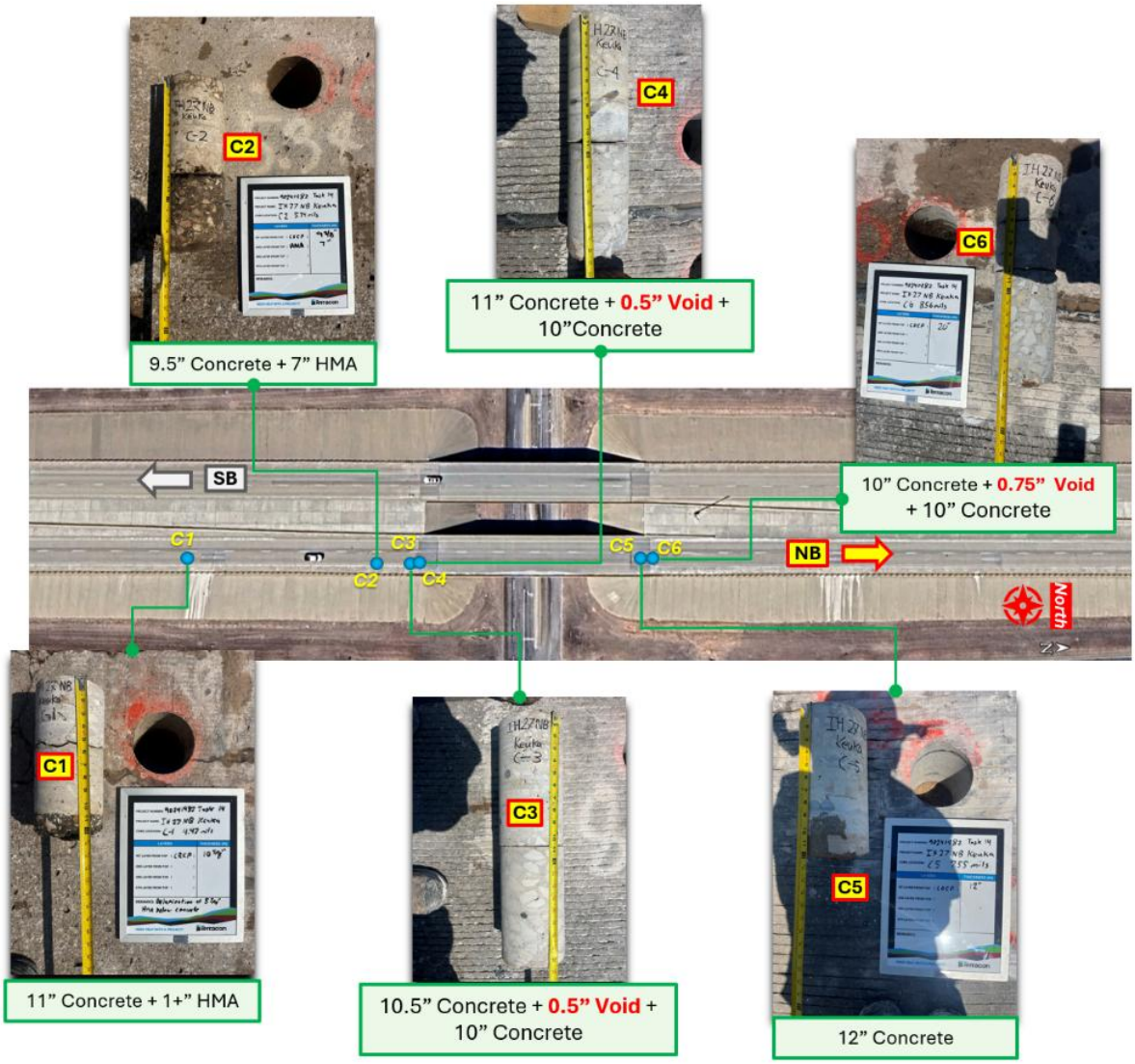


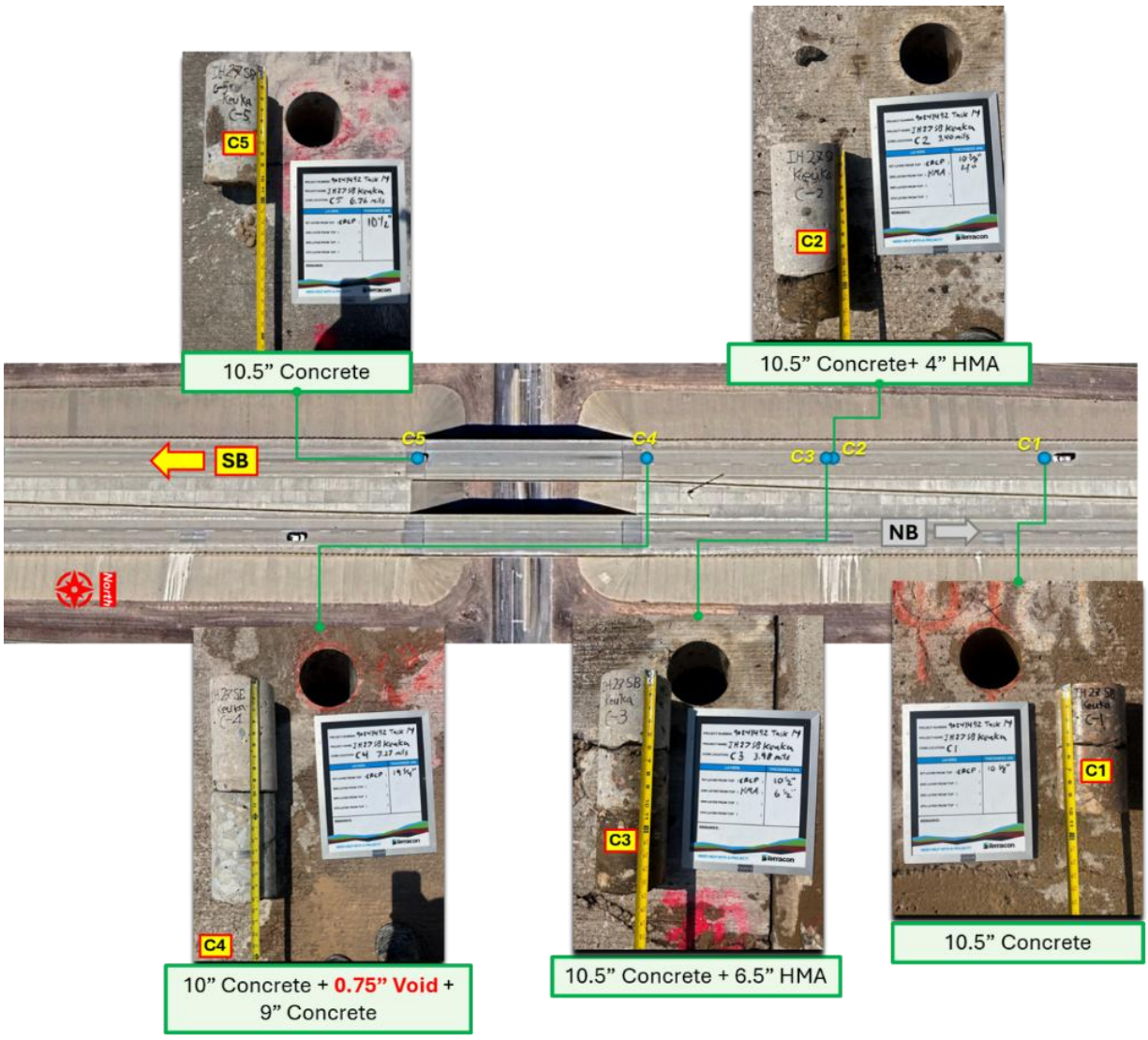
Figure 5-128. FWD deflection box plot summarizing data from all tested locations.

5.9.3 Coring

Coring was conducted at selected locations along both the northbound and southbound main lanes to verify layer thickness, and provide access for further testing activities like DCP, CPT and soil sampling. Five cores were extracted from southbound roads (both approach and departure) on Day 1 and additional six cores from northbound on Day 2. The locations and images for all the coring samples are presented in **Figure 5-129(a)** and **Figure 5-129(b)** for northbound and southbound respectively.


C2
C4
C6
9.5" Concrete + 7" HMA
11" Concrete + 0.5" Void + 10"Concrete
10" Concrete + 0.75" Void + 10" Concrete
SB
NB
C1
C3
C2
C4
C5
C6
North
C1
C3
C5
11" Concrete + 1+" HMA
10.5" Concrete + 0.5" Void + 10" Concrete
12" Concrete

(a)



(b)

Figure 5-129 Coring locations and images of core samples: (a) Northbound and (b) Southbound

The extracted cores generally confirmed that the surface layer structure of this site consisted of a 9- to 11-in CRCP underlain by a 5- to 7-in asphalt-stabilized or HMA base. The bridge approach slabs were typically 10 to 11 in thick and rested directly on a flex base layer without an asphalt layer. The sleeper slabs appeared as isolated concrete blocks without integral connection to the pavement structure.

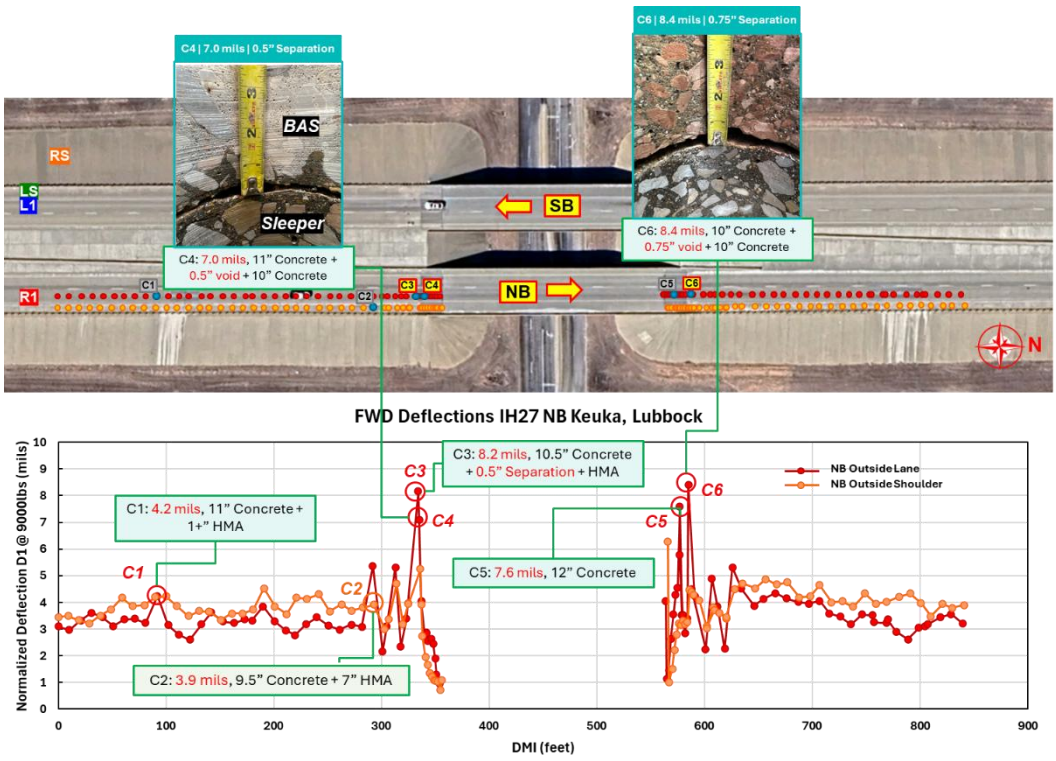
Figure 5-129(a) illustrates the coring locations and extracted cores for the northbound lanes. Cores C3, C4, and C6, taken near the BAS-pavement joint, showed visible separation between the BAS and the sleeper slab, ranging from 0.5 to 0.75 in, consistent with the elevated FWD deflection spikes in the same regions. Cores from the southbound lanes displayed similar trends. The

approach slab cores (e.g., C4 and C3) again showed separation (or void) of 0.5-0.75 in between the CRCP bottom and the sleeper slab. Photographic evidence of this separation for Southbound C4 is presented in **Figure 5-130**.

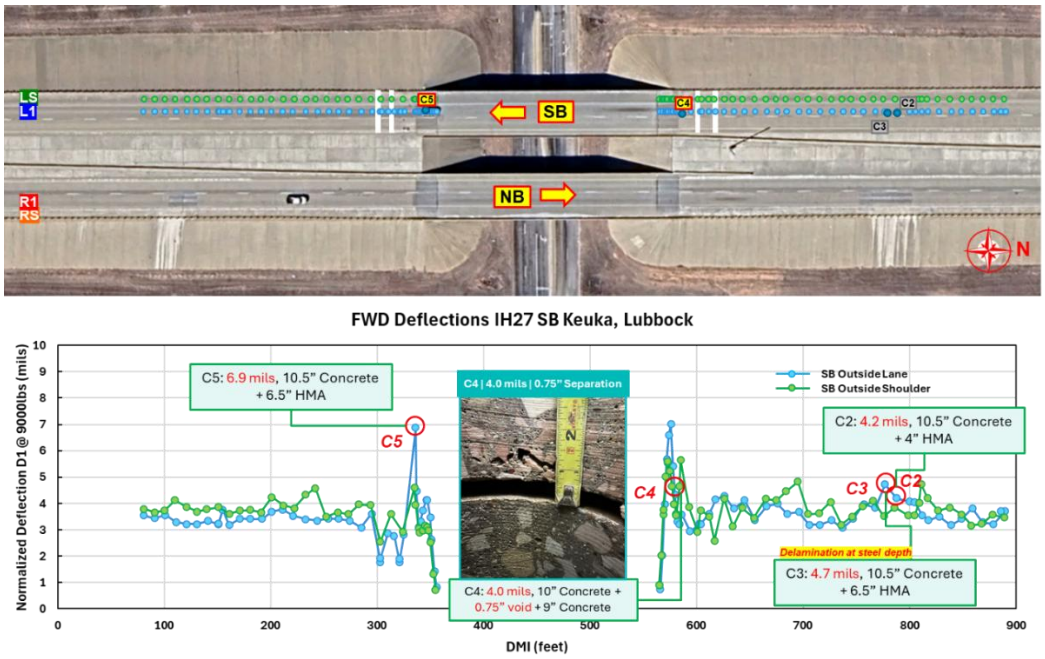


Figure 5-130. Photo of inside of C4 cored hole (0.5-in-thick void is observed between CRCP bottom and top of sleeper slab)

The voids observed at sleeper slab locations correlated directly with the high-deflection spikes observed in the FWD data. For instance, in the northbound lanes, Core C4 was taken from a location with a 7.0 mil deflection and revealed a 0.5-inch separation between the bridge approach slab and the sleeper slab. An even larger 0.75-inch separation was measured at Core C6, corresponding to the peak deflection of 8.4 mils. The southbound lanes showed the same distress; a 0.75-inch void was clearly documented in Core C4 (**Figure 5-131**), validating the high FWD measurements recorded at that location.



(a)



(b)

Figure 5-131. Separation between pavement and sleeper slab measured from coring in relation to FWD deflection at (a) southbound and (b) northbound roads

In addition to the loss of support due to voids, several cores revealed internal pavement distress. The core sample from C3 Southbound exhibited delamination at the depth of the reinforcing steel, often accompanied by visible corrosion on the longitudinal bars. This corrosion was also observed externally on the pavement surface near a longitudinal repair and at the southbound departure abutment (**Figure 5-132(a)** and **Figure 5-132(b)**, respectively). These conditions suggest that repeated deicing salt application has likely led to chloride ingress, accelerating the deterioration of the embedded steel and contributing to the delamination.

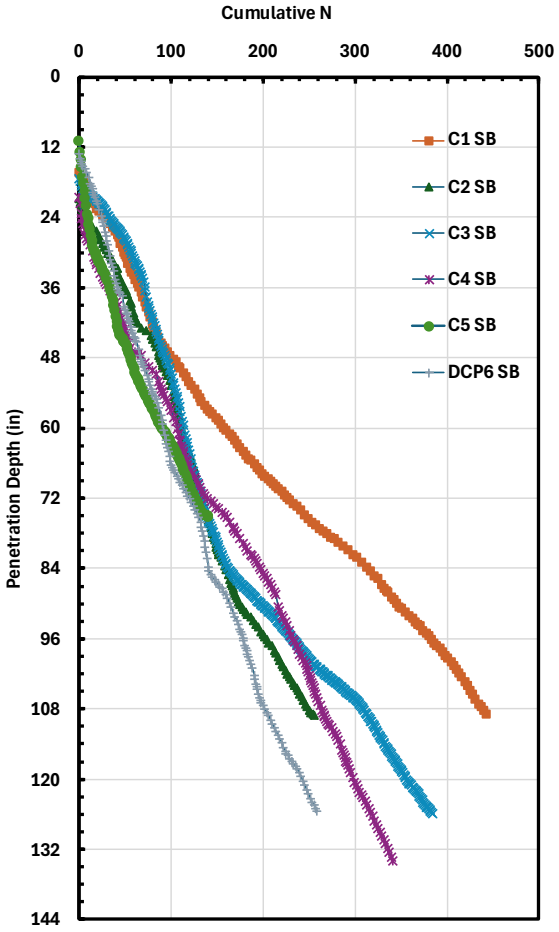


(a) (b)

Figure 5-132. Corrosion observed in (a) Pavement surface near longitudinal joint, (b) SB departure side Abutment (outside lane)

5.9.4 Dynamic Cone Penetration (DCP) tests

Following the coring, DCP tests were conducted through the cored holes to evaluate the in-situ strength and stiffness of the base and underlying embankment materials. The results are presented in two formats: plots of cumulative blows versus penetration depth, which illustrate the overall material resistance, and layer-wise bar charts that quantify the strength of discrete depth intervals. In the cumulative plots, a flatter slope indicates stiffer material, while a steep slope signifies weakness. In the bar charts, higher resistance values (green) represent competent material, while lower values (orange and red) indicate moderate and severe weakness, respectively. The results for the southbound and northbound lanes are presented in **Figure 5-133** and **Figure 5-134**, respectively.



(a)

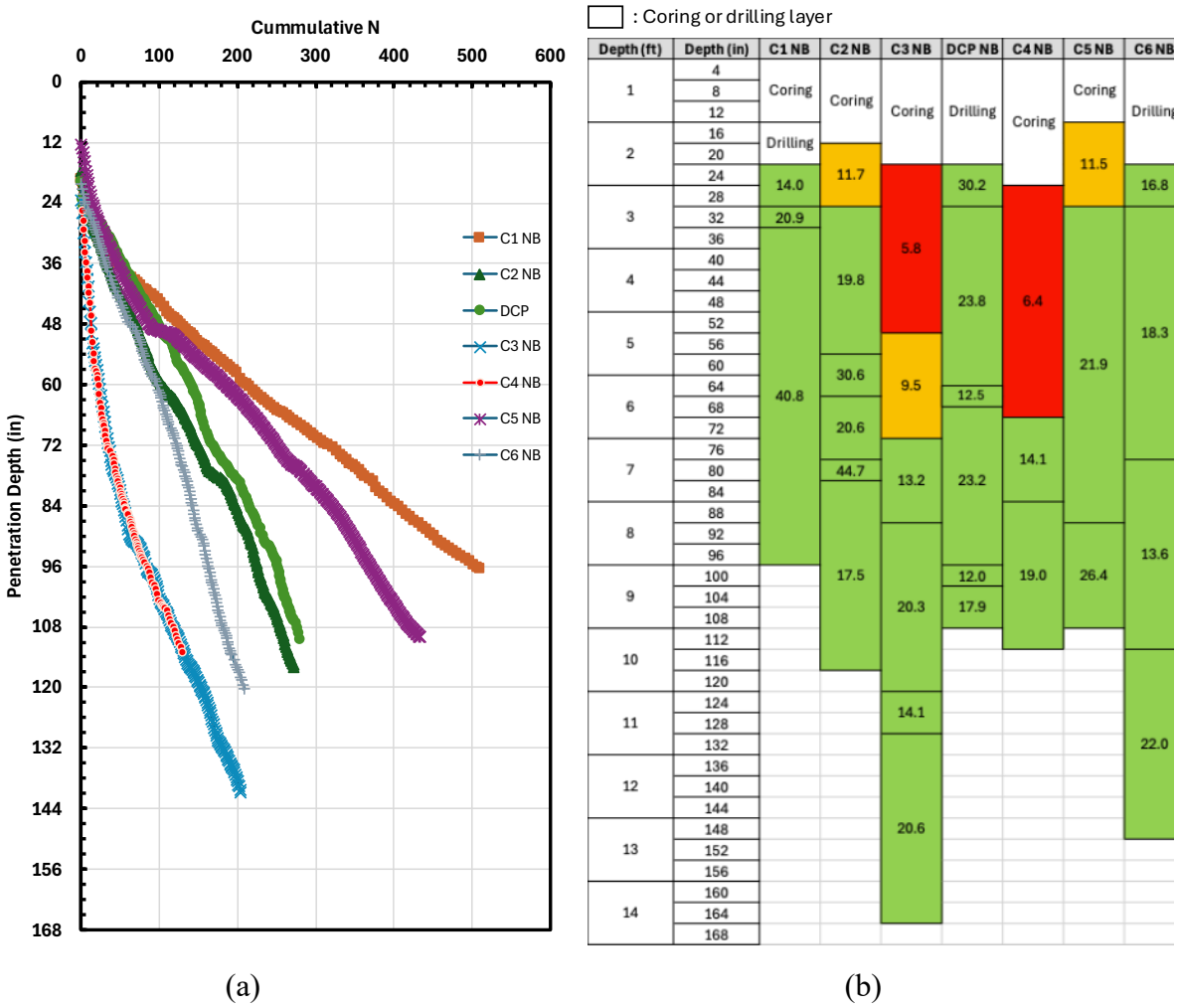
: Coring or drilling layer

Depth (ft)	Depth (in)	C1SB	C2 SB	C3 SB	C4 SB	C5 SB	DCP6 S
1	4	Coring	Coring	Coring	Coring	Coring	Drilling
	8	Drilling	Drilling				
	12						
2	16					8.6	
	20	25.1		29.7	10.6		
	24						
3	28						
	32	18.5				19.7	15.1
	36			19.8			
4	40				21.5	10.9	
	44						
	48	27.5					
5	52		21.7	12.3		20.9	
	56				16.5		11.4
	60						
6	64						
	68						
	72				30.9		22.4
7	76					61.2	
	80	35.6		18.9			9.8
	84						
8	88						
	92			34.7			
	96		26.1				
9	100				20.6		
	104	26.5					19.6
	108						
10	112						
	116						
	120			26.3			
11	124						
	128						
	132						
12	136						
	140						
	144						

(b)

Figure 5-133. DCP test results for Southbound main lanes (a) Cumulative N plot (b) Resilient modulus determined from DCP test

The DCP results for the southbound lanes show relatively consistent, but moderately weak, shallow depth soil support in the bridge approach slab area. The cumulative blow count plot (**Figure 5-133(a)**) shows that the profile at C1 SB, away from the bridge, is the flattest, establishing it as the stiffest baseline for the area. The other profiles are steeper and clustered together, indicating consistency throughout the testing limits. The layer-wise analysis in **Figure 5-133(b)** provides an easier interpretation. While the underlying layers are generally competent, the profiles at the departure slab (C4 SB) and approach slab (C5 SB) reveal zones of moderately weak material (orange) in the upper 2-4 feet, with M_r values of 10.6 and 8.6. This shallow softening and aligns with separation between pavement layer and sleeper slabs observed in these areas.



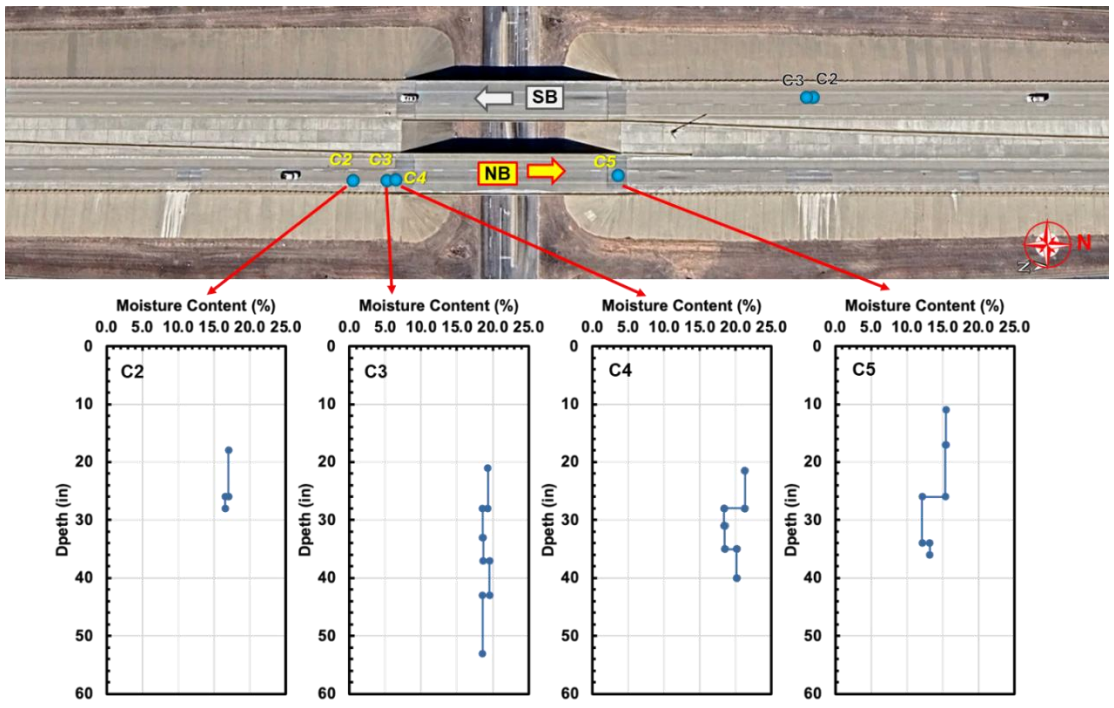
(a) (b)

Figure 5-134. DCP test results for Northbound main lanes (a) Cumulative N plot (b) Resilient modulus determined from DCP test

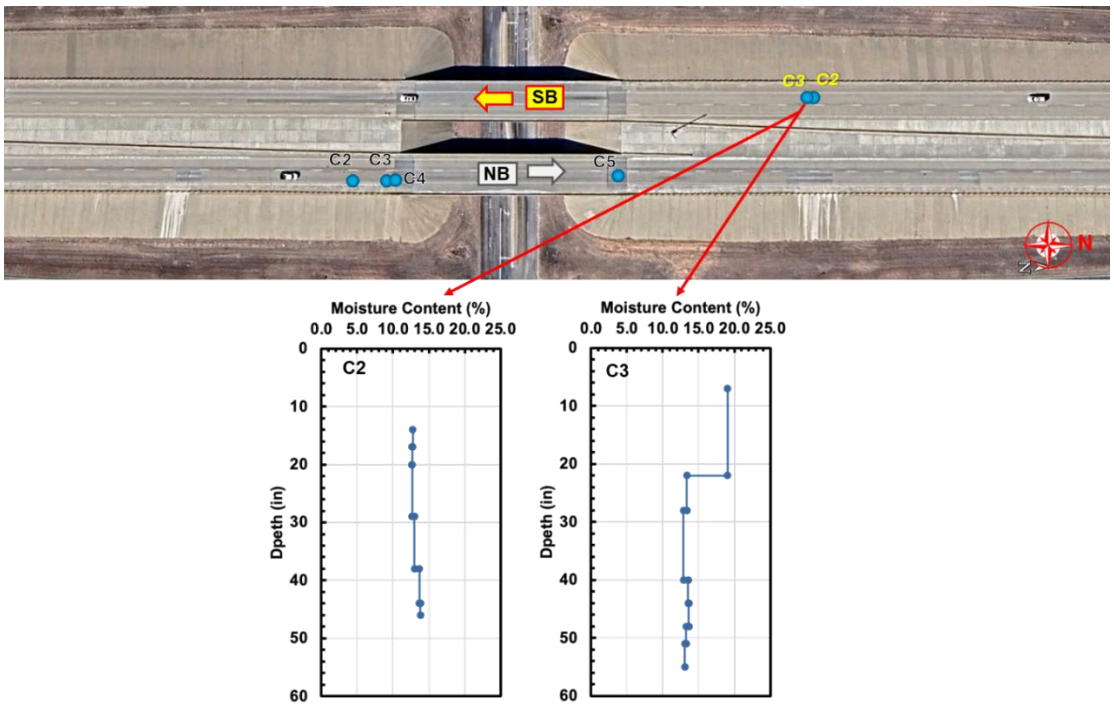
However, the northbound DCP data reveals highly localized weaker embankment layer profile. The cumulative blow count plot in **Figure 5-134(a)** immediately highlights that embankment soil in NB approach (C3 and C4) is exceptionally weaker. The layer-wise chart in **Figure 5-134** shows that profile at C4 and C3 NB contains a thick layer of extremely weak material (red) between approximately 2.5 and 6 feet deep, with a resistance value as low as M_r as low as 6.4 and 5.8 respectively.

5.9.5 Soil Sampling

Soil samples were collected at C2, C3, C4, and C5 from northbound road and C2 and C3 from southbound road. Standard laboratory tests including moisture content analysis, Atterberg limits (Liquid Limit and Plasticity Index), and particle distribution analysis were performed for these grab samples. The location for these cores for both northbound and southbound roads along with moisture content is presented in **Figure 5-135**.



(a)



(b)

Figure 5-135. Location of collected soil sample and moisture content at (a) Northbound and (b) Southbound Road

Southbound

The laboratory test results for the southbound samples are summarized in **Table 5-20**. The embankment material is predominantly composed of fine-grained soils, classified mostly as low-plasticity clays (CL) or clayey sands (SC), with AASHTO classifications of A-6.

Table 5-20. Summary of lab test results (Southbound)

Sampling Location (SB)	Sampling Type (Grab or Shelby tube)	Classification (USCS/ AASHTO[GI])	Sampling Depth (in)	Moisture Content (%)	Retained on #4 (%)	Passing #200 (%)	PI (%)	LL (%)
C2	Grab	-	14 - 17	12.8	-	-	-	-
	Grab	SC/A-6[3]	17 - 20	12.6	18	44	17	30
	Grab	CL/A-6[6]	20 - 29	12.7	1	52	19	33
	Grab	-	29 - 38	13.0	-	-	-	-
	Grab	CL/A-6[5]	38 - 44	13.7	8	54	17	28
	Grab	-	44 - 46	13.8	-	-	-	-
C3	Grab	CL/A-6[7]	7 - 22	19.0	6	52	21	34
	Grab	CL/A-6[10]	22 - 28	13.4	9	52	27	38
	Grab	CL/A-6[6]	28 - 40	12.9	1	52	19	30
	Grab	-	40 - 44	13.5	-	-	-	-
	Grab	CL/A-6[3]	44 - 48	13.6	8	50	14	27
	Grab	SC/A-6[5]	48 - 51	13.3	17	46	20	32
	Grab	-	51 - 55	13.1	-	-	-	-

The moisture content profiles, shown in **Figure 5-135(b)**, are relatively uniform, with most values falling between 12% and 14%. While one sample at C3 registered a higher moisture content of 19%, the overall trend suggests moderately and consistently moist conditions without evidence of localized saturation. The particle size distribution curves (**Figure 5-136**) also show a relatively uniform gradation across different depths and locations. Overall, the southbound embankment is constructed of consistent, moderately plastic, fine-grained material, which aligns with the fairly uniform DCP results for this direction.

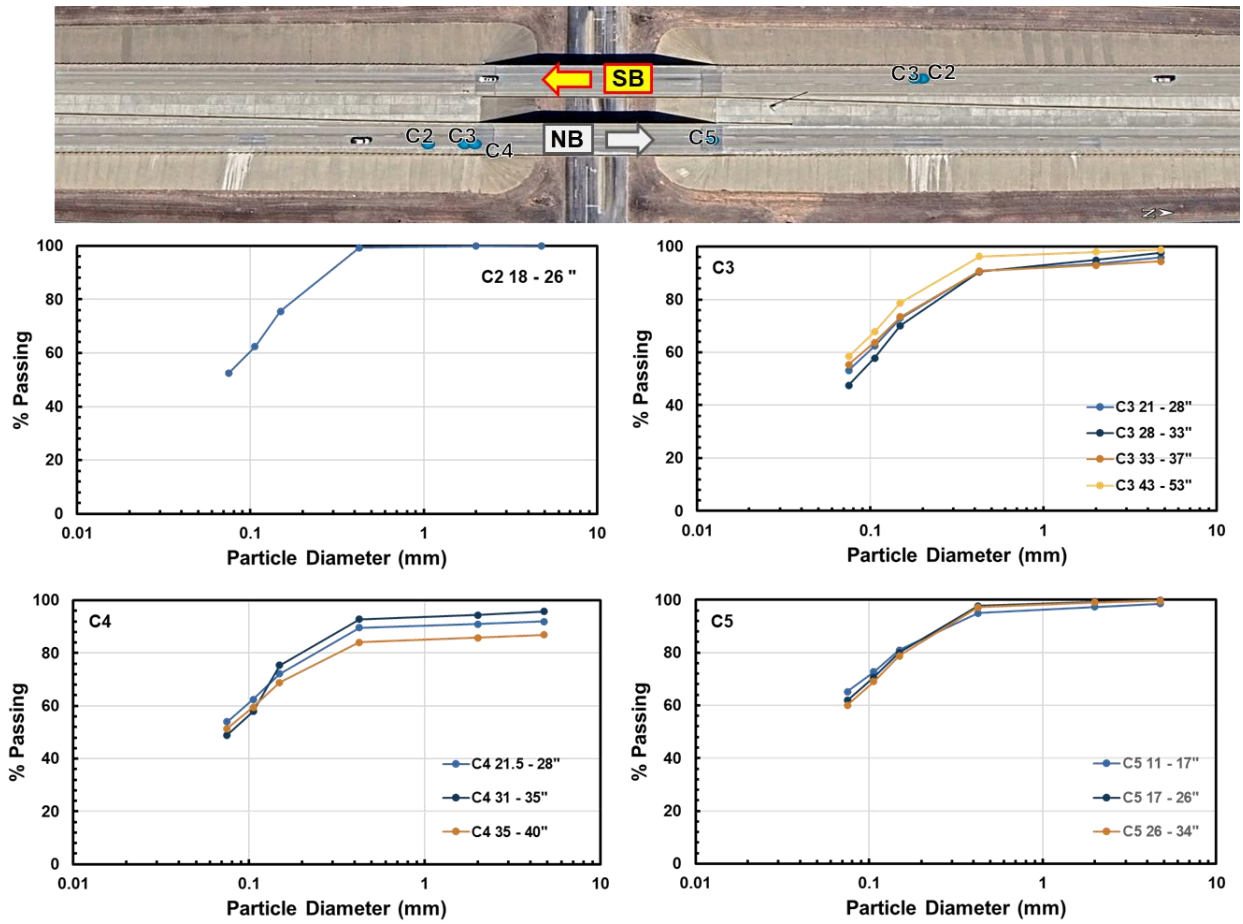


Figure 5-136. Particle Size Distribution for Southbound Soils

Northbound

While the soil types are similar to the southbound side, primarily CL and SC with A-6 and A-7 classifications (see **Table 5-21**), the moisture conditions are dramatically different.

Table 5-21. Summary of Laboratory Test Results for Northbound Soils

Sampling Location (NB)	Sampling Type (Grab or Shelby tube)	Classification (USCS/AASHTO[GI])	Sampling Depth (in)	Moisture Content (%)	Retained on #4 (%)	Passing #200 (%)	PI (%)	LL (%)
C2	Grab	CL/A-6[8]	18 - 26	17	0	53	21	38
	Grab	-	26 - 28	16.6	-	-	-	-
C3	Grab	CL/A-6[5]	21 - 28	19.3	4	53	16	27
	Grab	SC/A-6[4]	28 - 33	18.6	2	47	18	31
	Grab	CL/A-6[7]	33 - 37	18.7	6	55	20	32
	Grab	-	37 - 43	19.5	-	-	-	-
	Grab	CL/A-6[8]	43 - 53	18.6	1	59	19	33
C4	Grab	CL/A-6[7]	21.5 - 28	21.3	8	54	19	32
	Grab	-	28 - 31	18.4	-	-	19	33
	Grab	SC/A-6[6]	31 - 35	18.5	4	49	21	33
	Grab	CL/A-6[7]	35 - 40	20.1	13	51	21	33
C5	Grab	CL/A-6[7]	11 - 17	15.4	2	65	15	28
	Grab	CL/A-6[9]	17 - 26	15.4	0	62	20	32
	Grab	CL/A-6[9]	26 - 34	12.1	0	60	20	32
	Grab	-	34 - 36	13.2	-	-	-	-

The moisture content profiles in **Figure 5-135(a)** reveals that while locations C2 and C5 show moisture contents in the 12% to 17% range, locations C3 and C4 exhibit significantly higher moisture contents, approaching or exceeding 20%.

Specifically, at location C4, the moisture content at a depth between 21 and 40 inches (approximately 1.8 to 3.3 feet) is over 21%. This zone of high moisture content corresponds to the layer of extremely weak material (highlighted in red with a DCP M_r value of 6.4 ksi) identified in the DCP tests presented in **Figure 5-134(b)**. The presence of excess water in this fine-grained, plastic soil has led to a state of saturation, drastically reducing its stiffness. This explains why the DCP cone penetrated this layer so easily.

The particle size distribution curves for the northbound soils (**Figure 5-137**) confirm the fine-grained nature of the material, which makes it susceptible to significant loss of strength when saturated.

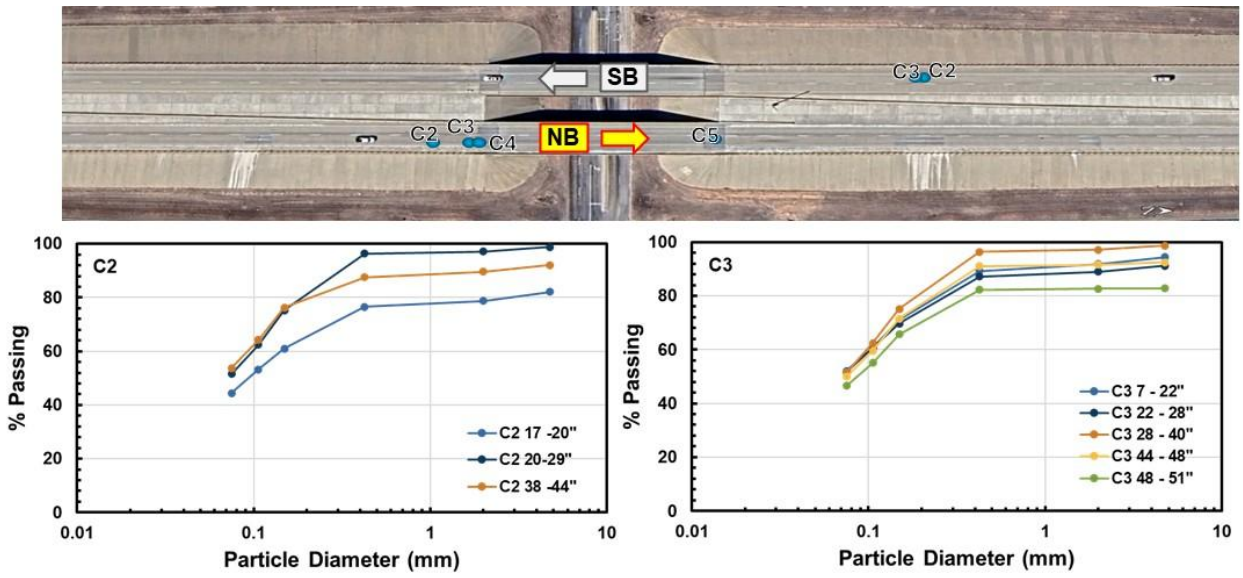


Figure 5-137. Particle Size Distribution for Northbound Soils

In summary, the laboratory testing added to the narration that the northbound bridge approach rests on a localized zone of saturated, weak embankment soil. The direct correlation between the high moisture content, the low DCP resistance values, the high FWD deflections due to separation between sleeper slab and pavement creates a coherent picture of the site's condition.

5.9.6 Potential Distress Mechanism

Based on the synthesis of the visual surveys, FWD data, coring findings, and material testing, the observed conditions at the IH 27 Keuka Street site appear to be the result of typical long-term embankment behavior and serviceability aging rather than structural or geotechnical failure. The distress mechanism is primarily defined by minor differential settlement at BAS.

The mechanism likely originated with the natural, long-term settlement of the embankment fill. The BAS serves as a bridge between the rigid, drilled-shaft-supported abutment and the flexible embankment soil. Over decades of service, the embankment fill, identified as fine-grained Clayey Sand and Lean Clay, has undergone minor consolidation. Because the abutment end of the BAS is fixed while the pavement end rests on the fill, the slab has experienced a slight rotation. This non-uniform support condition resulted in the settlement of the sleeper slab relative to the bridge deck, creating the mild bump observed at the interface. This differential movement created a distinct separation between the bottom of the BAS and the top of the sleeper slab, as illustrated in **Figure 5-138**. Coring investigations confirmed this gap, measuring voids ranging from 0.25 inches to 0.5 inches at the interface. The sleeper slab effectively acted as an isolated block settling with the soil, while the BAS remained partially suspended. This condition explains the specific deflection spikes (up to 8.4 mils) recorded during FWD testing at the BAS-pavement joint, despite the overall embankment remaining fairly stiff.

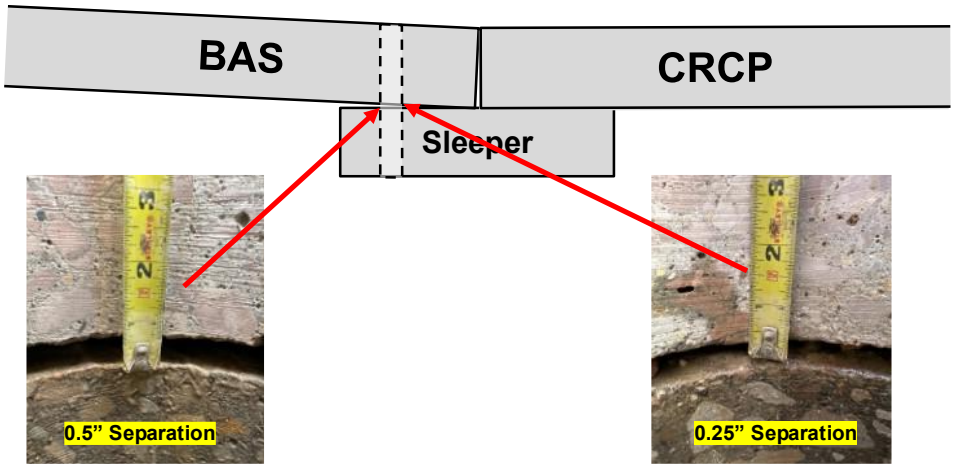


Figure 5-138. Observed separation at the BAS-sleeper slab interface.

Moisture infiltration appears to be a contributing factor to this settlement, particularly in the northbound lanes. Laboratory results identified a zone of elevated moisture content (> 21%) in the northbound approach embankment that aligned with lower stiffness values in the DCP profiles. The infiltration of surface water through the BAS joint likely softened the embankment soils locally, allowing for slightly more settlement in the northbound direction compared to the stiffer southbound section.

Additionally, the site exhibits signs of age-related durability distress common in mature pavements. The long-term application of deicing salts has led to chloride ingress, causing corrosion of the longitudinal steel and delamination at the reinforcement depth. While this has compromised the internal continuity of the slab and contributed to the observed longitudinal cracking, it is a secondary aging mechanism distinct from the settlement-driven behavior at the approach slabs.

5.9.7 Repair Recommendations

Based on the synthesis of field evaluation data, the distresses observed in IH 27 Keuka site may not be attributed to the condition of embankment. The observed distresses are the result of typical long-term embankment behavior over more than four decades of service, compounded by moisture infiltration in the northbound approach and age-related durability deterioration of the concrete pavement. The repair recommendations are therefore focused on restoring slab support at the BAS, preventing further moisture ingress, and addressing the secondary pavement durability issues.

Coring confirmed the separation ranging from 0.25 to 0.75 inches at the BAS-sleeper slab interface on both northbound and southbound approaches. To restore slab-support contact, undersealing with flowable fill (TxDOT Item 401) is recommended at all four BAS-sleeper slab joints. The flowable fill could be injected through the existing investigation core holes. During injection, the application team must monitor the bridge abutment joint and surrounding pavement for identifying leakage.

In addition, several localized areas along the outside edge of the outside lane showed punchout-like distress. These distresses were bound by transverse cracks, a longitudinal crack, and the longitudinal joint. Coring confirmed that the deterioration was primarily partial-depth in nature. Accordingly, partial-depth repair (Item 361) is recommended at these areas to remove the delaminated concrete and restore the slab surface. Crack and joint sealing should also be performed to limit further moisture and chloride infiltration. Epoxy patching (Item 720-7003) may be considered only for very small and shallow surface defects; however, it is not recommended as the primary treatment for the crack-bounded delaminated areas described above.

5.10 Section P-A-5: IH 27 Tulia, Lubbock

5.10.1 Overview

This section is located on Interstate 27 in Swisher County, Texas, within the Lubbock District, as shown in the location map in **Figure 5-139**. The site features a bridge overpass on an embankment approximately 32 feet high. The Research Team conducted a field evaluation on August 11 and 12, 2025, to investigate the causes of significant pavement distress observed at the bridge's approaches. A summary of the site information is provided in **Table 5-22.**

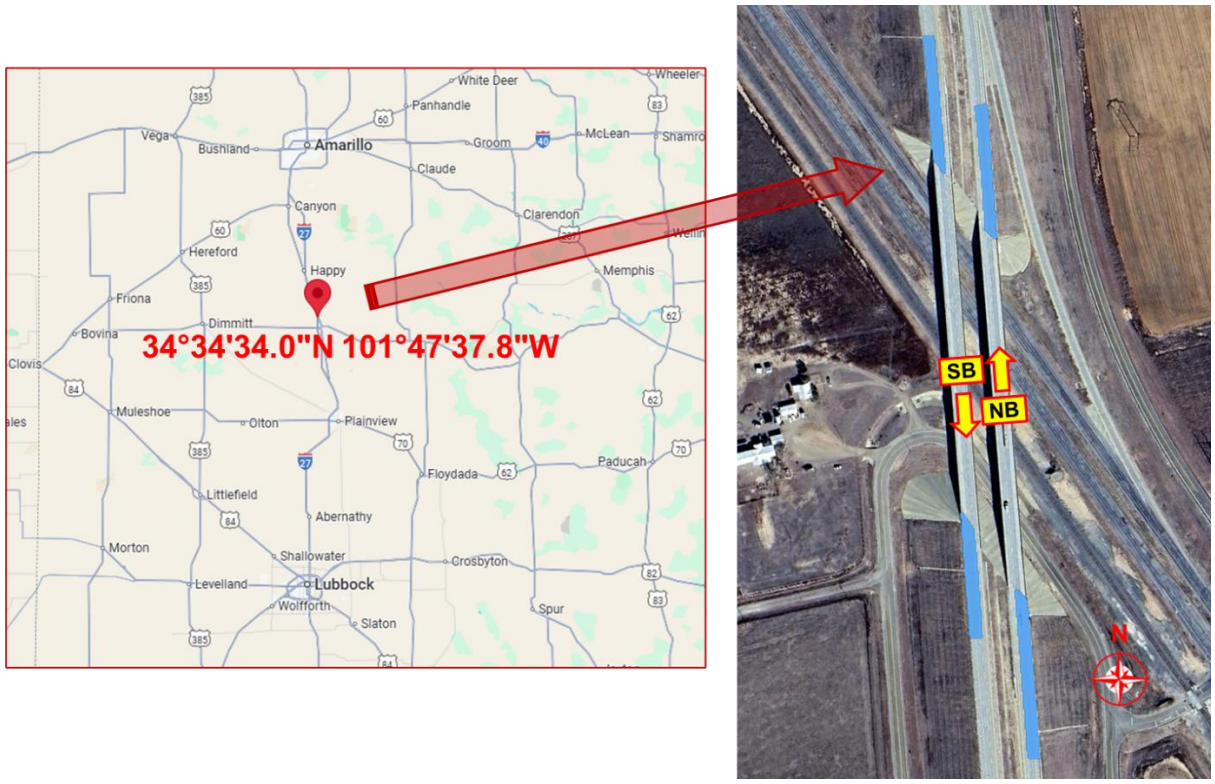


Figure 5-139. Location of Section P-A-5 on IH-27 in Tulia, Lubbock, Texas

Table 5-22. Detailed descriptions of Section P-A-5 on IH-27 in Tulia, Lubbock, Texas

Attribute	Information	Notes
District & Highway	Lubbock & IH-27	
CSJ	0067-02-031	
County	Swisher County	
Reference Marker	RM 77 + 0.90	
GPS Coordinates	34°34'34.0"N 101°47'37.8"W	
Date Work Begin	4/10/1985	
Date Completed	6/24/1988	
Pavement Type	CRCP (9-in)	
BAS Thickness	9-in	
Base Type	6-in ASB + 6" Flex Base (DC) (TY. F, GR. 4, CL. 2)	
Subgrade Type	2-in Emb. Matl. with PI less than 25	
Drainage Type	Side Drain / Ditch (Conc. RIPRAP)	
Embankment Height	~32in	
Length of Approach Slab	10-ft	Added in 2021
Distress Observed (Severity)	Longitudinal crack, lane separation, and spalling	

The original construction, completed between April 1985 and June 1988, featured a unique design that did not include a traditional, isolated bridge approach slab. Instead, the 9-inch continuously reinforced concrete pavement (CRCP) extended directly to the bridge abutment. As shown in the typical section in **Figure 5-140**, the pavement structure consists of the 9-inch CRCP placed over a two-layer base composed of 6 inches of asphalt-stabilized base (ASB) and 6 inches of flex base. To restrain thermal movements of the CRCP at the bridge interface, a five-lug terminal anchorage system was installed at the bridge ends. However, a 10-foot trapezoidal bridge approach slab was later added in 2021.

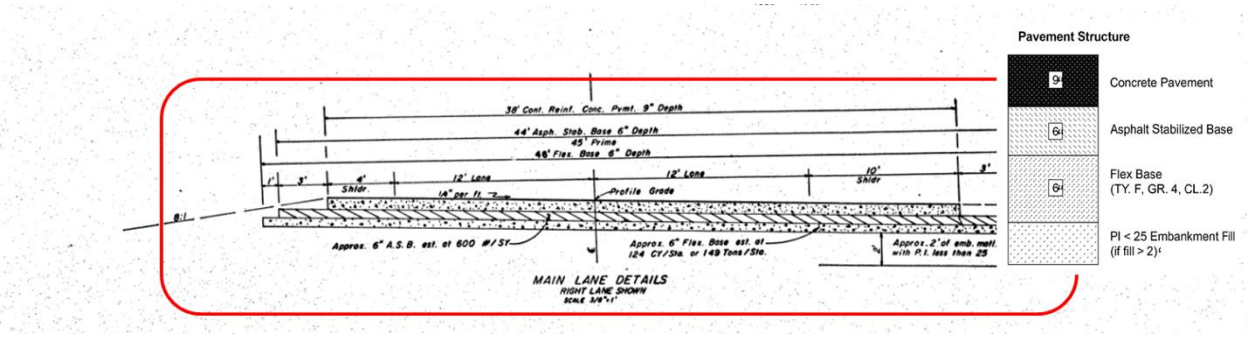


Figure 5-140. Typical section of Section P-A-5 on IH-27 in Tulia, Lubbock, Texas

A visual survey confirmed the presence of multiple surface distresses. Extensive longitudinal cracking was observed, most prominent in the inside lane. Additionally, the survey team noted significant map cracking distributed across the pavement surface, often accompanied by a distinct white powdery residue concentrated at cracks (**Figure 5-141**). Numerous PCC patches were also observed, indicating repairs to address spalling and what appear to be partial-depth punchouts. Unlike other sites in this study, significant settlement of the approach was not observed.



Figure 5-141. Observed white residue on the pavement surface.

The original investigation plan was designed to address the cause of the longitudinal cracking by focusing testing on the inside lane and the longitudinal joint. However, due to on-site traffic control constraints, the research team was unable to safely implement an inside lane closure. Consequently, the field investigation, including all testing and coring, was restricted to the outside lane and outside shoulder.

5.10.2 Falling Weight Deflectometer (FWD) tests

FWD tests were conducted on the outside lanes and outside shoulders of both the northbound (NB) and southbound (SB) main lanes to evaluate the structural capacity of the pavement system. The FWD results, presented in **Figure 5-142** (NB approach and SB Departure) and **Figure 5-143** (NB departure and SB approach), revealed a distinct and highly variable deflection pattern in the areas containing the CRCP terminal anchor lugs. This unique signature, consistent with observations

from the IH27 Keuka site, consists of low deflections directly over the stiff anchor lug structures followed by sharp deflection spikes in the pavement sections between them. This pattern strongly suggests a non-uniform support condition, likely caused by the formation of voids in the embankment material between the rigid lugs.

The FWD results for the northbound approach and southbound departure are presented in **Figure 5-142**. On the south side (**Figure 5-142**), the pavement sections away from the bridge exhibited relatively consistent deflections, generally ranging from 4 to 6 mils. As the tests entered the anchor lug zone, the deflections became highly erratic. The NB approach, for instance, showed deflections as low as 2 mils over the lugs before spiking to over 6 mils between them.

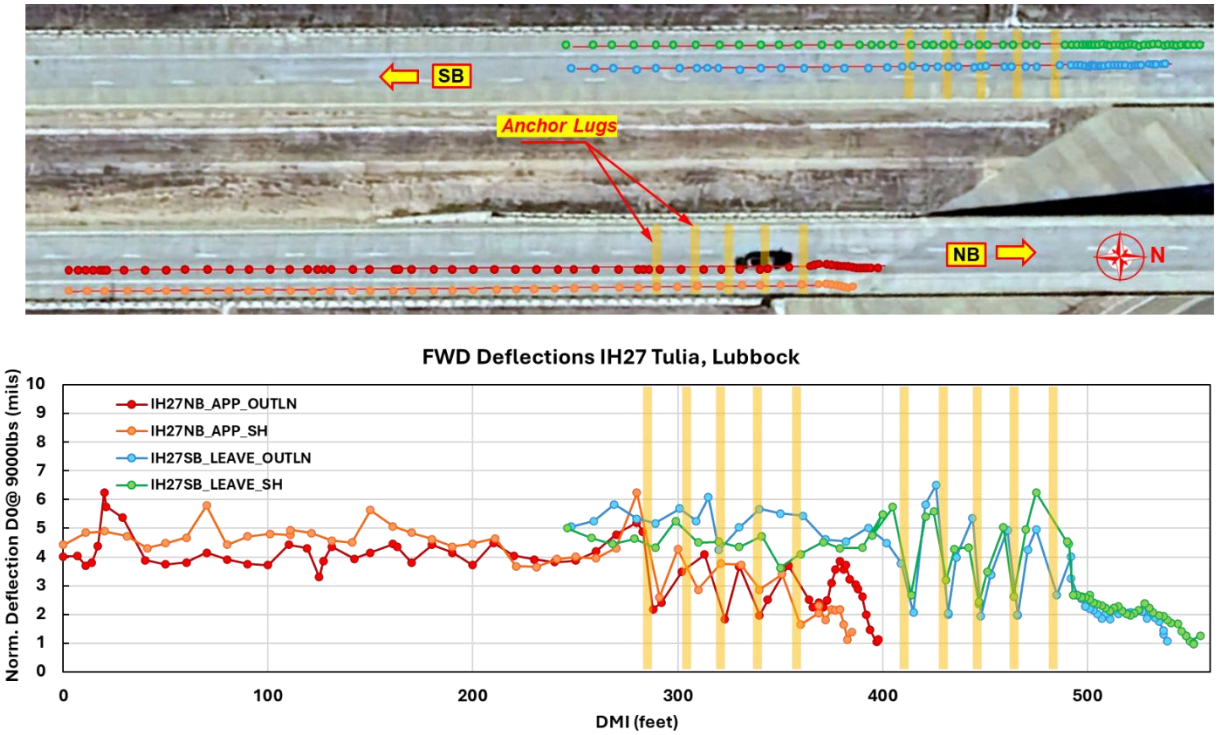


Figure 5-142. FWD deflections along outside lane and outside shoulder on NB approach and SB departure

North side (**Figure 5-143**) showed even more pronounced issues. The SB approach outside lane displayed the most severe condition, with deflection spikes reaching a maximum of over 10 mils, indicating a significant loss of slab support or potential lack of slab's integrity. The NB departure lane followed a similar trend of spiky deflections, although with slightly lower peak values generally ranging between 5 and 8 mils.

A noteworthy observation at this site is that the BAS sections consistently showed lower deflections than the adjacent pavement, reflecting improved support compared to the mainlane pavement.

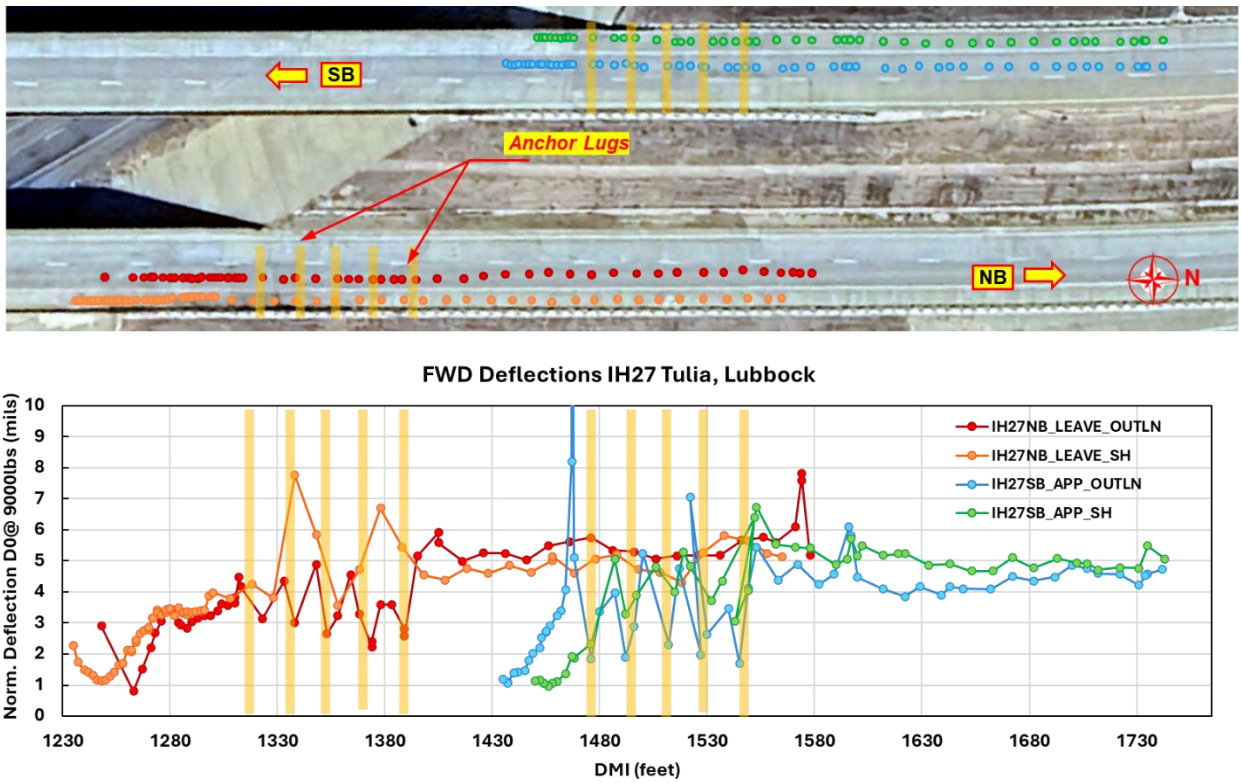


Figure 5-143. FWD deflections along outside lane and outside shoulder on NB departure and SB approach

5.10.3 Coring

Coring was performed at seven locations (C1–C7) along the southbound main lane near the bridge approach to verify pavement thickness and assess potential voids beneath the slab. The coring locations and corresponding photographs are shown in **Figure 5-144** for southbound approach side and in **Figure 5-145** for southbound departure side.



Figure 5-144. Coring locations and pavement structure for Southbound Approach



Figure 5-145. Coring locations and pavement structure for Southbound Departure

Core thicknesses ranged between 8.5 in and 10.5 in, consistent with the as-built design for the CRCP. Among the recovered cores, C2 exhibited a visible void at the bottom of the slab. The void was approximately 0.75 in. thick and contained a vapor barrier (plastic sheet) directly beneath the concrete (**Figure 5-144**). The presence of this sheet suggests that a vapor barrier was installed during the construction of the newly added BAS. The void space above the sheet was partially filled with moisture and loose soil, indicating potential loss of contact between the slab and underlying embankment material.

Two critical distress mechanisms were identified through the coring. The first was a loss of support near BAS-Pavement joint under the recently installed bridge approach slab. At location C2, a plastic sheet, presumably a vapor barrier for the new slab, was discovered at the base of the 10.5-inch concrete. A void was observed directly beneath this plastic sheet, which explains the elevated FWD deflection of 7.9 mils recorded at this specific point.

The second key finding was evidence of internal slab deterioration. Multiple cores, including C1, exhibited significant delamination at the depth of the reinforcing steel and corroded rebars. This internal cracking indicates a structural weakness within the CRCP itself, likely contributing to the surface distresses and erratic deflection behavior observed throughout the anchor lug zone. This type of delamination is often associated with stresses from slab movement or corrosion of the steel reinforcement.

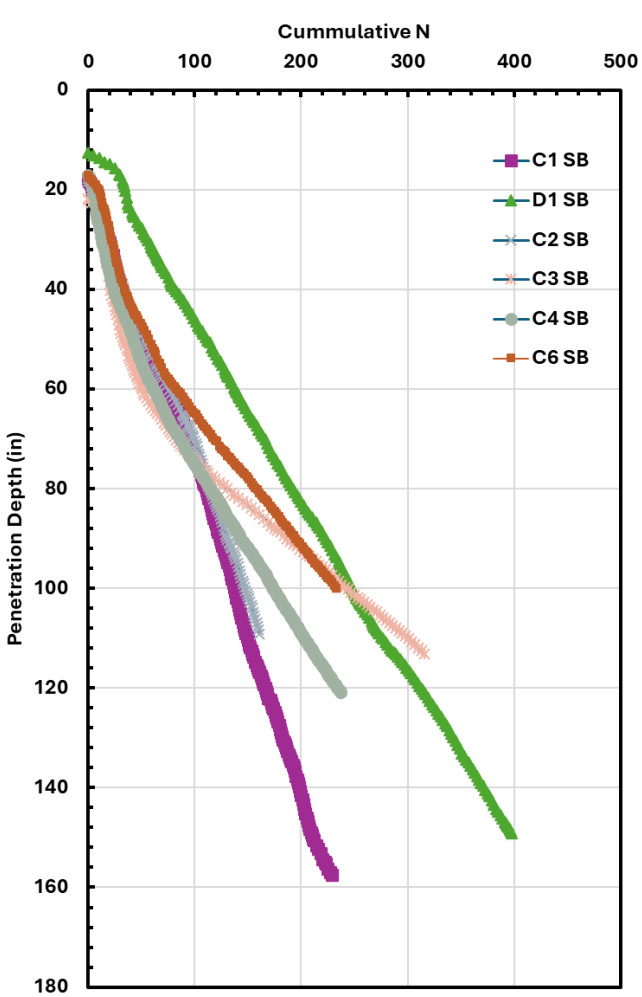
The remaining cores (C3–C7) generally showed sound concrete quality and no evidence of large voids at the slab-subgrade interface. Thicknesses were relatively consistent, ranging from 8.5 in. (C5, C6) to 10 in. (C3).

The coring results corroborate the FWD findings: the observed highly variable deflection pattern near the approach corresponds with the presence of voids and delamination zones beneath or within the slab. The detection of a vapor barrier at C2 strongly indicates that the bridge approach slab was added later and separated from the original pavement, which may have altered the drainage and moisture conditions beneath the BAS and contributed to partial loss of support.

5.10.4 Dynamic Cone Penetration (DCP) tests

Southbound

The DCP results for the southbound lanes (**Figure 5-146**) highlight the localized weak embankment material at BAS at shallow depth. At this location, a layer of very weak material (red) with a M_r value of only 5.1 ksi was found at a shallow depth of approximately 3 feet. This isolated pocket of poor material corresponds directly with a high-deflection area and demonstrates that while the embankment is not failing globally, it has localized weak spots that contribute to the non-uniform support beneath the slab.



: Coring or drilling layer

Depth (ft)	Depth (in)	C1 SB	D1 SB	C2 SB	C3 SB	C4 SB	C6 SB
1	4	Coring	Drilling	Coring	Coring	Coring	Coring
	8						
	12	Drilling			Drilling	Drilling	Drilling
2	16		31.8	Drilling		12.4	22.9
	20	11.8			19.4		
	24		9.0	12.6		9.8	10.8
3	28				5.1		
	32						
	36						
4	40						
	44				12.2	15.1	17.5
	48						
5	52	32.3		17.3		13.3	
	56						
	60				22.4	17.1	
6	64		19.6				
	68						24.5
	72						
7	76				32.8	20.6	
	80						
	84						
8	88			13.4			
	92						
	96						
9	100						
	104						
	108	17.0					
10	112						
	116						
	120						
11	124		21.2				
	128						
	132						
12	136						
	140						
	144						
13	148						
	152	10.9					
	156						
14	160						
	164						
	168						

(a) (b)

Figure 5-146. DCP Results – Southbound (a) Cumulative DCP blow counts vs. penetration depth below the pavement surface. (b) Resilient modulus determined from DCP tests

The northbound DCP data presented in **Figure 5-147** indicates more widespread and variable foundation conditions. The test at D6 NB was particularly notable, revealing a deep and continuous column of weak material extending from 3 feet to 16 feet below the surface. This extensive zone of poor embankment material provides an explanation for the high FWD deflections observed in this section.

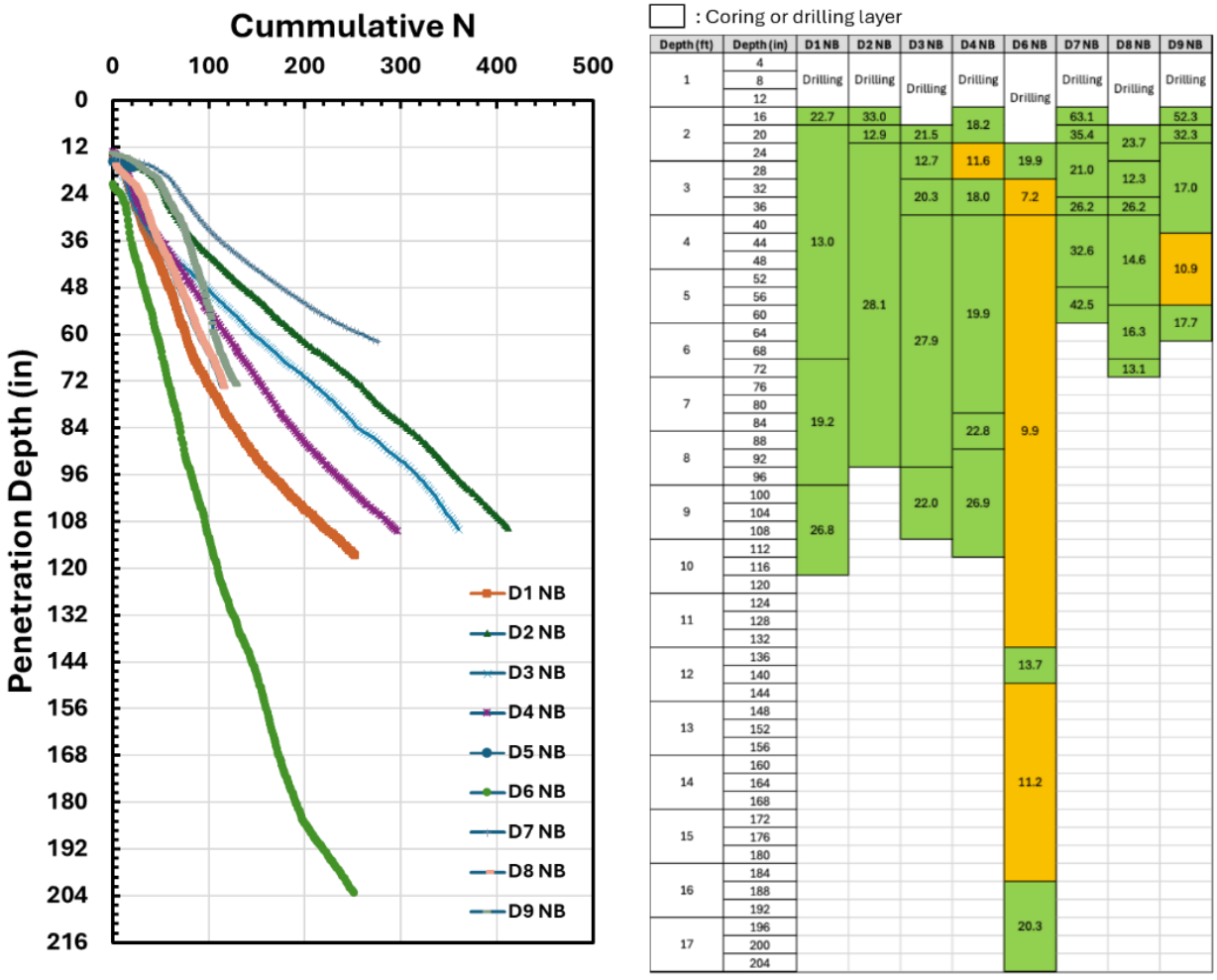


Figure 5-147. DCP results – Northbound (a) Cumulative DCP blow counts vs. penetration depth below the pavement surface. (b) Resilient modulus determined from DCP tests

In summary, while the primary distress mechanism at the IH27 Tulia site appears to be the internal structural deterioration of the concrete slab, the DCP tests confirm that this distress is exacerbated by localized zones of weak foundation material. The combination of a weakened slab and non-uniform support has led to the severe cracking, spalling, and high deflections observed in the field.

5.10.5 Potential Distress Mechanism

While the embankment at IH 27 Tulia exhibits localized weak embankment fill material, the global stability of the earth structure remains intact, evidenced by the lack of settlement despite the bridge's age (constructed in 1985). Instead, the observed pavement distress is attributed to a poor functional performance of a CRCP terminal anchorage system.

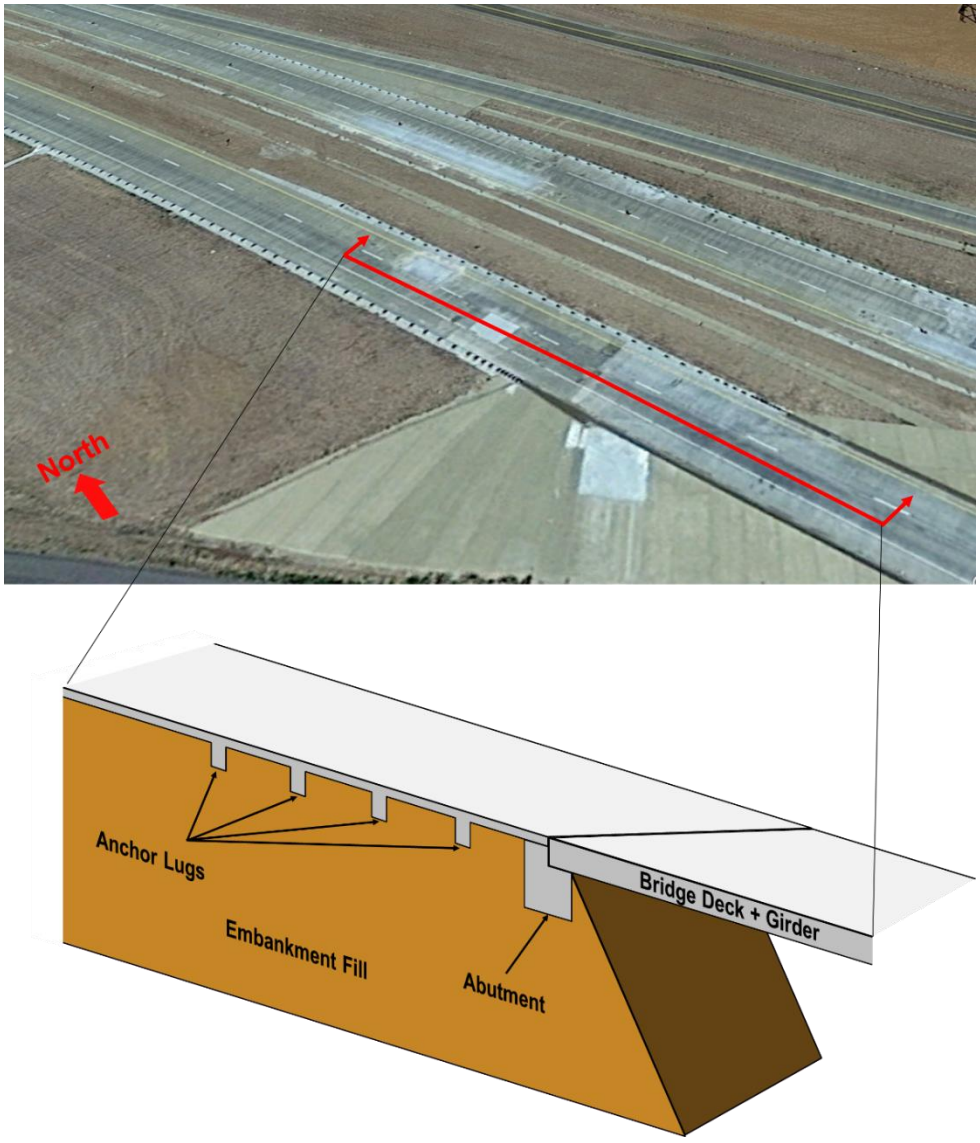


Figure 5-148. Illustration of IH27 Tulia site longitudinal cross section showing CRCP terminal anchor lug system

The original design relied on a multiple lug terminal anchorage system (as shown in **Figure 5-148**) to restrain the longitudinal expansion and contraction of the CRCP caused by daily and seasonal thermal cycles. Ideally, these lugs transfer the expansion forces into the embankment soil, using

the soil's passive resistance to immobilize the pavement end (**Figure 5-149)**. However, a critical incompatibility exists between the materials: the concrete pavement behaves elastically, expanding and contracting with temperature changes, while the embankment soil exhibits plastic deformation characteristics. As the pavement expanded, the anchor lugs compressed the adjacent soil faces. When the pavement subsequently contracted, the concrete returned to its original position, but the deformed soil did not fully rebound.

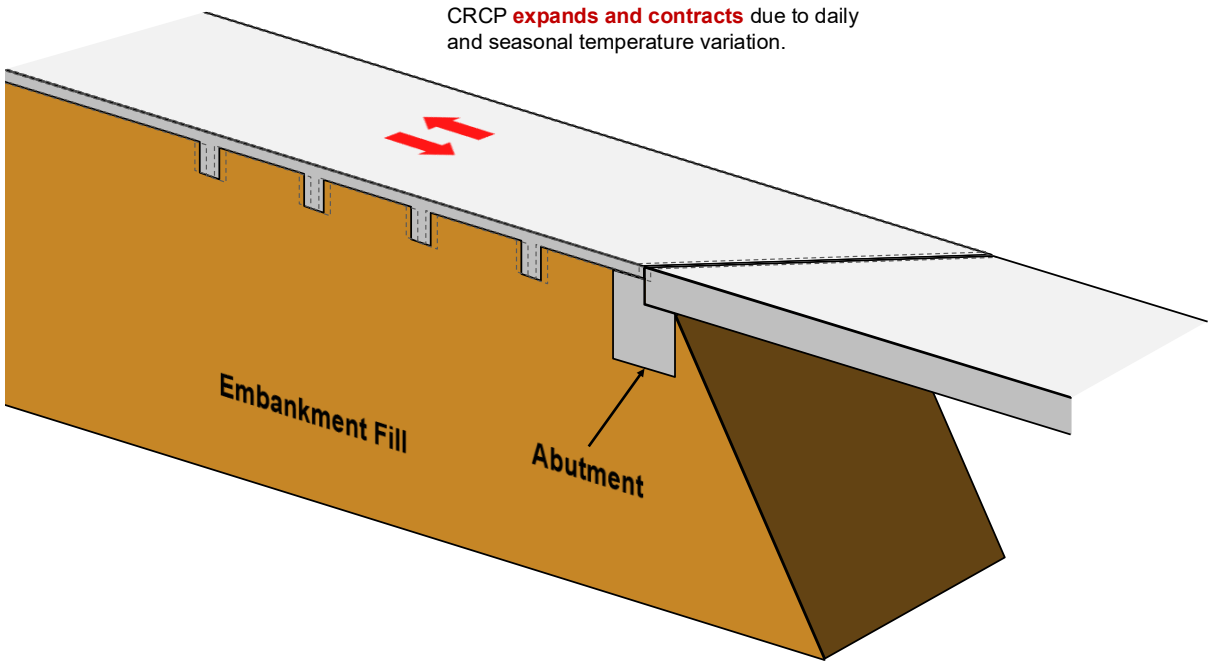


Figure 5-149. Longitudinal expansion and contraction of CRCP and anchorage system due to temperature variation

Over repeated thermal cycles, this differential behavior created permanent voids adjacent to the vertical faces of the anchor lugs and beneath the slab sections between the lugs. This phenomenon explains the distinct "spiky" deflection pattern observed in the FWD data shown in **Figure 5-142** and **Figure 5-143**, where low deflections were recorded directly over the rigid lugs, while significantly higher deflections were measured in the unsupported spans between them (illustrated in **Figure 5-150**) . Once these voids developed, the anchor lugs lost contact with the soil, resulting in a complete loss of the passive earth pressure required to restrain the pavement.

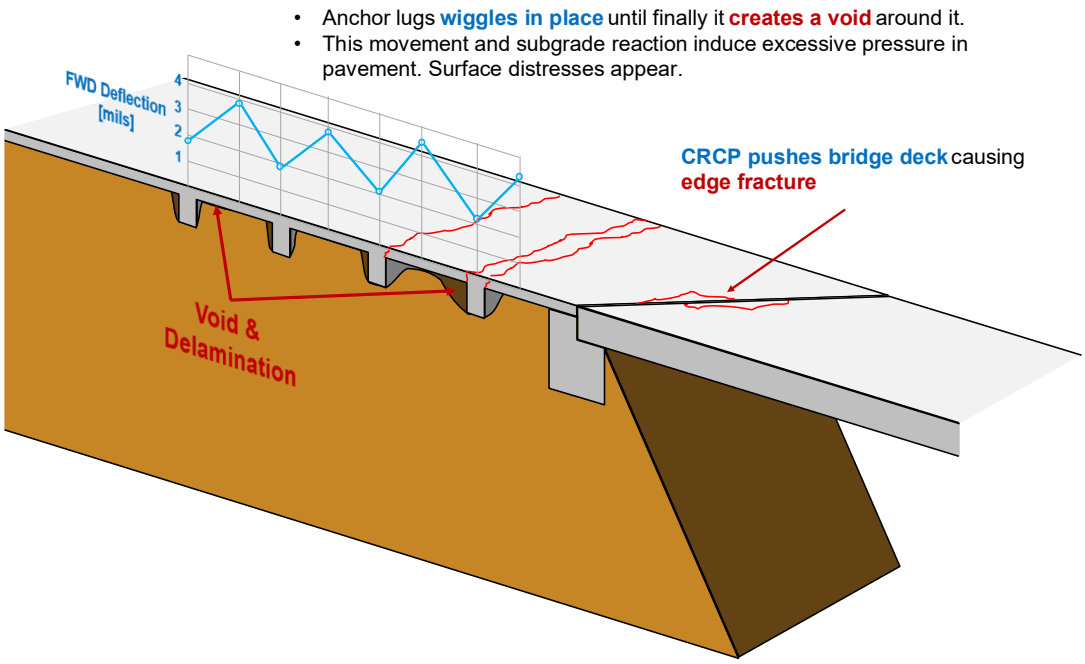


Figure 5-150. Illustration of formation of voids around anchor lugs due to cyclic thermal expansion and contraction of the CRCP.

Consequently, without the necessary restraint, the CRCP ends were free to expand longitudinally toward the bridge structure. This unrestricted movement exerted excessive compressive forces on the bridge abutment and approach interface, leading to the observed surface distresses, including cracking and spalling (**Figure 5-150**).

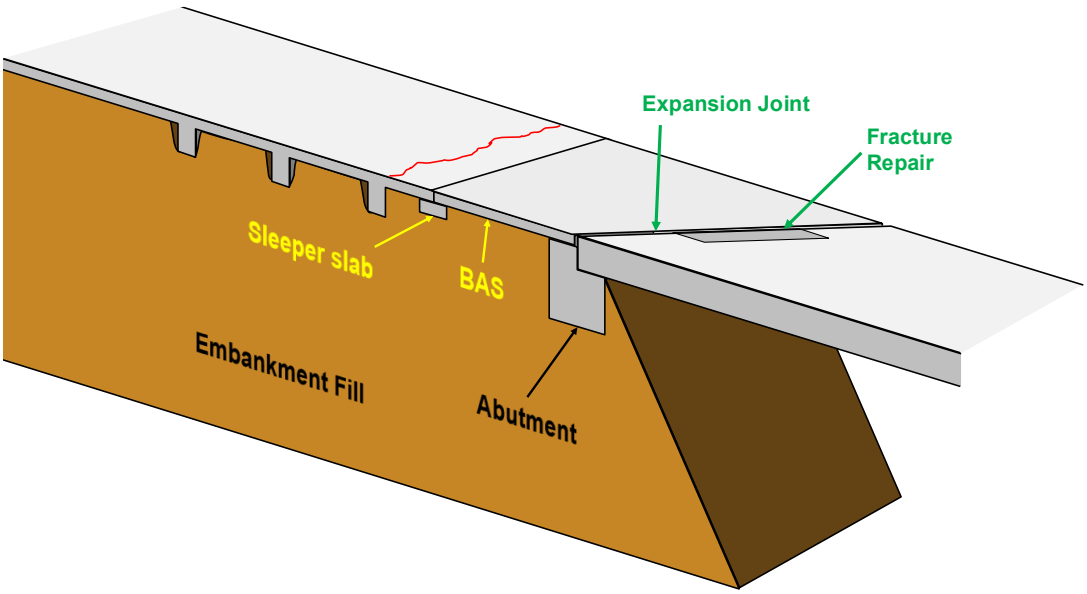


Figure 5-151. Addition of Bridge Approach Slab (BAS) and expansion joint to accommodate thermal expansion.

Ultimately, rather than attempting to reinforce the existing anchorage system, TxDOT repaired the section in 2021 (**Figure 5-151**) that involved partially removing the end of the terminal and replacing with a 10-foot BAS designed to accommodate pavement movement via an expansion joint rather than fighting the thermal forces.

5.10.6 Repair Recommendations

The IH 27 Tulia site presents a unique condition among the test sections evaluated in this study. The embankment remains globally stable with no significant settlement, despite the structure's age (constructed 1985–1988) and a height of approximately 32 feet. DCP and laboratory testing showed no clear evidence of washout or widespread stiffness deficiency. The primary distress mechanism at this site, failure of the CRCP terminal anchorage system due to cyclic thermal loading, was identified and addressed by TxDOT in 2021 through the removal of the terminal end and installation of a 10-foot bridge approach slab with an expansion joint.

The 2021 repair adopted a strategy to accommodate CRCP thermal movements rather than resist them. FWD testing conducted during the 2025 field evaluation confirmed that the BAS sections consistently exhibited lower deflections than the adjacent pavement in the anchor lug zone, indicating that the new BAS is structurally performing as intended.

Partial-depth repair in accordance with TxDOT Item 361 should be performed, as a short-term repair, at all locations exhibiting active spalling, punchouts, or delamination at the reinforcement depth. Based on the 2025 field evaluation, these locations are concentrated in the anchor lug zone on both the northbound and southbound approaches, particularly where previous PCC patches have been placed. This short-term strategy is intended to extend the serviceable life of the existing pavement rather than a permanent repair.

5.11 Section P-B-1: IH 35 Northbound Frontage Road in Waco

5.11.1 Overview

Section P-B-1 is the approach and departure side pavement on the northbound frontage road of IH 35 at Waco, McLennan County, TX. Texas. The location and typical section of Section P-B-1 are shown in **Figure 5-152** and **Figure 5-153**, respectively. Field evaluations of the pavement and embankment structures were conducted from 8/02/2022 by TxDOT, and following evaluation was performed from 1/18/2023 to 1/19/2023 by TTU research team.

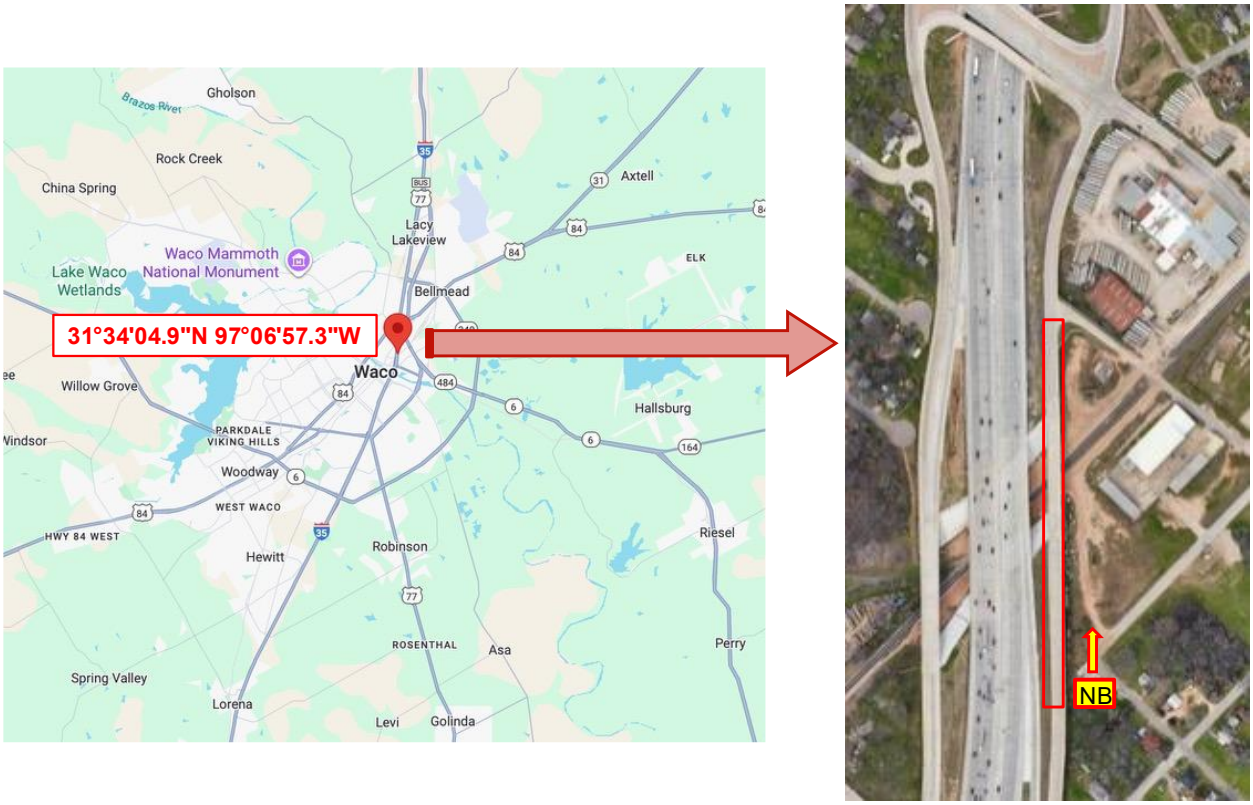


Figure 5-152. Location of the IH 35 Northbound Frontage Road in Waco, Texas.

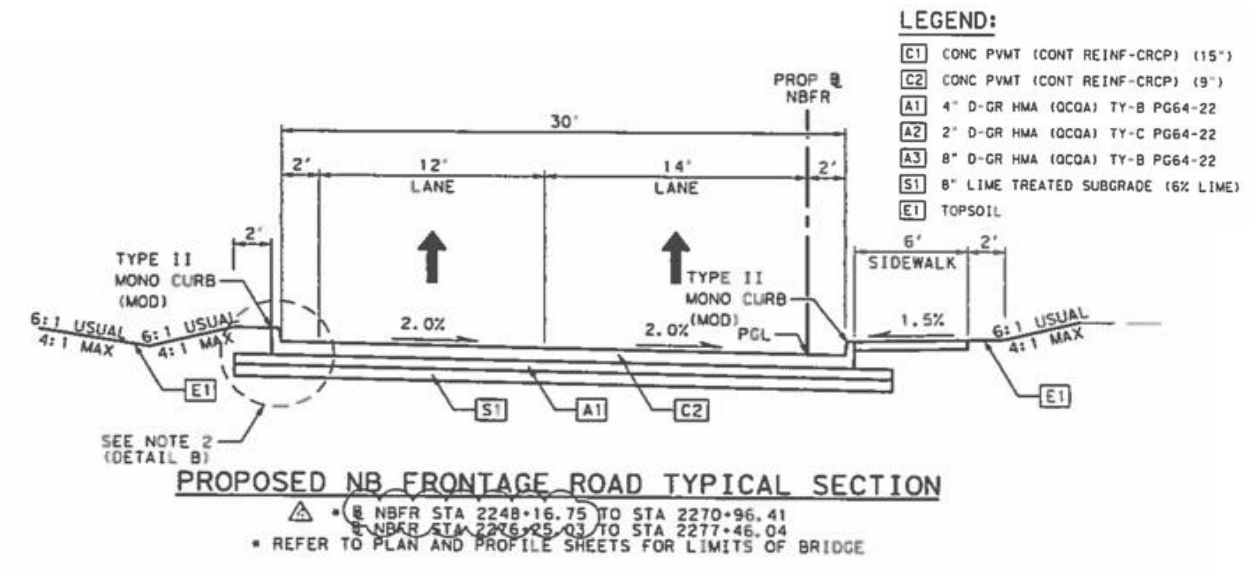


Figure 5-153. Typical section of Section P-B-1 on IH 35 in Waco. Texas

The test section was constructed on an embankment approximately 35 feet in height, supported by an MSE wall. The pavement structure consists of a 9-inch-thick Continuously Reinforced Concrete Pavement (CRCP) and a 4-in-thick hot mix asphalt (HMA) base, supported by a 9-inch-thick lime-treated subgrade (LTS). Detailed information regarding this section is provided in **Table 5-23**.

Table 5-23. Detailed descriptions of Section P-B-1 on IH 35 in Waco, Texas

Attribute	Information	Notes
District & Highway	Waco, IH 35	Northbound
CSJ	0015-01-229	
County	McLennan County	
Reference Marker	RM 335+0.867 to RM 336+0.694	
GPS Coordinates	31°33'58.2"N 97°06'57.9"W	
Date Work Begin	3/9/2015	
Date Completed	8/6/2019	
Pavement Type	Rigid - CRCP 9"	
BAS Thickness	9”	
Shoulder Type	No Shoulder	
Base Type	4” HMA (Type D)	
Subgrade Type	8” Lime Treated Subgrade (6% Lime)	
Drainage Type	Curb & Inlets	
Embankment Height at BAS	35 ft	Slope – MSE wall

Field observation revealed voids on the approach side of the BAS and severe longitudinal cracks near both the approach and leave sides of the BASs. The presence of High-Density Polyurethane Foam (HDPF) near the BAS indicates prior repair attempts to address settlement issues. Photos showing various distresses are presented in **Figure 5-154**.

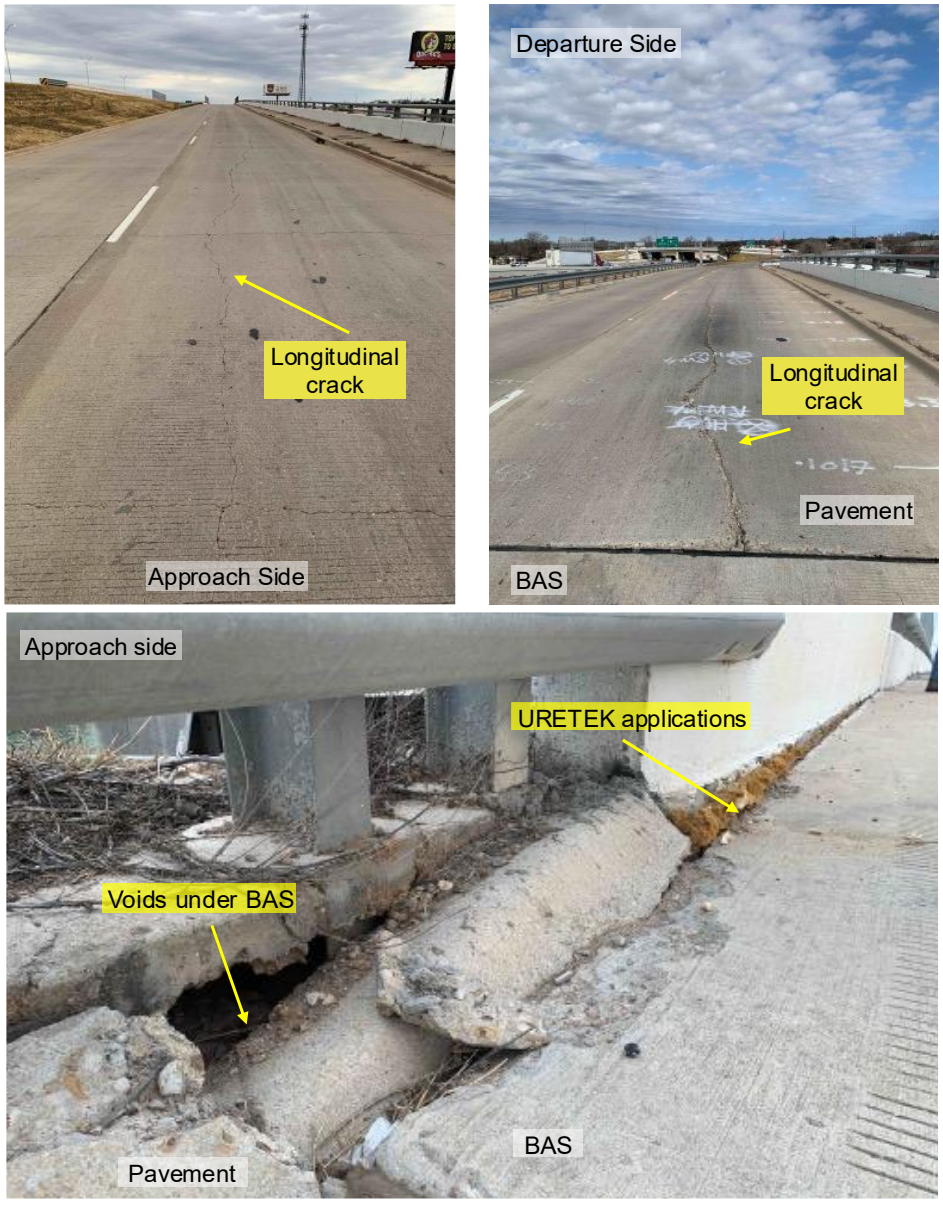


Figure 5-154. Observed distress on approach and departure side

5.11.2 Google Earth Satellite Image Investigation

Figure 5-155 shows Google Earth historical images of section P-B-1 from 10/31/2019 to 06/16/2022. Following the completion of the northbound frontage road, reconstruction of the adjacent highway and ramp was initiated. According to the historical images, the reconstruction

process appeared to have involved excavating the slope between the highway and the frontage road and installing soil nailing.

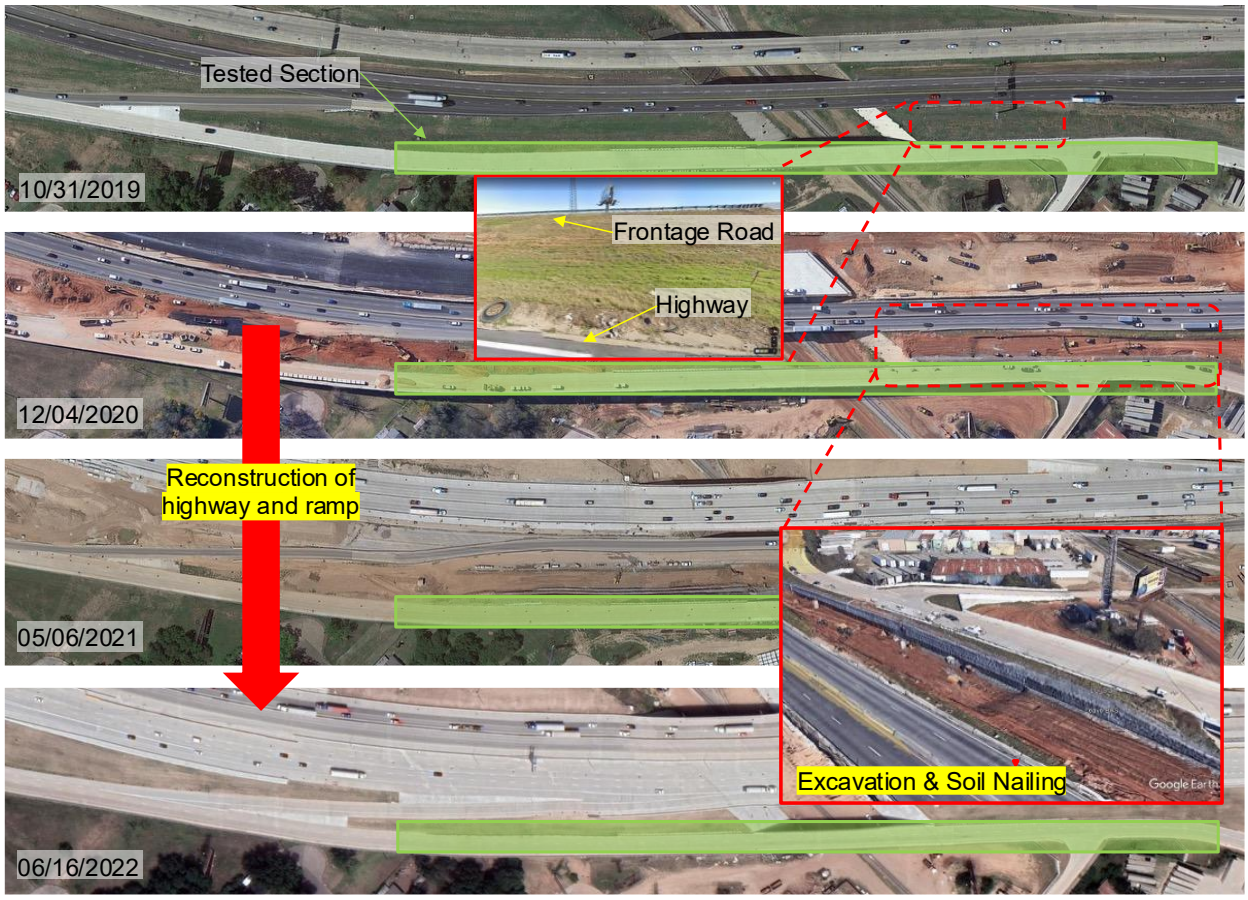


Figure 5-155. Reconstruction of main lanes and ramp on IH35 Waco site

The historical images further suggested that longitudinal cracks first appeared in December 2019, prior to the excavation work. However, these cracks significantly deteriorated during the reconstruction and excavation process (2019–2022) as shown in **Figure 5-156**.

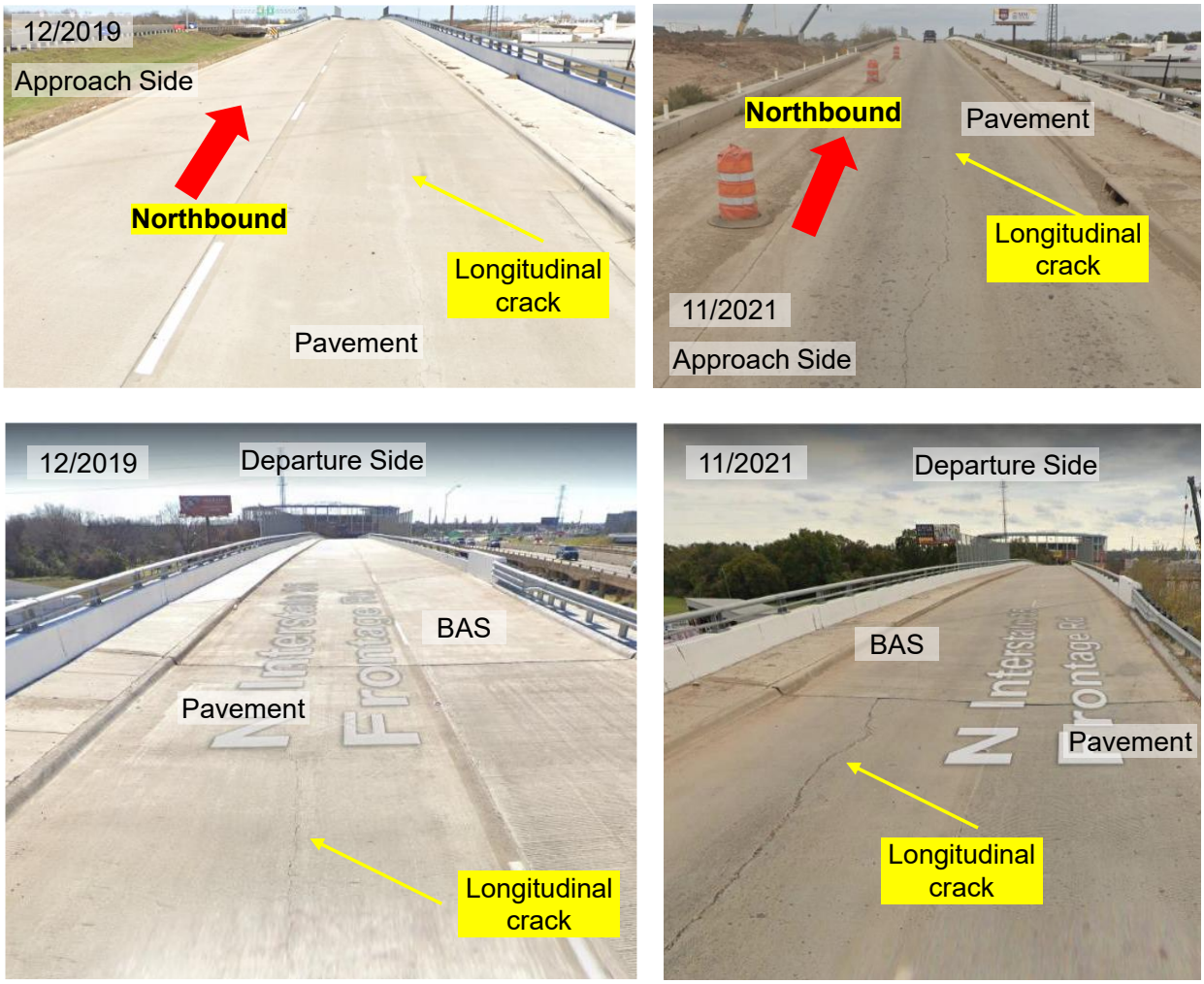


Figure 5-156. Google historical street view images on approach and departure side where longitudinal cracks were observed.

According to TxDOT standard (CRCP(1)-17), a sawed longitudinal construction joint is required when the pavement width exceeds 15 ft. Measurements indicated that the pavement width in the test section exceeded 16 ft, with some locations on the approach and departure sides exceeding 17 ft without a sawed joint (see **Figure 5-157)**. The locations exhibiting widths greater than 17 ft corresponded with the locations of the observed longitudinal cracks, suggesting the initial trigger of the longitudinal crack.

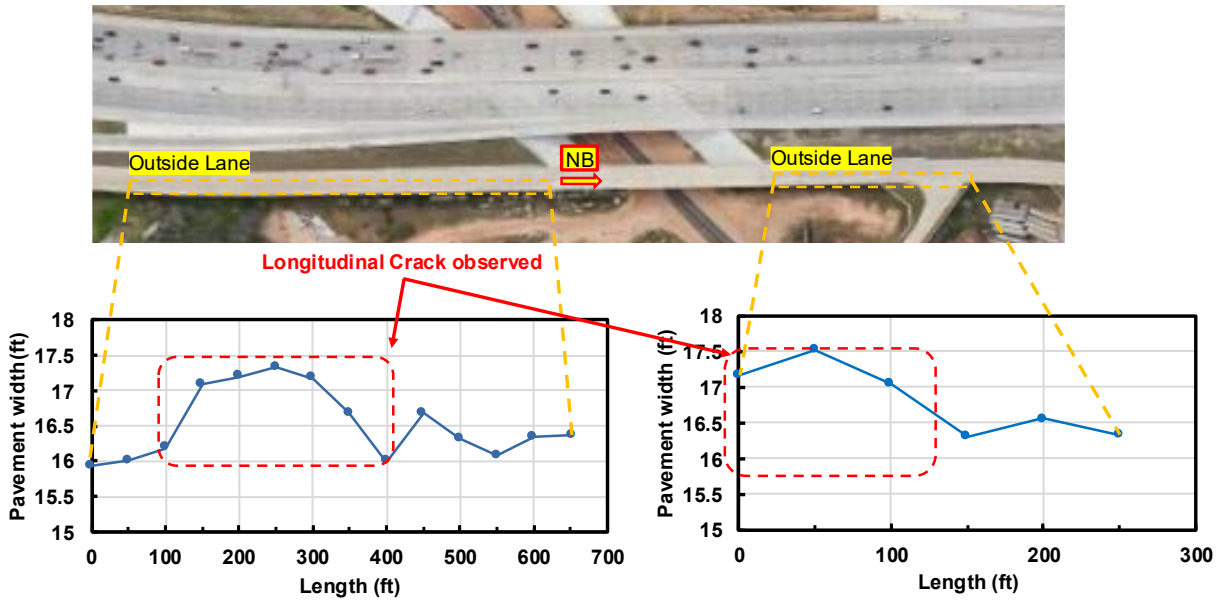


Figure 5-157. Pavement width of outside lane in approach and departure side.

5.11.3 Falling Weight Deflectometer (FWD) Tests

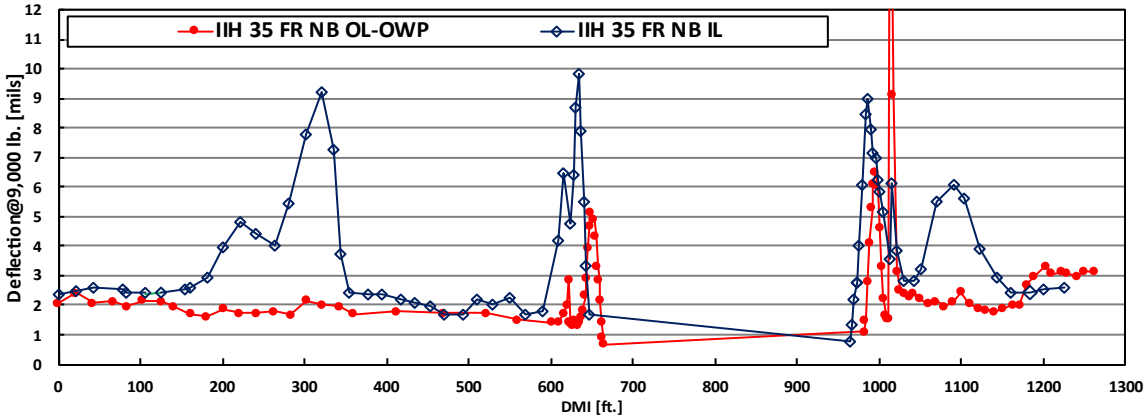
FWD tests were conducted by the TxDOT teams on the inside and outside lanes of both the approach and departure sides. Deflections were evaluated using a normalized 9,000-lb loading. **Figure 5-158** presents the FWD drop locations and the measured deflection profiles.

For the outside lane on the approach side, measured deflections in structurally sound areas (DMI 0 ft to 180 ft and 350 ft to 590 ft) were generally less than 3 mils. In contrast, deflections significantly increased in the section between DMI 180 ft and 350 ft, generally exceeding 4 mils. Peak deflections of 4.8 mils and 9 mils were recorded at approximately DMI 220 ft and 320 ft, respectively. Similarly, on the departure side of the outside lane, high deflections were recorded between DMI 1050 ft and 1130 ft, with a peak deflection of approximately 6 mils at DMI 1090 ft. In other sections of the departure side (DMI 1030 ft to 1050 ft and 1140 ft to 1230 ft), deflections remained low at approximately 3 mils. When comparing these results to the inside lane at similar DMI locations, the inside lane generally exhibited lower deflection values of approximately 2 mils.

A comparison of the FWD drop locations with the visual distress survey reveals a strong correlation between structural stiffness and longitudinal crack. The locations exhibiting higher deflections correspond closely with the areas where longitudinal cracks were observed (indicated by green lines in **Figure 5-158(a)**). Furthermore, elevated deflections were consistently observed at and near the BAS on both the inside and outside lanes for both the approach and departure sides. These higher deflections, relative to the baseline values of less than 4 mils observed in sound pavement sections, indicate insufficient structural support beneath the BAS and the immediately adjacent pavement.



(a)



(b)

Figure 5-158. FWD drop locations (a) and deflections (b) on bridge approach and departure side.

5.11.4 Coring

Coring operations were conducted prior to the execution of CPT and DCP tests. A total of five locations were selected for investigation, prioritizing areas exhibiting significant distresses, specifically longitudinal cracks and voids beneath the BAS identified during the initial TxDOT investigation. To ensure sample integrity and avoid damaging structural reinforcement, the MIRA system was utilized to detect the presence of rebar within the pavement. Consequently, coring locations were selected in areas free of reinforcement. The extracted core samples confirmed that the pavement structure consists of approximately 10 inches of CRCP overlying a 4-inch HMA base. **Figure 5-159** presents the detailed coring locations and images of the extracted core samples.



Figure 5-159. Coring locations and images of cored samples

5.11.5 Dynamic Cone Penetration (DCP) tests and CPT tests

To estimate the backfill and subgrade conditions within the embankment, DCP and CPT tests were conducted. TxDOT initially performed five DCP tests (D1 through D5) on the outside lane of the approach and departure sides on August 2, 2022. Subsequently, the TTU Research Team conducted additional five DCP tests between January 18 and 19, 2023: four on the inside lane (DCP1, DCP2, DCP4, and DCP6) and one on the outside lane (DCP5). To characterize embankment fill conditions for the entire embankment height, five CPT soundings (CPT1, CPT2, CPT4, CPT5, and CPT6) were performed. Detailed testing locations are presented in **Figure 5-160**.

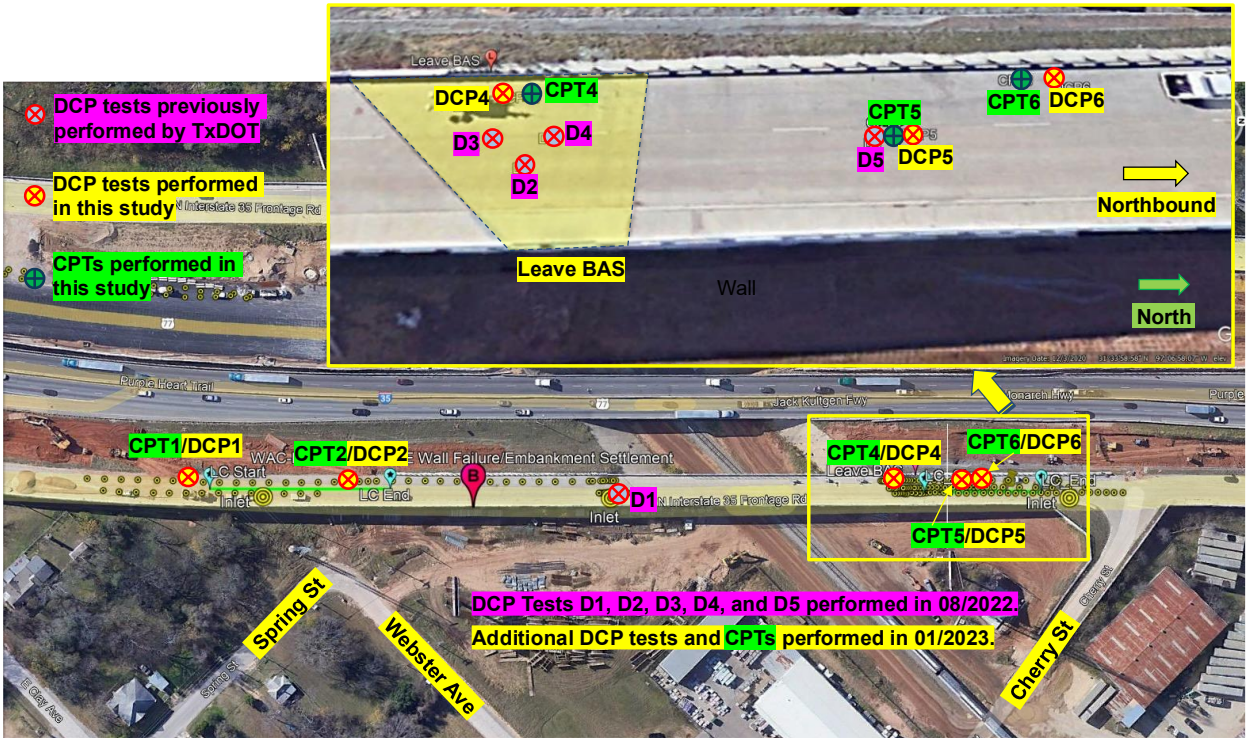


Figure 5-160. DCP and CPT testing locations. Testing layout for field investigation in I35 Waco site.

The resilient modulus values estimated from the initial five DCP tests (D1 though D5), performed by TxDOT, indicated varying soil stiffness (**Figure 5-161**). In general, the departure side exhibited M_r values greater than 10 ksi at shallow depths (approximately 38 inches from the pavement surface). However, at greater depths (approximately 5 ft), weaker soil conditions with M_r values less than 10 ksi were observed at locations D3, D4, and D5.

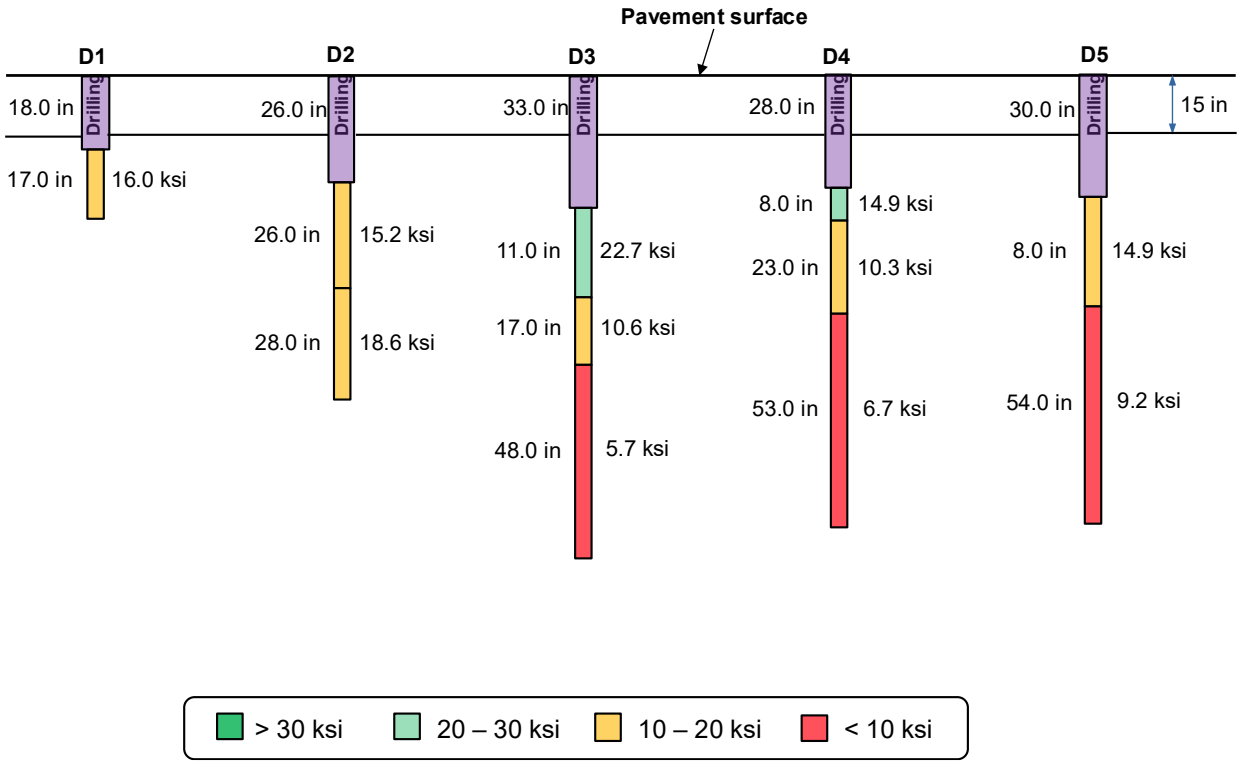


Figure 5-161. Resilient modulus of embankment fills from initial five DCP tests conducted by TxDOT (Note: the color scheme for M_r value is for illustrative purposes only.)

The resilient modulus values estimated from the additional five DCP tests (DCP1 through DCP5) conducted by TTU research teams are shown in **Figure 5-162**. Resilient modulus from 15 to 25 inches below the pavement surface were generally greater than 20 ksi at locations of DCP1, DCP2, and DCP6, whereas M_r values were smaller than 20 ksi at the location of DCP4 and DCP5. Especially, the modulus from DCP5 in entire testing depth were less than 20 ksi with a 31.5-in-thick layer with modulus of 8 ksi.

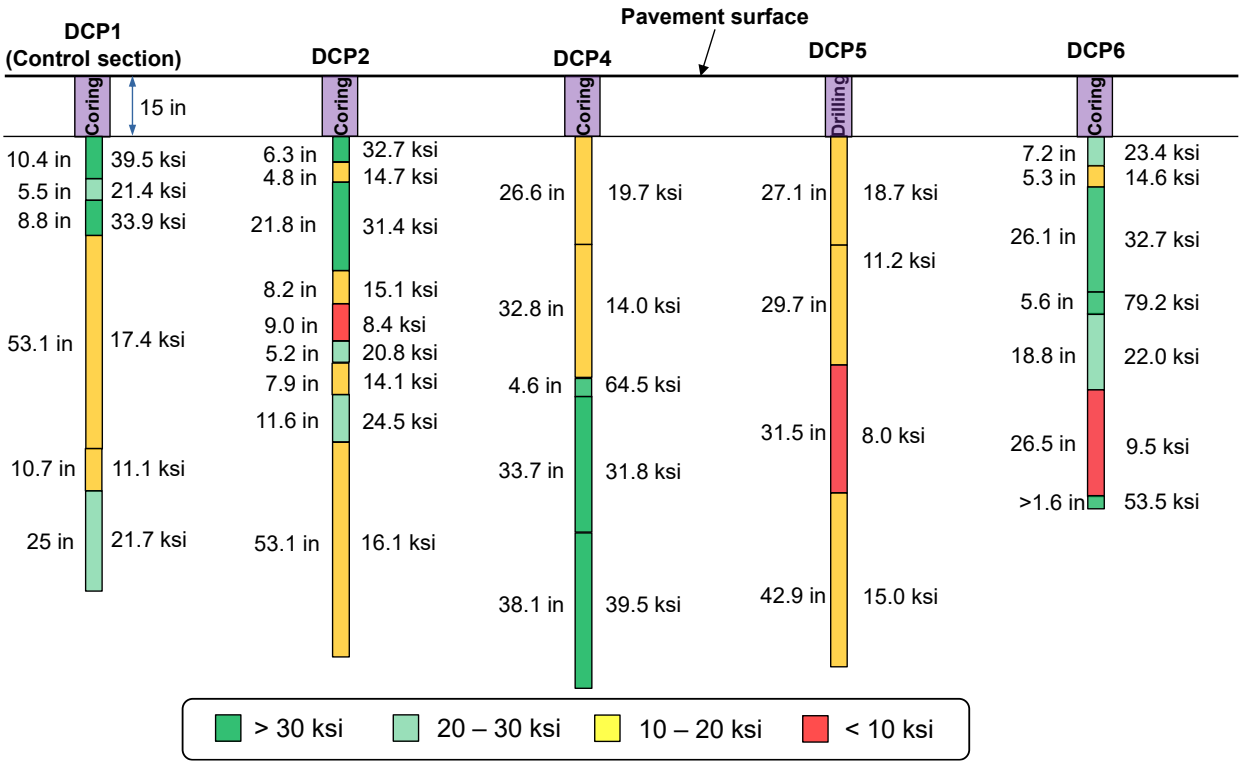


Figure 5-162. Resilient modulus of embankment fills from additional five DCP tests conducted by TTU research team (Note: the color scheme for M_r value is for illustrative purposes only.)

Cone resistance values from all CPTs are plotted in **Figure 5-163**. The measured cone resistance values are generally less than 200 tsf. Variations of cone resistance up to a depth of 12 ft (144 in), which was about maximum depth of DCP tests, are presented in **Figure 5-163** as well for better visualization. Overall, CPT5 showed the smallest cone resistance whereas CPT1, CPT2, and CPT6 showed slightly larger cone resistance than other locations.

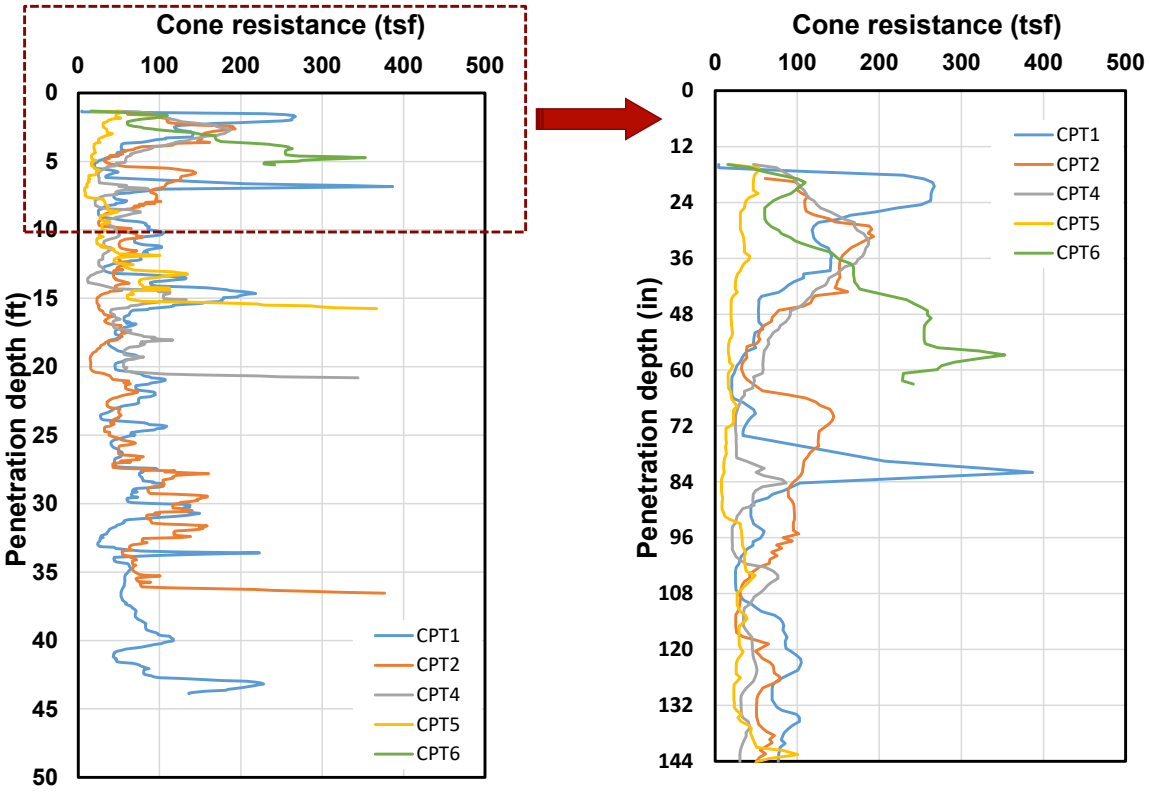
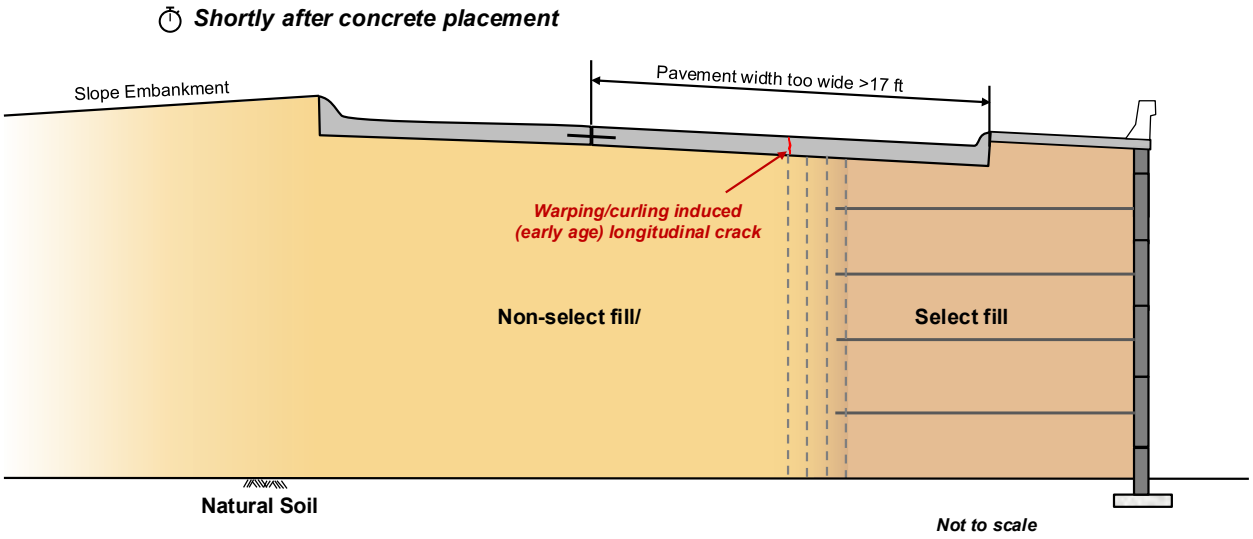


Figure 5-163. Cone resistance versus depth each CPT test location

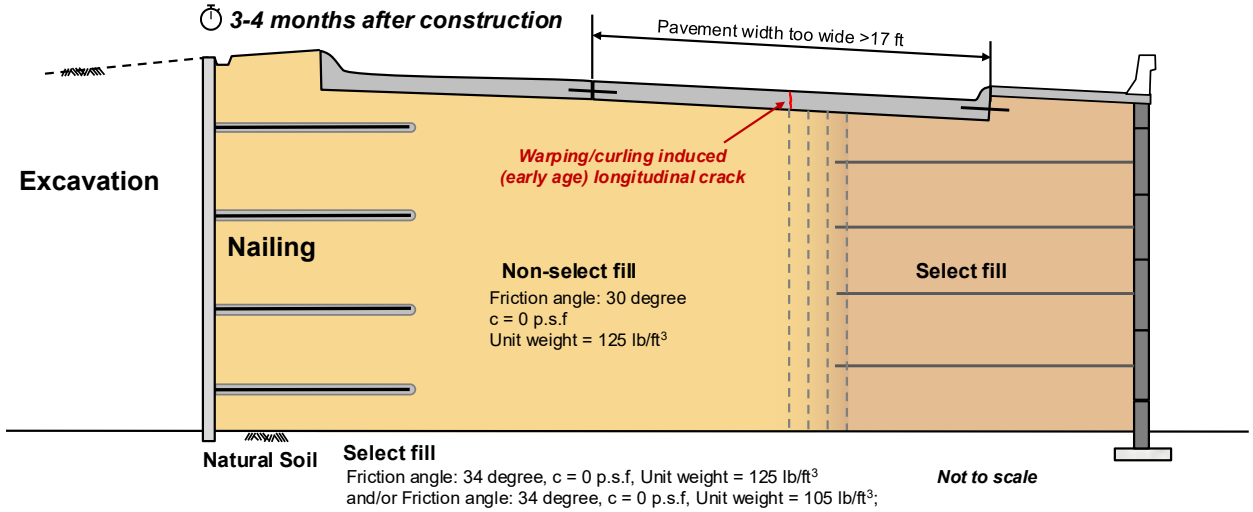
5.11.6 Potential Distress Mechanism

The potential distress mechanism governing the longitudinal cracking appeared to be a combination of initial geometric and thermal factors and subsequent exacerbation by adjacent excavation. **Figure 5-164** presents an illustration of the potential distress mechanism. The cracks initially appeared shortly after the construction near the location where the pavement width exceeds 17 ft, which is greater than the TxDOT standard requiring a sawed longitudinal construction joint at 15 ft. The absence of this joint subjected the wide pavement slab to excessive thermal stresses caused by transverse warping and curling, thereby initiating the cracks.

These initial cracks were significantly worsened following the excavation on the west side for the adjacent highway reconstruction. The excavation of the adjacent slope likely reduced the lateral confinement of this weaker fill material, causing lateral movement and settlement that compromised the pavement of necessary support and led to the further development of the longitudinal cracks. Furthermore, TxDOT Standard RW(MSE) specifies that the friction angle for granular select fills be 34 degrees while lower friction angles are allowed for non-select fills. Plan sets show that 30 degrees of friction angle was used for the non-select fills. The differences in material stiffness between select fills and non-select fills and, therefore, non-uniform slab support might have further contributed to the development of the longitudinal cracks.


Shortly after concrete placement
Slope Embankment
Pavement width too wide >17 ft
Warping/curling induced
(early age) longitudinal crack
Non-select fill/
Select fill
Natural Soil
Not to scale

(a)


3-4 months after construction
Pavement width too wide >17 ft
Excavation
Warping/curling induced
(early age) longitudinal crack
Nailing
Non-select fill
Friction angle: 30 degree
c = 0 p.s.f
Unit weight = 125 lb/ft3
Select fill
Natural Soil
Select fill
Friction angle: 34 degree, c = 0 p.s.f, Unit weight = 125 lb/ft3
and/or Friction angle: 34 degree, c = 0 p.s.f, Unit weight = 105 lb/ft3;
Not to scale

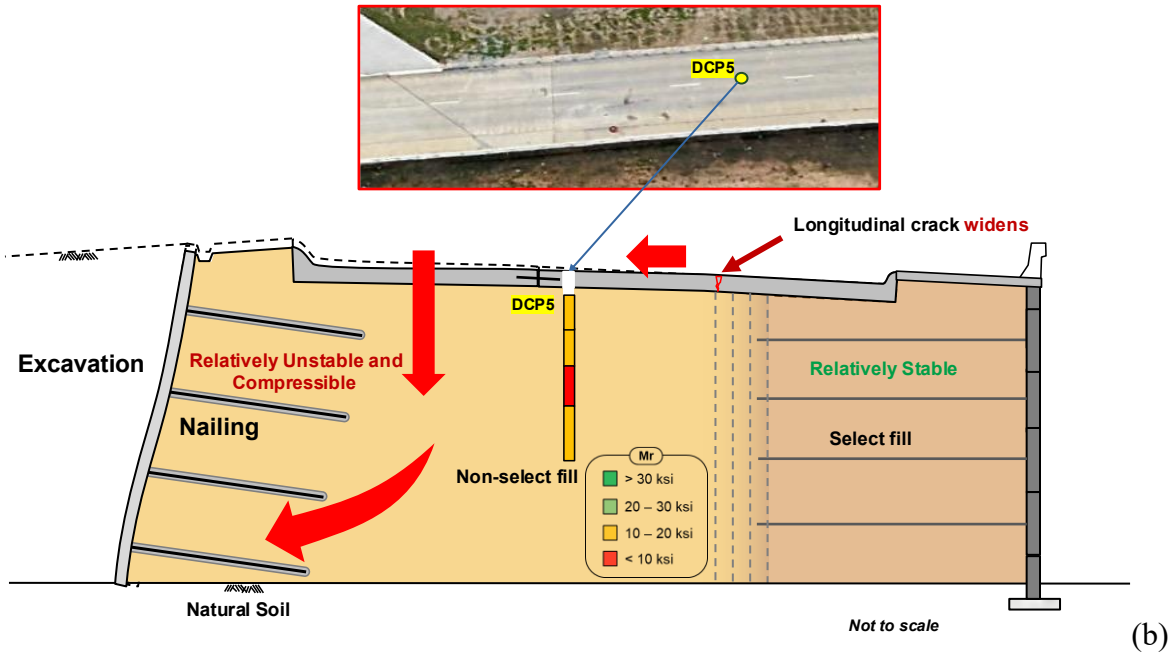


Figure 5-164. Distress mechanism for the observed longitudinal cracks: (a) initiation of early-age longitudinal crack due to warping/curling and (b) reduction of the lateral confinement due to excavation, causing lateral movement and settlement leading to widening of the longitudinal crack

(Notes: Excavation-induced lateral movement is exaggerated for illustration purposes; the color scheme for M_r value is for illustrative purposes only.)

5.11.7 Repair Recommendation

Based on the observed distresses and evaluation data analysis, the main causes of longitudinal cracks were identified as a pavement width exceeding 17 feet, weakened slab support caused the nearby excavation, and the presence of weak embankment fill materials.

For the BAS sections, replacements of both approach and departure side BASs are recommended. After removing materials from the pavement surface to a depth of 3 ft in the BAS areas, soil densification with HDPF (TxDOT SS 3086) should be employed by drilling a 4-ft-deep hole from the excavation bottom to densify embankment fills from 3 ft to 7 ft beneath the pavement surface. After the injection of HDPF, the excavated zone should be filled with Cement Stabilized Backfill (CSB), meeting Item 276, Class L specification, with a minimum thickness of 23 inches. Then, a 13-in CRCP should be constructed over the CSB.

For the CRCP section, a full-depth repair from the pavement surface to a depth of 7 ft is recommended. The reconstruction of CRCP must correct the initial geometric flaw by sawing a longitudinal joint wherever the lane width exceeds 15 feet. Also, DCP tests are recommended for the quality control testing to confirm layer stiffness when placing new embankment fill materials.

Chapter 6 Evaluation Guidelines

The field investigation presented in Chapter 5 combined falling weight deflectometer (FWD) testing, ground penetrating radar (GPR) scanning, coring, dynamic cone penetrometer (DCP) testing, cone penetration testing (CPT), and soil sampling with laboratory testing to characterize the condition of the bridge approach slab (BAS), adjacent pavement, and embankment fill at each section. This chapter presents the results of each method compared across sections and describes the key observations made from the field investigations. The chapter then develops interpretation guidelines for FWD, DCP, and CPT data, including a deflection-based screening threshold, a performance-based classification of embankment materials, and correlations for extending DCP-based classification to CPT data. The recommendations presented in these guideline sections are based on the field evaluation data collected at the time of the analysis and should be considered draft; they can be updated and further refined when additional datasets become available.

6.1 Observations from Field Investigation Program

The field testing methods employed in this study were applied in a deliberate sequence at most sections. FWD testing and visual surveys identified locations of elevated deflection or visible distress; coring at those locations verified layer thicknesses and confirmed or ruled out the presence of voids; DCP tests through the cored holes characterized the near-surface fill; CPT soundings extended the characterization through the embankment height; and soil samples supported laboratory classification and moisture testing. Control locations with low deflections and no visible distress were tested at most sections so that the results from distressed areas could be compared against a site-specific baseline. The following sections summarize the key observations we made from the field investigation program.

6.1.1 Falling Weight Deflectometer (FWD) Testing

The FWD testing in this study was conducted using a nominal target load of 9,000 lbs, representing a wheel load of an 18-kip single-axle truck. Because the actual applied load can vary slightly between drops, all measured deflections were normalized to a 9,000-lb reference load before analysis in this study. Mathematically, normalized D_0 can be calculated as:

$$D_0^{\text{norm}} = \frac{9000}{P_{\text{measured}}} \times D_0^{\text{measured}} \tag{3}$$

where, D_0^{norm} = normalized central deflection at 9000-lb load

D_0^{measured} = measured central deflection corresponding to actual applied load

P_{measured} = applied load during the FWD drop (lbs)

Each FWD test consists of a circular loading plate and an array of eight geophones spaced radially from the load center. The central geophone, located directly beneath the load plate, records the maximum surface deflection (D_0) and is therefore used as the key indicator of pavement structural response. All results discussed in this section refer to the normalized D_0.

Testing spacing varied by section type. On normal pavement sections constructed on embankment, the FWD test was performed at 10- to 20-ft intervals (typically 10 ft). On the BAS, where deflection gradients can change sharply, a closer spacing of 2 to 5 ft (typically 2 ft) was used to capture detailed variations across the slab length.

Across the evaluated sections, the FWD results consistently distinguished well-supported pavement from areas of support loss. At Section E-2, deflections on the CRCP main lanes were generally less than 2 mils, whereas deflections on the westbound BAS exceeded 6 mils at several locations. At Section P-A-3, deflections across most of the ramp remained near the statewide average, but a spike of 32.5 mils was recorded at a location where coring later confirmed a void and HDPF beneath the slab, and BAS peaks of 8.7 and 13.3 mils corresponded to voids of up to 4 in. At Section P-A-4, shoulder deflections of 2 to 4 mils rose to 7.5 mils on the BAS, where coring confirmed voids and HDPF. At Section E-4, the highest deflection of 21.5 mils occurred at a core location with a 1-in void near the pavement edge, while a control location with no void deflected only 1.8 mils. At Section P-B-1, deflections in structurally sound areas were generally less than 3 mils, and the zones exceeding 4 mils, with peaks of 4.8 and 9 mils on the approach side, corresponded closely to the areas where longitudinal cracks were observed.

The FWD results also revealed patterns that reflect structural configuration rather than localized voids. At Section E-5, deflections increased systematically across the roadway width, from an average of 3.4 mils on the inside lane to 12.3 mils on the middle lane and 17.5 mils on the outside lane adjacent to the mechanically stabilized earth (MSE) wall, indicating progressive loss of foundation support toward the wall rather than deterioration of the slab itself. At Sections E-1 and P-A-5, both constructed with CRCP terminal anchor lugs, the deflection profiles showed a distinctive signature of low deflections directly over the stiff lugs and sharp peaks between them, consistent with the formation of voids in the embankment material between the rigid lug structures reported in TxDOT Project 0-6326 (Jaiswal et al. 2012). At Section E-3, an asphalt-surfaced section, deflections ranged from about 2 to 33 mils and were governed largely by overlay thickness and subgrade condition, with the approach side of the bridge deflecting more than the leave side in the southbound direction.

Two aspects of the observed results carry forward into the interpretation guideline in Section 6.2. First, in general, wherever a sharp localized deflection spike was observed on a BAS, coring confirmed a void beneath that location. Second, elevated deflection alone does not identify the cause: comparable deflection levels resulted from voids, prior HDPF injection, thin slabs, weak near-surface fill, and, at Sections E-1 and P-A-5, internal slab deterioration. Distinguishing among these conditions requires the complementary methods described in the following sections.

6.1.2 Ground Penetrating Radar (GPR) Scanning

Ground-coupled ground penetrating radar (GC-GPR) with 350HS (350 Mhz) antenna was used at Sections S-11-8, P-A-3, P-A-4, and E-4 to scan subsurface anomalies over continuous areas, complementing the pointwise information from coring and penetration testing. GPR scans were run in longitudinal passes at 2-ft lateral spacing, with 8 to 18 passes per section, and the depth scale was calibrated against core measurements.

The GPR results served three functions. First, they located buried features that constrain both interpretation and test placement: at Section S-11-8, the scans delineated MSE wall reinforcing straps at a depth of about 40 in and a 3.5-ft-diameter drainage pipe at a depth of about 6 ft. Second, they identified voids and low-density repair materials. At Section P-A-3, strong negative reflections near two distress areas were confirmed by coring as HDPF beneath the CRCP and as a 4-in void. At Sections P-A-4 and E-4, the scans mapped the horizontal extent of prior HDPF injection, and, particularly, the E-4 scans identified the area of most severe settlement, which was verified by cores containing foam layers up to 4 in thick. Third, GPR scan results mapped slab thickness variation. At Section E-4, the GPR-derived CRCP thickness, verified by coring, showed that elevated deflections between two core locations corresponded to a reduced slab thickness of 10 to 12 in combined with HDPF, and the thickness data supported the deflection-thickness comparison developed in Section 6.2.

The S-11-8 results also illustrated the value of overlaying independent datasets. The FWD deflection profile closely followed the upper interface of a soft layer delineated by GPR, in an area where DCP testing measured subgrade moduli of 2 to 5 ksi, demonstrating that the surface deflection of asphalt pavements responds strongly to near-surface subgrade stiffness. A high-intensity reflection near the bridge suggested elevated moisture, which was subsequently verified by laboratory moisture contents and low DCP resistance in the same area. GPR results remained interpretive rather than quantitative, and anomalies required confirmation by coring before they could be attributed to voids, foam, or moisture.

6.1.3 Coring

Coring served four purposes in the field investigation program: verification of slab and pavement layer thicknesses, direct confirmation of voids at the slab base, retrieval of material for inspection and testing, and access for DCP tests, CPT soundings, and soil sampling. Core locations were selected primarily where FWD deflections or visible distress indicated potential problems, with additional cores at low-deflection locations serving as controls. The MIRA ultrasonic system was used to locate reinforcement so that cores could be taken without cutting rebars when necessary.

The cores confirmed the association between deflection spikes and voids. At Section E-2, voids 1.5 to 7 in thick were found beneath the concrete at all four core locations with high FWD deflections, and no voids were found at the two control locations. At Section P-A-3, cores at the BAS revealed voids up to 4 in; at Section P-A-4, all three BAS cores showed 2-in voids above 1.25- to 1.75-in-thick HDPF layers; and at Section E-4, voids of 0.5 to 3 in were found at five of the cored locations. At Section E-3, voids of about 0.4 to 0.7 in were limited to the northbound BAS. At Section E-1, cores taken near the BAS-pavement joints showed separations of 0.5 to 0.75 in between the approach slab and the sleeper slab, matching the deflection peaks recorded at those joints. Voids were almost always at the pavement-base interface or base-subgrade interface

The cores also revealed pavement structure and repair history that no surface measurement could identify. Measured CRCP thicknesses sometimes departed from design values and varied within single sections, for example, from 8.75 to 13.25 in on the P-A-3 ramp and from 10.125 to 14.5 in at Section E-4. HMA overlays 1 to 5 in thick above the concrete at Section E-2, overlay thicknesses

increasing toward the bridge at Section S-11-8 (total asphalt thicknesses of 15 to 21.9 in), and HDPF fragments in cores at Sections P-A-3, P-A-4, E-4, and E-5 all revealed prior repair attempts. At Section P-A-5, a core through the BAS encountered a plastic sheet, presumably a vapor barrier placed during the later addition of the approach slab, with a 0.75-in void directly beneath it.

Finally, coring exposed internal slab deterioration that might otherwise have been misattributed to support conditions. Cores at Sections E-1 and P-A-5 exhibited delamination at the depth of the reinforcing steel accompanied by corroded bars, consistent with chloride ingress from repeated deicing-salt application at these Panhandle-area sites. At Section P-A-5, this internal material deterioration, rather than weak embankment material, appeared to be the primary source of the erratic deflection behavior in the anchor-lug zone. This finding suggests that elevated deflections and surface distress must be checked against the condition of the slab itself before they are attributed to the embankment.

6.1.4 Dynamic Cone Penetrometer (DCP) and Cone Penetration Testing (CPT)

DCP and CPT testing were used together to characterize the stiffness of embankment fill and subgrade materials. The two methods are complementary in depth range. The DCP provides a continuous near-surface stiffness profile but becomes impractical beyond about 10 ft because of bending of the driving shaft, whereas roadway embankment heights at the evaluated sections are typically 20 to 35 ft; the CPT can penetrate the full embankment height unless refusal is met. DCP tests were performed through cored or drilled holes, with additional drilling where needed to reach untreated subgrade. The number of blows per depth interval was converted to a penetration rate and then to soil modulus (M_r) using the correlation of Webster et al. (1992); in the cumulative blow count versus depth plots, a flatter slope indicates stiffer material.

The DCP results across the sections showed a consistent association between distress and weak near-surface fill. At Section E-2, control locations maintained M_r values greater than 10 ksi over the full 9-ft investigation depth, whereas the locations with high deflections showed layers below 10 ksi, voids, or both. At Section E-3, northbound locations with M_r below 10 ksi were the two BAS locations C4 and C6, where voids were also found. At Section S-11-8, four locations showed M_r below 7 ksi within the 5- to 11-ft depth range. At Section P-A-4, a weak layer occupied the 4- to 6-ft depth range at the BAS, and one pavement location showed M_r of 5.7 ksi between 2 and 5.5 ft. At Section E-1, the northbound approach cores overlaid a layer with M_r as low as 5.8 to 6.4 ksi between about 2.5 and 6 ft, coinciding with moisture contents approaching or exceeding 20 percent in the same depth range. At Section P-A-5, a layer with M_r of 5.1 ksi was found at about 3 ft beneath the southbound BAS, and one northbound location showed weak material continuously from 3 to 16 ft. At Section E-5, two control locations yielded weighted average moduli of 15.8 and 17.8 ksi, while locations in the distressed area consistently fell below 10 ksi. At Section P-B-1, weak layers with M_r below 10 ksi appeared at about 5 ft at three locations, and one location showed a 31.5-in-thick layer with a modulus of 8 ksi.

Section E-4 was the exception. The embankment fill there exhibited high penetration resistance at nearly all locations, including locations where voids were observed, and the subgrade beneath existing HDPF layers was similarly stiff. The presence of voids above stiff, dense fill suggests that

support might have been lost through the lateral displacement of the soil mass accompanying MSE wall movement rather than through compression of weak fill. A single location adjacent to the BAS joint, at the probable entry point for surface runoff, showed distinctly lower resistance.

CPT soundings extended the characterization to depths the DCP cannot reach and, at several sections, identified conditions of the deeper embankment fills and founding soils. At Section E-2, six CPTs to a maximum depth of 32.7 ft found cone tip resistance generally below 30 tsf, and moduli estimated through a site-specific DCP-CPT correlation were below 10 ksi over most of the embankment depth. At Section P-A-3, the cone resistance at one location dropped below about 12 tsf beyond 20 ft, suggesting weak foundation soils that could have contributed to long-term settlement; at Section P-A-4, resistance fell below 10 tsf below about 19 and 23 ft at two locations. At Section E-5, five CPTs showed consistently low resistance (less than 15 tsf) within the embankment, and the sounding at the most distressed location revealed weak founding soils extending well below the embankment. Several soundings met refusal in cement-treated layers, at Section P-A-3 in particular, which limited CPT coverage at some locations.

6.1.5 Soil Sampling and Laboratory Testing

Soil samples were collected using Shelby tubes or grab sampling from augered holes. Laboratory testing included USCS and AASHTO classification, Atterberg limits, moisture content, particle size distribution by sieve and hydrometer. At Section S-11-8, pocket penetrometer tests were performed on undisturbed samples from Shelby tubes. The laboratory results contributed to two things the in-situ tests cannot: confirmation of soil type and gradation evidence of material loss.

The soil classification tests inform the characteristics of the embankment fills. At most sections the fill was low-plasticity clay: CL soils with liquid limits of 27 to 48 and plasticity indices of 10 to 28 at Section E-2, CL/A-6 soils with plasticity indices of 15 to 23 at Section P-A-3, and CL/A-6 soils with liquid limits of 25 to 43 at Section P-A-4. Section E-5 differs sharply: the fill there was fat clay (CH, A-7-6) with liquid limits of 68 to 74, plasticity indices of 43 to 48, and natural moisture contents near 35 percent. At Section E-4, the fill classified as clayey sand (SC) and lean clay (CL).

The moisture content provided useful information about water infiltration. At Section E-1, the southbound embankment showed uniform moisture contents of 12 to 14 percent and correspondingly uniform DCP results, whereas the northbound approach showed moisture contents approaching or exceeding 20 percent, with over 21 percent measured at one location over the same depth interval as the weakest DCP layer, indicating higher degree of saturation. At Section S-11-8, moisture contents were higher near the bridge than away from it and higher in the inside lane than the outside lane, suggesting water flow directed toward the bridge and inside lane; the wettest locations coincided with the low-strength DCP results and the GPR moisture anomaly.

The gradation results provide the most direct laboratory evidence of material washout. At Section E-2, the percentage passing the No. 200 sieve at one sampling location increased from about 56 percent at 3 to 5 ft to about 92 percent at 13 to 15 ft, and the fill at the location with a void beneath the slab was coarser than at the no-void control at similar depth. The consistent pattern of coarser

soil at shallow depth suggests that fines have been washed out of the upper fill by infiltrating water, with the accompanying volume loss contributing to void formation. At Section S-11-8, the percentage passing the No. 200 sieve at one location dropped from 32.5 percent at 5 to 7 ft to 3 percent at 8 to 10 ft, the depth range where the drainage pipe is buried, again indicating localized washout of fines. Gradation anomalies of this kind cannot be detected by FWD, DCP, or GPR, and they carry direct mechanistic significance for the washout classification developed in Chapter 7.

6.2 Guideline for Interpreting FWD Data

6.2.1 Overall Deflection Distributions

Figure 6-1 presents the overall distribution of normalized D_0 for all tested sites. Each box represents the statistical spread of FWD measurements collected along the respective section. Across all sites, the normalized D_0 generally range between 2 and 10 mils, with several locations exhibiting wide interquartile ranges and numerous outliers. The broad spread of deflections indicates that pavement support conditions vary considerably within the pavement on embankment and bridge approach slabs. In general, higher deflections and greater variability tend to occur in sections near bridge approach slabs. This pattern reflects the influence of differential foundation stiffness, loss of materials causing possible loss of slab-subgrade contact, among others.

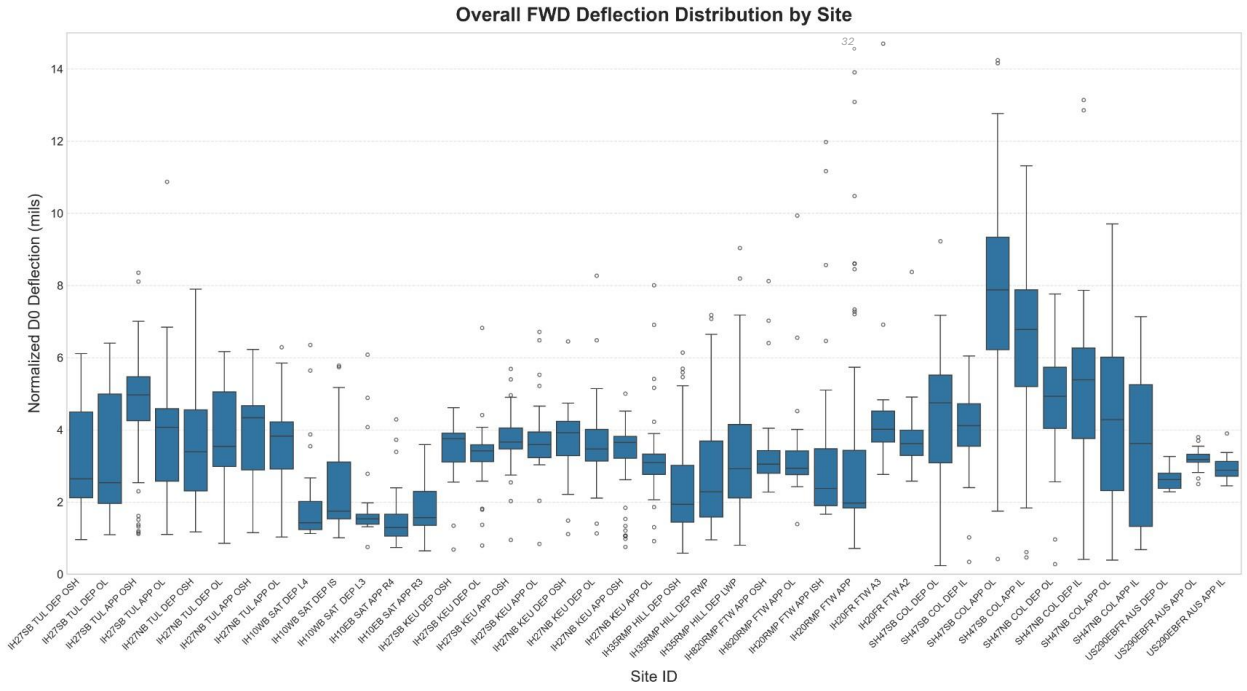


Figure 6-1. Overall FWD deflection distribution by site

Figure 6-2 compares the distributions of deflection data between BAS and the adjacent pavement on embankment (either CRCP or asphalt). In most CRCP systems, deflections data from the BAS are higher than those from the adjacent pavement. This can be attributed to distresses commonly

observed at BAS such as reduced slab-subgrade contact, void development, or inclusion of materials with a density less than pavement or soil such as HDPF. On the other hand, several sites experienced lower BAS deflections relative to the adjacent pavement, indicating well-supported slabs or sections where prior repairs improved contact. The overall pattern underscores that the bridge approach slab area remains the most structurally variable zone along each testing location.

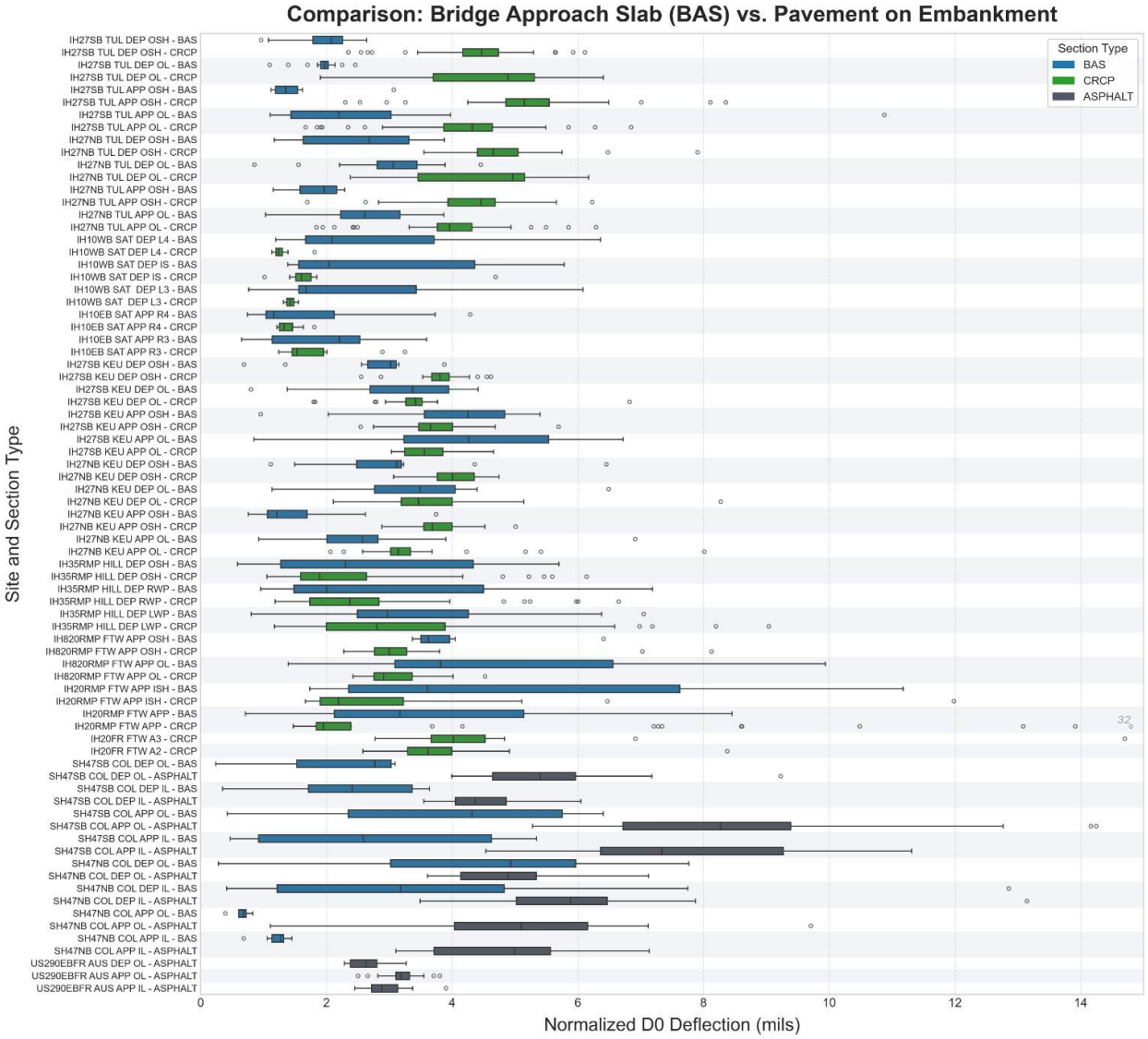


Figure 6-2. Comparison of deflection data obtained from Bridge Approach Slab (BAS) and pavement on embankment

Figure 6-3 and **Table 6-1** summarize the mean and standard deviation of normalized D_0 deflection for each site and section type. Most BAS sections in CRCP systems fall within deflection range of

3 to 6 mils, whereas adjacent pavement sections deflection typically range from 2 to 4 mils. The BAS sections also show larger variability, reflecting the irregular shape of the deflection response along the slab.

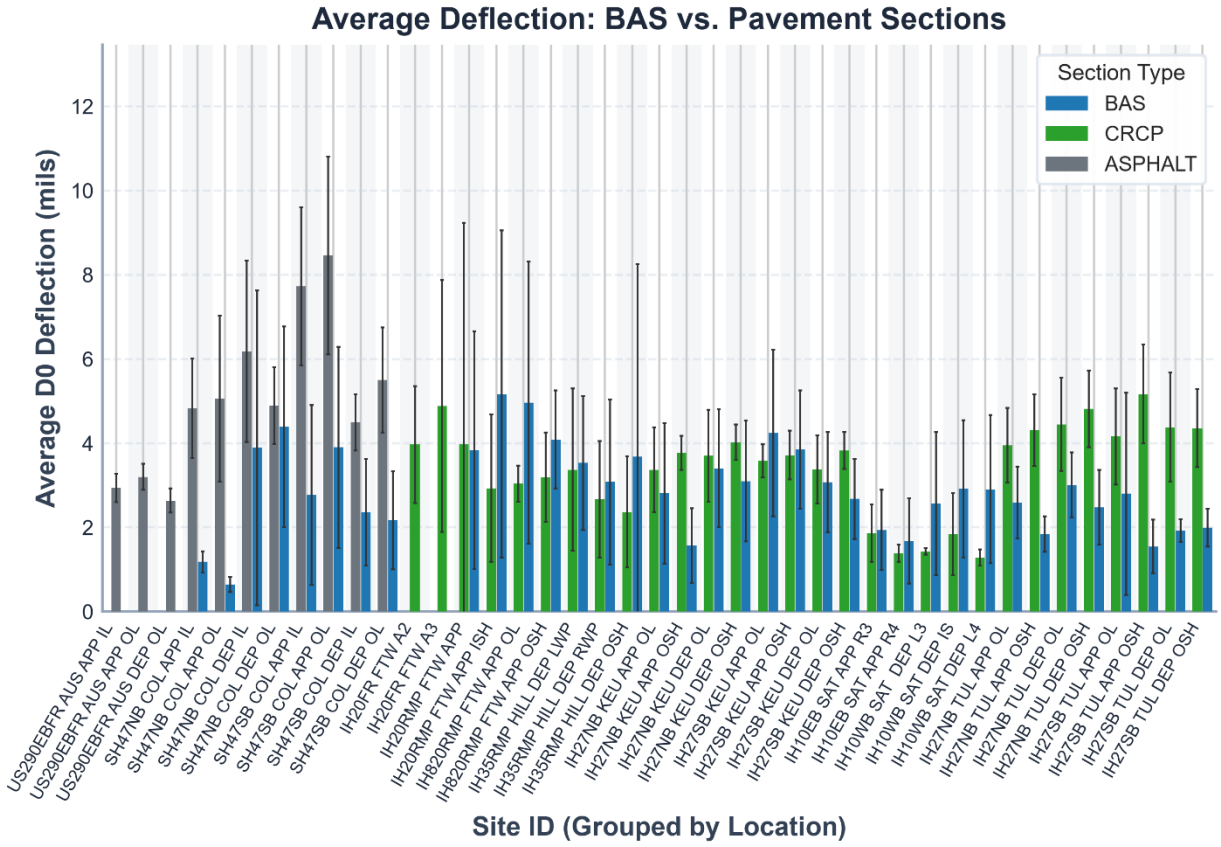


Figure 6-3. Average and standard deviation of normalized D_0 deflection by site

Table 6-1. Average and standard deviation of normalized D_0 from FWD by site

Site ID	Section Type	Average D_0 (mils)	Std. Dev. Of D_0	Avg. $D_{0,BAS}$ − Avg. $D_{0,Pavement}$
IH10EB SAT APP R3	BAS	2.0	0.9	0.1
	CRCP	1.9	0.7	
IH10EB SAT APP R4	BAS	1.7	1.0	0.3
	CRCP	1.4	0.2	
IH10WB SAT DEP L3	BAS	2.6	1.7	1.2
	CRCP	1.4	0.1	
IH10WB SAT DEP IS	BAS	2.9	1.6	1.1
	CRCP	1.8	1.0	
IH10WB SAT DEP L4	BAS	2.9	1.8	1.6
	CRCP	1.3	0.2	
IH20FR FTW A2	CRCP	4.0	1.4	-
IH20FR FTW A3	CRCP	4.9	3.0	-
IH20RMP FTW APP	BAS	3.8	2.8	-0.2
	CRCP	4.0	5.3	
IH20RMP FTW APP ISH	BAS	5.2	3.9	2.3
	CRCP	2.9	1.7	
IH27NB KEU APP OL	BAS	2.8	1.7	-0.6
	CRCP	3.4	1.0	
IH27NB KEU APP OSH	BAS	1.6	0.9	-2.2
	CRCP	3.8	0.4	
IH27NB KEU DEP OL	BAS	3.4	1.4	-0.3
	CRCP	3.7	1.1	
IH27NB KEU DEP OSH	BAS	3.1	1.4	-2.2
	CRCP	4.0	0.4	
IH27NB TUL APP OL	BAS	2.6	0.8	-0.3
	CRCP	3.9	0.9	
IH27NB TUL APP OSH	BAS	1.8	0.4	-0.9
	CRCP	4.3	0.8	
IH27NB TUL DEP OL	BAS	3.0	0.8	-1.3
	CRCP	4.4	1.1	
IH27NB TUL DEP OSH	BAS	2.5	0.9	-2.5
	CRCP	4.8	0.9	
IH27SB KEU APP OL	BAS	4.2	2.0	-1.4
	CRCP	3.6	0.4	
IH27SB KEU APP OSH	BAS	3.8	1.4	-2.3
	CRCP	3.7	0.6	
IH27SB KEU DEP OL	BAS	3.0	1.2	0.6
	CRCP	3.4	0.8	
IH27SB KEU DEP OSH	BAS	2.7	0.9	0.1
	CRCP	3.8	0.4	

Site ID	Section Type	Average D_0 (mils)	Std. Dev. Of D_0	Avg. $D_{0,BAS}$ − Avg. $D_{0,Pavement}$
IH27SB TUL APP OL	BAS	2.8	2.4	-0.4
	CRCP	4.2	1.1	
IH27SB TUL APP OSH	BAS	1.5	0.6	-1.1
	CRCP	5.2	1.2	
IH27SB TUL DEP OL	BAS	1.9	0.2	-1.4
	CRCP	4.4	1.3	
IH27SB TUL DEP OSH	BAS	2.0	0.4	-3.7
	CRCP	4.4	0.9	
IH35RMP HILL DEP LWP	BAS	3.5	1.6	0.2
	CRCP	3.4	1.9	
IH35RMP HILL DEP RWP	BAS	3.1	2.0	0.4
	CRCP	2.7	1.4	
IH35RMP HILL DEP OSH	BAS	3.7	4.6	1.3
	CRCP	2.4	1.3	
IH820RMP FTW APP OL	BAS	5.0	3.3	-2.5
	CRCP	3.0	0.4	
IH820RMP FTW APP OSH	BAS	4.1	1.1	-2.4
	CRCP	3.2	1.1	
SH47NB COL APP IL	ASPHALT	4.8	1.2	2
	BAS	1.2	0.2	
SH47NB COL APP OL	ASPHALT	5.0	2.0	0.9
	BAS	0.6	0.2	
SH47NB COL DEP IL	ASPHALT	6.2	2.1	-3.6
	BAS	3.9	3.7	
SH47NB COL DEP OL	ASPHALT	4.9	0.9	-4.4
	BAS	4.4	2.4	
SH47SB COL APP IL	ASPHALT	7.7	1.9	-2.3
	BAS	2.8	2.1	
SH47SB COL APP OL	ASPHALT	8.5	2.3	-0.5
	BAS	3.9	2.4	
SH47SB COL DEP IL	ASPHALT	4.5	0.7	-4.9
	BAS	2.4	1.3	
SH47SB COL DEP OL	ASPHALT	5.5	1.2	-4.6
	BAS	2.2	1.2	
US290EBFR AUS APP IL	ASPHALT	2.9	0.3	-
US290EBFR AUS APP OL	ASPHALT	3.2	0.3	-
US290EBFR AUS DEP OL	ASPHALT	2.6	0.3	-

In many bridge approach slabs, the deflection profile rises toward the sleeper-slab end and sometimes peaks near mid-slab, while significantly lower deflections are recorded near the

abutment on which the BAS is supported. Sharp localized spikes in the middle portion of the slab often correlated with voids or partial loss of subgrade contact beneath that region confirmed by coring operation. These features explain the higher variability in BAS deflection statistics. A typical example of this behavior can be seen in **Figure 6-4** (IH 10 WB SAT DEP L4), where the deflection increases sharply near the sleeper-slab end (indicated by BAS-pavement "Joint") and shows a secondary rise toward mid-slab before tapering near the abutment. Voids were observed in mid slab where spike in deflection was recorded. Although additional cores confirmed that the void extended over a larger portion of the approach slab, the lower deflection near the bridge abutment end is attributed to the load being transferred to the stiffer bridge structural member (abutment). In general, whenever a spike in deflection was observed in a BAS, voids were also found beneath that location between pavement and base layer.

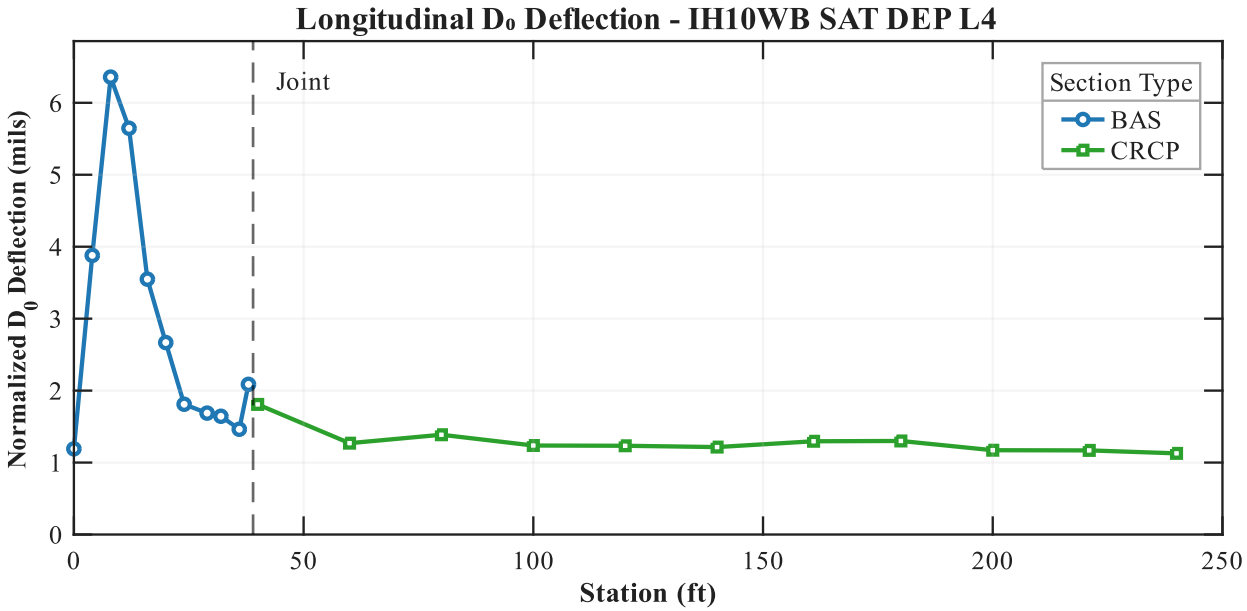


Figure 6-4. Longitudinal D_0 deflection profile: IH10WB SAT DEP L4

Additional examples exhibit a similar pattern. The IH820 ramp in Fort Worth (**Figure 6-5**) and the SH 47 NB College Station Departure (**Figure 6-6**) sections both show a mid-slab spike in deflection where voids were detected through coring. The dataset demonstrates that while many pavements exhibit relatively narrow range of deflections, localized soft or voided zones can significantly increase D_0, producing the long upper whiskers and multiple outliers seen in **Figure 6-1** and **Figure 6-2**.

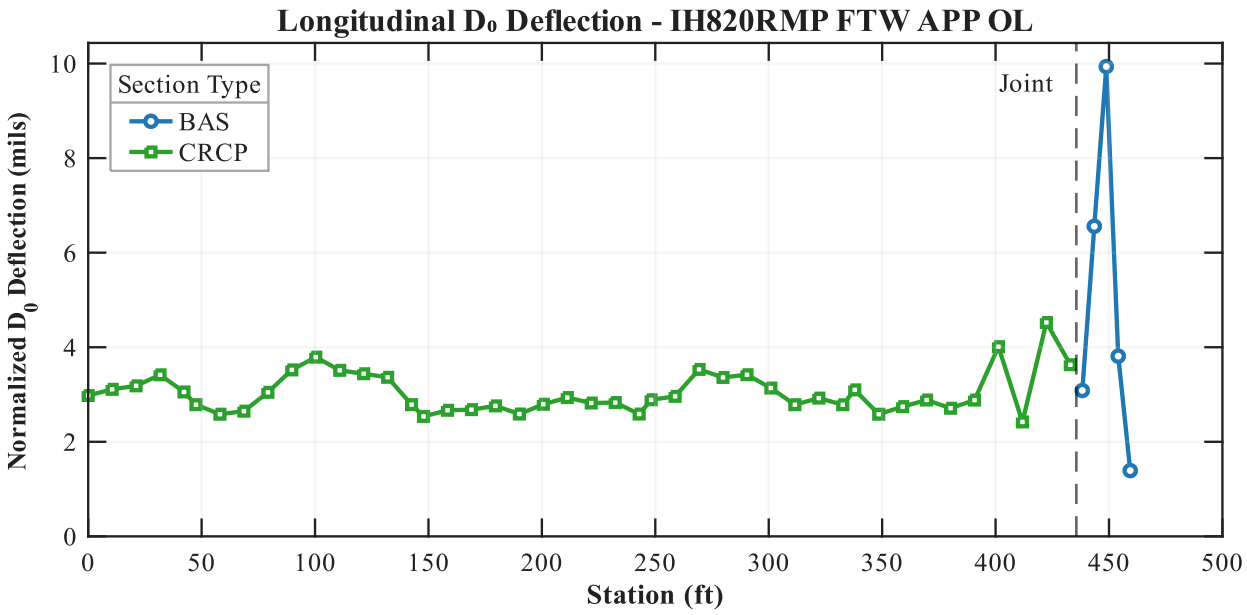


Figure 6-5. Longitudinal *D*₀ deflection profile: IH820RMP FTW APP OL

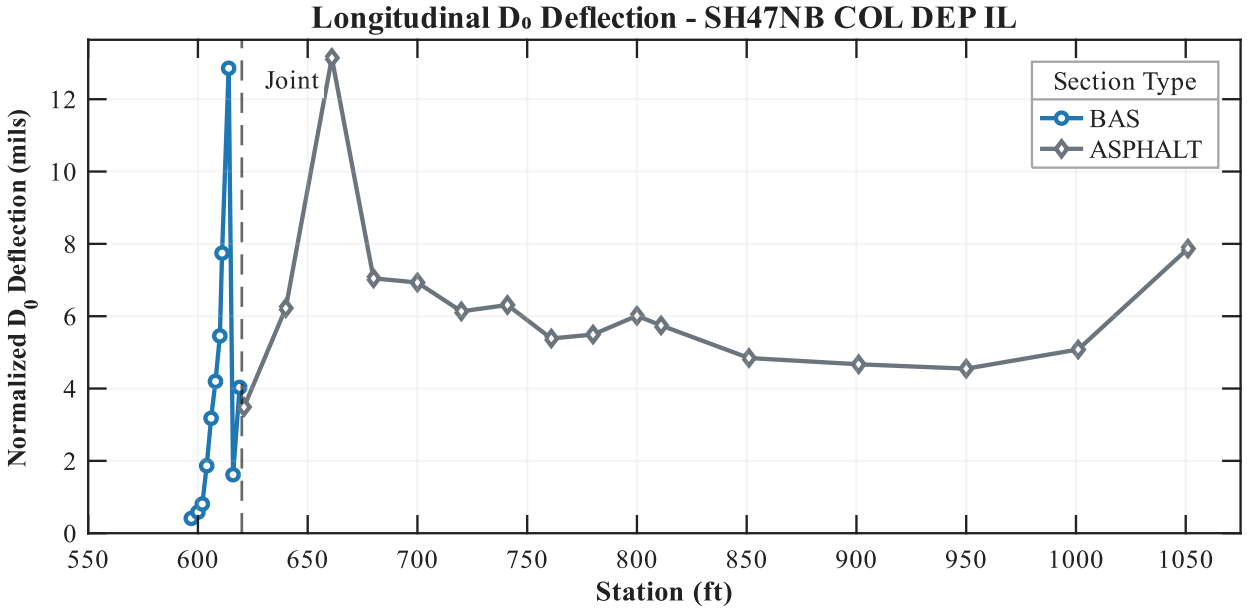


Figure 6-6. Longitudinal *D*₀ deflection profile: SH47NB COL Dep IL

Another recurring trend is the opposite case: lower BAS deflection than the adjacent pavement. This was often observed at sections where previous BAS rehabilitation successfully re-established slab-subgrade contact. The SH 47 NB College Station Approach (outside lane) is a clear example (**Figure 6-7**). This asphalt pavement section shows significantly lower deflection at the BAS and a generally reduced trend in the pavement near the approach, consistent with an asphalt overlay applied to correct earlier settlement. The deflection pattern correlates well with the asphalt overlay

thickness and demonstrates that pavement thickness strongly influences FWD response. No voids were detected along this BAS during coring.

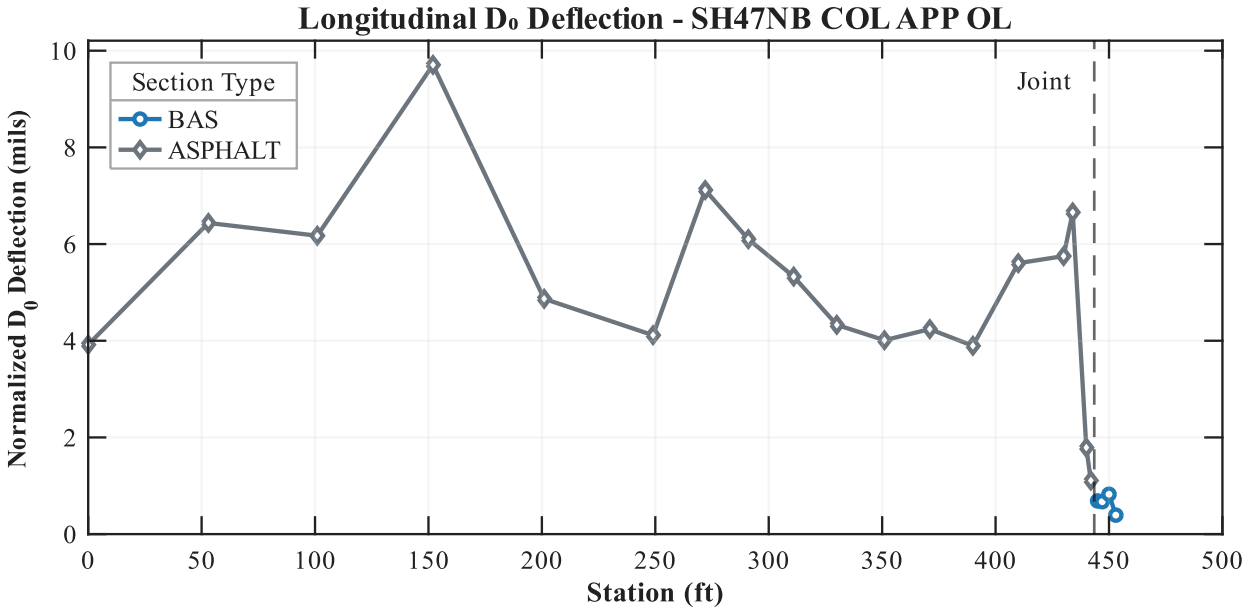


Figure 6-7. Longitudinal D_0 deflection: SH47NB COL APP OL

A similar condition was observed at IH 27 SB Tulia (**Figure 6-8**), where a bridge approach slab was added later to an originally continuous pavement. The addition appears to have maintained contact between the pavement and subgrade, as indicated by lower BAS deflection relative to the adjacent pavement and no evidence of the void presence.

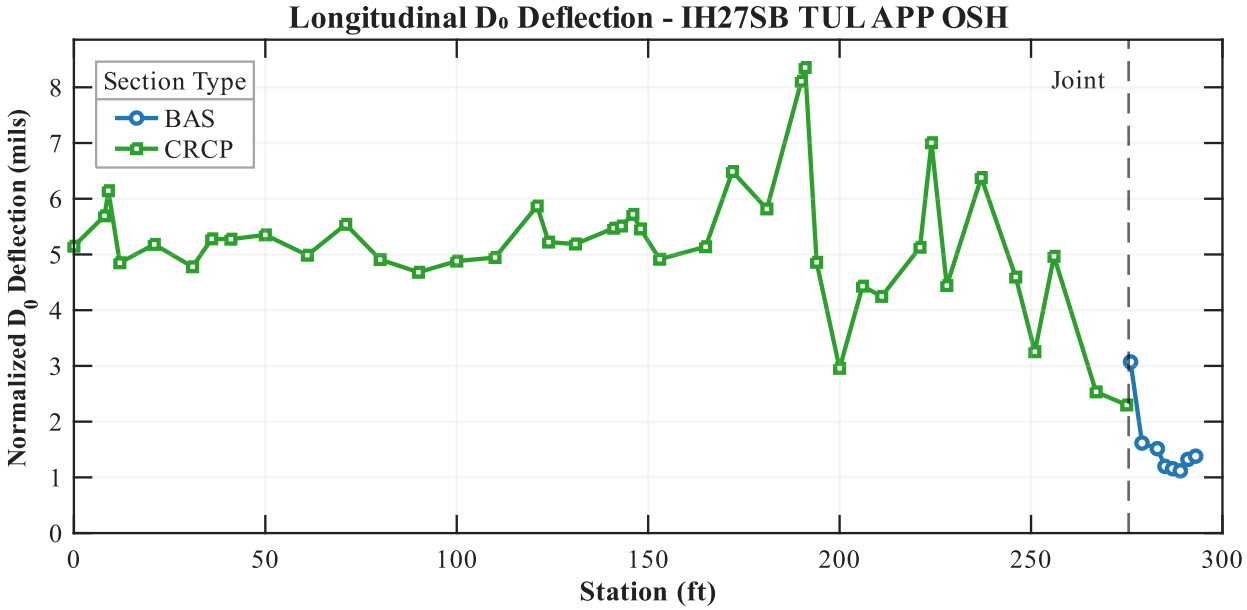


Figure 6-8. Longitudinal D0 Deflection: IH27SB TUL APP OSH

In summary, the FWD results demonstrate that bridge approach slabs exhibit greater deflection variability than the adjoining pavement on embankment, reflecting differences in pavement-subgrade contact conditions. The deflection typically rises toward the sleeper-slab end, sometimes peaks near mid-slab, and tapers toward the abutment, providing a reliable indicator of underlying support behavior. In some cases, localized spikes signify voids or partial separation beneath the slab, whereas uniform, lower responses correspond to well-supported approaches or successful rehabilitation.

6.2.2 Effect of Slab Thickness on Deflection

Slab thickness is one of the primary factors influencing the structural response of a pavement system under FWD loading. Thicker slabs distribute load over a wider area, reducing tensile stresses and surface deflection measured at the loading plate. To evaluate the effect of slab thickness on measured deflection, the statewide reference curve developed under TxDOT Research Project 0-5445 was adopted as a benchmark (*Won and Medina, 2008*). The study analyzed 27 CRCP sections across Texas and found a strong inverse relationship between slab thickness of well-performing CRCP and normalized central deflection (D_0) under a 9000-lb load. As shown in **Figure 6-9**, the statewide dataset can be expressed by an empirical relationship as follows:

$$D_0^w = 252.85 \times (t_{slab})^{-2.005} \quad (4)$$

where D_0^w= central deflection normalized with respect to 9000 load from FWD test performed on well-performing CRCP (in mils) and t_{slab} = thickness of CRCP (in inches). Note that the thickness of CRCP in the original dataset ranges between 8 in and 15 in.

For well-performing CRCP, the graph indicated that deflection decreased rapidly with increasing thickness; slabs thicker than about 13 in exhibited deflections typically less than 2 mils.

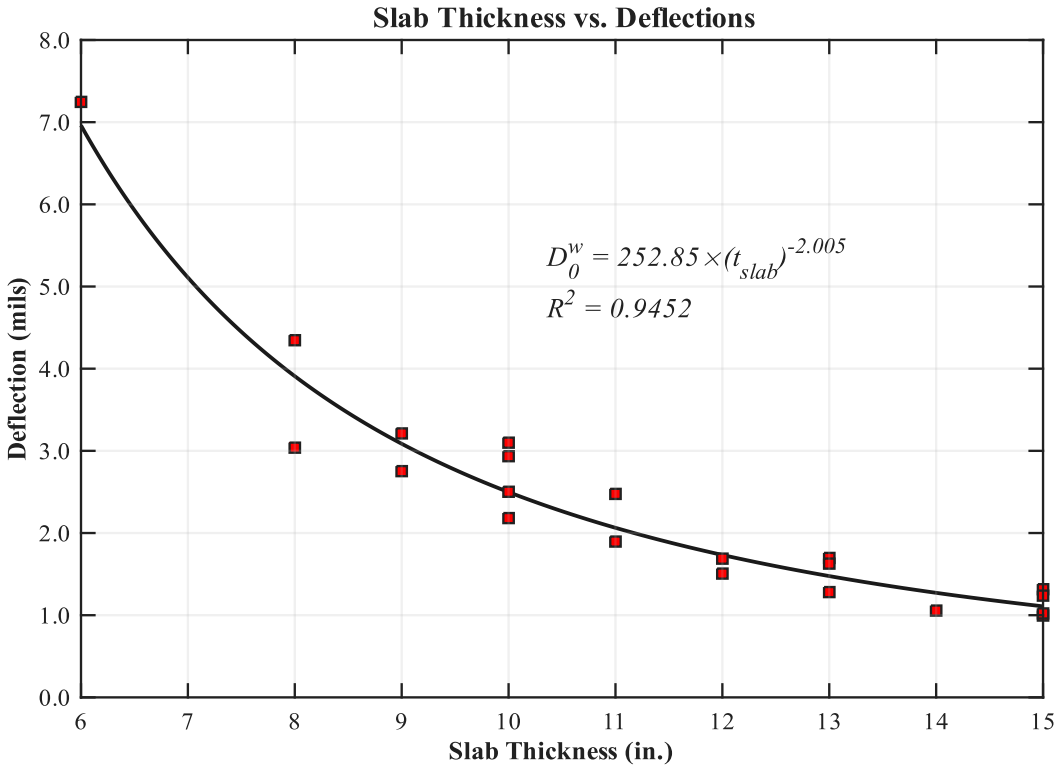


Figure 6-9. Slab thickness of well-performing CRCP vs normalized central deflection from FWD (modified after TxDOT Project 0-5445)

Figure 6-10 compares the deflection data obtained from FWD tests performed on the BAS and adjacent pavement during this study with the CRCP statewide average curve (benchmark) and 1.5, 2, and 3 times statewide average curves. Each data point in **Figure 6-10** represents the normalized D_0 from a single FWD drop plotted against the corresponding slab thickness obtained from coring or GPR scans where available. Thickness measured from GPR were calibrated using coring information as a ground truth at limited locations for accurate measurement. Locations without reliable GPR scans were excluded. Sections with asphalt surface, such as SH 47, US 290, and IH 10 (San Antonio overlay sections), were omitted because the surface deflection response of asphalt differs from that of concrete. Data points in **Figure 6-10** are color coded by observed support condition, classified from field investigation and coring into four categories: normal support, high-density polyurethane (HDPF) only, void only, and void + HDPF.

It was observed that about 81% of all data points located above the 1.5-times benchmark corresponded to drop locations where voids or HDPF injections were observed. Similarly, 95.5% of all data points that showed the FWD deflections 2-times or greater than the benchmark had voids or HDPF injections. Almost all data points (98.3%) above 3-times benchmark line had either a void or HDPF. Most well-supported CRCP slabs in this study aligned closely with the statewide average trend. A small subset of sections showed deflections well below the benchmark, typically

at bridge approach slabs near the bridge joint, where the slab is supported by a stiff abutment foundation providing minimal FWD deflection.

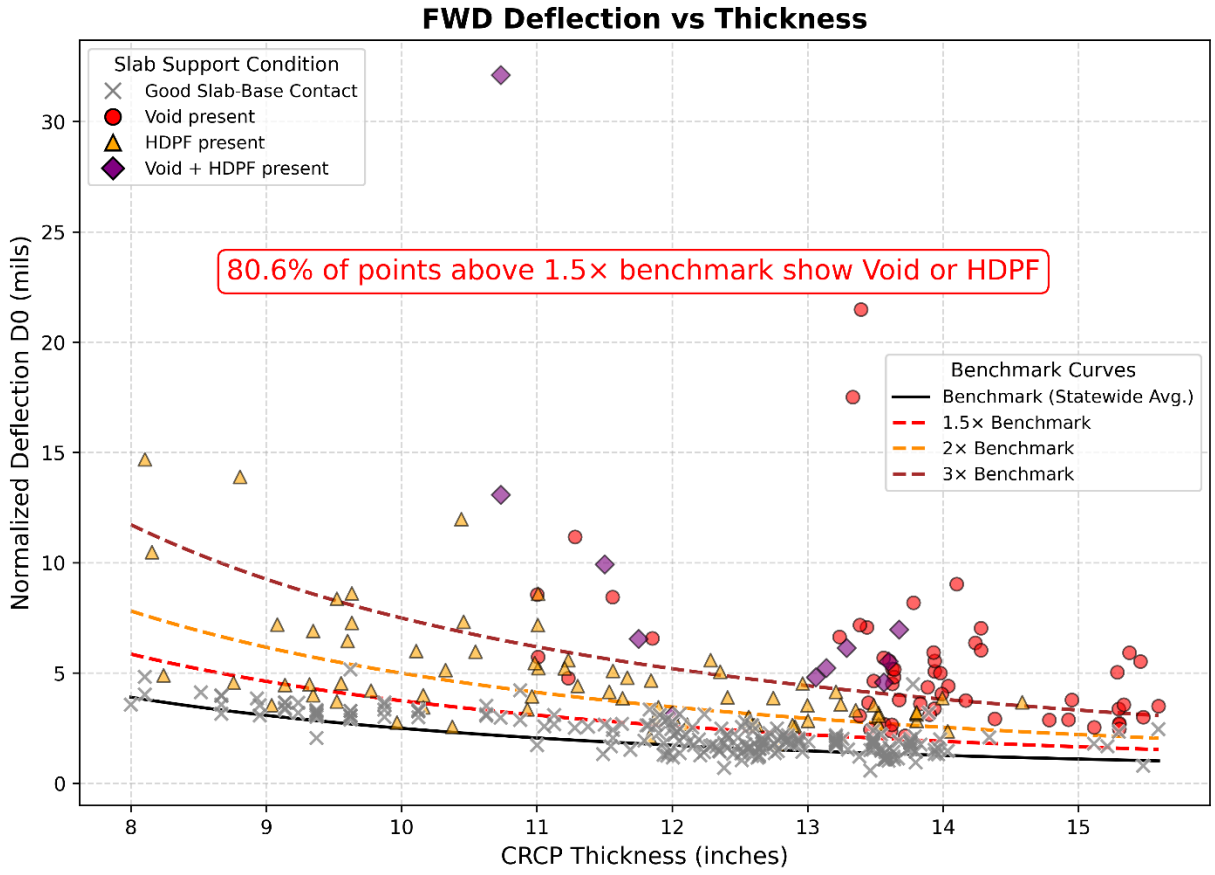


Figure 6-10. Observed FWD central deflection (D_0) vs CRCP thickness

The multiplicative factors of 1.5, 2 and 3 were selected as proportional thresholds to identify sections exhibiting significantly greater deflection than the statewide benchmark value. This proportional approach is preferred over an additive offset (e.g., +1 mil) because deflection varies nonlinearly with slab thickness due to the inverse-power relationship. Furthermore, field data show that the variability of deflection increases as slab thickness decreases. Thinner slabs exhibit a wider spread of deflections due to their greater sensitivity to local support conditions, whereas thicker slabs show tighter distributions around the mean. Applying a fixed additive threshold would fail to account for this scale-dependent variability. In contrast, a multiplicative threshold such as 1.5x the statewide benchmark provides a simple and consistent proportional measure of deviation across all thickness ranges and better aligns with the observed behavior of CRCP systems.

To further quantify these differences, the deflection ratio, defined as (measured D_0/benchmark D_0), was evaluated for each observation, and cumulative distributions were generated by support condition type in **Figure 6-11**.

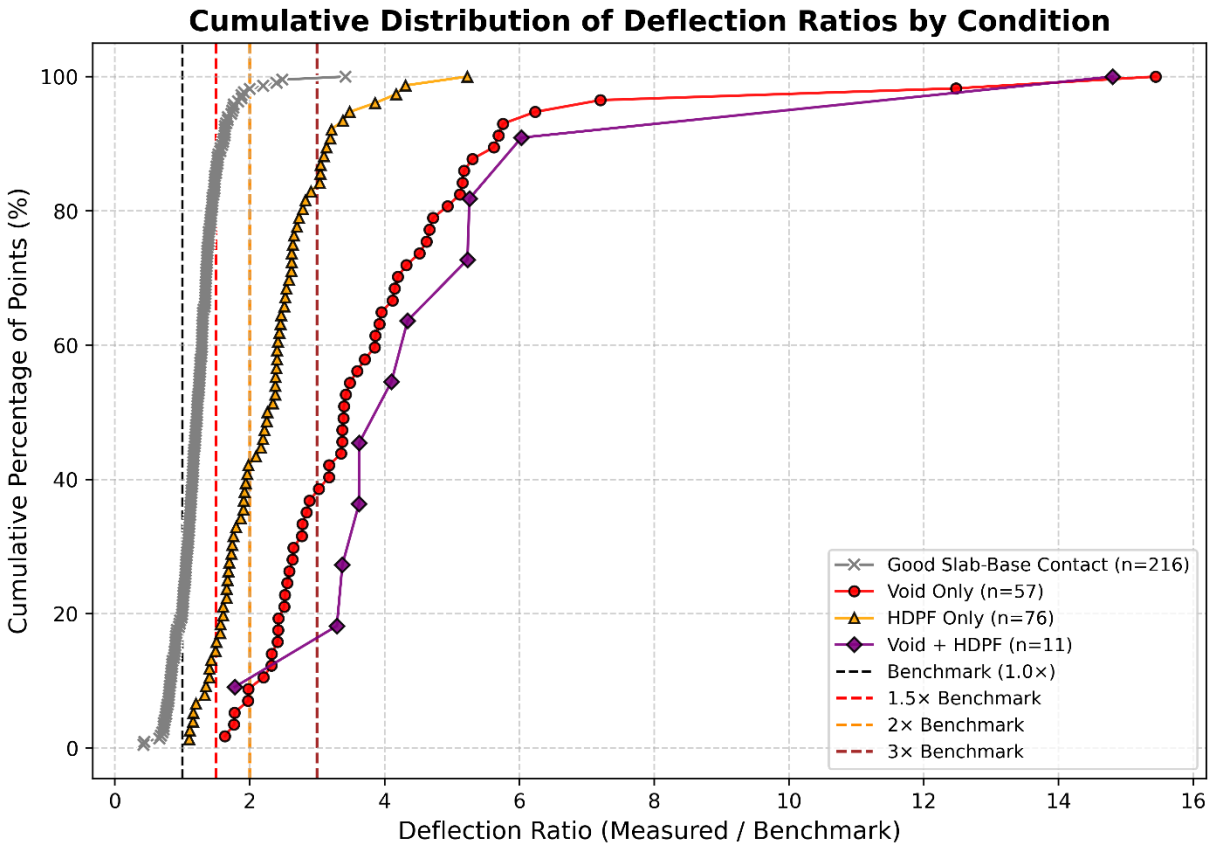


Figure 6-11. Cumulative distribution of deflection ratios by condition type

Points with no voids/HDPF were observed tightly around a ratio of 1.0, confirming agreement with statewide performance. Sections containing HDPF or voids exhibit significantly higher ratios, with many exceeding 1.5. About 95.5 % of all points with deflection greater than two times the statewide average benchmark value showed the presence of HDPF, void, or both. This threshold provides a practical quantitative indicator of the potential presence of void or HDPF when FWD results are interpreted relative to the statewide benchmark.

6.2.3 Segmentation of FWD Deflection

FWD deflection profiles often show noticeable variability even within the same site due to surface condition changes, surface defects, localized repair materials, variability in slab thickness, or different support conditions. These fluctuations can make the data appear noisy when viewed point by point. The goal of segmentation is to divide the continuous FWD deflection profile into zones that behave similarly, filtering out noise and emphasizing significant changes in structural response. Instead of interpreting every drop individually, the analysis identifies breakpoints: locations where the deflection trend changes significantly. This makes it possible to isolate areas that act differently from the rest of the slab (e.g., stiffer abutment support, HDPF-treated area) and to interpret the data in more informative manner.

A common approach to segmentation uses dynamic programming (DP) algorithm to identify the set of breakpoints that minimizes the total variation of deflection within each segment. Conceptually, the algorithm tests many possible ways of dividing the data into segments and selects the one that gives the smallest overall squared error within each group.

In practical terms:

- For each possible segment, the algorithm computes how "flat" the deflection data are inside it.
- A segment that contains data with consistent deflection will have a small internal cost (little variation).
- A segment that spans two different behaviors (for example, a stiff abutment end and a softer interior) will have a large cost.
- The DP method evaluates all combinations and picks the one that minimizes the total cost across the entire profile.

This can be written generally as:

$$\text{Total Cost} = \sum_{k} \sum_{i} (y_i - \overline{y_k})^2 \tag{5}$$

where y_i is the normalized deflection and $\bar{y}_k$ is the mean value within each segment k. The breakpoints are chosen such that this total cost is the smallest possible.

Adding more breakpoints always reduces the total error, but too many segments make the results noisy and difficult to interpret. To avoid over-segmentation, the "Elbow Method" was used to determine the optimum number of breakpoints. The Elbow Method plots the total segmentation cost versus the number of breakpoints. Initially, the cost drops rapidly as obvious discontinuities are captured. After a certain point, the improvement becomes marginal. The point where the curve "bends" (the elbow) is selected as the optimal number of segments.

Segmenting the deflection profile provides a macro-level view of how the pavement system behaves:

- Short, high-deflection segments usually indicate a localized problem, such as a void or partial loss of support beneath the slab.
- Longer, elevated segments suggest a broader soft zone or HDPF-treated region. If an area shows deflections higher than 1.5x the benchmark over a long stretch, it is unlikely to be a small void and more likely to represent a systematic support issue or HDPF injection.

Figure 6-12 shows a typical cost-versus-segment relationship and the selected elbow point used to determine the optimal segmentation. How the algorithm works is illustrated in **Figure 6-13** by taking IH20 Fort Worth as an example. **Figure 6-13** shows a series of intermediate segmentation results for increasing numbers of breakpoints (from two to six). As the number of segments

increases, large-scale changes are captured first (e.g., abutment vs. main pavement), followed by smaller refinements until the elbow point is reached.

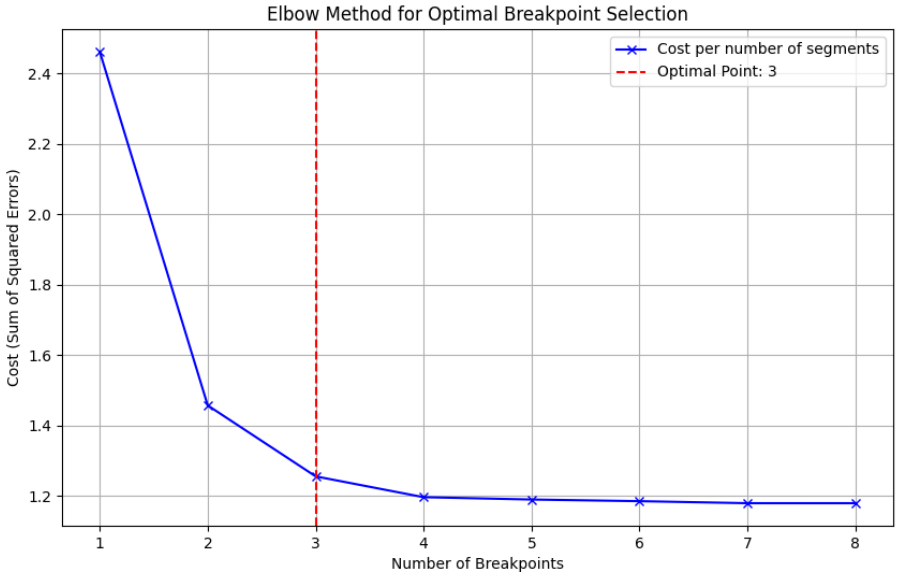


Figure 6-12. Typical example of "elbow method" for determining the optimal number of segments

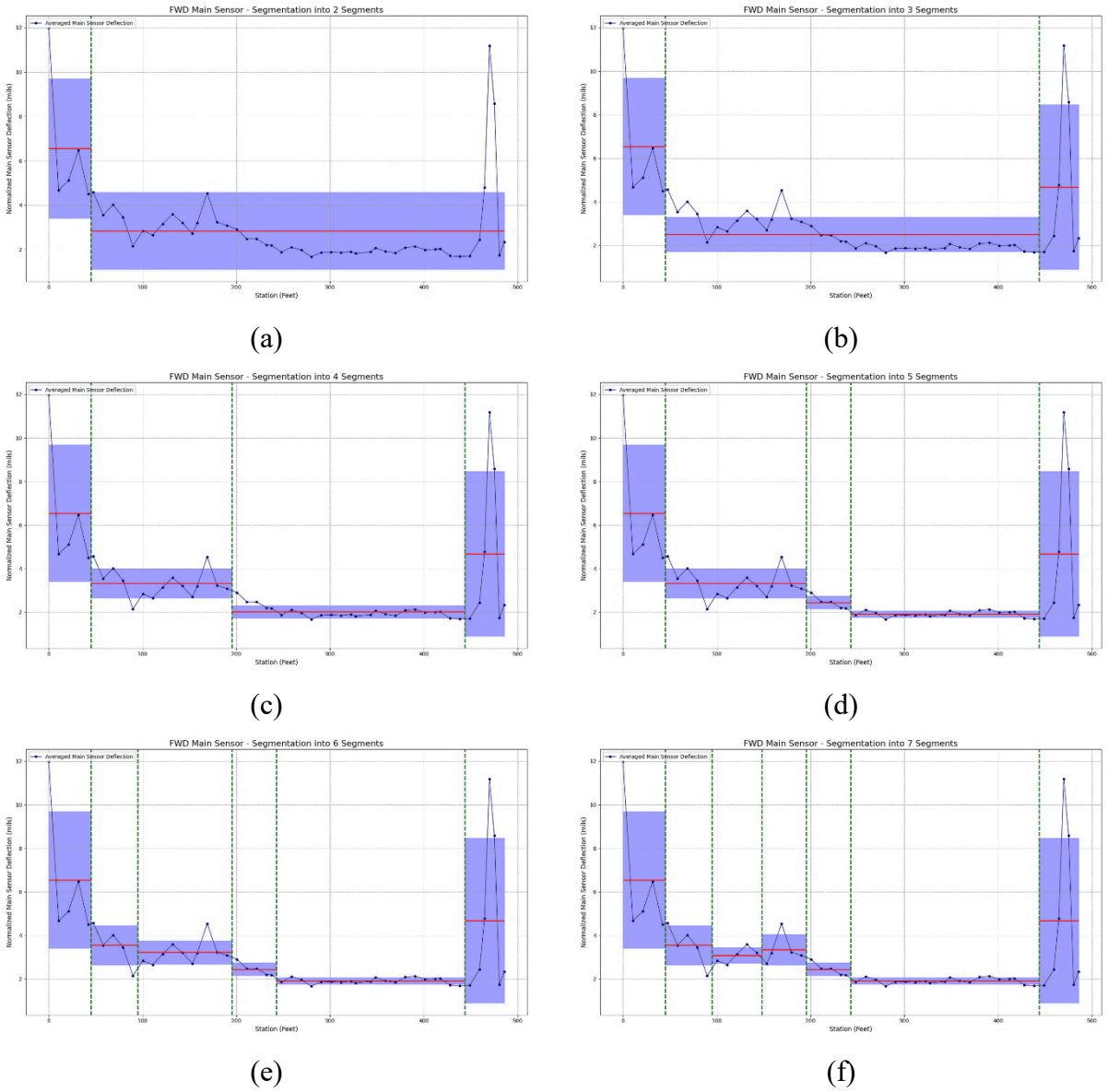


Figure 6-13. Iterative segmentation examples showing progression toward optimal segmentation (IH-20 Fort Worth Ramp)

Figure 6-14 presents one representative case of IH20 Fort Worth ramp where the segmentation results were verified through GPR and coring. This section corresponds to a ramp with variable slab thickness and a mix of HDPF-treated and voided regions. The dashed blue and green horizontal lines in **Figure 6-14** represent the statewide average deflection for well-performing CRCP sections of equivalent thickness, 2.49 mils for a 10-in slab and 1.47 mils for a 13-in slab, based on the statewide deflection-thickness relationship presented in Eq. (4). These values served as reference points for interpreting the magnitude of measured deflection. The deflection profile

was segmented into four distinct zones that align with the structural conditions observed in the field:

1. Segment 1: Thinner Slab with HDPF (≈ 10 in) – The first zone displayed high normalized deflections (6–8 mils). GPR scans indicated a thinner slab (~10 in) and negative reflections beneath the surface corresponding to HDPF injection. The consistently elevated deflection pattern is typical of soft, HDPF-treated support rather than a discrete void.
2. Segment 2: 13-in Slab with HDPF – The next segment exhibited moderate deflections (3–4 mils) over a long length. Coring confirmed a thicker slab (~13 in) still supported by HDPF. The uniform but higher deflection response than the state-wide average for 13-in-thick CRCP suggests a repaired but flexible base.
3. Segment 3: 13-in Slab with Normal Support – The third segment maintained low, consistent deflections (~2 mils) across nearly 200 ft, representing well-bonded slab–subgrade contact. No voids or repairs were identified here.
4. Segment 4: Bridge Approach Slab with Voids – The final segment near the abutment showed a steep deflection rise and greater variability. GPR revealed strong negative reflections, and coring confirmed voids under the slab. The algorithm correctly isolated this zone as a separate high-deflection region.

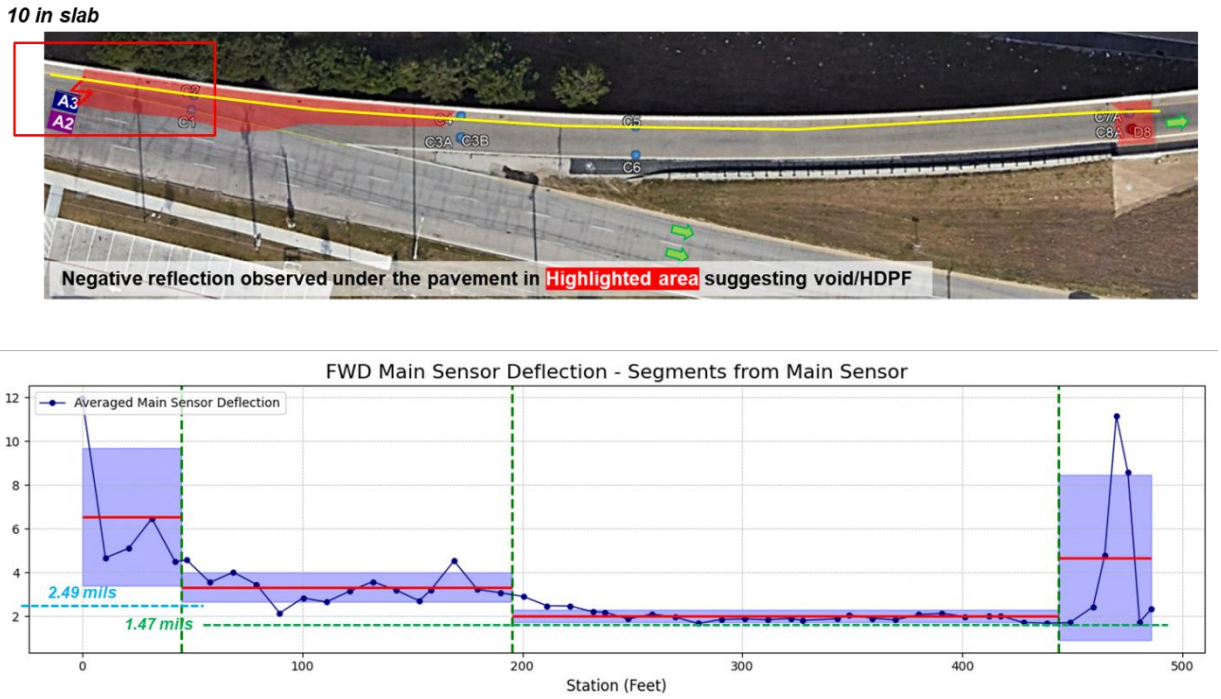


Figure 6-14. Field-validated segmentation isolating thinner slab, HDPF, normal support, and voided bridge-approach regions (IH-20 Ramp)

The segmentation matched the field conditions remarkably well, confirming that the method reliably distinguishes between thinner slabs, HDPF-treated zones, normal support, and true voids.

6.3 Guideline for Interpreting Dynamic Cone Penetrometer (DCP) Test Data for Evaluation of Embankment Fill Conditions

6.3.1 Overview

Dynamic Cone Penetrometer (DCP) testing was carried out at each test site to evaluate the in-situ stiffness of the subgrade and embankment fill materials beneath the pavement structure. At each test location, the number of blows required to drive the cone through successive depth intervals was recorded and later converted into penetration index values, which were subsequently correlated to soil modulus (M_r) using empirical relationships. The DCP-derived M_r profile provided continuous vertical stiffness distribution with depth at each test location.

To interpret how these properties relate to pavement performance, each DCP test location was georeferenced and mapped directly to field distress observations recorded during the site investigations. Distress types were classified as cracks, settlement, voids, material washout, and pavement material deterioration. DCP tests at locations where no distress was observed also performed as controls.

6.3.2 Minimum M_r value at different DCP locations.

After obtaining M_r profile at each location from DCP tests, the lowest M_r value from the test location was extracted to represent the weakest layer within that profile. The minimum M_r value from each test location was then associated with the distress types to examine how the subgrade stiffnesses varied between controls and distressed areas. These results were plotted and analyzed with distress type, layer depth, and thickness of the weakest layer to gain insights into the relation between M_r value and embankment/BAS performance.

Figure 6-15 presents the lowest M_r values identified from each test location and the observed distress types near the DCP test location. **Figure 6-15** indicates that control/no-distress locations generally maintain minimum M_r values greater than 10 ksi (79% of control locations where no distress was observed show M_r values greater than 10 ksi). By contrast, 86% of DCP test locations where settlements were observed show the minimum M_r values less than 10 ksi. Similarly, all DCP locations with longitudinal or diagonal /half-moon cracking and 83% of those with material washout show a minimum M_r value of less than 10 ksi. These observations indicate that pavement or BAS distresses observed at the test sites are consistently associated with M_r values below approximately 10 ksi, and the dashed horizontal line in **Figure 6-15** represents the threshold value (i.e., M_r = 10 ksi).

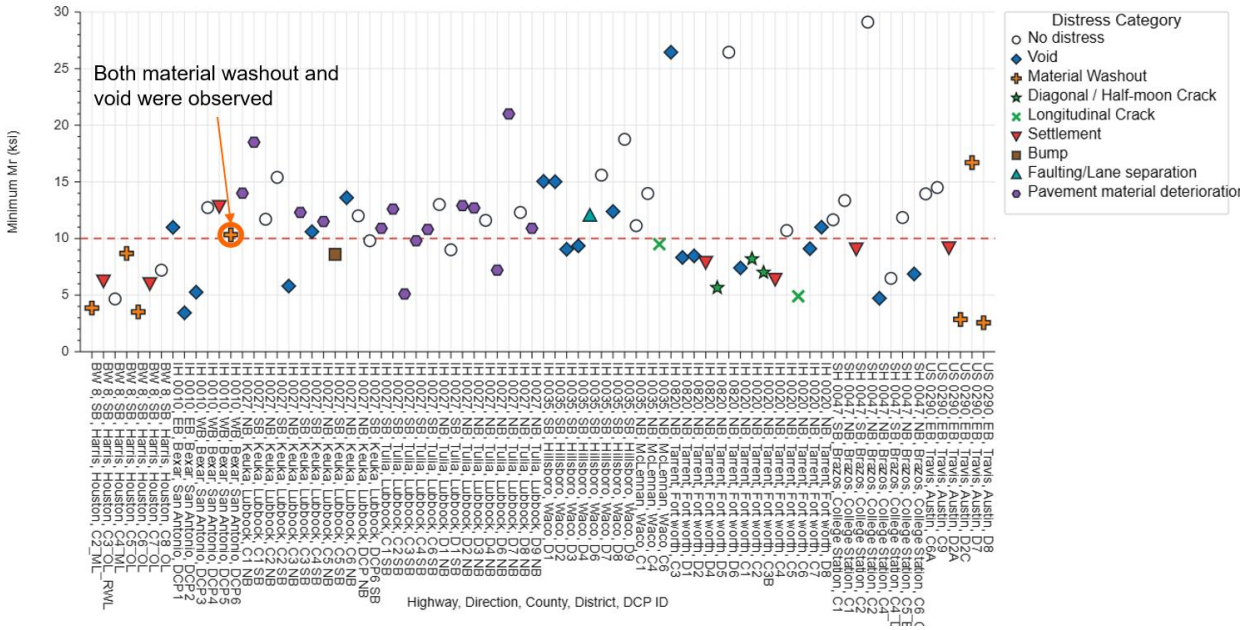


Figure 6-15. Minimum M_r value at each test location associated with distress types

Figure 6-15 also includes data points for the distress type categorized as 'pavement material deterioration,' represented by purple hexagonal symbols, and most of them are located above the threshold line at M_r = 10 ksi. As presented in Chapter 5.10, the DCP tests and coring performed at these locations in IH27 in Tulia revealed that the distresses observed on the pavement surface were primarily due to deterioration of concrete rather than poor embankment materials. Accordingly, these data points are excluded in the subsequent analysis to focus on the evaluations of embankment materials.

Some DCP test locations where voids were observed showed minimum M_r values above 20 ksi, and this requires further explanation. As stated previously, the M_r value in **Figure 6-15** is the minimum value of the embankment materials *beneath* the void. When voids are present, the pavement/BAS is partially or fully unsupported because voids are typically at the pavement-base interface or base-subgrade interface. Therefore, at test locations where voids were observed, distresses at pavement/BAS observed in the vicinity of such locations are most likely caused by the lack of slab support due to the presence of voids, and the M_r values at deeper depths beneath the void become less relevant to the distresses.

To consider the lack of slab support due to the presence of voids, refined interpretation rules were applied. In **Figure 6-16**, test locations where voids were present are assigned an effective M_r value of 0 ksi, reflecting the fact that the void beneath the slab provides no structural support regardless of deeper stiffer materials. Note that DCP6 location from IH10 San Antonio, categorized as "material washout" (circled with orange in **Figure 6-15**), shows an M_r value dropped to zero ksi in **Figure 6-16** as both the void and material washout were observed at this location.

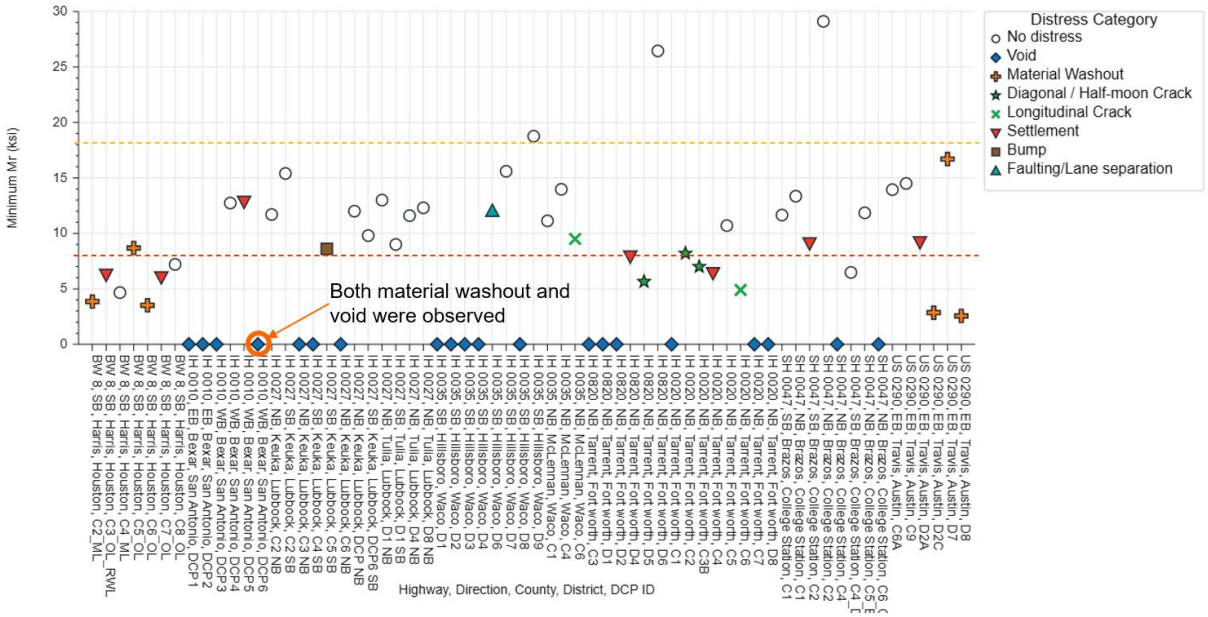


Figure 6-16. Minimum M_r value at each test location associated with distress types; Minimum M_r value was assigned to zero for locations with voids.

After refining the interpretation rules, **Figure 6-16** suggests that the two minimum threshold M_r values, represented by two horizontal dashed lines at 8 ksi and 18 ksi, can be used as guidelines for evaluation of embankment materials. Of the 40 distressed locations included in the analysis, 31 locations (78%) had effective minimum M_r values below 8 ksi. These locations included voids, settlements, material washout, and longitudinal and diagonal/half-moon pavement cracks. The remaining 9 distressed locations (23%) had effective minimum M_r values between 8 ksi and 18 ksi and included settlements, material washout, pavement cracks, a bump, and faulting/lane separation. When the minimum M_r values were greater than 18 ksi, no distresses related to poor embankment materials were observed.

6.3.3 Spatial context and thickness of layer corresponding to minimum M_r

The spatial context of the weak layer associated with the low M_r value is analyzed in this section. **Figure 6-17** presents the minimum M_r value versus the depth corresponding to the M_r value (*i.e.*, mid-depth of the weak layer associated with the minimum M_r value). According to **Figure 6-17**, control locations tend to have their weakest layer at greater depth (typically 40 to130 in below the pavement surface), and even M_r values for those "weakest" layers usually remain greater than 8 ksi, (shown as Region A in **Figure 6-17**). Distressed locations, in contrast, commonly show their minimum M_r within the upper 20 to 70 in (shown as Region B in **Figure 6-17**). This confirms that poor performance of pavement and BAS is controlled not only by how weak subgrade is but also by how shallow and continuous the weak layer is.

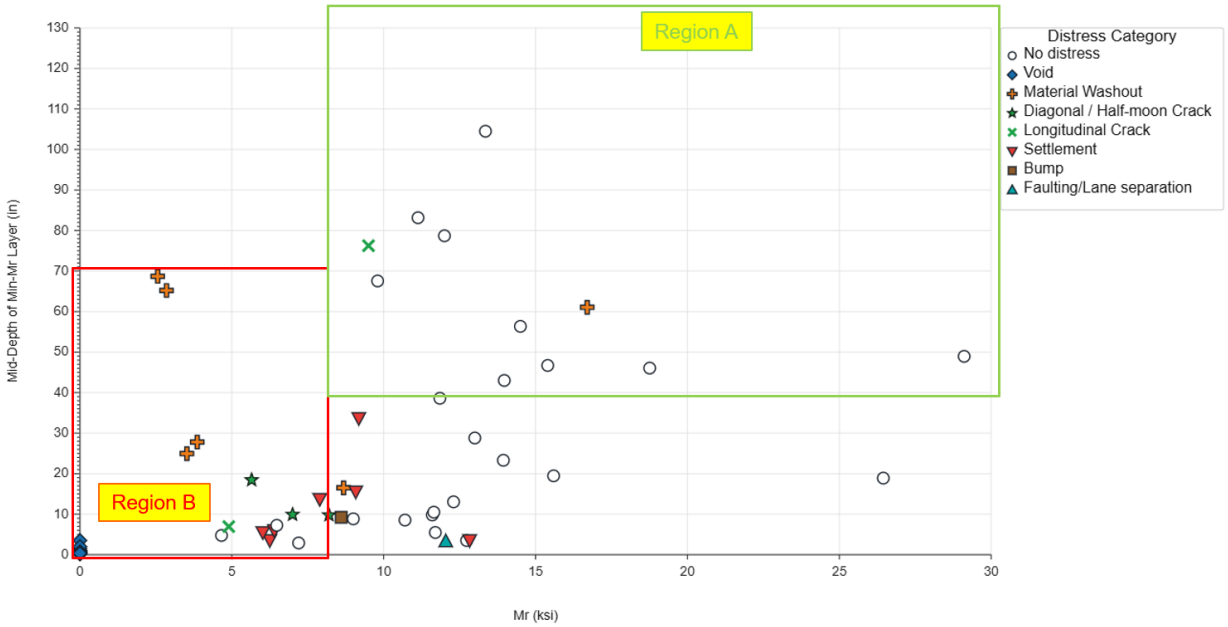


Figure 6-17. Minimum M_r value at each test location vs. mid depth of the layer corresponding to the M_r.

Figure 6-18 presents the minimum M_r value versus the thickness of the weak layer corresponding to the M_r value. **Figure 6-18** shows that the weak layers with the M_r value less than 8 ksi had a thickness generally ranging from 7 in (0.58 ft) to approximately 44 in (3.65 ft) . More specifically, data points for 'settlement' and 'cracking' are generally associated with weak layers with M_r value less than 8 ksi and thickness ranging between 8 to 30 in. On the other hand, data points for 'material washout' are generally associated with weak layers with M_r value less than 8 ksi and thickness ranging between 16 to 44 in. The fact that the thicknesses of the weak layers at the distressed locations varied as little as 0.58 ft to as large as 3.65 ft suggests that the presence of weak material with M_r value less than 8 ksi in the embankment makes it susceptible to various distresses, regardless of how thin the weak layer is.

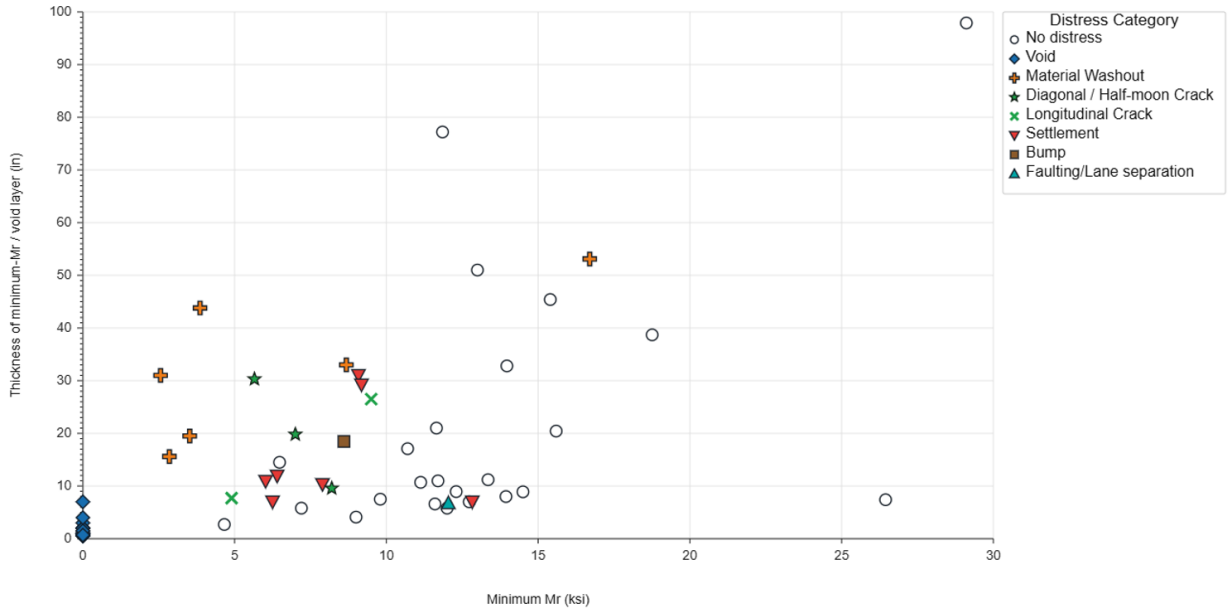


Figure 6-18. Minimum M_r value at each test location vs. thickness of the layer corresponding to the M_r.

6.3.4 Performance-based classification of embankment materials

Results from our analysis on DCP-derived M_r value and performance of roadway embankment indicate that:

- Well-performing roadway embankments with no observed distresses on BAS/pavement structure maintain an M_r value generally greater than about 18 ksi;
- Roadway embankments with observed voids, settlements, material washout, or pavement cracks generally have weak layers with M_r value less than 8 ksi within the upper 2 to 5 ft beneath the pavement structure;
- The thicknesses of the weak layers at distressed locations vary from 8 to 42 in; and
- The presence of voids provides no or very limited slab support, and they are observed at shallow depths, typically at the pavement-base interface or base-subgrade interface.

Recommendations for evaluation of embankments fill materials using DCP are presented in **Table 6-2** based on these findings. Note that these recommendations have been derived from the data collected at the time of writing this report and should be considered as *draft*. They can be updated with inclusion of more datasets and further refined analysis in future studies. Also, the values in parenthesis in **Table 6-2** reflect a practical consideration of the precision of DCP test.

Table 6-2. Recommended classification for evaluation of in-service roadway embankments using DCP data (draft).

Classification	M_r value from DCP tests performed on embankment fill/subgrade materials	Observed Field Behavior	Recommendations
Acceptable	≥ 18 ksi (20 ksi)*	No distresses were observed.	Maintain the current status.
Fair	8 – 18 ksi (10 – 20 ksi)*	23% of collected data points exhibited settlement, material washout, or pavement cracks.	Short-term: Perform targeted repair such as drainage/joint repair to minimize water infiltration into the embankment or asphalt overlay to cope with settlement. Perform HDPF injection, if deemed necessary. Long-term: Perform HDPF injection, soil densification, or replacement of backfill materials.
Poor	< 8 ksi (10 ksi)*	78% of collected data points exhibited the presence of void, settlement, material washout, or pavement cracks.	Perform immediate repair such as HDPF injection, soil densification, or replacement of backfill materials.

* *The values in parenthesis are conservative values that consider practical precision/repeatability/variability of DCP tests.*

6.4 Guideline for Interpreting Cone Penetration Test (CPT) Data for Evaluation of Embankment Fill Conditions

6.4.1 Overview

Although DCP tests have been widely used to determine moduli and thicknesses of subgrade layers for pavement evaluations, performing DCP tests to a depth deeper than 10 ft is very challenging due to the bending of the driving shaft, whereas roadway embankment heights are typically much greater than 10 ft, often exceeding 25 ft. Cone penetration tests (CPT) can be an alternative solution to this problem because CPT can be performed through the entire embankment height, unless obstructions are encountered, and, thus, providing conditions of embankment materials for the whole embankment depth.

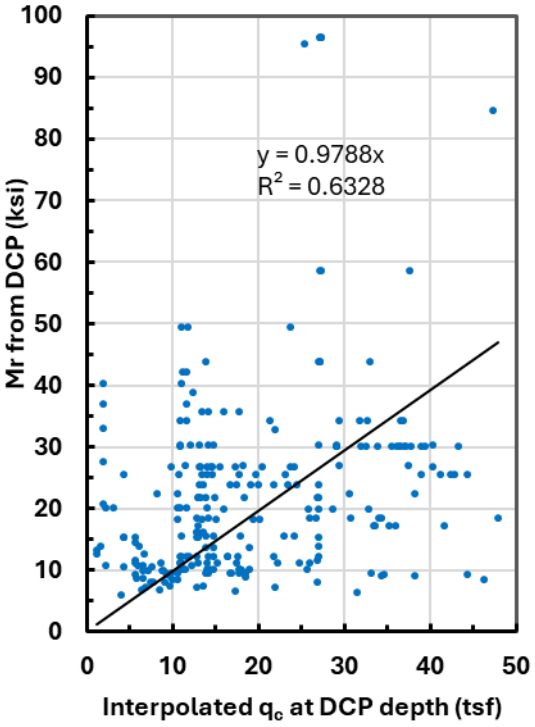
To establish a reliable relationship between DCP and CPT results, field investigation data from multiple sites were analyzed to correlate DCP-derived soil modulus (M_r) value with the CPT cone resistance (q_c). To minimize local variations of soil conditions at the testing locations, DCP and CPT tests were carried out within 1 ft of each other.

The datasets gathered in this study included six representative locations: IH45 SRA - Navarro, IH 20 in Fort Worth, IH 820 in Fort Worth, IH 10 in San Antonio, IH 35 in Waco, and BW8 in Houston, covering a range of soil types from low-plasticity clays (CL) to high-plasticity clays (CH) to sandy soil. IH45 SRA - Navarro site was not a roadway embankment, but side-by-side CPT and DCP tests were performed at this site as part of another project and, hence, data from the site were included in our datasets.

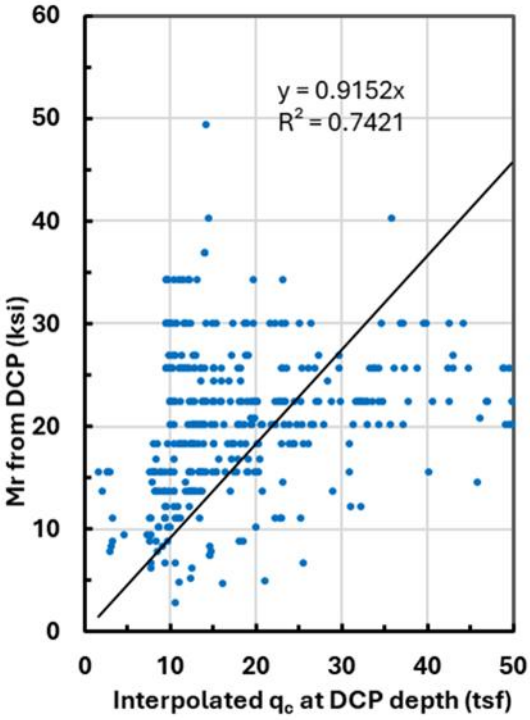
Each site's data were processed and compared in three different ways: (1) point-wise interpolation, where q_c values were interpolated at each DCP penetration depth; (2) layer-wise q_c averaging, using layer boundaries identified from DCP; and (3) depth-binned analysis at 6-in and 12-in intervals to determine q_c and reduce local variability. The goal was to evaluate how consistently CPT and DCP measurements reflect soil stiffness and whether q_c threshold values can be established across embankment materials using a unified or soil-specific correlation. The following sections present detailed analysis.

6.4.2 Point-wise interpolation

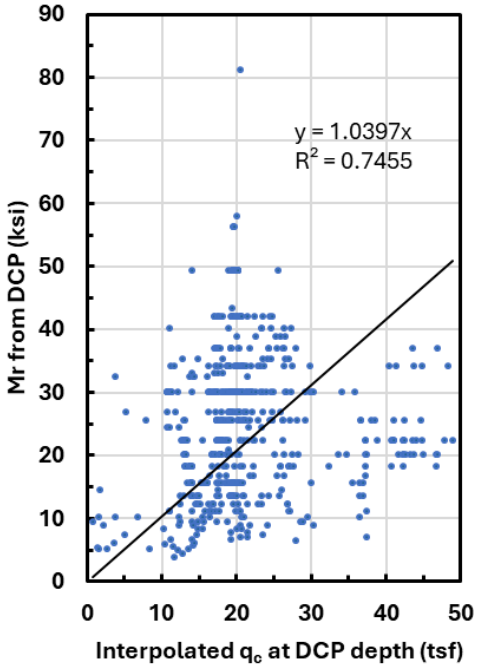
Figure 6-19 presents the relationship between DCP-derived M_r value and q_c from CPT following the point-wise interpolation approach. In this approach, every M_r value determined from two successive DCP blow counts measured over the corresponding penetration depth is paired with a q_c value determined from the CPT at the same depth. This produces a dense scatter that captures the full vertical variability of the embankment. Then, the regression analyses were performed to establish correlation between M_r and q_c. The results from the regression analysis are summarized in **Table 6-3**.


y = 0.9788x
R² = 0.6328
Mr from DCP (ksi)
Interpolated qc at DCP depth (tsf)

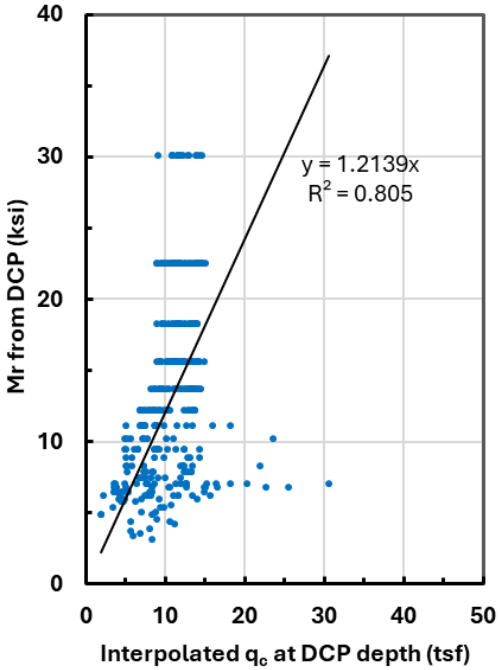
(a)


y = 0.9152x
R² = 0.7421
Mr from DCP (ksi)
Interpolated qc at DCP depth (tsf)

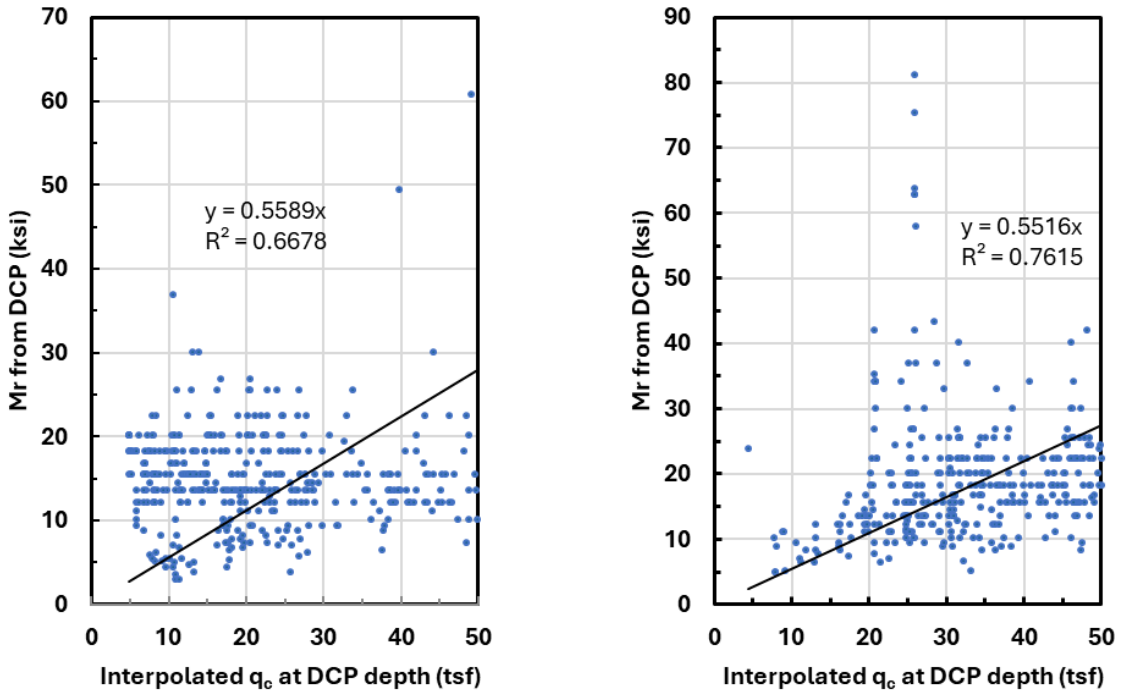
(b)


y = 1.0397x
R² = 0.7455
Mr from DCP (ksi)
Interpolated qc at DCP depth (tsf)

(c)


y = 1.2139x
R² = 0.805
Mr from DCP (ksi)
Interpolated qc at DCP depth (tsf)

(d)



(e) (f)

Figure 6-19. Regression analysis between Mr from DCP and qc from CPT at the same depth using a pointwise data: (a) IH-20, Fort Worth (b) IH-820, Fort Worth (c) IH-45, Navarro (d) BW-8, Houston (e) IH-10, San Antonio, and (f) IH-35, Waco.

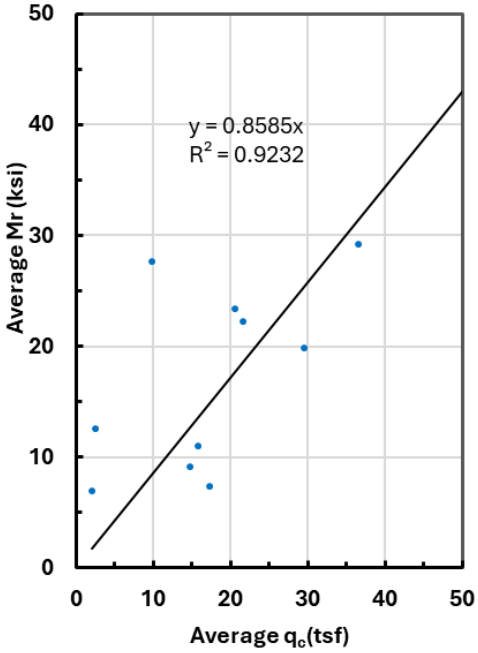
Table 6-3. Summary of regression analysis using pointwise data for all sites

Site	Predominant Soil Type	Correlation Equation (M_r=A·q_c)	R^2
IH 20, Fort Worth	CL	M_r [ksi] = 0.9788q_c [tsf]	0.63
IH 820, Fort Worth	CL	M_r [ksi] = 0.9152q_c [tsf]	0.74
IH 45, Navarro	CH	M_r [ksi] = 1.0397q_c [tsf]	0.74
BW 8, Houston	CH	M_r [ksi] = 1.2139q_c [tsf]	0.80
IH 10, San Antonio	CL	M_r [ksi] = 0.5589q_c [tsf]	0.66
IH 35, Waco	Sandy soil	M_r [ksi] = 0.5516q_c [tsf]	0.76

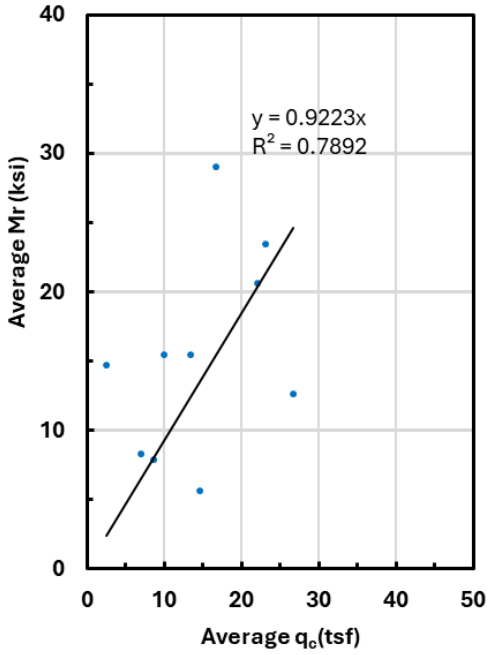
Four sites, IH 20 (CL), IH 820 (CL), IH 45 (CH), and BW 8 (CH), exhibited the regression coefficient (i.e., slope coefficient) of about 1.0 for linear relationship between M_r (in ksi) and q_c (in tsf), with correlation equations ranging from $M_r = 0.9152q_c$ to $M_r = 1.2139q_c$. The remaining two sites, IH-10 (CL) and IH 35 (Sandy soil), demonstrated a significantly lower regression coefficient, with equations clustered around $M_r = 0.5\,q_c$. Across all sites, the coefficient of determination R^2 values ranged from 0.63 to 0.80, indicating a generally positive and moderate-to-strong linear relationship even at the point-wise level of comparison.

6.4.3 Layer-wise method

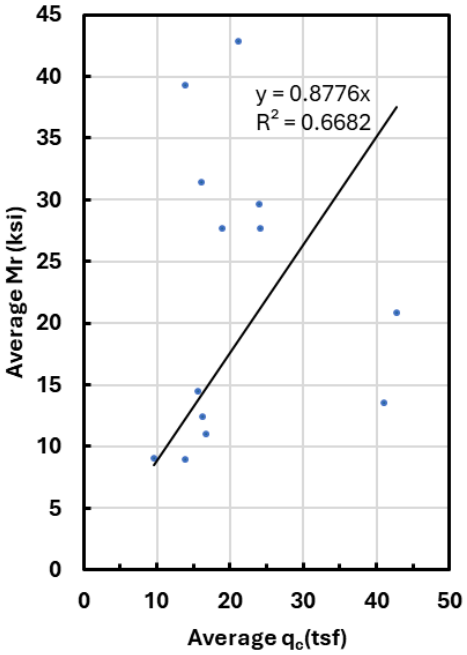
Figure 6-20 plots the relationship between the layer-averaged M_r value and the average value of q_c within the same layer, effectively smoothing out short-range spikes and representing the average behavior of each stratum. The layer-averaged M_r value was determined from the slope changes of the cumulative DCP blow counts vs. depth plot. The results from the regression analyses between the layer-averaged M_r and q_c are summarized in **Table 6-4**.



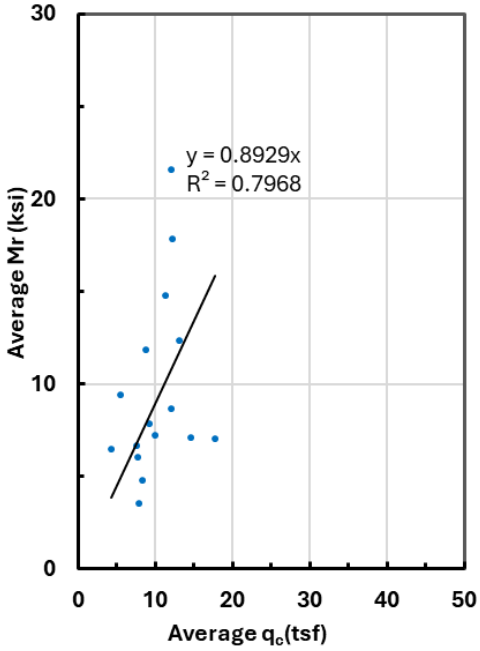
(a)



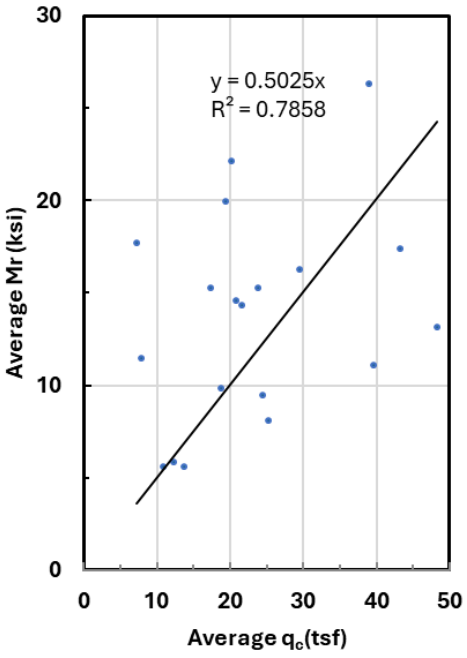
(b)



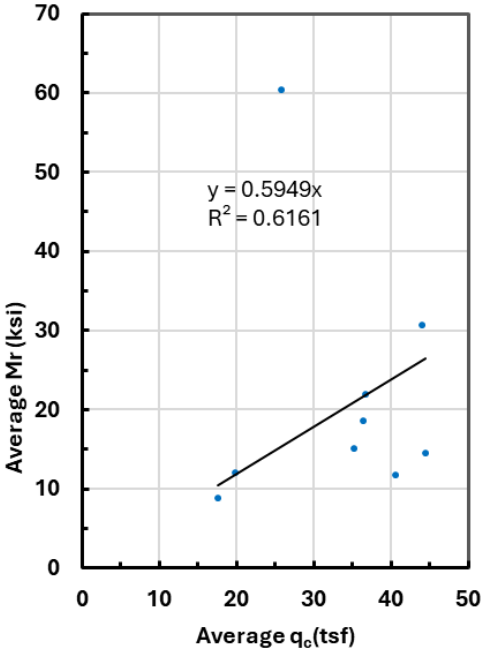
(c)



(d)



(e)



(f)

Figure 6-20. Regression analysis between M_r from DCP and q_c from CPT at the same depth using layer-wise data: (a) IH-20, Fort Worth, (b) IH-820, Fort Worth, (c) IH-45, Navarro, (d) BW-8, Houston, (e) IH-10, San Antonio, and (f) IH-35, Waco.

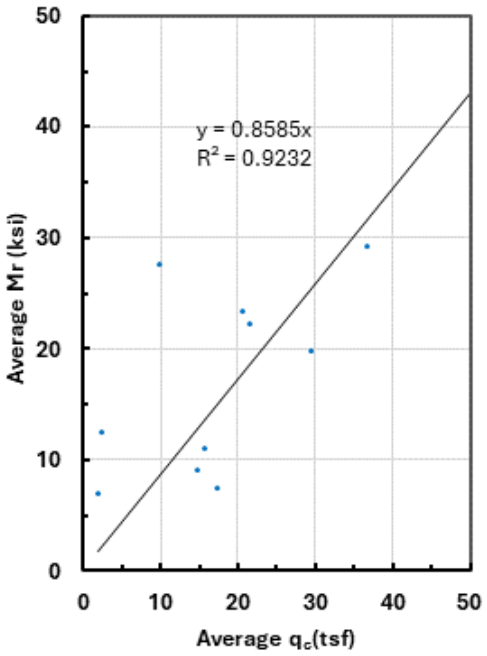
Table 6-4. Summary of correlation for DCP layer-wise averaging.

Site	Predominant Soil Type	Correlation Equation ($M_r = A \cdot q_c$)	R^2
IH-20, Fort Worth	CL	M_r [ksi] = 0.8585q_c [tsf]	0.92
IH-820, Fort Worth	CL	M_r [ksi] = 0.9223q_c [tsf]	0.79
IH-45, Navarro	CH	M_r [ksi] = 0.8776q_c [tsf]	0.66
BW-8, Houston	CH	M_r [ksi] = 0.8929q_c [tsf]	0.79
IH-10, San Antonio	CL	M_r [ksi] = 0.5025q_c [tsf]	0.78
IH-35, Waco	Sandy soil	M_r [ksi] = 0.5949q_c [tsf]	0.61

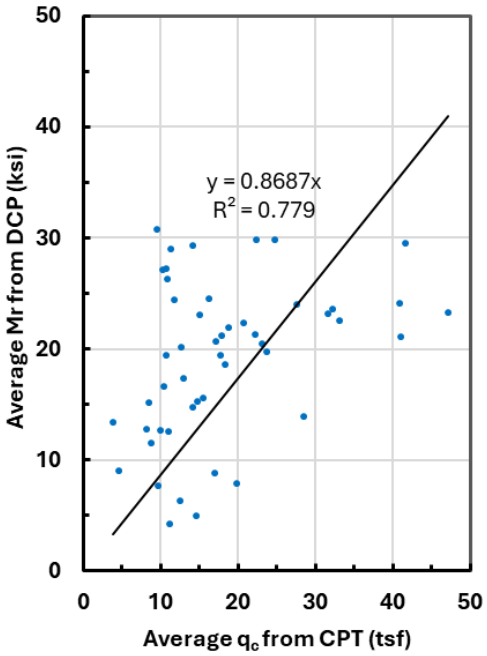
For the four sites [IH-20 (CL), IH-820 (CL), IH-45 (CH), and BW-8 (CH)] that exhibited a near 1:1 relationship between M_r and q_c in the point-wise analysis, the layer-wise data clustered more tightly (the slope coefficient ranging from 0.8585 to 0.9223) than the broader point-wise range (the slope coefficient ranging from 0.9152 to 1.2139). Moreover, the coefficient of determination (R^2) obtained from the point-wise approach for IH 20 was 0.63, whereas the layer-wise method yielded a higher value of 0.92. Similarly, for IH-10, the R^2 value increased from 0.66 using the point-wise method to 0.78 using the layer-wise method. Conversely, the R^2 for IH-45 and IH-35 slightly decreased from 0.74 and 0.76 (pointwise method) to 0.66 and 0.61 (layer-wise method), respectively.

6.4.4 Depth-binned analysis

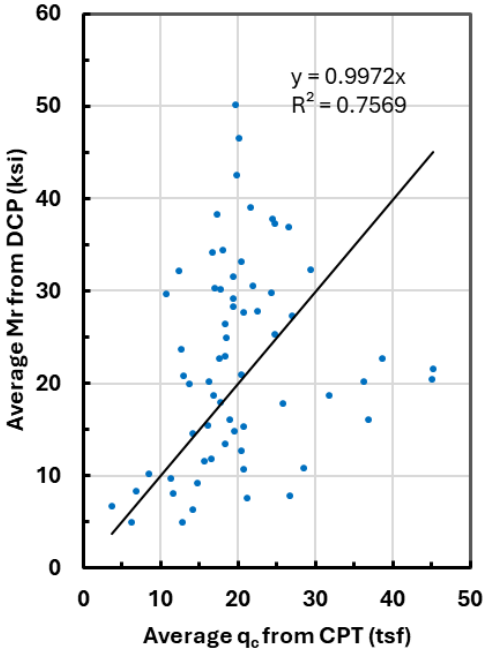
Figure 6-21 and **Figure 6-22** present correlations between M_r and q_c based on the smoothing methodology with 6-inch bin and 12-inch bin respectively. In this approach, M_r and q_c values were averaged over the same 6-inch and 12-inch layer intervals.


y = 0.8585x
R² = 0.9232
Average Mr (ksi)
Average qc(tsf)
0
10
20
30
40
50

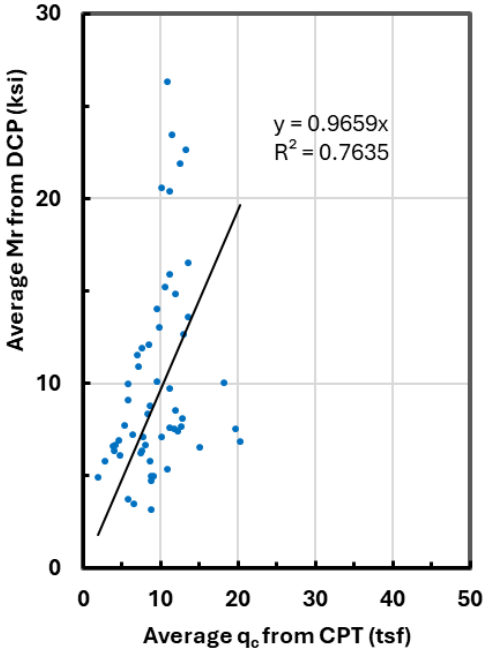
(a)


y = 0.8687x
R² = 0.779
Average Mr from DCP (ksi)
Average qc from CPT (tsf)
0
10
20
30
40
50

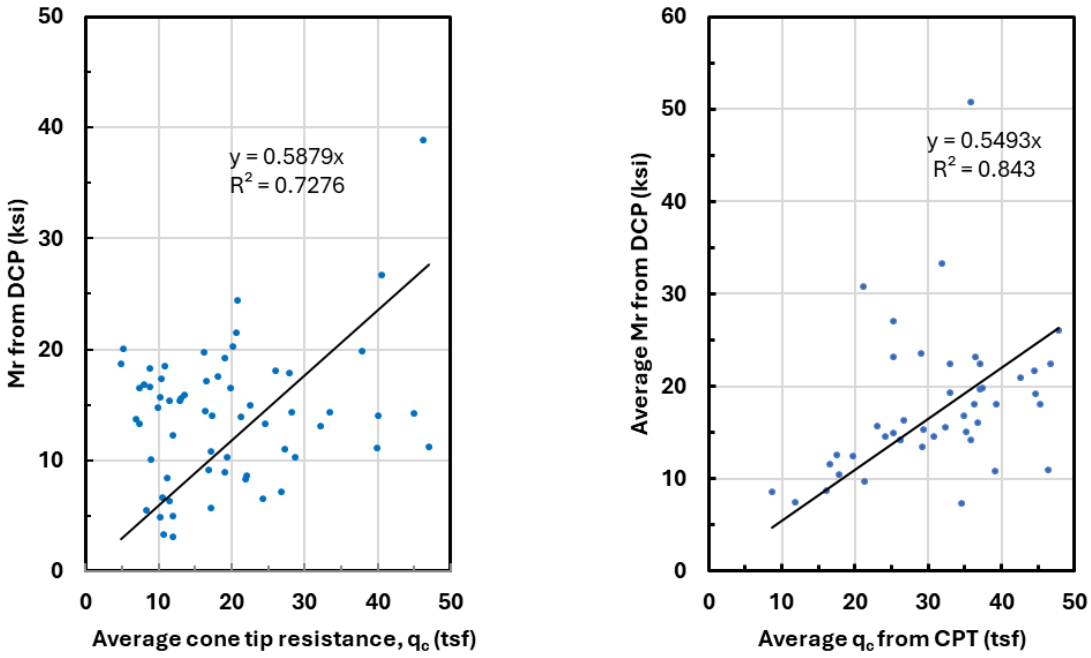
(b)


y = 0.9972x
R² = 0.7569
Average Mr from DCP (ksi)
Average qc from CPT (tsf)
0
10
20
30
40
50
60

(c)

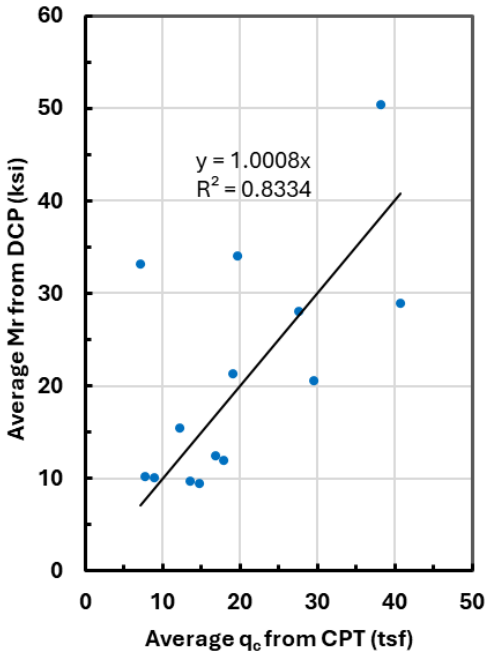

y = 0.9659x
R² = 0.7635
Average Mr from DCP (ksi)
Average qc from CPT (tsf)
0
10
20
30
40
50

(d)

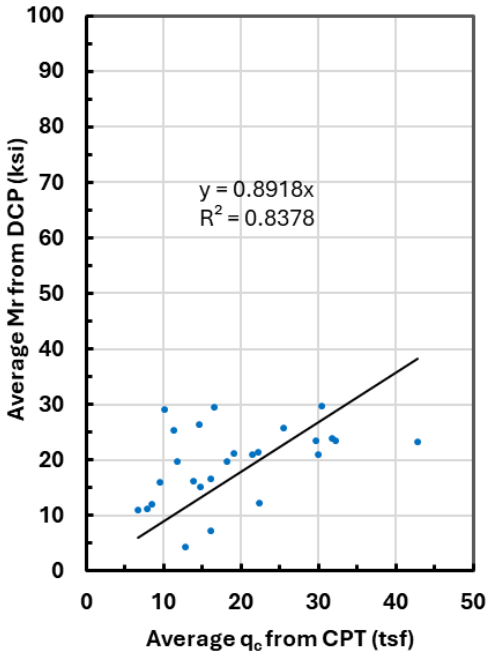


(e) (f)

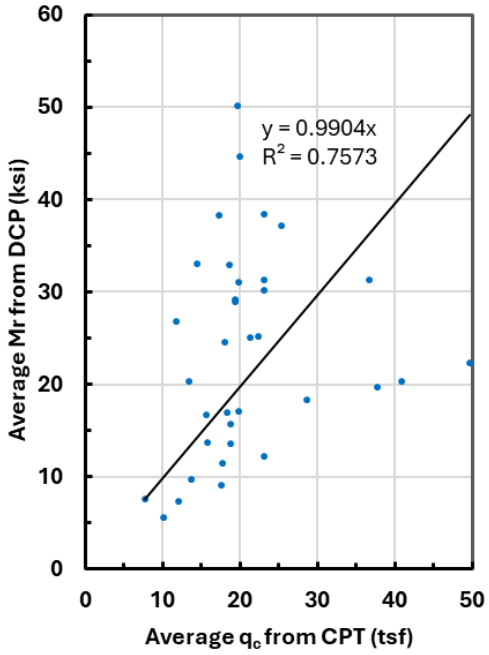
Figure 6-21. Regression analysis between M_r from DCP and q_c from CPT averaged for 6-in layer interval: (a) IH-20, Fort Worth, (b) IH-820, Fort Worth, (c) IH-45, Navarro, (d) BW-8, Houston, (e) IH-10, San Antonio, and (f) IH-35, Waco.


y = 1.0008x
R² = 0.8334
Average Mr from DCP (ksi)
Average qc from CPT (tsf)
0
10
20
30
40
50
60

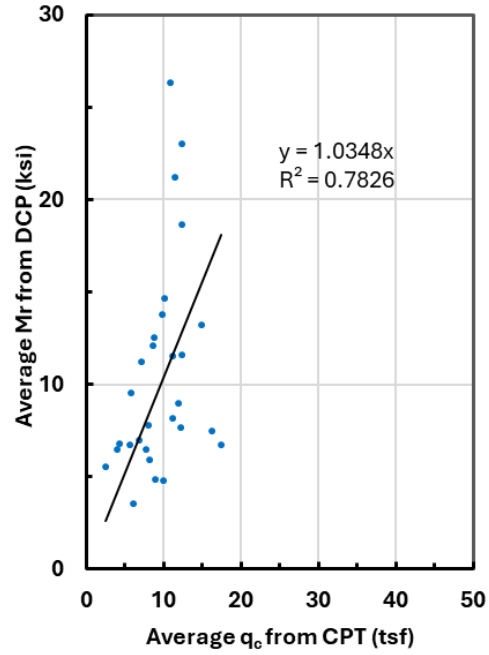
(a)


y = 0.8918x
R² = 0.8378
Average Mr from DCP (ksi)
Average qc from CPT (tsf)
0
10
20
30
40
50
60
70
80
90
100

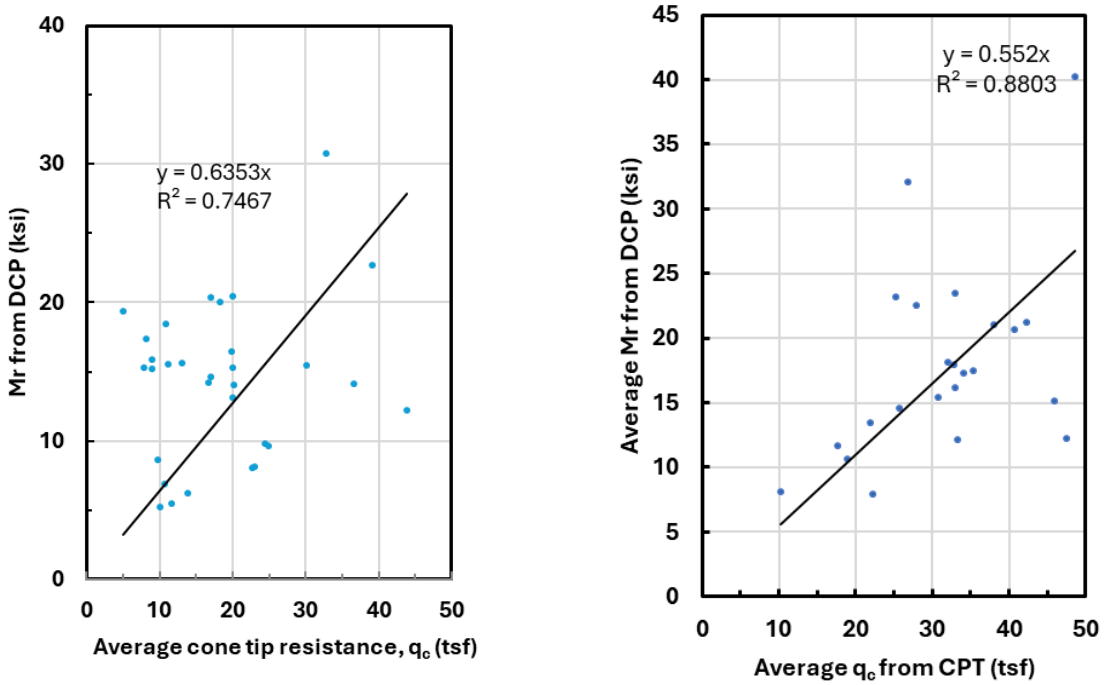
(b)


y = 0.9904x
R² = 0.7573
Average Mr from DCP (ksi)
Average qc from CPT (tsf)
0
10
20
30
40
50
60

(c)


y = 1.0348x
R² = 0.7826
Average Mr from DCP (ksi)
Average qc from CPT (tsf)
0
10
20
30
40
50

(d)



(e) (f)

Figure 6-22. Regression analysis between M_r from DCP and q_c from CPT averaged for 12-in layer interval: (a) IH-20, Fort Worth, (b) IH-820, Fort Worth, (c) IH-45, Navarro, (d) BW-8, Houston, (e) IH-10, San Antonio, and (f) IH-35, Waco.

Results from the regression analyses based on depth-binned approach (6-in and 12-in layer intervals) are summarized in **Table 6-5**. The resulting analysis confirms the trends from the layer-wise and point-wise analyses but yields higher coefficients of determination R^2.

Table 6-5. Summary of correlation for 6" and 12" averaged data.

Site	Predominant Soil Type	Bin size	Correlation Equation ($M_r = A\ q_c$)	R^2
IH-20, Fort Worth	CL	6"	M_r [ksi] = 0.8582q_c[tsf]	0.73
		12"	M_r [ksi] = 1.0008q_c[tsf]	0.83
IH-820, Fort Worth	CL	6"	M_r [ksi] = 0.8687q_c[tsf]	0.78
		12"	M_r [ksi] = 0.8918q_c[tsf]	0.84
IH-45, Navarro	CH	6"	M_r [ksi] = 0.9972q_c[tsf]	0.75
		12"	M_r [ksi] = 0.9904q_c[tsf]	0.75
BW-8, Houston	CH	6"	M_r [ksi] = 0.9659q_c[tsf]	0.78
		12"	M_r [ksi] = 1.0348q_c[tsf]	0.76
IH-10, San Antonio	CL	6"	M_r [ksi] = 0.5879q_c[tsf]	0.72
		12"	M_r [ksi] = 0.6353q_c[tsf]	0.74
IH-35, Waco	Sandy soil	6"	M_r [ksi] = 0.5493q_c[tsf]	0.84
		12"	M_r [ksi] = 0.5520q_c[tsf]	0.88

The four clay sites, IH 20, IH 820, IH 45, and BW 8, exhibited the slope coefficients close to or slightly above 1.0 at the 12-in bin level, suggesting a near one-to-one relationship between M_r (in ksi) and q_c (in tsf) when averaged over a 1 ft. On the other hand, the IH35 Waco site was predominantly sandy soil and demonstrated the highest R^2 values among all sites for both bin sizes (0.84 for 6 in and 0.88 for 12 in). Furthermore, the slope coefficient (= 0.55) from IH35 Waco site (sandy soil) was significantly lower than those from the four clay sites.

IH10 San Antonio site was also clayey soil (CL), but the slope coefficient (= 0.64) from the 12-in-bin regression analysis was significantly lower than the other four clay sites and rather close to that of sandy soil observed at IH35 Waco. This is because there was a significant amount of coarse-grained soils at the depth range where M_r–q_c comparisons were performed. According to the lab tests presented in **Table 5-3**, the clay soil had about 44% of coarse-grained soils. Therefore, the cone resistance measured at IH10 San Antonio reflects the presence of the significant amount of coarse-grained soils and, hence, the lower slope coefficient was observed from the regression analysis compared to other predominantly clay sites.

6.4.5 Summary and recommendations

Results from the previous regression analyses show that the correlation between M_r value determined from DCP and q_c measured from CPT is strongest when the measured data are analyzed over 1-ft layer intervals (i.e., 12-in-bin-depth approach). Therefore, further regression analysis was performed using all 12-in-layer-interval data from the four, predominantly clay sites, and the analysis results are presented in **Figure 6-23**.

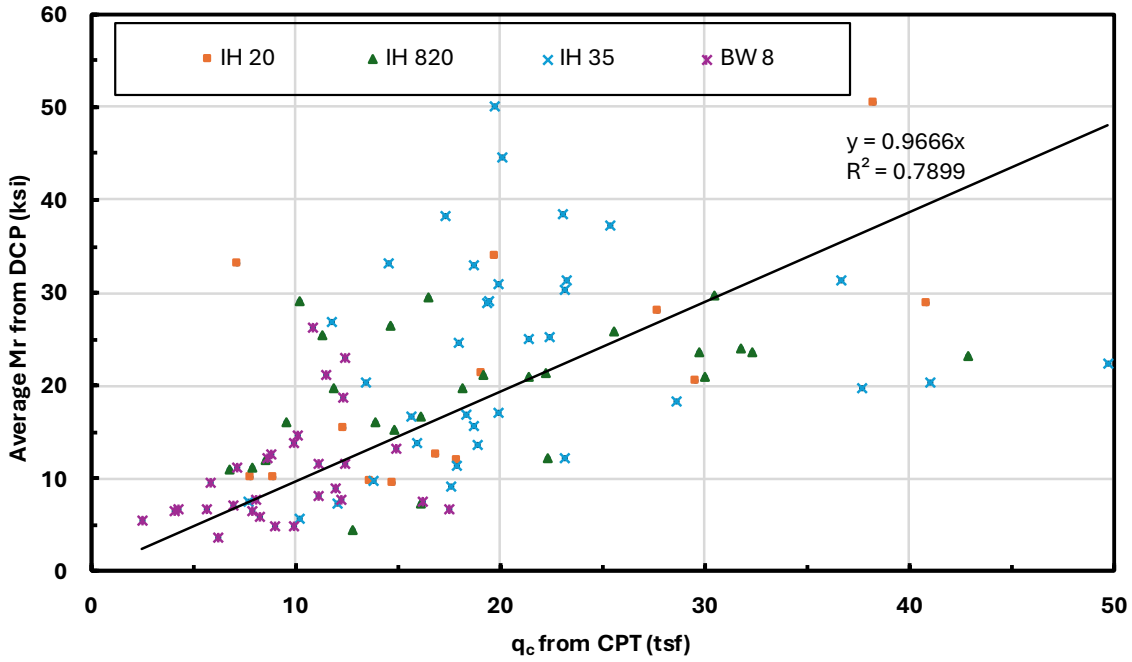


Figure 6-23. Combined regression analysis between M_r from DCP and q_c from CPT averaged for 12-in layer interval from four predominant clay sites (IH 20, Fort Worth; IH 820, Fort Worth; BW-8, Houston; and IH 35 Navarro)

Based on the regression analysis, the following correlation is proposed for predominantly clayey soils:

$$M_r[ksi] = 0.97q_c \text{ [tsf]} \ (R^2 = 0.79; \text{ Data points} = 104) \quad (6)$$

There was only one test site (IH 35 Waco) where the embankment fill materials were predominantly sandy soils. Accordingly, the correlation resulted from the 12-in-bin analysis using IH 35 Waco data (see Table 6-5) is proposed that **for predominantly sandy soils**:

$$M_r[ksi] = 0.55q_c \text{ [tsf]} \ (R^2 = 0.88; \text{ Data points} = 23) \quad (7)$$

Using the correlation Eqs. (6) and (7) in conjunction with the threshold M_r values presented in **Table 6-2**, recommendations for evaluations of embankment fill materials using CPT data are presented in **Table 6-6**. Note that these recommendations are based on the data collected at the time of writing this report and should be considered as *draft*. These can be updated with inclusions of more datasets and further refined analysis in future studies.

Table 6-6. Recommended classification for evaluation of in-service roadway embankments using CPT data (draft).

Classification	**M_r value from DCP (ksi)**	**q_c value from CPT (tsf)**
Acceptable	≥ 18 ksi (20 ksi)*	≥ 19 tsf (21 tsf)* for predominantly clayey soils ≥ 33 tsf (37 tsf)* for predominantly sandy soils
Fair	8 – 18 ksi (10 – 20 ksi)*	9 – 19 tsf (11 – 21 tsf)* for predominantly clayey soils 15 – 33 tsf (19 – 37 tsf)* for predominantly sandy soils
Poor	< 8 ksi (10 ksi)*	< 9 tsf (11 tsf)* for predominantly clayey soils < 15 tsf (19 tsf)* for predominantly sandy soils

** The values in parenthesis are conservative values that consider practical precision/repeatability/variability of DCP tests.*

Chapter 7 Distress Mechanisms and Classification

Chapter 5 presented the field and laboratory data collected at the evaluated test sections and discussed potential distress mechanisms. Based on the probable causes of the distresses observed at each test section, this chapter classifies them by underlying mechanism and examines the interactions among root causes, mechanisms, and the distresses visible at the surface.

7.1 Classification of distress mechanisms

The potential distress mechanisms identified from the test sections are classified as follows:

- Compression of materials (fill materials or founding soils)
- Loss of materials (erosion or washout)
- Lateral stress buildup behind the retaining wall
- Non-uniform slab support

The following sections present the details of each distress mechanism.

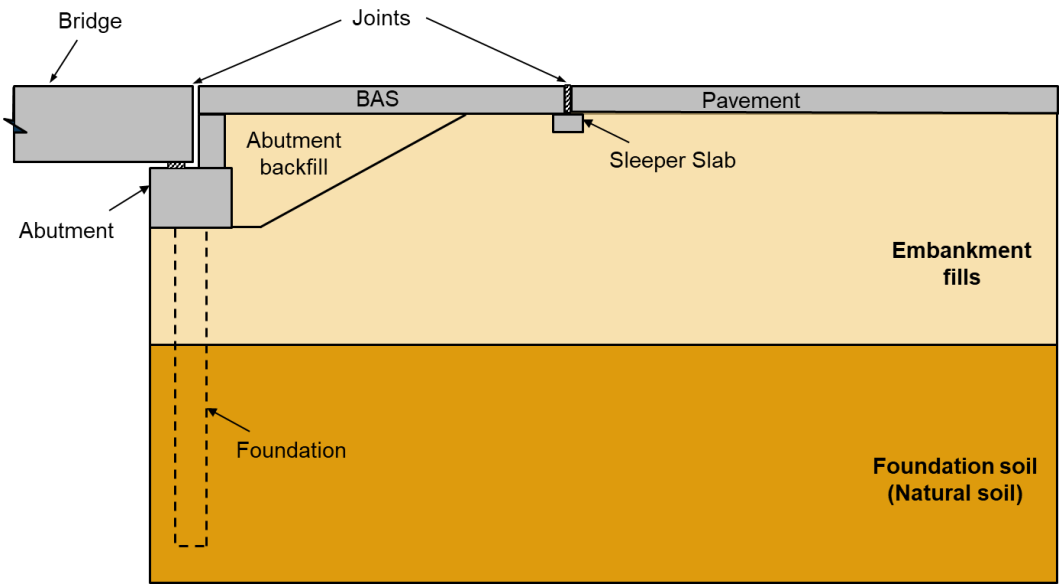
7.1.1 Compression of materials

Distresses commonly observed at BAS and adjacent pavement are typically related to settlement of underlying soils, which, in turn, resulted from compression of embankment fills or founding soils beneath the embankment. The following subsections present visual representation of distress mechanisms related to compression of materials.

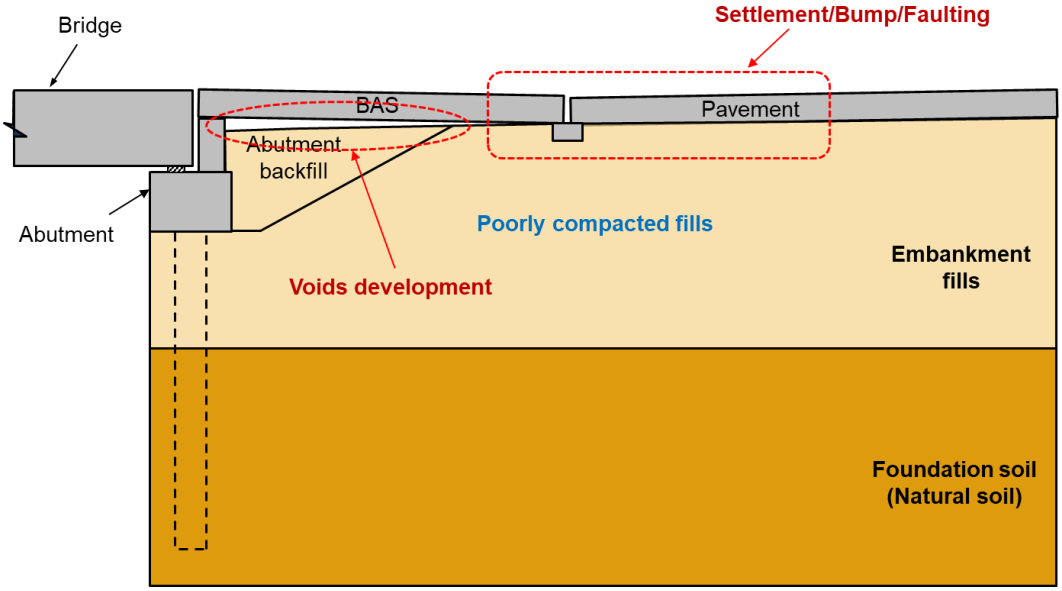
7.1.1.1 Compression of fill materials

Embankment fills are compacted in lifts via one of the two compaction methods specified in TxDOT Item 132: (i) Ordinary Compaction or (ii) Density Control. Inadequate compaction can be caused by either compacting the soils in lifts that are too thick or not achieving the required density (Briaud et al. 1997). Inadequate compaction of the embankment fill leads to a higher void ratio, and the void ratio decreases over time due to dynamic traffic loads and self-weight of the fill after construction. This creates compression of the fill material, and it is the major contributing factor that induces settlement/bump as well as void formation at BAS and adjacent pavement (Briaud et al. 1997).

As shown in **Figure 7-1(a)**, one end of the BAS is supported on the bridge abutment and the other end on the sleeper slab. Poor compaction causes the compression of the embankment fill and settlement under traffic loads. However, settlement of the BAS on the abutment side is less than that on the pavement side because the abutment wall is supported on a series of drilled shafts. Consequently, voids develop beneath the BAS and bump, faulting, or excessive settlement are commonly observed in the BAS area and adjacent pavement (see **Figure 7-1(b)**).



(a)



(b)

Figure 7-1. Illustration of distress mechanism for compression of fill materials: (a) embankment condition right after construction; (b) resulting embankment condition

7.1.1.2 Compression of founding soils

The compression of the embankment fill under traffic loads might be minimized if proper compaction is achieved. However, embankment fills are placed on the existing natural soils, and when the natural founding soil beneath the embankment is soft or weak, it can lead to a settlement of the BAS and adjacent pavement after the placement of the embankment fill. If the founding soil

beneath the embankment is clay, it is likely to experience the time-dependent consolidation settlement due to the weight of the embankment fill. The higher the embankment fill is, the greater settlement of the founding soil is expected.

Figure 7-2 visually illustrates the distress mechanism for compression of the founding soils. When the soft founding soil undergoes a compression, the embankment fill above the founding soil settles down, contributing to void development, bump, faulting, or excessive settlement in the BAS area and adjacent pavement.

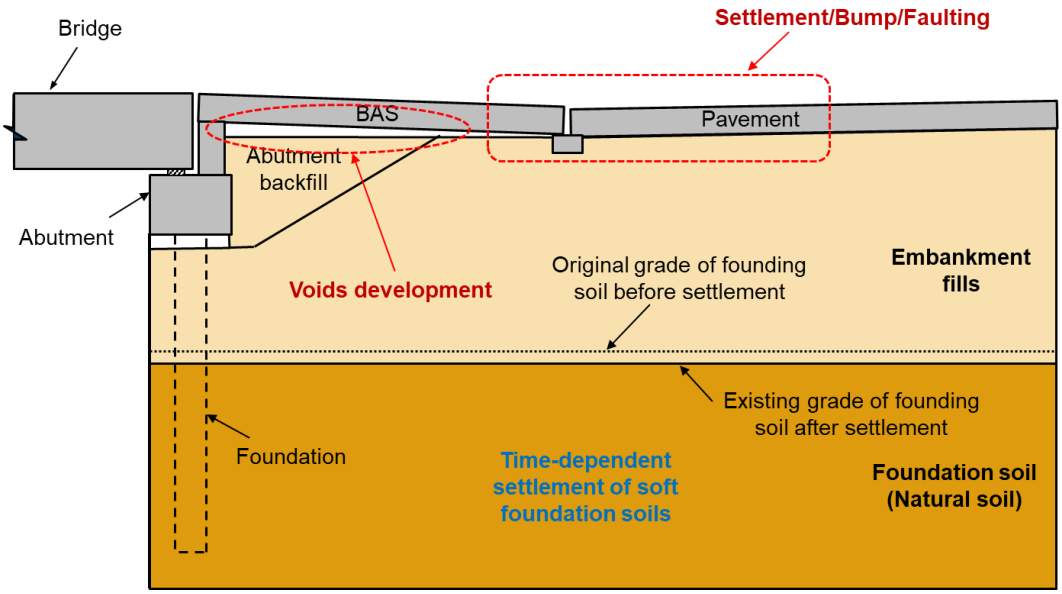


Figure 7-2. Illustration of distress mechanism for embankment condition resulted from compression of founding soil over time

7.1.2 Loss of materials (Washout)

The intrusion of surface water through faulty joints or cracked pavement sections can not only weaken the embankment fill but also cause internal erosion because the fines can be washed out from the fill material. As shown in **Figure 7-3**, washout of fines in the fill materials leads to the development of void or further settlement of the fill under repeated traffic loads. The formation of void and ensuing settlement can cause bumps, cracks, or other distresses due to insufficient slab support.

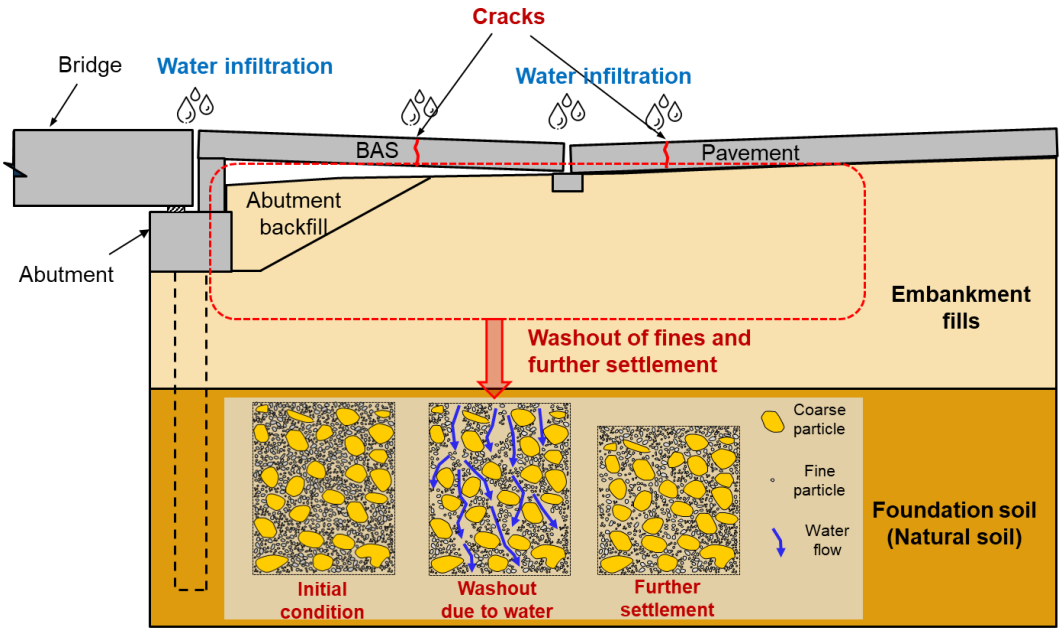
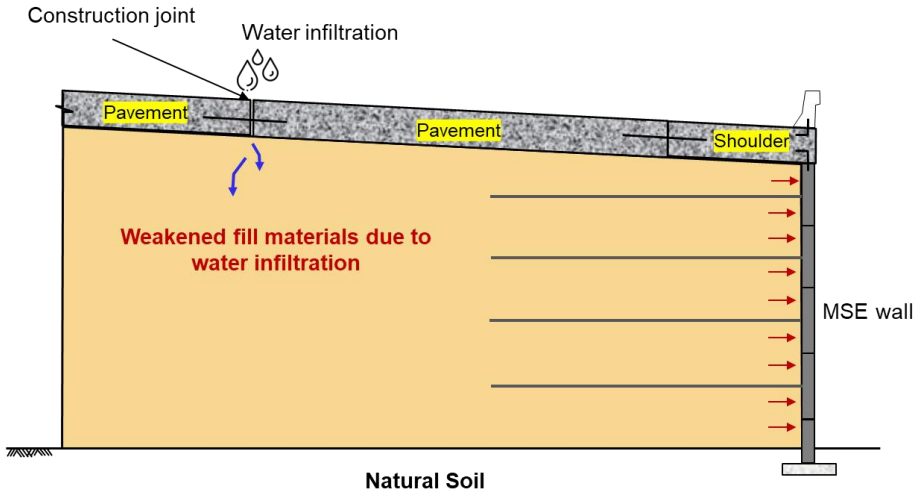


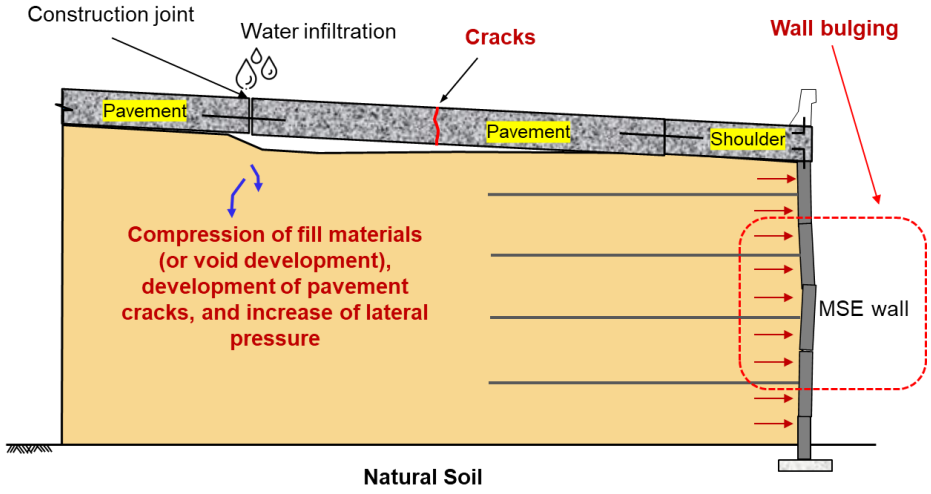
Figure 7-3. Illustration of distress mechanism for loss of materials (washout)

7.1.3 Lateral stress buildup behind the retaining wall

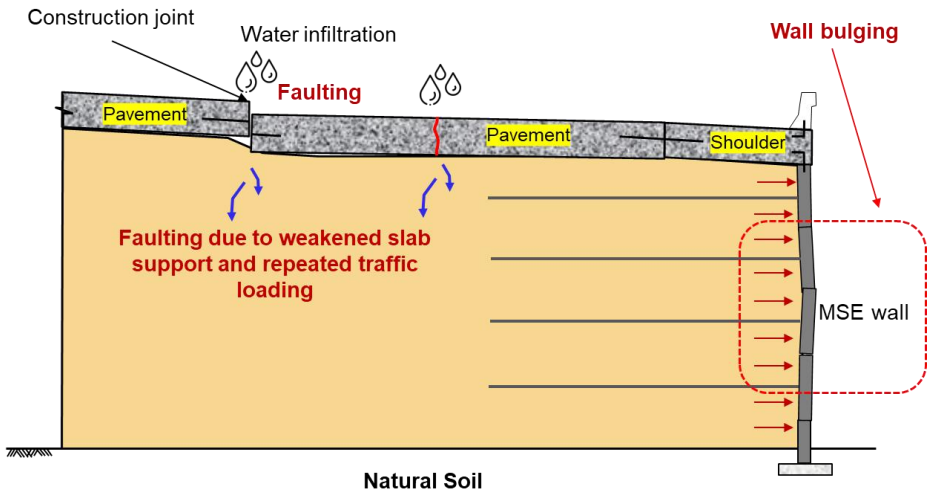
Water infiltration into the fill materials can cause not only the weakening or erosion of fill materials but also increased hydrostatic pressure on the retaining wall (see **Figure 7-4(a)**). The weakened fill materials undergo settlements, potentially leading to formation of voids and development of pavement cracks, due to the repeated dynamic traffic loads and other environmental factors. Furthermore, the increased lateral pressure due to water can push the wall away from the retained fill materials, causing the lateral movement, tilting, or bulging of retaining wall (see **Figure 7-4(b)**). The weakened slab support and/or formation of the voids causes a significant downward movement of the pavement slab under heavy traffic loads, causing shear failure of tie-bars and faulting (see **Figure 7-4(c)**). Continuous water infiltration, now facilitated by the faulting and pavement cracks, induces even greater build of lateral pressure behind the retaining, causing lane separation and further lateral movement, tilting, or bulging of retaining wall. (see **Figure 7-4(d)**).


Construction joint
Water infiltration
Pavement
Pavement
Shoulder
Weakened fill materials due to water infiltration
MSE wall
Natural Soil

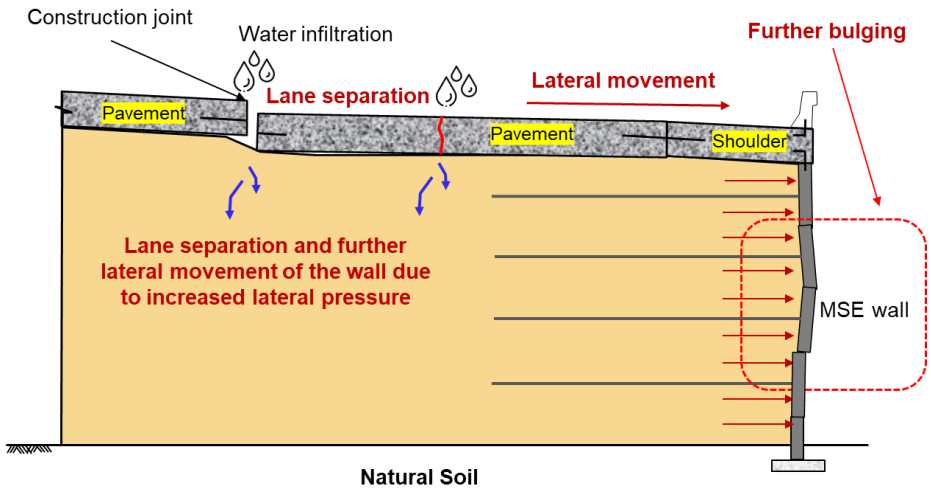
(a)


Construction joint
Water infiltration
Cracks
Wall bulging
Pavement
Pavement
Shoulder
Compression of fill materials (or void development), development of pavement cracks, and increase of lateral pressure
MSE wall
Natural Soil

(b)



(c)



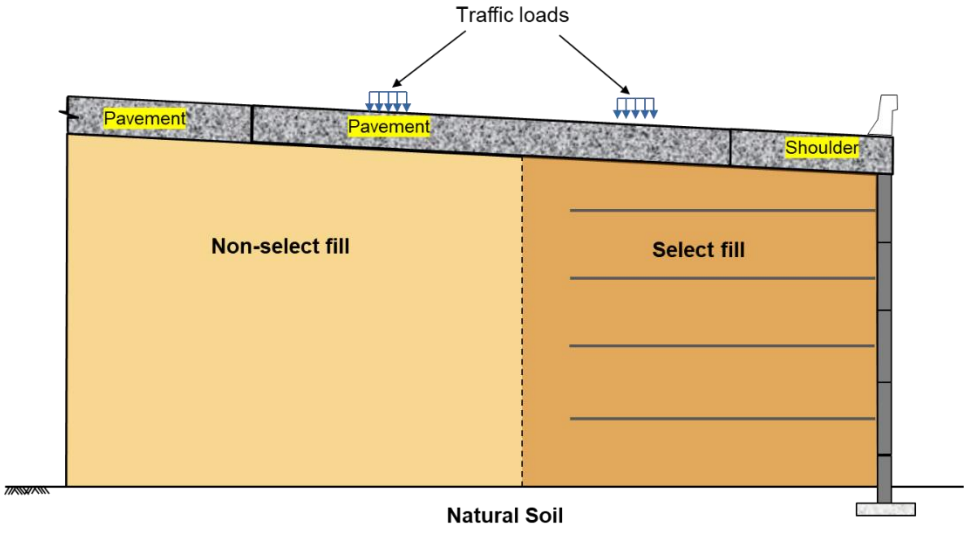
(d)

Figure 7-4. Illustration of distress mechanism for lateral stress buildup: (a) weakening of fill materials due to water infiltration, (b) compression of fill materials (or void formation), development of pavement cracks, and lateral movement of wall due to increase of lateral pressure, (c) faulting due to weakened slab support and repeated traffic loading, and (d) lane separation and further lateral movement of the wall due to increased lateral pressure.

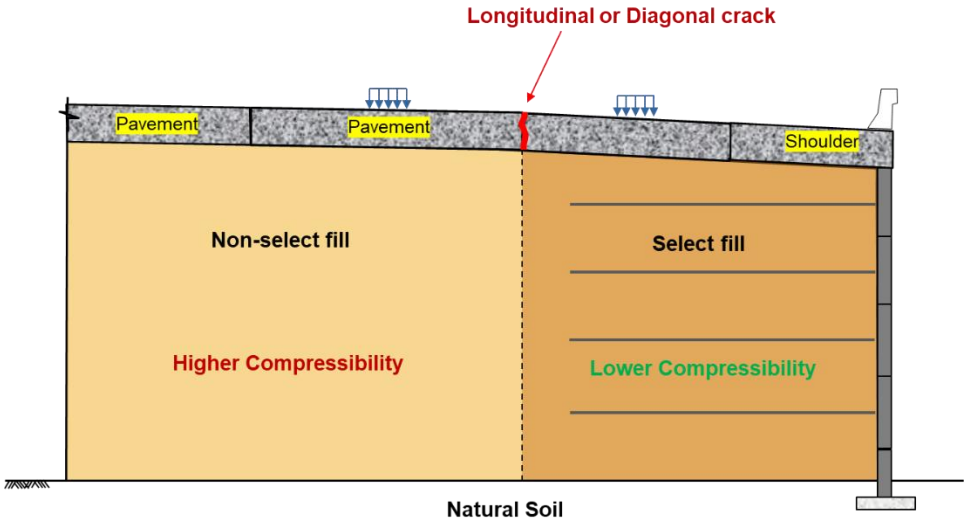
7.1.4 Non-uniform slab support

Fill materials used for construction of MSE-wall-type embankment consist of two types of fills: select fill and non-select fill (see **Figure 7-5**). Select fills are usually more permeable than non-select fills and often require more strict compaction control than non-select fills. This inconsistency in material types and compaction quality often leads to differential settlement over

time. Such differential settlement causes non-uniform support beneath the pavement and can induce longitudinal or diagonal cracks.



(a)



(b)

Figure 7-5. Illustration of distress mechanism for non-uniform slab support: (a) typical section of MSE-wall-type roadway embankment and (b) development of pavement cracks due to non-uniform slab support

7.1.5 Frequency of distress mechanisms observed from test sites

Figure 7-6 presents the distress mechanisms identified at each test site. It should be noted that the test sites investigated in this study often showed *multiple* distress mechanisms. Compression of materials (including both the embankment fills and founding soils) was the most frequent distress

mechanism (8 sites), followed by material washout (3 sites) and lateral stress buildup (3 sites). Although 8 sites exhibited compression of fill materials or founding soils, the other mechanisms are limited to three or less sites, requiring additional field evaluations to complement the dataset collected so far.

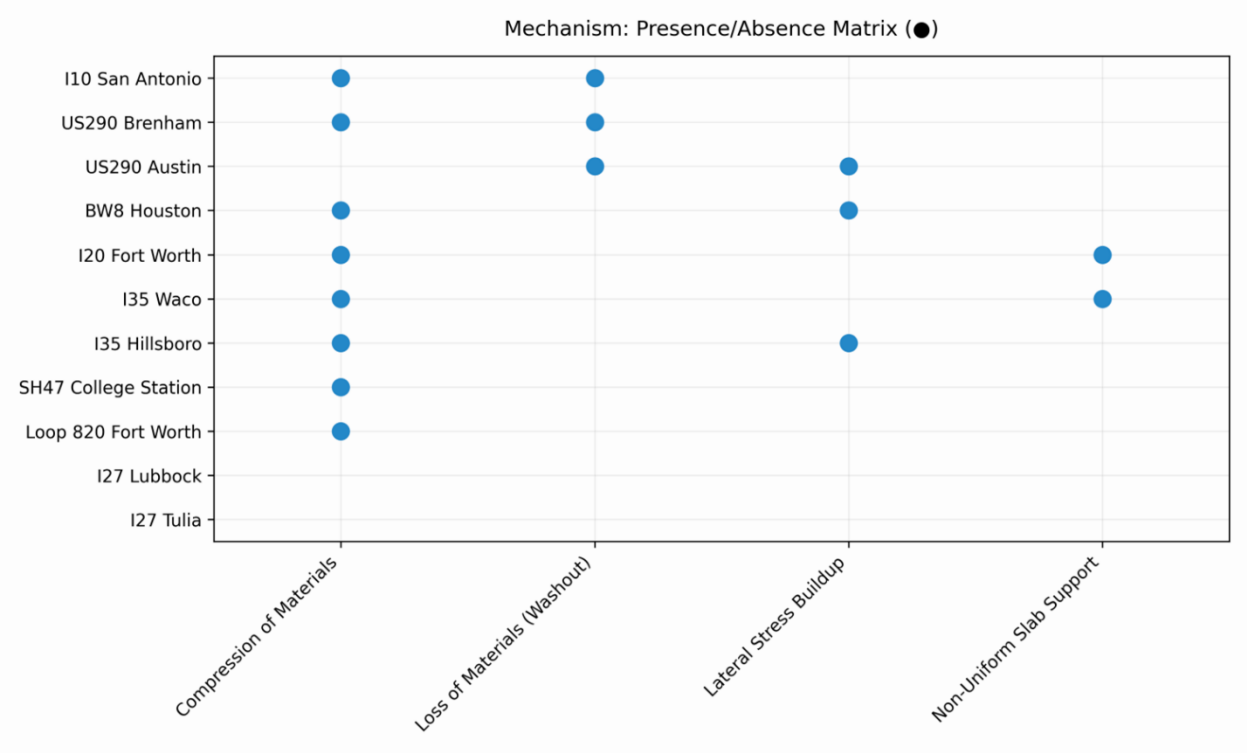


Figure 7-6. Distress mechanisms identified at each site

7.1.6 Interaction of Root Causes, Mechanisms, and Embankment Distresses

At a bridge approach, the BAS is supported by the bridge abutment on one end and a sleeper slab/adjacent pavement support on the other end. This transition can create non-uniform support, even before any deterioration occurs. If settlement develops in the embankment fill or founding soil, the support condition becomes more uneven, and the most common outcome is a bump at the end of the bridge (and related cracking, separation, or voids).

In this chapter, for simplicity, the term “embankment” is used to collectively refer to the BAS, adjacent pavement, embankment wall system (if present), and the embankment slope/fill mass. The performance of this combined system is subjected to construction quality, traffic loading, rainfall/infiltration, time-dependent consolidation, and environmental effects. Depending on the soil conditions and construction quality, the system may respond through different physical processes and eventually show visible distresses.

The interaction between an embankment and the forces acting upon it is very complex. A single distress is rarely the result of a single isolated issue; rather, it is usually the product of multiple

overlapping factors. To visually explain this complexity, the behavior is categorized into three layers as shown in **Figure 7-7**:

- **Layer 1: Root Causes (Invisible Triggers):** These are the initial conditions or events that set the instability in motion. They range from construction-phase issues, such as inadequate fill compaction or poor joint sealing, to natural processes like founding soil consolidation.
- **Layer 2: Mechanisms (Physical Processes)**: This layer represents how the embankment system responds. These are the "unseen" physical changes including washout & erosion, settlement, subgrade volume change, non-uniform support, increased pavement stress due to environmental loading, and increased lateral pressure behind the retaining wall.
- **Layer 3: Visible Distresses (Site Symptoms)**: These are the distresses that are visually observed, such as voids, railing-pavement separation, BAS bump, halfmoon cracks, longitudinal crack, wall bulge/movement, faulting, and lane separation.

A single root cause can trigger multiple mechanisms, and those mechanisms can combine to produce an array of surface distresses. It is important to note that this is a circular process: for example, once a distress like a lane separation appears, it can loop back to become a trigger for further water infiltration, accelerating the deterioration of the entire system.

In **Figure 7-8**, the highlighted pathway is used to show a common "loop" observed at bridge approach with MSE wall configuration, and IH35 Hillsboro is a clear example of that sequence. In this case, water infiltration likely entered through open joints/cracks, increasing moisture in the backfill. As moisture built up, it contributed to increased lateral earth pressure, which can drive wall bulge/movement and lateral displacement of the retained soil mass. That movement can create voids and loss of support, producing non-uniform support and differential movement under traffic, which then shows up as faulting and lane separation (often with associated cracking such as halfmoon/longitudinal patterns). Once lane separation/faulting develops, it further opens the system to more infiltration, which feeds back into the same highlighted loop and accelerates deterioration.

Ultimately, this cycle highlights why focusing only on surface repairs is often insufficient; unless the root cause is addressed, the system will likely continue to deteriorate. Effective repairs should target the underlying root causes and active mechanisms (e.g., infiltration pathways, drainage performance, support loss, and wall stability) rather than only correcting the surface distress, since treating symptoms alone often allows the same deterioration loop to continue and reappear.

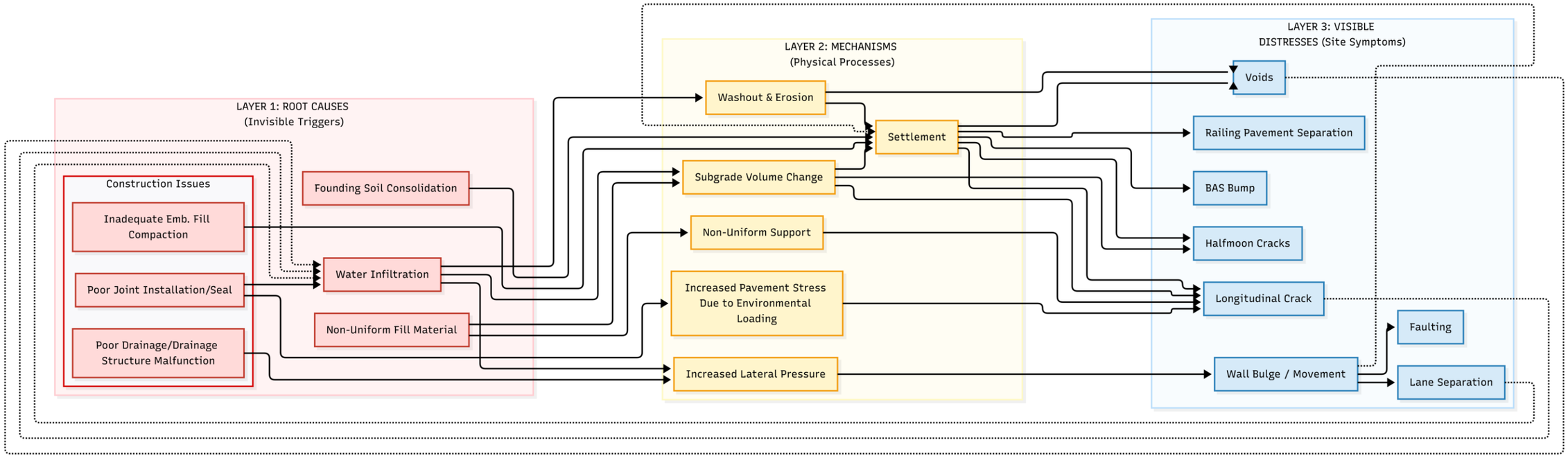


Figure 7-7. Three-layer interaction diagram showing how root causes (Layer 1) can trigger embankment response mechanisms (Layer 2) that manifest as visible distresses (Layer 3) at bridge approach transitions.

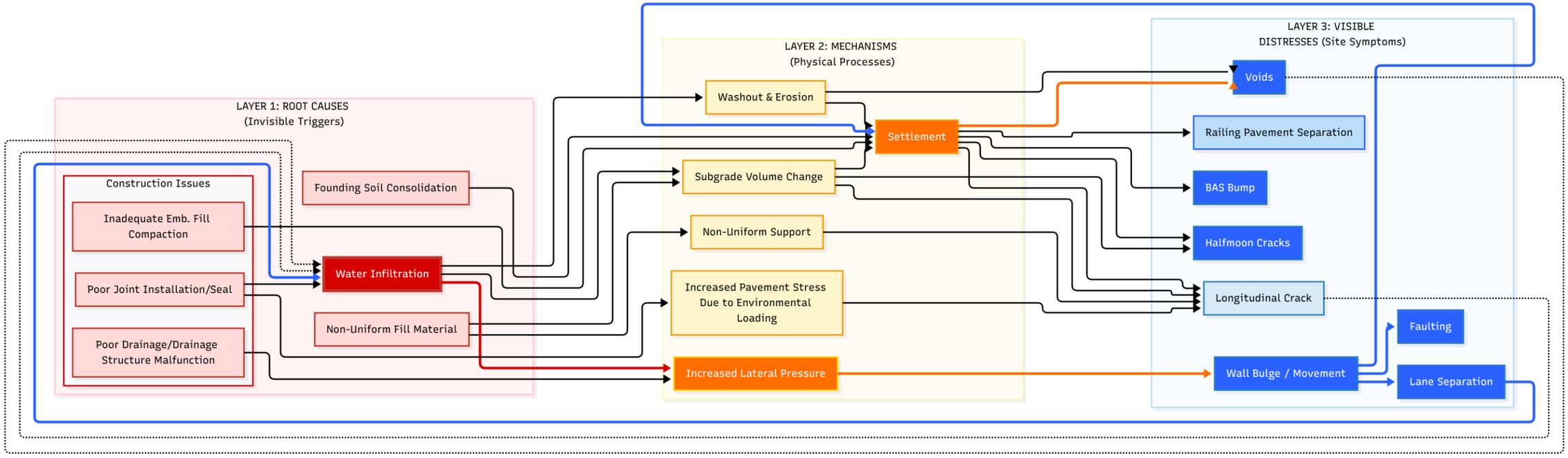


Figure 7-8. Interaction of Root Causes, Mechanisms, and Visible Distresses with Highlighted Deterioration Loop for the IH-35 Hillsboro Site.

Chapter 8 Maintenance and Repair Strategies

The deterioration of a bridge approach system, comprising the BAS, adjacent pavement, and underlying fill, is a complex process in which hidden physical mechanisms produce a wide variety of visible surface distresses. The same surface symptom, whether a bump, a faulted joint, a longitudinal crack, or a void beneath the slab, can be caused by different underlying mechanisms. Chapter 7 documented this behavior across the evaluated test sections, classified the observed mechanisms into four categories, and showed that a single distress is rarely the product of a single mechanism. Because of this complexity, a repair decision cannot be made from the surface distress alone. Surface-level repairs such as leveling a bump, sealing a crack, or overlaying a faulted joint restore the visible condition but do not treat the underlying mechanism. When that mechanism remains active, the repair is temporary, and the same distress is likely to recur on a timescale set by the underlying process rather than by the quality of the repair workmanship.

Two objectives therefore apply to any repair action at a BAS or embankment-pavement site. The first objective is a primary repair directed at the active deterioration mechanism: where ongoing compression, active washout, continuing wall movement, or persistent differential support is still driving deterioration. The priority is to intervene in that process, by restoring drainage, sealing infiltration pathways, densifying weak fill, or stabilizing the wall, before treating the surface. The second objective is a secondary, or residual, repair that restores the surface to serviceable condition: once the active mechanism has been addressed, the remaining bumps, voids, cracks, or faulting can be treated with conventional methods to restore ride quality, structural capacity, and resistance to water infiltration.

This chapter presents the maintenance and repair strategy developed based on these principles. The maintenance/repair strategy is organized in three levels: identification of the active distress mechanism from field and laboratory data (Level 0), primary repair actions directed at the root cause and active mechanism (Level 1), and residual repair of the remaining surface distresses (Level 2). Each level is supported by decision flowcharts covering the four distress mechanisms and the common surface distresses documented in Chapter 7. This chapter also describes the individual repair methods referenced in the framework, presenting the applicable TxDOT specifications, application procedures, triggers for use, and limitations.

8.1 Principles for selecting a repair strategy

Two objectives follow for any repair action at a BAS or embankment-pavement site:

(1) **Primary repair to address active deterioration mechanism.** If an underlying mechanism is still driving deterioration, which includes ongoing compression, active washout, continuing wall movement, or persistent differential support, the priority is to intervene in the ongoing mechanism. The intervention activities include restoring drainage, sealing water infiltration pathways, densifying weak fill, or stabilizing the wall prior to treating the surface.

(2) Secondary (residual) repair to restore the surface to serviceable condition. Once the active mechanism has been intervened, the remaining surface distresses, such as bumps, voids, cracks, or faulting, can be addressed with conventional repair methods to restore ride quality, structural capacity, and resistance to water-infiltration.

Whether an underlying mechanism is active or has been stabilized is therefore a central input to repair selection, and it is one that cannot be made from surface observation alone. It requires field evaluation (such as FWD, GPR, DCP, and/or coring) described in Chapter 5 as well as regular monitoring of the development of the distresses.

8.2 Mechanism-Based Decision Flowchart for BAS and Embankment Repair Selection

The maintenance strategy developed under this task is organized as a three-level decision framework, as illustrated in **Figure 8-1**. Level 0 diagnoses the active distress mechanism from field and laboratory data. Level 1 selects primary repair actions that address the root cause of the deterioration. Level 2 selects residual repairs for the surface distresses that remain after the mechanism has been addressed. The three levels are intended to be followed in sequence. The following section outlines the repair procedure based on the identified mechanism and the distresses observed in the field.

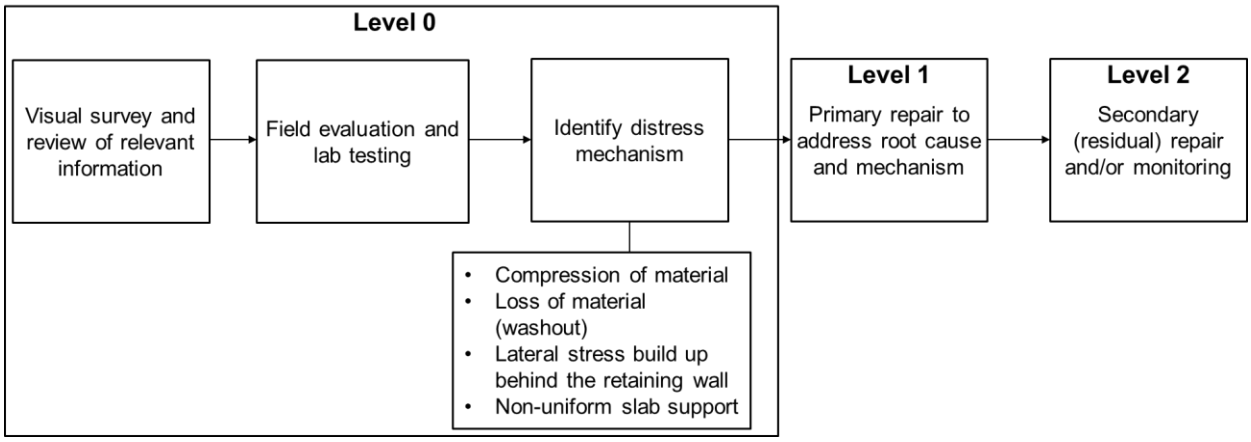


Figure 8-1. Three-level procedural framework for evaluating and repairing distress in BAS and embankment-pavement structures.

8.2.1 Level 0: Identification of distress mechanism

Selection of a repair strategy begins with a diagnosis of the active distress mechanism. This requires rigorous field evaluation utilizing ground-penetrating radar (GPR), falling weight deflectometer (FWD), dynamic cone penetrometer (DCP) or cone penetration testing (CPT), coring, and laboratory testing on collected soil samples. The field and laboratory evaluation procedures required to establish this diagnosis and guidelines for data interpretations are presented in Chapter 5 and 0, and the mechanism classification is presented in Chapter 7. The four primary distress mechanisms identified in the field are as follows:

- Compression of material.
- Loss of material (washout).
- Lateral stress build-up behind the retaining wall
- Non-uniform slab support

The coexistence of multiple mechanisms is common. At IH-35 Hillsboro, for example, water infiltration, lateral pressure buildup, and non-uniform support were all active, and the surface distresses (faulting, lane separation, void under BAS and half-moon cracking) could not be attributed to only one mechanism. When more than one distress mechanism is active, the Level 1 flowcharts presented in following sections are intended to be applied in sequence.

8.2.2 Level 1: Repair for root cause and mechanism

One or a combination of the four primary distress mechanisms may be active in the embankment and nearby pavement structure that initiates the instability and distress. Without addressing the root causes and mechanism of distress, like poor drainage, water infiltration, weak support, and unstable walls, addressing the visible distress alone may lead to the recurrence of the distress and can even deteriorate the structure furthermore.

A set of flowcharts is presented to provide guidance on various distress mechanisms before repairing the visible distress in the embankment-pavement system. **Note that the flowcharts presented in the subsequent sections are for illustrative purposes only. It should not be interpreted as strict specifications for repairs.**

8.2.2.1 Compression of fill materials

The current condition of the fill material should first be evaluated using DCP results. If the soil modulus M_r of the fill material is less than 8 ksi, which is considered the minimum acceptable threshold, remedial action is required. In such cases, the appropriate options are densification or full-depth repair.

The selection of full-depth repair should be based on several additional factors, including the depth of the predominant weak layer, the feasibility of repair under traffic and budget constraints, and the condition of the pavement and/or bridge approach slab (BAS). If the depth of the weak fill layer is 5 feet or less and the condition of the slab is unsalvageable due to severe cracking, full-depth repair (FDR) in accordance with TxDOT Item 361 becomes the most logical option.

Otherwise, densification using HDPF in accordance with TxDOT Special Specification 3008 is the preferred alternative. After the underlying fill condition has been addressed, the surface-level distresses can then be treated, as discussed in the subsequent sections.

Figure 8-2 illustrates the decision criteria for the selection of the appropriate method.

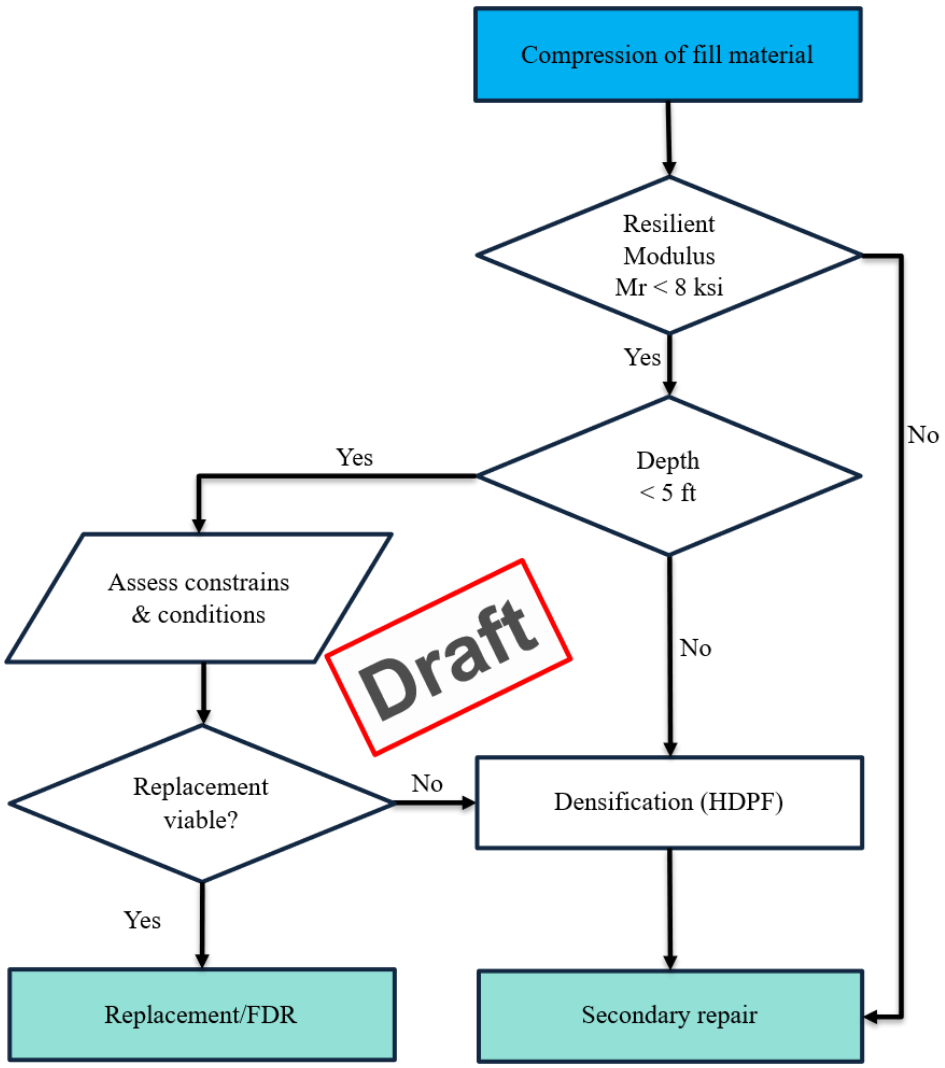


Figure 8-2. Flowchart to address compression of material for embankment-pavement system repair (this flowchart is for illustrative purposes only).

8.2.2.2 Loss of material (washout)

Loss of material refers to the erosion and removal of fine soil particles caused by water flowing through joints, cracks, drainage defects, or other seepage paths within the embankment system. This process can lead to the formation of voids, reduction in soil support, and deterioration of the structural integrity of the embankment-pavement system. As a result, settlement and other associated distresses may develop.

Where washout of material is identified as main distress mechanism, the initial repair action should be to identify and correct the pathway of water infiltration or seepage. Widened joints and deteriorated sealing materials should be repaired to prevent further infiltration. The drainage system should be restored by measures such as replacing the filter media from weepholes, repairing inlets, and improving drainage provisions where necessary. After these root causes are addressed

and fixed, the remaining visible distresses in the embankment-pavement system can be addressed through the appropriate corrective measures. **Figure 8-3** shows the steps to address the loss of material.

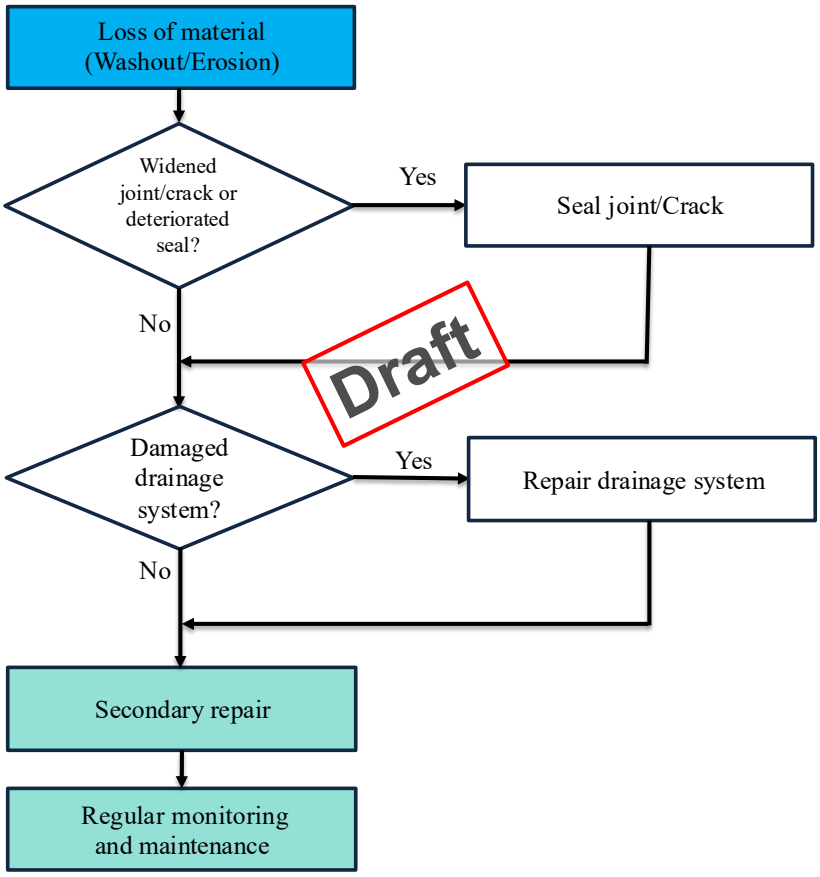


Figure 8-3. Flowchart to address loss of materials for embankment-pavement system repair (this flowchart is for illustrative purposes only).

8.2.2.3 Lateral stress buildup behind the retaining wall

Excessive lateral pressure behind a retaining wall can be caused by water infiltration through joints, cracks and/or inadequate drainage performance as well as poor compactions of fill materials. This buildup of lateral pressure can induce wall movement, which may subsequently lead to additional distresses in the embankment-pavement system. Therefore, the repair approach should focus on both eliminating the source of water infiltration and mitigating the excessive wall movement.

Where excessive wall movement is observed, the initial repair action should be to stabilize the wall, through the construction of a berm or buttress (or any other proper measures) to reduce ongoing movement. Once the wall movement is controlled, widened joints and deteriorated sealing

materials should be repaired to prevent further water infiltration. The drainage system should be restored by measures such as unclogging weepholes, repairing inlets, and improving drainage provisions where necessary. After these issues are addressed, corrective measures can be applied to the visible surface and structural distresses within the embankment-pavement system along with regular monitoring of the retaining wall movement. The overall process is illustrated by **Figure 8-4**.

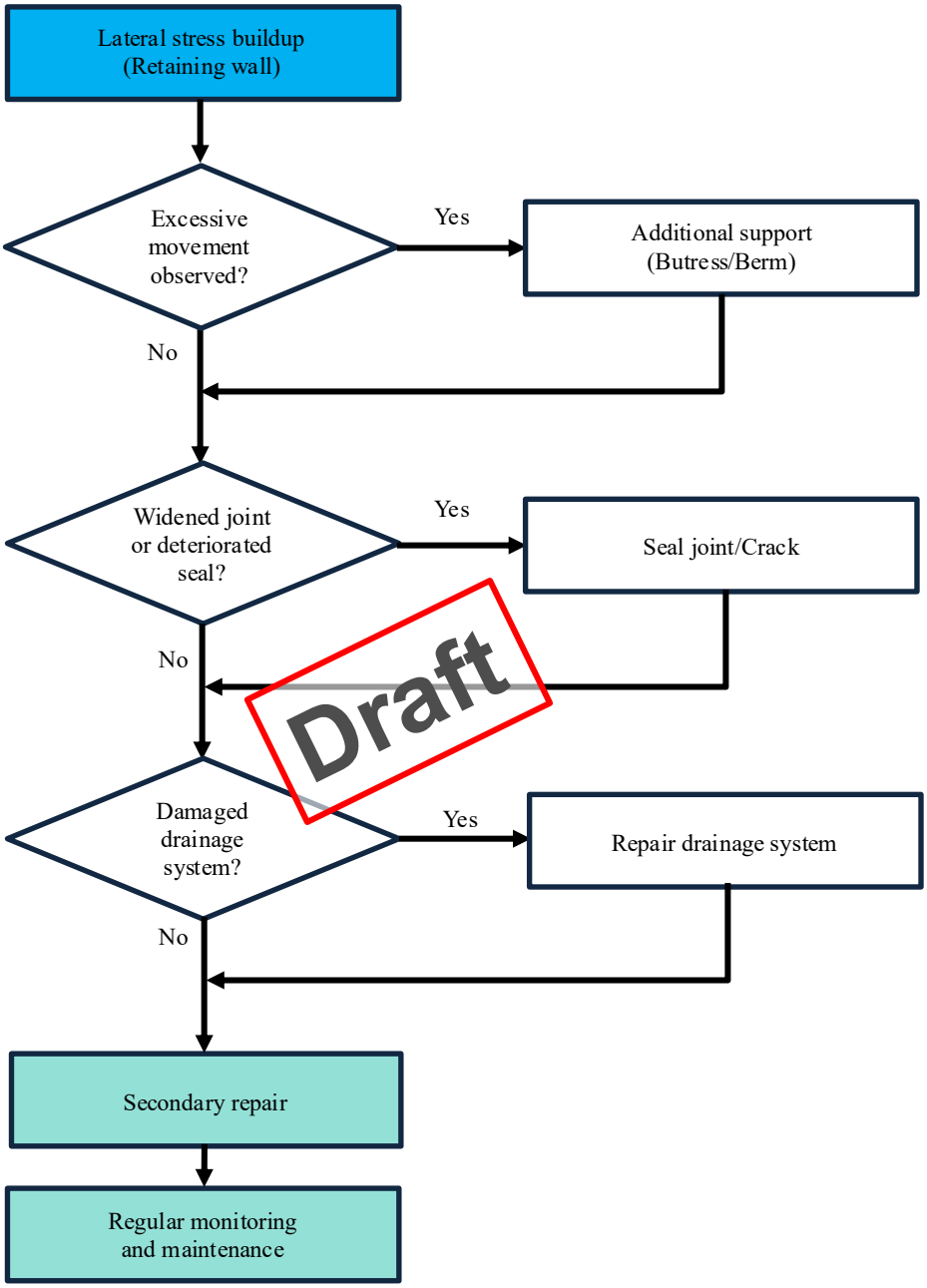


Figure 8-4. Flowchart to address lateral stress buildup behind the retaining wall for embankment-pavement system repair (this flowchart is for illustrative purposes only).

8.2.2.4 Non-uniform slab support

The interface between select fill and non-select fill may induce longitudinal cracking and faulting as a result of non-uniform slab support. Accordingly, the DCP results obtained from the select fill and non-select fill zones should be analyzed to assess the variation in support condition across the interface. If the soil modulus M_r of the non-select fill is found to be less than 8 ksi, densification of the weak material is recommended. This densification should be performed through the application of HDPF in accordance with the applicable TxDOT special specifications. Once the support condition has been improved, the visible surface-level distresses should be addressed through the appropriate corrective measures described in the subsequent section. **Figure 8-5** shows the steps to address the non-uniform support condition.

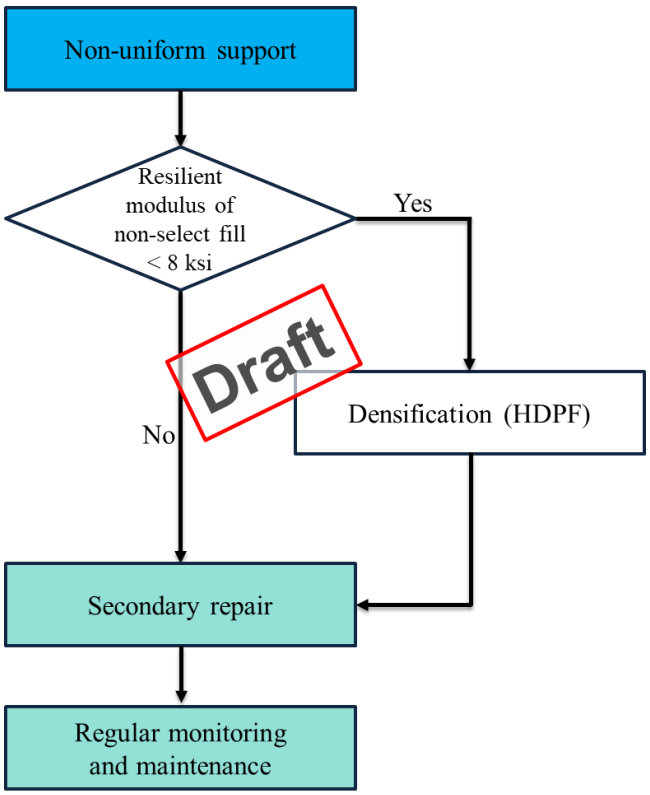


Figure 8-5. Flowchart to address non-uniform slab support for embankment-pavement system repair (this flowchart is for illustrative purposes only).

8.2.3 Level 2: Corrective repair measures

After addressing the root cause of the distresses, the next step is to address the visible distresses. These distresses may include settlement and bumps, faulting, lane separation, longitudinal crack, diagonal/half-moon shaped crack, and voids underneath BAS and/or pavement.

8.2.3.1 Voids beneath BAS/pavement

Voids beneath the pavement or BAS may be filled using flowable fill in accordance with TxDOT Item 401 or High-Density Polyurethane Foam (HDPF) in accordance with Special Specification 3010 (SS 3010). First, the size and the extent of the void is estimated using GPR and coring. Flowable fill is appropriate for large, continuous, and laterally extensive voids where the embankment is stable and the dead load from the application of the flowable fill is not a concern for the stability of the embankment. In cases where the void conditions are less suitable for flowable fill, or where a lighter and more adaptable material is needed, HDPF may be used in accordance with TxDOT Special Specification 3010 (SS 3010) as the preferred void-filling option. This is illustrated in the flowchart given in **Figure 8-6**.

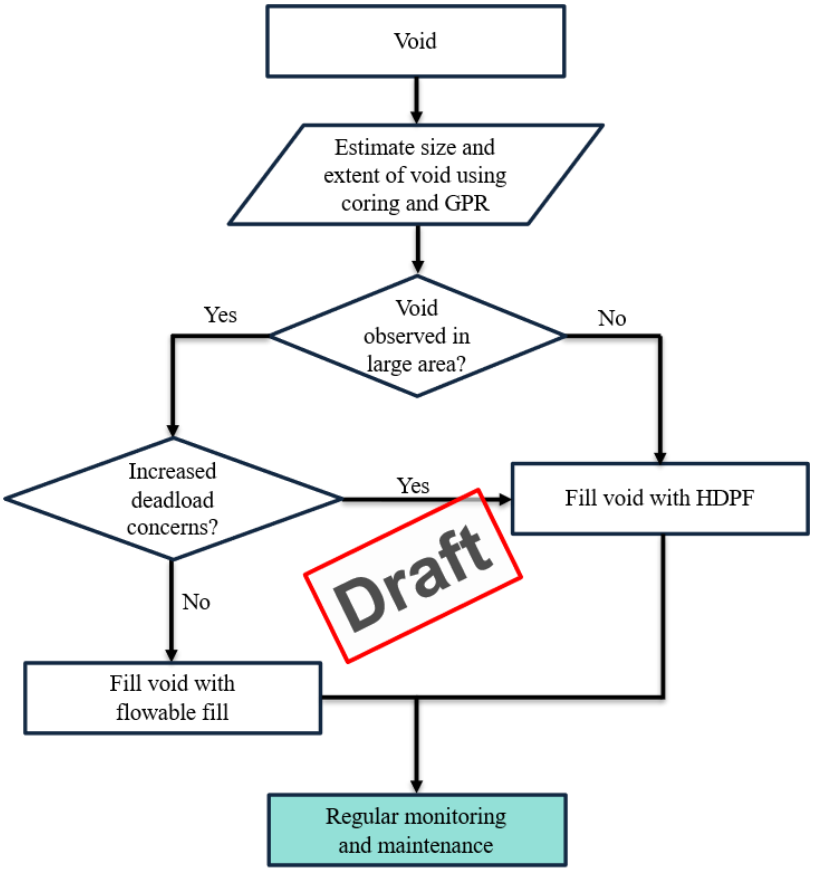


Figure 8-6. Repair flowchart for void (this flowchart is for illustrative purposes only).

8.2.3.2 Settlement/Bump

For addressing BAS/pavement settlement and associated surface bumps, the repair strategy must be selected based on the severity of the distress and the condition of the underlying support system. The initial step involves evaluating the severity of the distress. If the observed settlement or bump is considered severe, soil densification and slab jacking utilizing High-Density Polyurethane Foam (HDPF) are recommended, subject to site-specific conditions. Conversely, if the distress is minor, hot mix asphalt (HMA) overlay/level-up may be sufficient. Following the implementation of the selected repair, the site must be routinely monitored to verify whether the settlement has stabilized or further settlement recurs. The complete decision-making process and repair criteria are illustrated in the flowchart in **Figure 8-7**.

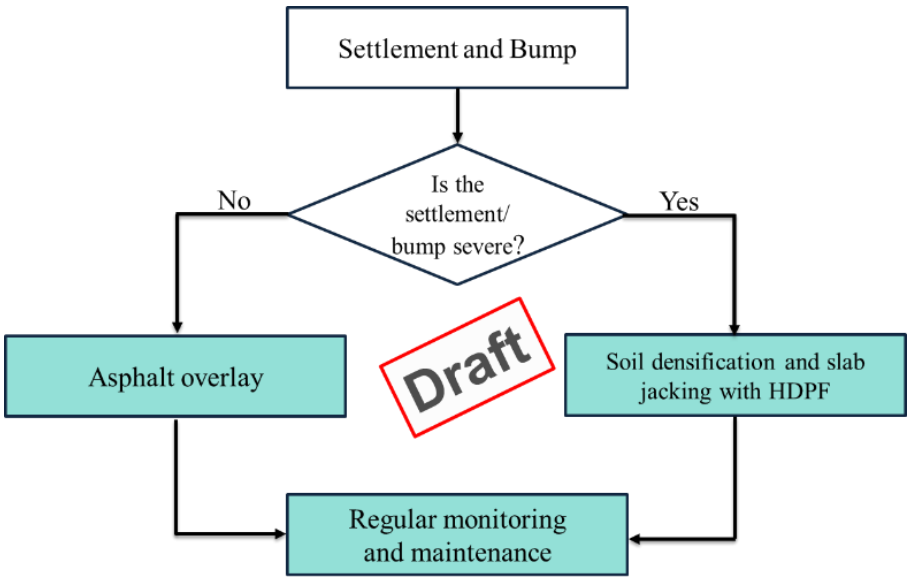


Figure 8-7. Repair flowchart for settlement and bump (this flowchart is for illustrative purposes only).

8.2.3.3 Faulting and lane separation

Figure 8-8 illustrates the repair decision process for faulting and lane separation. Faulting is addressed through slab jacking using HDPF in accordance with TxDOT Special Specification 3008 (SS 3008) and Special Specification 3010 (SS 3010). Repair for lane separation may include dowel bar retrofit, slot stitching, or cross stitching depending on site conditions and the judgment of the site engineer.

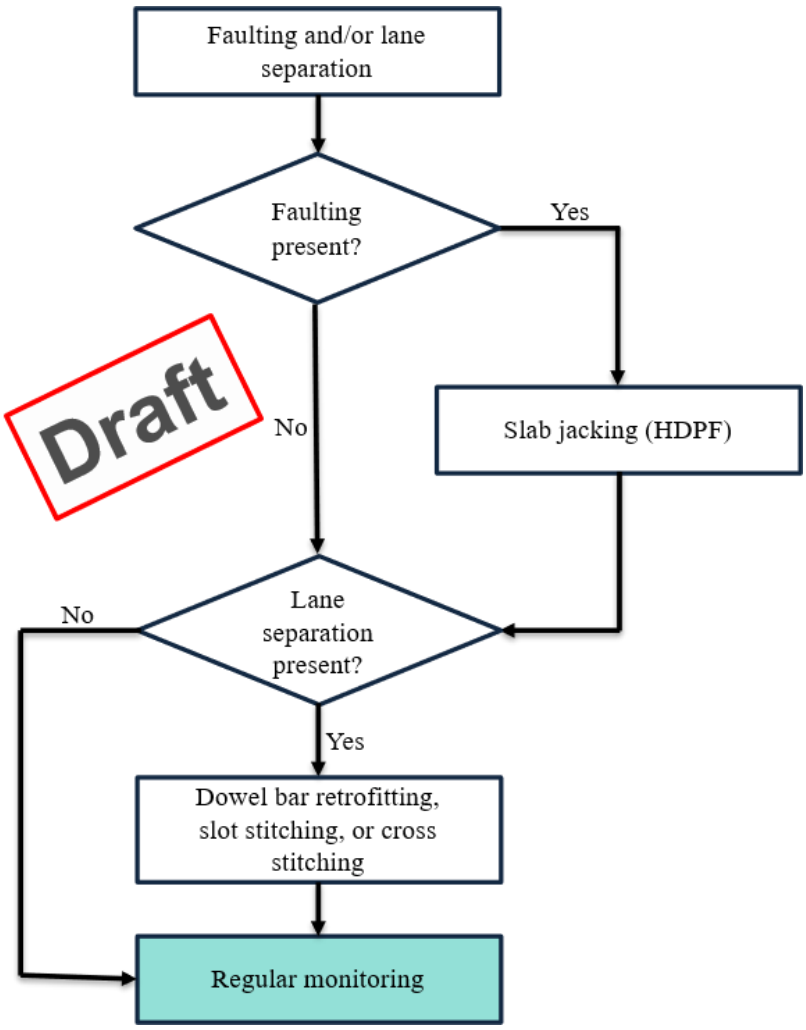


Figure 8-8. Repair flowchart for faulting and lane separation (this flowchart is for illustrative purposes only).

8.2.3.4 Longitudinal crack, half-moon shaped crack and diagonal crack

If the underlying causes for the initiation and development of crack have already been addressed based on the identified distress mechanism following Sections 8.2.3.1 through 8.2.3.3, the repair decision for longitudinal, half-moon shaped, and diagonal cracks is recommended to be based on the severity of cracking. If the crack width is wide enough to permit water penetration, crack sealing should be performed; otherwise, regular monitoring is recommended.

8.3 Commonly Used Repair Methods

Commonly used methods for repair of BAS and nearby pavement structures include:

- HMA level-up and overlay
- Flowable fill
- Grouting
- Polyurethane foam injection
- Full/partial depth repair
- Dowel bar retrofit, slot stitching, and cross stitching.

The following sections present the details of each repair method.

8.3.1 HMA Level-up and Overlay

Hot mix asphalt (HMA) overlay is a widely implemented maintenance technique used to remediate ride quality issues resulting from settlement. HMA overlay typically refers to a continuous layer of asphalt placed over an entire pavement section. Its primary goal is to improve overall ride quality and protect the underlying structure from moisture infiltration. HMA level-up refers to a localized application of asphalt specifically used to fill depressions or "dips" in the pavement. It is frequently used at the "bump at the end of the bridge" where the approach slab has settled.

This method is categorized as one of the most cost-effective and least time-consuming repair options available among TxDOT districts. However, it is primarily recommended for correcting surface irregularities when no underlying soil erosion, weakened subgrade, or void issues are present.

8.3.1.1 TxDOT specification

- TxDOT Item 341 (Dense-Graded HMA)
- Special Specification 7074 (SS 7074) Blade Level-Up with Asphalt concrete
- Special Specification 8011 (SS 8011) Dense-Graded Hot-Mix Asphalt (Materials Only)
- TxDOT Item 341 or Item 344 (Superpave). For thin applications (<1 inch), Item 347 (Thin Overlay Mixtures) is utilized.

8.3.1.2 Trigger for use

HMA serves as a suitable preservation material primarily when the objective is to extend the service life of a roadway that has reached approximately 90% of its primary embankment consolidation (Fortunatus 2018). The application of HMA is specifically triggered when surface irregularities are identified as the primary distress mechanism and field evaluations confirm the absence of active underlying soil erosion or large void formation (FHWA 2015; Ghorbanpoor et al. 2007). In these stabilized scenarios, HMA effectively restores ride quality by smoothing

differential settlements and providing a waterproof seal to prevent further moisture infiltration into the embankment (Jayawickrama et al. 2005).

8.3.1.3 Limitations

HMA repairs are not recommended for pavements categorized as poor or bad condition, specifically those exhibiting transverse joint faulting more than 3.8 mm or an International Roughness Index (IRI) greater than 2.70 m/km (Fortunatus 2018). A critical limitation is the "Band-Aid" effect, where HMA is used to mask active, progressive settlement. In high-plasticity clay environments, the additional weight of thick HMA applications can increase the dead load on the embankment, potentially accelerating secondary settlement (White et al. 2007). Furthermore, HMA should not be utilized as a primary corrective measure if active material washout or large voids (greater than 0.5 inches) are detected beneath the slab, as the lack of structural support will lead to rapid reflective cracking or "shoving" against the rigid abutment (Ghorbanpoor et al. 2007).

8.3.2 Flowable Fill

Flowable fill, also referred to as Controlled Low-Strength Material (CLSM) or "flow fill," is a self-leveling and self-compacting cementitious slurry. It is primarily used as an embankment backfill material to fill large, estimated voids without the need for conventional mechanical compaction (Puppala et al. 2011; Abu-Hejleh et al. 2006).

8.3.2.1 TxDOT specifications

TxDOT Item 401 Flowable Backfill.

8.3.2.2 Trigger for use

Flowable fill is highly recommended as a mitigation technique for filling specific, large void spaces beneath concrete pavement, approach slabs, and shoulders after they have been detected, mapped, and volumetrically estimated by tools like GPR (Puppala et al. 2011). It is specifically triggered when restoring pavement-base contact is required at the BAS-sleeper slab joints where water infiltration and material washout have created significant cavities beneath the concrete pavement.

8.3.2.3 Limitations

A primary limitation of flowable fill is the long-term performance uncertainty regarding how the BASs interact with the newly placed rigid material under dynamic traffic loads (Puppala et al. 2011). Furthermore, because it introduces a significant mass of wet material, there are concerns about its application over highly plastic, compressible fill material where moisture and added dead load are critical factors. To achieve high flowability, flowable fill requires a high-water content. As the material sets, it releases bleed water. If the surrounding embankment soils are highly moisture-sensitive (high plasticity clays), the bleed water can saturate the subgrade, potentially reducing its shear strength (ACI 229). While flowable fill effectively addresses the voids caused by water intrusion (Jayawickrama et al., 2005), it creates a rigid CLSM block over a potentially

settling subgrade. If the deep-seated embankment continues to settle, the rigid block may separate from the subgrade, requiring subsequent repairs.

Because the material is highly flowable, the application team must actively monitor the bridge abutment joints, sleeper slab interfaces, and surrounding pavement coping, MSE wall panel joints and riprap during injection to identify and prevent any unwanted leakage of the slurry. **Figure 8-9** shows leakage of flowable fill from riprap.



Figure 8-9. Leakage of flowable fill from riprap. (Image source: TxDOT Maintenance Division)

8.3.3 Polyurethane Foam Injection

High Density Polyurethane Foam (HDPF) is widely used to strengthen base and subgrade soil and fill the voids under concrete pavement and BAS. The injection of HDPF is furnished with two parts, 1:1-by-volume HDPF (Diphenylmethane Diisocyanate and Resin). This water resistance foam will densify the underlying soils at specific locations with real time surface monitoring to prevent over-heaving or unintended pavement displacement. HDPF injection process are shown in **Figure 8-10**.



Figure 8-10. HDPF injection process (Image source: *https://www.uretekusa.com/blogs/*)

8.3.3.1 TxDOT specifications

- Special Specification 3008 (SS 3008) Soil Densification and Raising Concrete Slabs with High-Density Polyurethane Foam (HDPF)
- Special Specification 3010 (SS 3010) Raising and Undersealing Concrete Slabs with Foam Systems

8.3.3.2 Trigger for use

HDPF serves as a suitable preservation tool primarily when the objective is to remediate pavement settlement and stabilize subgrade soils that exhibit localized instability or loss of support (Gaspard & Morvant 2004). The application of HDPF is specifically triggered when surface irregularities such as bridge approach depressions, faulted joints, or slab settlement are identified as the primary distress and field evaluations, such as FWD, DCP, GPR or visual void inspection, confirming the presence of subsurface voids or low-density base material (Abu al-Eis & LaBarca 2007; Opland & Barnhart 1995). HDPF effectively restores ride quality by lifting concrete slabs to the required grade and providing a hydro-insensitive, closed cell matrix that prevents further moisture infiltration and mitigates future erosion of the embankment (Ellis 2015; Opland & Barnhart 1995).

8.3.3.3 Limitations

HDPF should not be utilized as a primary corrective measure if extensive load transfer failure is detected. As the material's relatively low compressive strength (minimum 60 psi) and lack of rigidity compared to cementitious systems may result in resettlement or the development of unintended voids in adjacent, un-injected slabs (Gaspard & Morvant 2004; Opland & Barnhart 1995).

A critical limitation is the risk of non-uniform support; field evaluations indicate that the foam may fail to fully penetrate the entire width and depth of open-graded aggregate subbases, potentially creating a "bridging" effect where localized voids remain and compromise the long-term load-bearing capacity of the pavement system (Vennapusa et al., 2016). In complex subsurface environments, the high impermeability of the closed-cell foam can inadvertently block established drainage paths, trap moisture and potentially accelerate the deterioration of adjacent soil zones (Ellis 2015). HDPF repairs are not recommended for those already categorized as structurally failed, as the expansion pressures required for leveling can induce significant tensile stresses that lead to immediate longitudinal cracking and a reduction in the slab's remaining service life (Abu al-Eis & LaBarca 2007; Gaspard & Morvant 2004).

8.3.4 Full and Partial-Depth Repair

Full depth repair (FDR) and partial depth repair involves removing some or all of an approach slab and pavement, and can be done with full depth patching, a concrete pour, or precast panel (Jayawickrama et al., 2005). Although full and partial depth repair technique is often most expensive method and takes the longest amount of time to complete compared with the other methods (Al-Eis & LaBarca, 2007), this methods are commonly used as method of repair because it includes improvement of both ride quality and structural integrity (Chen & Won, 2008).

8.3.4.1 TxDOT specifications

- Item 361 Repair of Concrete Pavement
- Special Specification 3203 (SS 3203) Partial Depth Repair for Concrete Pavement

8.3.4.2 Trigger for use

Full-depth repair (FDR) serves as a suitable repair method primarily when the objective is to remediate severe structural distresses such as punchouts, shattered slabs, or deep spalling that compromise the pavement's integrity. The application of FDR is specifically triggered when surface irregularities including transverse cracks in CPCD or localized concrete depressions in CRCP are identified as the primary distress and field evaluations, such as visual pumping observations, falling weight deflectometer (FWD) testing, or coring, confirms the presence of subsurface voids, poor subgrade at shallow depth, or structural failure extending through the full depth of the slab. Partial depth repair (PDR) can be used for situations where the deteriorated concrete extends to the mid-depth of the slab.

8.3.4.3 Limitations

Full-depth and partial-depth repairs involve removing some or all of an approach slab and pavement to improve ride quality and structural integrity (Jayawickrama et al., 2005; Chen & Won, 2008). However, these techniques are often the most expensive methods and take the longest amount of time to complete compared with other maintenance options (Al-Eis & LaBarca, 2007).

A primary limitation of full-depth repair (FDR) is the risk of damaging the surrounding infrastructure during the removal process, specifically the potential to spall or fracture concrete adjacent to the repair area. Furthermore, there is a high risk of disturbing the underlying base materials; therefore, slabs must be lifted out with minimal disturbance, and any loose base material must be completely removed or recompacted. Scheduling is also a constraint, as concrete placement should follow full-depth saw-cutting by no more than seven days to prevent further slab degradation. Additionally, the complexity of restoring structural continuity requires epoxy-grouted tie bars to meet a pullout strength of at least 3/4 of the yield strength, necessitating simulated job condition testing before work begins.

Partial-depth repairs (PDR) are strictly limited to surface-level distresses, such as spalling or delamination in the upper portion of the slab and cannot address deep-seated structural issues. If a partial-depth patch is applied over a "working crack" that extends through the full depth of the pavement, the repair will likely suffer from reflective cracking and debonding. Consequently, partial-depth methods are an unsuitable solution for distresses originating at the bottom of the slab or those involving unstable base conditions.

8.3.5 Dowel-bar Retrofit, Slot Stitching, and Cross Stitching

Dowel bar retrofit (DBR), slot stitching, and cross stitching are pavement level repair methods used to restore or improve load transfer efficiency (LTE) across joints and cracks in concrete pavements. Although they are not soil-improvement methods, they can improve the performance of bridge approach slab and pavement repairs by stabilizing cracks and joints and enhancing slab-to-slab load transfer. In practice, these methods are most effective when used together with other repairs that address the underlying support condition, such as void filling, slab stabilization, or subgrade densification.

8.3.5.1 TxDOT specifications

Special Specification 3012 (SS 3012) Dowel Bar Retrofit

Special Specification 3013 (SS 3013) Slot-Stitching Longitudinal Joints in Concrete Pavement

8.3.5.2 Trigger for use

These methods fit best for repair of faulting, lane separation, and longitudinal cracking after the active distress mechanism has already been identified and addressed. They should therefore be treated as corrective pavement repair measures, not as root-cause repairs for embankment-related distresses.

8.3.5.3 Limitations

The limitation of these methods is that they do not address the underlying root cause of distress. like poor support condition or lateral movement of wall due to stress buildup. If the underlying distress mechanism is active, such as void formation, pumping, washout, embankment settlement, or lateral wall movement, then these repairs alone are likely to be insufficient.

Chapter 9 Conclusions and Recommendations

9.1 Summary of the Research

Bridge approach slabs (BAS) and the adjacent pavement supported on roadway embankments are a recurring maintenance concern for TxDOT. The embankment fill and the founding soil beneath it undergoes settlement in service under traffic loading, self-weight, and water infiltration, while the bridge, supported on deep foundations, experiences less settlement. The resulting distresses, settlement and bumps, faulting, cracking, lane separation, and voids beneath the slab, affect ride quality, safety, and maintenance cost across the state. Current TxDOT practice, however, does not provide guidance for connecting an observed distress to the mechanism producing it before a repair is selected. Because visually similar distresses can arise from different underlying mechanisms, repairs selected from surface symptoms alone frequently treat the visible condition while the process that produced it remains active, and the distress recurs.

Project 0-7173 was undertaken to close this gap. The Research Team reviewed the literature and the current state of practice for evaluating and repairing in-service roadway embankments; surveyed TxDOT districts on current identification, evaluation, and repair practice; reviewed 30 potential field test sections and selected 11 final sections encompassing a range of distress types, pavement structures, and embankment configurations; conducted field and laboratory evaluations at the test sections using falling weight deflectometer (FWD) testing, ground penetrating radar (GPR), coring, dynamic cone penetrometer (DCP) testing, cone penetration testing (CPT), and laboratory soil testing; classified the mechanisms responsible for the observed distresses into four categories; and developed a mechanism-based maintenance and repair framework, together with draft guidelines for interpreting the field evaluation data. The summary findings and recommendations for implementation are presented below.

9.2 Summary of Findings

9.2.1 Current Practice and the Need for Evaluation Guidance

The district survey, with 30 responses representing 22 of the 25 TxDOT districts, documented both the extent of the problem and the character of current practice.

a) Settlement, heave, and faulting, including the bump at the end of the bridge, were reported by every responding district, followed by partial or entire joint failure (57 percent), longitudinal cracks (43 percent), and transverse cracks (40 percent). Half of the respondents indicated that distresses begin to appear within five years of construction.
b) Districts identify sections needing repair almost entirely through visual observation (100 percent), public complaints (87 percent), and rideability (80 percent), and 63 percent of respondents reported no specific criterion for making repair decisions. Condition evaluation of the BAS and pavement likewise relies first on visual inspection (100 percent), with coring (57 percent), GPR (53 percent), and FWD (40 percent) applied less frequently.
c) Evaluation of the embankment fill itself is limited. In-situ testing that measures the stiffness or strength of in-service fill is not common practice: 37 percent of respondents reported using

the DCP, and smaller shares reported the Texas cone penetrometer, CPT, or standard penetration test, while 17 percent indicated that no evaluation activities are conducted for in-service fills or that they were unsure whether any are.

d) Districts attribute the distresses primarily to settlement of backfill due to poor compaction (80 percent), poor drainage and soil erosion due to water infiltration (60 percent), settlement of the foundation soils (57 percent), and poor construction practices (47 percent). Considering that void formation can be caused by washout, the factors associated with water infiltration together account for 80 percent of the responses.
e) Repairs are dominated by surface-level measures, led by level-up of the approach slab (50 percent), full- or partial-depth repair (40 percent), and polyurethane foam injection (37 percent), and they recur: 80 percent of respondents reported repairing the same section again within 10 years of the previous repair, and 33 percent within 5 years.

The literature review reached a consistent conclusion from the published record: the commonly used repair methods, HMA overlay, slab replacement, slab jacking, grouting, and polyurethane foam injection, generally perform well in the short term, but their long-term performance is variable, and no single method is suitable for all conditions. Studies in Texas and other states repeatedly associate poor long-term repair performance with unaddressed subgrade, base, drainage, or erosion conditions. The survey and the literature together define the gap the project addressed: distress identification is visual, the embankment is rarely evaluated, repair selection is not tied to cause, and repairs recur on a timescale consistent with untreated mechanisms.

9.2.2 Field Evaluation Methods and Interpretation Guidelines

Field investigations were conducted at 11 test sections. The evaluated sections encompassed slope and retaining-wall embankment configurations, embankment heights from 11 to 35 ft among the selected sections, and both CRCP and asphalt pavement structures. The findings on the evaluation methods are as follows.

a) Each method resolves a distinct and bounded part of the problem. FWD testing locates zones of poor structural response rapidly and over long lengths; GPR maps voids, repair materials, buried utilities, and thickness variation over continuous areas but requires core calibration; coring provides definitive point-wise confirmation of thickness, voids, repair history, and slab condition; DCP testing quantifies near-surface fill stiffness; CPT extends the stiffness characterization through the embankment height and into the founding soils; and laboratory testing determine soil composition, through moisture and plasticity, and detects material loss through gradation analysis.
b) Elevated deflection alone does not identify the cause. Comparable deflection levels at the evaluated sections resulted from voids, prior foam injection, thin slabs, weak near-surface fill, and internal slab deterioration. Conversely, at the sections evaluated, sharp localized deflection spikes on a BAS consistently corresponded to voids confirmed by coring. A measured central deflection exceeding 1.5 times the thickness-matched statewide benchmark for well-performing CRCP provides a practical screening indicator of potential voids or prior foam injection, and exceedance of 2.0 times the benchmark provides a strong

indicator. These thresholds are draft and based on the data available at the time of the analysis.

c) The DCP data support a draft three-tier, performance-based classification of in-service embankment materials: acceptable for minimum soil modulus M_r of 18 ksi or greater, fair for 8 to 18 ksi, and poor below 8 ksi, with conservative alternative values of 20 ksi (acceptable), 10 to 20 ksi (fair), and 10 ksi (poor), respectively. At the evaluated sections, no distress attributable to poor embankment materials was observed where the minimum resilient modulus exceeded 18 ksi, and 74 percent of distressed locations fell below 8 ksi. The depth of the weak layer matters as much as its stiffness: distressed locations commonly showed their weakest layer within the upper 20 to 60 in.
d) Draft correlations extend the DCP classification to CPT data, permitting evaluation over the full embankment height: M_r [ksi] = $0.97q_c$ [tsf] for predominantly clayey fills and M_r [ksi] = $0.55q_c$ [tsf] for predominantly sandy fills, the latter resting on a single site and particularly in need of additional datasets.

9.2.3 Distress Mechanisms

The distresses observed at the test sections trace to four recurring mechanisms: (i) compression of materials, comprising both embankment fill and founding soils; (ii) loss of materials through erosion and washout; (iii) lateral stress buildup behind the retaining wall; and (iv) non-uniform slab support.

a) Compression of materials was the most frequently identified mechanism, at eight sections, followed by material washout and lateral stress buildup at three sections each. More than one mechanism was active at most sections, and a single distress could rarely be attributed to a single cause.
b) Visible distress type alone is an unreliable indicator of mechanism. Settlement at the evaluated sections was traced variously to compression of poorly compacted fill, washout of fines by infiltrating water, consolidation of founding soils, and lateral displacement of stiff fill accompanying retaining-wall movement, and the appropriate repair differs in each case.
c) Not all observed distress originates in the embankment. At two sections, coring identified delamination at the reinforcing steel with corroded bars, an internal slab deterioration process, and at one of them the primary mechanism was the interaction between a CRCP terminal anchorage system and the embankment soil under thermal cycling. Attributing surface distress to the embankment by default can misdirect the repair in the same way as treating symptoms without diagnosis.
d) The interaction among root causes, mechanisms, and visible distresses is circular. Water infiltration weakens fill, raises lateral pressures, and creates voids; the resulting cracks, faulting, and lane separation open wider paths for infiltration; and the deterioration accelerates. This loop explains the recurrence of surface-only repairs documented in both the survey and the site histories, where repeated overlays at several sections managed the symptom for years while the underlying condition progressed.

9.2.4 Maintenance and Repair Strategy

The repair framework developed from these findings is organized in three levels, applied in sequence: identification of the active distress mechanism from field and laboratory data (Level 0), primary repair actions directed at the root cause and active mechanism (Level 1), and corrective repair of the remaining surface distresses (Level 2).

a) The central prescription of the framework is its ordering. Whether a mechanism is active or has stabilized cannot be determined from surface observation alone, and repairs applied without addressing an active mechanism are temporary. Where the mechanism has been stabilized, a conventional surface repair can perform well, as observed at a section where an earlier level-up and foam injection remained serviceable years later; where it has not, the primary repair, restoring drainage, sealing infiltration pathways, densifying weak fill, or stabilizing the wall, must come first.
b) Each commonly used repair method has defined triggers and limitations. HMA level-up and overlay suit minor, stabilized settlement but mask active settlement and add dead load; flowable fill suits large, mapped voids on stable embankments; HDPF injection suits void filling, slab jacking, and densification of weak fill within its effective depth, with limited improvement in soil stiffness; full-depth repair suits shallow weak layers beneath unsalvageable slabs and severe structural distress; and dowel bar retrofit, slot stitching, and cross stitching restore load transfer after the support condition has been addressed.
c) Where retaining-wall movement is involved, the stability of the wall governs the repair sequence: pavement repairs at such sections are contingent on verifying the global stability of the wall, and wall stabilization precedes surface restoration.

9.3 Recommendations for Implementation

The following recommendations are directed at TxDOT district and division practice for in-service BAS, adjacent pavement, and embankments.

a) It is recommended that repair selection at recurring-distress sites be preceded by a staged field evaluation rather than visual observation alone. The staged sequence developed in this research is: FWD screening of the deflection profile against the thickness-matched statewide benchmark; targeted coring at locations of elevated or spiking deflection, with control cores at sound locations; DCP testing through the core holes to classify the near-surface fill; CPT soundings where the embankment height warrants characterization beyond the DCP depth; and laboratory testing of soil samples where moisture accumulation or material washout is suspected. Slab condition should be checked in the cores before distress is attributed to the embankment.
b) It is recommended that the mechanism-based three-level framework be used for repair selection. The active mechanism should be identified first from the evaluation data; the primary repair should address that mechanism, including drainage restoration, joint and crack sealing, densification of weak fill, or wall stabilization; and corrective surface repairs should follow. Joint sealing and drainage maintenance is particularly important, since the

factors associated with water infiltration account for 80 percent of the contributing factors districts identified and water participates in all four mechanism categories.

c) It is recommended that the draft DCP- and CPT-based classification of embankment materials be applied, with its draft status retained, when evaluating in-service embankments. The classification provides screening thresholds for acceptable, fair, and poor materials and links each tier to a level of repair response.
d) It is recommended that DCP testing be incorporated into repair construction practice, in two roles documented in this research: quality-control testing of new fill lifts during reconstruction, with acceptance tied to a specified modulus, and paired before-and-after testing to verify what an injection treatment changed.
e) It is recommended that repaired sections be monitored after repair to establish whether the treated mechanism has stabilized, through periodic FWD testing at repaired BAS and pavement sections and periodic measurement of railing-pavement separation and wall movement at wall-supported sections. Where movement or separation recurs, the mechanism diagnosis and, where applicable, the wall stability should be re-evaluated before further repair.

9.4 Limitations and Recommendations for Future Research

The guidelines and framework developed in this project are based on the sections evaluated and carry the limitations of that dataset.

a) The FWD screening thresholds, the DCP classification, and the DCP-CPT correlations are draft recommendations derived from the data available at the time of the analysis. They should be refined as additional datasets become available. The correlation for predominantly sandy fills, in particular, rests on a single site.
b) The mechanism classification rests on a dataset in which compression of materials is well represented, at eight sections, but the other mechanisms are represented at three or fewer sections. Additional field evaluations at sections exhibiting washout, wall-related movement, and non-uniform support would strengthen the classification and the repair guidance tied to it.
c) The Level 1 and Level 2 decision flowcharts are illustrative guidance, not repair specifications, and their thresholds inherit the draft status of the evaluation guidelines.
d) The site-specific DCP-CPT correlations developed at individual sections were presented for information purposes and should not be transferred to other sites without verification.
e) The assessment of the effect of HDPF injection was based on DCP tests performed about 2 to 3 hours after injection, and the effect of set time on the measured moduli was not evaluated. Additional testing at longer set times is needed before firm conclusions are drawn about the effect of HDPF on fill stiffness.
f) Long-term field performance of various repair methods commonly used in practice should be evaluated to optimize repair strategies.

Within these limitations, the project provides TxDOT with a consistent, evidence-based procedure for evaluating BAS, pavement, and embankment conditions and for selecting repair strategies directed at the mechanism driving the distress rather than at its surface symptoms alone.

REFERENCES

Abu-Farsakh, M. Y. and Chen, Q. (2014). "Field demonstration of new bridge approach slab designs and performance." *Final Report Number FHWA/LA. 13/520*, Louisiana Transportation Research Center. https://rosap.ntl.bts.gov/view/dot/27323

Abu-Hejleh, N., Hanneman, D., White, D. J. and Ksouri, I. (2006). "Flowfill and MSE Bridge Approaches: Performance, Cost and Recommendations for Improvements." *Report No. CDOT-DTD-R-2006-2*. Colorado Department of Transportation, Denver.

Alavi, S., LeCates, J. F., and Tavares, M. P. (2008). "Falling Weight Deflectometer Usage." *NCHRP Synthesis 381*. Transportation Research Board.

Al-Eis, K. A., & LaBarca, I. K. (2007). *Evaluation of the URETEK method of pavement lifting*. Wisconsin Department of Transportation, Division of Transportation Systems

American Association of State Highway and Transportation Officials. (1993). Chapter 3 Guidelines for Field: 3.5.5 Use in Slab Void Detection, pp. III-41 to III-45. In AASHTO Guide for Design of Pavement Structures. Washington: AASHTO.

American Concrete Pavement Association (2001). Stitching concrete pavement cracks and joints. *Special Report-Concrete Pavement Technology & Research, SR903P, Skokie, IL*.

Azari, H. (2016). "Condition Assessment of Concrete Bridge Deck Using GPR." *LTBP News*. Federal Highway Administration.

Battaglia, I. K., Bischoff, D., & Peters, J. (2012). *Partial Depth Repair of Concrete Pavements in Wisconsin*. Wisconsin Department of Transportation, Division of Transportation System

Bozozuk, M. (1978). "Bridge Foundations Move. Transportation Research Record 678: Tolerable Movements of Bridge Foundations, Sand Drains, K-Test, Slopes, and Culverts." Transportation Research Board, National Research Council, Washington, D.C. 17–21.

Briaud, J. L., James, R. W., & Hoffman, S. B. (1997). "Settlement of Bridge Approaches (The Bump at the End of the Bridge)." *NCHRP Synthesis of Highway Practice 234*. Transportation Research Board, Washington, DC.

Cai, C. S., Voyiadjis, George Z., & Shi, Xiaomin. (2005). *Determination of interaction between bridge concrete approach slab and embankment settlement*. Louisiana Transportation Research Center.

Caltrans. (2021). Mechanically Stabilized Embankment (Caltrans Pre-Designed). In. https://dot.ca.gov/programs/engineering-services/manuals/geotechnical-manual: Caltrans.

Chen, D., and Won, M. (2008). Field performance monitoring of repair treatments on joint concrete pavements. *Journal of Testing and Evaluation*, *36*(2), 119-127.

Chen, D. H. and Scullion, T. (2007). "Using Nondestructive Testing Technologies to Assist in Selecting Optimal Pavement Rehabilitation Strategies." Journal of Testing and Evaluation 35(2): 211-219, Paper ID JTE100136, DOI: 10.1520/JTE100136

Chen, D.-H., Lin, H.-H., & Sun, R. (2011). Field performance evaluations of partial-depth repairs. *Construction and Building Materials*, *25*(3), 1369-1378.

Chen, D.-H., Won, M., & Hong, F. (2009). Investigation of settlement of a jointed concrete pavement. *Journal of performance of constructed facilities*, *23*(6), 440-446.

Chen, D-H, and Yi, Y. (2015) "Performance of Settled Bridge-Approach Slabs with Polyurethane-Foam Injection." *Journal of Testing and Evaluation* 43(6): 1338–49. https://doi.org/10.1520/JTE20140431.

Colorado DOT. (2023). 2023 Standard Specifications book. In. https://www.codot.gov/business/designsupport/cdot-construction-specifications/2023-construction-specifications/2023-specs-book/: Colorado DOT.

Darter, M. (2017). *Concrete repair best practices: a series of case studies*. Report No. cmr 17-013, Missouri Department of Transportation

Das, S. C., R. M. Bakeer, J. Zhong, and M. Schutt. 1999. Assessment of mitigating embankment settlement with pile-supported approach slabs. LA. 01/349. New Orleans, LA: Dept. of Civil and Environmental Engineering, Tulane Univ.

Dupont, B. and Allen, D. (2002). "Movements and Settlements of Highway Bridge Approaches." *Rep. No. KTC-02-18/SPR-220-00-1F*, Kentucky Transportation Center Report, Lexington, KY.

ElBatanouny, M. K., Hawkins, K. A., and Krauss, P. D. (2021). "Practices for Bridge Approach Systems." *NCHRP Synthesis of Highway Practice 566*. Transportation Research Board, Washington, DC. https://doi.org/10.17226/26196.

Ellis, W. (2015). *Assessment of Uretek deep injection process*.

FHWA (2000). "Priority, Market-Ready Technologies and Innovations." *Rep. No. FHWA-HRT-04-053*. Federal Highway Administration

FHWA. (2015). Bridge Maintenance Reference Manual. NHI Course Number 130108, Publication No. FHWA-NHI-14-050. In: United States Department of Transportation.

Fortunatus, M. (2018). Evaluation of the performance of polyurethane foams in rigid pavement preservation.

Galvan, M. (2007). Retaining Wall Design and Construction Issues. Presented at 2007 Design & Bridge Conference, Corpus Christi, Texas [https://ftp.txdot.gov/pub/txdot-info/des/presentations/desbrgconf07/galvan%20retaining_wall_issues.pdf]. (Accessed on 2/1/2023)

Galvan, M. (2011). "MSE Retaining Wall Design Considerations." Presented at 85th Transportation Short Course, Bryan, Texas [https://static.tti.tamu.edu/conferences/tsc11/presentations/struct-hydraulics-1/galvan.pdf]. (Accessed on 2/1/2023)

Gaspard, K., & Morvant, M. (2004). *Assessment of the Uretek process on continuously reinforced concrete pavement, jointed concrete pavement, and bridge approach slabs: technical assistance report*.

Ghorbanpoor, A., Koutnik, T. E., & Helwany, S. (2007). Evaluation of bridge approach settlement mitigation methods.

Ha, H. S., Seo, J., and Briaud, J-L. (2002). Investigation of Settlement at Bridge Approach slab Expansion Joint: Survey and Site Investigations. Report No. 4147-1. Texas Department of Transportation.

Hamakareem, M. I. *12 Factors Influencing Bearing Capacity of Soils*. The Constructor. Retrieved November 28th from *https://theconstructor.org/geotechnical/factors-bearing-capacity-soils/35343/*

Heintz, K. (2003). Follow up of injected polyurethane slab jacking.

Henderson, B., J. Dickes, G. Cimini, and C. Olmedo. (2016). FHWA LTPP Guidelines for Measuring Bridge Approach Transitions Using Inertial Profilers, Report No. FHWA-HRT-16-072, Federal Highway Administration, Washington, DC. Available online: https://www.fhwa.dot.gov/publications/research/infrastructure/pavements/ltpp/16072/160 72.pdf.

Hopkins, T. C. (1973). "Settlement of Highway Bridge Approaches and Embankment Foundations: Bluegrass Parkway Bridges over Chaplin River" *Interim Rep. No. KYHPR-64-17; HPR-1(8)*, Kentucky Transportation Center, Lexington, Kentucky

Hopkins, T.C. (1969). "Settlement of Highway Bridge Approaches and Embankment Foundations." *Interim Rep. No. KYHPR-64-17; HPR-1(4)*, Kentucky Transportation Center, Lexington, Kentucky

Hoppe, E.J. (1999). "Guidelines for the Use, Design, and Construction of Bridge Approach Slabs." Rep. No. VTRC 00-R4, Virginia Transportation Research Council, Charlottesville, VA.

Hsi, J. P. (2007). "Managing Difficult Ground-Case Studies." Proceedings of First Sri Lankan Geotechnical Society International Conference on soil and Rock Engineering, Colombo.

Iowa DOT. (2016). Bridge Maintenance Manual. Project No. TR-646.

Iowa DOT. (2023). Iowa DOT Standard Specifications Division 24 Section 2432 Mechanically Stabilized Earth (MSE) Retaining Wall. In. https://www.iowadot.gov/erl/current/gs/content/2432.htm: Iowa DOT.

Jayawickrama, P., Nash, P., Leaverton, M., and Mishra, D. (2005). "Water Intrusion in Base/Subgrade Materials at Bridge Ends." *Final Research Report FHWA/TX-06/0-5096-1*, Texas Department of Transportation.

Krauss, P. D., Lawler, J. S., & Steiner, K. A. (2009). Guidelines for selection of bridge deck overlays, sealers and treatments. *NCHRP Project*, 20-07.

Lenke, L. R. 2006. Settlement issues–bridge approach slabs. Final Rep. Phase 1. Rep. No. NM04MNT-02. Albuquerque, NM: New Mexico Dept. of Transportation.

Long, J.H., Olson, S.M. and Stark, T.D. (1998). "Differential Movement at Embankment/Bridge Structure Interface in Illinois." Transportation Research Record No. 1633, Transportation Research Board, Washington, D.C., 53-60.

Louisiana DOT (1999). Geotechnical Design Guide 8: Mechanically Stabilized Earth Wall (MSEW) Design Guide. In. http://wwwsp.dotd.la.gov/Inside_LaDOTD/Divisions/Engineering/Pavement_Geotechnical/MSE%20Walls/Geotechnical%20Design%20Guide%208.pdf. Louisiana Department of Transportation and Development.

Lu, Q., Li, M., and Xin, C. (2018). "Best Practices for Construction and Repair of Bridge Approaches and Departures." *Final Report No. BDV25-977-31*. Florida Department of Transportation.

Luna, D., Robison, J. L., and Wilding, A. J. (2004). "Evaluation of Bridge Approach Slabs, Performance and Design." Finap Project Report: RDT 04-010. Missouri Department of Transportation.

Marr, W. and Stulgis, R. (2013). Selecting backfill materials for MSE retaining walls. Draft Final Rep. NCHRP 24, 22.

McGhee, K. (2002.) A new approach to measuring the ride quality of highway bridges. VTRC 02-R10. Charlottesville, VA: Virginia Transportation Research Council.

Medina-Martinez, C. J., Sandoval Herazo, L. C., Zamora-Castro, S. A., Vivar-Ocampo, R., & Reyes-Gonzalez, D. (2023). Use of Sawdust Fibers for Soil Reinforcement: A Review. *Fibers*, *11*(7), 58.

Mekkawy, M., White, D.J., Souleiman, M.T., and Sritharan, S. (2005). "Simple Design Alternatives to Improve Drainage and Reduce Erosion at Bridge Abutments." *Proceedings of the 2005 Mid-Continent Transportation Research Symposium*, Ames, Iowa.

Miller, G. A., Hatami, H., Cerato, A., and Osborne, C. (2013). "Applied approach slab settlement research, design/construction." *Final Report: FHWA-OK-13-09*. Oklahoma Department of Transportation.

Mishra, D., J. McAtee, S. Chowdhury, B. Chittoori, E. Tutumluer, and J. Nicks. 2021. Statistical analysis of pavement profiler data to evaluate the bump at the end of the bridge. FHWA-HRT-21-037. McLean, VA: Federal Highway Administration. Office of Infrastructure Research and Development.

Mishra, D., J. McAtee, M. S. Chowdhury, B. C. S. Chittoori, and E. Tutumluer. (2020). TechNote: Synthesis—The Reduction and Analysis of Pavement Profiler Data to Quantify the Bump at the End of the Bridge, Report No. FHWA-HRT-20-021, Federal Highway Administration, Washington, DC. Available online: https://www.fhwa.dot.gov/publications/research/infrastructure/structures/bridge/20021/20021.pdf, [Last accessed June 5, 2020].

MoDOT. (2004). *Void Detection With the Falling Weight Deflectometer. [Report No. RDT04-004; RI99-044]*. Missouri Department of Transportation. https://rosap.ntl.bts.gov/view/dot/39792

Nicholson, P. G. (2014). *Soil improvement and ground modification methods*. Butterworth-Heinemann.

ODOT. (2023). Bridge Maintenance Manual: Preventative Maintenance Repair Guidelines for Bridges and Culverts. In: State of Ohio Department of Transportation.

Ohio DOT. (2007). Supplemental Specification 840: Mechanically Stabilized Earth Wall. In. https://www.dot.state.oh.us/Divisions/ConstructionMgt/Specification%20Files/840_01192007_for_2005.PDF: Ohio DOT.

Olmedo, C., B. Henderson, G. Cimini, and J. Springer. (2015). Bump Determination at Bridge Approach Transitions Using Inertial Profilers. Presented at the 2015 Conference of the Transportation Association of Canada, Charlottetown, Prince Edward Island. Available online: http://conf.tac-atc.ca/english/annualconference/tac2015/s18/olmedo.pdf.

Onyango, M., McLean, A., Owino, J., Fomunung, I., & Elliot, L. (2018). *Improving Rigid Pavement Smoothness using PolyLevel*.

Opland, W. H., & Barnhart, V. T. (1995). *Evaluation of the URETEK method for pavement undersealing*. Research and Technology Section, Materials and Technology Division, Michigan

Phares, B. M., White, D. J., Bigelow, J., Berns, M., and Zhang, J. (2011). Identification and evaluation of pavement-bridge interface ride quality improvement and corrective strategies. *Report No. FHWA/OH-2011/1*. Ohio Department of Transportation. *https://rosap.ntl.bts.gov/view/dot/18573*

Puppala, A. J., Archeewa, E., Saride, S. and Nazarian, S. and Hoyos, L. (2011). "Recommendations for Design, Construction, and Maintenance of Bridge Approach Slabs." *Final Research Report FHWA/TX-11/0-6022-2*. Texas Department of Transportation.

Roshan, M. J., Rashid, A. S. A., Wahab, N. A., Tamassoki, S., Jusoh, S. N., Hezmi, M. A., . . . Azmi, M. (2022). Improved methods to prevent railway embankment failure and subgrade degradation: A review. *Transportation Geotechnics*, *37*, 100834.

Ryu, S., Choi, P., Zhou, W., Saraf, S., & Won, M. C. (2012). *Improvements of Full Depth Repair Practices for CRCP Distresses*.

Ryu, S. W., Choi, P., Choi, S., & Won, M. C. (2013). Improvements of full-depth repair practices for distresses in continuously reinforced concrete pavement. *Transportation research record*, *2368*(1), 102-113.

Scherer, S. D., & Gay, R. L. (2000). Compaction grouting: three midwest case histories. In *Advances in Grouting and Ground Modification* (pp. 65-82).

Seo, J. (2003). "The Bump at the End of the Bridge: An Investigation." Dissertation submitted in partial fulfillment of the requirements for the degree of the Doctor of Philosophy, Texas, A&M University, College Station, Texas.

Soltesz, S. (2002). *Injected polyurethane slab jacking*.

Stevenson, J. (2021a). *Pavement Manual 2021-2: Section 6 HMA Overlays*. TxDOT. Retrieved November 2023 from *http://onlinemanuals.txdot.gov/TxDOTOnlineManuals/TxDOTManuals/pdm/hma_overlays.htm#i1009968*

Stevenson, J. (2021b). *Pavement Manual 2021-2: Section 7 Dowel Bar Retrofit*. TxDOT. Retrieved November 2023 from *http://onlinemanuals.txdot.gov/TxDOTOnlineManuals/txdotmanuals/pdm/dowel_bar_retrofit.htm*

Szynakiewicz, T. (2016). Compaction Grouting for Ground Improvement and Structure Rehabilitation. Rocky Mountain Geo-Conference 2016,

Tadros, M.K. and Benak, J.V. (1989). *Bridge Abutment and Approach Slab Settlement (Phase I Final Report)*. University of Nebraska, Lincoln

TxDOT. (2014a). Special Specifications 3025 Raising and Undersealing Concrete Slabs with Foam Systems. In. *https://www.txdot.gov/business/resources/txdot-specifications.html*.: Texas Department of Transportation.

TxDOT. (2014b). Special Specifications 3086 Soil Densification and Raising Concrete Slabs with High Density Polyurethane Foam (HDPF). In. *https://www.txdot.gov/business/resources/txdot-specifications.html*: Texas Department of Transportation.

Texas Department of Transportation (2014). *Standard Specifications for Construction and Maintenance of Highways, Streets, and Bridges*. Texas Department of Transportation, Austin, TX.

Texas Department of Transportation (2019). "Loss of Backfill in Mechanically Stabilized Earth Retaining Walls." https://ftp.txdot.gov/pub/txdot-info/library/pubs/bus/bridge/loss_backfill.pdf [Accessed on 11/2/23]

Texas Department of Transportation (2022). *Bridge Division Standard – Mechanically Stabilized Earth Retaining Wall (RW-MSE-22).* Texas Department of Transportation.

Texas Department of Transportation (2023). *Bridge Design Guide*. Texas Department of Transportation Bridge Division.

Thiagarajan, G., Gopalaratnam, V., Halmen, C., Ajgaonkar, S., Ma, S., Gudimetla, B., and Chamarthi, R. (2010). *Bridge approach slabs for Missouri DOT looking at alternative and cost efficient approaches* (No. OR 11.009). Missouri. Department of Transportation.

Umar, M., Kassim, K. A., & Chiet, K. T. P. (2016). Biological process of soil improvement in civil engineering: A review. *Journal of Rock Mechanics and Geotechnical Engineering*, *8*(5), 767-774.

Vennapusa, P. K., & White, D. J. (2015). Field assessment of a jointed concrete pavement foundation treated with injected polyurethane expandable foam. *International Journal of Pavement Engineering*, *16*(10), 906-918.

Vennapusa, P. K., Zhang, Y., & White, D. J. (2016). Comparison of pavement slab stabilization using cementitious grout and injected polyurethane foam. *Journal of Performance of Constructed Facilities*, *30*(6), 04016056.

Verma, H., Ray, A., Rai, R., Gupta, T., & Mehta, N. (2021). Ground improvement using chemical methods: A review. *Heliyon*, *7*(7).

Wahls, H. E. (1990). *NCHRP Synthesis of Highway Practice No. 159: Design and Construction of Bridge Approaches*. Transportation Research Board, National Research Council, Washington, D.C.

Wang, Y., Li, H., & Xie, J. (2023). "Evaluation of bridge approach slab condition using sub-mm 3D laser imaging technology." *Journal of Transportation Engineering, Part B: Pavements*, 149(2), 04023017.

White, D. J., Mekkawy, M. M., Sritharan, S., & Suleiman, M. T. (2007). "Underlying" causes for settlement of bridge approach pavement systems. *Journal of Performance of Constructed Facilities*, *21*(4), 273-282.

White, D. J., Sritharan, S., Suleiman, M. T., Mekkawy, M., and Chetlur, S. (2005). "Identification of the Best Practices for Design, Construction, and Repair of Bridge Approaches." *Research Report for CTRE Project 02-118 and Iowa DOT Project TR-481*. Iowa Dept. of Transportation.

Wilson, B., Scullion, T., & Faruk, A. (2015). *Evaluation of design and construction issues of thin HMA overlays*.

Zada, U., Jamal, A., Iqbal, M., Eldin, S. M., Almoshaogeh, M., Bekkouche, S. R., & Almuaythir, S. (2023). Recent advances in expansive soil stabilization using admixtures: current challenges and opportunities. *Case Studies in Construction Materials*, e01985.

Zang, K., J. Shen, H. Huang, M. Wan, and J. Shi. 2018. *Assessing and Mapping of Road Surface Roughness Based on GPS and Accelerometer Sensors on Bicycle-Mounted Smartphones*. Sensors, 18 (3), 914. Available online: https://doi.org/10.3390/s18030914

Zhang, J. (2016). "BRIDGE END SETTLEMENT EVALUATION AND PREDICTION". Theses and Dissertations--Civil Engineering. 40. *https://uknowledge.uky.edu/ce_etds/40*

APPENDIX A: Survey Questionnaire

Survey description:

The Research Team at Texas Tech University (TTU) is performing a research project titled "*0-7173 Develop Guidelines for Evaluation of Embankment Conditions in Bridge Approach Slabs and Pavement Structures,*" under the sponsorship of Texas Department of Transportation (TxDOT).

The purpose of this questionnaire is to document practices used by each district and division for the evaluation and maintenance of in-service roadway embankments/retaining walls on which bridge approach slabs and nearby pavement structures are supported. The results of this questionnaire will be incorporated into synthesis of state-of-the-practice on evaluation and repair of in-service roadway embankments/retaining walls, with the intent of helping TxDOT further improve the current practices.

Please complete and submit this questionnaire by Friday, April 19, 2024. We estimate that it should take approximately 15 minutes to complete and highly appreciate your valuable inputs. **If results of this study are published or presented, your name will remain confidential**.

If you have any questions related to this questionnaire, please contact the principal investigator Dr. Hoyoung Seo, P.E. at *hoyoung.seo@ttu.edu* or directly at (806) 834-5690.

Thank you for your time and expertise in completing this important questionnaire.

Contact Information:

Please provide the following contact information:

- Name: _____
- Position: _____
- District: _____
- Email: _____

1. What are the common problems you encountered at the bridge approach slabs and nearby pavement structures in embankments/retaining walls? Check all that apply.

   - ❑ Settlements/Heaves/Faulting (including bumps)
   - ❑ Longitudinal cracks
   - ❑ Transverse cracks
   - ❑ Lane separations
   - ❑ Partial or entire joint failure
   - ❑ Other_____

2. When do you typically start noticing/observing problems in bridge approach slabs or nearby pavement structures in embankments/retaining walls?

   - ❑ Less than a year after completion of the construction
   - ❑ 1 to 5 years after completion of the construction
   - ❑ 5 to 15 years after completion of the construction
   - ❑ More than 15 years after completion of the construction
   - ❑ Not sure

3. How do you identify bridge approach slabs and nearby pavement sections in embankments/retaining walls that need repair? Check all that apply.

   - ❑ Visual observations
   - ❑ Bridge condition ratings such as Item 65 (Approaches)
   - ❑ Rideability
   - ❑ International roughness index (IRI)
   - ❑ Public complaints
   - ❑ Other_____

4. Do you have any specific criterion when making decisions for repair of bridge approach slabs and nearby pavement sections in embankments/retaining walls?

   - ❑ No
   - ❑ Yes. Please specify: _____

5. What activities do you conduct to evaluate the conditions of the bridge approach slabs and nearby pavement section in embankments/retaining walls? Check all that apply.

   - ❑ Visual inspection
   - ❑ Falling Weight Deflectometer (FWD)
   - ❑ GPR (Ground Penetrating Radar)
   - ❑ Lidar
   - ❑ Coring through pavement structure
   - ❑ Other _____

6. What activities do you conduct to evaluate the conditions of the embankment fills that are already in service? Check all that apply.

   - ❑ Dynamic Cone Penetrometer (DCP) Test
   - ❑ Cone Penetration Test (CPT)
   - ❑ Standard Penetration Test (SPT)
   - ❑ Texas Cone Penetrometer (TCP) Test
   - ❑ Soil Sampling and Laboratory Test
   - ❑ Other _____

7. What are the main properties that you want to determine for in-service embankment fills when assessing their conditions? Check up to 2 items.

   - ❑ Resilient modulus (Mr)
   - ❑ Modulus of subgrade reaction (k)
   - ❑ California Bearing Ratio (CBR)
   - ❑ Degree of compaction
   - ❑ Dry density
   - ❑ Plasticity index (PI)
   - ❑ Others _____

8. In your opinion, what would be the major factors contributing to the distresses of bridge approach slabs and nearby pavement in embankments/retaining walls? Check up to 3 items.

   - ❑ Settlement of foundation soils (i.e., natural soils) beneath the embankment/retaining wall
   - ❑ Settlement of backfills due to poor compaction
   - ❑ Poor backfill materials (such as backfill soils not meeting specifications)
   - ❑ Poor construction practices
   - ❑ Poor drainage and soil erosion due to water infiltration
   - ❑ Void formation
   - ❑ Movements of retaining walls
   - ❑ Others _____

9. Please check the most common repair/maintenance measures taken in your District for bridge approach slabs and nearby pavement in embankments/retaining walls. Check up to 2 items.

   - ❑ Level-up of approach slab
   - ❑ Injection of polyurethane foam (e.g., Uretek)
   - ❑ Asphalt overlay
   - ❑ Full or partial depth repair
   - ❑ Treatment of the backfill/subgrade
   - ❑ Replacement of backfill
   - ❑ Installation of effective drainage system
   - ❑ Joints repair
   - ❑ Others _____

10. What is the typical frequency of performing repairs on a previously repaired section of bridge approach slabs and nearby pavement in embankments/retaining walls?

    - ❑ Repaired the same section again in less than one year.
    - ❑ Repaired the same section again between 1 and 5 years.
    - ❑ Repaired the same section again between 5 and 10 years.
    - ❑ No further repairs were needed.
    - ❑ Other _____

11. Do you have any distressed bridge approach slabs and nearby pavement sections in embankments/retaining walls that you would like the Research Team to investigate? If you do, please provide approximate GPS coordinates.

    ❑ No, we do not need any investigation.
    ❑ Yes, their locations are:
    (1) Longitude: _____; Latitude: _____ ( )
    (2) Longitude: _____; Latitude: _____ ( )
    (3) Longitude: _____; Latitude: _____ ( )
    Example: Longitude -97.116090; Latitude 31.566162; (IH35 North Bound Frontage Road)

12. Do you have any bridge approach slabs and nearby pavement sections in embankments/retaining walls that you previously repaired and have been performing well since then? If you do, please provide approximate GPS coordinates.

    ❑ No, we do not such sections.
    ❑ Yes, their locations are:
    (1) Longitude: _____; Latitude: _____ ( )
    (2) Longitude: _____; Latitude: _____ ( )
    (3) Longitude: _____; Latitude: _____ ( )
    Example: Longitude -97.116090; Latitude 31.566162; (IH35 North Bound Frontage Road)

13. Do you have any specific recommendations (a) for fill materials for embankments/retaining walls or (b) for construction practices to further improve performance of bridge approach slabs and nearby pavement structures in embankments/retaining walls?

    _____

    _____

    _____

    _____

_____

_____

14. Do you have any specific recommendations for repair practices to further improve performance of bridge approach slabs and nearby pavement structures in embankments/retaining walls?

_____

_____

_____

_____

_____

_____

APPENDIX B: Value of Research (VoR)

Benefit Areas

Project 0-7173 provides TxDOT with consistent guidelines for evaluating embankment-related distress at bridge approach slab (BAS) and adjacent pavement as well as mechanism-based repair framework. The savings that are estimated for Value of Research (VoR) assume that maintenance/repair costs can be decreased because the evaluation guidelines and repair framework can reduce the repetitive temporary repairs and increase service life.

For the estimation of the VoR, a summary of selected benefit areas of Project 0-7173 is shown in **Table B-1**.

Table B-1. VoR Benefit Areas.

Benefit Area	Qualitative	Economic	Both	TxDOT	State	Both	Definition in context to the Project Statement
Level of Knowledge	X			X			This project will enhance state-of-the-practice understanding of the root causes governing embankment, bridge approach slab (BAS), and approach pavement distresses.
Management and Policy	X			X			The evaluation sequence, classification thresholds, and three-level repair strategy developed in this project will enable more uniform inspection procedure so that maintenance decisions are consistent across all TxDOT districts.
System Reliability		X		X			Mechanism-based evaluation and repair selection can reduce recurrence of BAS settlement, faulting, subsurface voids, and lane separation, improving the reliability of bridge approach transitions.
Increased Service Life		X		X			Addressing the active mechanism before restoring the surface can improve treatment durability and extend re-intervention intervals at problematic bridge ends.
Improved Productivity and Work Efficiency		X		X			A staged testing sequence and evaluation guidelines developed in this project will help districts streamline field investigation, avoid unnecessary testing, and minimize trial-and-error diagnosis.
Reduced Construction, Operations, and Maintenance Cost		X			X		Better diagnosis and mechanism-matched repairs using the guidelines developed in this project can reduce repeated expenditure on temporary 'surface only' repairs that do not address active root causes.
Materials and Pavements		X			X		The evaluation guidelines developed in this project will allow districts to systematically assess conditions of pavement near BAS and in-service embankment fill materials and to select optimum repair strategy.
Safety and Quality of Life			X			X	More reliable bridge approach profiles and fewer recurring work zones will improve ride quality and reduce exposure to abrupt bumps, lane separation, and maintenance activities in traffic.

Estimation of VoR

According to TxDOT Bridge Facts (FY24), there are 56,620 bridges in Texas: 35,973 on-system bridges, 20,647 off-system bridges, and 33 international highway bridges. Because on-system bridges are maintained by TxDOT and bridges generally have two approach slabs (approach-side BAS and departure-side BAS), it is estimated that there are 71,946 BASs statewide managed by TxDOT.

There is no publicly available information about number of approach slabs repaired per year, but TxDOT Project 0-6022 cited that annual costs for BAS settlement repairs in Texas are around $7 million. Because repair costs vary widely depending on repair actions (ranging from routine asphalt overlay at about $10,000 to full slab replacement at about $50,000), the actual number could reasonably range from about 140 to 700 repairs. Based on this estimate, the Research Team assumed 360 BAS repairs per year (corresponding to 14 repairs per year per district) for the purpose of VoR estimation.

The expected annual benefit amount was estimated from the costs associated with potential reduction of recurring repairs and extension of repair intervals, improved selection of the initial repair, and avoided lane-closures and road-user delay. Because 80 percent of surveyed districts reported repairing the same section again within 10 years, 50 percent of annual BAS repairs were assumed to occur at previously repaired locations. The staged evaluation and mechanism-based repair framework was then assumed to prevent 15 percent of these repeat repairs, or approximately 27 avoided repairs per year. The resulting annual savings were estimated at about $674,494 (27 times $25,000 per repair per year). Since 63 percent of the survey respondents reported applying no specific criterion when deciding how to repair, improved diagnosis was also assumed to redirect 5 percent of annual repair actions to a more appropriate initial repair, at an average savings of $10,000 each, producing an estimated $179,865 per year. Both amounts, totaling $854,359, are reported under *Reduced Construction, Operations, and Maintenance Cost*.

For repeat repairs that were not avoided (153 out of 180 repairs), the framework was assumed to extend the repair interval by two years. The value of this extended repair interval, calculated at a 5 percent discount rate, was estimated at $355,346 per year and is reported under *Increased Service Life*. Finally, avoiding approximately 27 repeat-repair work zones was estimated to reduce road-user delay by $142,453 per year, based on 8,000 affected vehicles per work zone, an average delay of 0.033 hour (2-minutes) per vehicle, and a value of travel time of $20 per vehicle-hour, reported under *Reduced User Cost*.

The combined expected annual value of these four benefit components was approximately $1.35 million. Repairs avoided outright and repairs only deferred are counted separately, so no saving is claimed twice.

Figure B-1 presents the input and output values used in VoR estimation for this project. The estimated total savings by conducting this project is approximately $25 million, corresponding to a net present value (NPV) of approximately $15.4 million (see **Figure B-2**) and cost benefit ratio 22, with expected value duration of 20 years and payback period of about 0.5 years.

Texas Department of Transportation	**Project #**	0-7173		
	Project Name:	Develop Guidelines for Evaluation of Embankment Conditions in Bridge Approach Slabs and Pavement Structures		
	Agency:	TTU/TechMRT	**Project Budget**	$ 716,614
	Project Duration (Yrs)	3.0	**Exp. Value (per Yr)**	$ 1,352,157
Expected Value Duration (Yrs)		20	**Discount Rate**	5%
Economic Value				
Total Savings:	$ 24,974,376	**Net Present Value (NPV):**		$ 15,427,280
Payback Period (Yrs):	0.529978	**Cost Benefit Ratio (CBR, $1 : $___):**		$ 22

Figure B-1. Input and output values used in VoR analysis for Project 0-7173

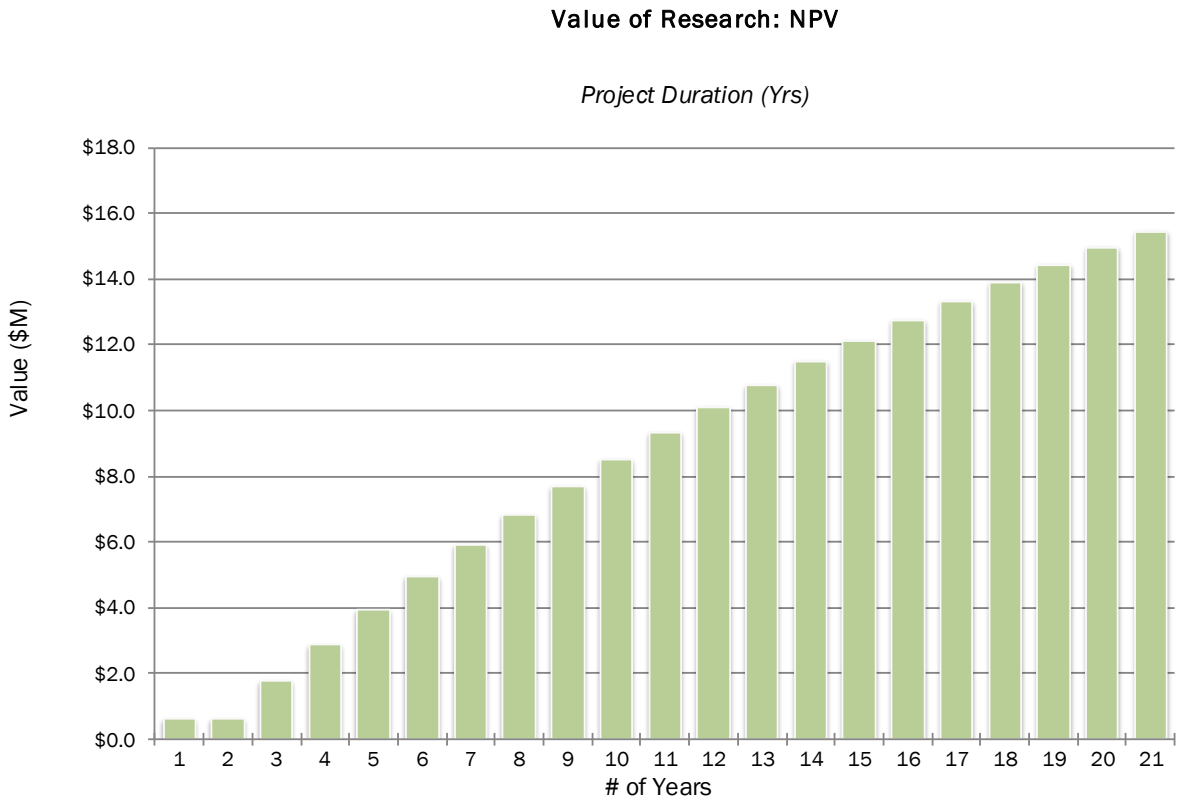


Figure B-2. Estimates of Net Present Value (NPV) of Project 0-7173